The expression and localisation of membrane transporters and P450 enzymes along the longitudinal and crypt-villus axes of the rat intestine and their response to oral imatinib

Megan Jo Webster MRes. B.Sc. (Hons)

Submitted for the degree of Doctor of Philosophy

Epithelial Research Group

Institute for Cell and Molecular Biosciences

The Medical School

University of Newcastle upon Tyne

September 2014

Abstract

A reduction in oral bioavailability of a wide range of drug compounds may occur following efflux of drug substrates into the intestinal lumen mediated by ATP dependent ABC transporters MDR1, MRP2 and BCRP and/or by enteric metabolism of drug compounds by CYP450 enzymes. Furthermore, inter-individual variability in the expression and function of key drug disposition proteins, which may occur following a regime of drug treatment, has the potential to cause altered pharmacokinetic profiles leading to failure of therapy.

This thesis aimed to establish mRNA and protein expression of key drug transporter proteins and CYP450 enzymes both along the length of the intestine and across the crypt-villus axis using NanoString mRNA technology and immunohistochemistry. Key findings include; a) evidence for cytoprotection of the crypt cells distinct from enterocytes, b) a lack of correlation between Mrp2 mRNA and protein expression in the rat small intestine, with a paucity of brush-border protein in all regions, c) using the M70 antibody, Bcrp protein was immunolocalised to the lateral cell membranes of cryptal epithelial in the duodenum, jejunum and ileum with no apparent protein expression above the crypt-villus junction.

Oral administration of the tyrosine kinase inhibitor imatinib mesylate was found to cause significant induction of Cyp1a1 mRNA expression with maximal induction in ileum samples showing an average 169-fold increase in expression. Immunohistochemistry indicates an associated increase in Cyp1a1 protein levels. In addition intestinal exposure to imatinib was found to cause significant changes in mRNA expression levels of genes including Mdr1a and Bcrp.

This thesis presents key differences with regards to protein localisation of ABC transporters proposed to play an important role in conferring intestinal drug resistance between rat and human tissues and highlights the high levels of complexity associated with oral drug delivery and intestinal absorption.

Acknowledgements

Firstly I would like to thank my supervisor Prof. Nicholas Simmons for his support, commitment and motivation throughout my PhD studies. I wish to thank Dr Gary Wilkinson not only for his input and supervision throughout my placement at AstraZeneca but also for his continued support throughout my studies whilst based at Newcastle University.

I would like to acknowledge several employees of AstraZeneca, without whom I would have been unable to utilise novel technologies and equipment whilst based at the Alderley Edge site. I wish to thank Margaret Veldmann-Jones, for her expertise and advice on design and implementation of NanoString mRNA analysis technology, Janet Kelsall for her advice surrounding molecular biology techniques and Kevin Randall for his support with immunohistochemical work. Thanks must also go to Peter Jones, Patricia Pimlott and Kathryn Pickup for their help in design and implementation of the *in vivo* work carried out during this project. I would also like to thank Constanze Hilgendorf for her help in obtaining human intestinal samples.

Finally, I would like to thank my friends and family for their motivational speeches in my hour of need and for helping to make this experience enjoyable.

Abbreviations

Ab	Antibody
ABC	ATP binding cassette
ABL	Abelson tyrosine kinase gene
aCa	Calcium activities
ACE	Angiotensin - converting enzyme
ACTB	β-actin
ADME	Absorption Distribution Metabolism and Excretion
ADP	Adenosine di-phosphate
Adr	Adriamycin
AhR	Aryl hydrocarbon receptor
Akt	Protein kinase B
ALPH	Alkaline phosphatase
AMP-PNP	Adenylyl-imidodiphosphate
ANOVA	Analysis of variance
ARG	ABL related gene kinase
ARNT	AhR nuclear translocator
Asn	Asparagine
ATCC	American Type Culture collection
ATP	Adenosine tri-phosphate
AUC	Area under curve
B2M	β-2-microglobulin
BCA	bi-cinchronic acid
BCR-ABL	Breakpoint cluster- Abelson tyrosine kinase gene
BCRP	Breast cancer resistance protein
Caco2	Colonic adenocarcinoma cell line
CAR	Constitutive androsterone receptor
CBC cells	Crypt-base columnar cells
cc1	cell conditioning treatment 1
cc2	cell conditioning treatment 2
CD147	cluster of differentiation 147 protein
cDNA	complementary DNA
CFTR	Cystic fibrosis transmembrane conductance regulator
CHO	Chinese Hamster Ovary cell line

c-Kit	proto-oncogene c-Kit (also known as Mast/stem cell growth factor receptor)
Cmax	Maximal concentration
CML	chronic myeloid leukaemia
cMOAT	Canalicular multispecific organic anion transporter
CNT	Concentrative nucleoside transporter
Crkl	Crk-like protein
cRNA	Complementary RNA
CsA	Cyclosporin A
Ct	Cycle threshold
CYP	Cytochrome
CYP450	Cytochrome P450
DAB	3, 3'-Diaminobenzidine
Dpm	Disintegrations per minute
Dt	Total disintegrations per minute
DTT	Dithiothreitol
E.Coli	Escherichia Coli
E3S	Estrogen-3-sulphate
ECACC	European Collection of Cell Cultures
ECL	Electrochemical luminescence
EDTA	Ethylenediaminetetraacetic acid
EGTA	Ethylene glycol tetraacetic acid
FCS	Fetal calf serum
FTC	Futrimorgan C
FXR	Farnesoid X Receptor
GAPDH	glyceraldehyde-3-phosphate dehydrogenase
GIST	gastrointestinal stromal tumours
GPR49	G-protein receptor 49
GUSB	glucuronidase-β
HA-	hemagglutinin
HBSS	Hanks balanced salt solution
HEK	Human Embryonic Kidney
HEK293	Human Embryonic Kidney293 cells
HIEC	Human intestinal epithelial cells
HMBS	Hydroxymethylbilane synthase

HPLC	High performance liquid chromatography
HPRT1	Hypoxanthine phosphorbosyltransferase 1
HRP	Horseradish peroxidase
HS	Horse Serum
HSCs	Hematopoietic stem cells
HSKP	Housekeeping
HSP90	Heat shock protein 90
$J_{(a-b)}$	Flux (apical to basolateral)
$J_{(b-a)}$	Flux (basolateral to apical)
J_{net}	Net flux ($J_{(b-a)} - J_{(a-b)}$)
KB	Kraftbrühe
KO	Knock out
K0143	(3*S*,6*S*,12a*S*)-1,2,3,4,6,7,12,12a-Octahydro-9-methoxy-6-(2-methylpropyl)-1,4-dioxopyrazino[1',2':1,6]pyrido[3,4-*b*]indole-3-propanoic acid 1,1-dimethylethyl ester
LAP	Leucine amino peptidase
LAP3	Leucine amino peptidase 3
LGR5	Leucine-rich repeat-containing G-protein coupled receptor 5
LogP	Partition coefficient
mBcrp	Mouse breast cancer resistance protein
MCT1	Monocarboxylate transporter 1
MDCK	Madin Darby Canine Kidney cell
MDR1	Multidrug resistance transporter 1
MDR1A	Multidrug resistance transporter isoform a
MDR1B	Multidrug resistance transporter isoform b
MEM	Modified eagles medium
MeOH	Methanol
MOPS	3-(N-morpholino)propanesulfonic acid
Mr	Molecular weight
mRNA	messenger ribonucleic acid
MRP	Multidrug resistance protein
MSD	Membrane spanning domain
MTS	3-(4, 5-dimethylthiazol-2-yl)-5-(3-carboxymethoxyphenyl)-2-(4-sulfophenyl)-2H-tetrazolium
MXR	Mitoxantrone resistance transporter

NADPH	Nicotinamide adenine dinucleotide phosphate
NBD	Nucleotide binding domain
NBF	Neutral buffered formalin
NEAA	Non-essential amino acids
Nkcc1	Na-K-Cl cotransporter 1
NR	Nuclear-receptor
OAT	Organic anion transporter
OATP	Organic anion-transporting polypeptide
OCT/OCTN	Organic cation transporter
P.D.	Potential difference
Papp	Apparent permeability
PBS	Phosphate buffered saline solution
PCNA	Proliferating cell nuclear antigen
PCR	Polymerase chain reaction
PDGFR	Platelet derived growth factor receptor
PEPT1	Peptide transporter 1
PFA	Paraformaldehyde
PFO	Perfluorooctanesulfonate
P_i	Inorganic phosphate
PI3K	Phosphatidylinositol-4, 5-bisphosphate 3-kinase
PK	Pharmacokinetic
PMEA	Para-methoxyl-N-ethylamphetamine
PNGase F	Peptide -N-Glycosidase F
pNPP	4-nitrophenyl phosphate
PPAR	Peroxisome proliferator-activated receptor
PXR	Pregnane-X-receptor
qPCR	Quantitative polymerase chain reaction
RAR	Retinoic acid receptor
RIN	RNA integrity value
RNA	Ribonucleic acid
Rpm	Revolutions per minute
RT-PCR	Real time – polymerase chain reaction
RXR	Retinoid-X-receptor
SEM	Standard error of the mean

SEYFP	Super enhanced yellow fluorescent protein
SGLT1	Sodium glucose co-transporter 1
Ship	SH2-containing Inositol 5'-Phosphatase
SLC	Multi-specific solute carrier
SLCO	Solute Carrier Organic Anion
SP	Side population
Stat5	Signal Transducer and Activator of Transcription 5
SUR1	Sulfonylurea receptor 1
SUR2	Sulfonylurea receptor 2
TBS	Tris-buffered saline
TCDD	2, 3, 7, 8-Tetrachlorodibenzodioxin
TEER	Transepithelial electrical resistance
TF	Transcription factor
TEM	Transmission electron microscopy
TK	Tyrosine kinase
Tm	melting temperature
TNFα	Tumour necrosis factor - α
TR-	Transport deficient
TUBA1	Tubulin alpha 1
VDR	Vitamin D receptor
XRE	Xenobiotic response element

Note: Consistent with HUGO Gene Nomenclature Committee guidelines human gene symbols and related mRNA and protein expression are presented with all letters in uppercase type (MDR1) whilst gene symbols, mRNA and protein designations of mouse, rat and canine are presented with only the first letter in uppercase with remaining letters in lower case (e.g. Mdr1).

Contents

Figures

Tables

Appendices

1. Introduction

1.1 The intestinal epithelium lining; an enterocytic barrier

The intestine can be subdivided into two regions; the small and large intestine. The small intestine is divided into the duodenum, jejunum and ileum which extend distally toward the ileocaecal junction and show differences with regard to intestinal absorption and secretion, whilst the large intestine comprises the colon (Boron and Boulpaep, 2009 p884, Lin et al., 1999). The primary purpose of the intestine, particularly the small intestine, is the digestion and absorption of a full complement of nutrients, both macro and micro, which are essential for maintaining life (Boron and Boulpaep, 2009 p883, Snoeck et al., 2005). The intestine therefore serves to allow storage and digestion of food substances and subsequent absorption of nutrients, released by digestion, across the epithelium lining of the lumen. Nutrients absorbed across the intestinal lining include sugars, fatty acids, peptides, amino acids, minerals and micronutrients such as vitamins (Boron and Boulpaep, 2009 p883).

Absorption of nutrients across epithelial cells mainly occurs by specialised membrane transport systems, which typically provide sufficient affinity to extract these components with high capacity, examples include the di and tri-peptide transporter PepT1 and the Na-glucose uptake transporter SGLT1 (Freeman et al., 1995, Yoshikawa et al., 2011). Following absorption, nutrients move into the extracellular fluid, lymph and blood which underlies the intestine (Barrett et al., 2010 p451). Once in blood, nutrients are transported via the hepatic portal vein to the liver (Boron and Boulpaep, 2009 p432).

In addition to the release of beneficial nutrients, intestinal digestion causes the release of potentially toxic compounds which must be excluded from blood plasma. As such, physiological mechanisms are required within the intestinal lining to prevent intracellular accumulation and subsequent absorption of such compounds (Snoeck et al., 2005). Furthermore, a barrier must exist to protect against invasion from bacteria and pathogens which constitute the intestinal microbiota that allow digestion of otherwise indigestible materials (Ohland and MacNaughton, 2010, Snoeck et al., 2005).

Such absorptive processes also apply to orally delivered pharmaceuticals. New drug entities may be hydrophilic in nature and achieve high bio-availability by mimicking nutrient substrates to aid compound absorption (Gomez-Orellana, 2005), e.g. angiotensin converting enzyme (ACE) inhibitors which contain a peptide bond and are good substrates for PEPT1 (Thwaites et al., 1995). Alternatively highly potent compounds are often lipophilic in nature and show ability to diffuse into the lipid membrane of intestinal enterocytes. A major advancement in the understanding of such problems in drug oral bioavailability has been the realisation that

the action of ATP binding cassette (ABC) transporters present within the intestinal mucosa limit absorption via recirculation of drug compounds back into the intestinal lumen and from the understanding that ABC transporters and cytochrome P450 (CYP450) enzymes, such as CYP3A4, may act synergistically to lower absorption of both drug molecules and potentially toxic compounds (Benet, 2009)

Membrane transport proteins belonging to the ABC superfamily, multidrug resistance transporter (MDR1), multidrug resistance protein 2 (MRP2) and the breast cancer resistance protein (BCRP) are responsible for the active efflux of potentially toxic compounds, including oral drugs, out of epithelial cells lining the intestine and into the intestinal lumen, thereby lowering drug absorption and promoting secretion (Szakacs et al., 2008). As such, MDR1, MRP2 and BCRP contribute to the physiological maintenance of the enterocyte barrier (Snoeck et al., 2005, Szakacs et al., 2008).

The enterocyte barrier is composed of a single layer of epithelial cells which line the intestine and defend against invasion from foreign and potentially toxic xenobiotics (Snoeck et al., 2005). In addition to expression of apical efflux transporters MDR1, MRP2 and BCRP, epithelial cells of the enterocyte barrier are now known to express a complement of metabolising enzymes which are able to biotransform xenobiotic molecules, rendering them inactive or more amenable to transporter mediated extrusion (Benet, 2009, Paine et al., 2006). With regards to expression of human metabolising enzymes the CYP3A family seem to be of significant importance in both hepatocytes and enterocytes (Paine et al., 2006, Suzuki and Sugiyama, 2004).

A series of studies summarised by Benet (2009) have shown synergistic actions of ABC transporters, specifically MDR1, and CYP3A enzymes, which caused reduced absorption of active drug compounds across enterocytes for example cyclosporine, tacrolimus, sirolimus, and K77. Studies have shown that dual MDR1 and CYP3A substrates were shown to be extensively metabolised, both *in vitro* and *in vivo*, when both proteins were functionally active, however inhibition of MDR1 significantly reduced compound metabolism and hence increased absorption of the parent drug molecule (Benet, 2009). For example, the extraction ratio (defined as the amount of drug metabolised relative to the amount of drug which could be accessed by the metabolising enzyme) of an investigational cysteine protease inhibitor, K77, was decreased from 33 to 14% when MDR1 was inhibited (Benet, 2009).

Given the reported apical expression of BCRP and MRP2/Mrp2 on villus enterocytes (Maliepaard et al., 2001, Mottino et al., 2000, Sandusky et al., 2002) and their known abilities to efflux drug compounds, these transporters may, in addition to MDR1, contribute toward

enterocytic recirculation of drug compounds. The proposed mechanistic interplay of ABC transporters and CYP450 enzymes is summarised in figure 1.1.

Even when the intestinal barrier is circumvented, the portal circulation, into which intestinal blood vessels drain, transports absorbed xenobiotic compounds to the liver (Boron and Boulpaep, 2009 p432). The liver encompasses extensive metabolic and secretory capacity, such that uptake from the portal circulation leads to subsequent hepatic biotransformation and biliary secretion into the intestinal lumen, a so called first pass metabolism phenomenon (Lin et al., 1999, Suzuki and Sugiyama, 2004).

Therefore although the enterocyte barrier and first pass metabolism are essential in protection against orally consumed toxic and foreign compounds and invasion by gut microbiota, they serve as a major barrier for oral drug delivery (Chan et al., 2004). Despite alternative drug delivery methods oral administration remains the preferred route for several reasons, although mainly due to high levels of patient compliance (Gomez-Orellana, 2005). Oral drug delivery also provides a cost effective mechanism for administration of pharmaceutical compounds without the need for hospitalisation or a sterile environment (Sastry et al., 2000). Furthermore, oral administration allows delivery of a diverse range of drug molecules and thus proves attractive to pharmaceutical companies (Sastry et al., 2000). Problems arise, however, due to intestinal efflux and metabolism and first pass metabolism of oral drug compounds since these physiologically protective mechanisms reduce systemic drug concentrations. As such, it is vital to understand how drug compounds interact with ABC efflux transporters and CYP450 enzymes in the intestine to ensure delivery of adequate drug concentrations and prevent the onset of adverse effects whilst ensuring achieved systemic concentrations lie within the desired therapeutic range. Further complications for oral administration arise due to inter-individual differences in expression and function of these proteins and/or potential for interaction and induction between co-administered drug compounds and dietary constituents (Gomez-Orellana, 2005, Suzuki and Sugiyama, 2004, Urquhart et al., 2007).

The main purpose of the present work has been to examine in detail the intestinal expression of selective nutrient transporters involved in drug absorption, ABC transporters and metabolic enzymes in the intestine to provide a framework for understanding potential interactions in the rat. In addition since expression of key elements of this model are not fixed but may be induced in response to oral (drug) challenge an *in vivo* study was also undertaken to explore aspects of multiple dosing with the anti-cancer agent imatinib.

Figure 1.1:

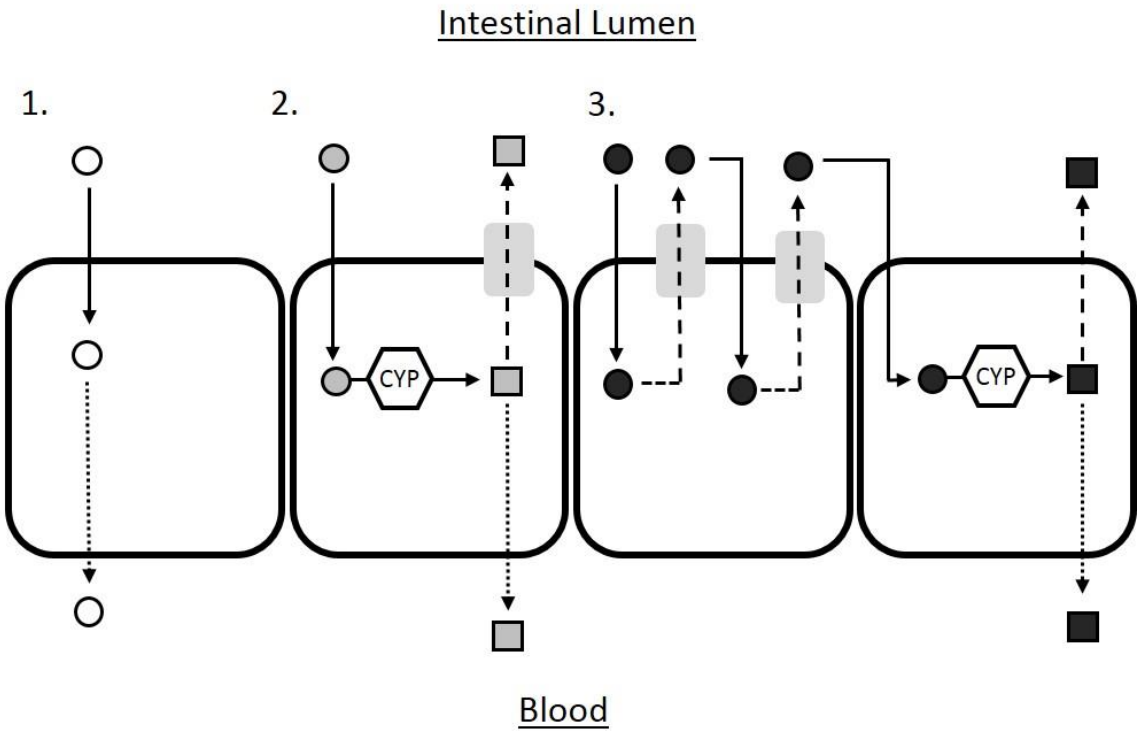

Figure 1.1 Schematic representation of the synergistic actions of ABC transporters and CYP450 enzymes active within the enterocyte barrier.

1. A drug molecule present within the lumen (open circle) is absorbed via the transcellular pathway from the intestinal lumen into the underlying blood by either facilitated diffusion due to its physiochemical properties or via access to nutrient transporters due to structural mimicking of physiological substrates. **2.** A drug molecule (grey circle) transverses the apical cell membrane and is biotransformed by cytochrome P450 (CYP) enzymes present within the cytoplasm thus rendering the metabolised drug molecule (grey square) more amenable to ABC mediated efflux, increasing overall capacity of the export process. **3.** Luminal drug molecule (black circle) transverses the apical cell membrane and if a substrate for ABC transporters is effluxed back into the intestinal lumen. The effluxed drug molecule is then free to be reabsorbed back across the apical cell membrane allowing enterocytic recirculation. Enterocytic recirculation increases potential for interaction between the drug molecule (black circle) and CYP450 enzymes, as such the drug is metabolised and subsequently effluxed or absorbed across the cell membrane. Absorbed drug metabolites likely show altered affinity at drug targets thereby altering drug pharmacokinetic profiles, as such enterocytic recirculation reduces absorption of parent drug molecule via promotion of interaction between drug molecules and CYP enzymes. Image adapted from (Benet, 2009).

1.1.1 Intestinal morphology; the longitudinal and crypt-villus axes

Lined by a single layer of epithelial cells, known as the enterocyte barrier, the mucosa of the intestine is not homogenous, rather it is folded to give finger like projections, known as villi (singular villus), which project into the intestinal lumen and submucosal invaginations which form structures known as crypts (Barker et al., 2008, Boron and Boulpaep, 2009 p934, Pinto and Clevers, 2005). Whilst the most proximal few inches of the duodenum lack villi the remainder of the small intestine possess both villi and crypts, with an increasing villus height observed with distal progression from the duodenum to the jejunum, such that folding of the small intestinal mucosa dramatically increases the surface area available for absorption (Boron and Boulpaep, 2009 p935). Unlike the small intestine, the mucosa of the colon has a flattened appearance (Pinto and Clevers, 2005), and does not possess villi but rather has an abundance of crypt structures which burrow deep into the submucosa (Barker et al., 2008). Like the small intestine the mucosa of the colon is essentially a single layer of epithelial cells.

The enterocyte barrier is composed entirely of epithelial cells and is generated by intestinal stem cells which reside within the crypt units (Snoeck et al., 2005). Each villus is populated by several crypt units each of which contain between 4-6 stem cells (Marshman et al., 2002). Despite a common origin, regional differences are apparent with regards to both physiological function and cell expression along the length of the intestine. Brunner's glands, for example, show a duodenal restrictive expression pattern where they act physiologically to secrete an alkaline rich mucus into the duodenum to neutralise the acidity of chyme and fluids received from the stomach (Boron and Boulpaep, 2009 p908-909). Brunner's glands are not found in any other region of the intestine. Similarly, Peyer's patches, aggregations of lymphoid tissue, are found only in the ileum of the small intestine. Whilst the small intestine serves as the main site of absorption, regional differences in nutrient transporter expression are evident with distal progression from the duodenum to the ileum (Boron and Boulpaep, 2009 p951). For example, differences in the intestinal absorption of calcium, folate and iron are also evident, with active absorption of these substances only in the duodenum, whilst active uptake of bile acids is apparent only in the ileum (Boron and Boulpaep, 2009 p951). Given that all cells of the enterocyte barrier originate from a common source, the intestinal stem cells, yet display differences with regards to cell types and transporter expression it is not unreasonable to suggest that such regional differences may also be apparent for drug transporter proteins and CYP450 enzymes.

By definition, stem cells should possess the ability to maintain proliferative status over prolonged time periods (longevity), be able to generate cell types of various lineages (pluripotency) and be self-regulated such that stem cell number remains constant within each

crypt (Barker et al., 2008, Marshman et al., 2002). As such, crypt stem cells must regenerate, to maintain tightly regulated stem cell numbers whilst also producing daughter cells which differentiate into the four lineages required for normal intestinal physiology (Barker et al., 2008, Marshman et al., 2002).

Intestinal stem cells are responsible for the generation of both absorptive and secretory epithelial cells which line the intestinal lumen (Pinto and Clevers, 2005). The absorptive cell component comprises intestinal enterocytes whilst the secretory component is made up of mucus secreting goblet cells, hormone producing enteroendocrine cells and Paneth cells (small intestine only), as such intestinal stem cells are pluripotent (Barker et al., 2008, Pinto and Clevers, 2005). Additionally M-cell expression is evident within some crypt units found adjacent to Peyer's patches (Marshman et al., 2002). M-cells are localised to the follicular associated epithelium of Peyer's patches within the ileum and evoke an immune response via endocytosis of luminal antigens and subsequent presentation to immune cells including macrophages and lymphocytes.

Using a Cre-activated LacZ promoter Barker et al., (2007) showed migration of blue stained daughter cells up the villus with an apparent origin of blue stained cell ribbons shown to be localised to the base of the crypt region. Furthermore, the presence of blue stained cells was apparent for up to 60 days, with an increasing crypt cell percentage observed with time, thus suggesting intestinal stem cells to be capable of long term maintenance (Barker et al., 2007). It is reported that prolonged presence of stem cells was observed for periods up to 12 months post study initiation (longevity) (Barker et al., 2008). As such intestinal stem cells have shown properties consistent with those required of a stem cell niche; pluripotency and longevity.

Two alternative models have been presented with regards to localisation and identification of crypt stem cells, known as the +4 position and the stem cell zone models (Barker et al., 2008). The +4 model is based on the localisation of stem cells four cells up from the crypt bottom, with Paneth cells occupying the three bottommost spaces (Barker et al., 2008). Past studies have shown these cells to be extremely sensitive to radiation and to carry the ability to retain genetic labels, indicative of ability to undergo proliferation. In 1977, Potten reported the presence of cells located at the crypt base which are hypersensitive to both X and γ radiation. Increased sensitivity of stem cells to radiation would ultimately protect against genetic damage, such that daughter cells would not be mutated and may therefore serve as a key mechanism responsible for preventing development of potentially harmful cells (Barker et al., 2008). It is speculated that stem cell progeny either migrate up the villus (enterocytes, goblet cells and enteroendocrine cells) or migrate toward the crypt base to form Paneth cells which reside within the crypt for up to twenty days (Barker et al., 2008, Pinto and Clevers, 2005). This

model, however, remains uncertain since it has not been possible to experimentally track the progeny of these proposed +4 stem cells, a trait required to confirm stemness of the identified niche (Barker et al., 2008).

Intestinal stem cell specific markers have long since eluded researchers, however realisation of the correlation between the WNT signalling pathway and intestinal epithelial cell differentiation and fate led to the immunohistochemical investigation of 80 WNT signalling molecules (Barker et al., 2008, Pinto and Clevers, 2005). Whilst the majority of WNT signalling molecules tested were found to be expressed throughout the crypt, the G-protein coupled receptor Lgr5 (leucine-rich repeat-containing G-protein coupled receptor 5) was shown to be expressed only in a distinct number of crypt cells. Generation of a Lrg5-LacZ heterozygous mouse allowed the study of Lgr5 expression in adult mice and showed Lgr5 protein to be restricted to a distinct subset of cells in tissues including the intestine, hair follicles, mammary glands and the adrenal gland. Furthermore a knock in Lgr5 allele carrying an integrated fluorescent green protein allowed visualisation of Lgr5 positive cells to the base of crypt units in both the small intestine and colon. Cryptal stem cells were distinct from Paneth cells and rather appeared to be interspersed amongst Paneth cells at the very base of intestinal crypts (Barker et al., 2008, Barker et al., 2007) This localisation is complementary to crypt base columnar (CBC) cycling cells, which were originally reported over thirty years ago (Cheng and Leblond, 1974). Presence of stem cells at the base of the crypt lead to the generation of the stem cell zone model (Barker et al., 2008).

The stem cell zone model speculates the presence of a mixed cell (MIX) population immediately above the cryptal Paneth cells. This MIX cell population is believed to originate from Lgr5 positive/CBC cells found interspersed at the crypt base (Barker et al., 2008). From within the MIX cell population bidirectional migration, as speculated in the +4 model, occurs, allowing movement and residence of Paneth cells at the crypt base and migration and subsequent differentiation of enterocytes, endocrine cells and goblet cells up the villus (Barker et al., 2008, Pinto and Clevers, 2005).

Stem cell progeny undergo up to six rounds of cell division as they migrate toward the crypt villus junction. Upon reaching the crypt-villus junction the fate of daughter cells, with regards to their intestinal cell lineage is decided and cells begin to terminally differentiate. Enterocytes, endocrine cells and goblet cells then progressively migrate up the intestinal villus where they undergo constant differentiation with regards to cellular protein expression and morphology. In compensation for continuous migration of cells from the crypt, cells are shed from the villus tip and are lost into the intestinal lumen by an apoptotic process (Barker et al., 2008). The

entire process, from initial cell division to loss at the villus tip has been shown to take 5 days in both human and mouse intestine (Barker et al., 2008, Pinto and Clevers, 2005).

Whilst the crypt unit is responsible for cell production, and consequently contains either proliferative or poorly differentiated cells (Barker et al., 2008, Pageot et al., 2000, Pinto and Clevers, 2005), the intestinal villus is responsible for numerous physiological processes including hormone production, secretion of digestive enzymes, absorption of nutrients and protection against foreign and drug compounds (Barker et al., 2008, Boron and Boulpaep, 2009 p933-935, Jakab et al., 2010). As such, gene expression and cellular protein composition differ remarkably and are altered as a direct result of differentiation up the crypt-villus axis (Anderle et al., 2005, Mariadason et al., 2005).

A possible explanation for such regional differences, both along the longitudinal and crypt-villus axes, is the axial patterning and graded expression of homeobox proteins, particularly Cdx1, Cdx2 and Pdx1, in the intestine. Homeobox proteins are peptides which bind to DNA promotor sequences of target genes and regulate target gene expression levels (Silberg et al., 2000). Following initial identification of homeobox genes in the *Drosophila melanogaster* they have since been shown to be vital during fetal development due to their ability to induce spatial and time dependent transcription of genes, however a major reduction in homeobox gene expression is reported toward the end of fetal life (Freund et al., 1998b). Given the requirement for regeneration of the intestinal epithelium, crypt-villus differentiation and regional gene expression along the longitudinal intestinal axis, homeobox genes, including Cdx1, Cdx2, and Pdx1, remain active in the intestine throughout adult life to allow cell renewal and remodelling (Silberg et al., 2000, Suh and Traber, 1996).

Cdx1 and Cdx2 are members of the caudal family of homeobox transcription factors as they show high sequence similarity with the *Drosophila melanogaster Caudal* gene which is known to play a key role in regulating anterior-posterior gene expression and early development (Freund et al., 1998b, Silberg et al., 2000). During intestinal organogenesis the embryonic lateral plate mesoderm and the visceral endoderm associate to allow development of the intestine, with the mesoderm being responsible for the formation of intestinal mesenchyme, amongst other anatomical features (Freund et al., 1998b). The ability of homeobox genes, expressed within the mesenchyme, to induce longitudinal axial patterning has been shown using a rat *in vivo* model. Dulec et al., (1994) determined the fate of the colonic endoderm, responsible for generation of the colon epithelium lining, following association of the colonic endoderm with either the colonic or small intestinal mesoderm. Since Cdx1 and Cdx2 are known to be expressed within mesenchyme, it was concluded that expression levels of Cdx1 and Cdx2 directly influence longitudinal axial patterning and the fate of intestinal epithelium,

with colonic mesoderm-colonic endoderm association giving a typical colonic phenotype whilst association of small intestinal mesoderm with colonic endoderm resulted in a phenotype displaying crypt-villus morphology with associated sucrose-isomaltase activity, reflective of small intestinal physiology (Duluc et al., 1997).

Additional to the role of Cdx1 and Cdx2 in fetal development, both homeoproteins remain expressed in intestinal tissues throughout adult life with undetectable levels of Cdx1 and Cdx2 mRNA in other mouse tissues (Suh and Traber, 1996). Both genes show differential expression levels along the longitudinal axis of the small intestine, with both Cdx1 and Cdx2 showing increased mRNA transcript expression from the duodenum to ileum (James and Kazenwadel, 1991). mRNA expression levels of both genes were found to be considerably higher in murine colonic samples, with Cdx1 and Cdx2 showing highest levels of expression in the proximal and distal colon respectively (James and Kazenwadel, 1991). Similarly, Cdx mRNA expression was found to be highest in the colon of rat tissues, with a decreasing expression gradient reported with anterior regression from the colon to the duodenum, however it is not known whether the 1.7Kb and 6.5Kb mRNA transcripts detected encode a single gene or represent two genes of close homology, as evident in murine tissues (Freund et al., 1998a). Studies performed on human tissue found expression of nine and sixteen homeobox mRNA transcripts in the duodenum and ileum respectively, with highest expression levels reported for Cdx1, Cdx2 and Pdx1, therefore supporting data presented for both mouse and rat intestine (Walters et al., 1997). The pancreatic/duodenal homeobox gene (previously known as Ipf-1, Idx-1 or somatostatin transcription factor Spf1), regulates the transcription of insulin and somatostatin in the pancreas and has previously been reported to show duodenal restricted intestinal expression in murine tissues, indicating a role for this homeobox protein in intestinal patterning (Miller et al., 1994, Walters et al., 1997).

It is reported that past studies have shown interactions between the intestinal specific homeobox gene Cdx2 and sucrose-isomaltase, calbindin-D9K, and carbonic anhydrase I which show distinct intestinal expression patterns (Lambert et al., 1996, Suh et al., 1994) strongly indicating a role for homeobox genes in intestinal regional patterning. Ability of homeobox genes to control transcriptional regulation of intestinal transporters indicates potential for homeobox gene regulated transcription of other intestinal transporters and enzymes, including those involved in drug disposition, and as such highlights the role of the nuclear proteins in intestinal axial patterning.

1.2 The ABC superfamily of proteins

The ABC superfamily is composed of 49 membrane bound proteins and is divided into seven subfamilies designated A through to G, based on their structural homology. ABC transporters are known to be involved in many physiological processes (Dean et al., 2001, Vasiliou et al., 2009). The ABC superfamily is composed of regulated ion channels (i.e. CFTR), membrane transporters and receptors (Dean et al., 2001). The importance of ABC transporters in maintenance of normal cell physiology is exemplified by their expression in every human cell studied thus far (Lee et al., 2009). Of key interest here are three widely expressed members of the ABC family belonging to the ABCB (MDR1), ABCC (MRP1-7) and ABCG (BCRP) subfamilies, which have previously been shown to cause resistance to drug compounds, either via apical intestinal efflux or translocation of substrates across the basolateral membrane in target cells. These transporters therefore alter the pharmacokinetic profile of orally administered drugs (Dietrich et al., 2003). Specific focus will be placed on MDR1, MRP2 and BCRP in this thesis due to their reported ability to confer intestinal drug resistance (Szakacs et al., 2008).

1.2.1 ABC transporters; structure and mechanism of action

ABCB, ABCC and ABCG family members share a common core structure composed of two membrane spanning domains (MSD) and two nucleotide binding domains (NBD), with all four units required to allow transporter functional activity (Higgins and Linton, 2004, Szakacs et al., 2008). Each MSD is composed of six membrane spanning α-helices which interact to form a central cavity through which substrates are transported (Higgins and Linton, 2004, Smith et al., 2002). Signature consensus sequences conserved within the ABC family, including the Walker A and B and signature 'S' motifs, in addition to H and Q loops involved in ATP transporter function are present within the amino acid sequences of these transporters (Higgins and Linton, 2004, Smith et al., 2002, Zhou, 2008). In addition to the two core MSDs, MRP2 and some other members of the ABCC subfamily also include a third MSD (long proteins), composed of five α-helical transmembrane domains, known as MSD_0, which gives rise to an extracellular N-terminal domain and an additional intracellular linker region, L_0 (Fukuda and Schuetz, 2012, Jedlitschky et al., 2006). Unlike MDR1 and MRP2, BCRP exists as a so called ''half protein'', in that it is composed of only one MSD and one NBD (Fukuda and Schuetz, 2012). As such homo- or hetero- dimerisation of the BCRP protein is required to confer functional transporter activity (discussed in detail in section 1.2.3.2) (Kage et al., 2002). Schematic representation of the predicted structures of MDR1, MRP2 and BCRP are shown in figure 1.2.

As indicated by their name, ATP *binding* cassette transporters bind and hydrolyse ATP to allow active transport of substances (Szakacs et al., 2008). The great difficulty to crystalise membrane proteins has impeded the study of the ABC transporter mechanism of action, nevertheless an ATP switch model is currently accepted as the mechanism by which ATP transporters efflux substrates out of the cell (Higgins and Linton, 2004, Szakacs et al., 2008). Given its ability to transport a wide range of substrates, and earlier identification and cloning, most work to ascertain ABC transporter mechanism of action has focused on the MDR1 transporter. Electron crystallography work performed by Rosenberg et al., (2003) showed presence of high density membrane spanning α-helical structures surrounding a central pore. Orientation of the transmembrane α-helices appeared to form a central cavity which was exposed to the extracellular milieu but occluded intracellularly due to the slanted orientation of surrounding TMD α-helices. The use of non-hydrolysable AMP-PNP (adenylyl-imidodiphosphate), to replace ATP, showed reorganisation of the pore surrounding membrane spanning domains upon binding of the AMP-PNP molecule such that whilst still enclosing a central pore perpendicular alignment of membrane spanning helices resulted in the formation of a gap within the transmembrane domain such that the central pore became accessible throughout the entire perpendicular length thereby exposing the transporter pore to the lipid membrane interface with an associated lack of intracellular pore occlusion (Rosenberg et al., 2003). This allows for acceptance of substrates into an internal binding pocket directly from within the lipid membrane in addition to substrate acceptance from the intracellular aqueous phase (Fukuda and Schuetz, 2012, Rosenberg et al., 2003). Given the lipophilic nature of many MDR1, MRP2 and BCRP substrates, it is likely that they will diffuse into the lipid bilayer therefore reorganisation of the membrane spanning proteins allows accessibility of membrane integrated substrates to the central transporter pore (Al-Shawi and Omote, 2005), permitting substrate transport.

Binding of transporter substrates to the MSD increases the affinity of ATP for the intracellular NBDs (Higgins and Linton, 2004). ATP binding initiates dimerisation of the two NBDs of the protein, causing formation of an intracellular NBD dimer with a subsequent conformational shape change to give an outwardly facing orientation of the central pore. The outward facing orientation allows release of substrates into the extracellular milieu (Fukuda and Schuetz, 2012). Hydrolysis of ATP to adenosine diphosphate (ADP) + P_i (inorganic phosphate) initiates dissociation of the NBD dimer and return to the inwardly facing conformation (Szakacs et al., 2008).

Similarly, BCRP homology modelling suggests arrangement of two monomeric MSDs to form a central cone like cavity, which in its closed conformation appears to be open toward the

intracellular NBD and closed to the extracellular membrane (Li et al., 2007). As such it is proposed that ABC transporters operate via an alternating access model, allowing translocation of lipophilic molecules (and more hydrophilic conjugates) from within the cell membrane to the extracellular milieu, via conformational shape changes of the protein MSDs which surround a central substrate binding cavity (Szakacs et al., 2008).

Figure 1.2:

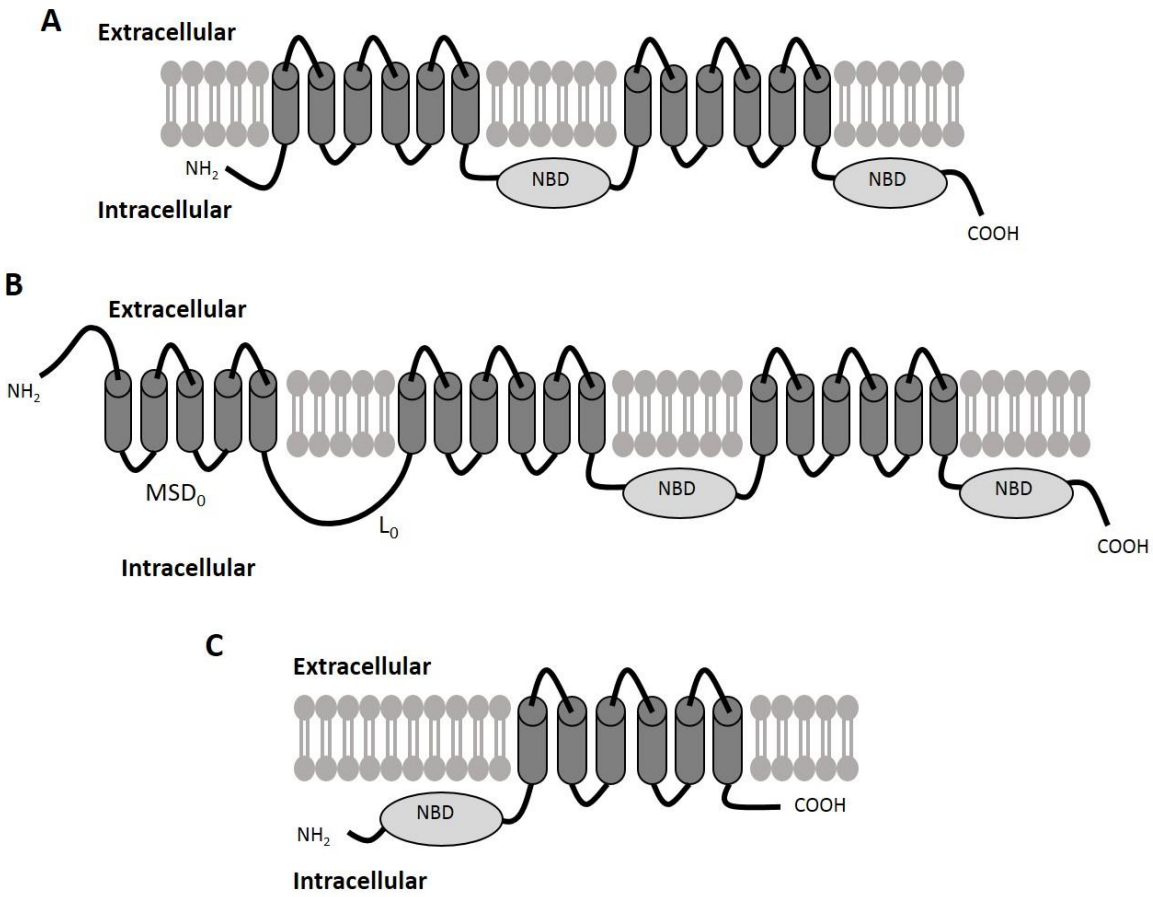

Figure 1.2 Schematic representation of predicted MDR1, MRP2 and BCRP protein structures

(A) MDR1 transporter structure showing two membrane spanning domains (MSD) and two nucleotide binding domains (NBD) with an intracellular N- and C-terminal. **(B)** MRP2 protein structure, note the additional MSD (MSD_0) and intracellular linker region L_0. Addition of MSD_0 forces an extracellular N-terminal domain. **(C)** BCRP half transporter, showing only one MSD and one NBD. The BCRP half transporter must dimerise to allow functional activity. Figure adapted from (Webster, 2011).

Figure 1.3:

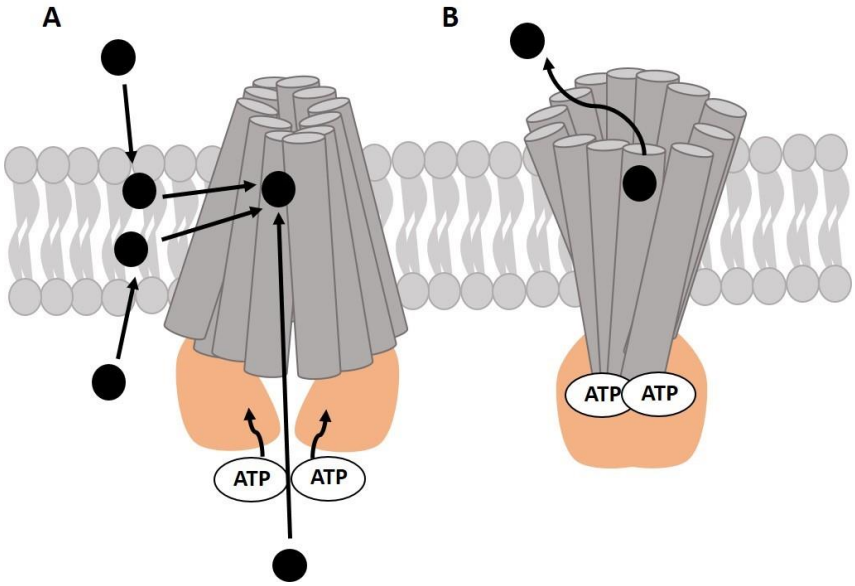

Figure 1.3 Schematic representation of the ABC switch/alternate access model proposed to be the mechanism of action for ABC transporters

(A) Binding of ATP causes rearrangement of the transmembrane domains (TMDs) (grey) such that a central pore is formed which is occluded to the extracellular domain but allows access of substrates to the transporter binding site both from within the lipid bi-layer and the intracellular aqueous phase. **(B)** Substrate binding increases affinity of ATP molecules for the nucleotide binding domains (orange), promoting dimerisation of the NBDs and subsequent rearrangement of TMDs to give an outward facing orientation with occlusion of the central pore to both the intracellular environment and the lipid interface of the membrane, allowing efflux of the substrate into the extracellular milieu.

1.2.2 MDR1; The permeability glycoprotein, P-gp

The multidrug resistance transporter, MDR1 (otherwise known as P-gp) is encoded by the ABCB1 gene, located on human chromosome 7 (position q21.1) and has a molecular size of approximately 170KDa (Vasiliou et al., 2009). Originally cloned from a Chinese hamster ovary (CHO) cell line which showed resistance to the natural product drug colchicine (Juliano and Ling, 1976), MDR1 is now known to confer resistance to a large variety of structurally unrelated substrates including drug molecules from classes including anti-arrythmics, anthracyclines, kinase inhibitors, anti-depressants, anti-virals, antibiotics, calcium channel blockers and immunosuppressants (Szakacs et al., 2008).

Cloning of MDR1 followed realisation that a membrane protein was responsible for altered membrane permeability in cells which showed cross resistance to a large number of structurally unrelated compounds (Juliano and Ling, 1976). Using galactose oxidase-boro [^{3}H] hydride surface labelling, Juliano and Ling, showed expression of a 170KDa protein on the cell membrane of drug resistant cells which was largely absent from drug sensitive AUX B1 cells, a mutant auxotrophic cell line which requires glycine, adenosine and thymidine, and reported strong correlation (0.86) between expression of this protein and drug resistance in colchicine resistance subclones of the parental AUX-B1 line. Due to its ability to alter membrane permeability this protein was named P-glycoprotein (later re-named MDR1) (Juliano and Ling, 1976). In this report ABCB1 will be referred to as MDR1.

MDR1 is ubiquitously expressed throughout the body with Langmann et al., (2003) showing highest levels of mRNA (messenger ribonucleic acid) expression to be evident in the adrenal gland, with lower level expression in the kidney, uterus, prostate, placenta, small intestine, spleen, liver, testis, brain, lung and colon by RT-PCR (real time polymerase chain reaction. Furthermore, expression of MDR1 on the apical membrane of secretory epithelial cells within the intestine, kidney, liver, and placenta and, also on the apical side of blood-tissue barriers indicates a physiological protective role of the transporter and further enforces the importance of this transporter in determination of drug pharmacokinetic profiles (Blokzijl et al., 2007, Hodges et al., 2011, Zhou, 2008).

A detailed description regarding intestinal mRNA and protein expression of MDR1 can be found in chapters 4 and 5 respectively. Conflicting literature is presented with regards to mRNA expression of MDR1, however the general consensus indicates an increased mRNA abundance from the proximal to distal ends of the small intestine with a drop in expression observed in the colon (Englund et al., 2006, Hilgendorf et al., 2007, Langmann et al., 2003). In agreement with the function of MDR1 as an efflux transporter, MDR1 protein expression has

been localised to the apical membrane of enterocytes within both the human duodenum and ileum (Blokzijl et al., 2007, Glaeser et al., 2007), with Western blot analysis showing increased protein expression from the duodenum to the ileum (Mouly and Paine, 2003). Furthermore, transport of the MDR1 fluorescent substrate Rhodamine123 from the serosal to mucosal surface of mounted mouse and rat intestinal segments was shown to be up to 5-fold higher in the ileum than in other intestinal regions, with transport showing sensitivity to the MDR1 inhibitor verapamil (Chianale et al., 1995, Yumoto et al., 1999).

1.2.3 The multidrug resistance protein family

In addition to MDR1, several members of the ABCC family of ABC transporters have been shown to confer resistance to a number of pharmaceutical compounds, particularly with regard to chemotherapeutic agents (Kruh and Belinsky, 2003). The ABCC family of transporters has a total of thirteen members including ten multidrug resistance proteins (MRP1 - MRP10), the transmembrane conductance regulator, CFTR (ABCC7), and the two sulphonylurea receptors, SUR1 and SUR2 (ABCC8 and ABCC9) (Deeley et al., 2006). Unlike other ABC protein family members CFTR (ACC7) is an ATP dependent Cl^- ion channel whilst the two sulphonylurea receptors, SUR1 and SUR2 (ABCC8 and ABCC9) are ATP dependent regulators of K^+ ion channels (Deeley et al., 2006). CFTR, SUR1 and SUR2 do not play a role in drug resistance (Deeley et al., 2006), and will therefore not be discussed further with regards to intestinal drug bioavailability.

Ten multidrug resistance proteins (MRP) have been identified to date, and have been shown to be vital in the transport of organic anions and in conferring resistance to a broad range of drug compounds including natural product drugs (anthracyclines, vinca alkaloids and taxanes) and their conjugates (Cole and Deeley, 1998, Deeley et al., 2006). In addition to their role in drug resistance, several MRP transporters are known to have specific physiological functions (described below) with loss of function mutations shown to cause pathophysiological conditions thus highlighting the clinical importance of the MRP family (Deeley et al., 2006, Kruh and Belinsky, 2003). Of specific interest with regards to oral bioavailability is the ABC transporter MRP2, due to its reported expression on the apical membrane of intestinal enterocytes (Mottino et al., 2000, Sandusky et al., 2002).

1.2.3.1 MRP2; an apical resistance transporter

MRP2 was identified following isolation, cloning and characterisation of the MRP1 transporter to which MRP2 is 45% identical (Deeley et al., 2006). Indeed the physiological profile of MRP2, with regards to its expression at the canalicular membrane of hepatocytes and substrate specificity, was unknowingly determined prior to cloning of any MRP family member following

characterisation of the canalicular multispecific organic anion transporter, cMOAT (canalicular multispecific organic transporter) which was later renamed MRP2 (Borst et al., 2000, Deeley et al., 2006, Mayer et al., 1995, Mirski et al., 1987).

cMOAT was shown to be highly expressed at the hepatocyte canalicular membrane where it was responsible for the efflux of conjugated organic anions, including bilirubin, from hepatocytes into bile (Borst et al., 2000, Mayer et al., 1995). Despite a clear overlap in substrate profiles, analysis of normal rat liver showed detection of two different Mrp mRNA sequences, with localisation to both lateral and canalicular membranes of hepatocytes shown using immunofluorescence (Mayer et al., 1995). In comparison the transport deficient (TR-) rat mutant, shown to lack cMOAT and be deficient in bilirubin-glucoronide secretion, expressed only one mRNA sequence with localisation being confined to lateral cell membranes (Borst et al., 2000, Mayer et al., 1995). Later cloning of the canalicular Mrp isoform by Buchler et al., (1996) using the previously isolated cDNA (complementary DNA) fragment from normal rat liver identified a protein, 1,541 amino acids in length with a molecular mass of approximately 170KDa which was absent in the TR^- mutant rat, this protein was named MRP2. Mutations in the ABCC2 gene (which encodes the MRP2 protein) that cause inactivation of human MRP2 are shown to be responsible for the development of a phenotype similar to that observed in TR- mutant rats, known as Dubin-Johnson syndrome (Borst et al., 2000). Dubin-Johnson syndrome presents as jaundice due to a lack of biliary bile-glucoronide secretion via the MRP2 canalicular membrane excretion pathway (Kruh and Belinsky, 2003), further clarifying clinical importance of MRP2.

As mentioned previously, in addition to the four core domains the MRP2 protein carries an additional MSD known as MSD_0 which is composed of five α-helical transmembrane domains (Borst et al., 2000). MSD_0 gives rise to an extracellular N-terminal domain and an additional intracellular linker region L_0, shown in figure 1.2 (Fukuda and Schuetz, 2012, Jedlitschky et al., 2006). The physiological relevance of this additional membrane spanning domain is currently unknown, however studies have shown MSD_0 is not required for functional activity (Borst et al., 2000). It should however be noted that the intracellular linker region, L_0, is conserved in those MRPs which do not possess MSD_0 (MRP4 and MRP5), suggesting a physiological role of this linker region (figure 1.2)(Borst et al., 2000).

Following addition of polar moieties to xenobiotics by CYP450 enzymes in phase I metabolism the majority of compounds enter phase II metabolic reactions which are mediated by UDP-glucoronosyl transferase, sulfonyl transferases and glutathione-S-transferases (Suzuki and Sugiyama, 2004). Phase II conjugation reactions make xenobiotics more amenable to MRP2

transport, since MRP2 shows affinity for glutathione, glucoronide and sulphate conjugated substrates, thus indicating this transporter to be important in the efflux of metabolic products (Deeley et al., 2006). Furthermore, expression of MRP2 on bile canalicular membrane supports the ability of this transporter to increase biliary excretion of drug compounds metabolised by the liver, as such MRP2 may potentially play an important role in influencing intestinal absorption and first pass metabolism of drug compounds (Jedlitschky et al., 2006). Previous *in vitro* and *in vivo* studies have shown MRP2 expression and functional activity to cause resistance to a wide range of anti-cancer drugs from several different drug classes including doxorubicin, daunorubicin, vinblastine, paclitaxel and mitoxantrone (Borst et al., 2000, Deeley et al., 2006, Kruh and Belinsky, 2003). Additionally MRP2 is able to transport saquinivir and indinavir, the HIV protease inhibitors, and the antiepileptic phenytoin (Deeley et al., 2006, Jedlitschky et al., 2006).

In addition to high levels of hepatic MRP2 expression, MRP2 has been localised to the apical membrane of polarised renal, gall bladder, small and large intestine and the blood brain barrier epithelial cells and to the apical membrane of placental syncytiotrophoblasts, (Deeley et al., 2006, Langmann et al., 2003, Maher et al., 2005, Nies and Keppler, 2007). Furthermore, low to very low level expression is reported in the testis, spleen and colon (Langmann et al., 2003). With regards to intestinal expression of MRP2, mRNA has been detected in all regions on the small intestine (duodenum, jejunum and ileum) whilst MRP2 mRNA expression in the colon is shown to be lacking (Englund et al., 2006, Langmann et al., 2003, Zimmermann et al., 2005). Immunohistochemical studies have shown localisation of MRP2 protein to the apical membrane of intestinal enterocytes both in humans (Sandusky et al., 2002) and rats (Mottino et al., 2000), however only faint antibody immunoreactivity was shown by Sanduskey et al., (2002) prior to MRP2 protein induction and Mottino et al., (2000) failed to show images confirming such expression.

1.2.3.2 Multidrug resistance proteins; MRP1, -3, -4, -5,-6 and -7

In addition to MRP2 several members of the ABCC subfamily of transporters are known to confer resistance to a wide range of compounds, however their role in intestinal drug resistance is proposed to be less critical than that of MRP2 given their localisation to the basolateral cell membrane of intestinal enterocytes (Fricker and Miller, 2002, Kruh and Belinsky, 2003). Expression of MRP proteins at the basolateral membrane of enterocytes contributes toward absorption of drug molecules and translocation of hydrophilic substances across the basolateral membrane into underlying blood vessels (Barrett et al., 2010 p451, Fricker and Miller, 2002). As such intestinal expression of MRP transporters other than MRP2 may in fact aid in absorption of drug compounds as opposed to the active efflux and

enterocytic recirculation mediated by MRP2. However, since intestinal blood flow is to the portal vein, this allows transported substrates to be taken up by the liver and subjected to further metabolism and/or biliary elimination.

MRP1 functional activity is believed to be important for transport of phase II metabolites given its ability to transport a wide variety of structurally diverse organic anion conjugates of glutathione, glucoronide and sulphate, including steroids and bile salts (Deeley et al., 2006, Kruh and Belinsky, 2003). MRP1 is shown to confer resistance to a similar drug profile as that detailed for MRP2, including doxorubicin, daunorubicin, vinblastine, paclitaxel, mitoxantrone and methotrexate (Borst et al., 2000, Deeley et al., 2006, Kruh and Belinsky, 2003). MRP1 expression is high at key barrier locations including Leydig and Serotoli cells of the testis, the blood-brain barrier, placental syncytiotrophoblasts and epithelial cells of the endoplacental yolk sac (Deeley et al., 2006). Overall high mRNA expression levels are reported in uterus, spleen, prostate and trachea (Langmann et al., 2003). Moderate MRP1 expression has been shown in the colon and lower levels are reported in the small intestine (Langmann et al., 2003). In contrast to MRP2 however, MRP1 is localised to the basolateral membrane of intestinal epithelial cells (Kruh and Belinsky, 2003) and as such is less important with regards to intestinal drug resistance.

MRP3 is an organic anion transporter which shows a strong structural identity to MRP1 (58%) and as such displays overlaps with regard to transport of glutathione and glucoronate conjugates (Kruh and Belinsky, 2003). Whilst the full drug resistance profile mediated by MRP3 is hard to determine due to a lack of *in vitro* cell lines which over-express the transporter, low level resistance has been shown to natural drug compounds etoposide and teniposide (Borst et al., 2000, Kruh and Belinsky, 2003) whilst short term exposure to mitoxantrone was shown to induce MRP3 mediated resistance to this drug compound (Borst et al., 2000). Little correlation exists however between MRP3 expression levels and tumour resistance (Borst et al., 2007), the role of MRP3 in drug resistance therefore requires further enquiry. A ubiquitous expression profile is reported for MRP3 with mRNA expression reported in the lung, prostate, bladder, kidney, pancreas, spleen, placenta, gall bladder, adrenal gland, splenic cells and stomach (Borst et al., 2007, Deeley et al., 2006, Kruh and Belinsky, 2003, Langmann et al., 2003). Little information is available regarding intestinal expression of MRP3 although mRNA transcripts have been detected in all regions of the intestine, with a substantial rise in expression toward to terminal ileum and colon (Maher et al., 2005). Distinct basolateral protein localisation has been confirmed in the ileum and colon (Borst et al., 2000), indicating a role for this transporter in the efflux of drug compounds into blood (Rost et al., 2002).

Discovered in the same way as MRP3, MRP4 and MRP5 were first reported in 1997 following mining of the EST database (Deeley et al., 2006). Unlike other MRP transporters (see below) MRP4 and MRP5 lack the additional MSD_0 domain and consequently show slight alterations in substrate profile, both physiologically and with regards to drug resistance (Kruh and Belinsky, 2003). Transfection and over-expression of MRP4 cDNA has been shown to result in a cellular resistance to many anti-cancer and anti-viral drug compounds, with recent additions of BCRP substrate quercitin and resveratrol supporting complex interplay between drug resistance transporters (Borst et al., 2007). MRP4 and MRP5 confer resistance to drugs including para-methoxy-N-ethylamphetamine (PMEA), an acyclic nucleotide drug indicated for the treatment of hepatitis B, and anti-cancer nucleotide analogues 6-mercaptopurine and 6-thioguanine, primarily used in the treatment of childhood lymphoblastic leukaemia (Kruh and Belinsky, 2003). Like other MRP transporters, MRP4 and MRP5 are reported to have a ubiquitous expression profile (Borst et al., 2007). Controversy regarding protein localisation of MRP4 and MRP5 is apparent, since these transporters have been localised to both the apical and basolateral cell membranes. It is believed that membrane localisation of MRP4 and MRP5 is tissue dependent for example, MRP4 has been localised to the apical cell membrane of renal proximal tubule cells however basolateral expression was apparent in human and murine brain samples (Borst et al., 2007). Similarly although MRP5 showed trafficking to the basolateral membrane of MDCK (Madin Darby Canine Kidney) cells, *in vivo* studies showed apical expression of the transporter in brain capillary endothelial cells (Borst et al., 2007). As such, although MRP4 and MRP5 are proposed to localise to the basolateral membrane of enterocytes further studies are required to confirm membrane expression (Borst et al., 2000). Little information is available with regards to intestinal expression levels, although mRNA expression of both transporters has been reported in all regions of the intestine (duodenum, jejunum, ileum and colon) (Taipalensuu et al., 2001, Zimmermann et al., 2005).

Less information exists regarding drug specificity of MRP6 and MRP7 although past studies have shown transfection of MRP6 to cause low level resistance against etoposide, teniposide, cisplatin and anthracyclins in CHO cells (Kruh and Belinsky, 2003). Drug sensitivity assays performed by Hopper-Borge et al., (2004) showed an ability of MRP7 to confer resistance to a wide range of drug compounds. A resistance profile including taxanes (docetaxel and paclitaxel), anthracyclines such as doxorubicin and the vinka alkaloids vincristine and vinblastine was identified (Hopper-Borge et al., 2004). Langmann et al., (2003) report moderate to low level expression of MRP6 mRNA detected using RT-PCR in a wide range of human tissues, including kidney, liver, lung, trachea, small intestine and colon. A low level ubiquitous expression mRNA profile if reported for MRP7, including mRNA detection in the

small intestine and colon (Deeley et al., 2006, Kruh and Belinsky, 2003, Langmann et al., 2003). Very little information exists regarding intestinal expression of MRP6 and MRP7, although MRP6 mRNA has been detected in the jejunum (Taipalensuu et al., 2001).

1.2.4 Breast cancer resistance protein (BCRP)

1.2.4.1 Cloning of BCRP and the BCRP protein structure

BCRP was first cloned from the mitoxantrone resistant cell line MCF7-AdrVp following prolonged exposure of human breast cancer carcinoma MCF7 cells to the anthracycline, Adriamycin (Adr) (Doyle et al., 1998). The MCF-AdrVp cell line showed cross resistance to several drug compounds following co-incubation of MCF7 cells with 1µg/ml Adr and 2.5µg/ml verapamil (Doyle et al., 1998). Cells were incubated with verapamil to select for drug resistance mechanisms unique from MDR1 (Doyle et al., 1998). MCF7 cells transfected with and expressing a 2.4-kb mRNA sequence, found to be over-expressed in the MCF-AdVrp cell line by RNA fingerprinting, developed resistance to compounds including mitoxantrone, daunorubicin and doxorubicin, now known to be BCRP substrates (Doyle et al., 1998). Consistent with ABC family characteristics BCRP protein sequence analysis revealed a conserved Walker A motif with a hydrophilic amino and carboxy-terminal (Doyle et al., 1998). The BCRP protein sequence was found to show homology with both MDR1 and the MRP subfamily whilst cell lines transfected with BCRP cDNA showed decreased accumulation of the fluorescent dye Rhodamine123 compared with vector control transfected cells (Doyle et al., 1998). Furthermore, restoration of Rhodamine123 accumulation was observed following depletion of cellular ATP, strongly indicating ATP to be required for functional transporter activity (Doyle et al., 1998). It was therefore concluded that the protein responsible for drug resistance in the MCF7-AdrVp cell line belonged to the ABC transporter family and conferred resistance by efflux of drug compounds (Doyle et al., 1998).

At about the same time as the cloning of the BCRP protein by Doyle et al., (1998), Allikmets et al., (1998) identified two sequences belonging to the ABC family in human placenta (named ABCP) by reverse transcription PCR and cDNA sequencing. Like BCRP, these sequences showed homology with the Drosophila white (w) gene family (Allikmets et al., 1998). Furthermore, Miyake et al., (1999) showed increased mitoxantrone accumulation in drug sensitive S1 human colon carcinoma cells compared with the S1-M1-80 cell line which had been pre-selected using 80µM mitoxantrone, with similar findings also apparent in the MCF7/AdrVp cell line. Two clones, MXR1 (mitoxantrone resistance transporter) and MXR2 identified by Northern blot analysis and found to be over-expressed in S1-M1-80 cells, showed distinctive ABC transporter features. Again 27% identity with Drosophila white protein was reported (Miyake et al., 1999). Later sequence analysis revealed BCRP, ABCP, MXR1 and MXR2 to be almost identical and the

protein was assigned the common name of ABCG2 by the human genome nomenclature committee (Robey et al., 2009). For the purpose of this review the transporter shall be referred to as BCRP.

A member of the ABCG subfamily of ABC transporters, the ABCG2 gene is located at chromosomal region 4q21-4q22 and encodes a protein of 655 amino acids with a molecular weight of 72KDa (Robey et al., 2009). The higher molecular weight reported by Doyle et al., (1998) may reflect post-translational modifications. Structural analysis of the BCRP protein sequence showed presence of a single conserved Walker A motif, whilst hydrophobicity analysis identified only six transmembrane domains, comprising a single MSD (Allikmets et al., 1998, Doyle et al., 1998, Miyake et al., 1999). Identification of a single MSD highlights a key difference between BCRP and MDR1/MRP2 in that the transporter is homologous to only one half of the core structure of the MDR1/MRP2 proteins. It is for this reason that BCRP is known as the half transporter and has a reduced size in comparison to MDR1 and MRP2 (Doyle et al., 1998, Fukuda and Schuetz, 2012, Robey et al., 2009). Furthermore, BCRP differs with regards to arrangement of the core domains. Whilst the NBD of BCRP is the most N-terminally located feature, MDR1 and MRP proteins are arranged such that a MSD is N-terminal, as shown in figure 1.2.

1.2.4.2 Dimerisation of the BCRP half transporter is required for functional protein activity

To allow functional activity, ABC transporters must possess two NBDs and two MSDs, therefore BCRP must form a homo- or hetero- dimer *in vivo* to allow the transport of substances (Kage et al., 2002, Robey et al., 2009). Early studies support protein dimerisation with detection of high molecular weight protein bands by immunoblot *in vitro*. Kage et al., (2002) showed transfection of the PA317 cell line with Myc- or HA- (hemagglutin) tagged BCRP by Western blot, alone and in combination, allowed the detection of a 140KDa band under non reducing conditions using anti-Myc, anti-HA and anti-BCRP antibodies, protein solubilisation with DTT (dithiothreitol) and 2-mercaptoethanol however reduced the 140KDa protein to a molecular weight of approximately 72KDa, very similar to that of the BCRP monomer. Similarly, Litman et al., (2002) showed detection of a protein band of molecular weight 72KDa in cells known to over-express BCRP in the presence of the reducing agent beta-mercaptoethanol. However, under non-reducing conditions migration of the detected protein to higher molecular weights (>180KDa) was observed, consistent with formation of BCRP dimers/oligomers (Kage et al., 2002, Litman et al., 2002). Furthermore immunoprecipitation with the anti-Myc antibody and subsequent Western blot of precipitated samples showed reactivity with both anti-BCRP and anti-HA antibodies, suggesting potential dimerisation of the Myc- and HA- tagged BCRP monomers (Kage et al., 2002). Finally, co-transfection of PA317 cells with a non-functional

BCRP mutant and the Myc-BCRP protein imparted an increased cell sensitivity to both SN38 and mitoxantrone (BCRP substrates) compared with Myc-BCRP transfects alone (Kage et al., 2002). As such dominant-negative inhibition of BCRP function, as shown by increased sensitivity, confirms the requirement of BCRP dimerisation to allow functional activity of this membrane transporter.

The lack of a higher molecular weight band under reducing conditions suggests BCRP dimerisation to result from disulphide bond formation between BCRP monomers (Kage et al., 2002). Xu et al., (2004) however, showed only approximately 50% of total BCRP protein present in isolated membrane preparations to exist as a dimer under non-reducing conditions. Since around half of the expressed BCRP protein exists in monomer form it is suggested that disulphide bond formation results from *in vitro* sample preparation, with an emphasis on the oxidising conditions used during protein extraction (Xu et al., 2004). In support of this theory Shigeta et al., (2010) later showed functional BCRP activity in PA317 cells transfected with a triple mutant BCRP protein C608S;C603S;C592S. Despite inability to dimerise through disulphide bond formation, these cells were shown to reduce intracellular mitoxantrone accumulation compared with the control PA317 parental cell line suggesting functionality of the protein to be unaltered despite the inability to form disulphide bonds (Xu et al., 2004). Furthermore a loss of apparent BCRP mediated mitoxantrone efflux was observed following mutant transporter knockdown using siRNA (Shigeta et al., 2010). Despite measured functional activity, cysteine residue mutation reduced membrane BCRP localisation and altered the FTC (Futrimorgan C) inhibition properties of BCRP (Shigeta et al., 2010). These data indicate that the cysteine residues play a role in normal BCRP expression and function but are not essential for dimer formation and transporter activity *in vivo*.

It has also been proposed that BCRP may in fact form higher-order oligomers (Xu et al., 2007). Extraction of BCRP from MCF7/AdrVp cell lines using the ionic detergent PFO prevents breakage of any covalent bonds and hence allows a more accurate determination of oligomeric states. Xu et al., identified two high molecular weight bands following PFO extraction and Western blot of 285KDa and 790KDa which were proposed to represent a BCRP protein tetramer and higher order oligomer respectively. Further cross linking experiments in live cells supported BCRP tetramer formation (Xu et al., 2007). Whilst it is accepted that BCRP must dimerise to allow functional activity further work is required to determine how BCRP forms such complexes *in vivo* and to ascertain if indeed BCRP does form higher order oligomers.

1.2.4.3 Localisation of BCRP throughout the body

Like MDR1 and MRP2, BCRP mRNA expression has been reported across many different tissue types, with detection of BCRP mRNA at key sites involved in drug disposition and with barrier

functions including the brain, prostate, small intestine, testis, ovary, colon and liver (Doyle et al., 1998). Additionally BCRP is expressed at high levels in the placenta and has been localised to tumorous tissues and stem cells (Aust et al., 2004, Scharenberg et al., 2002, Staud and Pavek, 2005). Langmann et al., (2003) detected BCRP mRNA in many tissues, with highest levels in the uterus and prostate followed by the placenta and small intestine; much lower mRNA expression was apparent in the colon.

A detailed review of current literature regarding intestine mRNA and protein expression can be found in chapters 4 and 5 respectively, however the general consensus indicates BCRP mRNA expression to increase from the duodenum to the ileum with lower levels of expression detected in the colon (Englund et al., 2006, Gutmann et al., 2005, Hilgendorf et al., 2007). Maliepaard et al., (2001) have shown apical BCRP expression on enterocytes in both the small intestine and colon of human samples.

1.2.4.4 Expression of BCRP in the side population of stem cells; a protective role for the transporter?

Whilst many studies suggest a physiological role for BCRP in the efflux of pharmacological agents thereby promoting their excretion at key physiological barrier locations, the transporter is also responsible for the generation of the so called 'side population' (SP) of stem cells. SP cell isolation was performed based on the unique ability of hematopoietic progenitors to efflux the fluorescent dyes Hoechst33342 and Rhodamine123, both of which are known substrates of the ABC transporter family (Scharenberg et al., 2002). The ability of this cell line to efflux Hoechst33342 from the cell allows isolation based on low Hoechst33342 dependent fluorescence determined using flow cytometry (Zhou et al., 2001). The SP dependent Hoechst33342 efflux was shown to be diminished by ATP depletion. Whilst moderate inhibition of Hoechst33342 efflux was observed in the presence of low verapamil concentrations (specific to MDR1) incubation of SP cells with high verapamil concentrations or with the specific BCRP inhibitor FTC was shown to reduce Hoechst33342 accumulation to a greater level. Furthermore, it was shown that the SP cell phenotype remained evident in Mdr1a/Mdr1b -/- mouse models which were shown to express BCRP, at least at an mRNA level (Zhou et al., 2001). Additionally, BCRP mRNA expression levels were shown to be higher than those of MDR1 and MRP in murine hematopoietic stem cells displaying an SP phenotype (Scharenberg et al., 2002, Zhou et al., 2001). It is therefore concluded that BCRP contributes substantially toward the SP cell population phenotype and has been shown to be expressed at high levels in progenitor stem cells across a range of tissues indicating a potential role for BCRP in the protection of stem cells due to their need to undergo lifelong proliferation.

Given the presence of stem cells within the crypt region, and their vital role in the population of the enterocyte barrier it is proposed that BCRP may also be expressed within this stem cell niche. BCRP expression within cryptal stem cells, or in fact within the crypt region, may potentially allow for protection of this poorly differentiated and proliferative unit.

1.3 Cytochrome P450 enzymes and their contribution to intestinal drug metabolism

As discussed earlier, it is established that interplay between MDR1 and CYP3A enzymes is especially apparent within the intestinal enterocyte barrier, with such synergistic activities causing reduced bioavailability of oral drug compounds (Benet, 2009). However, given that many different isoforms of the CYP450 family are now known to be expressed in intestinal epithelial cells alongside the apparent localisation of BCRP and MRP2 to the apical enterocyte membrane and their ability to efflux a wide range of substrates, it is becoming increasingly recognised that the intestinal enterocyte barrier contributes substantially toward first pass absorption and metabolism of drug compounds (Benet, 2009, Chan et al., 2004, Lin et al., 1999, Paine et al., 2006).

Drug metabolism can be divided into two phases; phase I metabolic enzymes include alcohol and aldehyde dehydrogenases, NADPH-P450 reductase, esterases and CYP450 enzymes amongst others (Suzuki and Sugiyama, 2004). For the purpose of this thesis focus will be placed on the CYP450 enzymes due to their role in metabolism of clinically used drugs (Suzuki and Sugiyama, 2004). CYP450 enzymes are haemproteins and as such contain a haem molecule which binds two oxygen atoms and catalyses the production of water and a drug compound derivative known as the metabolite. Drug metabolites are formed following oxidation, hydroxylation, dealkylation or reduction of parent compounds (Martignoni et al., 2006), and can exhibit a reduction or alteration of pharmacological activity compared to the parent drug (Wilkinson, 2005). Phase II biotransformation occurs when the functional groups from phase I react with endogenous ligands to form highly hydrophilic conjugates e.g. by glucuronidation, sulphation or acetylation. Increased hydrophilicity of phase II metabolic products makes them more amenable to transport by membrane proteins, such as the MRP family (Deeley et al., 2006, Kruh and Belinsky, 2003, Suzuki and Sugiyama, 2004). Given the importance of the potential coupling between ABC transport and P450 action, consideration will be focussed on the CYP450 family of enzymes (Benet, 2009).

Whilst the liver serves as the main site of phase I drug metabolism (oxidation, reduction, hydrolysis and dealkylation of drug compounds) due to extremely high levels of CYP450 expression (Paine et al., 2006), it is also proposed that CYP450 mediated biotransformation

contributes toward detoxification of drug compounds outside of hepatocytes (Martignoni et al., 2006, Suzuki and Sugiyama, 2004). Indeed CYP450 enzymes have been localised to tissues including the lung, kidney, testis and brain with the intestine serving as the major site of extrahepatic drug metabolism (Martignoni et al., 2006, Paine et al., 2006).

Unlike other superfamilies, naming of CYP450 enzymes follows strict guidelines. Identified sequences which show greater than 40% identity are categorised into the same family, i.e. CYP1, CYP2, and CYP3. Families are then subdivided such that proteins with > 55% identity are placed within the same subfamily and are named using a consecutive numbering system, e.g. CYP1A1 and CYP1A2. Genes showing between 40 and 55% identity fall into the same family but are categorised under different subfamilies (Anzenbacher and Anzenbacherova, 2001, Martignoni et al., 2006).

The majority of CYP450 enzymes identified have been shown to be functionally active and metabolise of a range of endogenous substrates including fatty acid molecules, steroids, bile acids, retinoids and vitamin A derivatives (Nebert and Russell, 2002). In addition to their physiological role, CYP450 enzymes are known to metabolise foreign compounds including drugs, secondary diet-derived metabolites, and environmental pollutants. Of particular importance with regards to xenobiotics are the CYP1, CYP2 and CYP3 families of enzymes, with a lesser contribution from the CYP4 family (Nebert and Russell, 2002).

The human CYP3A family comprises four members, CYP3A4, CYP3A5, CYP3A7 and CYP3A43, although CYP3A7 is expressed only in fetal livers and expression and tissue restricted activity of CYP3A43 is apparent (Paine et al., 2006). In contrast, CYP3A4 and CYP3A5 are the most abundant CYP450 isoforms of both the human liver and the human intestine, with expression levels of CYP3A accounting for 29% of the total hepatic content and up to 84% of intestinal CYP450 expression (Mitschke et al., 2008, Paine et al., 2006). The CYP3A family is proposed to account for metabolism of approximately 50% of administered drug compounds (Martignoni et al., 2006). Enteric expression of CYP3A reportedly represents only 1% of that expressed in the liver, yet studies have shown intestinal CYP3A activity to contribute significantly toward drug metabolism, with enteric contributions matching hepatic metabolism of some drugs (Paine et al., 2006).

Given the wide substrate profile of CYP3A and overlap between MDR1 and CYP3A substrates it is vital to determine the contribution of the CYP3A family to intestinal metabolism of drug compounds (Anzenbacher and Anzenbacherova, 2001, Benet, 2009). Furthermore, Paine et al., (2006) showed detection of CYP2B6, 2C9, 2C19, 2D6, 2J2, 3A4 and 3A5 protein in human

intestinal microsomes using Western blot analysis, further emphasising the need to accurately determine expression and function of CYP450 enzymes within the intestine.

1.4 Solute carrier family of transporters – SLC proteins

In addition to the ABC transporter family it is established that several members of the solute carrier (SLC) family expressed within the intestine may act as drug transporters (Sai, 2005). The SLC series of transporters is extremely extensive and comprises 43 subfamilies (SLC1-SLC43) with a total of 298 genes (Hediger et al., 2004). Intestinal SLC proteins play a vital physiological role in regulating uptake of digestive products including sugars, amino acids and nucleotides (Hediger et al., 2004). Exploitation of the physiological role of SLC transporters has proven key in establishing successful intestinal drug delivery systems. Addition of chemical moieties to drug compounds allows them to mimic natural substrates of SLC transporters, thereby increasing oral bioavailability and intestinal absorption of hydrophilic molecules (Gomez-Orellana, 2005).

A key example of an SLC family member involved in drug absorption is PEPT1 (SLC15A1), an apically localised di-/tri- peptide transporter reportedly expressed in both the small and large intestine (Ford et al., 2003, Freeman et al., 1995, Steffansen et al., 2004, Thwaites et al., 1995). PEPT1 facilitates the uptake of drugs including ACE inhibitors, β-lactam antibiotics, cephalosporins and the prodrugs acyclovir and ganciclovir (Steffansen et al., 2004). Due to broad substrate specificity of PEPT1 various attempts have been made to target this transporter for intestinal drug uptake.

Concentrative nucleoside transporters (CNT) CNT1, CNT2 and CNT3, which belong to the SLC family, physiologically scavenge and mediate the uptake of hydrophilic purine and pyrimidine nucleosides from within the intestinal lumen but are targeted as drug delivery systems for structurally related nucleoside like drug molecules (Steffansen et al., 2004). Examples of CNT targeted drug compounds include antivirals used in the treatment of HIV, hepatitis and solid tumours (Gray et al., 2004).

Furthermore, the organic anion (OATs) and organic cation transporters (OCTs) transporters play important roles in disposition of xenobiotics and drug compounds including tetraethylammonium, acyclovir, ganciclovir, amantadine, memantidine, cimetidine, quinidine, verapamil and methotrexate (Sai and Tsuji, 2004).

It is therefore of interest to gain a better understanding of the role of these transporters in drug delivery and their expression profiles along the length of the intestine, since specific targeting of drug molecules may allow for increased oral bioavailability. Moreover,

determination of how expression of these transporters correlates with expression of ABC transporters and CYP450 enzymes may give a more thorough understanding of potential drug-transporter interactions.

1.5 Interindividual variability in response to oral drug administration and potential for ABC/CYP450 mediated drug interactions

As described earlier the expression of drug transporters and CYP450 enzymes within epithelial cells lining the intestinal lumen directly influences the oral bioavailability of drug compounds (Chan et al., 2004, Paine et al., 2006, Szakacs et al., 2008). Furthermore the proposed interplay between ABC transporter mediated enterocytic recirculation and CYP450 metabolism of drug compounds adds a considerable degree of complexity with regards to oral dosing (Benet, 2009). Although the enterocyte barrier and first pass metabolism of drug compounds is known to reduce bioavailability by up to 50% (Wilkinson, 2005), a good level of understanding regarding a drug's pharmacokinetic (PK) profile allows achievement of therapeutic doses via oral administration. However, inter-individual differences with regard to expression and function of key genes involved in drug disposition shows potential for the development of unpredictable adverse effects, which may prove toxic and potentially life threatening (Marchetti et al., 2007). The severity of inter-individual differences is exemplified by the high number of patients (10%) who are admitted to hospital due to drug related illness (Marchetti et al., 2007).

Inter-individual differences with regards to drug disposition are dependent on age, organ function, concomitant therapies, genetics and drug-drug, drug-food and drug-herb interactions (Kerb, 2006). Of particular interest here is the ability of drug compounds to induce expression of drug disposition proteins thereby leading to changes in the PK profiles of administered drugs, particularly with regard to polypharmacy (Tirona and Kim, 2005).

It is established that proteins involved in phase I and phase II metabolism, in addition to ABC transporters, share common mechanisms which regulate transcriptional activation and induced gene expression (Nakata et al., 2006). One such mechanism is the binding of nuclear receptors (NR) to the promoter regions of target genes (Tirona and Kim, 2005). The nuclear receptor family of ligand activated transcription factors is reported to comprise 48 members, including orphan nuclear receptors and endocrine receptors (Nakata et al., 2006). Orphan nuclear receptors are localised within the cell cytoplasm and show ability to bind specific receptor ligands, with subsequent heterodimerisation with the retinoid-X-receptor (RXR) and translocation into the cell nucleus (Tirona and Kim, 2005). Orphan nuclear receptors include RXR, retinoic acid receptor (RAR), constitutive androsterone receptor (CAR), vitamin D receptor

(VDR) and the peroxisome proliferator-activated receptors (PPAR) α and γ (Nakata et al., 2006, Tirona and Kim, 2005).

With regards to drug compound mediated induction, xenobiotics diffuse across the cell membrane and bind to cytoplasmic NR (Tirona and Kim, 2005). Following ligand binding the NR monomer dissociates from co-repressors and translocates to the nucleus were it dimerises with RXR to form a heterodimeric complex. NR heterodimers then bind to the promoter regions of target genes and induce gene expression via RNA polymerase (Tirona and Kim, 2005, Urquhart et al., 2007). Given their ability to interact with xenobiotics, including drug compounds, the PXR and CAR receptors are often referred to as the xenobiotic receptors. In addition the bile acid receptors FXR and VDR are also able to bind xenobiotics (Nakata et al., 2006). Transcriptional regulation of drug disposition proteins is extremely complex. For example, PXR is known to cause induction of many ABC transporters and CYP450 genes, including the CYP3A family, CYP2C9, CYP2C19, MDR1, MRP1, MRP2, MRP3 and BCRP. In addition the RARs induce MDR1 expression, whist PPARs induce expression of both MRP2 and BCRP, with the VDR causing increased transcription of CYP3A4 and MDR1 (Nakata et al., 2006). Furthermore, the aryl-hydrocarbon receptor (AhR), a member of the bHLH-PAS transcription factor (TF) superfamily, is reported to regulate transcription of several drug disposition proteins via a similar mechanism and is discussed in detail in chapter 6 (Deb and Bandiera, 2009, To et al., 2011, Wang et al., 2011).

A very good example of nuclear receptor mediated induction is the interaction between the cardiac glycoside digoxin and the tuberculosis treatment rifampin. Greiner et al., (1999) showed reduced AUC (area under the curve) and Cmax (maximal plasma concentration) parameters for digoxin following oral administration of rifampin ($AUC_{(0\text{-}3h)}$ng/h/ml control versus rifampin administration 8.8 ± 2.9 and 5.0 ± 1.1 respectively, and Cmax 5.4 ± 1.9 versus 2.6 ± 0.7 ng/ml). This has been modelled using the T84 human intestinal cell line, where rifampin pre-treatment increases MDR1 mRNA expression, MDR1 protein expression at the brush-border and secretory transport capacity, so reducing the absorptive permeability $P_{(a\text{-}b)}$ for digoxin (Haslam et al., 2008). Using the T84 model a number of inducing agents including St John's Wort have been identified with a strong substrate overlap between PXR and MDR1 (Haslam et al., 2008).

Rifampin administration appears to have multiple actions mediated by PXR activation in vivo; upregulation of both mRNA and protein expression of MRP2 and CYP3A4 in addition to MDR1 was noted in human intestinal duodenal samples following oral administration of 600mg rifampin in healthy volunteers (Fromm et al., 2000). Similar effects can be seen with herbal

remedies such as St John's Wort which has been shown to induce both MDR1 and CYP3A expression in healthy subjects (Dresser et al., 2003, Haslam, 2007).

Dresser et al., (2003) showed reduced Cmax concentrations for both midazolam, a CYP3A substrate which is essentially entirely eliminated by metabolism, and fexofenadine, a non-metabolised MDR1 substrate, following oral administration of St John's Wort. Altered function and expression of MDR1 and MRP2 in concert reinforces the complexity of response with regards to drug transporters and intestinal drug resistance, particularly considering the proposed roles of both proteins in intestinal drug efflux.

Similarly, induction or inhibition of CYP450 enzymes, particularly CYP3A can cause reduced or increased plasma drug concentrations respectively. Indeed several drugs have been withdrawn from the market due to CYP450 mediated drug-drug interactions including the non-sedating anti-histamines terfenadine and astemizole and the calcium channel block mibefradil (Lynch and Price, 2007). Given that an extensive number of drug compounds are substrates for both MDR1 and CYP3A, interactions are likely to occur when two, or more, medications are co-administered. As such care must be taken in understanding drug interactions and designing treatment regimens where polypharmacy is common e.g. in the elderly and cancer patients.

In the context of the present thesis, given the likely complexity of the in vivo response to repeated dosing, it was of interest to consider mapping changes in both drug transporter and CYP450 enzymes in response to a single drug where such issues of induction and drug resistance have been identified.

1.6 Thesis aims and objectives

1) In order to investigate the transport and metabolic capabilities of villus enterocytes compared to crypt cells, a method to isolate villus and crypt enriched cell populations is required. Of importance to any data derived from such a method is validation of the technique by microscopy and biochemical measurements. Ideally the cell preparations would be viable allowing measurements of membrane transport. The species chosen should reflect one of the main animal models used in Pre-Clinical drug testing and should allow the generation of sufficient experimental material from a single animal to ensure minimal animal usage.

2) Using the ability to isolate villus and crypt fractions to investigate the distribution of expression of key transporters involved in drug disposition at the mRNA level (including members of the SLC and ABC transporter families with particular focus on Mdr1, Mrp2 and Bcrp) and metabolic enzymes (cytochrome P450 family) between the villus and the crypt. Correlation between mRNA expression data of Mdr1, Mrp2, and Bcrp and Cyp450 enzymes in rat intestine will provide insight into potential interplay between these two protein families. Co-expression will augment the existing data on the validity of the Benet model. The method chosen should ideally allow multiple determinations of gene expression from the same sample and provide quantitative data.

3) Correlate the level of mRNA expression with the extent and location of protein expression of key drug resistance transporters Mdr1, Mrp2 and Bcrp. Protein localisation will allow the analysis of the importance of these ABC transporters in influencing oral bioavailability of drug compounds.

4) Determine the *in vivo* response to multiple oral dosing on the extent of bioavailability of a target drug, imatinib mesylate. Imatinib has been reported to act as an MDR1/BCRP substrate/inhibitor and is shown to induce ABC transport up-regulation. Given the overlap in substrate specificity and transcriptional regulation of gene expression, the interplay between levels of expression of ABC transporters and Cyp450 enzymes are important in assessing the effects of imatinib on pharmacokinetic profiles in dosed animals.

2. Materials and Methods

2.1 Materials

All cell culture flasks and culture plates were purchased from Corning Costar (High Wycombe, UK). Cell culture medium and supplements were purchased from Sigma Aldrich (Poole, UK). All reagents were purchased from Sigma Aldrich (Poole, UK) unless stated otherwise. All NuPAGE immunoblotting reagents were purchased from Life Technologies (Paisley, UK).

2.1.1 Buffer Solutions

Ringer's buffer solution: 140mM NaCl, 10mM $KHCO_3$, 0.4mM KH_2PO_4, 2.4mM K_2HPO_4, 1.2mM $MgCl_2$ and 1.2mM $CaCl_2$.

Crypt villus isolation buffer: 112mM NaCl, 5mM KCl, 30mM Na_2-EDTA, 0.5mM DTT, 20mM HEPES. pH adjusted to 7.1 using Tris-Base.

Krebs buffer: 137mM NaCl, 5.4mM KCl, 1mM $MgSO_4$, 0.3mM KH_2PO_4, 0.3mM NaH_2PO_4, 10mM D-Glucose, 10mM HEPES, and 2.8mM $CaCl_2$, pH adjusted to 7.4 with TRIS-base.

2mM $ZnCl_2$ Krebs buffer: 135mM NaCl, 5.4mM KCl, 1mM $MgSO_4$, 10mM D-Glucose, 10mM HEPES, 2.8mM $CaCl_2$ and 2mM $ZnCl_2$, pH 7.4 with TRIS-base.

KB medium: 85mM KCl, 30mM K_2HPO_4, 5mM $MgSO_4$, 5mM Na_2ATP, 5mM Pyruvic acid, 5mM β-OH-butyric acid, 5mM Creatine, 20mM Taurine, 20mM Glucose, 50g/l Polyvinypyrollidone (PVP40), 10mM EGTA and 1.95mM $CaCl_2$. Adjusted to pH 7.2 with KOH and with EGTA to pCa (pCa = -log $[Ca^{2+}]$) 7.5 (aCa_o 30nM (calcium activities extracellular).

2.2 Methods

2.2.1 Routine cell culture

All cells were cultured in flasks of surface area 75cm^2 and were maintained at 37˚C, 5% CO_2 in a sterile humidified incubator. All cell culture work was performed inside a Class II laminar flow hood (Safeflow 1.2, Bioaire Instruments, Italy). Cell bathing medium was routinely changed every 3-4 days, unless otherwise stated.

MDCKII cells used in the present study were obtained as described by Barker and Simmons, (1981) and were maintained as frozen stocks in the laboratory from this point forward. Transfected MDCKII cell lines were a generous gift from the Netherlands Cancer Institute. Native MDCKII and MDCKII cells stably transfected with MDR1 and MRP2 ABC transporters were grown in Minimum Essential Eagles Medium (MEM), supplemented with 10% fetal calf serum (FCS) (v/v), 1% non-essential amino acids (NEAA) (v/v), 2mM L-glutamine, 100 U/ml penicillin and 100µg/ml streptomycin. MDCKII cells stably transfected with mBcrp (mouse Bcrp) were grown in MEM, supplemented with 20% FCS (v/v), 1% NEAA (v/v), 2mM L-glutamine, 100U/ml penicillin and 100µg/ml streptomycin.

All MDCKII cell lines were passaged every 5-7 days upon reaching confluency. Once confluent cell growth medium was removed and cells washed three times with sterile phosphate buffered saline solution (PBS) to remove FCS. Cells were incubated for approximately 20-25 minutes at 37°C with 0.25% trypsin-EDTA (ethylenediaminetetraacetic acid) until cells began to detach from the culture flask base, at which point fresh medium was added to neutralise trypsin-EDTA. Remaining cells were then mechanically rinsed from the culture flask base to form a cell suspension. Cell suspensions were centrifuged at approximately 1200rpm for 5minutes, cell medium was removed and cells resuspended in fresh medium using a wide bore needle and syringe, giving a uniform cell suspension. Cell counts were determined and continuation flasks seeded as required.

2.2.2 Animal housing and sacrifice

All animals were allowed to become acclimated for a minimum of three days prior to initiation of the study. Animals were housed in polycarbonate cages and provided with R&M No1 Modified Irradiated Diet (Special Diet Services), used in all toxicological studies, and water ad libitum. The R&M No1 modified irradiated diet is subject to contamination testing and contains a protein level of 14.7% (Tucker, 1997). Room temperature and humidity were monitored, and animal rooms subjected to a 12 hour light/12 hour dark cycle.

Male Sprague Dawley and Han Wistar rats were sacrificed according to Schedule 1 of the Animals Scientific Procedures Act, 1986, and were able to access food ad libitum until time of sacrifice. Animals were sacrificed either by increasing isoflurane/CO_2 inhalation with death confirmed by cervical dislocation (AstraZeneca, Alderley Edge, UK), or by concussion with cervical dislocation (Newcastle University, UK). All animals were male, aged 8-10 weeks and were purchased from Charles River laboratories (UK) or Harlan laboratories (UK). For all experimental work the entire intestinal length from the pyloric sphincter to the anus was removed and immediately placed in ice cold L-15 Liebovitz's medium + L-Glutamine (Gibco, life technologies) (AstraZeneca, Alderley Edge, UK) or Ringer's solution (Newcastle University, UK).

2.2.3 Acquirement of duodenal, jejunal, ileal and colonic mucosal scrapes

Following washing with PBS, rat intestines were opened along the longitudinal axis to expose the mucosal surface. Duodenal intestinal mucosal scrapes were taken from the 4cm of intestine immediately distal to the pyloric sphincter, down to the ligament of Trietz. Jejunal intestinal scrapes were taken from the 5-6cm of intestine distal to the ligament of Trietz. Mid-ileal scrapes were taken from a length of intestine approximately 10cm long mid-way along the ileum and terminal colon scrapes taken from the length of intestine approximately 6cm proximal to the anus. Intestinal scrapes were frozen rapidly using liquid nitrogen and stored at -80°C until required.

2.2.4 Crypt-villus isolation and preparation validation

The crypt-villus isolation procedure is a modified version of that used by McNicholas et al., 1994. Mid-ileum sections were procured and the intestinal lumen washed three times using either L-15 Liebovitz's medium + L-Glutamine or Ringer's solution (as above) to remove faecal matter. Intestinal lumens were then flushed with crypt-villus isolation buffer (detailed in section 2.1). Excised intestinal sections were everted and carefully threaded onto a glass spiral such that the intestinal mucosa was outward facing, as shown in figure 2.1. Intestine was vibrated at approximately 50Hz into ice cold crypt-villus buffer (as above). Ten fractions were collected by replacing the crypt-villus buffer at timed intervals. Fractions were collected at cumulative incubation times of 2 x 30 seconds, 2 x 1 minute, 4 x 3 minutes and 2 x 7 minutes, such that the final fraction had been vibrated for a total of 29 minutes. Fractions were collected by centrifugation at 600 x g for 5 minutes at 4°C. Fractions for RNA and protein extraction were frozen rapidly using liquid nitrogen and were stored at -80°C until required. Fractions for enzyme analysis were frozen at -20°C.

2.2.4.1 Morphological assessment of crypt-villus fractions using light microscopy and transmission electron microscopy

Following collection of samples by centrifugation, fractions were mounted onto glass slides and imaged using a Nikon TMS Inverted phase contrast microscope with a 10x objective. All fractions were imaged to confirm morphological separation of villus and crypt enterocytes.

Additional to light microscopy, fractions 1 and 2 and fractions 9 and 10 were combined to give villus tip and crypt preparations respectively, and were imaged using transmission electron microscopy (TEM). Sample preparation for TEM and subsequent imaging was performed by the Electron Microscopy Research Unit at Newcastle University, UK. Following isolation, samples were combined and fixed in 2% gluteraldehyde in sodium cacodylate buffer (TAAB Lab. Equip, Berks, UK). Sodium cacodylate buffer was subsequently replaced three times and samples were incubated overnight. Samples were washed with deionised water and post-fixed for one hour using 1% osmium tetroxide (Agar Scientific, Essex, UK). Fixed samples were dehydrated using a series of increasing acetone concentrations (25%, 50%, 75% and 100%). Embedding of samples was performed using TAAB (laboratories) epoxy resin kit (TAAB Lab. Equip, Berks, UK) and samples impregnated in series with 25% resin in acetone, 50% resin in acetone, 75% resin in acetone and 100% resin for one hour per concentration. Samples were then further impregnated three times with 100% resin, prior to a final embedding stage in 100% fresh resin at 60°C for 24 hours.

Following dehydration and embedding of samples, survey sections of 1µm were cut and stained with 1% Toludine Blue in 1% Borax. Post staining, ultrathin (approximately 70nm) sections were cut using either a RMC MT-XL ultramicrotome or a Leica EM UC7 ultramicrotome, and stretched with chloroform. Sections were stretched with chloroform prior to mounting on Pioloform filmed copper grids (Agar Scientific, Essex, UK) to prevent section compression. Heavy metal staining using 2% aqueous uranyl acetate and lead citrate (Leica UK Ltd, Milton Keynes, UK) was used to stain sections and ensure high contrast staining. Sections were imaged using an AMT CCS camera (Deben) and a Phillips CM 100 Compustage (FEI) Transmission Electron Microscope.

2.2.4.2 Measurement of alkaline phosphatase and leucine aminopeptidase activity in crypt-villus fractions.

Fraction enzyme profiles for alkaline phosphatase (Alph) and leucine aminopeptidase (Lap) were deduced using enzyme substrates 4-nitrophenyl phosphate disodium salt hexahydrate (pNPP) and L-leucine-p-nitroanilide respectively. Alph and Lap activities were measured in all isolated fractions. ALPH catalyses the conversion of pNPP to p-nitrophenol whilst LAP hydrolyses leucine-p-nitroanilide to give p-nitroaniline with both reactions forming a soluble product, which is yellow in colour. The formation of p-nitrophenol and p-nitroaniline and the associated colour change can be measured (absorbance 410nm) to determine enzyme activity. Early experiments showed minimal formation of p-nitrophenol by alkaline phosphatase, however addition of 2mM $ZnCl_2$ to Krebs solution restored enzyme activity. Fractions were therefore resuspended in Krebs buffer + 2mM $ZnCl_2$ prior to homogenisation.

Following isolation and collection of samples by centrifugation, all samples were resuspended in Krebs buffer containing 2mM $ZnCl_2$. Phosphate was removed from Krebs buffer due to zinc mediated phosphate precipitation. Samples were homogenised using a hand held TissueRuptor (Qiagen, UK) and aliquots of fraction homogenate transferred in triplicate to a 96 well plate.

As described previously by Feruzza et al., (2011) pNPP was dissolved to 5mg/ml in 100mM diethanolamine, 150mM NaCl and 2mM $MgCl_2$ to give a working pNPP solution which was pH adjusted to 9.5 using HCl prior to the addition of pNPP. An Alph assay buffer was prepared by combining pNPP solution with a TRIS-HCl based assay collection buffer (10mM TRIS-HCl, 150mM NaCl, pH 8.0) at a ratio of 3:1 to give a final pNPP concentration of 10mM with a resultant pH of 9.3 (Ferruzza et al., 2011). Buffer solutions were warmed to 37°C prior to assay initiation. 150µl of assay buffer was added to the 96 well plate containing fraction homogenate at timed intervals and the enzyme reaction stopped following a 10 minute incubation period at 37° by the addition of 50µl of 0.5M NaOH.

L-leucine-p-nitroanilide was dissolved to a concentration of 25mM in a phosphate based buffer solution (84mM Na_2HPO_4, 67mM KH_2PO_4 final pH of 7.4). LAP phosphate buffer was warmed to 37°C and 150µl added to the 96 well plate containing fraction homogenate as described above. Enzyme reactions were stopped following 10 minute incubation at 37°C by the addition of 1.5M acetic acid (50µl). Product formation was determined by measuring absorbance at 410nm on a FLUOstar Omega microplate reader (Alph) or a Tecan infinit-pro200 plate reader (Lap). Sample protein concentrations were determined using the Pierce BCA (bi-cinchronic acid) protein assay (Pierce, Thermo Scientific, UK). The BCA protein assay relies on the detection of Cu^{1+} by bi-cinchronic acid (BCA) following reduction of Cu^{2+} to Cu^{1+} by protein present within the solution being analysed (Walker, 2009). An intense water soluble purple coloured precipitate is formed as a result of the chelation of one Cu^{1+} ion by two BCA molecules. The resultant colour change is then measured spectrophotometrically. Standard calibration curves were produced and unknown protein concentrations calculated using linear regression following measurement of absorbance at 562nm using a FLUOstar microplate reader. An example BCA calibration curve is shown in figure 2.2. Change in absorbance (compared with blank well absorbance) due to enzyme mediated substrate formation was calculated per µg of protein per minute assuming linearity of enzyme activity. Substrate concentrations formed were calculated using enzyme extinction coefficients of 18.5 and 9.9 for alkaline phosphatase and leucine aminopeptidase respectively. Values were adjusted to give µM concentrations; allowing comparison between fractions.

Figure 2.1:

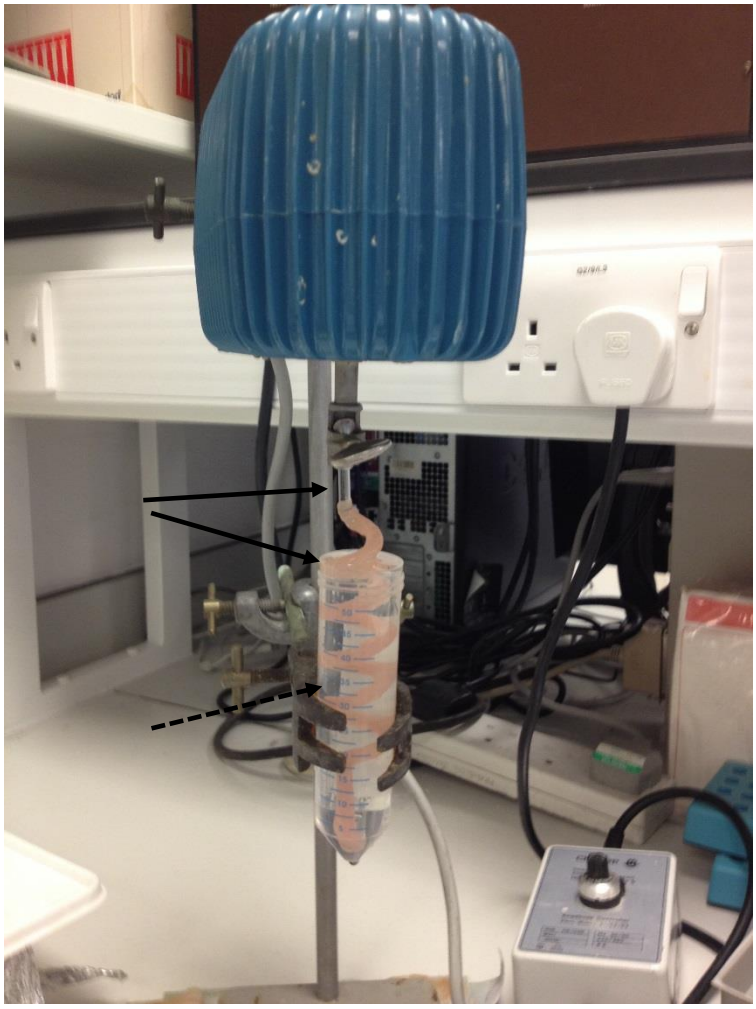

Figure 2.1 Intestinal crypt-villus isolation; experimental apparatus and tissue set-up.

Mid-Ileum section is shown everted with mucosal surface outward facing on glass spiral mounted in vibrating apparatus (solid black arrows). Specially designed glass coil is suspended in ice cold crypt villus isolation buffer to ensure collection of chelated enterocytes (dashed black arrow).

Figure 2.2:

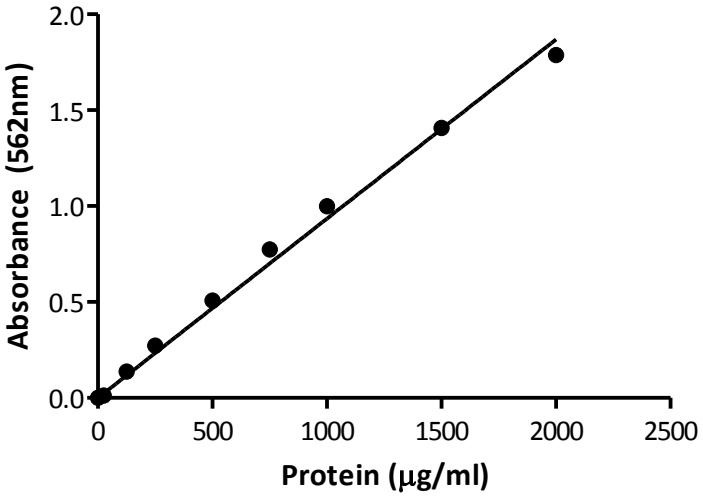

Figure 2.2 BCA standard calibration curve with linear regression analysis.

BCA protein standard calibration curve was produced using known protein concentrations and utilised for calculation of concentrations of unknown protein samples using linear regression analysis.

2.2.4.3 Assessment of cell viability in villus tip and crypt fractions using the Live-DEAD cell assay and fluorescence microscopy.

The Live-DEAD cell assay employs the two nucleic acid stains, DEAD Red (ethidium homodimer-2) and SYTO 10 (Molecular probes, Invitrogen). DEAD Red, is a membrane impermeant dye and therefore will only bind to nucleic acids of those cells with compromised membranes whilst SYTO 10 is membrane permeant and will label all cells. The relative binding affinities and concentrations of these two nucleic acid stains are balanced such that live cells are stained with SYTO 10 and fluoresce green, whilst dead cells will fluoresce red when excited due to DEAD Red cellular staining.

Working solutions of DEAD Red and SYTO 10 were prepared by diluting and mixing both dyes (1:50) in one volume of Hanks Balanced Salt Solution (HBSS). Crypt-villus isolation medium was carefully removed from fractions, and fractions 1 and 2 and fractions 9 and 10 combined to give villus tip and crypt preparations. Samples were separated to give three aliquots allowing determination of cell viability either immediately following isolation or following incubation in Krebs buffer solution for 30 minutes at room temperature or 37°C. Following incubation cell samples were combined with working dye solutions and were incubated in complete darkness, at room temperature for 15 minutes, at which point cells were resuspended in fresh HBSS.

To maintain cellular morphology dyed cells were mounted onto glass slides using CyGEL (Biostatus, UK). CyGEL is unusual in that it is a thermoreversible gel used to immobilise live cells which liquefies when cooled. CyGEL was prepared according to manufacturer's instructions and cooled on ice until a liquid state was reached. CyGEL was combined with pre-dyed crypt-villus fractions using a cooled pipette tip. CyGEL/fraction suspensions were streaked across the glass slide surface and cooled on ice allowing CyGEL to liquefy and spread out beneath the mounted cover clip. Slides were removed from ice allowing CyGEL to solidify and were stored in darkness at room temperature until imaged. Samples were imaged using a Zeiss Axioimager microscope, and were excited using light of wavelengths 450-490nm and 540-552nm to visualise SYTO10 (live) and DEAD Red (dead cells) respectively.

Pixel intensity measurements were made using ImageJ software with a consistent standard pixel intensity threshold applied to all images. All images analysed were of the same size and ratios calculated by division of SYTO10 pixel intensity by pixel intensity of DEAD Red.

2.2.4.4 Determination of intracellular Na/K concentrations using flame photometry

Flame photometry was performed by Professor Nicholas Simmons, University of Newcastle, UK. The Na-K ATPase transporter expressed on the basolateral membrane of epithelial cells is responsible for maintenance of membrane gradients for Na and K such that intracellular K is

approximately 120-150mM and Na is present at a concentration of 5-20mM (Simmons, 1981), with reversal of this gradient indicating a loss of membrane integrity and as such cell viability, or lack of Na-K ATPase activity. We therefore determined K and Na concentrations in isolated mid-villus fractions, fractions 3-8. Na-K ATPase activity was assessed only in mid-villus fractions since isolated villus tip and crypt samples were used for determination of enzyme activities and morphological analysis. Following centrifugations fractions were combined and incubated at 4°C, 20°C or 37°C for either 40 or 120 minutes in either Krebs or KB medium (section 3.2.1). Mid-villus fragments were then washed twice in 200 times volume of ice cold Krebs buffer in which Na and K had been substituted with mannitol and iso-osmolality maintained. Fractions were then extracted in 0.5ml distilled water and Na and K ion concentrations determined by flame photometry. Flame cytometry allows determination of ion concentrations via quantification of the photoelectric current using a series of filters specific to each ion. Unknown ion concentrations are determined by measurement of the flame intensity which is reliant upon the energy required to vaporise atoms present within a sample and subsequent comparison with flame intensities of solutions with known ion concentrations.

2.2.4.5 Assessment of cell viability in crypt-villus fractions using the MTS colourimetric assay

The MTS colourimetric assay was utilised to measure cell viability, based on the metabolic activity of cells, following crypt-villus isolation. The MTS compound [3-(4,5-dimethylthiazol-2-yl)-5-(3-carboxymethoxyphenyl)-2-(4-sulfophenyl)-2H-tertrazolium, inner salt; MTS] is a soluble tetrazolium compound which is reduced by electron transfer from NAD(P)H to give an insoluble purple precipitate, known as formazan (Promega, UK). NAD(P)H is produced by metabolically viable cells. The formation of the coloured precipitate, formazan, and subsequent measurement of sample absorbance at 490nm therefore allows measurement of cell viability.

Following isolation and collection by centrifugation, fractions 1 and 2 and fractions 9 and 10 were combined to give villus tip and crypt preparations. Fractions were resuspended in 1ml of Krebs buffer solution or KB medium (see section 2.1.1) and incubated at 37°C for 30 minutes. Following incubation 10µl of fraction homogenate were transferred to a 96 well plate and combined with 200µl of MTS reagent. Absorbance at 490nm was measured kinetically over a ten minute period and absorbance change per minute calculated (assuming substrate formation to be linear).

2.2.5 Measurement of functional MDR1 and mBcrp/BCRP transporter activity using the Hoechst33342 dye retention assay

A known substrate for both MDR1 and mBcrp/BCRP (Scharenberg et al., 2002, Shapiro et al., 1997), the lipophilic cationic dye, Hoechst33342, can be used to determine functional MDR1 and BCRP activity in intact cells. Hoechst33342 is able to diffuse passively across the cell membrane and intercalate with cellular DNA causing a dramatic shift in the emission spectra of the dye. A shift in the emission spectra is also observed following diffusion and binding of Hoechst33342 into the phospholipid bilayer (Müller et al., 2007). The shift in absorbance following binding of Hoechst33342 to either DNA or the phospholipid bilayer is associated with an intense increase in fluorescence compared with fluorescence measured at the same wavelength when the Hoechst33342 dye is free in solution (Müller et al., 2007).

MDR1 and BCRP are able to actively transport Hoechst33342 from within the lipid bilayer and extrude the dye into the aqueous extracellular environment thereby reducing measured cellular fluorescence. Inhibition of MDR1 or BCRP using either of the inhibitors Cyclosporine A (CsA) or K0143 at concentrations specific to each transporter or by competitive substrate mediated transporter inhibition will cause a reduction in functional transporter activity and result in an increased cellular accumulation of Hoechst33342, either intracellularly or within the lipid bilayer causing a subsequent increase in cellular fluorescence. The measured increase in fluorescence in the presence of transporter inhibition is relative to functional activity, since when active, MDR1 and BCRP will efflux Hoechst33342 from the cell. The movement of Hoechst33342 out of the cell will ultimately reduce cellular fluorescence. This is summarised in figure 2.3.

2.2.5.1 Cell culture for Hoechst33342 dye retention assays in MDCKII cell lines

MDCKII cell lines were seeded at a density of 20,000 cells per well on 96 well tissue culture plates. Cells were cultured for 5-7 days and cell medium was replaced 24 hours prior to experimentation.

2.2.5.2 Characterisation of MDR1 and mBcrp functional activity using Hoechst33342 dye retention assay in native and transfected MDCKII cell lines

Cellular Hoechst33342 dye retention assays were performed on a temperature regulated hotplate at 37°C and all solutions used were warmed to 37°C to maintain physiological relevance. To begin, cells were washed twice using Krebs buffer solution and then incubated with Krebs buffer solution in the presence or absence of specific MDR1 and mBcrp transporter inhibitors, CsA and K0143, or Imatinib mesylate (dissolved in DMSO) at specified concentrations for 40 minutes to allow equilibration. Solutions were removed and replaced

with Krebs buffer solution +/- CsA, K0143 or Imatinib mesylate in the presence or absence of 3µM Hoechst33342. A 3µM Hoechst33342 concentration was deemed optimal based on previous work in our laboratory (Webster, 2011, Wright, 2011). Following a further 40 minute incubation period cells were again washed using Krebs buffer solution and cellular fluorescence measured. Hoechst33342 dye retention was measured using a Tecan infinite-pro200 plate reader. Cells were excited at optimal wavelength of 361nm with resultant emitted fluorescence being measured at 486nm. Data were normalised for background cellular fluorescence determined in the absence of Hoechst33342.

2.2.5.3 Characterisation of Mdr1 and Bcrp functional activity using the Hoechst33342 dye retention assay in villus tip and crypt fractions isolated from rat ileum

To determine functional transporter activity of Mdr1 and Bcrp in villus tip and crypt fractions, fractions 1 and 2 and fractions 9 and 10 were combined post isolation and resuspended in Krebs buffer. Fractions were resuspended to give a uniform suspension and were incubated in the presence or absence of the specific Mdr1 and Bcrp inhibitors, CsA and K0143, and 3µM Hoechst33342. Pre-incubation with specific inhibitors was not performed due to a lack of cell viability following isolation. Following a 30 minute incubation period fractions were again resuspended and aliquots transferred, in triplicate, to a 96 well plate. Hoechst33342 dependent fluorescence was measure using a FLUOstar Omega microplate reader (excitation 355nm, emission 485nm). Due to differences in the instrument used to determine cellular fluorescence it was not possible to measure the fluorescence of cultured cell lines and isolated fractions using the same wavelengths, however all wavelengths used fall within the excitation and emission peaks of Hoechst33342.

Figure 2.3:

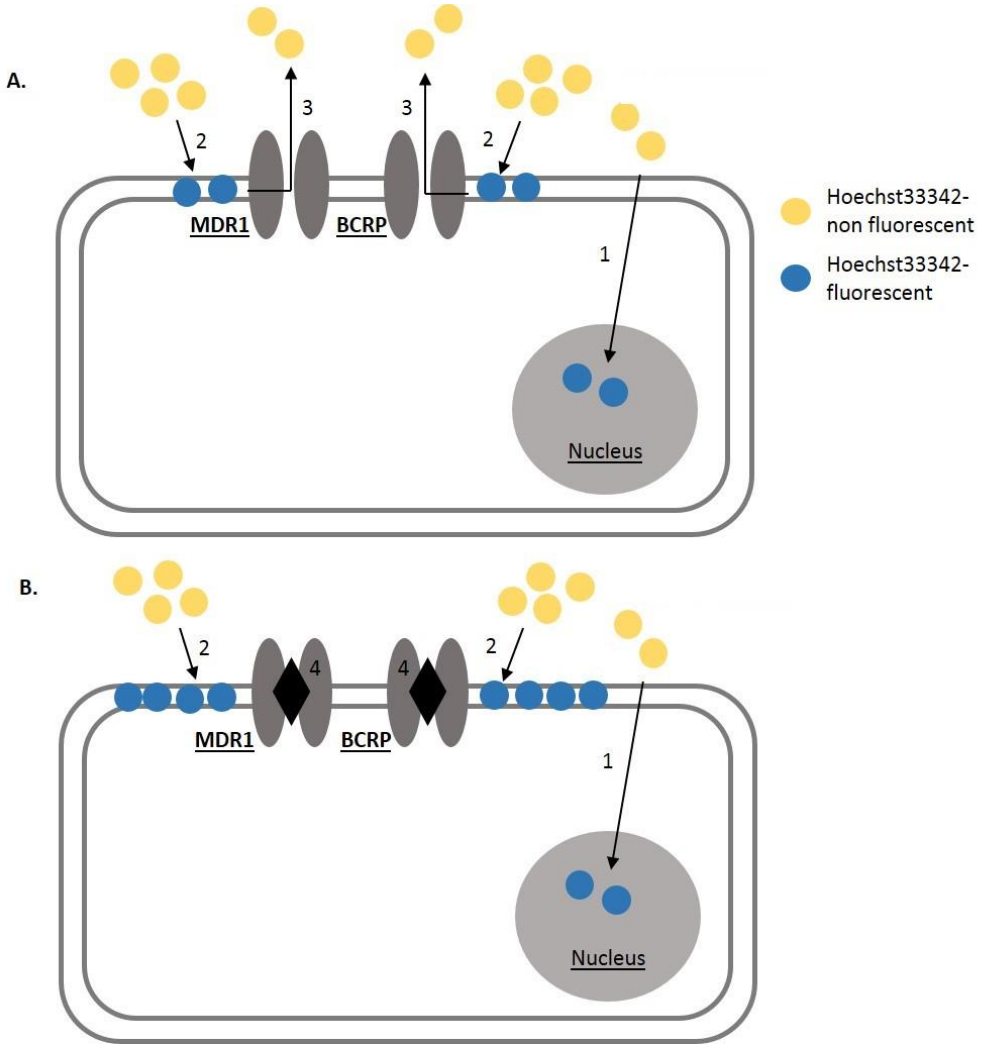

Figure 2.3 Schematic representation of the Hoechst33342 dye efflux assay in the absence (A) and presence (B) of MDR1 and BCRP transporter inhibition.

(1) Hoechst33342 (yellow) diffuses across the cell membrane and intercalates with cellular DNA (blue) causing an intense shift in fluorescence (2) Hoechst33342 diffuses into the cell membrane and undergoes an intense shift in fluorescence. (3) Hoechst33342 is effluxed from within the lipid bilayer by MDR1 and BCRP, lowering cellular fluorescence via movement of Hoechst33342 into solution. (4) Inhibition of transporter activity prevents efflux of Hoechst33342 from the lipid bilayer and instead the dye accumulates within the cell membrane, further increasing fluorescence intensity.

2.2.6 Determination of mRNA expression levels of key intestinal drug transporters and cytochrome P450 enzymes in rat intestine using NanoString technology

2.2.6.1 Total RNA extraction from rat intestinal samples and RNA quality control

Prior to RNA extraction all specimens were kept on dry ice during initial processing, to prevent thawing and RNA degradation. Approximately 30mg of tissue was weighed and immediately placed in 700µl of Qiazol solution (Qiagen, UK). Tissues were disrupted and homogenised in Qiazol using a Polytron 3100 homogeniser. Chloroform (140µl) was added and the tissue suspensions centrifuged to allow phase separation. The colourless aqueous phase was then removed and RNA extracted as per the Qiagen RNA mini plus protocol. Briefly the homogenised lysate was spun through a gDNA eliminator column to remove DNA contamination. Column flow through was combined at a 1:1 volume ratio with 70% ethanol, samples were bound to RNAeasy spin column membranes and contaminants removed using Qiagen RNA mini plus kit supplied wash buffers.

To determine RNA concentrations, all extracted RNA samples were analysed using a Nanodrop 2000 spectrophotometer (Thermo Scientific, UK). Nanodrop spectrophotometry measures the absorbance at 230, 260 and 280nm and calculates a 260:280nm and a 260:230nm ratio for each sample. Resultant ratios give an indication as to sample purity, since nucleic acids and protein have absorbance maxima of 260nm and 280nm respectively, with absorbance readings at 230nm assumed to result from other contaminants. Nanodrop 260:280nm ratios ≈ 2 are deemed to reflect pure RNA.

Additionally, total RNA samples were analysed using Eukaryotic total RNA analysis on an Agilent 2100 bioanalyser to determine sample integrity. The Agilent 2100 bioanalyser allows separation of samples in a size dependent manner by on chip gel electrophoresis. Samples are run alongside a ladder of known band size to allow size quantification. Fluorescent dye added during chip preparation intercalates with sample RNA allowing detection using laser induced fluorescence, prior to translation of results to give a gel like image and a corresponding electropherogram. Example gel images and an electropherogram are shown in figure 2.4 and figure 2.5. RNA integrity (RIN) values calculated by the Agilent 2100 bioanalyser, using the entire electrophoretic trace of the RNA samples (including the presence or absence of degradation products) allow assessment of RNA integrity across samples.

Figure 2.4:

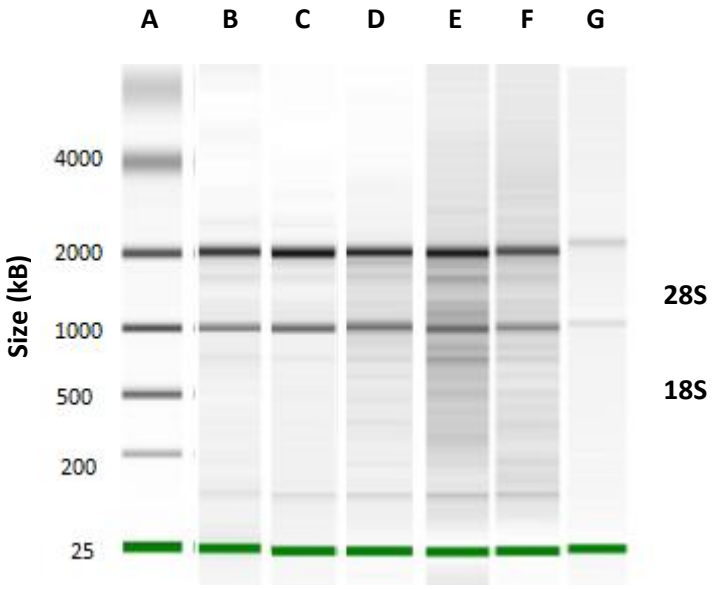

Figure 2.4 Representative gel image following on chip gel electrophoresis of rat samples from villus tip and crypt total RNA samples using an Agilent 2100 bioanalyser.

On chip gel electrophoresis was performed using an Agilent 2100 bioanalyser. A ladder of known RNA sizes is shown (A) alongside villus tip (B-D) and crypt (E-G) samples for three animals with clear distinct bands apparent at 28S and 18S, indicating RNA remains intact.

Figure 2.5:

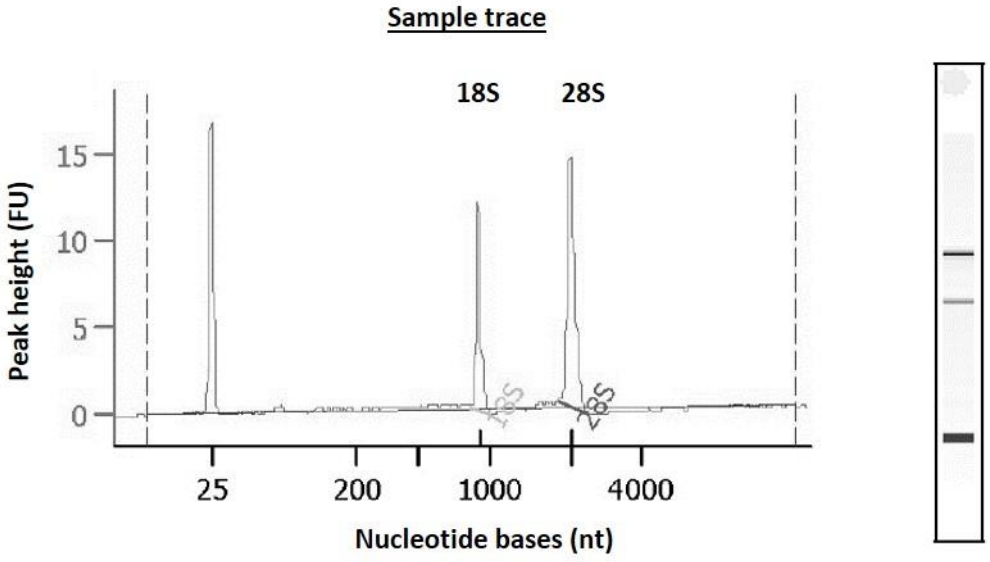

Figure 2.5 Representative electropherogram following Eukaryotic total RNA analysis using Agilent 2100 Bioanalyser alongside respective gel electrophoresis image.

Calculated RIN value for sample = 9.5 (maximum obtainable RIN value = 10).

2.2.6.2 NanoString

For full details regarding NanoString technology please see Geiss et al., 2008. mRNA expression levels of key drug transporters and Cyp450 enzymes in intestinal regions, villus tip, crypt, duodenum, jejunum, ileum and colon were determined using NanoString technology. NanoString technology allows for determination of gene expression levels using a multiplexed probe library which allows simultaneous measurement of mRNA expression levels of up to 800 gene targets within one total RNA sample, without the need for reverse transcription and target amplification (Geiss et al., 2008). The removal of requirement to transcribe RNA to cDNA and subsequent enzymatic based amplification, as necessary in qPCR (quantitative PCR), allows direct correlation between NanoString counts and sample mRNA transcript expression, whilst greatly reducing potential for introduction of human and technological errors. NanoString technology is highly sensitive and can detect mRNA concentrations as low as 0.1 - 0.5fM, making the technique arguably more quantitative than qPCR.

Target libraries, known as codesets are designed by NanoString technologies, based on user preference against the desired species of interest. Target mRNA sequences are screened to identify potential 100-base regions, complementary to the target gene, which present minimal base repeats and low GC content. These 100-base regions are divided to give two 50-base probes, designated capture and reporter probes. All probes are pre-screened for cross hybridisation, with those probes showing greater than 85% cross hybridisation, or greater than 15 continuous complementary bases to non-target mRNA being rejected. Probe sequences are adjusted to give optimal melting temperatures (Tm), with a lower cut off value of 35 bases (Geiss et al., 2008).

Reporter and capture probes are each 35-50 bases in length and are complementary to the target mRNA sequence. The capture probe carries a 3' biotin affinity tag which permits immobilisation of target-probe complexes to streptavidin-coated slides, allowing imaging and data collection. The target reporter probe carries a molecular barcode. The molecular barcode of the reporter probe is a target unique fluorescent colour coded tag ligated to a single stranded DNA backbone. The reporter probe and associated molecular barcode allows measurement of target gene mRNA expression via NanoString Digital Analyser based imaging. Additionally, the capture and reporter probe contain 3' and 5' repeats required for post-hybridisation purification.

An excess of capture and reporter probes for multiple gene targets, are mixed with a single total RNA sample and hybridisation buffer in solution and the mix incubated at 65°C. This hybridisation step facilitates the binding of target mRNA to specific reporter and capture

probes, forming a tripartite structure as shown in figure 2.6. The suspension of mRNA and NanoString probes within solution gives a higher level of sensitivity than micro arrays, ensuring maximal detection of mRNA transcripts.

Following hybridisation samples are transferred by the NanoString prep station to individual flow cells of the NanoString sample cartridge. Samples are affinity purified using magnetic beads and the 3' and 5' repeats found on the capture and reporter probes respectively, allowing the removal of excess unbound probes. Remaining tripartite complexes are bound to streptavidin-coated slides via the 3' biotin molecule of the capture probe and an electrical current applied to microfluidic channels within the nCounter sample cartridge, to stretch and align tripartite structures. Alignment and stretch immobilises probe-mRNA complexes in an elongated state to allow counting of molecular barcodes. Purification and immobilisation steps described are handled robotically on the NanoString Technologies Prep Station.

NanoString sample cartridges are then placed in the Digital analyser (NanoString technology), which counts the number of times each molecular barcode appears using four different excitation wavelengths, corresponding to fluorescent spots of the molecular probe. Control criteria must be met for spot sequences to be recorded as a reporter probe, including spot-to-spot spacing, acceptable linearity and orientation requirements, ensuring accurate counting of mRNA transcripts.

Additional to user-defined gene targets the NanoString codeset contains several positive controls which are synthetic RNA molecules spiked into the codeset at known concentrations ranging from 0.125fM to 128fM. Positive controls are used to normalise for assay efficiency, including hybridisation and purification steps and permit comparison of results across different assays. Positive controls are also used as standard references to allow calculation of target gene concentrations. Negative synthetic RNA controls, for which no target sequences exist, are also spiked into the reaction. Since no target mRNA exists for the negative reporter and capture probes it is assumed that any binding and subsequent detection of unique molecular barcodes associated with these negative controls results from mis-hybridisation thereby allowing correction for mismatched hybridisation and declaration of target genes to be present or absent.

2.2.6.3 NanoString CodeSet design

The NanoString codeset used in this project was designed based on current literature, and key intestinal drug transporters and drug metabolising cytochrome P450 enzymes were carefully selected. Whilst RNA concentration and RNA integrity were controlled, three potential

housekeeping (HKSP) genes were selected and included in the NanoString codeset to allow normalisation of target gene expression against expression levels of genes expected to be constitutively expressed across all samples, irrelevant of tissue type or experimental treatment (Vandesompele et al., 2002a). Finally, several genes with known intestinal expression patterns reported in the literature were included in the codeset as experimental controls. The NanoString codeset used throughout this project is shown in table 2.1.

Figure 2.6:

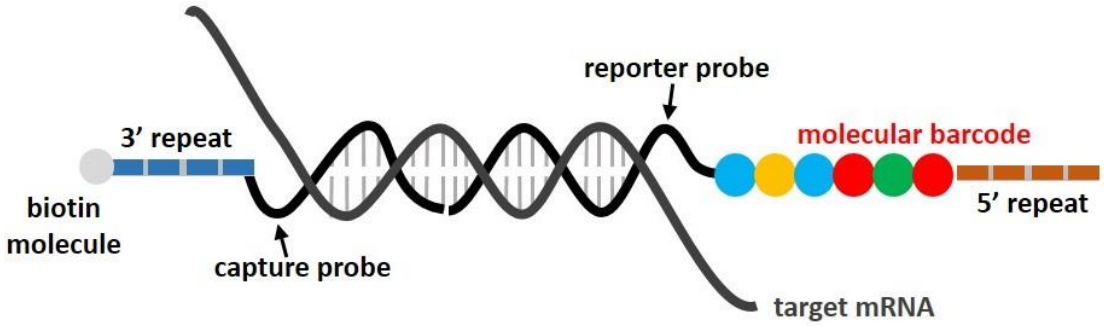

Figure 2.6 NanoString tripartite structure showing hybridisation of capture probe, reporter probe and target mRNA sequence.

Table 2.1:

Target identifier	Gene	Accession	Probe target region	Capture Probe Tm	Reporter probe Tm	Notes
Mdr1a	Abcb1a	NM_133401.1	4428-4528	85	85	
Mdr1b	Abcb1b	NM_012623.2	202-302	85	83	
Mrp1	Abcc1	NM_022281.2	3491-3591	84	83	
Mrp2	Abcc2	NM_012833.1	2887-2987	85	81	
Mrp3	Abcc3	NM_080581.1	1098-1198	84	83	
Mrp4	Abcc4	NM_133411.1	448-548	82	86	
Mrp5	Abcc5	NM_053924.1	1554-1654	82	87	
Mrp6	Abcc6	NM_031013.1	5660-5760	85	80	
Mrp7	Abcc10	NM_001108201.1	245-345	85	80	
Bcrp	Abcg2	NM_181381.2	1609-1709	83	85	
Cyp1a1	Cyp1a1	NM_012540.2	2164-2264	85	80	
Cyp2b1/2b2	Cyp2b2	NM_001198676.1	1691-1791	80	84	Targets Cyp2b1 (NM_001134844) with 98% homology
Cyp2c11	Cyp2c11	NM_019184.2	1105-1205	79	79	
Cyp2c6v1/2c7	Cyp2c6v1	NM_001013904.1	1072-1172	86	82	Targets Cyp2c7 (NM_017158) with 85% homology
Cyp2d1/2d5/2d9	Cyp2d1	NM_153313.1	661-761	85	81	
Cyp2d3	Cyp2d3	NM_173093.1	577-677	82	80	
Cyp2d4/2d6	Cyp2d4	NM_138515.2	697-797	83	82	
Cyp2j4	Cyp2j4	NM_023025.2	21-121	88	87	
Cyp2s1	Cyp2s1	NM_001107495.1	1915-2015	85	86	
Cyp3a18	Cyp3a18	NM_145782.1	1465-1565	84	80	
Cyp3a1/3a2/3a23	Cyp3a23/3a1	NM_013105.2	14-114	90	90	Targets Cyp3a2 (NM_153312) with 93% homology
Cyp3a62	Cyp3a62	NM_001024232.1	1578-1678	84	80	
Cyp3a9	Cyp3a9	NM_147206.2	1549-1649	84	82	
Cnt2	Slc28a2	NM_031664.1	22-122	86	83	
Pept1	Slc15a1	NM_001079838.1	349-449	83	81	
Oct1	Slc22a1	NM_012697.1	1004-1104	83	85	
Octn1	Slc22a4	NM_022270.1	974-1074	85	85	
Octn2	Slc22a5	NM_019269.1	1746-1846	88	87	
Oatp-b	Slco2b1	NM_080786.1	2736-2836	85	83	
Oat3	Slc22a8	NM_031332.1	1315-1415	84	85	
Oatp-3	Slco1a5	NM_030838.1	101-201	85	85	
Alph	Alph	NM_013059.1	1863-1963	86	85	Experimental control gene
Lap3	Lap3	NM_001011910.1	1270-1370	86	83	Experimental control gene
Villin	Vil1	NM_001108224.2	2986-3086	80	80	Experimental control gene
Sglt1	Slc5a1	NM_013033.2	2325-2425	82	81	Experimental control gene
Pcna	Pcna	NM_022381.3	526-626	85	85	Experimental control gene
Ca2	Ca2	NM_019291.1	984-1084	84	84	Experimental control gene
Nkcc1	Slc12a2	NM_031798.1	1640-1740	80	77	Experimental control gene
Cftr	Cftr	NM_031506.1	1274-1374	80	82	Experimental control gene
Gapdh	Gapdh	NM_017008.4	991-1091	84	90	Houskeeping gene
Hmbs	Hmbs	NM_013168.2	460-560	82	84	Houskeeping gene
Hprt1	Hprt1	NM_012583.2	679-779	82	84	Houskeeping gene

Table 2.1 NanoString CodeSet used throughout project to determine intestinal mRNA expression levels both in untreated and *in vivo* treated animals.

Target identifier names are shown alongside gene details and NCBI accession numbers. Target sequence regions against which capture and reporter probes are designed are noted with respective Tm values. Probe target pairs homologous to multiple gene targets are identified.

2.2.6.4 NanoString protocol

The NanoString protocol requires minimal user input thereby reducing the probability of human error. NanoString hybridisation buffer (130µl) was added directly to a manufacturer supplied tube containing codeset reporter probes to give a Master Mix solution. Master Mix solution was then divided between 12 sample tubes in 20µl aliquots. 5µl of total RNA (~50ng/µl) was added to each reaction, with the ability to adjust data for RNA concentration during post experimental analysis. Despite high loading concentrations binding density values determined by the nCounter digital analyser showed all samples to fall within the concentration range for which reporter and capture probes are present within excess to maximise potential for tri-partite structure formation. 5µl of Capture ProbeSet was added to each sample tube immediately prior to incubating the final mix at 65°C, to allow hybridisation. Sample strip tubes were incubated at 65°C in a thermocycler for between 20-24 hours and samples immediately transferred to the nCounter Prep-station for post-hybridisation robotic processing. Excess probes were removed and samples purified and aligned prior to digital imaging on the nCounter digital analyser. Following post-hybridisation processing, samples were quantified using unique, fluorescent colour coded barcodes attached to target reporter probes, described in detail in section 2.6.6.2.

2.2.6.5 Data analysis, normalisation and statistics

Data from the NanoString digital analyser is output in Microsoft Excel format, allowing easy post-assay manipulation and post-experimental analysis. As suggested by NanoString, data was initially normalised against positive synthetic RNA levels to correct for differences in assay efficiency, since experimental restraints forced samples to be run across multiple assays. Positive control sample counts were summed, and normalisation factors calculated by dividing the average assay positive control count (n=12 samples) by respective assay summed sample counts. All target gene and negative control counts were multiplied by assay normalisation factors, allowing comparison across multiple assays. An example showing the calculation of assay normalisation factors is shown in figure 2.7. Negative control counts were summed and subtracted from target gene counts to adjust for background noise, and false readings.

2.2.6.6 Housekeeping gene selection and validation

Additional to normalising for differences between assays, three housekeeping genes were included in the design of the NanoString codeset to allow normalisation of target gene expression for RNA concentration and quality. Normalisation against a single, or a group of, chosen housekeeping (HSKP) genes permits comparison of gene expression levels across samples, allowing direct comparison between villus tip and cryptal expression for example (Wang et al., 2010).

Geometric mean (geomean) values were calculated from Gapdh (glyceraldehyde-3-phosphate dehydrogenase), Hprt1 (hypoxanthine phosphoribosyltransferase 1) and Hmbs (hydroxymethylbilane synthase) for each individual sample. The geometric mean indicates the central tendency of a set of numbers and therefore controls for differing expressions of HSKP genes and potential outlying value (Vandesompele et al., 2002b). NanoString data obtained from control animals (villus tip, crypt, duodenal, jejunal, ileal and colonic samples) and data obtained from *in vivo* studies were normalised independently. The geomean was then determined from n=48 respective samples, and this value was divided by each sample geomean to give individual sample normalisation factors. All target gene counts were normalised against individual sample HSKP gene normalisation factors. An example showing HSKP gene normalisation is shown in figure 2.8.

Following normalisation, NanoString counts were converted to fmol/sample concentrations using positive control standards. Average positive control counts, at each concentration (128fM – 0.125fM), were determined and respective standard curves produced (figure 2.9). All standard curves gave a correlation coefficient > 0.998. Fmol/sample concentrations were calculated for each target mRNA NanoString count using GraphPad prism 5.0.

Prior to analysis of statistical difference between intestinal regions Levene's test was applied to normalised data to determine if regional gene populations showed equal or unequal variance. Sample variance was determined since Student's t-test assumes both populations show equal variance and may therefore give erroneous statistical results should populations be unequal. Where populations were unequal Welche's correction was applied, removing the equal population assumption. Statistical tests used are noted alongside respective tables and figures. All statistical analysis was performed using Excel SigmaXL 2010 or GraphPad Prism 5.

Fold change values were calculated by determination of expression ratios between two regions of the intestine. Calculation of $\log_2$ fold change values allows easy identification of fold changes between regions, whether gene expression is up or down regulated. For example, should gene expression show a 2-fold increase data can be easily interpreted however a 2-fold decrease in expression is represented as a 0.5 fold change, by taking the binary log of these two fold change values $\log_2$ data shows values of 1 and -1 for the fold increase and decrease respectively. Log_2 transformations therefore allow representation of fold changes relative to each other, irrelevant of direction of change.

Figure 2.7:

A

	Concentration (fM)	NanoString counts Sample 1	Sample 2	Sample 3	Sample 4
	128	18161.8	15116.1	24793.2	27327.9
	32	5703.8	4249.1	6152.2	7259.9
	8	1629.8	1262.1	1792.2	1945.9
	2	373.8	281.1	377.2	492.9
	0.5	57.8	49.1	82.2	89.9
	0.125	18.8	21.1	48.2	53.9
Sum	=SUM(C4:C9)	20978.7	33245.3	37170.2	

B

	Concentration (fM)	NanoString counts Sample 1	Sample 2	Sample 3	Sample 4
	128	18161.8	15116.1	24793.2	27327.9
	32	5703.8	4249.1	6152.2	7259.9
	8	1629.8	1262.1	1792.2	1945.9
	2	373.8	281.1	377.2	492.9
	0.5	57.8	49.1	82.2	89.9
	0.125	18.8	21.1	48.2	53.9
Sum		25945.9	20978.7	33245.3	37170.2
Average	=AVERAGE(C11:F11)				

C

	Concentration (fM)	NanoString counts Sample 1	Sample 2	Sample 3	Sample 4
	128	18161.8	15116.1	24793.2	27327.9
	32	5703.8	4249.1	6152.2	7259.9
	8	1629.8	1262.1	1792.2	1945.9
	2	373.8	281.1	377.2	492.9
	0.5	57.8	49.1	82.2	89.9
	0.125	18.8	21.1	48.2	53.9
Sum		25945.9	20978.7	33245.3	37170.2
Average		29335.0			
Normalisation Factor	=$C$12/C11		1.40	0.88	0.79

Cont.

Figure 2.7 Calculation of assay normalisation factors

Example of the calculation used to determine assay normalisation factors for each sample; example shows n=4 samples whilst actual assay normalisation factors were calculated across n=12 samples per assay. **A**. Sum of positive control counts for each sample. **B**. Average of all sample positive control counts within one assay determined. **C**. Normalisation factors calculated by dividing average of all sample positive control counts by respective summed sample positive control counts.

Figure 2.8:

A

	BM	BN	BO	BP	BQ	BR
81	Endogeno	**Octn2**	10060.0	15158.6	10233.9	5232.7
82	Endogeno	**Oat3**	90.9	141.2	120.2	65.6
83	Endogeno	**Cnt2**	31447.8	21236.9	41489.5	14684.1
84	Endogeno	**Sglt1**	148771.7	262905.1	49978.7	97990.2
85	Endogeno	**Oatp-3**	29.7	38.5	46.3	21.5
86	Endogeno	**Oatp-b**	217.9	338.5	266.0	555.9
87	Endogeno	**Villin**	64452.4	103568.1	63633.1	72251.7
88						
89						
90	Housekee	**Gapdh**	59241.4	83318.4	73832.6	69695.9
91	Housekee	**Hmbs**	597.5	881.7	569.4	910.5
92	Housekee	**Hprt1**	546.1	645.3	683.7	707.6
93						
94		**Geomean**	=GEOMEAN(BO90:BO92)	**3619.15**	**3063.28**	**3554.32**
95						

B

	BM	BN	BO	BP	BQ	BR
81	Endogeno	**Octn2**	10060.0	15158.6	10233.9	5232.7
82	Endogeno	**Oat3**	90.9	141.2	120.2	65.6
83	Endogeno	**Cnt2**	31447.8	21236.9	41489.5	14684.1
84	Endogeno	**Sglt1**	148771.7	262905.1	49978.7	97990.2
85	Endogeno	**Oatp-3**	29.7	38.5	46.3	21.5
86	Endogeno	**Oatp-b**	217.9	338.5	266.0	555.9
87	Endogeno	**Villin**	64452.4	103568.1	63633.1	72251.7
88						
89						
90	Housekee	**Gapdh**	59241.4	83318.4	73832.6	69695.9
91	Housekee	**Hmbs**	597.5	881.7	569.4	910.5
92	Housekee	**Hprt1**	546.1	645.3	683.7	707.6
93						
94		**Geomean**	**2683.72**	**3619.15**	**3063.28**	**3554.32**
95		**Average**	=AVERAGE(BO94:BR94)			

C

	BM	BN	BO	BP	BQ	BR
81	Endogeno	**Octn2**	10060.0	15158.6	10233.9	5232.7
82	Endogeno	**Oat3**	90.9	141.2	120.2	65.6
83	Endogeno	**Cnt2**	31447.8	21236.9	41489.5	14684.1
84	Endogeno	**Sglt1**	148771.7	262905.1	49978.7	97990.2
85	Endogeno	**Oatp-3**	29.7	38.5	46.3	21.5
86	Endogeno	**Oatp-b**	217.9	338.5	266.0	555.9
87	Endogeno	**Villin**	64452.4	103568.1	63633.1	72251.7
88						
89						
90	Housekee	**Gapdh**	59241.4	83318.4	73832.6	69695.9
91	Housekee	**Hmbs**	597.5	881.7	569.4	910.5
92	Housekee	**Hprt1**	546.1	645.3	683.7	707.6
93						
94		**Geomean**	**2683.72**	**3619.15**	**3063.28**	**3554.32**
95		**Average**	3230.12			
96		**Norm. Factor**	=$BO$95/BO94	0.89	1.05	0.91
97						

D

98						
99	Endogeno	**Octn2**	=BO81*BO$114	13529.1	10791.3	4755.4
100	Endogeno	**Oat3**	109.5	126.0	126.7	59.6
101	Endogeno	**Cnt2**	37850.6	18954.0	43749.2	13344.7
102	Endogeno	**Sglt1**	179061.3	234644.6	52700.7	89052.1
103	Endogeno	**Oatp-3**	35.7	34.4	48.8	19.5
104	Endogeno	**Oatp-b**	262.2	302.1	280.5	505.2
105	Endogeno	**Villin**	77574.8	92435.3	67098.9	65661.3
106						
107						
108	Housekee	**Gapdh**	59241.4	83318.4	73832.6	69695.9
109	Housekee	**Hmbs**	597.5	881.7	569.4	910.5
110	Housekee	**Hprt1**	546.1	645.3	683.7	707.6
111						
112		**Geomean**	**2683.72**	**3619.15**	**3063.28**	**3554.32**
113		**Average**	3230.12			
114		**Norm. Factor**	1.20	0.89	1.05	0.91
115						

Figure 2.8 Calculation of housekeeping gene normalisation factors

Figure 2.8 shows an example of the calculation used to determine housekeeping gene normalisation factors for each sample, example shows n=4 samples whilst actual assay housekeeping gene normalisation factors were calculated across n=48 samples. **A**. Geomean of Gapdh, Hprt1 and Hmbs calculated. **B**. Average geomean value determined from all samples. **C**. Normalisation factors calculated by dividing average of all sample geomean values by respective sample geomean value. **D**. Target gene NanoString counts multiplied by sample housekeeping gene normalisation factors to correct for RNA concentration and quality

Figure 2.9:

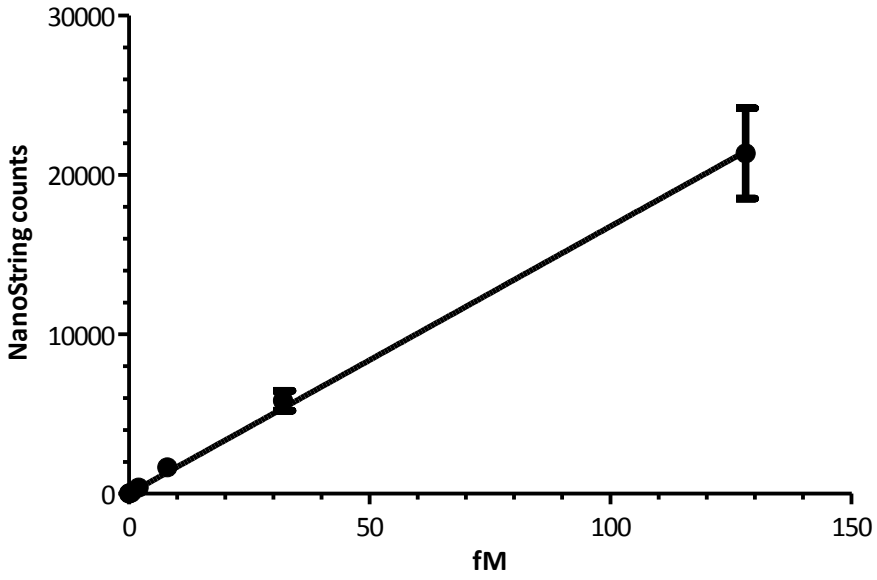

Figure 2.9 Representative standard curve produced using positive synthetic RNA spiked into a NanoString reaction.

Linear regression analysis (GraphPad Prism 5.0) was used to determine target mRNA fmol/sample concentrations from respective positive sample standard curve.

2.2.7 Western blot analysis

2.2.7.1 Protein extraction and quantification

MDCKII cell lines were cultured in 6 well plates and were seeded at a density of 60,000 cells per well. All cell lines were grown for 7 days prior to protein extraction and cell medium replaced 24 hours prior to experimentation. Following culture, cells were washed using PBS and were stored at -80°C for a minimum of 24 hours.

Protein was extracted from cell lines as follows; one cOmplete Mini protease inhibitor tablet (Roche, UK) was dissolved in 10ml of RIPA lysis buffer (Pierce, Thermo Scientific) and 0.5ml of resultant lysis solution added directly to the six well plate containing cells. Cells were shaken vigorously at 4°C for approximately 30 minutes. Cells were scraped from the plate base using a rubber policeman and transferred to an Eppendorf. Cell lysates were centrifuged at 4°C, 12,000 rpm (revolutions per minute) for 20 minutes to pellet cell debris. Supernatant was removed and the soluble cellular protein quantified using the BCA protein assay (Pierce, Thermo Scientific, UK) described previously (section 2.2.3.2).

For tissue protein extraction all samples were kept on dry ice during initial processing to prevent tissue degradation. Sigma protease inhibitor cocktail (SPIC) (0.1ml per 100ml of buffer) was added to RIPA lysis buffer and 0.5ml of the resultant solution was combined with approximately 35mg of tissue sample. Samples were homogenised using a Polytron 3100 homogeniser. Protein homogenate was centrifuged at 4°C, 13,000 rpm for 10 minutes. Supernatant was removed and cellular protein quantified using the BCA protein assay.

2.2.7.2 Immunoblotting

The NuPAGE system (Invitrogen, Life Technologies, UK) was used for immunoblotting of MDR1/Mdr1, MRP2/Mrp2 and Bcrp in both transfected cell lines and rat tissues. Following protein quantification samples were prepared for immunoblotting as follows; sample proteins (at specified concentrations) were combined with 4X NuPAGE LDS sample buffer, 10X NuPAGE sample reducing agent, and final volumes diluted to 25µl using molecular grade water. Samples were denatured at 70°C for 10 minutes and immediately placed on ice. NuPAGE Novex, 4-12% BIS TRIS 12-well gels, 1mm standard thickness, were loaded into electrophoresis tanks with NuPAGE MOPS (3-(N-morpholino-propanesulfonic acid) SDS running buffer. The inner chamber of the electrophoresis tank also contained NuPAGE antioxidant. Samples were loaded alongside protein ladders of known molecular size (Novex sharp pre-stained ladder, Invitrogen, Life Technologies, UK). Samples were separated by electrophoresis at 200V for approximately 50 minutes. Protein transfer from gel to PDVF/nitrocellulose membranes was performed using either an iBlot Gel Transfer device and iBlot Gel Transfer stacks (Invitrogen,

Life Technologies, UK) (AstraZeneca, Alderley Edge, UK) or wet protein transfer using a BioRad transfer tank and NuPAGE transfer buffer containing 10% MeOH. Those proteins transferred using the wet protein transfer method were transferred for approximately 50 minutes at 70V. Following transfer, gels were stained using Bradford reagent to confirm transfer of protein to nitrocellulose/ PDVF membranes.

Membranes were blocked using 5% milk TBS-tween 0.1% or 5% milk PBS-tween 0.1% at room temperature for approximately one hour. Primary antibodies were incubated on a roller mixer at specified dilutions in blocking solutions overnight at 4°C (table 2.2). For the immunoblotting of MDR1/Mdr1, membranes were probed with either C19 (diluted 1:50) (Santa Cruz, Biotechnology) or C219 (diluted 1:100) (Calbiochem, UK). MRP2/Mrp2 was detected using primary antibody M2-III-6 (diluted 1:100) (AbCam, UK). For the detection of mBcrp, membranes were probed with either M70 (diluted 1:100) (Santa Cruz, Biotechnology, UK) or BXP9 (diluted 1:100) (AbCam, UK). Rat Bcrp protein was detected using the M70 primary antibody at a dilution of 1:200. Membranes were washed using TBS-tween 0.1% or PBS-tween 0.1% for a minimum of 3 x 10 minutes at room temperature. Membranes were then incubated with secondary horseradish peroxidase-conjugated antibodies (HRP-conjugated) at concentrations specified in table 2.2 for one hour at room temperature. Membranes were exposed to either ECL (electrochemical luminescence) prime (GE healthcare, UK) or pico-chemiluminescence solutions (Thermo Scientific, UK) for approximately five minutes and membranes developed using X-ray film and an automatic developer. For the membrane probed with M70 and BXP9, membranes were stripped following M70 immunoblotting using membrane stripping buffer for 15 minutes (Thermo Scientific, UK) and reblocked using 5% milk PBS-Tween 0.1% for one hour at room temperature. Membranes were probed with BXP9 (diluted 1:100) overnight at 4°C on a roller mixer. Membranes were then processed as above and BXP9 primary antibody detected with anti-Rat HRP conjugate (diluted 1:3000).

Where possible, membranes were stripped using stripping buffer (Restore^{TM}, fluorescent western blot stripping buffer, Thermo Scientific, UK) for 15 minutes at room temperature, and re-blocked using 5% milk as above. Membranes were incubated with anti α-actin antibody (diluted 1:2000) (Santa Cruz Biotechnology, UK) for 3 hours at room temperature as a loading control and remaining protocol performed as above. Anti α-actin was detected using a anti-Goat HRP secondary antibody (diluted 1:3000).

2.2.7.3 mBcrp deglycosylation

Deglycosylation of protein from MDCKII-mBcrp cells was performed using the PNGase F kit (New England BioLabs). PNGase F (Peptide -N-Glycosidase F) is an amidase enzyme which cleaves high mannose, hybrid and complex N-glycans from glycoproteins. As described

previously, MDCKII-mBcrp cells were seeded at a density of 60,000 cells per well in 6-well culture plates and grown for 5-7 days. Following growth, protein was extracted (above) and immediately treated with PNGase F. Following cell lysis and protein quantification, 10µg of protein from whole cell MDCKII-mBcrp lysate (adjusted with RNase free water to total volume of 9µl) was combined with 10X Glycoprotein denaturing buffer (1µl), samples were briefly vortexed and denatured at 100°C for 10 minutes. Samples were cooled on ice for 1 minute and the following reagents added: 10X G7 reaction buffer (2µl), 10% NP40 (2µl), PNGase F (500,000 U/ml) (2µl) and final volume adjusted to 20µl using molecular grade water. Samples were incubated at 37°C for one hour, and were used immediately in immunoblotting experiments. Final sample protein content was 5µg.

Densitometric analysis of Western blot results was performed using ImageJ software. Individual lanes were selected and peak intensities determined for all bands present. Relative peak areas were then used to determine protein expression ratios between samples.

Table 2.2:

	1° Antibody		2° Antibody	
Protein	**Antibody**	**diution**	**Antibody**	**dilution**
MDR1	C19	1:50	anti-Goat HRP conjugate	1:3000
MDR1	C219	1:100	anti-Mouse HRP conjugate	1:3000
MRP2	Ab3373	1:50	anti-Mouse HRP conjugate	1:3000
mBcrp	M70	1:100	anti-Rabbit HRP conjugate	1:3000
mBcrp	BXP9	1:100	anti-Rat HRP conjugate	1:3000
α-Actin	I-19	1:2000	anti-Goat HRP conjugate	1:3000

Table 2.2 Primary and secondary antibody combinations and dilutions used for immunoblotting of MDR1/Mdr1, MRP2/Mrp2, mBcrp and α-actin.

2.2.8 Immunocytochemistry

Indirect immunocytochemistry was employed for antibody validation experiments using native and ABC transporter transfected MDCKII cell lines.

2.2.8.1 Culture and fixing of cells for immunocytochemistry

MDCKII cell lines were cultured on permeable polycarbonate membrane filters with cell growth area of 1.14 cm^2 (Transwell, Corning Co-star, 3401). All cells were seeded at a density of 500,000 per filter and were grown for 5-7 days. Cell medium was replaced 24 hours prior to fixation of cells. Following culture, permeable membrane supports were washed using PBS to remove cell medium. For immunocytochemical Bcrp detection in MDCKII native and MDCKII-mBcrp cell lines, cells were fixed using ice cold MeOH for 15 minutes. To allow the detection of MDR1 and MRP2, MDCKII native, MDCKII-MDR1 and MDCKII-MRP2 cells were fixed using 4% paraformaldehyde (PFA) (w/v) diluted in PBS. Cells were incubated on ice in 4% PFA for 10 minutes and were then washed using PBS. Cells were washed using 50mM NH_4Cl (Sigma-Aldrich, Poole, UK) to quench remaining PFA and permeabilised using 1% Triton-X-100 dissolved in PBS for approximately five minutes. All fixed cells were stored in PBS at 4°C until used for staining.

2.2.8.2 Immunocytochemical detection of MDR1, MRP2, mBcrp and Ezrin

Details of all antibodies used throughout this project are shown in table 5.1. Prior to initiation of transporter staining polycarbonate membrane filters were quartered such that four conditions were tested using each individual membrane. All cells were washed with fresh PBS solution and were subject to a primary blockade using 3% horse serum (HS) dissolved in PBS for one hour at room temperature. Primary antibodies were diluted in 3% horse serum and applied to Transwell® filters overnight at 4°C, final primary antibody dilutions are noted in table 2.3. Following primary incubation, cells were washed with PBS and were subject to a secondary blockade using either 3% donkey or 3% goat serum, dependent upon the secondary antibody used. Secondary antibodies were applied at dilutions specified in table 2.3 and incubated at room temperature for one hour. Propidium iodide (1µM) or Hoechst33342 (10µg/ml) nucleic acid stains were used to stain cell nuclei following secondary antibody incubations. Filter membranes were mounted onto glass slides using VectaShield and imaged using a Leica TCS SP2 UV confocal microscope, confocal sections were imaged at approximately 1µm thickness. Cells were viewed and imaged using either a HCX 40X Plan Apo NA 0.85 or a HCX X63 Plan Apo NA 1.32 (oil) lens. For all antibodies except C19, native MDCKII cells were used as a negative control and as such fluorescence gain settings for relevant secondary antibody detection wavelengths were adjusted such that background fluorescence

was minimal, allowing a direct comparison following transporter transfection. All gain settings were adjusted within the limits of primary omitted/secondary only controls for each antibody combination. C19 gain settings were adjusted only against primary omitted controls due to high level expression of constitutive dog Mdr1.

Table 2.3:

			Primary antibody				Secondary antibody		
	Cell line	**1° block**	**1° antibody**	**dilution**	**stock concentration**	**2° block**	**2° antibody**	**dilution**	**stock concentration**
MDR1 and Ezrin	MDCKII-MDR1	3% HS	C19	1:25	200µg/ml	3% DS	donkey anti-goat 488nm (AbCam, UK)	1:50	2mg/ml
			H276	1:50	200µg/ml		donkey anti-rabbit 566nm (SantaCruz, UK)	1:50	2mg/ml
MDR1 and Ezrin	MDCKII-MDR1	3% HS	C219	1:25	72.3µg/ml	3% DS	donkey anti-mouse 647nm (AbCam, UK)	1:50	2mg/ml
			H276	1:50	200µg/ml		donkey anti-rabbit 488nm (AbCam, UK)	1:50	2mg/ml
MRP2 and Ezrin	MDCKII-MRP2	3% HS	Ab3373	1:25	250µg/ml	3% DS	donkey anti-mouse 546nm (AbCam, UK)	1:50	2mg/ml
			H276	1:50	200µg/ml		donkey anti-rabbit 488nm (AbCam, UK)	1:50	2mg/ml
mBcrp	MDCKII-mBcrp & MDCKII-hBCRP	3% HS	M70	1:25	200µg/ml	3% DS	donkey anti-rabbit 488nm (AbCam, UK)	1:50	2mg/ml
mBcrp	MDCKII-mBcrp	3% HS	BXP-9	1:25	unknown	3%GS	goat anti-rat 488nm (SantaCruz, UK)	1:50	
mBcrp	MDCKII-mBcrp & MDCKII-hBCRP	3% HS	B-25	1:25	100µg/ml	3% DS	donkey anti-rabbit 488nm (AbCam, UK)	1:50	2mg/ml
mBcrp	MDCKII-mBcrp & MDCKII-hBCRP	3% HS	D20	1:25	200µg/ml	3% DS	donkey anti-goat 488nm (AbCam, UK)	1:50	2mg/ml
hBCRP	MDCKII-mBcrp & MDCKII-hBCRP	3% HS	MAB4146 (BXP-21)	1:25	250µg/ml	3% DS	donkey anti-mouse 647nm (AbCam, UK)	1:50	2mg/ml
hBCRP	MDCKII-hBCRP	3% HS	MAB4155 (Clone5d3)	1:25	1000µg/ml	3% DS	donkey anti-mouse 647nm (AbCam, UK)	1:50	2mg/ml
mBcrp and hBCRP	MDCKII-mBcrp & MDCKII-hBCRP	3% HS	Ab63907	1:25	1000µg/ml	3% DS	donkey anti-rabbit 488nm (AbCam, UK)	1:50	2mg/ml
mBcrp and hBCRP	MDCKII-mBcrp & MDCKII-hBCRP	3% HS	10180-1-AP	1:25	166.6µg/ml	3% DS	donkey anti-rabbit 488nm (AbCam, UK)	1:50	2mg/ml
mBcrp and hBCRP	MDCKII-mBcrp & MDCKII-hBCRP	3% HS	Ab63907	1:25	1000µg/ml	3% DS	donkey anti-rabbit 488nm (AbCam, UK)	1:50	2mg/ml
mBcrp and hBCRP	MDCKII-mBcrp & MDCKII-hBCRP	3% HS	10180-1-AP	1:25	166.6µg/ml	3% DS	donkey anti-rabbit 488nm (AbCam, UK)	1:50	2mg/ml

Table 2.3 Protocol used for immunocytochemical staining of MDR1, MRP2 and mBcrp including primary and secondary antibodies and dilutions.

2.2.9 Immunohistochemistry

2.2.9.1 Preparation of rat intestinal sections for immunohistochemistry

Following removal of rat intestine (as described in 2.2.3) and excision of relevant sections, intestine was opened along the longitudinal axis to expose the mucosal surface. Tissues were immersed in 10% neutral buffered formalin (NBF) (supplied in house by AstraZeneca) (containing 4% PFA by weight) solution to increase viscosity and allow sections to be carefully rolled using the Swiss roll technique, previously described by (Moolenbeek and Ruitenberg, 1981). The Swiss roll technique allows preparation of tissue samples such that the mucosal surface is outward facing, and when sectioned a transverse view of the entire section length is possible. Intestine segment Swiss rolls were then secured around the outer circumference using thread, to maintain the Swiss roll structure, and segments fixed in buffered formalin for 24 hours. A stained Swiss roll section is shown in figure 2.10. Following a 24 hour fixation period samples were transferred to 70% ethanol prior to paraffin embedding and storage at 4°C. From this point onwards all tissues were processed and sectioned by Jane Reeves, AstraZeneca, Alderley Edge, UK. Tissues were loaded into histology cassettes and processed using the Shadon Hypercenter XP tissue processor (Thermo Scientific) to allow hot paraffin permeation. Tissues were taken through the following steps, 70% ethanol (20 minutes), 95% ethanol (20 minutes x2), 100% ethanol (20 minutes x2), Xylene (20 minutes x2), paraffin (65°C) (30 minutes) and finally paraffin (65°C) (30 minutes with vacuum). Paraffin processed tissues were then embedded in paraffin blocks and stored at room temperature. Paraffin blocks were cooled prior to sectioning and 4μm sections cut. Sections were floated onto glass slides which were later heated at 65°C for 20 minutes allowing intestinal tissues to bond.

2.2.9.2 Human intestinal material

Human material was kindly donated by Constanze Hilgendorf, AztraZeneca, Sweden and was paraffin embedded at AstraZeneca in Sweden as described above (section 2.2.9.3). Human intestinal tissues were collected from surgical resections and their use approved by the regional Ethical Committee in Gothenburg (Sweden). Informed written consent was obtained from each donor prior to tissue collection and all patients were hospitalised at Östra Sahlgrenska, University Hospital, Sweden. Jejunal samples were obtained from patients undergoing laparoscopic Rous-en-Y gastric bypass and colonic tissues obtained from colon cancer patients.

2.2.9.3 Ventana staining platform and immunohistochemical detection

All immunohistochemical staining carried out at AstraZenenca, Alderley Edge, UK was performed using either a Ventana BenchMark XT or Ventana BenchMark Ultra fully automated

IHC/ISH slide staining system (Ventana, Roche, UK). Both staining platforms allow simultaneous processing of up to 30 slides, improving consistency of staining across multiple sections. Detailed protocols for final staining procedures are shown in appendix 9.1. In brief, the Ventana Benchmark XT and Ultra staining platforms progress through six stages to ensure high quality staining of IHC slides. Initially slides undergo baking, followed by a dewaxing stage and subsequent cell conditioning. Several Ventana supplied reagents were used to allow antigen retrieval and optimisation of primary antibody binding. Antigen retrieval protocols vary between antibodies and utilise cell conditioning treatment 1 (CC1), a tris based buffer solution, cell conditioning treatment 2 (CC2), a citric acid based solution, and protease enzymes 1, 2 and 3, either alone or in combination. CC1 and CC2, when heated, are capable of breaking covalent bonds formed by formalin. Method development steps were performed to ensure optimal antigen retrieval and primary antibody binding.

Following cell conditioning, slides are set up for staining and finally the staining stage is run. Manual primary antibody titration was performed, with primary antibodies diluted using antibody diluent (Ventana, Roche, UK). Primary antibodies were detected using species specific OmniMap HRP peroxidase conjugate reagents in combination with a ChromoMap DAB (3, 3'-Diaminobenzidine) kit, which includes DAB and H_2O_2 as peroxidase substrates. Following Ventana based IHC staining, slides were counterstained using a Shandon Varistain Gemini ES counterstaining platform (Thermo Scientific, UK). Slides were subject to a series of incubations as follows: Carazzi's Haemotoxylin (1 minute) (ClinTech LTD, UK), running water (1 minute), 95% ethanol (2 minutes), 100% ethanol (2 minutes x2), and 100% xylene (2 minutes x3). Coverslips were mounted using Shandon ClearVue Glass Coverslipper (Thermo Scientific, UK). Following processing slides were scanned electronically using a ScanScope AT slidescanner (Aperio, Vista, CA, USA) to allow easy image manipulation using Aperio ImageScope software version 11. All staining was run alongside primary negative controls, and where possible IgG purified serum negative controls. Rabbit IgG purified serum was used as a negative control for M70, a rabbit IgG polyclonal anti-Bcrp antibody and mouse IgG_{2a} purified serum was used as a negative control for M2-III-6, a mouse IgG_{2a} monoclonal anti-Mrp2 antibody.

Immunohistochemical staining carried out at Newcastle University was done using a BenchMark classic Ventana automated staining platform. Following the same principles as the BenchMark XT and BenchMark Ultra the BenchMark classic allows simultaneous, consistent staining of multiple slides. The detection system employed by the BenchMark differs slightly in that a universal ultraView DAB detection kit is used for the detection of primary antibodies raised in both mouse and rabbit. Slides were counterstained using Ventana blueing agent and haematoxylin. Following staining, slides were manually washed with detergent to remove oil

and were dehydrated. For dehydration, slides were immersed in 50% ethanol (3 minutes), 75% ethanol (3 minutes), 100% ethanol (3 minutes) and 100% Xylene (3 minutes x2). Following dehydration coverslips were manually mounted on slides using DPX mountant.

Details of antibodies used for immunohistochemical detection are shown in table 2.4 and table 5.1.

Figure 2.10:

Figure 2.10 Transverse section of a rat colon Swiss roll following DAB and Haematoxylin IHC staining.

Table 2.4:

	1° Antibody		2° Antibody	
Protein	**Antibody**	**dilution**	**Antibody**	**dilution**
MDR1	C19	1:50	anti-Goat HRP conjugate (SigmaAldrich, UK)	1:3000
MDR1	C219	1:100	anti-Mouse HRP conjugate (SigmaAldrich, UK)	1:3000
MRP2	Ab3373	1:50	anti-Mouse HRP conjugate (SigmaAldrich, UK)	1:3000
mBcrp	M70	1:100	anti-Rabbit HRP conjugate (SigmaAldrich, UK)	1:3000
mBcrp	BXP9	1:100	anti-Rat HRP conjugate (SigmaAldrich, UK)	1:3000
α-Actin	I-19	1:2000	anti-Goat HRP conjugate (SigmaAldrich, UK)	1:3000

Table 2.4 Primary antibodies and detection systems used for Ventana platform immunohistochemical staining.

2.2.10 Determination of transepithelial flux of radiolabelled MDR1 and mBcrp substrates, digoxin and ciprofloxacin

In addition to investigation of imatinib mesylate (imatinib) effects on Hoechst33342 MDR1 and mBcrp mediated transport more direct assessments of interaction between imatinib and MDR1/mBcrp were made by measurement of transepithelial transport of MDR1 substrate ^{3}H-digoxin (Cavet et al., 1996) and BCRP substrate ^{14}C-ciprofloxacin (Griffiths et al., 1993), as described previously (Wright, 2011).

2.2.10.1 Cell culture and TEER measurements for transepithelial flux experiments

MDCKII cell lines (native, MDCKII-MDR1 and MDCKII-mBcrp) were routinely cultured as described in section 2.2.1. Following passage, cells were seeded at a high density (5 x 10^5 cells per filter) onto 12-well permeable polycarbonate membranes (Corning, Transwell, 3401, 12mm diameter, 0.4µm, 1.14cm^2 growth area). MDCKII cells were cultured for 5-7 days post seeding with medium replacement 24 hours prior to experimentation. To allow efficient measurement of substrate transport formation of confluent, polarised epithelial monolayers with a functioning tight junction network is essential. We therefore determined transepithelial electrical resistance measurements (TEER) prior to experimentation using an EVOM voltohmmeter (World Precision Instruments). MDCKII cells were deemed to be sufficiently confluent upon recording TEER values of > 100Ω.cm^2.

2.2.10.2 Measurement of transepithelial potential differences (P.D.) to ensure cell monolayer confluency

Given the leaky nature of MDCKII cells, transepithelial P.D. were measured osmotically via generation of bi-ionic gradients across the cell monolayer following replacement of NaCl with choline chloride (ChCl) in the basolateral bathing medium. Paracellular diffusion of choline is restricted due to the molecular size of the molecule therefore preventing movement from the basolateral to apical chamber compartments. Conversely, Na^+ is able to diffuse from the apical bathing compartment to the basolateral chamber by both paracellular and transcellular diffusion thereby generating an electropositive P.D. Measurement of positive P.D values therefore indicates monolayer integrity due to inability of choline to diffuse from the basal to apical chamber. We found normal P.D. values to range between 30-50mV, with bi-ionic potentials greater than 25mV being considered acceptable (Carr et al., 2010) .

2.2.10.3 Experimental measurement of MDR1 and mBcrp transepithelial mediated transport

Cell monolayers were initially washed with Krebs buffer solution (section 2.1.1) warmed to 37°C and were maintained on a temperature sensitive hotplate at 37°C throughout experimentation to maintain physiological relevance. Apical to basal (A to B) and basal to

apical (B to A) flux was determined by addition of either apical (A to B) or basolateral (B to A) Krebs bathing medium with so called donor solutions comprising Krebs buffer containing either 0.1µCi/ml ^{3}H-digoxin (specific activity 20 Ci/mmol) or 0.3µCi/ml ^{14}C-ciprofloxacin (specific activity 260µCi/mmol). Following addition of donor solutions to respective compartments Krebs buffer solution was added to the acceptor chambers such that final volumes in the apical and basolateral chambers were 0.5ml and 1ml respectively. To determine if imatinib is an MDR1/mBcrp substrate/competitive inhibitor known MDR1 and mBcrp inhibitors CsA and K0143 were added to both the apical and basolateral chambers. 50µl aliquots were taken from the acceptor chamber at timed intervals over a three hour period to allow measurement of apical to basal and basal to apical substrate flux per hour.

50µl aliquots were taken from both the apical and basal chambers at timed intervals and were added to 1ml of liquid scintillation cocktail (OptiPhase ''Hisafe'' 2 Liquid Scintillation Cocktail). Samples were collected over a three hour experimental period and sample activity measured using a radioactive liquid scintillation counter (Beckman LS 5000 Liquid Scintillation System).

2.2.10.4 Calculation of apical to basal, basal to apical and net flux

Calculation of apical to basal flux ($J_{(a-b)}$), basal to apical flux ($J_{(b-a)}$) and net flux ($J_{net} = J_{(b-a)} - J_{(a-b)}$) was performed as follows:

$$J_{(a-b)} = \frac{Db \times M}{Dt \times S}$$

$$J_{(b-a)} = \frac{Da \times M}{Dt \times S}$$

$$J_{net} = J_{(b-a)} - J_{(a-b)}$$

Where Dt is the total dpm (disintegrations per minute) present in the donor compartment (apical or basal) on initiation of experiment. Da and Db are the dpm activities of apical or basolateral acceptor chambers per hour. M is the number of moles of substrate present and S is the surface area of the polycarbonate filter (1.14cm^2 for 12-well plate) (Wright, 2011).

2.2.11 *In vivo* study

Many thanks go to Peter Jones, Patricia Pimlott and Kathryn Pickup (Alderley Edge, AstraZeneca, UK) for their help and expertise in the design and implementation of this *in vivo* study.

2.2.11.1 Animals and animal sacrifice

All animals used were male Sprague Dawley rats aged approximately 8 weeks (Harlan, UK) (study start weight 310g – 379g). Animals were housed and sacrificed as detailed in section 2.2.2, except to accommodate sampling. Animal weight and individual animal health condition was reported three days prior to study initiation during the acclimatisation period and throughout the study.

2.2.11.2 Compound formulation and animal dosing

Imatinib mesylate was obtained from AstraZeneca, Alderley Edge and was of the highest purity. Imatinib was formulated to a 30mg/ml dose in PBS with a maximal administrative animal dose volume of 5ml/kg. Final administered dose levels were 150mg/kg per day. Animal weight was recorded prior to dosing and used to determine correct dosing volumes. Dose concentrations were validated using high performance liquid chromatography – mass spectrometry (HPLC-MS) against a concentration curve of known imatinib concentrations. Treated animals were dosed with 150mg/kg imatinib dissolved in PBS and control animals dosed with PBS vehicle only for 5 consecutive days.

2.2.11.3 Blood sampling and animal necropsy

Whole blood samples (0.2ml) were taken on day 1 and day 4 of dosing from the rat tail vein. Sample times were as follows, t = 0, t = 0.5, t = 1, t = 2, t = 4, t = 6, t = 12 and t = 24 where (time of dosing is represented as t = 0 hours), with final blood samples been taken prior to day 2 and day 5 of dosing respectively. Animals were sacrificed 4 hours post final dose on day 5 by isoflurane/CO_2 inhalation. Cardiac puncture was performed immediately following sacrifice and intestinal necropsy from the pyloric sphincter to the anus carried out. Excised tissues were removed and immediately placed into ice cold Liebovitz's medium + L-glutamine.

2.2.11.4 Post study tissue and blood sample processing

Following isolation, intestines were processed as described in sections 2.2.6 and 2.2.9 for RNA extraction and NanoString mRNA analysis (n = 3) and IHC analysis (n = 2). Blood samples were collected in EDTA blood tubes and centrifuged at 10,000 rpm for 2 minutes at 4°C to isolate blood plasma. Plasma samples were stored temporarily at -20°C and transferred for long term storage at -80°C until required.

2.2.11.5 High pressure liquid chromatography mass spectrometry (HPLC-MS)

To allow quantification of imatinib concentrations in rat plasma samples a standard curve of known imatinib concentrations was produced and quality controls incorporated into analysis. Quality controls were included, interspersed between samples measurements, to ensure determination of unknown drug concentrations did not deviate significantly from the standard curve throughout the entirety of the mass spectrometry analysis.

Imatinib concentrations within rat plasma samples were determined from neat samples, and also from samples diluted 1:10 and 1:100 to ensure plasma imatinib concentrations could be accurately predicted using the calibration curve. MeOH was added to precipitate proteins within samples (crashing) and an internal standard compound (dissolved in acetonitrile) added to ensure standardisation of injection volumes onto the HPLC-MS system.

HPLC-MS compound optimisation was performed for imatinib with daughter compound detection at a mass of 394.10 using positive ionisation mode with a cone voltage of 60.0V and collision energy of 25.0V. A solvent containing 10mM ammonium acetate dissolved in 95% H_2O: 5% methanol was used for the polar mobile phase with a 30µl sample injection volume and a flow of 0.750 ml/minute. The internal standard control was detected at a daughter compound molecular weight of 174.09 with a cone voltage of 40.0V and collision energy of 25.0V. Data was processed using QuanLynx software (Waters Inc.) with sample peak integration and subsequent quantification being performed using MassLynx software (Waters Inc.).

Analysis and quantification of HPLC detected compound was done using a calibration line spanning an imatinib concentration range of 50-100,000nM, with a lower limit of quantification at 50nmol/L. Quality controls included in the HPLC experimental run were acceptable. Following quantification and calculation of plasma imatinib concentrations non-compartmental analysis was performed using WinNonLin Phoenix v6.3 and area under curve (AUC) and Cmax concentrations calculated. Data analysis was performed by Dr Gary Wilkinson, iMed oncology, DMPK, AstraZeneca.

3. Drug transporter models and the isolation of villus tip and crypt populations

3.1 Introduction

During the drug development process it is estimated that approximately 5000 potential drug compounds enter pre-clinical testing for each single drug approved for therapeutic use (Kraljevic et al., 2004). Furthermore, the development of new drug discovery technologies highlights the need for high throughput, consistent screening assays for pre-clinical drug testing (Irvine et al., 1999, Kraljevic et al., 2004). Since oral drug administration is the preferred route of delivery, *in vitro* models utilising epithelial cell lines are standard protocol in early drug screening phases. Epithelial cell models are used due to their ability to imitate intestinal enterocyte barrier functions (Walter and Kissel, 1995). The most commonly used cell lines are the human colonic adenocarcinoma, Caco2, and the Madin Darby Canine Kidney, MDCK, cell lines. Both the Caco2 and MDCKII cell lines are known to possess morphological and biochemical characteristics which strongly reflect small intestinal columnar cells, including formation of confluent, polarised monolayers with tight junctional complexes and apical brush border membranes making them attractive cell models for permeability assays (Irvine et al., 1999, Volpe, 2008).

Originally isolated for cancer studies the Caco2 cell line showed characteristics consistent with both enterocytic and colonocytic cellular morphologies, however culture of the Caco2 cell line on permeable supports promotes functional differentiation, improved cellular morphology and the formation of highly functional epithelial barriers, thereby permitting determination of apparent drug permeabilities and membrane transport function (Irvine et al., 1999). With shorter culture periods than Caco2 cells, the MDCKII cell line provides an attractive alternative for early stage intestinal permeability assays. The MDCK cell line was originally cloned by Madin and Darby in 1958 (Madin and Darby N, 1958) from a seemingly normal female cocker spaniel, with two MDCK subclones being described later (Barker and Simmons, 1981). Despite low endogenous transporter expression levels, stable transfection of MDCK cells with drug transporters, including MDR1, BCRP and MRP2 make them ideal for assessing compound absorption properties. Irvine et al., (1998) showed good correlation ($R^2 = 0.79$) between P_{app} (apparent permeability) values of 55 compounds measured in Caco2 and MDCK cell lines using monolayer transport assays (Irvine et al., 1999).

Despite the ease of cell culture and high throughput screening permitted by the use of MDCK and Caco2 cell lines, both are problematic with regards to subpopulation heterogeneity resulting from spontaneous cell transformation, differences in cell culture and experimental

conditions and/or passage number between laboratories (Barker and Simmons, 1981, Volpe, 2008).

The Caco2 cell line is a heterogeneous cell line with many subclones. Numerous cell culture factors are known to directly influence Caco2 cell mosaicism, including passage number, seeding density, growth supports, medium composition and cell growth time (Volpe, 2008). For example, MDR1 expression was found to decrease with increasing cell density and in the presence of high glucose concentration medium (Volpe, 2008). Furthermore, our laboratory found a lack of BCRP RNA and protein in high passage Caco2 cells (Wright, 2011) however functional BCRP expression was apparent in low passage Caco2 cells (Wright et al., 2010). Lack of, or changes in both MDR1 and BCRP activity (amongst others) as a result of experimental pressures highlights the disadvantages and liabilities in using such a heterogeneous cell line.

Similar results have been reported regarding the MDCK cell line, with protein expression and morphology being directly dependent on passage number, cell seeding density, membrane supports and monolayer age (Volpe, 2008). Of note, are the changes in MDR1 functional activity in apparently stably transfected cell lines following an initial low seeding density (Volpe, 2008).

Varying data is presented with regards to correlation between compound P_{app} values in the two cell lines and percent human compound absorption (R^2 = 0.54 human absorption vs Caco2 and R^2 = 0.58 human absorption vs MDCK) (Irvine et al., 1999). Several compounds, displaying high percent absorption in humans (>94%) displayed only very small P_{app} values in both Caco2 and MDCK cell lines, highlighting discrepancies between drug compound transport in model systems and *in vivo* (Irvine et al., 1999). Strain differences and contradictory data suggest that the Caco2/MDCKII cell lines do not accurately reflect the *in vivo* system, however they do serve a clear purpose in the initial screening of drug compounds despite lacking the complex integrity of the intestine.

Membrane vesicle preparations, formed from cells known to express drug resistance transporters such as MDR1 and BCRP, amongst others, are a commonly used tool in pharmaceutical research (Glavinas et al., 2008). The ability to measure drug translocation or transporter activity allows high throughput study of drug transporter interactions, at a relatively low cost compared with other techniques (Hegedus et al., 2009).

Vesicular ATPase assays, which allow the measurement of inorganic phosphate formation following ATP (adenosine tri-phosphate) hydrolysis by the ATP binding domain of the transporter, allow study of compounds with a high or low passive permeability (Hegedus et al., 2009). The orientation of inside-out vesicles and membrane lamellae allows direct access of

drug compounds and ATP to their relative binding sites, which are hidden in right way-out vesicles (Hegedus et al., 2009). ATP hydrolysis and associated P_i formation, as determined spectrophotometrically following formation of colourimetric inorganic phosphate, allows direct measurement of ABC transporter activity. Although useful in the measurement of ATP turnover initiated by highly transported substrates the ATPase assay is less useful in measuring ATPase and P_i formation by slowly transported substrates (Hegedus et al., 2009). The transporter substrate interactions of poorly transported compounds must therefore be determined by their ability to reduce maximal P_i formation in competition experiments with well-known, highly transported substrates. Whilst poorly transported substrates will reduce P_i formation under these conditions it is not possible to conclude whether these compounds are indeed transporter substrates or transporter inhibitors/modulators.

Therefore, despite the lower cost of the ATPase assay, measurement of substrate translocation by vesicular transport assays is preferred (Hegedus et al., 2009). Inside out vesicles facilitate the transport of substrates into the vesicles central lumen (Glavinas et al., 2008). This accumulation can be determined using fluorescently or radioactively labelled substrates or by HPLC analysis of cold drug compounds. A major problem with vesicular transport assays arises with the measurement of highly lipophilic substrates. Since many ABC transporter substrates are able to freely diffuse across the cell membrane, once translocated, substrates often diffuse back into the extracellular medium, reducing vesicular accumulation (Hegedus et al., 2009). Accumulation measurements may therefore underestimate substrate translocation. Again, competition experiments are employed to study low permeability compounds. The inability to classify compounds as substrates, inhibitors or transporter modulators is problematic with vesicular assays, particularly with regards to drug-drug interactions.

Given their preparation from cell membranes, membrane vesicles do not accurately reflect the complex interplay between drug transporters and metabolising enzymes which occurs *in vivo*. Expression of drug transporters and metabolic enzymes (particularly CYP450s) in the enterocyte barrier is known to provide a first line barrier of defence to drug absorption through uptake, efflux and metabolism of drug compounds (Benet, 2009, Paine et al., 2006, Szakacs et al., 2008). Since many substrates show a strong overlap between transporter and CYP450 interactions, it is vital that these interactions be studied together.

Transporter knockout mice models have been genetically engineered to allow determination of drug-transporter interactions, whilst maintaining an otherwise functioning network of metabolising enzymes. These models are however extremely low throughput, require extensive hands on time periods, extremely expensive, and are seldom used even in late stage drug discovery (Glavinas et al., 2008).

The lack of complexity shown by *in vitro* models, and low throughput of knockout animals highlights a strong need for alternative drug screening assays to decipher substrate pharmacokinetic parameters. The ability to investigate drug permeability properties using functional primary intestinal tissues would be of great advantage since isolated tissues would better reflect the complex nature of the intestinal epithelium. On isolation, it is believed that primary intestinal cells express a full complement of drug transporters and metabolising enzymes (Giacomini et al., 2010). The inability to culture isolated intestinal cells however is a major barrier for their use in *in vitro* studies, since maintenance of an *in vivo* like morphology, for prolonged time periods, requires cell transformations and highly complicated growth medium and is likely to alter cell protein expression (Pageot et al., 2000).

Of interest with regards to intestinal enterocytes, three primary cultures described by Pageot et al., (2000) were proposed to provide a system complementary to epithelial cell populations of the functional intestinal unit, the crypt-villus axis. Human intestinal epithelial cells (HIEC) isolated from the ileum by thermolysin-based dissociation allowed successful culture of undifferentiated, yet proliferative, crypt like cells. These cells expressed the 350KDa crypt specific MIM-1/39 protein and lacked typical morphological characteristics associated with differentiated enterocytes and were therefore suggested to allow study of crypt cell physiology *in vitro* (Pageot et al., 2000). A second primary cell isolation method using temperature sensitive cell transformation was also proposed to allow study of the differential properties of the crypt niche. Temperature sensitive transformation of human fetal crypt cells using a SV40 T-Ag mutant was suggested to allow study of the proliferative, undifferentiated stem cell like crypt population at 32°C. When cultured at 39°C however, a loss of cellular proliferation was shown, with a switch to a differentiating phenotype, including acquisition of morphological characteristics consistent with differentiated epithelium (Pageot et al., 2000).

Use of the dissociating medium, Matrisperse™, and gentle agitation allowed isolation of complete villus epithelial sheets free from mesenchymal contamination (Perreault and Beaulieu, 1998). Interestingly, when cultured on collagen coated supports these villus sheets adhered, proliferated and formed confluent monolayers which appeared unchanged up to 5 to 6 days post plating (Perreault and Beaulieu, 1998). Morphological analysis showed presence of cell tight junctions and a well-defined brush border membrane (Perreault and Beaulieu, 1998). A degree of cryptal contamination was apparent in the cultured monolayer, highlighted by the detection of the crypt marker MIM-1/39. To our knowledge, none of these primary cell models are reported to show functional activity, particularly with regards to drug absorption and metabolism. Furthermore the low throughput nature of these models and potential for differences in isolation and culture conditions may alter cellular properties, potentially

increasing variation between preparations/laboratories and resulting in a lack of correlation with *in vivo* physiology.

Recent growth of single stem cell derived organoids and isolated crypts has been reported (Sato et al., 2009). Isolation of murine crypt cells and dissociation and culture of single Lgr5 positive crypt stem cells was shown to produce cellular organoids which are reflective of the normal gut (Sato et al., 2009). Resultant organoids showed cryptal fission when grown under strict culture conditions such that final structures possessed around 40 crypt units which all served to populate a central lumen lined by villus-like epithelia (Sato et al., 2009). E-Cadherin staining of organoids showed structures to be free from underlying mesenchymal contamination and to be lined by a single cell layer, as is observed with the enterocyte barrier *in vivo*. Production of cell lineages consistent with the crypt-villus axis was evident, with presence of Paneth cells at the base of crypts and dispersion of enterocytes, goblet cells and enteroendocrine cells within the organoid structure (Sato et al., 2009). Furthermore, positive villin localisation identified mature brush borders, with apoptotic cells shown to be shed into the central lumen, reminiscent of the self-sacrifice and shedding of intestinal epithelia (Sato et al., 2009). The functionality of these organoids has yet to be reported and growth medium proves extremely expensive due to the complexity of components required to maintain proliferation and long term culture of these structures.

The isolation of crypt units was described as early as 1969, where a combination of 5mM EDTA and intestinal distention allowed total removal of the crypts from rat intestine (Harrison and Webster, 1969), with Weiser, (1973) describing successful isolation of two distinct cell populations, villus tip and crypt in 1973. Using a combination of sodium citrate (27mM) and low EDTA concentration (1.5mM) with accompanying intestinal incubation at 37°C, Weiser, (1973) isolated epithelial cell fractions representative of a villus to crypt gradient. A decrease in activity of the brush border enzyme, alkaline phosphatase, and an increase in thymidine kinase activity were apparent from fraction 1 to fraction 9 (upper villus to crypt). Variations and improvements on the Weiser technique have since been reported to improve cellular dissociation, including mechanical intestinal vibration, increased EDTA isolation concentrations and a decrease in isolation temperature from 37°C to 4°C (Bjerknes and Cheng, 1981, Flint et al., 1991, McNicholas et al., 1994).

Bjerknes and Cheng, (1981) reported multiple methods for the isolation of structurally intact epithelial sheets, free from nonepithelial contamination, which were proposed to be viable. Interestingly, they also successfully isolated villi and crypt distinct populations following perfusion of mice with high (30mM) and low (1mM) EDTA concentrations and later mounting of intestinal tissues on glass rods with tissue vibration. Photomicrograph images showed

distinct separation of the two populations, however numerous steps were required throughout the protocol, exposing it to potential experimental variations and resultant villus fractions included broken villi (Bjerknes and Cheng, 1981). Flint et al., (1991) showed a reduction in isolation temperature from 37°C to 4°C to increase membrane integrity and cellular adhesion. Clear differences in RNA integrity were also apparent, with a lack of distinct ribosomal subunits (18 and 28S) being evident in cells isolated at 37°C, indicating cellular RNA to be of low quality when extracted at this temperature (Flint et al., 1991).

Further modifications were made to the original Weiser, (1973) technique by McNicholas et al., in 1994. Combining several previous alterations, McNicholas et al., (1994) successfully isolated duodenal epithelial cells across the crypt-villus axis, from the villus tip to the crypt. Following isolation duodenal segments were everted and threaded onto glass spirals prior to glass spiral suspension and vibration into surrounding isolation buffer containing 30mM Na_2-EDTA at 4°C. Isolation buffer was replaced such that 10 sequential fractions were isolated. Scanning electron microscopy confirmed distinct isolation of villus tips, free from underlying mesenchymal tissues, and crypt units. Supported by biochemical assessment showing decreasing alkaline phosphatase activity and increased radiolabelled thymidine incorporation by thymidine kinase from fraction 1 to 10, the method described by McNicholas et al., (1994) was deemed successful in the isolation of a gradient of epithelial cells from the villus tip to the crypt.

Given that epithelial cells of the crypt-villus axis serve as the functioning unit of the intestinal enterocyte barrier, the aim of this chapter was to isolate primary rat intestinal epithelial cells from along the crypt-villus axis in an attempt to allow immediate functional assessment of ABC transporter activity in cells expressing a full complement of physiological proteins. The protocol described by McNicholas et al., (1994) has therefore been used to successfully isolate epithelial cells reflective of the crypt-villus axis allowing segregation of distinct villus and crypt epithelia and independent study of these two cell populations.

3.2 Methods

3.2.1 Crypt-villus isolation and preparation validation

All methods used in this chapter are detailed in materials and methods section 2.2.4

3.2.2 Incubation of isolated fractions in KB medium in an attempt to restore metabolic activity

Cardiac myocytes have long been studied in isolation following their extraction from heart tissue, however exposure to extracellular calcium concentrations where Ca activity > 0.1mM, was shown to induce a phenomenon described as the calcium paradox. Isenberg and Klockner, (1982) suggest exposure to extracellular concentrations of Ca in the millimolar range not only causes hypercontraction of cardiac myocytes but also results in significant elevation of intracellular Ca activity. Although electrophysiological measurements show an apparent renormalisation of intracellular calcium concentrations it is proposed that mitochondrial Ca uptake is in fact responsible for the observed depletion of intracellular Ca. TEM images showed swelling of mitochondria present within cardiac myocytes and associated loss of mitochondrial cristae, in addition to myofilament fragmentation. Accumulation of Ca within mitochondria, and the associated loss of cristae ultimately inhibits production of ATP by oxidative phosphorylation. Restoration of calcium tolerability and an increased yield of calcium tolerant myocytes was observed following incubation of cardiac myocytes with a ''Kraftbrühe'' (KB) medium (Isenberg and Klockner, 1982).

Kraftbrühe translates from German to English as power soup. KB medium is a complex solution containing several components shown to directly increase the yield of calcium tolerant cardiac myocytes. KB medium has a composition as follows: 85mM KCl, 30mM K_2HPO_4, 5mM $MgSO_4$, 5mM Na_2ATP, 5mM pyruvic acid, 5mM β-OH-butyric acid, 5mM creatine, 20mM taurine, 20mM glucose, 50g/l polyvinypyrollidone (PVP40), 10mM EGTA and 1.95mM $CaCl_2$, pH 7.2 with KOH, aCa_o (extracellular calcium activity) 30nM. Incubation of cardiac myocytes with low Ca medium containing 5mM $MgSO_4$ and subsequent addition of 5mM Na_2-ATP was shown to increase the yield of calcium tolerant myocytes from 16 to 41% of the cells tested. Furthermore, taurine was also found to restore calcium tolerance in cardiac myocytes (Isenberg and Klockner, 1982).

Given the high frequency of mitochondria which showed swelling and breakdown in isolated villus tip and crypt fractions in early experiments, and the requirement of ATP hydrolysis for Mdr1 and Bcrp functional activity, villus tip and crypt cells were incubated in KB medium with the hypothesis that KB medium components would restore cellular metabolic activity and functional activity of ABC transporters. Following isolation and collection of fractions by

centrifugation, cells were resuspended in KB medium and incubated at 37°C for 30 minutes (unless specified otherwise). Following incubation cells were immediately assayed for metabolic viability and ability to retain Hoechst33342 as described in methods section 2.2.4.5 and 2.2.5 respectively.

3.3 Results

3.3.1 Isolation of intestinal cells across the crypt-villus axis of the rat ileum

A modified Weiser technique (Weiser, 1973) utilising EDTA based chelation with mechanical vibration was used to isolate epithelial cells of the crypt-villus axis (methods section 2.2.4). Collected fractions were imaged by phase contrast microscopy (figure 3.1) and TEM (figures 3.2 and 3.3) to assess cellular morphology and show effectiveness of the crypt-villus preparation. Similar morphology to that reported by Flint et al., (1991) and McNicholas et al., (1994) was observed. Villus tips are clearly visible by phase contrast microscopy in fractions 1 to 3 whilst epithelial sheets are present with progression to later fractions, and associated movement down the crypt-villus axis to yield crypt structures in fractions 9 and 10 (figure 3.1, black arrows). Detailed assessment of fractions by phase contrast microscopy showed appearance of crypt units from fraction 5 onwards, with (McNicholas et al., 1994) reporting similar observations in duodenal rat samples where crypt cells were visible from fraction 6 onwards. Whole villus sheets, with crypt units attached are visible in fractions 6 and 7, whilst an abundance of crypt units are evident in fractions 8, 9 and 10. Crypt units present with a characteristic tubular appearance, almost identical in morphologically to those isolated by (Flint et al., 1991).

High magnification morphological analysis using TEM was conducted following fixation and heavy metal staining of villus tip and crypt fractions, as described in section 2.2.4.1. Figure 3.2 shows TEM analysis of a combined fraction 1 and 2 sample (villus tip). Several columnar epithelial cells with a prominent brush border membrane (figure 3.2A black arrow) are shown in combination with higher magnification of microvilli (figure 3.2C). Numerous mitochondria are visible within the cell cytoplasm (figure 3.2A). Occlusion of extracellular space between neighbouring villus epithelial cells by zonula occludens (ZO) associated proteins indicates retention of functional barrier activity by villus enterocytes following chelation based isolation (figure 3.2B).

TEM micrographs taken from the crypt preparation (fractions 9 and 10 in combination) identify a single crypt unit (figure 3.3A) with multiple cells surrounding a central crypt lumen. A sparse brush border membrane, with short microvilli, is shown projecting into the crypt lumen. Intact mitochondria similar to those observed in villus enterocytes (fractions 1 and 2) are shown within the cell cytoplasm (figure 3.3B) with maintenance of tight junctions between adjacent crypt epithelial cells (figure 3.3B).

Figure 3.1:

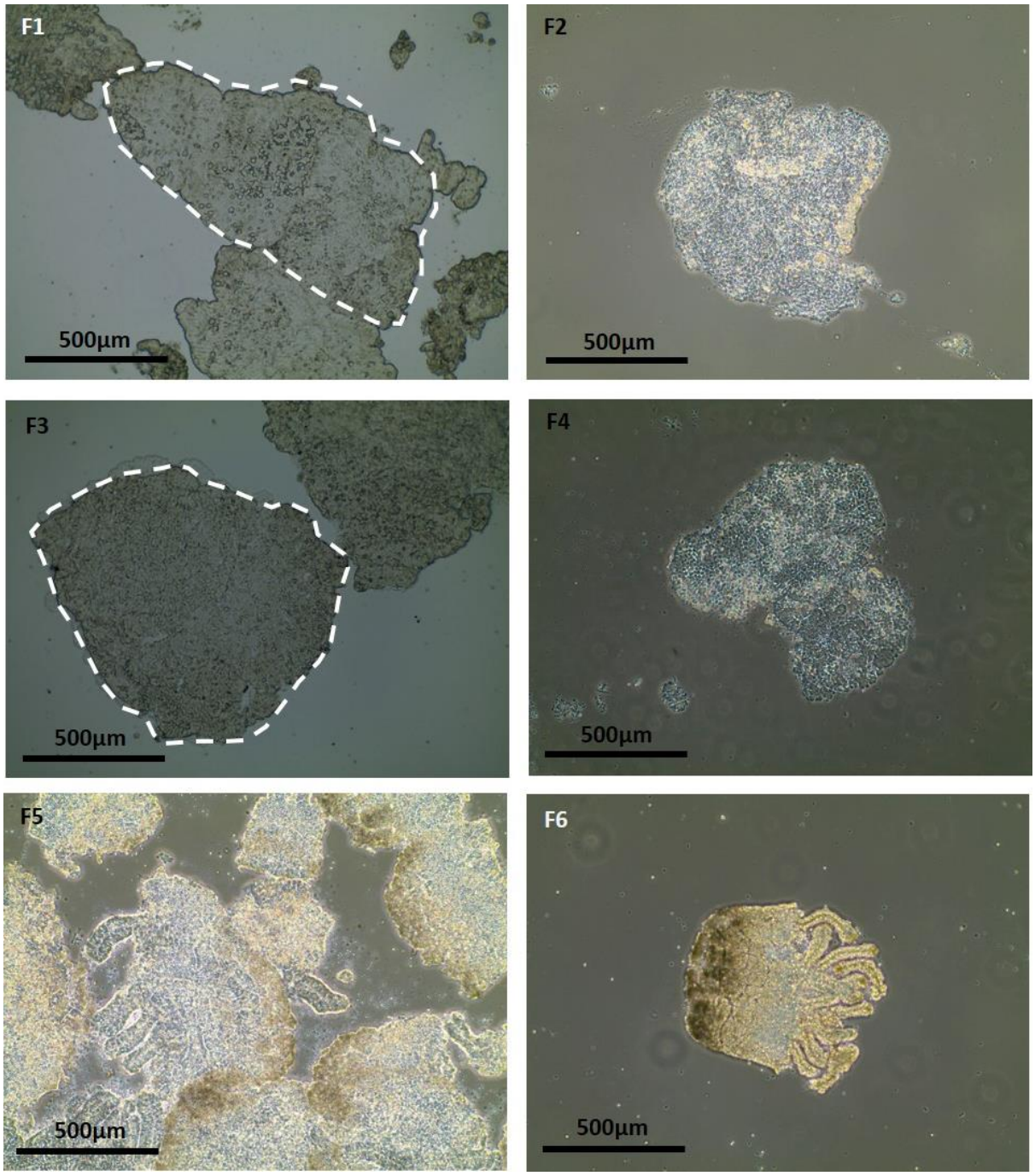

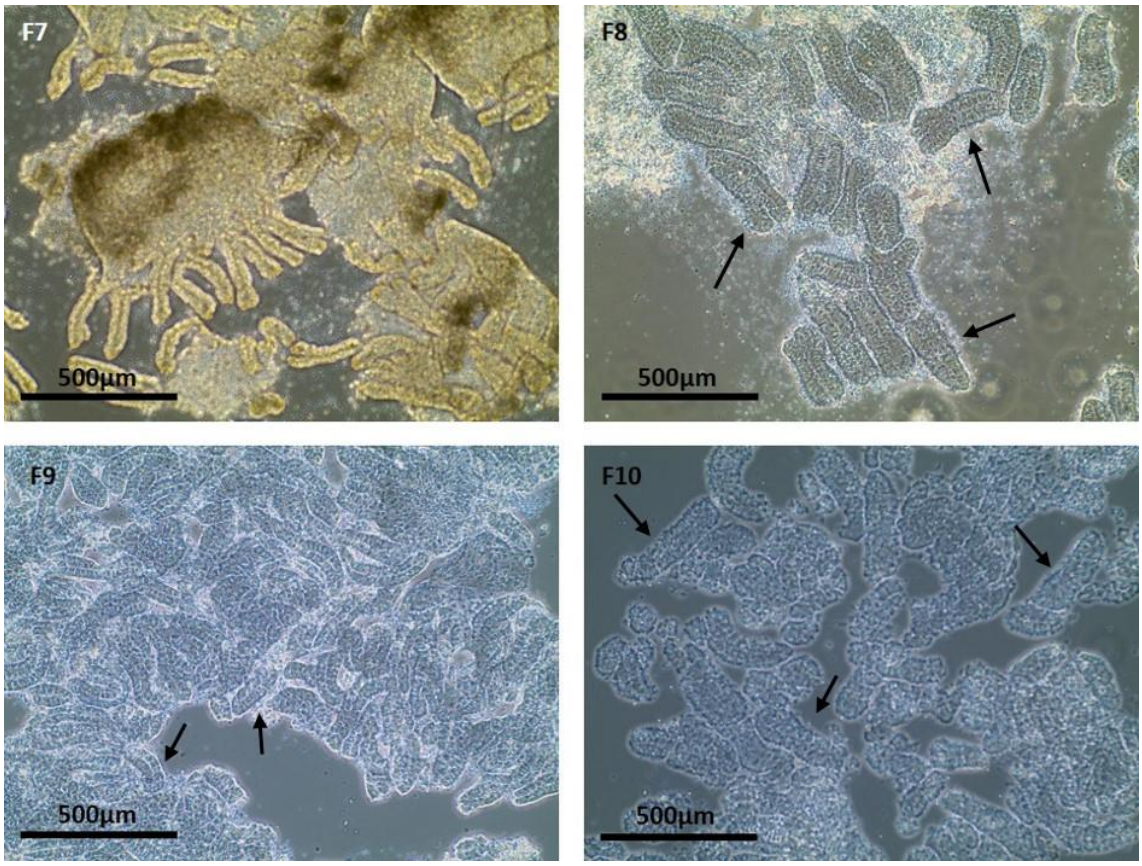

Figure 3.1 Phase-contrast photomicrographs of tissue fragments released sequentially in the crypt villus isolation procedure (fractions 1 to 10)

Samples from fractions isolated using EDTA chelation with mechanical vibration (see methods), were mounted on glass-slides with coverslips, immediately following isolation, and viewed using phase-contrast microscopy. Images shown are taken from multiple preparations and are representative of many individual experiments. Villus tips are clearly shown in fractions 1 and 3 (white dashed lines) with epithelial sheets evident in fractions 4 through 7. Crypt structures (black arrows) are clearly visible in fractions 8, 9 and 10.

Figure 3.2:

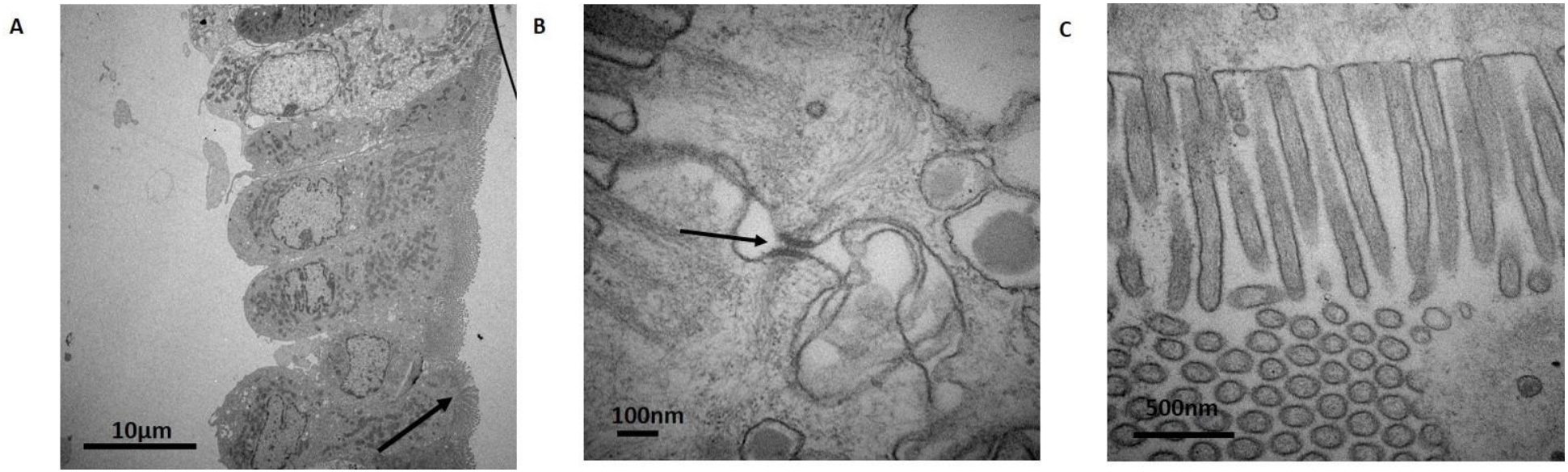

Figure 3.2 Transmission electron microscopy (TEM) images taken from villus tip fractions (F1/F2) showing detail of enterocyte morphology

Fractions 1 and 2 were combined to give villus tip preparation. **(A)** Shows isolated sheet of villus cells detached from the basal lamina with a prominent brush border membrane (black arrow) **(B)** Shows apical junctional area between two adjacent cells showing zona occludens, sub-junctional desmosome and lateral space (black arrow) **(C)** High-power image of the epithelial brush-border.

Figure 3.3:

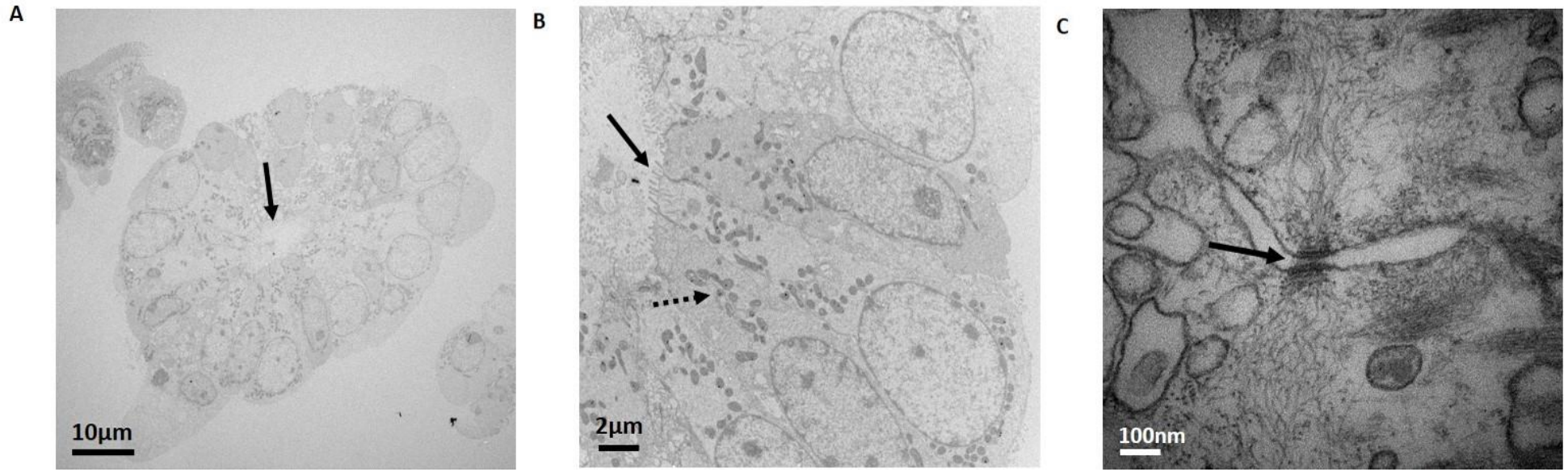

Figure 3.3 Transmission electron microscopy (TEM) images of crypt-enriched fractions (F9/F10)

(A) Traverse section across single crypt with brush border localised to the crypt lumen (black arrow). **(B)** Mid- magnification image showing sparse brush border of crypt cells in comparison to villus enterocytes (figure 3.2) (black solid arrow). Mitochondria can be seen within the cells and appear to be intact (dotted arrow). **(C)** Apical junctional area showing intact zona occludens and desmosome between two adjoining crypt cells (black arrow).

3.3.2 Biochemical assessment of villus tip and crypt cell populations

Although assay validation experiments showed substrate formation and an associated colour change for Alph with fresh intestinal mucosal scrapes and brush border membrane vesicles no measured activity was apparent in fractions isolated using EDTA based chelation (data not shown). EDTA is a chelating agent and will therefore readily sequester metal ions, including Zn^{2+} and Mg^{2+}. Replacement of Zn^{2+} chelated by EDTA in isolated fractions was found to restore Alph activity. Lap activity was not affected by either EDTA or $ZnCl_2$ and was therefore measured following suspension of isolated fractions in Krebs buffer containing 2mM $ZnCl_2$.

Biochemical assessment of enzyme markers Alph and Lap in isolated fractions, following re-suspension of material in Krebs buffer solution containing 2mM $ZnCl_2$, was performed to substantiate the effective isolation of two distinct populations, villus tip and crypt. We observed highest levels of product formation, p-nitrophenol and p-nitroaniline for Alph and Lap respectively, in fraction 2 (1.90 ± 0.26 and 10.67 ± 1.60 µmol. min^{-1}. µg $protein^{-1}$ respectively, mean ± SEM, n=9 wells), with similar activities being measured in fractions 1 and 3. Both enzymes display a similar trend of activity across fractions, however measured absorbance levels were greater for Lap than for Alph (results not shown). Combination of fractions showed increased enzyme activity in villus tip preparations for both Alph and Lap compared with respective cryptal activity. Formation of p-nitrophenol in villus tip and crypt samples was 1.49 ± 0.20 and 0.64 ± 0.06 µmol. min^{-1}. µg $protein^{-1}$ respectively (n=9 replicates ± SEM) (figure 3.4A). Higher levels of Lap activity are suggested in villus tip preparations due to increased concentration of the Lap product p-nitroaniline, with calculated concentrations of 9.24 ± 1.10 and 4.18 ± 0.32 µM. min^{-1}. µg $protein^{-1}$ (n=18 replicates ± SEM) in villus tip and crypt samples respectively (figure 3.4B). The difference in enzyme activity between villus tip and crypt preparations was found to be significant using Student's t-test with Welche's correction, ** p = 0.0018 for Alph and *** p = 0.0008 for Lap. For Alph and Lap, 31.2% & 34.7% and 15.8% & 14.3% of total enzyme activity was measured in villus tip and crypt preparations respectively.

Figure 3.4:

A

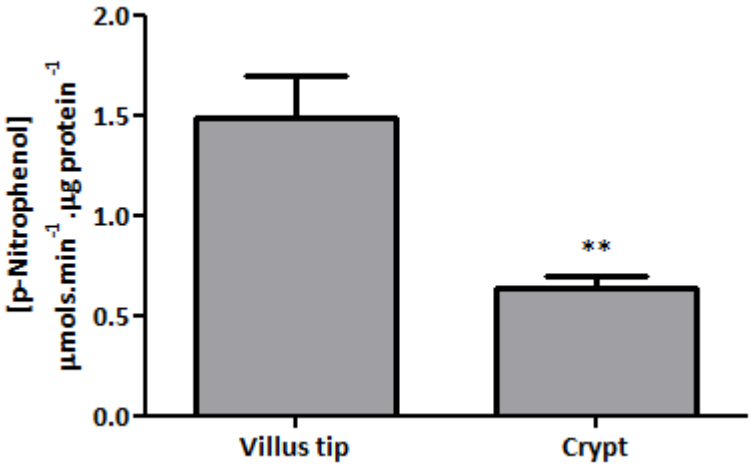

B

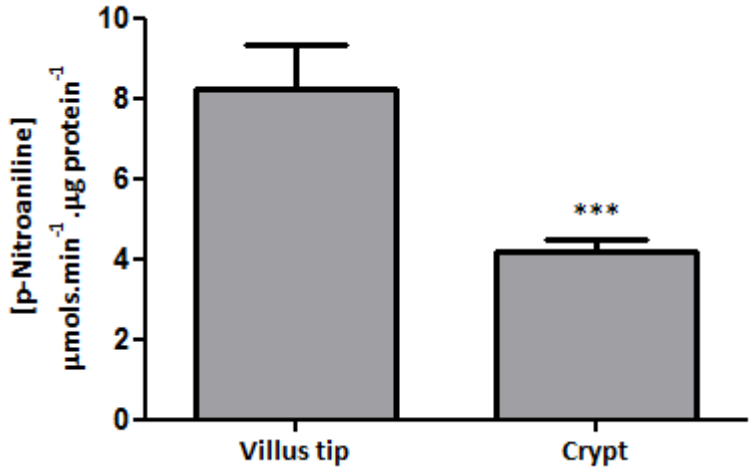

Figure 3.4 Measurement of [p-nitrophenol] and [p-nitroaniline] formation by alkaline phosphatase and leucine amino peptidase in villus tip and crypt fractions

Results show mean **(A)** [p-nitrophenol] and **(B)** [p-nitroaniline] substrate formation per minute per µg protein following a 10 minute incubation period with respective enzyme substrates from a total of n=9 replicates taken from N = 3 independent crypt-villus preparations ± SEM. Note measurement of greater p-nitroaniline formation by Lap compared with p-nitrophenol formation by Alph. ** $p > 0.01$ *** $p > 0.001$ villus tip vs. crypt, unpaired, Student's t-test.

3.3.3 Functional assessment of MDR1 and mBcrp activity in MDCKII cell lines and of Mdr1 and Bcrp in isolated rat villus tip and crypt samples

To allow the assessment of functional Mdr1 and Bcrp transporter activity in villus tip and crypt fractions the Hoechst33342 dye retention assay was employed. As described in methods section 2.2.5 Hoechst33342 is a lipophilic dye which is subject to MDR1 and BCRP mediated efflux from within the lipid bilayer (Scharenberg et al., 2002, Shapiro et al., 1997). The lipophilic nature of Hoechst33342 allows diffusion of the dye into the lipid bilayer, upon which an intense increase in Hoechst33342 dependent fluorescence is observed. Functionally active ABC transporters, MDR1 and BCRP, transport Hoechst33342 from within the lipid bilayer to the extracellular milieu with an associated decrease in fluorescence. As such, cellular Hoechst33342 fluorescence is directly related to functional ABC transporter activity, with inhibition of transporters leading to a rise in cellular dye retention. In addition to increased fluorescence associated with movement of Hoechst33342 into the lipid bilayer, diffusion of the dye across the lipid membrane and subsequent intercalation with cellular DNA also increases measured fluorescence.

Cultured MDCKII cell lines +/- stable transfection of MDR1 and mBcrp were used to confirm Hoechst33342 to be a substrate of MDR1 and mBcrp prior to the assessment of transporter activity in isolated villus tip and crypt preparations and to illustrate the behaviour of viable epithelial cells in this assay. Transfection of MDCKII cells with either MDR1 or mBcrp ABC transporters is expected to lower control fluorescence, due to increased efflux of Hoechst33342 from within the lipid bilayer compared with that of native (non-transfected) MDCKII counterparts. A decrease in fluorescence (Ex. 361nm, Em. 486nm) from 599.4 ± 56.3 to 313.8 ± 26.8 arbitrary units (mean n=18 wells ± SEM) was observed between native MDCKII cells and MDCKII-MDR1 transfected cell lines in the absence of CsA transporter inhibition under control conditions (figure 3.5). Incubation of MDCKII-mBcrp cells with Hoechst33342 in the absence of K0143 decreased measured fluorescence to 60.9 ± 9.8 from 267.8 ± 30.0 (mean n=18 wells ± SEM) compared with native MDCKII cells (figure 3.6). The observed decrease in fluorescence resulting from MDCKII transfection is consistent with Hoechst33342 acting as a substrate for both MDR1 and mBcrp, as reported previously (Kim et al., 2002, Müller et al., 2007).

To ascertain functional cellular activity of MDR1 and mBcrp the effect of pharmacological inhibitors, CsA and K0143, on cellular Hoechst33342 retention was determined. CsA and K0143 are known to selectively inhibit MDR1 and mBcrp respectively at transporter specific concentrations (Ejendal and Hrycyna, 2005, Matsson et al., 2009). Therefore, in the presence of CsA and K0143 Hoechst33342 efflux from the cell will be reduced and an increased

fluorescence measured. Measured cellular fluorescence was shown to increase in the presence of higher CsA and K0143 concentrations. A significant increase in fluorescence above that measured in the absence of transporter inhibition (control) was evident following incubation of transfected cell lines with CsA and K0143 respectively (figure 3.5 and 3.6). Whilst CsA showed no significant effect on cellular Hoechst33342 retention in native MDCKII cells below 30μM, a 2-fold increase ($p < 0.001$) was observed with 1μM CsA in MDCKII-MDR1 transfected cells, presented as a rise in cellular fluorescence from 313.8 ± 26.8 to 640.1 ± 50.4 arbitrary units (mean n=18 wells ± SEM). Given the inability of lower CsA concentrations to increase retention of Hoechst33342 above the level of control in native MDCKII cells it is suggested that 30μM CsA may evoke a cytotoxic effect on normal cell membrane integrity, leading to increased binding of Hoechst33342 to both the cell membrane and DNA.

K0143 was shown to dramatically increase Hoechst33342 retention at concentrations as low as 0.1μM in mBcrp transfected cells, which gave a 6.2-fold increase above control fluorescence. Control fluorescence was measured to be 60.9 ± 9.8 and fluorescence measured in the presence of 0.1μM K0143 was 377.7 ± 69.2 arbitrary units (mean n=18 wells ± SEM). Conversely, a significant increase in fluorescence was only observed at concentrations >5μM in native MDCKII cells (figure 3.6).

Following preliminary experiments using the MDCKII cell lines, isolated villus tip (F1/F2) and crypt (F9/F10) preparations were incubated in the absence and presence of 1μM CsA and/or K0143 (figure 3.7). As detailed in methods section 2.2.5.3 no pre-incubation of isolated fractions with inhibitors was performed to reduce assay times and help attempt to maintain viability. No significant difference between control fluorescence and fluorescence measured in the presence of transporter inhibition was observed either alone or in combination (two-way analysis of variance (ANOVA) with Bonferroni post-tests) (figure 3.7). The inability of CsA and K0143 to cause a rise in measured fluorescence is indicative of an absence of functional Mdr1 and Bcrp transporter activity within isolated villus tip and crypt fractions. The apparent lack in transporter activity may be attributable to a lack of cell viability following isolation, a hypothesis supported by the loss of Alph activity as a result of EDTA chelation and mitochondrial breakdown, experiments were therefore performed to determine viability of isolated fractions.

Figure 3.5:

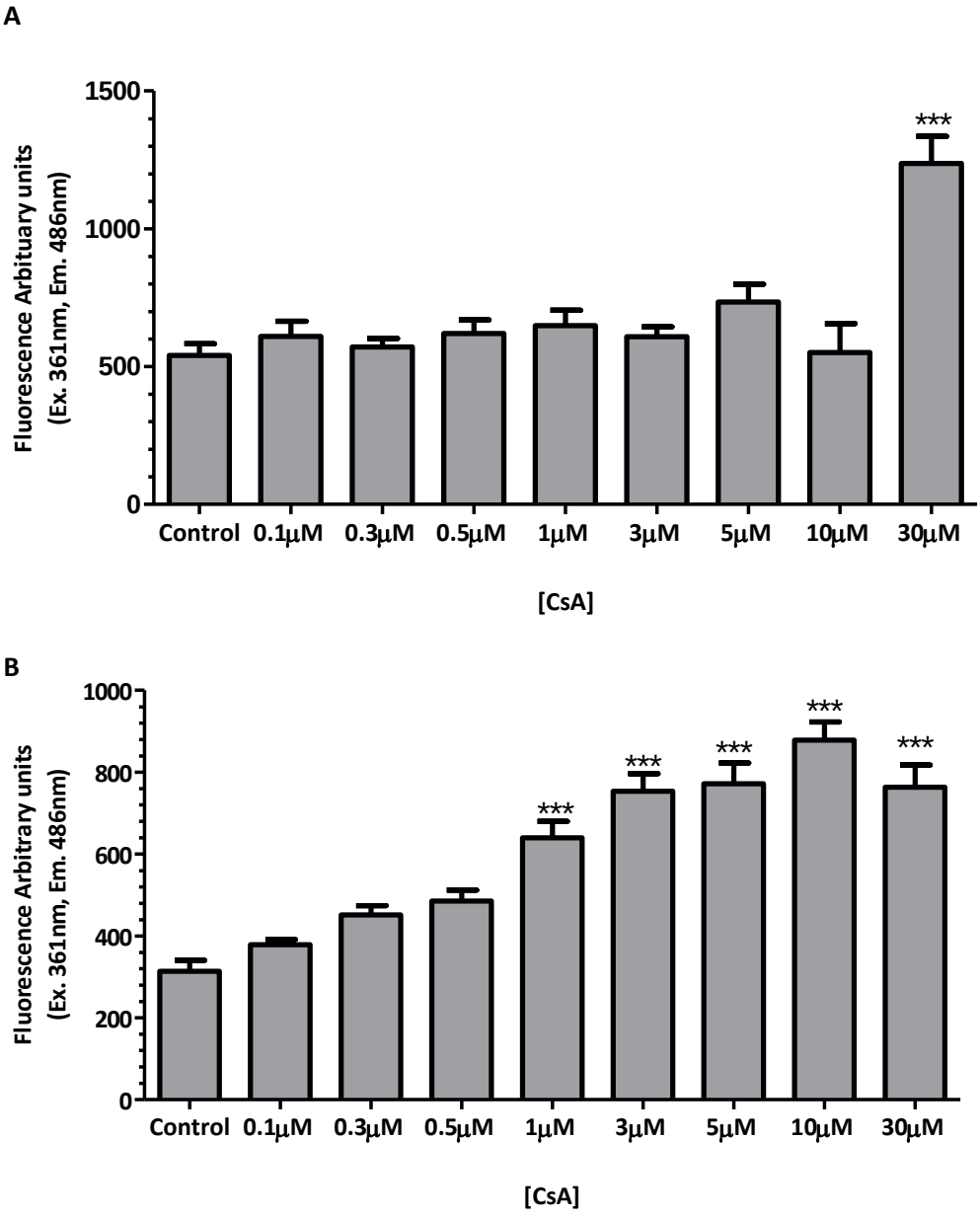

Figure 3.5 Concentration dependent effect of CsA on intracellular Hoechst33342 dye retention in native MDCKII and MDCKII-MDR1.

Hoechst33342 retention was measured in a fluorescence-dependent manner in **(A)** native MDCKII and, **(B)** MDCKII-MDR1 cell lines following incubation with CsA at specified concentrations. Hoechst33342 was used at a concentration of 3μM. Cells were excited at 361nm and emitted fluorescence at 486nm measured. Cells were grown on 96 well plates for 5-7 days, data shown represent mean n=18 wells from three independent experiments ± SEM. *** $p < 0.001$, one-way ANOVA with Bonferroni post-tests vs. control.

Figure 3.6:

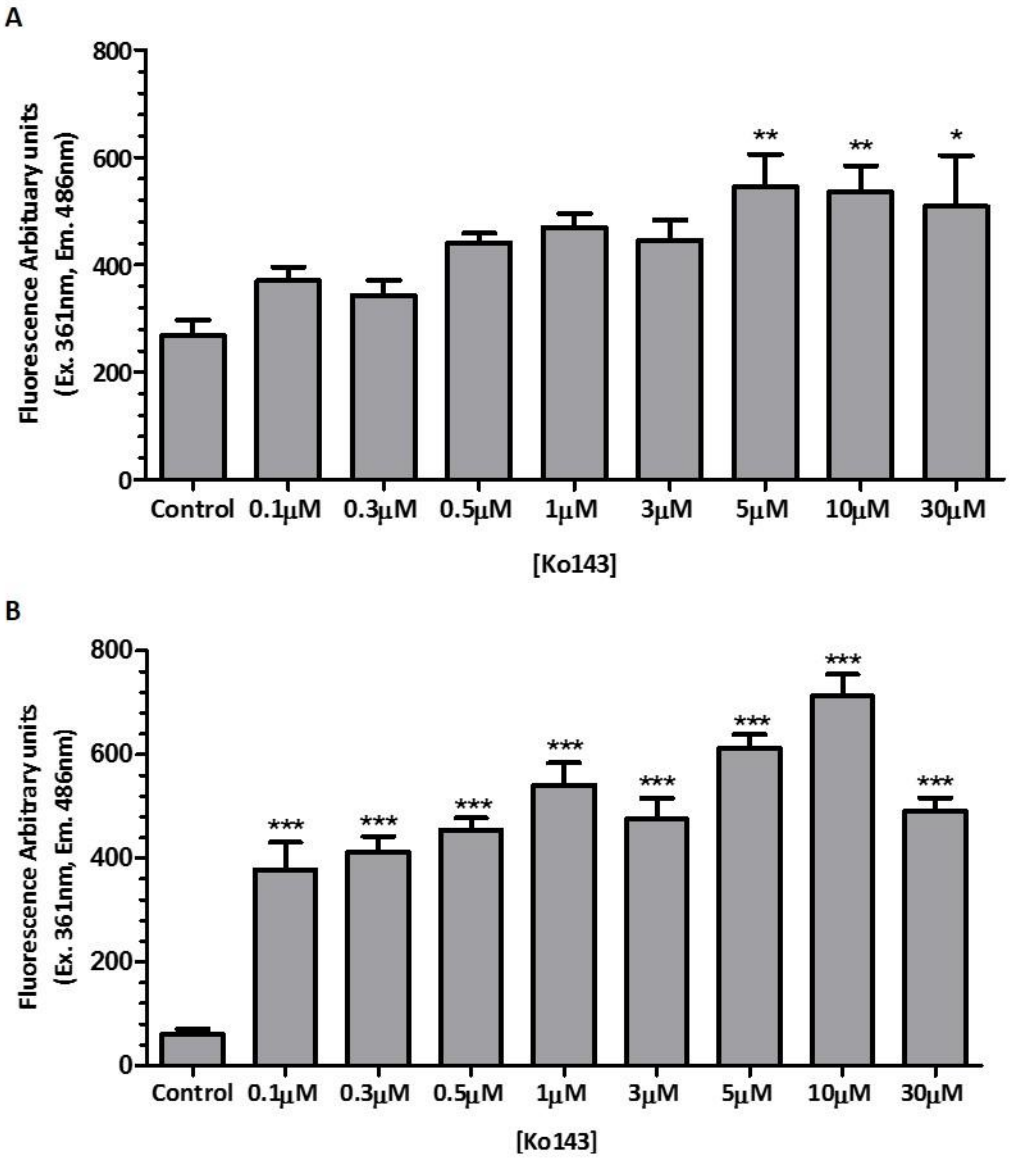

Figure 3.6 Concentration dependent effect of K0143 on intracellular Hoechst33342 dye retention in native MDCKII and MDCKII-mBcrp cells.

Hoechst33342 retention was measured in a fluorescence dependent manner in **(A)** native MDCKII and **(B)** MDCKII-mBcrp cell lines following incubation with increasing concentration of K0143. Hoechst33342 was used at a concentration of 3µM. Cells were excited at 361nm and emitted fluorescence at 486nm measured. Cells were grown on 96 well plates for 5-7 days, data shown represent mean minimum n=12 wells from three independent experiments ± SEM. *$p < 0.05$, ** $p< 0.01$, *** $p < 0.001$ one-way ANOVA with Bonferroni post-tests vs. control.

Figure 3.7:

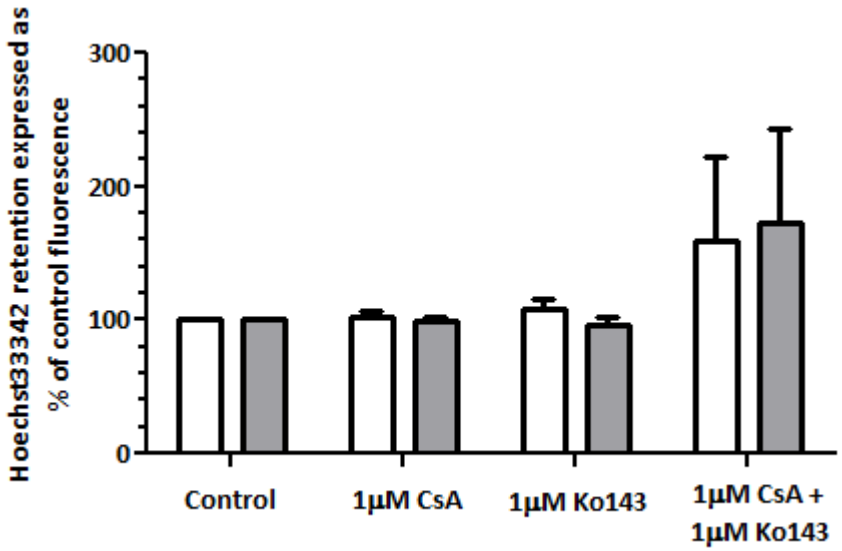

Figure 3.7 Intracellular Hoechst33342 dye retention in villus tip and crypt samples immediately following isolation in Krebs buffer.

Hoechst33342 retention was measured in a fluorescence dependent manner in villus tip (clear bars) and crypt (shaded bars) samples in the presence and absence of specific Mdr1 and Bcrp inhibitors CsA and K0143 alone or in combination. Hoechst33342 was used at a concentration of 3µM. Cells were excited at 381nm and emitted fluorescence at 485nm measured. Cells were incubated at 37°C in Krebs buffer solution, data shown represent mean n=9 replicates from three rat intestines ± SEM and have been normalised for control fluorescence (measured in absence of transporter inhibition). No significant difference is apparent between conditions.

3.3.4 Assessment of crypt-villus cell viability; TEM, Na^+/K^+ ratios, live-DEAD cell analysis and the MTS viability assay of crypt-villus preparations

Despite TEM micrographs in figures 3.2 and 3.3 suggesting isolated cells to be viable, further analysis of cells present within samples taken from the same villus tip and crypt populations suggested otherwise. Figure 3.8, shows the same villus tip preparation as displayed in figure 3.2, with all images being taken at the same time, however a loss of the classic columnar cell shape is apparent here accompanied by extensive formation of cytoplasmic vacuoles toward the cell base. Sub-apical vacuolation is also apparent beneath the brush border membrane (figure 3.8C). Whilst the brush border membrane remains intact, mitochondrial organelles appear ruptured and cells lack a well maintained structure, contrasting with those shown in figure 3.2. Taken together, lack of a distinct cell structure, extensive breakdown, and rupture of mitochondrial membranes further indicate a loss of cellular viability within villus tip fractions. These differences suggest intra-preparation variability with regards to cell function.

Although not as detrimental as the loss of cell structure observed in the villus tip sample, cryptal morphology shown in figure 3.9 shows disruption to the already sparse brush border membrane and similar mitochondrial breakdown, with an increased organelle size resulting from mitochondrial swelling. A loss of lateral cell adhesion and structural organisation (figure 3.9B, long black arrow) indicates breakdown of tight junctions, with widening of the lateral space between adjacent cells (short black arrow, figure 3.9B). Bulging of the basal cytoplasm (figure 3.9C) is shown to contribute to the loss of normal cell structure discussed above. Similar to that observed in villus tip cells, cytoplasmic vacuolation is shown; however vacuoles appear to show a narrower diameter and are fewer in number than was observed in villus tip preparations (figure 3.9B, dotted arrow).

An alternative test of viability of the isolated cells was made using the Live-DEAD cell assay, figure 3.10 and figure 3.11. Isolated cells were incubated with nucleic acid stains DEAD Red and SYTO10 green as described in methods section 2.2.4.3. DEAD Red only stains nucleic acids contained within compromised cell membranes, whilst the highly permeant SYTO10 is able to stain nucleic acids of those cells with membranes which are not compromised. As can be seen from figure 3.10 there is a prominent DEAD Red staining of villus tips in all three experimental conditions, immediately following extraction and either 30 or 60 minutes incubation at 37 °C with Krebs buffer solution. With regards to cryptal cell populations, strong green SYTO10 fluorescence staining is apparent immediately following isolation, with a decreasing intensity being apparent with extended incubation times (figure 3.11). Assessment of pixel intensities for SYTO10 green (live) and DEAD Red (dead) fluorescence and calculation of mean live: dead (SYTO10:DEAD Red fluorescence) ratios for each incubation condition showed a decreased cell

viability of both villus tip and crypt populations following extended incubation for 30 and 60 minutes in Krebs buffer solution compared with immediate cell mortality analysis (figure 3.12). Decreased cell viability is represented as a decreased SYTO10: DEAD Red pixel intensity ratio due to increased intensity of measured fluorescence following excitation of DEAD Red at wavelength 540-552nm and/or decreased fluorescence following excitation of the SYTO10 dye using wavelength 450 – 490nm. Under all conditions mean pixel intensity values were higher for crypt populations than villus tips (figure 3.12), with a significant difference shown following incubation for both 30 and 60 minutes. Pixel intensity data is supported by fluorescence images showing an increased DEAD Red staining (red fluorescence) and a decreased SYTO 10 intensity with increasing incubation time in both villus tip and crypt preparations (figure 3.10 and 3.11).

A sensitive measure of loss of cell viability is the trans-plasma membrane ion gradients maintained by the activity of the Na-K ATPase. In normal cells the intracellular K concentration is in the order of 120-150mM with Na present at 5-20mM, giving a normal physiological ratio of K/Na ranging from six to thirty (Simmons, 1981). Loss of membrane integrity or a decrease in cellular ATP will reverse the normal cellular gradient to one where the intracellular Na concentration is greater than that of K. We therefore determined intracellular Na/K concentrations using flame photometry and calculated ionic ratios following incubation of mid-villus fractions (fractions 3-8 inclusive) in either Krebs or KB medium at 4°C and 37°C for 60 minutes. Fractions were resuspended in KB medium in an attempt to improve cellular viability and restore metabolic activity, as shown in cardiac myocytes (Isenberg and Klockner, 1982). For fragments incubated in Krebs at 37°C the Na content exceeded K (392 nmol/mg versus and 200nmol/mg respectively, giving a K/Na ratio 0.51) and at 4°C the ratio was 0.32. Reversal of the intracellular balance of Na and K indicates a loss of membrane integrity or inability of Na-K ATPase to maintain a physiological membrane gradient, likely due to depletion of intracellular ATP. In KB medium at 37°C the K/Na ratio was 5.4 whereas at 4°C it was 1.1. Incubation of villus fragments in KB medium for 120 minutes at 37°C decreased the K/Na ratio to 2.5. Cells incubated in Krebs medium therefore showed limited viability, with K/Na ratios lying below the normal range, with KB medium allowing partial but not prolonged recovery.

Metabolic cellular viability was determined using the MTS cell viability assay. As described in methods section 2.2.4.5 the MTS cell viability assay is dependent upon reduction of the MTS compound to allow formation of the insoluble, coloured precipitate formazan. Formazan formation was measured spectrophotometrically at 490nm. The MTS cell viability assay showed only low level formation of formazan in both villus and crypt cells with no significant difference observed between the two populations (figure 3.13A). A change in measured

absorption at 490nm of only 0.43 ± 0.14 and 0.46 ± 0.12 per µg of protein per minute in villus tip and crypt preparations respectively was observed following incubation with Krebs buffer solution, suggesting a lack of cell viability. Absorbance readings taken following 90 minutes incubation with MTS reagent for viable HK-2 cells and villus tip and crypt populations were 1.72, 0.72 and 0.53 arbitrary units respectively following the deduction of absorbance readings at time = 0 to allow comparison between villus and crypt samples and the HK-2 cell line (HK-2 cells data courtesy of Git Chung, Newcastle University, UK), reflecting a substantial loss of viability in isolated fractions.

Re-suspension of fractions and subsequent incubation in KB medium for 30 minutes at 37°C did not significantly increase MTS cell viability measurements in villus tip or crypt preparations compared with Krebs buffer. A significant difference is however shown between villus tip and crypt viability suggesting isolated crypt units to be of increased integrity (figure 3.13). Pre-incubation of isolated villus tips and crypt samples in KB medium failed to increase Hoechst33342 dye retention in the presence of transporter inhibition (figure 3.14) with both 1µM CsA and 1µM K0143 alone and in combination. These results indicate that incubation of isolated fractions in KB medium is unable to restore cell viability.

Figure 3.8:

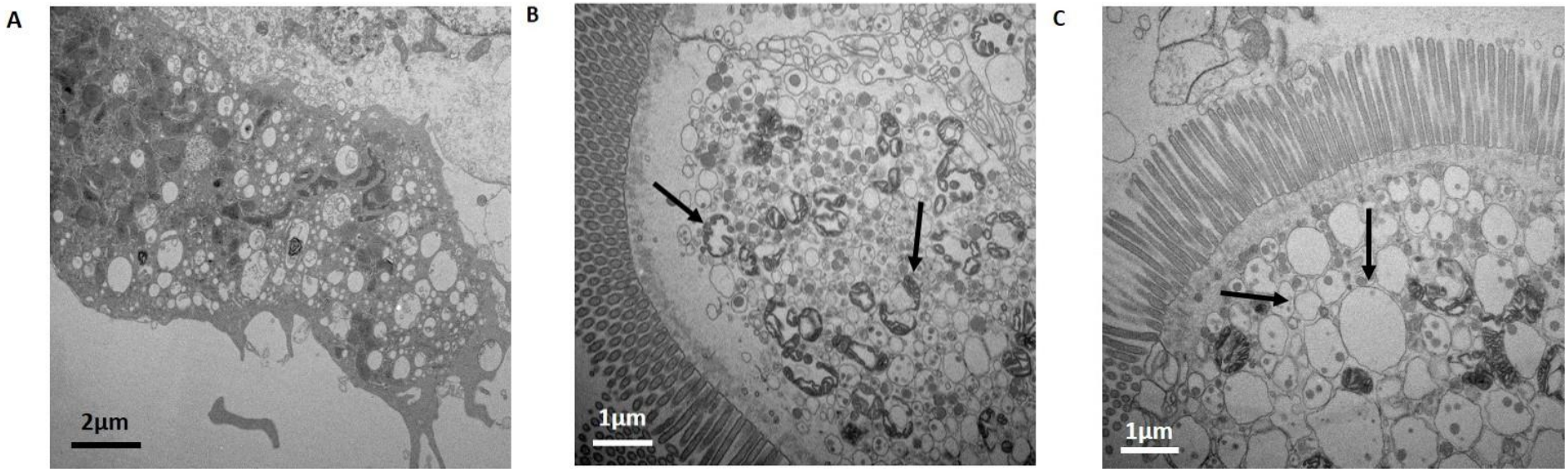

Figure 3.8 Evidence of disruption of enterocyte cyto-architechture in transmission electron microscopy (TEM) images taken from villus tip (F1/F2) preparations.

Fractions 1 and 2 were combined to give villus tip preparation. **(A)** Shows highly vacuolated cytoplasm at base of enterocyte with accompanying breakdown of villus epithelial cell membrane. **(B)** Extensive rupture and breakdown of cellular mitochondria (black arrows) and **(C)** excessive sub-apical intracellular vacuolation (black arrows).

Figure 3.9:

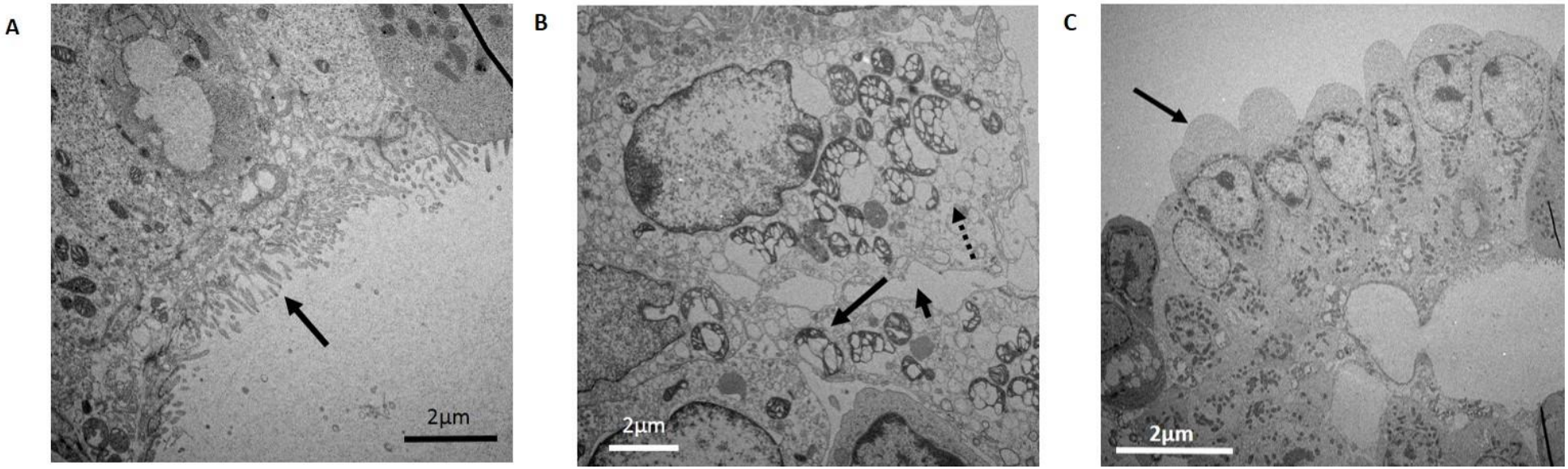

Figure 3.9 Transmission electron microscopy (TEM) images of crypt cells showing limited disruption of mitochondria and cyto-architechture

(A) Limited disruption of the brush border membrane of cryptal epithelial cells is evident (arrow) with **(B)** mitochondrial swelling and breakdown of mitochondrial cristae (long black arrow) and cytoplasmic vacuolation (dotted arrow), loss of lateral membrane cell adhesions is also shown (short black arrow). (**C)** Bulging of basal cytoplasm (arrow).

Figure 3.10:

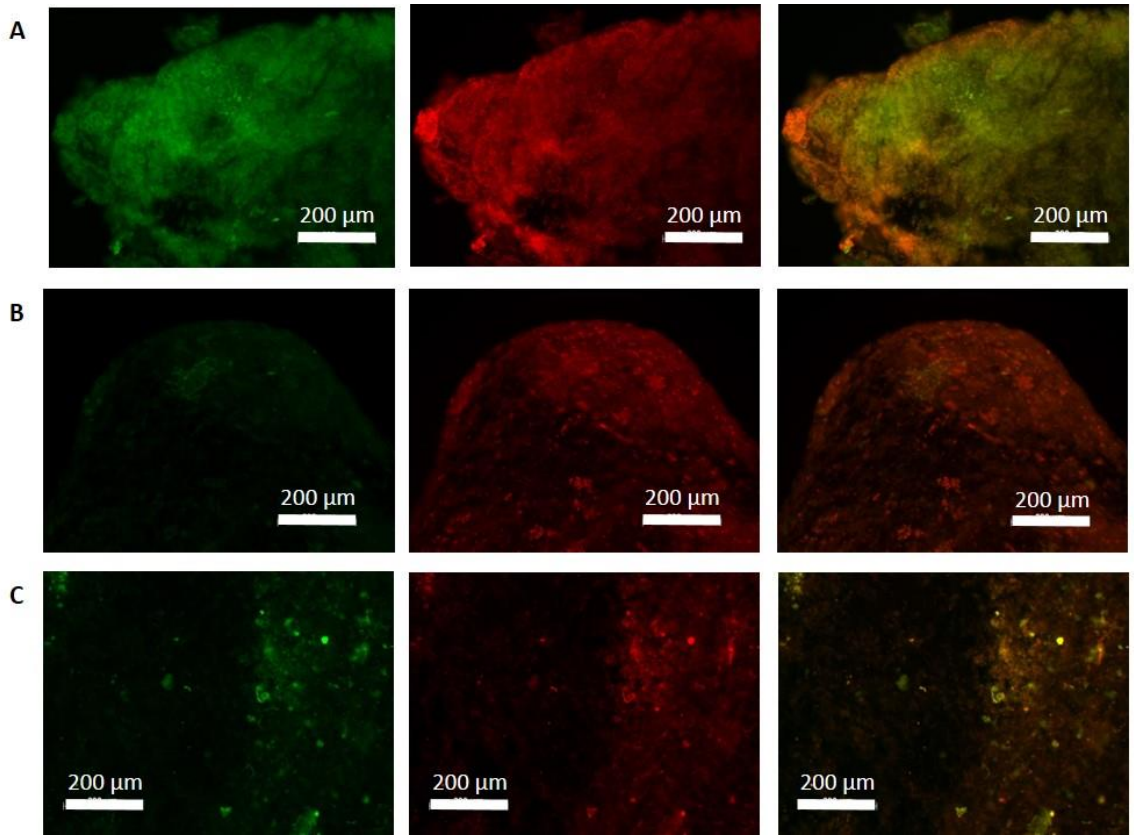

Figure 3.10 Live-DEAD cell assay using SYTO 10 green fluorescent stain and DEAD Red stain to assess cell viability with regards to live and dead cells in villus tip preparations.

Image shows SYTO 10 green fluorescent nucleic acid stain (left), DEAD Red (ethidium homodimer-2) nucleic acid stain (centre) and merged image (right). Fractions 1 and 2 were combined to give a villus tip enriched preparation. **(A)** Cell viability immediately following extraction. Note exclusion of DEAD Red at centre of villus tip. **(B)** Cell viability following 30 minute incubation in Krebs buffer at 37˚C. **(C)** Cell viability following 60 minute incubation in Krebs buffer at 37˚C.

Figure 3.11:

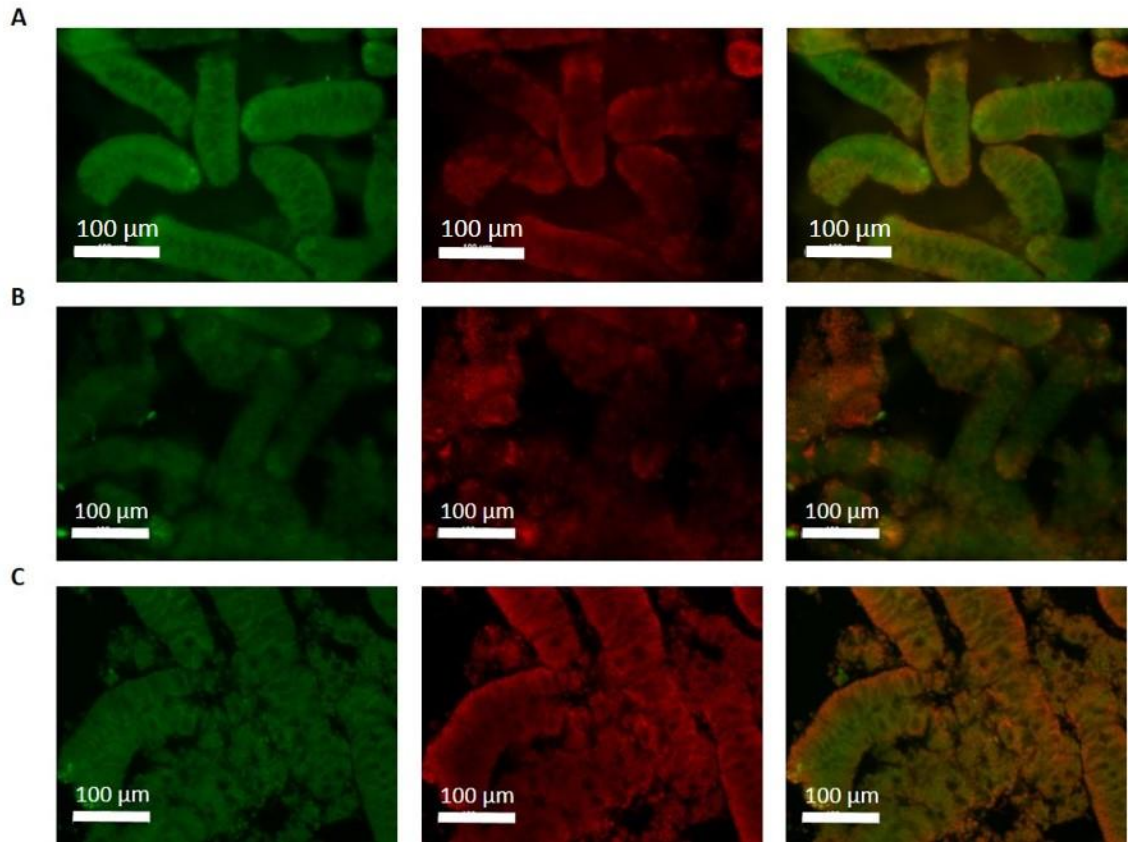

Figure 3.11 Live-DEAD cell assay using SYTO 10 green fluorescent stain and DEAD Red stain to show cell viability with regards to live and dead cells in crypt preparations.

Image shows SYTO 10 green fluorescent nucleic acid stain (left), DEAD Red (ethidium homodimer-2) nucleic acid stain (centre) and merged image (right). Fractions 9 and 10 were combined to give a crypt enriched preparation. **(A)** Cell viability immediately following extraction. Note prominence of SYTO10 green and exclusion of DEAD red. **(B)** Cell viability following 30 minute incubation in Krebs buffer at 37˚C. **(C)** Cell viability following 60 minute incubation in Krebs buffer at 37˚C.

Figure 3.12:

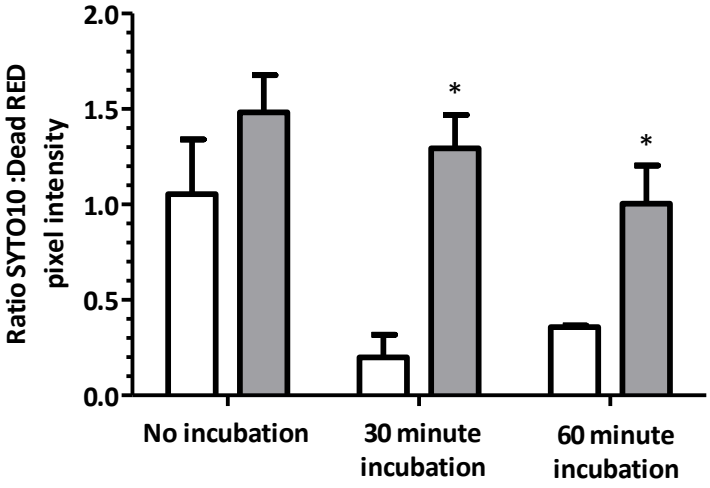

Figure 3.12 ratio of mean pixel intensity following staining of villus tip and crypt samples with SYTO10 and DEAD Red nuclear stains.

Cell mortality was assessed using the live-DEAD cell assay with villus tip (open bars) and crypt (shaded bars) fractions immediately following isolation and following 30 and 60 minute incubation periods in Krebs buffer solutions at 37°C. Data shown mean pixel intensity of between n=2 and n=8 wells as determined using ImageJ. Student's t-test analyses showed no significant difference in SYTO10: DEAD Red pixel intensity ratios between conditions for neither villus tip nor crypt. * $p < 0.05$ villus tip vs. crypt. Significant difference in SYTO10: DEAD Red ratio was observed between villus tip and crypt fractions following 30 and 60 minute incubation with Krebs buffer solution, indicating crypt preparations to be more viable than villus tip.

Figure 3.13:

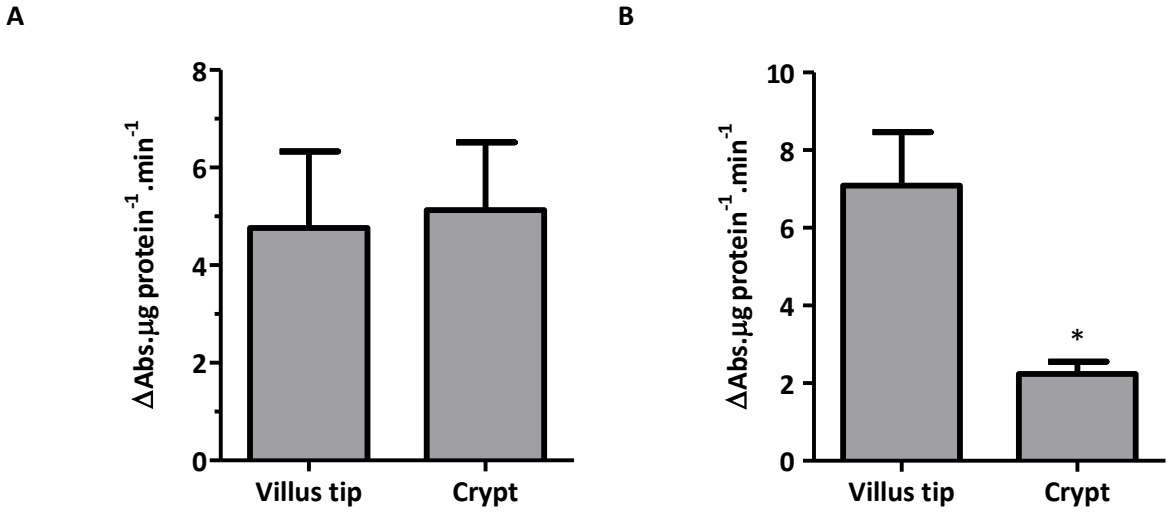

Figure 3.13 Assessment of villus tip and crypt cell viability using MTS cell assay following incubation in Krebs buffer solution and KB medium.

Assessment of metabolic cell viability measured as the change in absorbance at 490nm due to formation of formazan compound, following 30 minute incubation periods of villus tip and crypt fractions in Krebs buffer **(A)** or KB medium **(B)** at 37°C per minute. Data shown represent mean n=3 wells expressed as ΔAbs (490nm) per minute per µg of protein. Data were adjusted accordingly to allow ease of handling. * $p < 0.05$ Student's t-test villus tip vs. crypt following suspension in KB medium. No significant difference was apparent between fractions suspended in Krebs buffer or KB medium.

Figure 3.14:

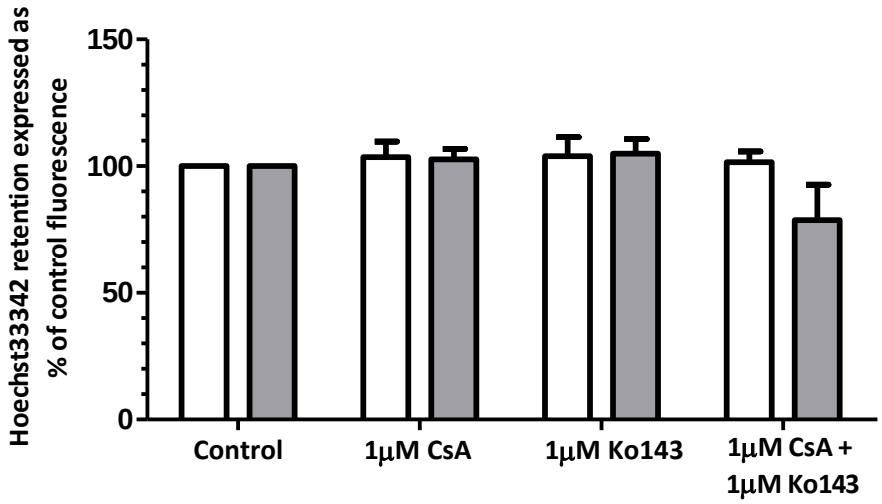

Figure 3.14 Intracellular Hoechst33342 dye retention in villus tip and crypt samples following 30 minute incubation in KB medium.

Hoechst33342 retention was measured in a fluorescence dependent manner in villus tip (open bars) and crypt (shaded bars) samples in the presence and absence of specific Mdr1 and Bcrp inhibitors CsA and K0143 alone or in combination with 3μM Hoechst33342. Cells were excited at 381nm and emitted fluorescence at 485nm measured. Cells were incubated at 37°C in KB medium solution, data shown represent mean n=9 replicates from three independent experiments ± SEM and have been normalised for control fluorescence (measured in absence of transporter inhibition). No significant difference is apparent between conditions.

3.4 Discussion

Currently the most popular methods used for the screening of early stage drug compounds are high throughput assays utilising the cultured cell lines Caco2 and MDCK (Irvine et al., 1999, Volpe, 2008). The growth of these two lines on permeable supports allows for measurement of apical and basolateral compound flux and the subsequent calculation of apparent drug permeabilities (Irvine et al., 1999). Cell culture allows high throughput screening protocols due to unlimited cell availability, coupled with the relatively short culture growth periods required for Caco2 and MDCK cells, these cell lines serve as an ideal choice for initial screening. Disadvantages are however evident, with differences in transporter expression and therefore apparent drug permeabilities being reported across different laboratories, likely due to differences in cell culture and experimental conditions leading to cellular mosaicism, particularly in the Caco2 cell line (Volpe, 2008). The cell models used fail to accurately reflect the complexity of *in vivo* absorption and elimination properties and therefore present difficulties with regards to translating data to *in vivo* studies. Furthermore, the origin of model cell lines should be considered. Since MDCK cells are a canine kidney derived cell line (Barker and Simmons, 1981) and the Caco2 cell line was extracted from colonic carcinoma tissue, whilst they prove useful in the study of transporter activity and interactions they are less useful for translation of findings to *in vivo* studies. The vast majority of primary cell models have thus far being unsuccessful due to limitations in culture of isolated preparations. We therefore aimed to isolate native rat ileal epithelial cells with the aim to allow functional assessment of key ABC transporters, Mdr1 and Bcrp, involved in drug efflux in an attempt to determine their functional influence in primary intestinal epithelia whilst maintaining some level of intestinal enterocyte complexity.

Isolation of primary epithelial cells was conducted according to a method previously described by McNicholas et al., (1994) (see methods section 2.2.4). Isolation allowed the obtainment of epithelial cells across the crypt villus axis therefore permitting study of two distinct cell populations derived from the villus tip and crypt (McNicholas et al., 1994). We have shown successful isolation of epithelial cell populations ranging from villus tip to crypt by phase contrast microscopy with cellular morphology indicating reproducible separation of epithelial cells showing progression from villus tips (fractions 1, 2 and 3) to epithelial sheets in mid fractions and an abundance of crypt units in fractions 8, 9 and 10. Further support for the isolation of distinct villus tip population is shown using TEM analysis of a combined F1/F2 sample. Columnar epithelial cells with a prominent brush border membrane alongside lateral cell membrane apposition with tight junctional proteins, classic characteristics of intestinal

enterocytes, were shown (Proulx, 1991, Volpe, 2008). The presence of such morphological features combined with phase contrast micrographs of villus tips strongly indicate successful isolation of a villus tip population in fractions 1 and 2.

Cryptal populations in fractions 9 and 10 are confirmed by the cylindrical arrangement of adjacent cells, such that their apical membrane surrounds a central lumen. A sparse brush border membrane, characteristic of poorly differentiated epithelial cells was shown to project from the apical cell membrane into the lumen. Combined with the presence of tube like crypt structures as visualised by phase microscopy and in agreement with isolated crypt morphologies described previously (Bjerknes and Cheng, 1981, Flint et al., 1991, McNicholas et al., 1994) it was confirmed that utilisation of the crypt-villus preparation achieved successful isolation of a distinct crypt cell population.

Alph, a membrane anchored metalloenzyme responsible for the hydrolysis of phosphomonoesters to inorganic phosphate and alcohol is highly expressed in intestinal mucosa (Coleman, 1992, Ensinger et al., 1978, Zhang et al., 2004). However, this study failed to measure functional Alph activity following fractional isolation despite McNicholas et al., (1994) reporting a clear decreasing gradient for Alph in fractions 1 to 10 using the same isolation procedure. In contrast high levels of p-nitrophenol formation by Alph in both fresh rat mucosal intestine scrapes and brush border membrane vesicles was evident using the same technique. The inability to measure functional Alph activity indicates a loss of enzymatic activity due to EDTA based chelation.

EDTA is a chelating agent, it sequesters and diminishes the activity of metal ions. We therefore propose that in the presence of high EDTA concentrations ALPH activity is decreased due to inhibition of catalytic activity, mediated by EDTA chelation, of the three metal ions found within the enzyme's active site (Conyers et al., 1967). Past studies have shown EDTA concentrations above 3mM to diminish intestinal human ALPH activity, with correlation between lack of human ALPH activity and increasing EDTA concentration (Conyers et al., 1967). Furthermore an alternative chelating agent 1,10-phenanthroline was shown to inhibit Escherichia Coli (E.Coli) Alph activity (Plocke and Vallee, 1962). Despite only 25-30% homology between human and E.Coli alkaline phosphatases, both enzymes show conservation of a catalytic serine residue, and of residues responsible for the co-ordination of two Zn^{2+} and one Mg^{2+} ions within the active site of each alkaline phosphatase monomer (Zhang et al., 2004). It is proposed that of the four Zn^{2+} ions found within the alkaline phosphatase dimer, two are involved in structural integrity whilst two are required for catalysis (Ensinger et al., 1978). It is therefore clear that human ALPH activity is dependent upon the presence of Mg^{2+} and Zn^{2+}, with isolation using 30mM EDTA causing a loss of activity due to the chelation of Zn^{2+} ions from

the enzyme active site. The addition of $ZnCl_2$ to Krebs buffer therefore allowed for to some extent the replacement of chelated Zn^{2+} and hence restoration of catalytic activity with similar findings being reported by Plocke and Vallee (1962).

Whilst Wesier (1973), Flint et al., (1991) and McNicholas et al., (1994) all show a decreased gradient of Alph activity from fraction 1 to fraction 10, Weiser (1973) used only 1.5mM EDTA during tissue isolation and incubated samples with 0.3mM $ZnCl_2$ prior to ascertaining enzyme activity whilst Flint et al., (1991), substitute EDTA chelation with a 27mM Na_2-citrate based isolation protocol, and therefore had no difficulty in measuring Alph activity. It is therefore surprising that McNicholas et al., (1994) were able to measure functional Alph enzyme activity in the absence of Zn^{2+} following isolation using 30mM EDTA. No mention of fractional re-suspension or incubation in solutions containing Zn^{2+} is detailed in the study.

LAP is a zinc metalloenzyme known to catalyse the hydrolysis of amino acids (Burley et al., 1990). The LAP hexamer is known to possess twelve Zn^{2+} ions which are localised within the catalytic site of the enzyme and prove essential for enzyme activity, with Cd^{2+} replacement of Zn^{2+} leading to a loss of enzyme hydrolysis (Burley et al., 1990, Himmelhoch, 1969). Although enzyme activity has been shown to decrease in the presence of group II metal chelating agents, EDTA was previously found to have no effect on LAP mediated hydrolysis of L-leucine-p-nitroanilide (Burley et al., 1990). Similarly, substrate formation was apparent here and could be measured spectrophotometrically following incubation of EDTA isolated fractions with L-leucine-p-nitroanilide without the need for zinc re-suspension.

Since Alph and Lap are brush border enzymes it was predicted that similar activity trends to those reported previously would be observed. Previous assessment of crypt-villus enzyme activity showed a progressive decrease in substrate formation from villus tip to crypt fractions. Despite recovery of low level Alph activity following resuspension in Krebs buffer containing $ZnCl_2$ this study failed to show a progressively decreasing gradient of either Alph or Lap activity from fraction 1 to 10, and rather a marked decrease was seen after fraction 3 (data not shown). This may be attributable to lack of Zn^{2+} availability preventing enzyme hydrolysis with regards to Alph despite attempts to replace Zn^{2+} ions within the enzymes active site. It was however shown that highest Alph and Lap activity levels were evident in fraction 2, with a significantly higher overall enzyme activity in villus tips than in crypt preparations (figure 3.4). Despite reported high intestinal mucosal expression levels for ALPH, Lap activity was found to be greater than that of Alph in all fractions. Taken together with morphological fraction assessment our data strongly supports successful isolation of two distinct epithelial cell populations which would allow study of the two distinct regions of the crypt-villus axis.

Hoechst33342, a lipophilic dye, is a known substrate of both MDR1 and BCRP (Scharenberg et al., 2002, Shapiro et al., 1997). The $LogD_{7.4}$ partition coefficient of Hoechst33342 is 3.1 indicating that the dye is able to diffuse into the plasma membrane. The binding of Hoechst33342 within the lipid bi-layer or to intracellular DNA causes an intense increase in fluorescence compared with the virtually negligible fluorescence measured in both extracellular and intracellular aqueous solutions (Shapiro et al., 1997). It is believed that Hoechst33342 is transported by MDR1 from within the lipid bi-layer (Shapiro et al., 1997), with similar reports suggesting BCRP to mediate substrate efflux in the same manner (Homolya et al., 2011). Using inside out membrane vesicles Shapiro & Ling (1997) present a model for Hoechst33342 MDR1 efflux in which Hoechst33342 binds to the lipophilic cell membrane and is transported directly from here into the extracellular medium causing a decrease in the measured fluorescence due to a shift in the emission spectrum of the dye (Shapiro et al., 1997). Hoechst33342 is also able to dissociate from the cell membrane and intercalate with cellular DNA (Müller et al., 2007), supporting its role as a nucleic acid stain. Furthermore, Shapiro & Ling, (1997) suggest this method to be utilised for the transport of all MDR1 substrates, indeed mitoxantrone efflux from within the lipid-bilayer by BCRP has also been reported suggesting a common mechanism of action between these drug resistance transporters (Homolya et al., 2011).

As expected, data is consistent with the proposed role of Hoechst33342 as a substrate for both MDR1 and mBcrp using transfected MDCKII cell lines. Transfection of cell lines with MDR1 and mBcrp resulted in a lowered cellular fluorescence, compared with native MDCKII counterparts, due to increased Hoechst33342 efflux limiting its accumulation within the lipid bilayer. Despite over-expression of MDR1 and mBcrp transporters fluorescence levels above those of transfected MDCKII cells alone measured in the absence of Hoechst33342 were detected following incubation of MDCKII-MDR1 and MDCKII-mBcrp cells with the dye, thus indicating that some Hoechst33342 dye remained bound to either the cell membrane or intracellular DNA despite high levels of transporter activity. Indeed, with over-expression of ABC transporters the limit of measured cellular fluorescence is determined by the ability of Hoechst33342 to rebind to cell membranes following clearance to the extracellular medium, or its intercalation with DNA (Shapiro et al., 1997).

Optimal inhibitory concentrations for CsA and Ko132 were identified as approximately 1µM CsA and 1µM K0143 using the preliminary experiments in the transfected cell lines and current literature. K0143, a FTC analogue, is a highly potent inhibitor of both BCRP and mBcrp at low micromolar concentrations, with 97% inhibition of human BCRP being reported at 0.5µM K0143 (Matsson et al., 2009). Matsson et al., (2009) report K0143 to selectively inhibit BCRP at

concentrations <1μM however it was also shown that K0143 inhibited MRP2 and MDR1 activity at higher pharmacological concentrations. Although MRP2 inhibition has been observed at mid-micromolar concentrations of K0143, Hoechst33342 is not a substrate of MRP2 (Matsson et al., 2009). K0143 therefore has no effect on cellular Hoechst33342 accumulation, and has no effect on the assay used here. MDR1 inhibition was evident only at K0143 concentrations > 1μM with an IC50 value > 10μM (Matsson et al., 2009). Consistent with reports of non-specific inhibition at concentrations greater than 1μM, increased Hoechst33342 retention was observed following incubation of native MDCKII cells with K0143 concentrations > 5μM. The rise in fluorescence observed here is likely due to nonspecific inhibition of endogenous canine transporters expressed in the native MDCKII cells for which Hoechst33342 is a substrate (Kuteykin-Teplyakov et al., 2010).

Similarly whilst CsA has been shown to inhibit MDR1 activity at low micromolar concentrations (Ejendal and Hrycyna, 2005), a loss of MDR1 selective CsA inhibitory effects at high concentrations (>10μM) has been shown (Xia et al., 2007), however this is not of concern in the present study since native MDCKII and therefore MDR1 transfected MDCKII cells do not endogenously express Bcrp (as shown in chapter 5). The increased fluorescence observed in native MDCKII cells may result from inhibition of canine Mdr1 activity, since canine Mdr1 is known to be endogenously expressed in this cell line (Kuteykin-Teplyakov et al., 2010), however the steep rise in measured fluorescence is reflective of a potential cytotoxic effect caused by high CsA concentrations leading to a lack of normal membrane integrity. In addition, previous work performed in our laboratory (Wright, 2011) showed a lack of cellular Hoechst33342 accumulation in MDCKII-MDR1 cells incubated in the presence of 1μM K0143 and similarly a lack of accumulation following incubation of MDCKII-mBcrp cells with 1μM CsA(Wright, 2011). We therefore conclude that 1μM K0143 and 1μM CsA specifically inhibit mBcrp and MDR1 and support the use of these concentrations in the pharmacological dissection of Mdr1 and Bcrp functional components in villus tip and crypt fractions.

Despite McNicholas et al., (1994) reporting functional activity of both villus tip and crypt fractions, with the incorporation of radiolabelled Rb^+ by the basolateral Na-K-Cl co-transporter shown in both preparations, this study failed to measure ABC transporter activity following incubation of villus tip and crypt fractions in either Krebs buffer or KB medium despite previous studies showing KB medium to restore cellular metabolic activity in cardiac myocytes (Isenberg and Klockner, 1982).

Assessment of cell viability using TEM and the MTS assay strongly indicates a loss of viability following EDTA-based isolation. Cellular vacuolation and a loss of cell structure was apparent

in both villus tip and crypt fractions with an accompanying rupture of mitochondrial membranes, and a loss of zona occludens between lateral membranes of adjacent cells. Low levels of formazan formation reported are likely due to low level cellular NAD(P)H production resulting from decreased cellular respiration and turnover of the citric acid cycle, supported by TEM evidence showing loss of mitochondrial cristae, demonstrating low levels of cellular metabolic activity.

It was proposed that incubation of isolated fractions in KB medium may restore cellular metabolic activity based on work performed by Isenberg and Klockner, (1982). Isolation of cardiac myocytes in low Ca^{2+} medium (aCa = 1μM) was shown to result in spontaneous hyper-contraction, and resultant disaggregation, with similar findings being shown in perfused isolated heart models (Isenberg and Klockner, 1982). A possible explanation of this Ca^{2+} paradox was a lack of cellular metabolic activity as a result of cellular Ca^{2+} overload. Specifically ATP-dependent Ca^{2+} transport into mitochondria, and therefore impairment of mitochondrial oxidative phosphorylation resulting in an increased consumption and a decreased production of ATP, causing cell rigour in isolated myocytes (Isenberg and Klockner, 1982). Findings of the present study, including rupture of mitochondria (as shown by TEM) and low levels of MTS reduction suggest reduced ATP availability within isolated fractions. ATP is required for functional ABC transporter and Na-K ATPase activity and therefore low levels of cellular ATP will limit transporter ATP hydrolysis and function. Whilst both cardiac resting and action potentials were restored following incubation of cardiac myocytes in KB medium, suggesting recovery of cellular metabolic activity (Isenberg and Klockner, 1982), no significant improvement of cellular metabolic activity was measured in villus tip and crypt epithelial preparations following incubation in KB medium when compared with metabolic activity measured following incubation of fractions in Krebs buffer. Rather, a non-significant fall in viability was measured in crypt fractions by the MTS assay. KB medium partially restored K/Na ratios however increased cell viability was not maintained. Confirmation of low cell viability was shown using the live-DEAD cell assay. The outer sufaces of the cell structures showed damage indicative/suggestive of cell death immediately following isolation with a rise in DEAD Red intensity shown with increasing incubation time for villus tip and crypt fractions, however such observations may be apparent due to adherence of and staining of, dead cell remnants to the outer edges of intact cells.

We have shown successful isolation of villus tip and crypt preparations from rat ileum sections using an EDTA based chelation method. Although able to measure membrane – associated functional enzyme activity (Lap), disappointingly, measurements of ABC transporter function were not possible due to a lack of cell viability. We therefore conclude that whilst this

preparation is not suitable for the originally proposed study of Mdr1 and Bcrp functional activity, the investigation of ABC transporter mRNA expression levels in villus tip and crypt preparations may be possible.

4. Determination of mRNA expression levels of drug transporters and cytochrome P450 enzymes

4.1 Introduction

A single layer of cells, composed of both absorptive and secretory cell types, lines the intestinal lumen and provides an enterocytic barrier which regulates the absorption of dietary nutrients whilst serving to protect underlying tissues against foreign and potentially toxic compounds (Ohland and MacNaughton, 2010, Snoeck et al., 2005). In addition to its physiological role in nutrient digestion and absorption the enterocyte barrier directly influences pharmacokinetic parameters of orally consumed drug compounds. For example, expression of SLC family members including organic cation transporters (OCT/OCTNs), concentrative nucleoside transporters (CNTs) and organic anion transporter proteins (OATPs) on the cell membranes of enterocytes increases the absorption of hydrophilic drug compounds across the epithelial cell layer by transporter facilitated movement (Gomez-Orellana, 2005, Sai and Tsuji, 2004, Steffansen et al., 2004). By designing drug molecules which imitate physiological substrates intestinal absorption does not solely rely on the ability of drug compounds to diffuse passively across the apical membrane (Gomez-Orellana, 2005). A similar approach is taken with hydrophilic peptidodimetic drugs which utilise amino acid transporters, such as PEPT1 (Thwaites et al., 1995), expressed on the cell membranes of epithelia lining the intestine. Alternatively, lipophilic molecules diffuse passively across into intestinal epithelial cells due to their ability to partition into the cell membrane.

Following absorption of drug compounds, both lipophilic and hydrophilic, oral bioavailability may be reduced due to the expression of ABC transporters and CYP450 enzymes within the epithelial cells of the enterocyte barrier.

The ABC family of transporters comprises several members which are known to induce drug resistance to a wide substrate profile both *in vitro* and *in vivo* (Dietrich et al., 2003, Kruh and Belinsky, 2003). Of particular interest with regards to intestinal drug resistance and pharmacokinetics are the three transporters MDR1, MRP2 and BCRP (Dietrich et al., 2003, Szakacs et al., 2008). MDR1, MRP2 and BCRP have been shown to be expressed at key physiological barrier locations (as detailed in chapter 1) where they are believed to protect against invasion from toxic and foreign compounds. Reported to be apically expressed on intestinal enterocytes these transporters are capable of transporting orally consumed substrates against their concentration gradient from the intracellular aqueous environment or directly from the lipid interface of the cell membrane into the intestinal lumen (Blokzijl et al., 2007, Glaeser et al., 2007, Maliepaard et al., 2001, Sandusky et al., 2002). The movement of

drug substrates into the intestinal lumen ultimately increases intestinal elimination of drug compounds and lowers the systemic drug concentration (Szakacs et al., 2008). As such it is vital that all potential drug compounds are screened to determine potential interactions with the ABC transporters, MDR1, MRP2 and BCRP to allow administered doses to be adjusted accordingly.

In addition to MDR1, MRP2 and BCRP other members of the MRP subfamily are known to transport drug substances and contribute to the development of drug resistance in some cell/tissue types (Borst et al., 2007, Borst et al., 2000, Kruh and Belinsky, 2003). MRP1, -3, -4, -5, -6 and -7 are however proposed to be localised to the basolateral membrane of intestinal enterocytes and are not therefore believed to contribute to increased intestinal elimination of drug compounds (Borst et al., 2007, Borst et al., 2000). However, basolateral expression of these transporters allows for the translocation of some hydrophilic drugs across the basolateral membrane and into the underlying sinusoidal blood (Kruh and Belinsky, 2003).

In addition to transporter proteins, enteric cytochrome P450 enzymes are known to contribute significantly to intestinal first pass metabolism of drug compounds (Paine et al., 2006). Expressed within the cell cytoplasm CYP450 enzymes are capable of metabolising drug compounds such that some resultant metabolites are inactive. Metabolism of oral drug compounds by intestinal CYP450 enzymes therefore results in lowered systemic concentrations of the parent drug molecule and may influence the therapeutic potential of the drug (Martignoni et al., 2006, Mitschke et al., 2008, Paine et al., 2006). It should be noted however that CYP450 enzymes are sometimes utilised by chemists in the delivery of prodrugs, which must undergo biotransformation before becoming therapeutically active, in an attempt to increase drug efficiency (Suzuki and Sugiyama, 2004).

Given the wide substrate specificities of ABC transporters and cytochrome P450 enzymes it is well established that substantial overlap in substrate recognition is apparent between the two protein families (Benet, 2009). Such overlap presents problematic with regards to oral drug bioavailability due to enterocytic recirculation of drug compounds (Benet, 2009). Drug molecules absorbed by transcellular diffusion must move through the cell cytoplasm, thereby increasing opportunity for interaction with CYP450 enzymes and subsequent CYP450 mediated metabolism. As discussed in chapter 1, MDR1, MRP2 and BCRP transporters are proposed to efflux xenobiotics across the apical cell membrane and into the intestinal lumen allowing recirculation of drug compounds into intestinal epithelial cells, since molecules will diffuse passively or be transported back across the apical membrane, as they progress down the intestine toward the colon. Reabsorption of drug molecules across the cell membrane will result in them being re-exposed to intracellular CYP450 enzymes, thereby potentiating

likelihood of CYP450 metabolism thus lowering systemic concentrations of parent drug molecules (Benet, 2009). Furthermore, CYP450 metabolism may render metabolites more susceptible to ABC transporter mediated efflux thereby increasing intestinal elimination of metabolic products and lowering potential therapeutic concentrations.

The crypt-villus axis serves as the functional unit of the intestine. Stem cells residing within the crypt region are responsible for the generation of all cell lineages which populate the intestine (see chapter 1 for more details) (Barker et al., 2008). Cell fate is decided upon reaching the crypt-villus junction where cells undergo rapid terminal differentiation (Barker et al., 2008, Pinto and Clevers, 2005). Cells undergo constant differentiation up the crypt-villus axis until they are shed into the intestinal lumen approximately 5 days post-initial cell division (Barker et al., 2008, Marshman et al., 2002, Pinto and Clevers, 2005). The loss of cells into the intestinal lumen is balanced by the constant production of new, undifferentiated cells within the crypt (Barker et al., 2008, Pinto and Clevers, 2005).

The extensive differentiation of cells across the crypt-villus axis results in a vast difference in gene and protein expression between cells found within the crypt and at the villus tip (Anderle et al., 2005, Mariadason et al., 2005). For example, the projection of intestinal villi into the lumen increases the potential for interaction between epithelial transporters and luminal content/substrates, as such the increased expression of digestive enzymes and nutrient transporters reported in the villus region is consistent with the absorptive capacity of the intestine. Conversely proteins involved in DNA replication are expressed at much higher levels within the proliferative crypt unit (Freeman et al., 1993, Himmelhoch, 1969, Jakab et al., 2010, Lenzen et al., 1996, Mariadason et al., 2005, McNicholas et al., 1994).

Although past studies have shown differentiation of cells as they migrate up the crypt-villus axis it is hypothesised that, in agreement with their proposed role in the enterocyte barrier, ABC transporters and/or CYP450 enzymes could potentially be expressed in the crypt unit to allow protection of this vital stem cell region since exposure of the intestinal crypt to drug compounds may potentially induce a toxic effect and lead to the development of cytotoxicity. Given that stem cell progeny are believed to undergo six rounds of cell division the loss of a single crypt stem cell can reduce total cell volume by 64 cells, (Barker et al., 2008, Marshman et al., 2002), it therefore seems logical that a protective mechanism exists to prevent toxic insult within this poorly differentiated region.

Past studies have shown involvement of BCRP in establishment of the SP phenotype of stem cells (Scharenberg et al., 2002, Zhou et al., 2001). The SP stem cell population show a reduced ability to efflux Hoechst33342 when exposed to the BCRP specific inhibitor K0143

(Scharenberg et al., 2002). Furthermore BCRP expression is confirmed in numerous stem cell lineages (Zhou et al., 2001). It is therefore hypothesised that Bcrp expression may be evident within the intestinal crypt region of rat intestine, with functional activity of the transporter proposed to protect the stem cell niche against toxic insult via the efflux of substrates out of cryptal epithelia. Such a hypothesis does not however exclude potential for expression of alternative drug transporters and/or cytochrome P450 enzymes to function within this region.

Despite the established role of drug transporters and metabolising enzymes in determination of drug pharmacokinetic profiles little is known with regards to comparative expression levels and localisation of these proteins in the intestine. Whilst some studies have examined transporter or cytochrome P450 expression along the length of the intestine, many focus only on a small subset of genes and do not provide quantitative and comparable expression levels. The main purpose of the studies described in this chapter therefore, has been to determine mRNA concentrations of key transporters (ABC and SLC family members) and CYP450 enzymes in the rat intestine, both along the longitudinal and crypt-villus axes of rat intestine using quantitative NanoString mRNA technology.

4.2 Methods

4.2.1 NanoString Codeset design

The NanoString codeset used in this project was designed based on current literature and key intestinal drug transporters and drug metabolising Cyp450 enzymes were carefully selected. NanoString codeset details are shown in table 2.1. Although RNA concentration and RNA integrity were controlled for, three housekeeping (HSKP) genes were selected and included in the codeset design to allow normalisation of target gene expression against expression levels of HSKP genes, believed to be constitutively expressed across all samples. Finally, several genes of known intestinal expression patterns were included in the codeset as experimental controls.

4.2.2 Sample preparation and determination of mRNA expression levels

Villus tip and crypt RNA samples were prepared as described in materials and methods section 2.2.4. Briefly, rat ileum was excised, inverted and threaded onto a glass spiral. Tissue was then vibrated at approximately 50Hz into a crypt-villus isolation buffer containing 30mM Na_2-EDTA. Epithelial cells were chelated from the ileal tissue at timed intervals to give a total of 10 fractions. Fractions 1 and 2 were combined and deemed villus tip, and fractions 9 and 10 combined as crypt samples. Mucosal scrapes were taken from the duodenum, jejunum, ileum and colon to allow assessment of mRNA levels within these regions (section 2.2.3). Trizol-based total RNA extraction was performed, and resultant RNA subjected to quality control checks. All samples used here had RIN values > 6 (range 6.1 to 8.8) except for duodenal samples, all of which showed RIN values < 1. Reasoning for the low RIN values of duodenal samples is unknown. Nanodrop 260/280 ratios were > 2 for all samples (data not shown) and as such all samples were deemed of suitable quality for RNA analysis. Samples were combined in solution with capture and reporter probes, and hybridised as per NanoString guidelines. Samples were loaded onto the NanoString prep station, and NanoString counts acquired as previously described (materials and methods section 2.2.6).

4.2.3 Normalisation and statistical analysis of NanoString mRNA expression data

To allow direct comparison between samples all data were adjusted against positive and negative assay controls and NanoString counts were normalised against expression levels of three housekeeping genes. NanoString counts were converted to fmol/sample concentrations, and fold change and $\log_2$ fold change values determined. A full description of NanoString data analysis, including housekeeping gene validation, can be found in materials and methods, section 2.2.6.

4.3 Results

4.3.1 Identification and validation of housekeeping reference genes as internal controls

Housekeeping genes (or internal control genes) are currently regarded as the gold standard with regards to normalisation of mRNA expression (de Jonge et al., 2007). Three potential housekeeping genes were identified based on their reported constitutive expression levels across different tissue samples including villus tip, crypt, de-epithelialised intestinal mucosa and whole intact mucosa (Wang et al., 2010). Wang et al., (2010) assessed the stability of thirteen commonly used housekeeping genes including β-actin (ACTB), β-2-microglobulin (B2M), glucuronidase-β (GUSB), GAPDH, HPRT1, HMBS and tubulin alpha 1 (TUBA1). GeNorm and NormFinder analysis showed HPRT1 and HMBS to be amongst the top five most stably expressed genes across all tissues (Wang et al., 2010). Of particular concern here was the selection of housekeeping genes present at similar expression levels in villus tip and crypt samples due to extensive enterocyte differentiation evident across the crypt villus axis (Barker et al., 2008). Additional to the high levels of stability reported for HMBS and HPRT1, both genes, in addition to GAPDH, displayed an overlap in real time PCR cycle threshold (Ct) values in villus and crypt samples (Wang et al., 2010). It was for these reasons that Gapdh, Hmbs and Hprt1 were included in the NanoString codeset as potential HSKP genes. Following selection, and determination of mRNA expression levels, validity of nominated housekeeping genes was confirmed to ensure constitutive expression of similar mRNA levels across all samples investigated.

It was expected that expression levels of the three selected housekeeping genes would not be significantly different between villus tip, crypt, duodenum, jejunum, ileum and colon samples, irrelevant of experimental treatment (Vandesompele et al., 2002b). Validation of chosen HSKP genes was performed by directly comparing mean HSKP mRNA expression counts from n=48 samples (combination of villus tip, crypt, duodenum, jejunum, ileum and colon samples taken from normal and *in vivo* treated experimental animals) with mean sample group expression (e.g. crypt) using an unpaired, two-tailed Student's t-test. No significant difference was reported between mean HSKP mRNA expression (n=48) and the mean mRNA expression of any segment group for Gapdh, Hprt1 or Hmbs (see section 2.2.6.6 for more details), validating the use of these genes as internal controls. Target gene counts were therefore normalised against Gapdh, Hprt1 and Hmbs expression levels to allow comparison of target gene expression between samples. An example of HSKP gene normalisation is shown in figure 2.8. It should be noted that NanoString data presented here showed little variation when normalised against

expression levels of HSKP genes alone or in different combinations, indicating data to be robust against variation in HSKP gene expression levels.

4.3.2 Experimental validation using control genes of known intestinal expression pattern

To ensure isolation of RNA samples specific to the region of interest (villus tip, crypt, duodenum, jejunum, ileum and colon) and confirm validity of NanoString based mRNA detection, several genes of known expression patterns were included in our codeset. Genes of known distribution along both the longitudinal and crypt-villus axes were identified and used to confirm experimental validity (appendix 9.2). Furthermore, in addition to phase and TEM microscopy and enzyme analysis results discussed earlier (chapter 3), inclusion of distinct villus tip and crypt cell markers allowed for further validation of the crypt-villus isolation technique discussed in chapter three (appendix 9.3).

Experimental control genes included in the design of the NanoString codeset were; Alkaline phosphatase (Alph); Leucine aminopeptidase (Lap3); Carbonic anhydrase 2 (Ca2); Sodium-glucose transporter 1 (Sglt1); Villin; Proliferating cell nuclear antigen (Pcna), Na-K-Cl co-transporter (Nkcc1) and the Cystic fibrosis transmembrane conductance regulator (Cftr). Details of mRNA concentrations for all regions studied are shown in appendices 9.2 and 9.3.

Alkaline phosphatase (Alph) is a brush border enzyme previously shown by others to have high levels of functional activity in villus tip fractions (Bjerknes and Cheng, 1981, McNicholas et al., 1994). In contrast to data presented by others, p-nitrophenol formation following crypt-villus isolation, in both villus tip and crypt samples, was low (chapter 3). In agreement with low level product formation NanoString data showed a lack of Alph mRNA expression both along the length of the intestine and across the ileal crypt villus axis (appendices 9.2 and 9.3). NanoString counts for Alph in crypt, jejunum and ileum samples were not significantly different to those of negative synthetic RNA controls ($p > 0.05$), for which no target genes exist. Average mRNA expression concentrations were < 0.1 fmol/sample in villus tip, duodenal and colonic samples. The lack of p-nitrophenol formation discussed earlier therefore likely results from low level Alph gene expression. As such p-nitrophenol formation measured in chapter 3 may result from the hydrolysis of pNPP by an unknown Zn^{2+} dependent enzyme as opposed to Alph dependent activity (section 3.4). All other experimental control genes showed significantly higher levels of expression compared with negative controls (Student's t-test) and were therefore deemed to be present in all regions of the intestine studied.

Villin is an actin bundling protein primarily involved in the assembly of the brush border membrane of epithelial cells (Friederich et al., 1990). In line with the rise in absorptive capacity of epithelial cells with distal progression along the longitudinal intestinal axis (Englund et al., 2006), increased villin expression was noted from the duodenum to ileum (••• $p < 0.001$) with concentrations of 183.5 ± 18.0, 301.2 ± 14.5 and 334.8 ± 12.5 fmol/sample in the duodenum, jejunum and ileum respectively, indicating increased brush border presence along the length of the small intestine. In agreement with Englund et al., (2006) a significant decrease in villin expression between the small intestine and colon was also detected (92.6 ± 20.3 fmol/sample, average n=4 animals ± SEM) (appendix 9.2)(Englund et al., 2006). Given the flattened appearance of the epithelium lining the colonic lumen and the lack of epithelial brush border assembly within this region, low level villin expression in the colon is not surprising (Pinto and Clevers, 2005).

Unlike many other genes, villin mRNA expression is independent of epithelial cell differentiation and is detected in epithelial cells of both the crypt and villus (Boller et al., 1988) however past studies have shown decreased expression of villin mRNA in the crypt region compared with that of the villus tip by both in situ hybridisation and microarray analysis (Boller et al., 1988, Mariadason et al., 2005). In agreement NanoString mRNA analysis shows significant (** $p < 0.01$) up-regulation of villin mRNA in villus tip compared with crypt samples. A 2.3 ± 0.4 fold change between villus tip and crypt expression levels was apparent with average mRNA concentrations of 624.3 ± 51.0 and 288.8 ± 40.7 fmol/sample within each respective area (appendix 9.3/figure 4.2)(average n=4 animals ± SEM). Increased villin mRNA within villus tip samples is supportive of epithelial cell differentiation from the crypt to villus tip (Barker et al., 2008). In support of lower cryptal villin mRNA expression, TEM studies (reported in chapter 3) showed presence of a limited brush border membrane on cryptal epithelial cells as opposed to the prominent microvilli identified in villus tip fractions (figures 3.2 and 3.3).

Similar to Alph, Lap is a brush border amino peptidase enzyme (McNicholas et al., 1994). The role of Lap3 in peptide cleavage supports its high level expression at the intestinal brush border (Himmelhoch, 1969). We found a highly significant (** $p < 0.01$) difference in mRNA expression between villus tip and crypt regions with a calculated fold change of 4.9 ± 1.4 (appendix 9.3/figure 4.2). Given the role of villin in formation of the brush border membrane and the function of Lap, it is not surprising to observe a significantly increased expression of the brush border enzyme Lap3 from the duodenum to the ileum. Increasing mRNA concentrations of 177.2 ± 14.9, 402.6 ± 13.6 and 529.4 ± 63.4 fmol/sample (average n=4 animals ± SEM) (appendix 9.2/figure 4.1) were measured in the duodenum, jejunum and ileum

with a significant fall in expression from all regions of the small intestine to 43.7 ± 1.8 fmol/sample in the colon (appendix 9.2). It should be noted that no significant difference in Lap3 mRNA expression was detected between the jejunum and ileum.

Similarly, Ca2 and Sglt1, involved in intestinal bicarbonate production and brush border associated Na^+ coupled glucose uptake respectively (Kivela et al., 2005, Yoshikawa et al., 2011), were detected at higher expression levels in villus tip than crypt fractions in line with their physiological functions. Only Ca2 however displayed a significant increase in mRNA expression between the two regions whilst Sglt1 mRNA expression levels were highly variable in villus tip samples investigated (appendix 9.3). Previous studies have shown in situ hybridisation of Sglt1 mRNA above the crypt villus junction in the duodenum, jejunum and ileum of rabbit intestine, with cryptal hybridisation signals falling below the level of detection (Freeman et al., 1993, Lenzen et al., 1996). Despite a lack of cryptal mRNA detection using in situ hybridisation techniques, Sglt1 mRNA was detected in both crypt and villus tip samples using NanoString technology (418.2 ± 26.1 and 1145.4 ± 342.5 fmol/sample respectively) (average n=4 animals ± SEM), with a calculated fold change of 2.7 ± 0.8 (appendix 9.3/figure 4.1) villus tip versus cryptal expression (non-significant). Detection of cryptal mRNA shown here may result from increased sensitivity of NanoString technology compared with in situ hybridisation techniques. In agreement with findings from Freeman et al., (1993) Sglt1 mRNA expression levels were found to be highest in the jejunum, 583 ± 69.7 fmol/sample, with a significantly higher expression measured within this region compared with the duodenum (* $p < 0.05$) and colon ($^{\#\#}$ $p < 0.01$), no significant difference is apparent between duodenal and ileal Sglt1 mRNA expression (average n=4 animals ± SEM) (appendix 9.2).

In agreement with current literature Ca2 expression was found to be highest in villus tip (46.7 ± 5.0) and in colon samples (186.8 ± 14.7) (appendix 9.2 and 9.3). In agreement with Kivela et al., (2005) and Maridason et al., (2005) who report significant upregulation (** $p = 0.0035$) of Ca2 in villus tip fractions compared with crypt samples we found significantly higher Ca2 expression in villus tip than crypt samples (** $p < 0.01$) with a calculated fold change of 3.6 ± 0.8 between the two regions (appendix 9.3/figure 4.2). Carbonic anhydrase catalyses the reversible conversion of carbon dioxide and water to bicarbonate and protons and ultimately drives turnover of the $Cl^-/HCO3^-$ and Na^+/H^+ exchangers present within the colon. Turnover of these transporters facilitates the reabsorption of NaCl from the intestinal lumen and as such drives osmotic reabsorption of water. High expression levels of Ca2 in the colon therefore provide a mechanism by which NaCl and H_2O are reabsorbed within the large intestine (Kivela et al., 2005). As such significantly higher expression of Ca2 in the colon compared with the jejunum and ileum is in agreement with the physiological function of this enzyme (appendix

9.2). Decreasing Ca2 expression along the length of the small intestine has previously been shown (Fleming et al., 1995), as is evident here from the duodenum to ileum (• $p < 0.05$), jejunum to colon ($^{\#}$ $p < 0.05$) and ileum to colon ($^{\#\#}$ $p < 0.01$).

Cftr is a chloride ion channel which allows the movement of Cl^- from the intracellular to the extracellular domain. Translocation of Cl^- ions by Cftr directly implicates this channel in the regulation of fluid and electrolyte absorption (Sheppard and Welsh, 1999). It was reported by Trezise et al., (1992) that Cftr and Mdr1a show opposing expression patterns across the crypt villus axis of rat intestine, with in situ hybridisation showing detection of Cftr mRNA within the crypt region only with an apparent lack of villus mRNA expression. A more recent study by Jakab et al., (2010) however showed Cftr protein to be expressed at the apical cell membrane of both villus and crypt epithelia in all regions of the rat intestine from the proximal duodenum to the distal colon, with densitometric analysis showing higher protein content in the duodenal villus relative to that detected in the crypt. Whilst assessment of mRNA expression levels was not performed by Jakab et al., (2010) presence of villus protein indicates a requirement for underlying mRNA, in agreement we show a 2.1 ± 0.3 fold change in the ratio between villus tip and cryptal Cftr mRNA expression, with mRNA concentrations of 29.2 ± 4.1 and 13.8 ± 1.5 fmol/sample in villus tip and crypt samples of the ileum respectively (average n=4 animals ± SEM) (appendix 9.3, figure 4.2). How such differences correlate with Cftr protein localisation and function remains to be established. We also show presence of Cftr mRNA in all regions of the intestine (appendix 9.2) supporting protein detection from the proximal duodenum to distal colon shown by Jakab et al., (2010).

As expected, significantly increased expression of Villin, Ca2, and Lap3 mRNA is apparent in isolated villus tip samples compared with cryptal expression levels, in combination with morphological analysis and biochemical data discussed previously (chapter 3) NanoString data confirms that a villus tip rich population was successfully isolated using the crypt-villus isolation procedure described earlier. In addition isolation of a crypt like cell population is confirmed, supported by significantly higher expression levels of both Pcna (*** $p < 0.001$) and Nkcc1 (** $p < 0.01$) within crypt compared with villus tip samples.

The proliferative nature of the crypt unit and the rapid cell division associated with the transit amplifying compartment are reflective of high levels of DNA replication (Barker et al., 2008, Pinto and Clevers, 2005). Given its known role in regulation of DNA replication (Moldovan et al., 2007) it is not surprising that Pcna mRNA is expressed at significantly higher levels in crypt samples than at the villus tip, with a $\log_2$ fold change value of -1.3 ± 0.2 (11.0 ± 1.3 fmol/sample villus tip and 27.2 ± 2.1 fmol/sample crypt)(appendix 9.3/figure 4.2)(average n=4

animals ± SEM). Similarly, Mariadason et al., (2005) showed increased Pcna mRNA expression in crypt samples following isolation using a modified Weiser technique with microarray analysis. In support of higher cryptal mRNA expression, we show immunoreactivity of the anti-Pcna antibody PC10 (see table 5.1 for details) to be strictly restricted to the crypt region of the rat small intestine (figure 4.3). Due to poor section morphology a villus-crypt profile for Pcna protein could not be obtained here, however past studies have shown distinct localisation of Pcna to the crypt of both rat and mouse intestine (Gu et al., 2001, Mariadason et al., 2005).

Similarly, as reported using in situ hybridisation (Jakab et al., 2010) higher mRNA expression levels of Nkcc1 are apparent in crypt samples in comparison to villus tip expression (6.5 ± 1.3 fmol/sample villus tip versus 34.8 ± 6.3 fmol/sample crypt) (appendix 9.3/figure 4.2) (average n=4 animals ± SEM). A $\log_2$ fold change of -2.4 ± 0.5 (** p = 0.0045) was calculated for Nkcc1 (appendix 9.3). Contrasting expression profiles of Cftr and Nkcc1 across the crypt-villus axis therefore suggests villus Cftr expression may not solely be associated with intestinal Cl^- (fluid) secretion. In contrast to other control genes studied, Nkcc1 expression is maintained along the length of the gut with an indicated non-significant increase in expression towards the colon (appendix 9.1/figure 4.1). Since basolateral Nkcc1 protein operates in conjunction with apical Cftr to mediate Cl^- (and hence fluid) secretion, its mRNA distribution reflects the ability of the small intestine and colon to secrete as well as absorb fluid (Jakab et al., 2010).

This summary of pre-existing mRNA expression data, obtained using a variety of experimental techniques, both across the crypt-villus and longitudinal axes is therefore broadly mirrored by the data obtained using NanoString technology which is presented here. The ability to replicate such data using NanoString technology strongly supports expression trends observed for other target drug transporters and Cyp450 enzymes in the rat intestine.

Figure 4.1:

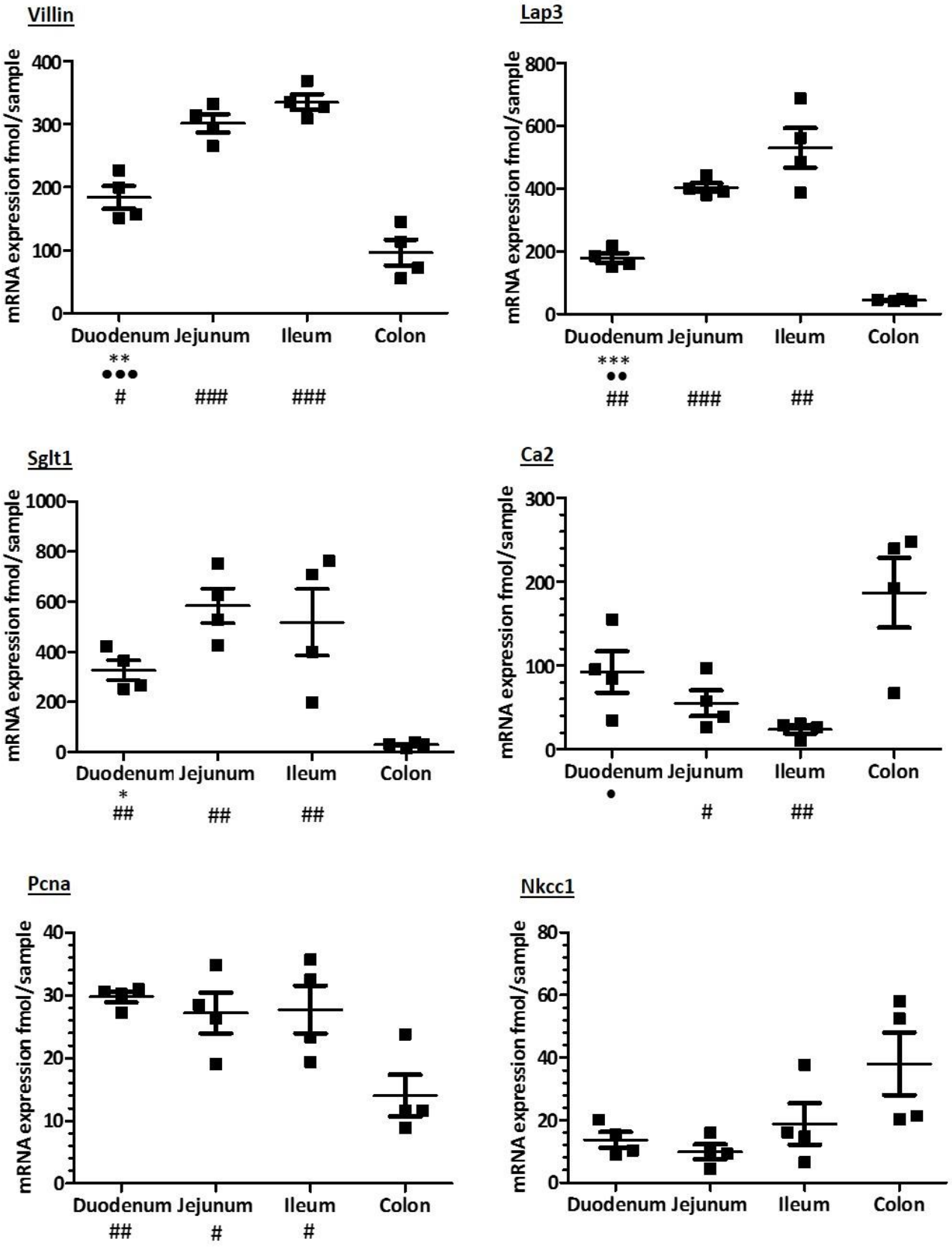
Villin
mRNA expression fmol/sample
400
300
200
100
0
Duodenum Jejunum Ileum Colon
**
●●●
#
###
###
Lap3
mRNA expression fmol/sample
800
600
400
200
0
Duodenum Jejunum Ileum Colon
***
●●
##
###
##
Sglt1
mRNA expression fmol/sample
1000
800
600
400
200
0
Duodenum Jejunum Ileum Colon
*
##
##
##
Ca2
mRNA expression fmol/sample
300
200
100
0
Duodenum Jejunum Ileum Colon
●
#
##
Pcna
mRNA expression fmol/sample
40
30
20
10
0
Duodenum Jejunum Ileum Colon
##
#
#
Nkcc1
mRNA expression fmol/sample
80
60
40
20
0
Duodenum Jejunum Ileum Colon

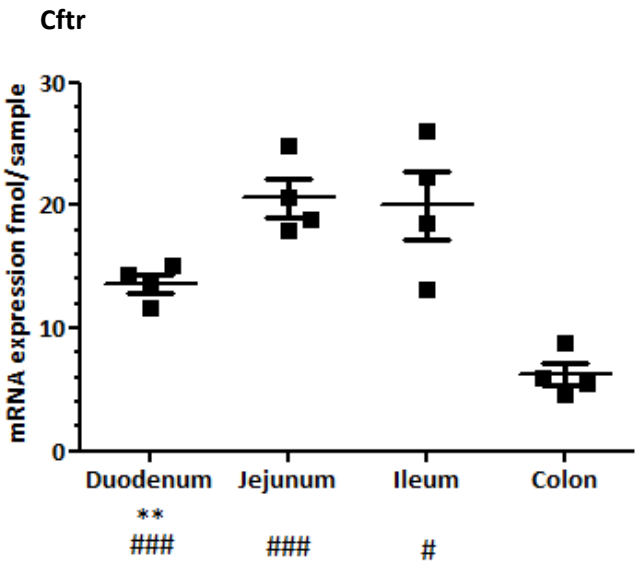

Figure 4.1 mRNA concentrations (fmol/sample) of experimental control genes in the duodenum, jejunum, ileum and colon of the rat intestine.

Data show individual animal replicate mRNA concentrations (fmol/sample) with mean concentration ± SEM. mRNA expression values have been normalised against assay controls and expression levels of Gapdh, Hprt1 and Hmbs HSKP genes. Following assessment of regional population variance using Levene's test, Student's t-test statistical analyses were performed, with Welche's correction applied where relevant. Welche's correction removes assumption of equal population variance of any two regions being compared and was applied to prevent occurrence of false statistical significance. Statitical analyses were performed between different intestinal regions and resultant summary statistics are shown below the x-axis, * $p < 0.05$, ** $p < 0.01$ *** $p < 0.001$ vs. jejunum, • $p < 0.05$, •• $p < 0.01$ and ••• $p < 0.001$ vs. ileum and # $p < 0.05$, ## $p < 0.01$ and ### $p < 0.001$ vs. colon.

Figure 4.2:

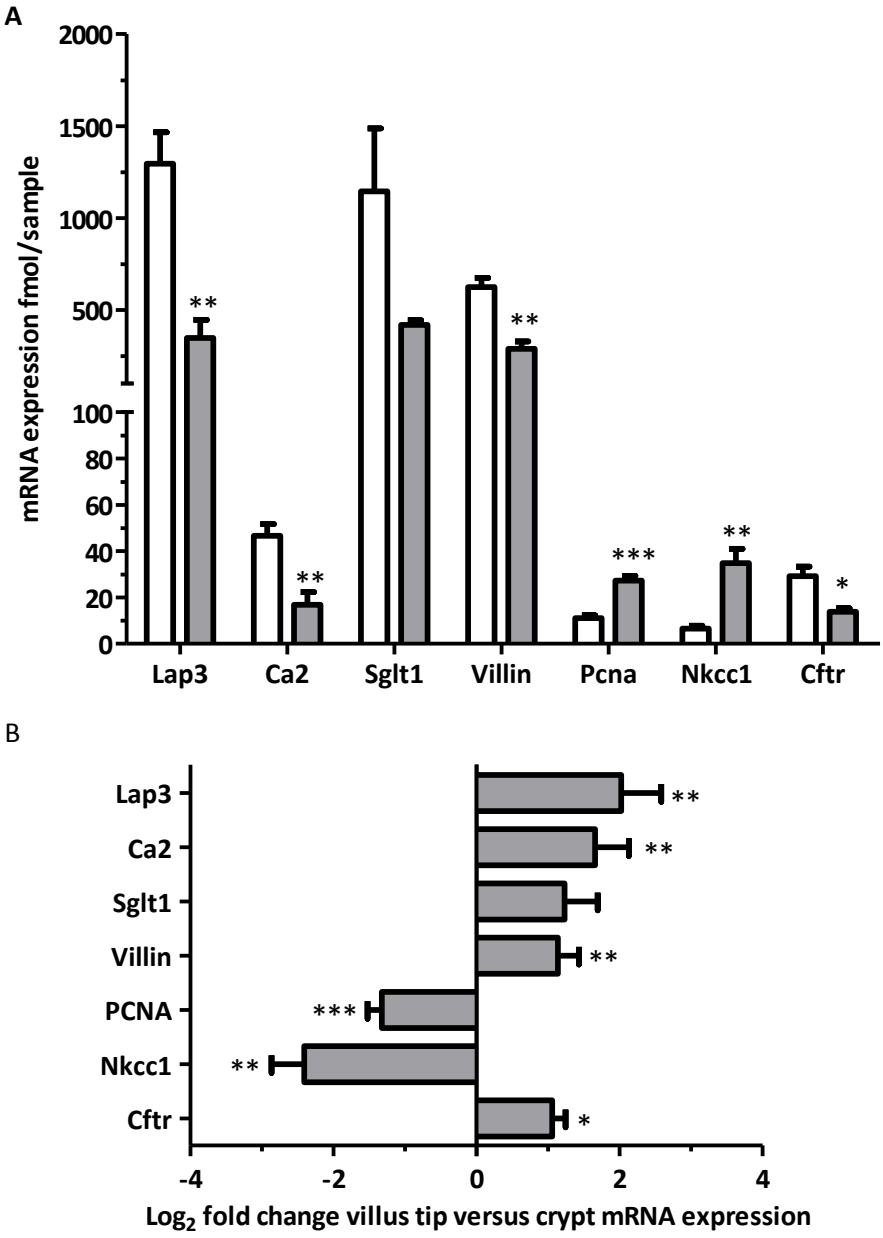

Figure 4.2 mRNA concentrations (fmol/sample) of experimental control genes in the villus tip and crypt regions and log_2 fold change villus tip versus crypt.

(A) Mean mRNA concentrations (fmol/sample) measured in rat ileal villus tip (clear bars) and crypt (grey bars) fractions **(B)** Log_2 fold change villus tip versus crypt. Data show mean mRNA concentration from n=4 male rats ± SEM and have been normalised against assay controls and expression levels of Gapdh, Hprt1 and Hmbs HSKP genes. Statistical analyses show Student's t-test analysis with Welche's correction applied where population variances were found to be unequal, * $p < 0.05$, ** $p < 0.01$, *** $p < 0.001$ villus tip vs cryptal expression.

Figure 4.3:

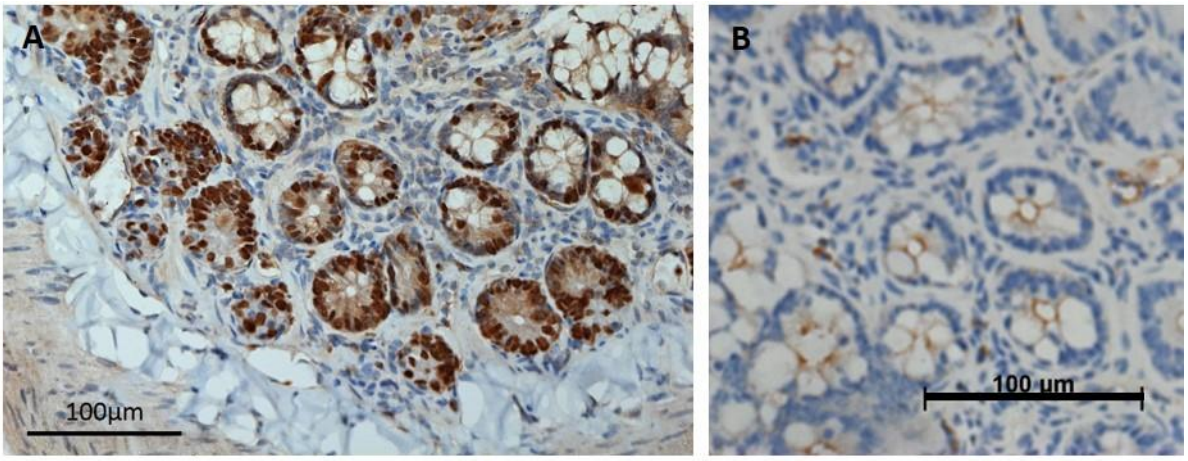

Figure 4.3 Cryptal localisation of Pcna protein using anti-PCNA PC10 antibody

(A) Cryptal localisation of Pcna in rat ileum sections using the PC10 anti-Pcna primary antibody (diluted 1:4000) **(B)** primary antibody omitted control. Staining was performed using a Ventana Benchmark staining platform and counterstained with Ventana blueing agent and haematoxylin. Post-staining sections were dehydrated using increasing alcohol concentrations. Sections were imaged using a Zeiss Axioimager.

4.3.3. Intestinal expression of ABC drug transporter mRNA from the duodenum to colon and across the crypt-villus axis

Given their role in multidrug resistance (Szakacs et al., 2008), and the lack of convincing evidence with regards to their intestinal distribution, mRNA expression levels of key drug transporters Mdr1, Mrp2 and Bcrp were quantified both across the crypt-villus axis and along the length of the rat intestine. In rat two Mdr1 isoforms have been reported, Mdr1a and Mdr1b (Zhou et al., 2001). NanoString targets directed against both isoforms were therefore included in the design of the NanoString codeset used here. Only very low mRNA concentrations for Mdr1b were detected along the length of the small intestine and across the crypt-villus axis with a maximum average concentration of 0.3 ± 0.1 fmol/sample in the villus tip of the ileum and in the duodenum (appendices 9.2 and 9.3). Expression levels in the jejunum, ileum and colon were not significantly different to those of negative synthetic RNA controls. It is therefore concluded that a lack of Mdr1b mRNA expression is apparent in rat intestine.

Mdr1a expression was shown to significantly increase along the length of small intestine from the duodenum to the ileum (appendix 9.2, figure 4.4). mRNA concentrations in the duodenum, jejunum and ileum were 2.4 ± 0.4, 4.5 ± 0.6 and 10.2 ± 2.2 fmol/sample (average n=4 animals ± SEM). As reflected by the SEM substantial variation is apparent in expression levels between animals however a significant difference in expression was found between duodenum and jejunum (* $p < 0.05$), duodenum and ileum (• $p < 0.05$) and, jejunum and ileum (* $p < 0.05$) (appendix 9.2, figure 4.4). Relative to expression levels of other ABC transporters Mdr1a mRNA expression is considerably low, particularly in the duodenum, where Mdr1a ranks lowest with regards to those ABC transporters deemed to be present in this region of the intestine (appendix 9.2). Colonic expression was shown to vary to a greater degree than expression in the duodenum and jejunum with an average concentration of 4.6 ± 1.6 fmol/sample (average n=4 animals ± SEM) (appendix 9.2, figure 4.4) with no significant difference being apparent between any region of the small intestine and the colon. Colonic mRNA expression levels appear to lie at a similar level to those measured in the duodenum/jejunum when taking into account the observed inter-animal variation.

Mrp2 expression shows greater inter-animal variation along the length of the small intestine than was observed with Mdr1a, with mRNA expression concentrations of 8.8 ± 2.0, 14.8 ± 2.9 and 14.5 ± 5.5 fmol/sample in the duodenum, jejunum and ileum respectively (average n=4 animals ± SEM). No significant difference in mRNA expression levels was measured between any two regions of the small intestine although data does suggest an increase in mRNA

expression levels toward the distal end of the small intestine (appendix 9.2/figure 4.4). In agreement with human MRP2 expression (Englund et al., 2006, Langmann et al., 2003, Zimmermann et al., 2005), Mrp2 mRNA is lacking in the rat colon with no significant difference between colonic Mrp2 and negative assay control values ($p = 0.62$). A significantly higher mRNA expression level is therefore measured in the duodenum and the jejunum compared with the colon ($^{\#}$ $p < 0.05$). Should inter-sample variation be reduced in the ileum, it is likely that a significant difference in Mrp2 expression between rat ileum and colon samples would also be evident. In comparison to other transporters Mrp2 mRNA expression levels rank highly along the length of the small intestine (appendix 9.2). High mRNA expression is somewhat surprising given the inability to detect Mrp2 protein expression in the rat intestine using immunohistochemistry (chapter 5).

In agreement with data reported by Englund et al., (2006) Bcrp mRNA expression levels were found to be much higher than corresponding levels of both Mdr1a and Mrp2 in all intestinal regions, with decreased variation between samples being observed (appendix 9.2 and 9.3). Inter-animal variation in the ileum is however still substantial (approximately 18%) (figure 4.4). Bcrp mRNA expression is ranked highest of all the ABC transporters studied in all regions of the small intestine and is lower than only Mrp3 expression in the colon (appendix 9.2 and 9.3). High mRNA expression levels of Bcrp compared with other transporters indicates an important role for Bcrp in rat intestinal physiology. As observed with Mrp2, Bcrp expression is shown to increase from the duodenum to ileum with mRNA expression concentrations of 24.2 ± 2.9 and 46.4 ± 8.4 fmol/sample (average n=4 animals ± SEM) for the duodenum and ileum respectively (• $p < 0.05$) (appendix 9.2). Furthermore, a significant decrease in expression is apparent from the jejunum and ileum to the colon ($^{\#}$ $p < 0.05$).

With regards to crypt-villus expression of Mdr1a, Mrp2 and Bcrp, all three transporters show higher mRNA expression levels in villus tip than crypt samples, however only Bcrp shows a significant increase in expression (** $p < 0.01$) (appendix 9.3/figure 4.5). It is likely that the lack of significance between villus tip and cryptal mRNA expression levels is apparent due to observed variation in mRNA expression levels within each region. Increasing animal numbers may therefore draw observed differences between villus tip and crypt mRNA expression levels of Mdr1a and Mrp2 into significance by reducing inter-region variation. Average expression levels in the villus tip region are 51.5 ± 13.2, 45.9 ± 14.8 and 144.7 ± 16.4 fmol/sample for Mdr1a, Mrp2 and Bcrp respectively (average n=4 animals ± SEM) (appendix 9.3/figure 4.5), with Bcrp showing significantly higher expression than Mdr1a and Mrp2 (** $p < 0.01$). Bcrp expression in the ileal crypt region is also higher than that of Mdr1a and Mrp2, as reflected by the decreased fold change (appendix 9.3, figure 4.5). Fold change values of 3.8 ± 0.9, 4.4 ± 1.3

and 3.2 ± 0.7 were calculated for Mdr1a, Mrp2 and Bcrp respectively. Inter-animal variation is however high with regards to cryptal Bcrp expression, with measured mRNA concentrations ranging from 35.3 to 84.3 fmol/sample (average n=4 animals ± SEM) (appendix 9.3). Without further information on protein expression and localisation this data would suggest that in the small intestine Bcrp function would be of paramount importance, followed by Mrp2 and Mdr1a in succession. In the colon order of importance would be Bcrp > Mdr1a > Mrp2.

In addition to Mdr1a, Mrp2 and Bcrp evidence suggests a potential role for other members of the MRP family of proteins in intestinal drug disposition (Deeley et al., 2006). mRNA expression levels of Mrp1, -3, -4, -5, -6 and 7 were therefore determined both along the length of the rat intestine and across the crypt-villus axis as shown in appendices 9.2 and 9.3. Expression levels of Mrp1 were low throughout the small intestine, with average expression reaching only 2.6 ± 0.7, 2.0 ± 0.2 and 2.5 ± 0.3 fmol/sample in the duodenum, jejunum and ileum respectively (average n=4 animals ± SEM) (appendix 9.2). Limited variation was observed between animals suggesting a consistent low level of Mrp1 mRNA in rat small intestine. Significantly higher Mrp1 concentrations (5.60 ± 1.45 fmol/sample) were shown in the colon ($^{\#}$ $p < 0.05$, $^{\#\#\#}$ $p < 0.01$ and $^{\#\#\#}$ $p < 0.001$ for the duodenum, jejunum and ileum respectively), indicating potential for a physiological role of this transporter in the large intestine.

Remarkably consistent expression levels of Mrp3 were detected in duodenum, jejunum and ileum rat mucosal scrapes with concentrations of 8.0 ± 0.7, 7.3 ± 0.3 and 9.3 ± 2.5 fmol/sample respectively (average n=4 animals ± SEM) (appendix 9.2, figure 4.6) as such no significant difference between mRNA expression levels in any two regions of the small intestine was observed for Mrp3 (figure 4.6). There is a significantly ($^{\#\#}$ $p < 0.01$) elevated expression of Mrp3 in the colon (41.8 ± 7.6 fmol/sample) compared to all regions of the small intestine (appendix 9.2/figure 4.6). Given its known basolateral localisation and ability to export glucoronide and glutathione conjugates within the cell to the blood (Borst et al., 2007, Borst et al., 2000) these high expression levels suggest a likely physiological role for this transporter in extruding conjugates from the epithelial cells of the colon into the underlying blood supply.

Mrp4 mRNA concentrations along the length of the intestine were very low, as such Mrp4 expression was concluded to be lacking in all regions of the intestine (appendix 9.2 and 9.3). Overall Mrp5 concentrations, like Mrp1, were low both in the small and large intestine with expression reaching a maximal concentration of 4.0 ± 0.5 fmol/sample in the colon (average n=4 animals ± SEM) (appendix 9.2). Although higher concentrations of Mrp6 were detected by NanoString analysis, considerable variation was observed between animals with detected concentrations of 12.6 ± 2.8, 13.0 ± 2.9 and 11.6 ± 2.3 fmol/sample (average n=4 animals ±

SEM) giving a standard error of approximately 20-25% total mRNA expression. As such no significant difference in Mrp6 expression was apparent between any two regions of the small intestine (appendix 9.2, figure 4.6). Colonic Mrp6 expression is virtually absent with a significant decrease in expression from the duodenum ($^{\#}$ $p < 0.05$), jejunum and ileum ($^{\#\#}$ $p < 0.01$) (appendix 9.2/figure 4.6). Mrp7 mRNA expression was below 5 fmol/sample in all regions of the small intestine and in the colon and showed a significant measured decrease from the jejunum and ileum to the colon ($^{\#}$ $p < .05$ and $^{\#\#}$ $p < 0.01$ respectively) (appendix 9.2).

All Mrp transporters show increased villus tip mRNA expression relative to that detected in the crypt. As with expression determined along the length of the intestine, villus tip and crypt concentrations of Mrp1 are low, with calculated average fold changes < 2 for villus tip versus crypt mRNA expression (* $p < 0.01$) (appendix 9.3). With an average fold difference of 5.5 ± 1.3, Mrp5 shows the greatest change with regards to crypt-villus expression profiles (** $p < 0.01$), with fmol/sample concentrations of 6.3 ± 0.9 and 1.3 ± 0.3 for villus tip and crypt respectively (average n=4 animals ± SEM) (appendix 9.3). Mrp7, Mrp6 and Mrp3 show decreasing fold difference values of 4.0 ± 0.7 (** $p < 0.01$), 3.9 ± 0.4 (* $p < 0.05$) and 2.0 ± 0.2 (** $p < 0.01$) between the villus tip and crypt region (appendix 9.3, figure 4.7), however it is Mrp6 which shows the greatest villus tip mRNA concentration at 36.3 ± 6.9 fmol/sample (appendix 9.3). High mRNA expression of Mrp6 in villus tip samples, indicates a potential role of this transporter in drug disposition, although levels of inter-animal variation were high (figure 4.7 and appendix 9.3). Mrp3 shows a 2-fold increase in expression from crypt to villus tip with fmol/sample concentrations of 9.6 ± 1.1 and 18.1 ± 1.0 (average n=4 animals ± SEM) in each respective region (figure 4.7, appendix 9.3).

Figure 4.4:

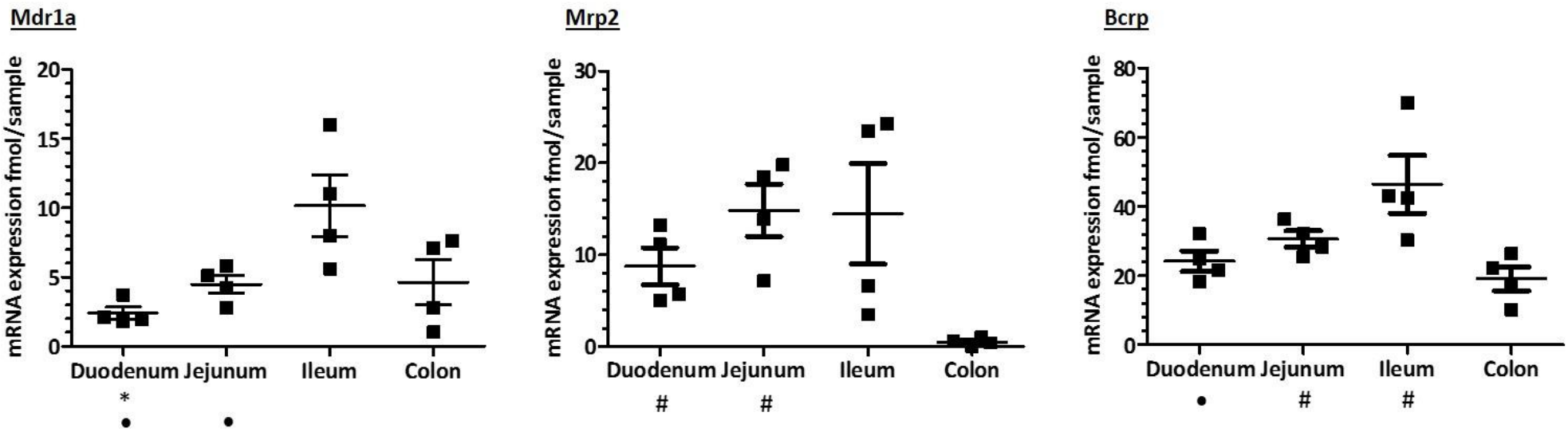

Figure 4.4 mRNA concentrations (fmol/sample) of Mdr1a, Mrp2 and Bcrp in the duodenum, jejunum, ileum and colon of the rat intestine.

Data show individual animal replicate mRNA concentrations (fmol/sample) with mean concentration ± SEM. mRNA expression values have been normalised against assay controls and expression levels of Gapdh, Hprt1 and Hmbs HSKP genes. Following assessment of regional population variance using Levene's test Student's t-test statistical analyses were performed, with Welche's correction applied where relevant, between different intestinal regions. Welche's correction removes the assumption of equal population variance of any two regions being compared, Welche's correction was therefore applied to prevent occurrence of false statistical significance. Resultant summary statistics are shown below the x-axis * $p < 0.05$ vs. jejunum, • $p < 0.05$ vs. ileum and # $p < 0.05$ vs. colon.

Figure 4.5:

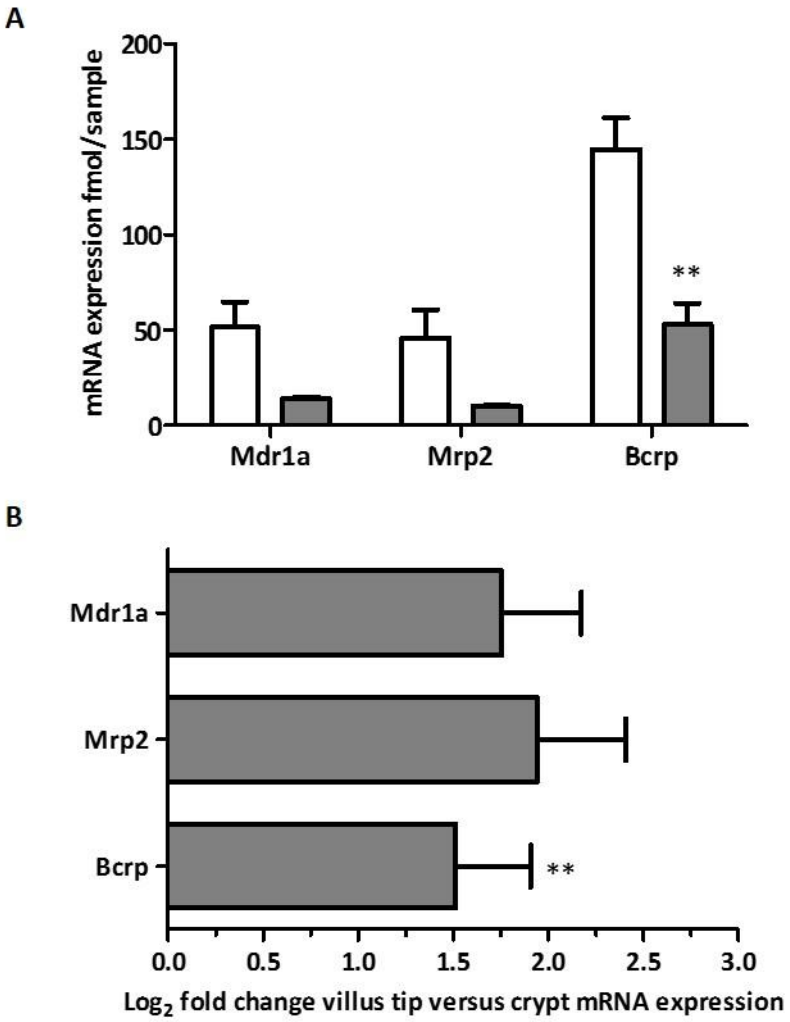

Figure 4.5 mRNA concentrations (fmol/sample) of Mdr1a, Mrp2 and Bcrp in the villus tip and crypt of rat ileum and log_2 fold change villus tip versus crypt.

(A) Mean mRNA concentrations (fmol/sample) measured in rat ileal villus tip (clear bars) and crypt (grey bars) fractions **(B)** Log_2 fold change villus tip versus crypt. Data show mean mRNA concentration from n=4 male rats ± SEM and have been normalised against assay controls and expression levels of Gapdh, Hprt1 and Hmbs HSKP genes. Statistical analyses show Student's t-test analysis with Welche's correction where required. ** $p < 0.01$ villus tip vs cryptal expression.

Figure 4.6:

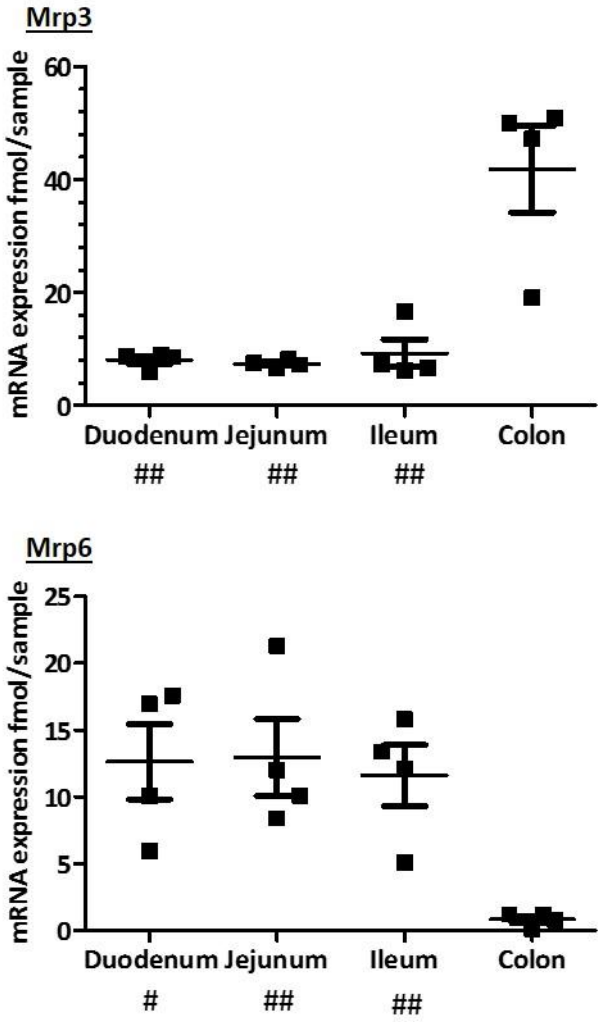

Figure 4.6 mRNA concentrations (fmol/sample) of Mrp3 and Mrp6 in the duodenum, jejunum, ileum and colon of the rat intestine.

Data show individual animal replicate mRNA concentrations (fmol/sample) with mean concentration ± SEM. mRNA expression values have been normalised against assay controls and expression levels of Gapdh, Hprt1 and Hmbs HSKP genes. Following assessment of regional population variance using Levene's test, Student's t-test statistical analyses were performed, with Welche's correction applied where relevant, between different intestinal regions. Welche's correction removes assumption of equal population variance of any two regions being compared and was applied to prevent occurrence of false statistical significance. Resultant summary statistics are shown below the x-axis, # $p < 0.05$ and ## $p < 0.01$ vs. colon.

Figure 4.7:

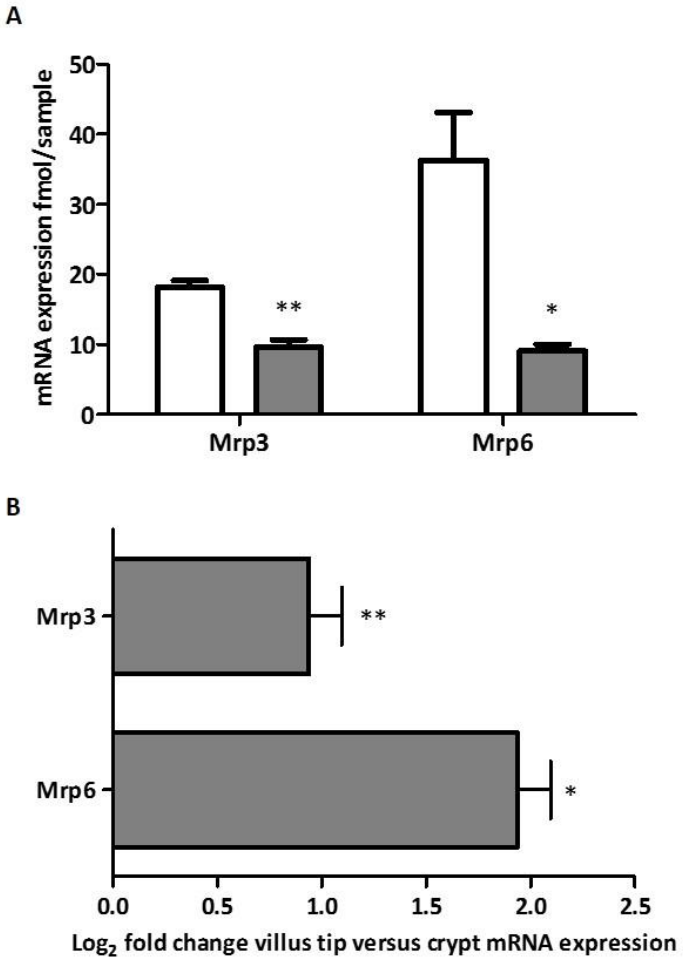

Figure 4.7 Average mRNA concentrations (fmol/sample) of Mrp3 and Mrp6 in the villus tip and crypt of rat ileum and log_2 fold change villus tip versus crypt.

(A) Average mRNA concentrations (fmol/sample) measured in rat ileal villus tip (clear bars) and crypt (grey bars) fractions. **(B)** Log_2 fold change villus tip versus crypt. Data show mean mRNA concentration from n=4 male rats ± SEM and have been normalised against assay controls and expression levels of Gapdh, Hprt1 and Hmbs HSKP genes. Statistical analyses show Student's t-test analysis with Welche's correction applied where required, * $p < 0.05$ and ** $p < 0.01$ villus tip vs cryptal expression.

4.3.4 Expression of selected SLC transporters in the intestine

In addition to expression of ABC transporters proposed to be involved in drug resistance mRNA expression levels of eight SLC transporters (PepT1, Oct1, Octn1, Octn2, Oat3, Cnt2, Oatp-3 and Oatp-b) were also investigated. Oat3 and Oatp-3 mRNA expression was found to be very low in the rat intestine with maximal concentrations of 0.9 ± 0.1 and 0.3 ± 0.0 fmol/sample respectively (appendix 9.2 and 9.3). No significant difference between Oat3 expression and negative controls was observed in crypt and duodenal samples nor between Oatp3 and negative controls in crypt, duodenal, jejunal and ileal samples ($p > 0.05$). As such it is concluded that mRNA expression is below the level of reasonable detection for these targets using NanoString technology and will not be discussed further.

Low level, but consistent, expression of Oatp-b was apparent from the proximal to distal small intestine and in the colon, with no significant difference observed between any two regions (appendix 9.2). Given such low levels of mRNA, and assuming equivalent translation of functional protein, it seems unlikely that Oatp-b contributes significantly to intestinal drug absorption in normal laboratory rats.

Expression levels of Cnt2 along the length of the small intestine were shown to be very high as would be expected for this important nucleoside uptake transporter (Gray et al., 2004), with average maximal jejunal expression of 192.6 ± 12.2 fmol/sample (average n=4 animals ± SEM) (appendix 9.2/figure 4.8). Data indicates one probable outlying value for Cnt2 expression in the ileum, as shown in figure 4.8, which is likely responsible for the large standard error observed between mRNA levels of Cnt2 within this region (129.1 ± 36.5 fmol/sample)(average n=4 animals ± SEM). There is a significantly reduced level of expression of Cnt2 mRNA in the colon compared with the duodenum, ($^{###}$ $p < 0.001$), jejunum ($^{###}$ $p < 0.001$) and ileum ($^{##}$ $p < 0.01$) respectively, in agreement with the known physiological role of this transporter in intestinal absorption of nucleoside analogues (Gray et al., 2004, Kis et al., 2009). Cnt2 mRNA was also measured at higher levels in the villus tip than in the crypt, with measured concentrations of 234.9 ± 60.3 and 50.9 ± 6.2 respectively, consistent with the role of this transporter in uptake of luminal nucleosides (Gray et al., 2004). A lack of significance is however apparent with regards to the crypt-villus expression profile of Cnt2 likely due to high levels of inter-animal variation in villus tip samples (appendix 9.3). Although lower than villus expression it should be noted that cryptal Cnt2 mRNA is still high in comparison with other transporters (appendix 9.3).

In contrast to other members of the SLC family investigated, Oct1 shows a non-significant decrease in mRNA expression levels from the duodenum to the jejunum and ileum with average concentrations of 11.1 ± 1.5, 9.5 ± 1.9 and 7.6 ± 0.9 fmol/sample in each respective region. A significant decrease in mRNA expression was apparent between all regions of the small intestine and the colon, with mRNA expression levels of only 1.8 ± 0.5 fmol/sample detected in this region (appendix 9.2/figure 4.8). Consistent with mRNA expression patterns of other transporters across the crypt-villus axis Oct1 showed a significant increase (* $p < 0.05$) in expression from the crypt to villus tip samples (5.9 ± 0.4 and 10.5 ± 1.2 fmol/sample respectively) (appendix 9.3/figure 4.9).

Expression levels of Octn1 were shown to increase from the duodenum to the jejunum (* $p < 0.05$) and from the duodenum to the ileum (•• $p < 0.01$) with mRNA concentrations of 3.7 ± 0.6, 6.5 ± 0.6 and 7.4 ± 0.6 fmol/sample (average n=4 animals ± SEM) in the duodenum, jejunum and ileum respectively (appendix 9.2). Colonic mRNA levels of Octn1 were significantly lower than those in all regions of the small intestine (appendix 9.2, figure 4.8). Whilst Octn2 also shows increasing mRNA expression levels from the duodenum to the jejunum and ileum a significant change in concentration was detected between the duodenum and ileum only (• $p < 0.05$), a significant decrease in expression was however observed between the jejunum and colon ($^{\#}$ $p < 0.05$) and the ileum and colon ($^{\#\#}$ $p < 0.01$) (appendix 9.2). As with the majority of target genes investigated, Octn1 (** $p < 0.01$) and Octn2 (* $p < 0.05$) were detected at higher concentrations in villus tip than the crypt samples (appendix 9.3/figure 4.9). Concentrations of Octn1 and Octn2 in villus tip samples were 18.7 ± 3.5 and 84.9 ± 15.9 fmol/sample and cryptal mRNA concentrations were 6.7 ± 0.3 and 16.3 ± 1.2 fmol/sample (average n=4 animals ± SEM). Expression levels of Octn2 therefore exceed those of Octn1 in all intestinal segments, particularly in the colon where Octn1 expression is virtually absent.

PepT1 mRNA expression was shown to increase from the duodenum to the jejunum (* $p < 0.05$) and from the duodenum to the ileum (• $p < 0.05$) with a significant decrease in expression measured between all regions of the small intestine and colon ($^{\#\#\#}$ $p < 0.01$ duodenum and ileum vs. colon and $^{\#\#}$ jejunum vs. colon) (appendix 9.2). Villus tip mRNA expression showed a significant 3.9 ± 0.9 fold increase (** $p < 0.01$) compared with those levels measured in crypt samples (143.2 ± 19.8 villus tip versus 43.0 ± 9.1 fmol/sample in the crypt, average n=4 animals ± SEM) (appendix 9.3/figure 4.9).

Figure 4.8:

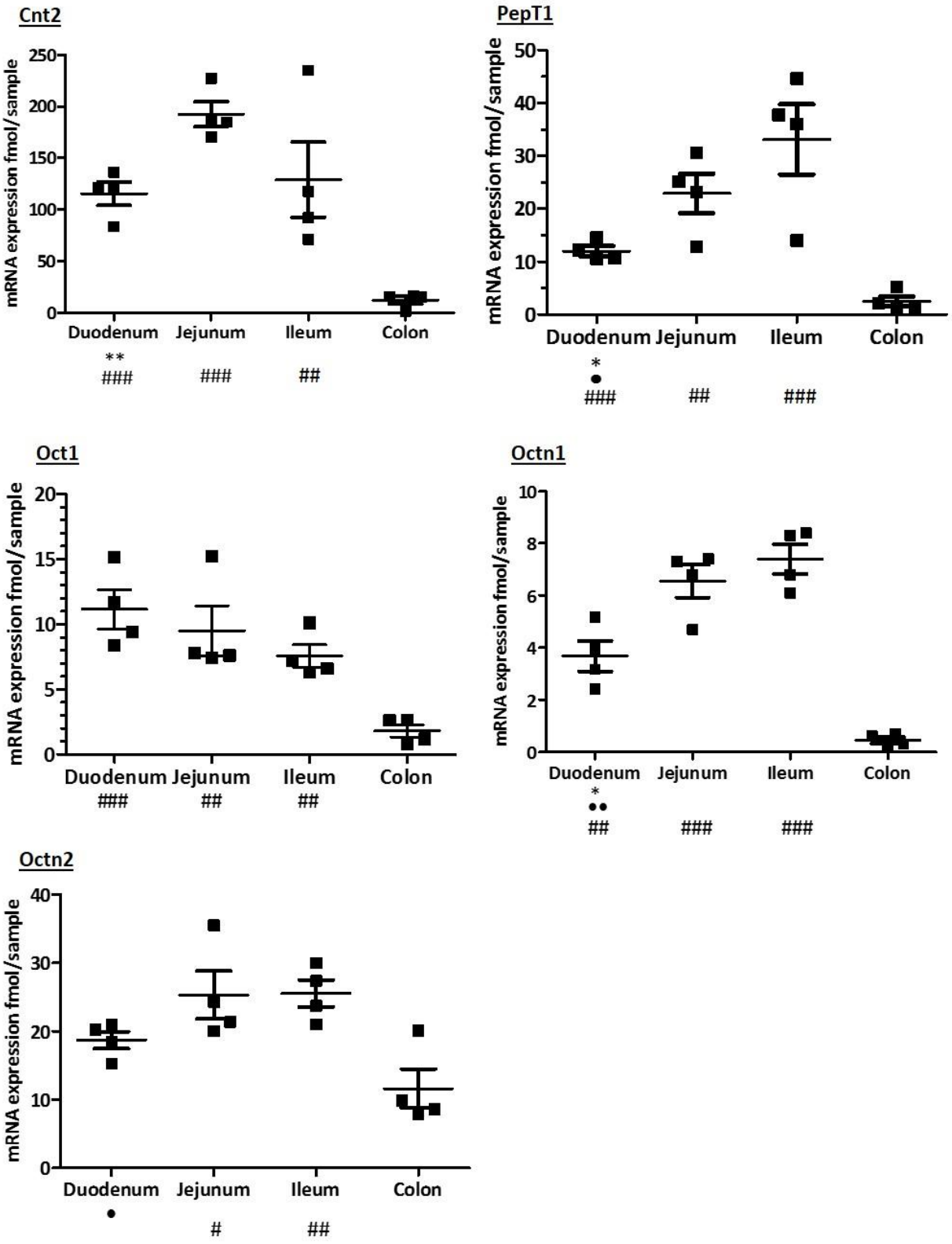
Cnt2
mRNA expression fmol/sample
250
200
150
100
50
0
Duodenum
Jejunum
Ileum
Colon
**
###
###
##
PepT1
mRNA expression fmol/sample
50
40
30
20
10
0
Duodenum
Jejunum
Ileum
Colon
*
###
##
###
Oct1
mRNA expression fmol/sample
20
15
10
5
0
Duodenum
Jejunum
Ileum
Colon
###
##
##
Octn1
mRNA expression fmol/sample
10
8
6
4
2
0
Duodenum
Jejunum
Ileum
Colon
*
##
###
###
Octn2
mRNA expression fmol/sample
40
30
20
10
0
Duodenum
Jejunum
Ileum
Colon
#
##

Figure 4.8 mRNA concentrations (fmol/sample) of selected SLC family transporters in the duodenum, jejunum, ileum and colon of the rat intestine.

Data show individual animal replicate mRNA concentrations (fmol/sample) with mean concentration ± SEM. mRNA expression values have been normalised against assay controls and expression levels of Gapdh, Hprt1 and Hmbs HSKP genes. Following assessment of regional population variance using Levene's test, Student's t-test statistical analyses were performed, with Welche's correction applied where relevant, between different intestinal regions. Welche's correction removes assumption of equal population variance of any two regions being compared and was applied to prevent occurrence of false statistical significance. Resultant summary statistics are shown below the x-axis, * $p < 0.05$, ** $p < 0.01$ vs. jejunum, • $p < 0.05$, •• $p < 0.01$ vs. ileum, # $p < 0.05$, ## $p < 0.01$ and ### $p < 0.001$ vs. colon.

Figure 4.9:

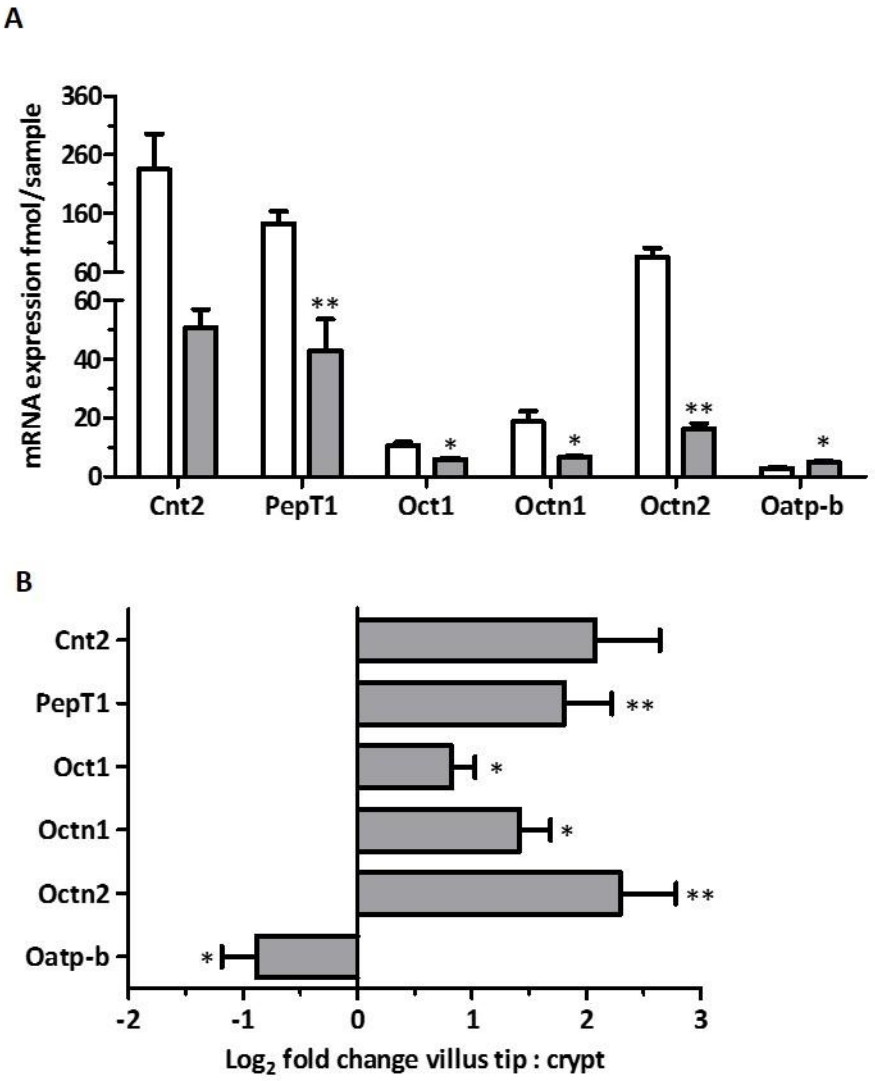

Figure 4.9 mRNA concentrations (fmol/sample) of SLC transporters in villus tip and crypt regions and log_2 fold change villus tip versus crypt.

(A) Mean mRNA concentrations (fmol/sample) measured in rat ileal villus tip (clear bars) and crypt fractions (grey bars) **(B)** Log_2 fold change villus tip versus crypt. Data show mean mRNA concentration from n=4 male rats ± SEM and have been normalised against assay controls and expression levels of Gapdh, Hprt1 and Hmbs HSKP genes. Statistical analyses show Student's t-test analysis with Welche's correction where required, * $p < 0.05$ and ** $p < 0.01$ villus tip vs cryptal expression.

4.3.5 Cytochrome P450 enzymes; intestinal expression patterns

The rat Cyp3a9 enzyme is homologous to human CYP3A4 which is indicated to be the most important CYP450 enzyme with regards to drug metabolism (Shin et al., 2009). We detected high mRNA expression of Cyp3a9 along the longitudinal and crypt-villus intestinal axes (appendix 9.2 and 9.3). Cyp3a9 showed highest mRNA concentration of all target genes investigated in the present study with a maximum average expression level of 389.7 ± 17.0 in the jejunum (average n=4 animals ± SEM). As such expression levels of Cyp3a9 are significantly higher than all other Cyp3a family members in all regions of the small intestine (* $p < 0.05$) (appendix 9.2 and 9.2). Measured mRNA concentrations for Cyp3a9 in the duodenum, jejunum, ileum and colon were 183.7 ± 22.7, 389.7 ± 17.0, 300.5 ± 99.7 and 121.0 ± 23.6 fmol/sample (average n=4 animals ± SEM) (appendix 9.2, figure 4.10). A highly significant difference in Cyp3a9 expression was measured between the duodenum and jejunum (*** $p < 0.001$) and between the jejunum and colon ($^{###}$ $p < 0.001$). Whilst inter-animal variation was apparent in the duodenum, jejunum and colon, ileal samples showed greatest variation in detected Cyp3a9 concentrations (SEM of approximately 30% of mean mRNA expression, figure 4.10). Observed variation is such that it was not possible to determine a predictive trend of Cyp3a9 expression in the small intestine. The reason for this segment specific variation is currently unknown, other than to note that Cyp3a9, like CYP3A4, may be highly inducible and subject to inter-individual variation in expression (Aiba et al., 2005, Martignoni et al., 2006, Matsubara et al., 2004).

In addition to Cyp3a9, current literature indicates Cyp3a1/3a23, Cyp3a18 and Cyp3a62 to be important in drug metabolism (Matsubara et al., 2004). Originally believed to encode two cytochrome P450 isoforms the Cyp3a1 and Cyp3a23 gene products were later shown to be identical by sequence analysis (Matsubara et al., 2004). Given the high level of sequence homology between Cyp3a1 and 3a2 it was not possible to design NanoString probes specific to the 3a1 isoform, as such the final probes used target Cyp3a1/3a23 (100% homology) and Cyp3a2 (93% homology). However, we failed to detect mRNA expression (< 0.20 fmol/sample) of Cyp3a1/3a23/3a2 in any region of the rat intestine studied and therefore conclude these genes to be below the level of detection for NanoString technology under non-inducing conditions. Similarly, Aiba et al., (2004) reported expression of Cyp3a2 in the liver but not in the intestine of male rats whilst Matsubara et al., (2004) did not detect Cyp3a1/3a23 expression in rat intestine using RT-PCR (reverse transcription polymerase chain reaction). The possibility of increased mRNA concentrations following exposure to xenobiotics cannot however be excluded.

Cyp3a18 and Cyp3a62 show increasing expression from the proximal to distal small intestine however no significant difference was apparent between regions of the small intestine except for Cyp3a18 between the duodenum and ileum (• $p < 0.05$), with substantial variation in mRNA expression being observed in all regions of the small intestine for both genes (appendix 9.2/ figure 4.10). A significant decrease in Cyp3a18 and Cyp3a62 mRNA concentration was measured between the jejunum and colon and between the ileum and colon (appendix 9.2).

All three detected metabolising enzymes, Cyp3a9, 3a18 and 3a62 were expressed at a significantly higher level in villus tip than crypt samples (appendix 9.3/figure 4.11) in agreement with increasing expression due to epithelial differentiation as epithelial cells migrate up the crypt-villus axis (Barker et al., 2008). Villus to crypt fold differences for Cyp3a9, 3a62 and 3a18 are 9.6 ± 3.1, 5.1 ± 1.4, and 4.2 ± 1.0 respectively with the high SEM value of Cyp3a9 reflecting inter-animal variation in mRNA expression (appendix 9.3/figure 4.11). High mRNA concentrations were measured in villus tip samples for Cyp3a18, Cyp3a62 and Cyp3a9 (89.0 ± 11.1, 179.3 ± 44.9 and 446.2 ± 104.3 fmol/sample, average n=4 animals ± SEM, appendix 9.3). Should mRNA expression be translated to functional protein, high levels of villus tip activity will ultimately increase interaction between the enzyme and substrates present within the lumen of the intestine thereby promoting metabolism of orally ingested compounds. Crypt mRNA expression levels were 25.9 ± 7.1, 37.3 ± 2.6 and 60.8 ± 16.1 fmol/sample (average n=4 animals ± SEM) for Cyp3a18, 3a62 and 3a9 respectively (appendix 9.3). As such mRNA concentrations of these Cyp450 enzymes exceed detected expression levels of other Cyp450 genes in the crypt region, indicating a potential functional role for these Cyp3a enzymes in crypt drug metabolism.

mRNA expression levels of several other P450 enzymes suggested to be expressed in the intestine were also determined. As with Cyp3a1 and Cyp3a2, Cyp2c6v1 and Cyp2c7 show high levels of sequence homology and as such the NanoString probes targeted against Cyp2c6v1 (100% homology) also target Cyp2c7 with 85% homology. Of those cytochrome P450 enzymes included in our NanoString codeset Cyp2c11, Cyp2c6v1/Cyp2c7 and Cyp2d3 in addition to Cyp3a1/3a23 discussed earlier were below the limit of detection using the NanoString technology (appendix 9.2). With regards to expression patterns many of the remaining Cyp450 enzymes analysed showed a very similar trend to Cyp3a9, with an increasing expression from the duodenum to jejunum and an approximately equal expression level between the jejunum and ileum, although significance is limited between regions of the small intestine and it is noted that some genes show considerable inter-animal variation (appendix 9.2). Colonic Cyp450 expression was generally found to be low (appendix 9.2/figure 4.12). Of interest is the significant rise in colonic expression of the Cyp2d1/2d9 enzyme ($^{\#\#}$ $p < 0.01$) with mRNA

concentrations of 5.0 ± 0.5, 6.5 ± 0.9, 3.9 ± 0.7 and 31.2 ± 5.3 fmol/sample ± SEM (average n=4 animals ± SEM) for the duodenum, jejunum, ileum and colon respectively. Cyp2d1/2d9 therefore, in combination with Cyp3a9 and Cyp3a62, appears to account for the majority of Cyp450 expression in the colon. Given that expression levels of Cyp3a9 and Cyp3a62 are high throughout the entire length of the intestine the rise in mRNA expression of Cyp2d1/2d9 in the colon suggests an important role of this enzyme in colon physiology. Unlike other Cyp450 enzymes Cyp2j4 expression remains constant along the length of the small intestine with mRNA concentrations of 22.2 ± 4.5, 25.8 ± 3.8 and 25.1 ± 5.6 in the duodenum, jejunum and ileum (appendix 9.2), however caution should be exercised in extrapolating mRNA levels to those of translated protein.

Other than those Cyp450 enzymes deemed to be absent from the rat intestine (Cyp2c11, Cyp2c6v1, Cyp2d3 and Cyp3a1/3a23) all Cyp450 enzymes investigated, except for Cyp2s1, show significantly increased villus tip mRNA expression compared with mRNA concentrations detected in the crypt (appendix 9.3). All Cyp450 enzymes (other than Cyp3a18) show greater than a 5-fold increase in mRNA expression from the ileal crypt to the villus tip (appendix 9.3), indicating a substantial rise in expression to result from epithelial cell differentiation. Villus tip and crypt mRNA concentrations and $\log_2$ fold differences of selected Cyp450 enzymes are shown in figure 4.13.

Quantitative measurement of mRNA expression levels of key genes involved in drug disposition has been performed and reported here. In addition to determination of expression levels along the length of the intestine we have characterised differences in expression between the crypt and villus tip regions. The majority of target genes investigated showed increased villus tip mRNA concentrations in line with increased expression due to epithelial cell differentiation on migration from the crypt to villus tip (Barker et al., 2008). Expression of Mdr1a, Mrp2 and Bcrp mRNA was identified in ileal crypt samples, supporting the earlier hypothesis of a physiological protective mechanism of ABC transporters within this region. Similarly, Cyp450 mRNA was detected in the crypt region indicating potential for ABC transporter: Cyp450 interplay.

Figure 4.10:

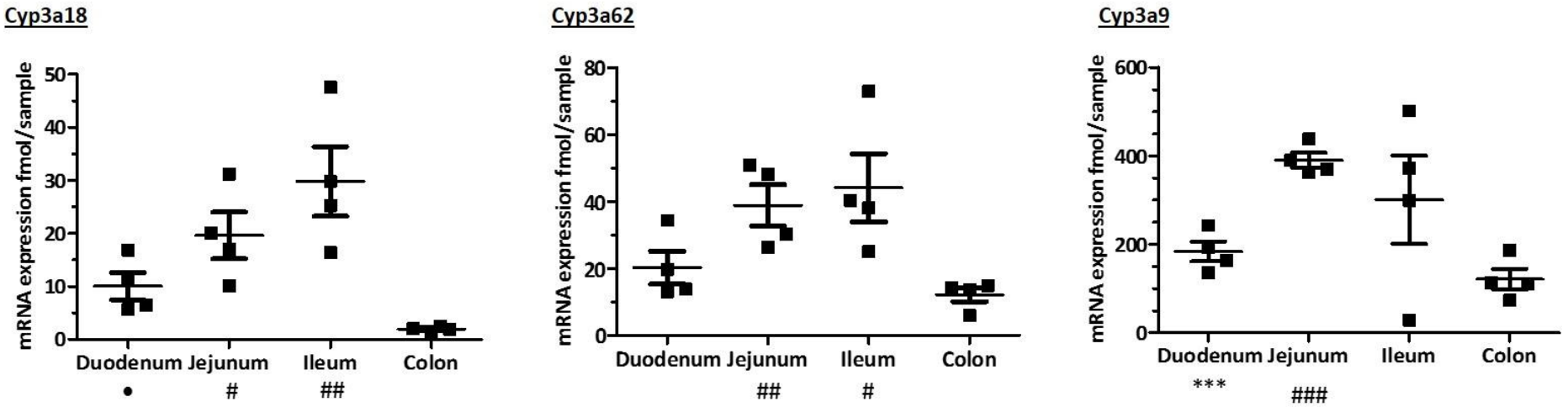

Figure 4.10 mRNA concentrations (fmol/sample) of Cyp3a18, Cyp3a62 and Cyp3a9 in the duodenum, jejunum, ileum and colon of the rat intestine.

Data show individual animal replicate mRNA concentrations (fmol/sample) with mean concentration ± SEM. mRNA expression values have been normalised against assay controls and expression levels of Gapdh, Hprt1 and Hmbs HSKP genes. Following assessment of regional population variance using Levene's test, Student's t-test statistical analyses were performed, with Welche's correction applied where relevant, between different intestinal regions and resultant summary statistics are shown below the x-axis, *** $p < 0.001$ vs. jejunum, • $p < 0.05$ vs. ileum, # $p < 0.05$, ## $p < 0.01$ and ### $p < 0.001$ vs. colon. Welche's correction removes assumption of equal population variance of any two regions being compared and was applied to prevent occurrence of false statistical significance.

Figure 4.11:

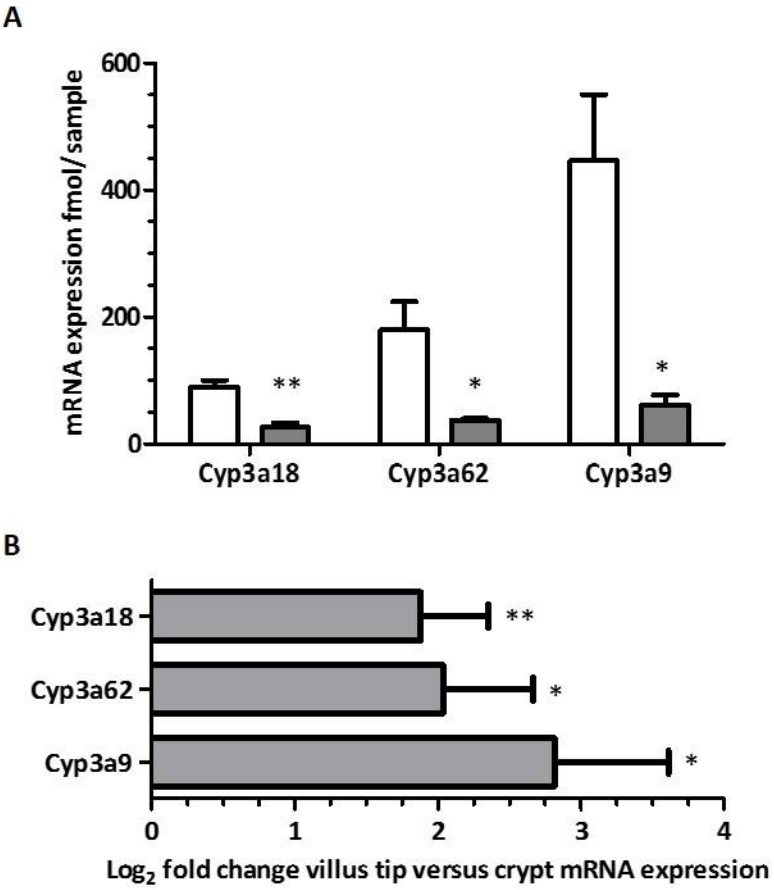

Figure 4.11 mRNA concentrations (fmol/sample) of Cyp3a18, Cyp3a62 and Cyp3a9 in villus tip and crypt of rat ileum and log_2 fold change villus tip versus crypt.

(A) Mean mRNA concentrations (fmol/sample) measured in rat ileal villus tip (clear bars) and crypt (grey bars) fractions **(B)** Log_2 fold change villus tip versus crypt. Data show mean mRNA concentration from n=4 male rats ± SEM and have been normalised against assay controls and expression levels of Gapdh, Hprt1 and Hmbs HSKP genes. Student's t-test analysis, with Welche's correction applied where required, * $p < 0.05$ and ** $p < 0.01$ villus tip vs cryptal expression.

Figure 4.12:

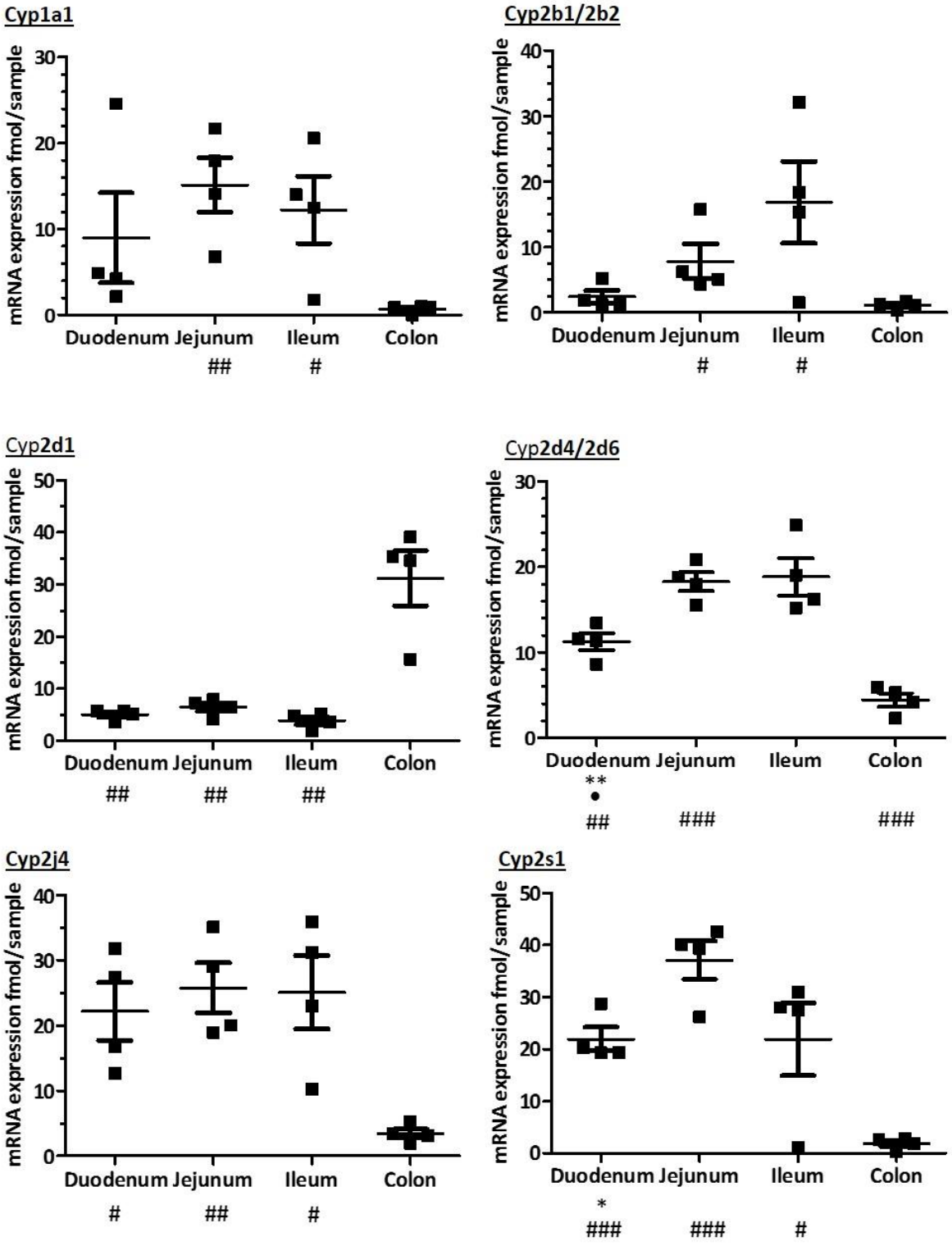
Cyp1a1
mRNA expression fmol/sample
30
20
10
0
Duodenum Jejunum Ileum Colon
#
Cyp2b1/2b2
mRNA expression fmol/sample
40
30
20
10
0
Duodenum Jejunum Ileum Colon
# #
Cyp2d1
mRNA expression fmol/sample
50
40
30
20
10
0
Duodenum Jejunum Ileum Colon
##
Cyp2d4/2d6
mRNA expression fmol/sample
30
20
10
0
Duodenum Jejunum Ileum Colon
** ## ### ###
Cyp2j4
mRNA expression fmol/sample
40
30
20
10
0
Duodenum Jejunum Ileum Colon
#
Cyp2s1
mRNA expression fmol/sample
50
40
30
20
10
0
Duodenum Jejunum Ileum Colon
* ### ### #

Figure 4.12 mRNA concentrations (fmol/sample) of Cyp1a1, Cyp2b1/2b2, Cyp2d1/2d9, Cyp2d4/2d6, Cyp2j4, Cyp2s1 in the duodenum, jejunum, ileum and colon of the rat intestine

Data show individual animal replicate mRNA concentrations (fmol/sample) with mean concentration ± SEM. mRNA expression values have been normalised against assay controls and expression levels of Gapdh, Hprt1 and Hmbs HSKP genes. Following assessment of regional population variance using Levene's test, Student's t-test statistical analyses were performed, with Welche's correction applied where relevant, between different intestinal regions and resultant summary statistics are shown below the x-axis, * $p < 0.05$ and ** $p < 0.01$ vs. jejunum, • $p < 0.05$ vs. ileum, # $p < 0.05$, ## $p < 0.01$ and ### $p < 0.001$ vs. colon. Welche's correction removes assumption of equal population variance of any two regions being compared, where statistical result was < 0.05 Welche's correction was applied to prevent occurrence of false statistical significance.

Figure 4.13:

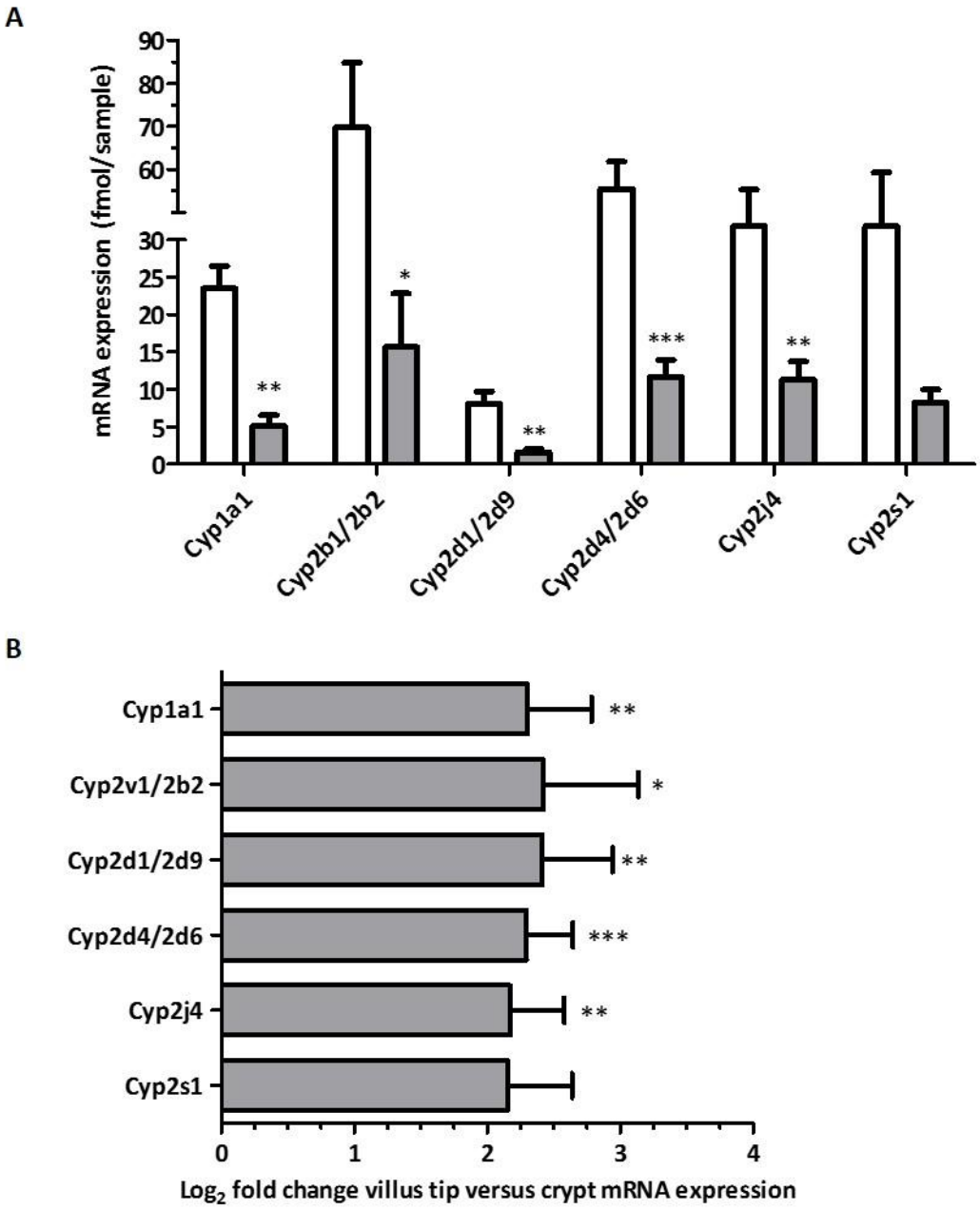

Figure 4.13 mRNA concentrations (fmol/sample) of cytochrome P450 enzymes in villus tip and crypt of rat ileum and log_2 fold change villus tip versus crypt.

(A) Mean mRNA concentrations (fmol/sample) measured in rat ileal villus tip (clear bars) and crypt (shaded bars) fractions **(B)** Log_2 fold change villus tip versus crypt. Data show mean mRNA concentration from n=4 male rats ± SEM and have been normalised against assay controls and expression levels of Gapdh, Hprt1 and Hmbs HSKP genes. Student's t-test analysis, with Welche's correction applied where required, * $p < 0.05$, ** $p < 0.01$ and *** $p < 0.001$ villus tip vs cryptal expression.

4.4 Discussion

Despite the existence of numerous alternative administration routes, oral drug delivery remains the preferred route due to low cost and high levels of patient compliance resulting from ease of administration (Chawla and Bansal, 2003, Gomez-Orellana, 2005, Sastry et al., 2000). Furthermore, formulation of orally active pharmaceuticals allows for versatility with regards to the type of drug candidate being delivered (Sastry et al., 2000). Given the complexity of oral dosing it has thus far proven difficult to rectify poor bioavailability associated with some drug compounds. Drug compound physiochemical properties, particularly lipophilicity, molecular size, pH dependent solubility and extent of drug compound ionisation contribute to determination of drug bioavailability (Chawla and Bansal, 2003). The physiochemical properties of a drug compound such as solubilisation and stability in regions of altered pH directly influences intestinal site specific absorption, with many drugs showing a non-uniform absorption rate along the intestine (Chawla and Bansal, 2003). In addition to pH, regional expression of drug transporters and cytochrome P450 enzymes within the intestinal enterocyte barrier will influence intestinal drug absorption and hence systemic drug concentration, discussed in chapter 1 (Chawla and Bansal, 2003).

Apical expression of ABC transporters, MDR1, MRP2 and BCRP, which are known to confer drug resistance, on the brush border membrane of intestinal enterocytes lining the lumen has the potential to lower drug bioavailability and increase intestinal elimination (Chan et al., 2004, Szakacs et al., 2008). MDR1, MRP2 and BCRP utilise energy generated by ATP hydrolysis to efflux orally administered substrates against their concentration gradient out of the enterocyte and into the intestinal lumen (Szakacs et al., 2008). Furthermore, intestinal expression of functionally active CYP450 enzymes has been shown to contribute significantly to extrahepatic intestinal metabolism and hence 'first pass metabolism' of drug compounds (Paine et al., 2006). Given the recognised overlap in ABC transporter and CYP450 enzyme substrates, and their ability to act synergistically to lower intestinal drug absorption (Benet, 2009, Chawla and Bansal, 2003), it is vital to obtain a complete understanding of drug transporter and CYP450 enzyme expression patterns in the intestine. Gaining an understanding of expression patterns both at an mRNA transcript and protein level may allow for production of oral drug compounds with increased bioavailability and help to ensure achievement of desired therapeutic systemic concentrations. Potential for the formulation of drugs with dissolution properties reliant on pH may ultimately allow drug absorption in regions of lower drug transporter/enzyme expression, thereby increasing drug bioavailability. Given the high use of rats in pre-clinical drug studies RNA expression patterns of key intestinal drug transporters and cytochrome P450 enzymes in the mucosa of the duodenum, jejunum, ileum and colon of male

rat intestine have been determined here. To assess how transporter and cytochrome P450 expression profiles are altered as a result of enterocyte differentiation (Barker et al., 2008) mRNA expression levels across the crypt-villus axis were also investigated.

In addition to determination of currently unknown mRNA expression levels of drug transporters and cytochrome P450 enzymes in the rat intestine we replicated literature reported expression patterns of several experimental control genes using NanoString technology along both the longitudinal and crypt-villus axes (section 4.3). The ability to reproduce previously published expression patterns strongly indicates NanoString mRNA technology to be a robust technique for determination of currently unknown target gene expression profiles.

Current understanding with regards to intestinal ABC transporter expression patterns is limited, with conflicting data presented by different laboratories and between species (section 4.1). Of particular interest with regards to intestinal drug resistance are MDR1, MRP2 and BCRP due to their reported apical localisation and ability to transport and confer resistance to a wide range of drug substrates (Chan et al., 2004, Szakacs et al., 2008). Studies performed using human tissue have shown increased expression of MDR1 from the proximal to distal small intestine (Berggren et al., 2007) although murine mRNA expression data determined using gene affymetrix showed consistent Mdr1a expression levels in all four regions of the intestine (Mutch et al., 2004), with Chianale et al., (1995) reporting a lack of murine duodenal Mdr1 expression thus highlighting discrepancies between reported data sets. Of the two Mdr1 isoforms expressed in rat, Mdr1a and Mdr1b (Zhou et al., 2001), Mdr1b mRNA transcript expression was not detected along the length of the gastrointestinal tract suggesting Mdr1a alone to be the isoform which contributes to intestinal drug resistance in the rat.

Similar to expression of MDR1 in human tissues, rat intestinal Mdr1a expression was shown to increase from the duodenum to the ileum (Berggren et al., 2007, Englund et al., 2006). NanoString data presented here is in agreement with qPCR data published by our laboratory which also showed increased expression of Mdr1 in rat intestine from the duodenum to the jejunum and ileum, and decreased expression in the colon (Haslam et al., 2011). Furthermore, as reported previously, decreased mRNA expression was measured in colon samples when compared with mRNA expression in the ileum (Blokzijl et al., 2007, Englund et al., 2006, Haslam et al., 2011, Zimmermann et al., 2005). Replication of reported human MDR1 expression patterns along the length of the rat intestine therefore supports the use of rats in preclinical screening of potential drug compounds. Immunolocalisation studies have previously shown immunoreactivity of anti-MDR1 antibodies at the apical membrane of villus enterocytes (Blokzijl et al., 2007, Glaeser et al., 2007), with our laboratory reporting similar findings in the

Caco2 cell line (Haslam, 2007). Furthermore, detection of MDR1 protein at the apical cell membrane of MDCKII-MDR1 transfected cells using immunocytochemistry is shown in chapter 5. It is therefore accepted that MDR1 localises to the apical membrane of intestinal enterocytes thus allowing efflux of drug compounds into the intestinal lumen. Our data show increased mRNA expression levels at the villus tip, therefore assuming translation to functional protein mRNA expression levels reported here support the role of Mdr1a in rat intestinal drug resistance.

Similar trends of mRNA expression were observed for Mrp2 and Bcrp. In contrast to low level MRP2 mRNA levels reported in human intestinal samples (Englund et al., 2006, Langmann et al., 2003, Zimmermann et al., 2005) higher levels of Mrp2 mRNA expression were detected in all regions of the small intestine than were observed for Mdr1a. Mrp2 mRNA was detected in all regions of the rat small intestine with a non-significant increase in expression observed from the duodenum to the jejunum in agreement with data reported previously (Englund et al., 2006, Langmann et al., 2003, Zimmermann et al., 2005). Ileal Mrp2 expression was approximately equal to that detected in the jejunum. Our data in the rat support the lack of colonic MRP2 mRNA expression reported by Englund et al., (2006) who found a 100-fold decrease in expression between the terminal ileum and colon of human subjects, with similar findings also reported by others (Langmann et al., 2003). We failed to determine a significant difference between expression of colonic Mrp2 mRNA in the rat and expression levels of negative controls included within the NanoString codeset, strongly indicating Mrp2 mRNA expression to be below the limit of NanoString detection within this region.

In agreement with data presented by Englund et al., (2006) who showed BCRP to be expressed at higher levels than MDR1 and MRP2 in human duodenum, jejunum, ileum and colon biopsies, Bcrp was found to be the highest expressed member of the ABC transporters investigated in all regions of the small intestine, with significantly increased expression compared to Mdr1a and Mrp2 in villus tip samples. Conflicting data reported by Gutmann, (2005) however shows human MDR1 mRNA expression to exceed that of BCRP in human duodenal tissues. Discrepancies between existing literature and mRNA expression profiles presented here are likely to represent a combination of experimental and inter-individual variation and species differences in transporter expression levels.

The current study shows increased Bcrp mRNA expression from the duodenum to ileum of the small intestine, with lowest levels of expression detected in the colon although it is noted that colonic mRNA expression does not differ significantly from levels measured in the duodenum. In agreement with data shown here our laboratory have previously reported increasing Bcrp mRNA expression in rat tissues from the duodenum to ileum, with a fall in colonic mRNA using

qPCR (Haslam et al., 2011). In addition to rat expression data, investigations performed in human tissues show increased human BCRP mRNA expression in duodenal samples relative to that in the colon (Gutmann et al., 2005, Hilgendorf et al., 2007) whilst Englund et al., (2006) show ileal mRNA expression to be greater than that in the duodenum in human samples. Increased BCRP mRNA expression in the ileum compared with the duodenum in human samples is in agreement with mRNA expression data in the rat presented here. Similarly both data presented here and by Englund et al., 2006 show a decreased colonic expression of Bcrp/BCRP mRNA to levels similar to those measured in duodenal samples when taking into account sample variation.

Expression of Mdr1a, Mrp2 and Bcrp in all regions of the small intestine, with a significant increase in expression observed from the crypt to the villus tip, supports the role of these transporters in intestinal drug resistance (Szakacs et al., 2008). Assuming direct correlation between mRNA expression and functional protein activity, data presented here suggests Bcrp to be of substantial importance in protection against invasion from potentially toxic xenobiotics and in determination of pharmacokinetic drug profiles. Furthermore mRNA expression of Bcrp, Mdr1a and Mrp2 within isolated crypt samples may indicate a currently unrecognised role for these transporters in protection of this undifferentiated region.

Although shown to mediate drug resistance in target tissues (Kruh and Belinsky, 2003), less literary emphasis is placed upon remaining members of the MRP family, likely due to reduced substrate profiles and/or basolateral transporter expression in intestinal enterocytes (Borst et al., 2007, Borst et al., 2000, Kruh and Belinsky, 2003). Very little information is currently available regarding intestinal expression patterns of Mrp1, -3, -4, 5, -6 and -7. Current literature indicates basolateral expression of MRP1, MRP3, MRP6 and MRP7 in intestinal enterocytes, however membrane localisation in intestinal epithelial cells has not yet been confirmed for MRP4 and MRP5, which are known to undergo tissue specific membrane localisation (Borst et al., 2007). In vitro studies have however shown MRP5 to localise to the basolateral membrane of MDCKII cells, as such it is expected that both proteins, like other family members, will be expressed basolaterally (Benet, 2009, Borst et al., 2007). Basolateral expression of MRP proteins indicates a role for these transporters in facilitating the absorption of endogenous and xenobiotic (drug) conjugates following phase II metabolism. Phase II metabolism (see chapter 1) mediates the production of glucoronides, sulphates and glutathione compounds which show increased affinity for MRP transporters (Borst et al., 2000, Deeley et al., 2006, Suzuki and Sugiyama, 2004). As such expression of MRP proteins on the basolateral membrane of enterocytes allows transport of parent molecules and organic conjugates into the underlying blood with subsequent transport via the hepatic portal vein to

the liver (Barrett et al., 2010, Deeley et al., 2006), where drug compounds are subject to uptake and further extensive metabolism, mediated by high levels of CYP450 enzymes (Paine et al., 2006, Suzuki and Sugiyama, 2004).

Despite a lack of data regarding expression of individual MRP transporters in the intestine two studies have established rank order expression profiles for the MRP family in human samples (Taipalensuu et al., 2001, Zimmermann et al., 2005). We have therefore ranked rat Mrp proteins in order of decreasing expression in the duodenum (Mrp6 > Mrp2 ~ Mrp3 >> Mrp5 ~ Mrp7 ~ Mrp1), jejunum (Mrp2 > Mrp6 > Mrp3 >> Mrp7 ~ Mrp5 ~ Mrp1), ileum (Mrp2 > Mrp6 > Mrp3 >> Mrp7 > Mrp1 > Mrp5) and colon (Mrp3 >> Mrp1 > Mrp7 ~ Mrp5 > Mrp6 > Mrp2). Data shown here contradicts that presented by others, for example, Zimmermann et al., (2005) showed MRP3 to be of higher expression than MRP2 in human duodenum samples (MRP6 expression was not measured) whilst Taipalensuu et al., (2001) report MRP2 to be of highest expression in the human jejunum, followed by MRP3 and MRP6, further highlighting variation in expression profiles of ABC transporters between species.

We have therefore shown some correlation between rat and human relative Mrp/MRP expression levels, particularly in the jejunum. Reversal of MRP3 and MRP2 relative expression levels between rat and human samples may reflect species differences. We found Mrp2 mRNA to be of highest expression relative to other ABCC genes in the ileum whilst it was surprisingly ranked as the lowest expressed gene in human samples (Zimmermann et al., 2005), further raising the spectre of substantial species differences and raising serious questions as to the use of rats in pre-clinical ADME assessment studies. In agreement with data presented here human colonic expression of MRP3 was shown to be much greater, and MRP2 to be much lower than other MRP proteins investigated (MRP1, -3, -4, -5 and 6) (Zimmermann et al., 2005).

We failed to detect expression of Mrp4 along the length of the intestine, with NanoString counts similar to those observed for negative assay controls. Similar findings of very low level MRP4 mRNA detection have been reported for human tissues using numerous techniques (Maher et al., 2005). Similarly, low level expression of Mrp5 along the length of the small intestine was shown, with increased expression in colon samples. A lack of substantial Mrp4/Mrp5 mRNA expression in rat tissues, like that observed in human intestine (Hilgendorf et al., 2007, Maher et al., 2005), indicates Mrp4/Mrp5 to be less important with regards to intestinal drug disposition compared with other family members, although caution must be practiced in assuming correlation between mRNA expression data and protein expression and functional activity.

Like Mrp5, Mrp1 shows only low level mRNA expression in the small intestine with an approximate 2-fold increase observed between the ileum and colon, similarly Maher et al., (2005) also found relatively low level expression of Mrp1 along the length of the mouse intestine. In contrast to the observed increase of Mrp1 mRNA between the small intestine and colon, human MRP1 expression was found to be fairly constant between the duodenum, terminal ileum and colon (Maher et al., 2005, Zimmermann et al., 2005).

We found expression levels of Mrp3 and Mrp6 along the small intestine to be higher than those of Mrp1, -5 and -7, with detection of concentrations similar to those of Mrp2. mRNA expression levels of Mrp3 and Mrp6 remain fairly consistent along the length of the small intestine. Upon reaching the colon however expression of Mrp6 decreases significantly such that concentrations are similar to those of negative controls. Contrastingly, a significant rise in Mrp3 mRNA levels between all regions of the small intestine and colon is evident ($^{\#\#}$ $p < 0.01$), with a calculated 4-fold increase in expression between the ileum and colon. Past studies have shown a high level expression of MRP3/Mrp3 in human and mice colon samples (Borst et al., 2000, Maher et al., 2005), and now replication of such data in the pre-clinical rat model is presented here. Given the lack of absorptive capacity associated with the flattened epithelium of the colon and the notion that the majority of orally consumed drugs are absorbed in the small intestine (Chawla and Bansal, 2003), it is likely that high colonic MRP3/Mrp3 mRNA expression plays a predominantly physiological role within this region as opposed to the involvement of this transporter in drug disposition. Indeed, past studies have indicated a role for MRP3 in absorption of steroid conjugates from the large intestine (Rost et al., 2002) and high mRNA expression levels determined by us support this physiological role.

As discussed in section 1.1.2 intestinal specific homeobox genes Cdx1 and Cdx2 related to the *Drosophila melanogaster Caudal* gene and the pancreatic/duodenal specific homeobox gene, Pdx1, have been implicated in regional intestinal patterning of gene expression in adults (Silberg et al., 2000, Suh and Traber, 1996). Extensive literature searching was therefore undertaken to determine if any of the genes investigated in the present study are transcriptionally regulated by these, or other, intestinal homeobox genes. Extensive literature review failed to find evidence of such regulatory mechanisms for all target genes included in the NanoString codeset, except for MDR1 and PEPT1. Recent studies have shown strong correlation between CDX2 and MDR1 in both the colorectal HT-29 cancer cell line and the gastric SGC7901/DDP cancer cell line (Takakura et al., 2010, Yan et al., 2015). Takakura et al., 2010 showed a 31.14-fold increase in MDR1 mRNA expression in HT-29 cells following transfection of the cell line with full length human CDX2 cDNA, with an associated increase in MDR1 protein detected using Western blot analysis. Furthermore, high levels of both MDR1

and CDX2 mRNA transcripts and protein were shown in six additional cell lines, including the Caco2 cell line, strongly indicating high levels of correlation between these two genes (Takakura et al., 2010). Immunohistochemistry using antibodies directed against MDR1 and CDX2 showed highly similar immunoreactivity in the colon of healthy human volunteers (Takakura et al., 2010). In addition to correlation at an mRNA and protein level Yan et al., (2013) report increased sensitivity of SGC7901/DDP cells to the MDR1 substrate doxorubicin following stable transfection of siRNA-CDX2 into cell line. The IC50 value of doxorubicin was reduced from 0.39 ± 0.15μg/mL in the parental SGC7901 cell line to 0.12 ± 0.05μg/mL in SGC7901 cells following CDX2 mRNA silencing Yan et al., (2015) thus indicating CDX2 to regulate functional activity of the MDR1 protein.

Freund et al., (1998a) showed presence of two Cdx mRNA transcripts in rat intestine and reported a decreasing transcript expression with anterior regression from the colon to the duodenum. Data presented here show increasing Mdr1a expression from the duodenum to the jejunum and ileum and as such reflect a similar mRNA expression pattern to that described for rat Cdx, however colonic Mdr1a expression was determined to be similar to that present in jejunal mucosal scrapes in contrast to Cdx which was previously shown to be expressed at highest levels in the rat colon (Freund et al., 1998a). As such, despite literature reports of strong correlation between CDX and MDR1, it appears that transcriptional regulation of intestinal genes does not exactly follow Cdx expression patterns suggesting presence of other regulatory mechanisms and highlighting the complex nature of intestinal epithelium.

In support of such a hypothesis, past studies have shown high levels of correlation between mRNA expression levels of the SLC PEPT1 transporter and CDX2 in human gastic tissue samples (Terada and Inui, 2007). Despite strong gene correlation the PEPT1 promotor was found to lack typical CDX2 binding sequences but rather expressed Sp-1 (specificity protein 1) binding sites indicating co-regulation of PEPT1 by CDX2 and SP-1 transcription factors (Terada and Inui, 2007). Like Mdr1a, rat intestinal PepT1 expression reported here appears to show correlation with previously reported Cdx2 mRNA expression along the length of the small intestine, with an increased concentration apparent from the duodenum to the ileum, but shows only low level expression in the colon.

In addition to ABC transporters, the solute carrier family of proteins play a crucial role in drug disposition, particularly PEPT1, CNT1-3 and members of the OCT (organic cation transporter) and OAT (organic anion transporter) families (Sai, 2005, Sai and Tsuji, 2004, Steffansen et al., 2004). Given the role of the SLC family in nutrient absorption additional to exploitation of these membrane proteins as drug delivery systems for poorly absorbed compounds (Gomez-Orellana, 2005) mRNA expression levels of several SLC genes have been determined in rat

intestine. Of those transporters investigated Oat3 and Oatp-3 were concluded to be below the level of detection using NanoString technology, with detected mRNA concentrations being very similar to those of negative controls. Only very low level expression of Oatp-b along the length of the intestine was evident, although this transporter was unique in that it showed higher levels of mRNA expression in the crypt than at the villus tip.

Nucleosides are known to act as signalling molecules in a number of physiological pathways and are precursors to nucleotides required for cellular synthesis of DNA and RNA (Gray et al., 2004). Due to their hydrophilic nature, nucleosides must be actively transported across the cell membrane (Gray et al., 2004). The SLC28 family of proteins known as the high affinity concentrative nucleoside transporters (CNTs) mediate the Na^+ coupled transport of nucleosides into the cell cytoplasm via utilisation of the Na^+ gradient (Gray et al., 2004, Steffansen et al., 2004). Salvage of nucleosides from the extracellular environment by CNTs requires lower energy expenditure than de novo synthesis, and as such serves as an important physiological mechanism by which cellular and systemic nucleoside concentrations are regulated (Gray et al., 2004, Lu et al., 2004). As with other transporters, the physiological function of CNTs has been exploited for drug development. CNTs mediate uptake of synthetic nucleoside analogues, including anti-viral drug compounds used in the treatment of HIV, hepatitis and solid tumours (Gray et al., 2004, Steffansen et al., 2004).

We determined intestinal expression levels of Cnt2, which transports nucleoside analogues including the anti-viral drug compounds didanosine and ribavirin, in the intestine (Benet, 2009, Kis et al., 2009). Very high level mRNA expression of Cnt2 was detected in the rat small intestine using NanoString technology. Given the role of CNTs in salvage of nucleoside analogues (Gray et al., 2004) high mRNA expression along the length of the small intestine is reflective of their physiological function. Dietary consumption of nucleotides in the form of dietary nucleoproteins yields intestinal nucleotides and nucleosides as a result of phosphatase mediated digestion (Uauy et al., 1994). High level expression of Cnt2 in the intestine is therefore likely to mediate uptake of dietary derived nucleosides to be used in DNA/RNA synthesis, and cellular signalling pathways (Gray et al., 2004). With regards to drug design, highest levels of Cnt2 were evident in the rat jejunum thus suggesting increased absorption of clinically important nucleoside analogues within this region. High mRNA concentrations were however apparent in all regions of the small intestine, as drug molecules designed to specifically target the Cnt2 uptake transporter would likely possess good oral bioavailability profiles.

PepT1 is an apically expressed co-transporter responsible for the uptake of small peptides composed of two or three amino acids (Freeman et al., 1995). The ability of PepT1 to transport

small peptide molecules is utilised in the oral drug delivery of peptidodimetic drugs which are recognised as substrates by PepT1 and transported across the apical enterocyte membrane into the cell (Ford et al., 2003, Steffansen et al., 2004). Given the absorptive nature of PepT1 it is not surprising that increased mRNA expression was measured at the villus tip. Mixed reports are however presented concerning the expression profile of PepT1 mRNA along the length of the intestine. Freeman et al., (1995) show in situ localisation of transporter mRNA to be confined to the rabbit small intestine, with an absence of expression in colon tissue samples, whilst others have shown colonic PepT1 mRNA expression by RT-PCR (reverse transcription – PCR), although expression was shown to be decreased compared with that of the small intestine (Ford et al., 2003). In agreement with the data presented by Freeman et al., (1995) this study detected PepT1 mRNA expression along the length of the rat small intestine however mRNA transcript expression was also detected in the colon, as reported by Ford et al., (2003). This indicates potential for differential PepT1 expression/activity between species, in support of such a theory microarray assays performed by Kim et al., (2007) showed high PepT1 mRNA levels in rat duodenal samples in contrast to low level expression in human duodenum samples providing some explanation as to the reported literary discrepancies.

Translocation of cationic drug compounds across cell membranes is limited by membrane restrictive passage due to their associated positive charge at physiological pH (Muller et al., 2005). Expression of organic transporters in the intestinal enterocyte barrier therefore directly influences oral drug bioavailability of cationic therapeutic compounds including clonidine, diphenhydramine, metformin and quinidine (Muller et al., 2005). The SLC22 sub-family are organic cation transporters and are known to influence bioavailability of many drug compounds. Oct1 was the first cloned member of the family which is now known to contain 11 functionally active transporters, including Oct1-3 and Octn1-3 (Koepsell and Endou, 2004). OCT transport organic cationic substrates across cell membranes in a sodium independent manner. The driving force for OCT mediated transport is determined solely by the electrochemical gradient of the ion being transported, as such, the direction of OCT mediated transport can be reversed (Koepsell and Endou, 2004). A second subgroup of the SLC22 family comprising OCTN1 and OCNT2 also exists. OCTN1 and OCNT2 transporters are both able to function as organic cation uniporters however OCNT1 is also known to act as a antiporter in which it transports organic cations in exchange for H^+ and OCNT2 is capable of functioning as a Na^+/carnitine cotransporter (Koepsell and Endou, 2004).

Despite the majority of drugs indicated for therapeutic being organic cations and the ability of the SLC22 family to transport a broad array of substrates (Koepsell and Endou, 2004, Muller et al., 2005), little is known with regards to their intestinal expression. Furthermore, much

attention has been focussed on OCTN1 and OCTN2 due to the association of gene polymorphisms with Crohn's and Ulcerative colitis diseases, as such information regarding intestinal expression of these transporters may allow improved management of such conditions. We have therefore determined intestinal expression of Oct1, Octn1 and Octn2 in the rat intestine. Of the three rat Slc22 family members investigated, Octn2 showed higher expression levels along the length of the small and large intestine. Octn2 mRNA expression was found to exceed that of Octn1 especially in the colon where expression levels are high. Oct1 and Octn1 appear to show contrasting expression patterns with decreased mRNA concentration of Oct1 from the proximal to distal small intestine and increased Octn1 mRNA expression from the duodenum to ileum, although data is not significant for Oct1.

Oct1 has been localised to the basolateral membrane of rat enterocytes (Koepsell and Endou, 2004). Following oral administration of a drug compound the electrochemical gradient is such that the transport of Oct1 substrates across the basolateral membrane and into underlying sinusoidal blood vessels is favourable, as such it is likely that Oct1 facilitates absorption of organic drug compounds with subsequent transport to the liver (Koepsell and Endou, 2004). Unlike Oct1, Octn1 and Octn2 are expressed on the apical membrane of small intestinal enterocytes where they exchange Na^+/carnitine or facilitate absorption of organic cations and weak bases from the intestinal lumen via acting as a uniporter or antiporter (Kato et al., 2006, Koepsell and Endou, 2004).

Following oral consumption of an organic cationic drug compound its absorption may therefore be influenced by apically expressed Octn1 and Octn2, once intracellular concentrations become high enough the Oct1 transporter expressed on the basolateral membrane will become active such that substrates are transported into the underlying sinusoidal blood. As expected for transporters associated with apical brush-border uptake, NanoString mRNA data shows increased expression in villus tip compared with crypt samples for all three transporters, thereby increasing potential for substrate absorption.

The 3A family of CYP450 enzymes is expressed in many tissues but are concentrated in the liver and the mucosa of the small intestine and are of major importance in the first pass metabolism of many drugs and xenobiotics (Paine et al., 2006). In man, over 25% of all CYPP450 activity is mediated by the 3A family with 3A4 being the most predominant enzyme (Paine et al., 1997). Expression of both cytochrome P450 enzymes and drug efflux transporters within enterocytes may ultimately reduce drug absorption due to enterocytic recirculation of drug compounds (discussed in detail in chapter 1) (Benet, 2009).

The contribution of enteric CYP450 enzymes to first pass metabolism of drug compounds is becoming increasingly recognised. Studies have shown human intestinal expression of CYP3A family members (3A4 and 3A5) to contribute significantly if not equally toward first pass metabolism, despite the dramatic reduction in CYP3A intestinal expression compared with that in the liver (Paine et al., 2006). In support of the important role of enteric CYP450 metabolism, tacrolimus and midazolam have been shown to undergo extensive metabolism in the intestine (Aiba et al., 2005). Past studies which have determined CYP expression and functional activity in human intestinal microsomes have shown the importance of the CYP3A family. Paine et al., (2006) found total specific content of the CYP3A family to represent 82% of the total proximal small intestine CYP450 content in humans.

As in humans the rat Cyp3a family is important in intestinal metabolism (Matsubara et al., 2004, Shin et al., 2009). Six genes were originally categorised as belonging to the rat Cyp3a family Cyp3a1, Cyp3a2, Cyp3a9, Cyp3a18, Cyp3a23 and Cyp3a62, however gene analysis showed Cyp3a1 and Cyp3a23 to be the same gene and hence encode the same protein (Matsubara et al., 2004). Intestinal expression patterns of all Cyp3a family members in the rat intestine have been investigated here.

Peculiarities have been reported with regards to intestinal metabolism of CYP3A4 substrates in rats in comparison to their hepatic metabolism profiles, indicating altered Cyp450 expression profiles between the two tissues (Aiba et al., 2005). Such differences are reported for Cyp3a1/3a23 and Cyp3a2. Midazolam is metabolised by CYP3A4 in humans and Cyp3a1/3a23 in rats but does not undergo biotransformation in rat intestine despite extensive metabolism in the human intestine (Mitschke et al., 2008). Whilst expression of both isoforms was evident in hepatic microsomes, a lack of Cyp3a2 specific antibody reactivity was observed in intestinal microsomes, with only minimal Cyp3a1/3a23 protein detected (Aiba et al., 2005). Similarly, Matsubara et al., (2004) were unable to detect expression of Cyp3a1/3a23 and Cyp3a2 mRNA by RT-PCR in any region of the rat intestine, despite predominant expression of these isoforms in rat liver. These data indicate that a lack of intestinal 3a1/3a23 expression accounts for the observed differences in Midazolam metabolism.

Given the high level of sequence homology between Cyp3a1 and 3a2 it was not possible to distinguish between the two isoforms using NanoString technology, however in agreement with others, no mRNA expression of Cyp3a1 or Cyp3a2 was detected in any region of the rat intestine in the present study. Tissue specific expression of Cyp450 isoforms is therefore vital in determination of metabolic profiles of drug compounds, prompting requirement for detailed analysis of Cyp450 intestinal expression patterns in an attempt to ascertain how intestinal metabolism influences the pharmacokinetic profiles of drug compounds.

Whilst Cyp3a1/3a23 is predominantly expressed in the liver and absent in the intestine, Cyp3a9 and Cyp3a62 are reported to be predominantly expressed in the rat intestine (Matsubara et al., 2004). Intestinal expression of Cyp3a18 is shown to be extremely variable, with indications of predominant hepatic expression for this enzyme (Aiba et al., 2005, Matsubara et al., 2004). Past studies have reported decreasing levels of mRNA, protein and function of CYP3A/Cyp3a family members from the proximal to distal intestine in both human and rat tissues (Martignoni et al., 2006, Matsubara et al., 2004, Paine et al., 2006). Although NanoString mRNA data presented here suggests Cyp3a mRNA expression to increase with distal progression along the small intestine no significant increase in expression levels is measureable. As such, differences between data reported here and that found within the literature may result from high levels of variability in mRNA expression levels between animals. Considerable inter-animal variation with regards to intestinal expression of the Cyp3a family is observed here. Approximate SEM values for Cyp3a18 and Cyp3a62 range from 15-26% of total expression content along the length of the small intestine. Although jejunal mRNA concentrations showed minimal inter-animal variation (4%), ileal Cyp3a9 expression shows a calculated SEM of 33%, likely due to low level expression noted in one animal.

Whilst reasoning for such variations remains to be identified, two common factors are reported to influence inter-individual variation in CYP450 enzyme expression and function, genetic polymorphisms and interindividual differences in gene induction. It may therefore be that observed inter-animal variations reported here result from differences in genetics and/or in response to xenobiotics present within the rat diet (Glaeser et al., 2007, Tirona and Kim, 2005). Members of the human CYP3A family are known to express PXR response elements within their regulatory region and as such are likely to be induced when the ligand-binding domain of the PXR is bound to substrates and activated (Nebert and Russell, 2002). Indeed CYP450 induction by food/drug compounds is known to cause often unpredictable food-drug and drug-drug interactions (Nakata et al., 2006, Tirona and Kim, 2005, Urquhart et al., 2007).

Whilst the Cyp3a/CYP3A family contributes substantially to the intestinal metabolism of drug compounds it is reported to account for only 26 and 49% of the rat intestinal CYP450 content in the rat duodenum and human jejunum (Paine et al., 2006). We therefore looked to determine expression levels of alternative Cyp450 enzymes in an attempt to establish potential contributors toward intestinal metabolism. Of those enzymes investigated expression of Cyp2c11, Cyp2c6v1/2c7 and Cyp2d3 was not detected.

Cyp1a1 is known to be predominantly expressed in rat intestine as opposed to rat liver, and as such is proposed to play an important role in the intestinal metabolism of xenobiotic compounds, although this is yet to be extensively validated (Lindell et al., 2003, Martignoni et

al., 2006, Rochat et al., 2008). mRNA expression of Cyp1a1 has been reported in all regions of the small intestine indicating a potential correlation between mRNA expression levels determined by us and relatively uniform protein expression previously observed along the length of the rat small intestine (Mitschke et al., 2008). Due to high levels of sequence homology it was not possible to distinguish between Cyp1a1 and Cyp1a2 using NanoString technology however since past studies have shown an absence or weak expression of CYP1A2/Cyp1a2 in extrahepatic tissues (Martignoni et al., 2006) Cyp1a1/1a2 will be referred to as Cyp1a1 only from this point forward.

Substantial inter-animal variation is apparent for Cyp1a1 mRNA expression within each respective region of the small intestine. Such variation may result from altered transcriptional regulation of Cyp1a1 mRNA. In fact it has been suggested that CYP1A1/Cyp1a1 is not constitutively expressed in human or rat intestine and expression is rather induced by dietary components and/or xenobiotics (Kaminsky and Zhang, 2003, Paine et al., 2006). Known to be under the transcriptional regulation of the aryl-hydrocarbon receptor (AhR), Cyp1a1 gene expression may be induced to differing extents between animals following ligand binding and activation of the AhR (Deb and Bandiera, 2009, Martignoni et al., 2006). Various substances are known to induce expression of human CYP1A1 including cigarette smoke, dietary components such as chargrilled food and polycyclic aromatic hydrocarbons (PAHs) and drug compounds such as omeprazole and thiabendazole (Martignoni et al., 2006, Wang et al., 2011). Since animals used in the present study were maintained under sterile laboratory conditions it is unlikely that induction of mRNA occurred following exposure to any such chemicals as those described above, however it is reported that constituents present within laboratory rat chow are capable of inducing Cyp1a1 transcription (Kaminsky and Zhang, 2003, Paine et al., 2006). We therefore suggest observed variation in mRNA concentrations of Cyp1a1 may result from differences in consumed levels of rat chow and/or inter-individual response to consumed transcription factor ligands, however it should be noted that all rats were of a similar weight at the time of sacrifice indicating that excessive consumption was not apparent for any single animal.

Given the high degree of similarity between Cyp2b1 and 2yp2b2 it was not possible to distinguish between them using NanoString technology, although it has been suggested that Cyp2b2 is absent from the rat intestine (Kaminsky and Zhang, 2003). Relatively limited information is available regarding Cyp2b intestinal expression patterns. Lindell et al., (2003) showed strong mRNA expression levels for Cyp2b1 in the duodenum, jejunum and ileum in agreement with the decreasing protein expression evident from the duodenum to terminal ileum reported by Mitschke et al., (2008). In contrast to other findings data presented here

suggests increased expression of Cyp2b1/2b2 from the duodenum to the jejunum and from the jejunum to the ileum. It should be noted however that substantial inter-animal variation is apparent and no significant increase in expression levels is measured as such data may not accurately reflect expression trends. Furthermore, absolute correlation between mRNA and protein expression levels is not definite. We found similar trends in expression for the cytochrome P450 enzyme Cyp2d4/2d6, with a significant increase in expression from the duodenum to the jejunum and duodenum to the ileum. Again inter-animal variation associated with these genes is pronounced in all regions of the small intestine.

Cyp2d1/2d9 the rat orthologue of human CYP2D6 and is known to be involved in the hepatic biotransformation of approximately 30% of drugs on the market despite accounting for only 4% of the total hepatic cytochrome P450 pie (Martignoni et al., 2006). We found low level Cyp2d1/2d9 mRNA expression in the small intestine, with Mitschke et al., (2006) reporting low level protein expression as determined by densitometric analysis of Western blots. Similarly, human intestinal CYP2D6 content is low (< 1% total content) (Paine et al., 2006) suggesting a role for CYP2D6/ Cyp2d1/2d9 in small intestinal drug metabolism is unlikely. Of interest however is the significant increase in mRNA expression between the small intestine and colon for Cyp2d1/2d9. A rise in Cyp2d1/2d9 protein expression was also shown by Mitschke et al., (2006) toward the distal ileum and colon. The high level mRNA expression of Cyp2d1/2d9 in the colon is in contrast to the measured decrease in expression of all other CYP450 enzymes from the small intestine to the colon. It is proposed that the diverse microbial population present within the colon, which is largely absent from the small intestine, is capable of metabolising Cyp450 substrates, removing requirement for enzyme expression within this region (Mitschke et al., 2008). Logical reasoning therefore suggests inability of the colonic microflora to metabolise Cyp2d1/2d9 substrates, promoting increased expression of this enzyme and hence increased mRNA concentrations of Cyp2d1/2d9 within this region.

Although originally cloned from rat intestine in 1997 (Zhang et al., 1997) very little information regarding the intestinal expression of CYP2J4 is available. Zhang et al., (1997) showed RNA expression of Cyp2j4 in the liver, small intestinal enterocytes and the olfactory mucosa, with an apparent lack of expression in heart, kidney and lung tissue. In agreement with mRNA expression data presented here, further investigation by Zhang et al., (1998) showed increased Cyp2j4 protein expression from the duodenum to the jejunum with a subsequent fall in expression in the ileum using immunoblot (Zhang et al., 1998). Our data indicate high levels of variation between individual animals with regards to Cyp2j4 mRNA expression, suggesting potential for interindividual variation of intestinal Cyp2j4 activity.

Cyp2s1 was originally identified and cloned from human and mouse tissues in 2001/2002 however little focus has been placed upon expression of this cytochrome P450 enzyme in rat intestine until recently (Deb and Bandiera, 2009). Although shown to be expressed in the human small intestine, to our knowledge no data exists regarding murine Cyp2s1 expression. Deb and Bandiera, (2009) report mRNA expression of Cyp2s1 in the duodenum, jejunum and ileum of male and female rats, with a relatively consistent expression between the different regions. In agreement the present study shows expression levels of Cyp2s1 to be similar in the duodenum, jejunum and ileum of rat intestine, taking into account the error of variation between animals. A significant decrease in mRNA expression is evident from the small to large intestine. Despite moderate expression of Cyp2s1 mRNA, Deb and Bandiera, (2009) failed to detect presence of Cyp2s1 protein in small intestinal microsomes, showing a poor correlation between mRNA and protein. Like Cyp1a1, Cyp2s1 is inducible by AhR ligands, and both mRNA and protein expression was shown to increase in rat lung following intraperitoneal injection of the carcinogen TCDD (2,3,7,8-Tetrachlorodibenzodioxin), an AhR ligand (Deb and Bandiera, 2009). It is therefore reasonable to suggest that oral exposure to AhR ligands may induce expression of intestinal Cyp2s1 mRNA and protein potentially allowing for large inter-individual differences in functional activity.

As shown here, the expression of intestinal Cyp450 enzymes, at least at the mRNA level, shows substantial variation between animals. It is therefore not surprising that differences in human CYP450 expression levels potentiate the likelihood of interindividual variation in response to treatment (Nakata et al., 2006, Urquhart et al., 2007). Furthermore, further differences may be apparent in enzyme function and/or due to induction of CYP450 enzymes by xenobiotics or dietary constituents.

Given the vital role of intestinal stem cells in population of the crypt-villus axis it is not unreasonable to suggest presence of a mechanism within the crypt region, by which these cells are protected from toxic insult and xenobiotics. The established role for Bcrp in the SP stem cell (Scharenberg et al., 2002, Zhou et al., 2001) niche indicates a potential role for ABC transporter expression and functionality in protection of the crypt region and the intestinal stem cell. We have therefore characterised transporter and CYP450 expression profiles within the crypt region for the first time.

Upon reaching the crypt-villus junction epithelial cells enter a state of differentiation and rapidly undergo terminal differentiation as they progress up the villus toward the intestinal lumen (Barker et al., 2008). A lack of data is apparent with regards to comparable expression levels of both drug transporters and CYP450s across the crypt-villus axis, mRNA expression levels of members of both families have therefore been determined to contribute toward the

filling of a gap in current knowledge. Given the extensive epithelial cell differentiation which occurs from the intestinal crypt to the villus tip it is not surprising that the vast majority of target genes investigated showed increased mRNA expression in isolated villus tip samples. Of the eighteen drug transporters and nine cyp450 enzymes found to be expressed in the rat intestine, only Oatp-b showed higher mRNA expression levels in the crypt region, although Oatp-b mRNA transcript concentrations were low in comparison to expression levels of other target genes. It remains to be determined if correlation exists between mRNA and protein expression of Oatp-b in the intestinal crypt region. Human OATP-B protein has been localised to the apical membrane of human villus enterocytes but this publication did not show images of crypts (Kobayashi et al., 2003) as such further protein localisation studies are indicated, especially in the rat. OATP-B mediates proton-linked uptake of organic anions and has been linked with drug uptake e.g. pravastatin, and may therefore have a physiological purpose in the crypt (Kobayashi et al., 2003).

Our data is in agreement with past studies which have shown increased villus tip Mdr1 mRNA expression using in situ hybridisation (Trezise et al., 1992). Furthermore, Anderle et al., (2005) showed increased expression of Cnt2 in villus epithelial cells compared with those of the crypt using RT-PCR (real time–PCR) following laser dissection of mouse ileum. In contrast to our findings in rat ileum, Anderle et al., (2005) show no difference in Mrp1 expression between villus and crypt epithelial cells and report higher cryptal mRNA expression for Mrp3. It should however be noted that no specific localisation with regards to micro-dissection of villus epithelial cells is described, examined epithelial cells may therefore originate from any region of the villus, ranging from the villus base to tip (Anderle et al., 2005).

Despite higher villus tip mRNA concentrations substantial levels of mRNA expression for some genes were apparent within ileal crypt samples. Of those transporters studied Bcrp, Mdr1a, Mrp2, Cnt2 and PepT1 are expressed at high levels in the crypt region, indicating potential for functional transporter activity within this region. Past studies have however indicated a lack of correlation between mRNA expression and protein translation (Maier et al., 2009), it therefore remains to be established how detected mRNA concentrations correlate with both protein expression and functional activity. Given the role of Bcrp, Mdr1a and Mrp2 in drug resistance and their expression at key protective barrier locations it is proposed that mRNA expression of these transporters in the intestinal crypt indicates a role in protection of the stem and poorly differentiated cells of this region. Protein expression and localisation of these transporters in both rat and human intestine sections has therefore been characterised using immunohistochemistry (chapter 5); immunoreactivity of anti-Mdr1 and anti-Bcrp antibodies within the crypt was observed.

In addition high level expression of the CYP450 enzymes, Cyp3a18, Cyp3a62 and Cyp3a9 is apparent in the intestinal crypt. It is believed that the Cyp3a9 protein is the rat homolog of human CYP3A4, with sequences of the two genes showing 81% sequence homology (Shin et al., 2009). Human CYP3A4 contributes toward metabolism of up to 50% of marketed drugs, and is well known to be the predominant CYP enzyme in both hepatic and intestinal tissues (Shin et al., 2009). We suggest that should high mRNA expression levels be reflected in the form of functional protein, expression of key Cyp3a enzymes shown to be involved in drug metabolism within the crypt may contribute toward detoxification of the crypt region via biotransformation of drug compounds.

It is well established that a complex interplay exists between ABC transporters and CYP450 enzymes. Expression of Mdr1a, Mrp2, Bcrp, Cyp3a18, Cyp3a62 and Cyp3a9 mRNA in the ileal crypt may therefore reflect co-operative activity of these proteins in protection of the stem cell niche. We propose that ABC transporters expressed within crypt epithelia or intestinal stem cells may mediate the efflux of both parent drug compounds and metabolites from the cell, thereby lowering intracellular drug accumulation. Cytoplasmic expression of CYP450 enzymes may further reduce cellular accumulation of active drug molecules via biotransformation of the parent drug compound. Both mechanisms, ABC transport and Cyp450 metabolism may therefore serve to protect the crypt region against cytotoxic insult.

5. Intestinal localisation of Mdr1, Mrp2 and Bcrp in rat and human tissues

5.1 Introduction

Previous work presented in this thesis shows detection of mRNA expression of key drug transporters and cytochrome P450 enzymes along the length of the gastrointestinal tract and the crypt-villus axis using NanoString technology (described in chapter 4). It was therefore of interest to determine how mRNA transcript expression correlates with protein and ultimately physiological activity. Whilst many studies assume mRNA expression levels to reflect not only protein expression but also functional activity it may not always be the case that such correlations are true (Aust et al., 2004). High mRNA expression levels do not always directly result in high levels of translated protein. In fact, the majority of studies have shown a weak correlation between mRNA expression data and protein levels (Maier et al., 2009). Furthermore, protein expression may be non-functional with regard to physiological activity since membrane proteins must be correctly assembled (as observed with obligate requirement of BCRP dimerisation) and successfully translocated through the Golgi network, packaged in the exocytic pathway and correctly inserted into the plasma membrane to allow functional activity (Boron and Boulpaep, 2009 p29-38, Kage et al., 2002).

As emphasised in chapter 1, oral drug bioavailability may be directly impacted by the action of three key ABC transporters, MDR1, MRP2 and BCRP which are known to confer multidrug resistance (Szakacs et al., 2008). Considered to be expressed at the apical membrane of enterocytes, these transporters act in concert with CYP450 enzymes such as the CYP3A family to constitute a biological barrier which precedes hepatic drug exposure and metabolism (Benet, 2009, Snoeck et al., 2005, Szakacs et al., 2008). The expression of ABC transporters and CYP450 enzymes within the enterocyte barrier contributes to the first pass metabolism of drug compounds (Benet, 2009). With regards to ABC transporters few studies have investigated both mRNA and protein levels together, with many opting only to study one or the other. A study by Berggren et al., (2007) sought to establish correlation patterns between mRNA and protein expression levels of key drug transporters MDR1 and MRP2 and the metabolising enzyme CYP3A4 in the human intestine. A strong correlation was observed between mRNA abundance and protein expression in human jejunum, ileum and colon for CYP3A4 (correlation coefficient = 0.779) however data for both MDR1 and MRP2 were less convincing (Berggren et al., 2007). When sample expression data from all regions were combined MRP2 did show some correlation, although this was lost when comparing individual intestinal sections alone. MDR1 mRNA and protein expression showed no correlation, with a correlation coefficient value of

0.115 (Berggren et al., 2007). Given the important role of ABC transporters in intestinal drug disposition it is vital to understand if high levels of mRNA transcript expression equates to high levels of expressed protein and vice versa, particularly for those transporters known to confer drug resistance. Knowledge of intestinal protein expression may potentially allow optimisation of oral drug delivery and uncover the physiological relevance of these transporters with regards to intestinal drug disposition (Anderle et al., 2005).

Extensive searching of current literature revealed a paucity of information with regards to intestinal transporter expression patterns at the protein level. Western blot analysis has shown MDR1 and Mrp2 protein to be expressed in all regions of the small intestine with an increased expression from the duodenum to ileum in human and rat respectively (Blokzijl et al., 2007, Glaeser et al., 2007, Mottino et al., 2000, Mouly and Paine, 2003). There are few reports of human intestinal MRP2 protein localisation and although Sandusky et al., (2002) reported apical membrane staining in the duodenum and colon they failed to present any images confirming this. Similarly, whilst Mottino et al., (2000) conclude Mrp2 expression along the length of the rat intestine from Western blot analysis immunohistochemical antibody immunoreactivity was very low with substantial levels of background staining. In contrast to Northern blots, which confirm mRNA expression in the upper villus with an 50% reduction in cryptal mRNA expression, relatively weak immunostaining was visible at the villus tip with an absence of immunoreactivity within the crypt region (Mottino et al., 2000) thus suggesting a lack of correlation between Mrp2 mRNA and protein expression in the rat. Strong evidence is however presented which confirmed apical expression of MDR1 on villus cell membranes (Blokzijl et al., 2007, Glaeser et al., 2007). Thiebaut et al., (1987) showed apical localisation of MDR1 in human jejunum and colon sections, whilst later studies showed up regulation of apically expressed MDR1 in human duodenum following oral consumption of rifampin (Greiner et al., 1999). Similarly, Rost et al., (2002) showed apical expression of Mdr1 on jejunal villus enterocytes, with a strong co-localisation of Mdr1 and Mrp2 in rat intestine. Comprehensive determination of Mdr1 and Mrp2 expression in all regions of the rat intestine is however presently lacking.

Despite the known ability of BCRP to efflux numerous drug compounds very few studies have investigated its expression in the intestine and rather a general assumption regarding localisation of BCRP to the apical enterocyte membrane is apparent. Apical localisation of BCRP has been shown in other tissues and studies have shown the transporter to be functionally active at the apical membrane in cultured cell lines (Aust et al., 2004, Wright et al., 2010). However, only a single study shows apical expression at the villus epithelial membrane in human small intestine and colon sections, whilst others have reported cytoplasmic BCRP

expression in many tissues including the small and large intestine (Fetsch et al., 2006, Maliepaard et al., 2001). Of the 116 papers citing Maliepaard et al., (2001) none replicate findings of intestinal apical expression. Whilst apical transporter expression would allow efflux of substrates into the intestine the role of BCRP in the cell cytoplasm is not understood. It is therefore vital to characterise BCRP protein expression in the intestine to help understand the influence of this transporter with regards to oral drug delivery and disposition.

The intestinal stem cell is responsible for the generation of the four intestinal cell lineages present within the enterocyte barrier (Barker et al., 2008, Pinto and Clevers, 2005). Numbers of intestinal stem cells and their location within the crypt have long since eluded researchers however two current consensus models; the +4 position and the stem cell zone models have been generated (Barker et al., 2008), see chapter 1 section 1.1.2. Given the important role of the stem cell in regeneration of the entire cell population of the enterocyte barrier it is not unreasonable to suggest that in addition to their proposed role in villus epithelia ABC transporters may serve to protect the stem cell niche of the intestinal crypt from toxic insult. The tight regulation of stem cell number further supports a need for protection of this crucial region. The gain or loss of a single stem cell has been shown to effect overall cell number by up to 64 cells, based on six rounds of cell division following generation of stem cell progeny (Barker et al., 2008, Marshman et al., 2002).

We believe the most likely ABC transporter to play a role in stem cell protection is BCRP, given its role in the development of the SP stem cell phenotype (Scharenberg et al., 2002) and higher mRNA expression compared with Mdr1 and Mrp2 in rat crypt samples (shown in chapter 4). The SP phenotype is characterised by the ability of these stem cells to efflux Hoechst33342 from the cell (Scharenberg et al., 2002). This decreased intracellular accumulation of the lipophilic dye is sensitive to inhibition by the BCRP specific inhibitor FTC (Scharenberg et al., 2002). It has since been shown that BCRP is expressed in a wide range of progenitor stem cells across many tissues suggesting BCRP mediated efflux to be important in this cell type (Scharenberg et al., 2002, Zhou et al., 2001).

Given the lack of current data regarding intestinal expression of the key ABC transporters, Mdr1, Mrp2 and Bcrp protein and the high mRNA expression levels of the transporters detected using NanoString technology (chapter 4) along the length of rat intestine, the aim of this chapter has been to determine relative transporter expression and localisation along the length of the rat small intestine and colon. Of considerable interest is ABC transporter expression in the crypt region in relation to stem cell protection, particularly following the detection of Mdr1, Mrp2 and Bcrp mRNA in this area (chapter 4). Knowledge regarding intestinal transporter localisation may further clarify the role of these transporters in intestinal

drug disposition and protection of the epithelial cells of the intestinal mucosa, especially in relation to stem cell protection.

5.2 Methods

5.2.1 Western blot

All Western blot experiments were performed as detailed in section 2.2.7 of materials and methods. Details of antibodies used are shown in table 5.1.

5.2.2 Immunocytochemistry

Immunocytochemistry was performed using the methods described in materials and methods section 2.2.8. Details of all antibodies used are shown in table 5.1.

5.2.3 Immunohistochemistry

All immunohistochemical staining was performed using a Ventana Benchmark classic, Ventana Benchmark XT or Ventana Benchmark Ultra staining platform. Full details of immunohistochemical methods and ethical approval are available in section 2.2.9 of materials and methods.

5.3 Results

5.3.1 Immunohistochemical detection of Mdr1 in rat intestine using the primary antibody C19

Mdr1 protein expression in rat intestine was investigated using both C219 and C19 anti-Mdr1 primary antibodies (figure 5.1). Although both antibodies were found to localise Mdr1 to the apical villus membrane, a higher intensity staining and increased specificity with respect to apical immunostaining were observed with C19 compared to C219 (figure 5.1). As detailed in table 5.1, C219 is a mouse monoclonal antibody indicated for the detection of the 170KDa MDR1 and MDR2/3 proteins in human, rat and mouse tissues. C19 is a goat affinity isolated polyclonal antibody indicated for the detection of Mdr1, Mdr2 and Mdr3 of rat and mouse origin and for the detection of MDR1 and MDR3 of human origin. C19 is also indicated for the detection of Mdr proteins of equine, canine, bovine and porcine origin.

MDR3, a member of the ABCB ABC transporter subfamily, is shown to be highly expressed (mRNA) in the human liver, with C219 showing localisation of the MDR3 protein to the bile canniculi (Scheffer et al., 2000, Smit et al., 1994). MDR3 mRNA expression was reported in the adrenal gland, heart, striated muscle, spleen and tonsil, with no mention of intestinal expression (Smit et al., 1994). Similar expression patterns for the homologous mouse Mdr2 protein have also been reported (Smit et al., 1993). Given the lack of MDR3/Mdr2 mRNA in the human and mouse intestine respectively it is expected that Mdr2 mRNA will also be lacking in the rat intestine, as such an absence of Mdr2 protein is predicted in this region (Smit et al., 1994, Smit et al., 1993). In rats Mdr3 is an alternative name for Mdr1a, an isoform of Mdr1 which will be detected with the antibodies used here (Teeter et al., 1990). Given the lack of MDR3 and Mdr2 intestinal expression and that Mdr3 is identical to Mdr1a, it is assumed that the use of the C219 and C19 antibodies in rat intestine will allow specific localisation of the Mdr1 protein. Works will therefore refer only to MDR1/Mdr1 detection from this point forward.

To ensure accurate assessment of Mdr1 expression in rat intestine, antibody specificity of C219 and C19 using Western blot and immunocytochemistry experiments was determined. The two antibodies selected for the detection of MDR1 are predicted to cross react with both human and rat variants, allowing the translation of antibody specificity validations from MDCKII-MDR1 transfected cell lines to rat tissues.

Western blot and immunocytochemical staining of native and MDR1 transfected MDCKII cells were performed to confirm antibody specificity. Figure 5.2 shows the detection of MDR1 by C219 and C19 in native and transfected MDCKII cells and of Mdr1 in rat ileum mucosal scrapes.

Proteins were extracted as described in methods section 2.2.7.1. Immunoblotting shows a C219 protein band present at approximately 170KDa in the MDCKII-MDR1 protein sample and in the rat ileum muscosal scrape sample, similar to the predicted molecular weight of MDR1. It is therefore likely that this band represents the MDR1 transporter. No band was detected by C219 in the native (dog) MDCKII cell protein sample however actin loading controls confirm successful loading and separation of protein samples by SDS gel electrophoresis (figure 5.2). The absence of a 170KDa band in the native MDCKII cell sample exposed to C219 suggests a lack of ability of this antibody to detect canine Mdr1 or that the level of Mdr1 protein expression is low as suggested by Hoechst33342 retention assays detailed in chapter 3. Bands of differing intensities are clearly visible at sizes below 170KDa in all three sample lanes, suggesting a possible lack of MDR1/Mdr1 specificity to be associated with the C219 antibody in these situations.

In contrast, the use of C19 in immunoblotting was shown to give specific, single intense bands at approximately 170KDa in all three samples (native MDCKII, MDCKII-MDR1 and rat ileum, figure 5.2). Unlike C219 no non-specific bands below 170KDa were apparent. Since no protein band was detected in the native MDCKII protein sample using C219, detection of Mdr1 in native MDCKII samples using C19 likely represents expression of endogenous canine Mdr1 protein. Actin loading controls confirm approximately equal loading of protein across all samples. The increased protein band density observed in the MDR1 transfected cell line therefore suggests cumulative detection of endogenous canine Mdr1 and stably expressed transfected human MDR1, compared with canine expression alone in the native MDCKII counterpart. Reactivity with rat Mdr1 is shown by detection of an intense band in the ileal mucosal sample at the same molecular weight to that detected in MDR1 transfected cells.

Western blot findings are supported by immunocytochemical detection of MDR1 in MDCKII-MDR1 cells (figures 5.3 to 5.6). Cells were cultured on permeable supports and fixed using 4% PFA as described in materials and methods section 2.2.8. Primary antibodies C219 and C19 were detected with secondary anti-mouse 647nm (figures 5.3 and 5.4) and anti-goat 488nm (figures 5.5 and 5.6) antibodies respectively (table 2.2). Cell nuclei were counterstained using either propidium iodide or Hoechst33342. Ezrin is a cytoskeletal protein known to be highly expressed at the apical brush border membrane of intestinal epithelial cells (Berryman et al., 1993) therefore primary antibodies were co-incubated with the anti-Ezrin H276 antibody to allow confirmation of apical localisation. Confocal gain settings were adjusted such that primary omitted control sections for Ezrin staining showed no background fluorescence, as shown in control panels of figure 5.3 (see methods section 2.2.8). Following indication of a lack of specific MDR1 expression by Western blot in native cells by C219, native C219

immunofluorescence was arbitrarily set to zero and MDR1 transfected cells imaged using the same confocal microscope gain settings. This allowed direct comparison of MDCKII-MDR1 cells with native counterparts. Co-localisation of MDR1 and Ezrin following immunostaining of MDR1 transfected MDCKII cells with C219 and anti-Ezrin antibody H276 in combination showed overlapping expression patterns and suggests apical cell membrane expression of MDR1 (merged image figure 5.4, XY and XZ focal plane images). Confocal imaging of native MDCKII cells using the same gain adjustment settings for C219 showed no cellular fluorescence (figure 5.3 XY, XZ focal plane C219 images). Lack of native MDR1 expression confirms reactivity of the C219 antibody with MDR1 since fluorescence is observed only following transfection. Note that only a subset of cells show immunostaining of MDR1 across the cell monolayer using the C219 antibody, suggesting low affinity of C219 with regards to protein binding since staining of filter quarters taken from the same permeable membrane support using C19 displayed a uniform MDR1 expression (figure 5.6).

In agreement with Western blot data, endogenous canine Mdr1 expression is shown by immunocytochemistry using the C19 antibody in native MDCKII cells (figure 5.5, XY and XZ focal plane image panels). C19 immunostaining in XZ optical sections show that it is primarily localised to the cell cytoplasm or lateral cell membranes. This is confirmed by apical Ezrin immunostaining with quite separate cellular localisation being evident in the super-imposed image. Due to apparent high levels of endogenous canine Mdr1 transporter expression gain adjustments were made against primary omitted controls only. Increased 488nm fluorescence intensity was however visible in MDR1 transfected cells compared with native counterparts with uniform transporter expression is shown throughout the cell monolayer (figure 5.5 and 5.6). Some level of co-localisation of MDR1 and Ezrin is observed at the apical cell membrane although, as observed using C219, co-localised staining is sporadic across the cell monolayer when viewed in the XZ optical plane (figure 5.6).

Taken together Western blotting and immunofluorescence data show that C219 and C19 antibodies react with MDR1 protein of both human and rat origin, however antibody validation experiments show the C19 antibody to be superior to C219. Western blot analysis using C19 showed only one band of the correct molecular weight for MDR1/Mdr1 whilst multiple bands were apparent with C219. We therefore determined intestinal expression of the Mdr1 protein in rat sections using the goat polyclonal C19 primary antibody.

Intestinal Mdr1 expression is localised to the villus apical membrane in all small intestine sections, duodenum, jejunum and ileum and to a lesser extent the apical membrane of the colon (figure 5.7). All sections were stained simultaneously using the Ventana XT staining platform removing inter-experiment variations and allowing direct comparison of staining

intensities across sections. Primary omitted negative controls are shown to the right hand side of each image pair for the respective intestine section. Mdr1 staining intensity, and associated protein expression, appear to be greatest in the ileum with increasing expression from the villus base to the villus tip (figure 5.7). C19 staining appears to visually show a decreasing stain intensity from the ileum, to the duodenum, jejunum and colon respectively (figure 5.7) suggesting ileal protein expression levels to be the highest of those areas studied. Quantification of staining intensities should be performed to confirm these visual observations, however no successful quantification methods were employed here.

Higher magnification images show distinct Mdr1 staining at the brush border membrane of enterocytes with an apparent lack of Mdr1 expression in epithelial cells below the crypt junction (figure 5.8). Mdr1 staining in the villus is localised to absorptive epithelial cells with no detection being apparent on villus goblet cell membranes. Despite a lack of uniform staining of Mdr1 expression below the crypt-villus junction, immunoreactivity is apparent in a very distinct region at the bottommost location of the crypt (figure 5.8B). Staining of Mdr1 is interspersed between those cells which form the bottommost crypt region which show signs of characteristics consistent with those of the proposed intestinal stem cell niche (figure 5.8B, inset). We also show Mdr1 expression at the apical membrane of follicular associated epithelium, with sporadic staining shown within the follicle (indicated by the black arrows in figure 5.8C).

The localisation of Mdr1 to a distinct subset of cells located within the crypt base lead us to determine the relation of this staining to the crypt stem cell population. Recent findings have indicated the G-protein coupled receptor Lgr5 to be a unique marker of crypt stem cells (Barker et al., 2007). We therefore used the anti-LGR5 antibody raised against the LGR5 protein to identify Lgr5 positive cells within rat intestinal sections. Figure 5.9 shows a darkened anti-Lgr5 dependent immunoreactivity in single cells of the crypt region. Additionally a distinct staining of some villus enterocytes is shown (figure 5.9). It should be noted however that potential nonspecific staining is observed in the mid villus and basement membrane regions. In contrast primary omitted controls show no immunoreactivity. Although attempts were made to detect Lgr5 protein using Western blot they were unsuccessful using this anti-Lgr5 antibody.

Table 5.1:

Antibody	Supplier	Recommended for the detection of	Type	Epitope; amino acid residues	Immuno mapped to	Cross reactivity		
						Human	Rat	Mouse
PC-10	AbCam	Pcna of mouse,rat, chicken, human, pig, monkey and more	Mouse IgG monoclonal	unknown	rat Pcna fusion protein obtained from PC2T; unknown	X	X	X
C19	Santa-Cruz	Mdr1, Mr2 and Mdr3 of mouse and rat origin MDR1 and MDR3 of human origin also reacts with equine, canine, bovine	Goat IgG polyclonal	Epitope located within the c-terminal region	MDR1 of human origin; unknown	X	X	X
C219	Calbiochem	MDR1 and MDR3 of human, rat, mouse and hamster origin	Mouse IgG_1 monoclonal	unknown	multidrug resistance CHO cell line and multidrug resistance human cell line; unknown	X	X	X
Lgr5 (ab75850)	AbCam	Lgr5 (GPR49) of mouse, rat and human origin	Rabbit IgG monoclonal	unknown	Synthetic peptide corresponding to residues in human LGR5	X	X	X
M2-III-6	AbCam	MRP2 of human and rat origin	Mouse IgG_{2a} monoclonal	residues 1339 - 1541, internal epitope	Bacterial fusion protein of human MRP2 containing the carboxy-terminal region; unknown	X	X	
M70	Santa-Cruz	Bcrp of rat and mouse origin	Rabbit IgG polyclonal	internal topological domain	Mouse Bcrp; amino acids 301-370		X	X
BXP9	AbCam	Bcrp of mouse origin	Rat IgG_1 monoclonal	topological domain	Fusion protein containing fragment of mouse Bcrp; amino acids 221-394			X
Clone5d3 (MAB4155)	Millipore	BCRP/Bcrp of human and rat origin	Mouse IgG_{2b}	Extracellular peptide sequence	3T3 cells expressing human BCRP; unknown	X	X	
B25	Santa-Cruz	BCRP/Bcrp of human, rat and mouse origin	Rabbit IgG polyclonal	unknown	Human BCRP; unknown	X	X	X
D20	Santa-Cruz	Bcrp of rat and mouse origin	Goat IgG polyclonal	Peptide sequence located toward N-terminal region	unknown		X	X
10180-1-AP	Protein tech	BCRP/Bcrp of human , rat and mouse origin	Rabbit IgG polyclonal	intracellular peptide sequence	Human BCRP; amino acids 0-249	X	X	X
BXP21 (MAB4146)	Millipore	BCRP of human origin	Mouse IgG monoclonal	intracellular peptide sequence	Human BCRP; amino acids 271-396	X		
H276	Santa-Cruz	Ezrin of mouse, rat and human. Also reactive with equine, canine, bovine and porcine	Rabbit IgG polyclonal	Epitope located within the c-terminal region	Human Ezrin; amino acids 311-586	X	X	X
I19	Santa-Cruz	Broad range of Actin isoforms of mouse, rat, human and more	Goat IgG polyclonal	Epitope located within the c-terminal region	Human Actin; unknown	X	X	X
AB111868	AbCam	CYP1A1 and 1A2 of mouse and human, predicted to work with rat	Mouse IgG_1 monoclonal	Unknown	Unknown	x	predicted	X

Table 5.1 Details of all antibodies used in the current study, including host species, reactivity and immunogen details.

Figure 5.1:

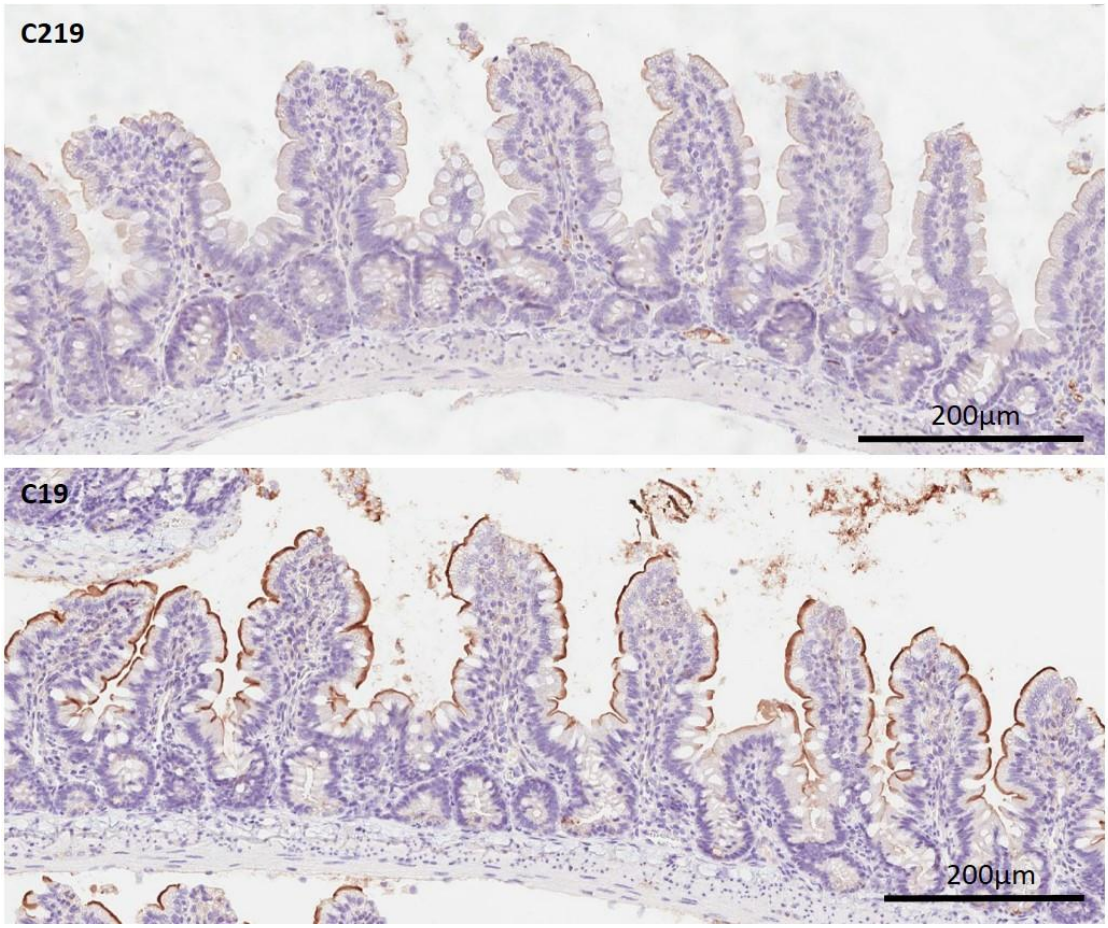

Figure 5.1 Immunohistochemical detection of Mdr1 in rat ileum paraffin embedded sections using the mouse monoclonal C219 and goat polyclonal C19 antibodies.

Images show Mdr1 localisation using anti-Mdr1 antibodies C219 and C19 diluted 1:25 in formalin fixed, paraffin embedded ileal male Sprague-Dawley rat intestinal sections of 4µm thickness. Staining is shown at the apical cell membrane of villus epithelial cells using both C219 (top) and C19 (bottom). An increased intensity of staining is shown with the C19 antibody compared to that observed with C219. Images are representative of two rat ileum sections taken from two animals. Sections were stained using an automated Ventana benchmark XT staining platform with Tris-based antigen retrieval, DAB antigen stain and haematoxylin counter stain. Sections were rehydrated and cover slips mounted. Slides were then scanned electronically using an Aperio ScanScope.

Figure 5.2:

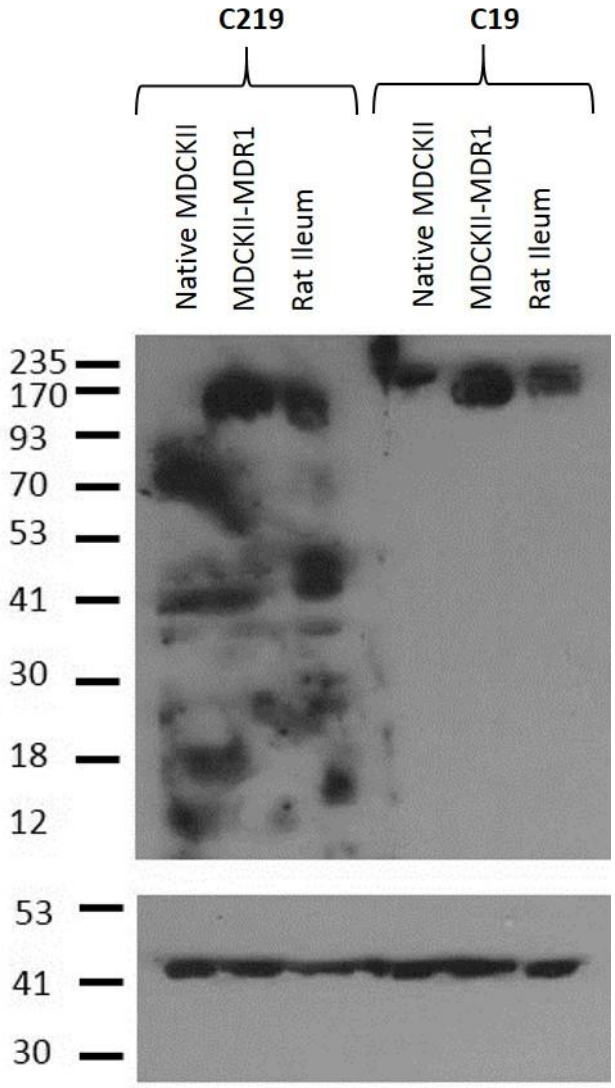

Figure 5.2 Western blot analysis of MDR1/Mdr1 expression in native MDCKII, MDCKII-MDR1 cell lines and male rat mucosal ileum scrapes.

Image shows native MDCKII (20µg protein loaded), MDCKII-MDR1 (20µg loaded protein) and rat ileum (20µg loaded protein) MDR1/Mdr1 protein expression. Following transfer, nitrocellulose membranes were probed with mouse monoclonal C219 primary antibody, diluted 1:100 (left) or goat polyclonal C19 primary antibody diluted 1:50 (right) overnight at 4˚C. Primary antibodies were detected using anti-mouse and anti-goat HRP conjugated secondary antibodies. C219 and C19 antibodies yield bands at approximately 170KDa. Membranes were stripped and re-probed using a cross species anti-actin I-19 antibody as a loading control (43KDa). Western blot image shown is one gel and was performed only once to confirm antibody specificity.

Figure 5.3:

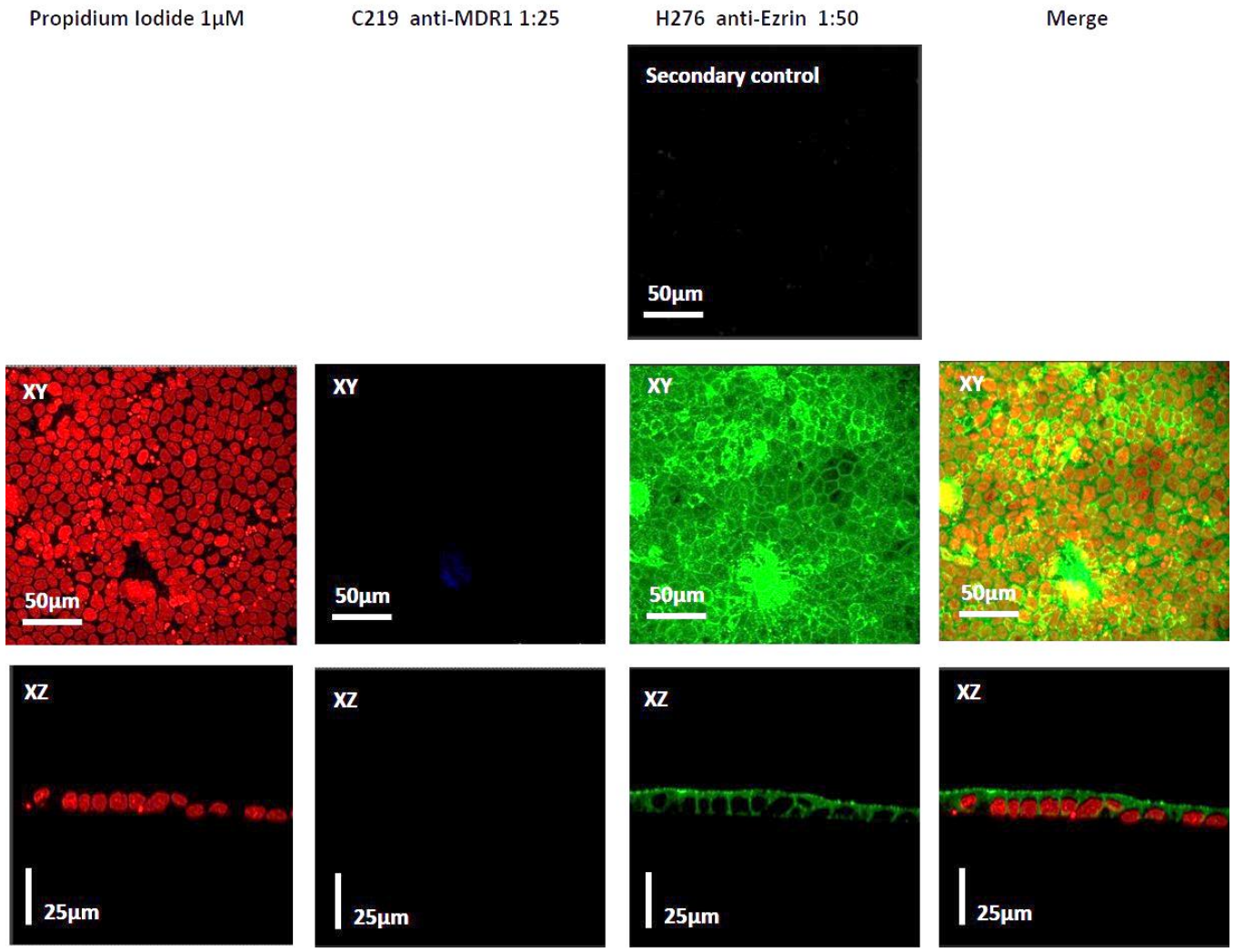
Propidium Iodide 1µM
C219 anti-MDR1 1:25
H276 anti-Ezrin 1:50
Merge
Secondary control
50µm
XY
50µm
XY
50µm
XY
50µm
XY
50µm
XZ
25µm
XZ
25µm
XZ
25µm
XZ
25µm

Figure 5.3 Immunocytochemical detection of MDR1 and Ezrin in native MDCKII cell monolayers using anti-MDR1 antibody C219 and anti-Ezrin H276

Native MDCKII cells were cultured on transwell filters for a period of seven days. Filters were co-stained for MDR1, (C219 mouse monoclonal primary antibody, 1:25), and Ezrin (H-276 rabbit polyclonal primary antibody, 1:50). Secondary antibodies directed against C219 and H-276 were donkey anti-mouse 647nm (AbCam, UK) and donkey anti-rabbit 488nm (AbCam, UK) respectively. Cell nuclei were counterstained using propidium iodide (1µM). Merged image shows propidium iodide nuclear stain, MDR1 and Ezrin expression. Gain settings were adjusted accordingly to within the limits of secondary only controls such that native 647nm fluorescence was arbitrarily set to zero, allowing direct comparison between native MDCKII and MDCKII-MDR1. Images were taken using Leica CS SP2 UV confocal laser scanning microscopy with a x63 oil immersion objective, sections were approximately 1µm thick. XY images show a stack of images taken throughout the cell monolayer and XZ images confirm apical localisation of Ezrin. Image brightness has been increased to allow fluorescence to be viewed, both figure 5.3 and 5.4 were subject to identical brightness adjustments to allow comparison.

Figure 5.4:

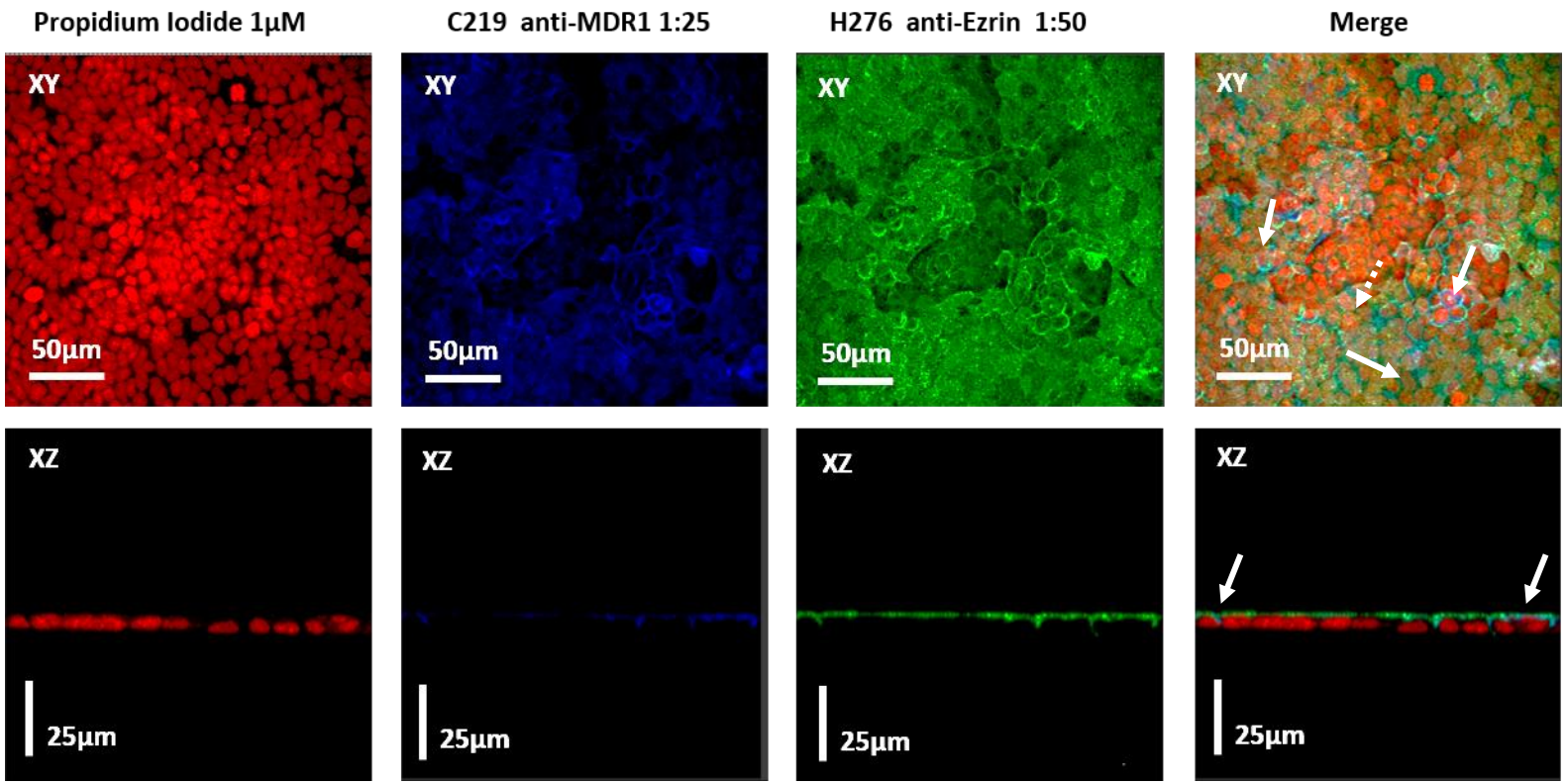
Propidium Iodide 1µM
C219 anti-MDR1 1:25
H276 anti-Ezrin 1:50
Merge
XY
XZ
50µm
25µm

Figure 5.4 Immunocytochemical detection of MDR1 and Ezrin in MDCKII-MDR1 cell monolayers using anti-MDR1 antibody C219 and anti-Ezrin H276

MDCKII-MDR1 cells were cultured on transwell filters for a period of seven days. Filters were co-stained for MDR1, (C219 mouse monoclonal primary antibody, 1:25), and Ezrin (H-276 rabbit polyclonal primary antibody, 1:50). Secondary antibodies directed against C219 and H-276 were donkey anti-mouse 647nm (AbCam, UK) and donkey anti-rabbit 488nm (AbCam, UK) respectively. Cell nuclei were counterstained using propidium iodide (1µM). Merged image shows propidium iodide nuclear stain, MDR1 and Ezrin expression. White solid arrows indicate co-localisation of MDR1 and Ezrin whilst the white dashed arrow shows a lack of MDR1 expression to be apparent in some areas of the cell monolayer. Gain settings were adjusted accordingly to within the limits of secondary only controls to allow direct comparison between native MDCKII and MDCKII-MDR1. Images were taken using Leica CS SP2 UV confocal laser scanning microscopy with a x63 oil immersion objective, sections were approximately 1µm thick. XY images show a stack of images taken throughout the cell monolayer and XZ images show inconsistent co-localisation (solid white arrows) of Mdr1 and Ezrin at the apical cell membrane. Image brightness has been increased to allow fluorescence to be viewed, both figure 5.3 and 5.4 were subject to identical brightness adjustments to allow comparison.

Figure 5.5:

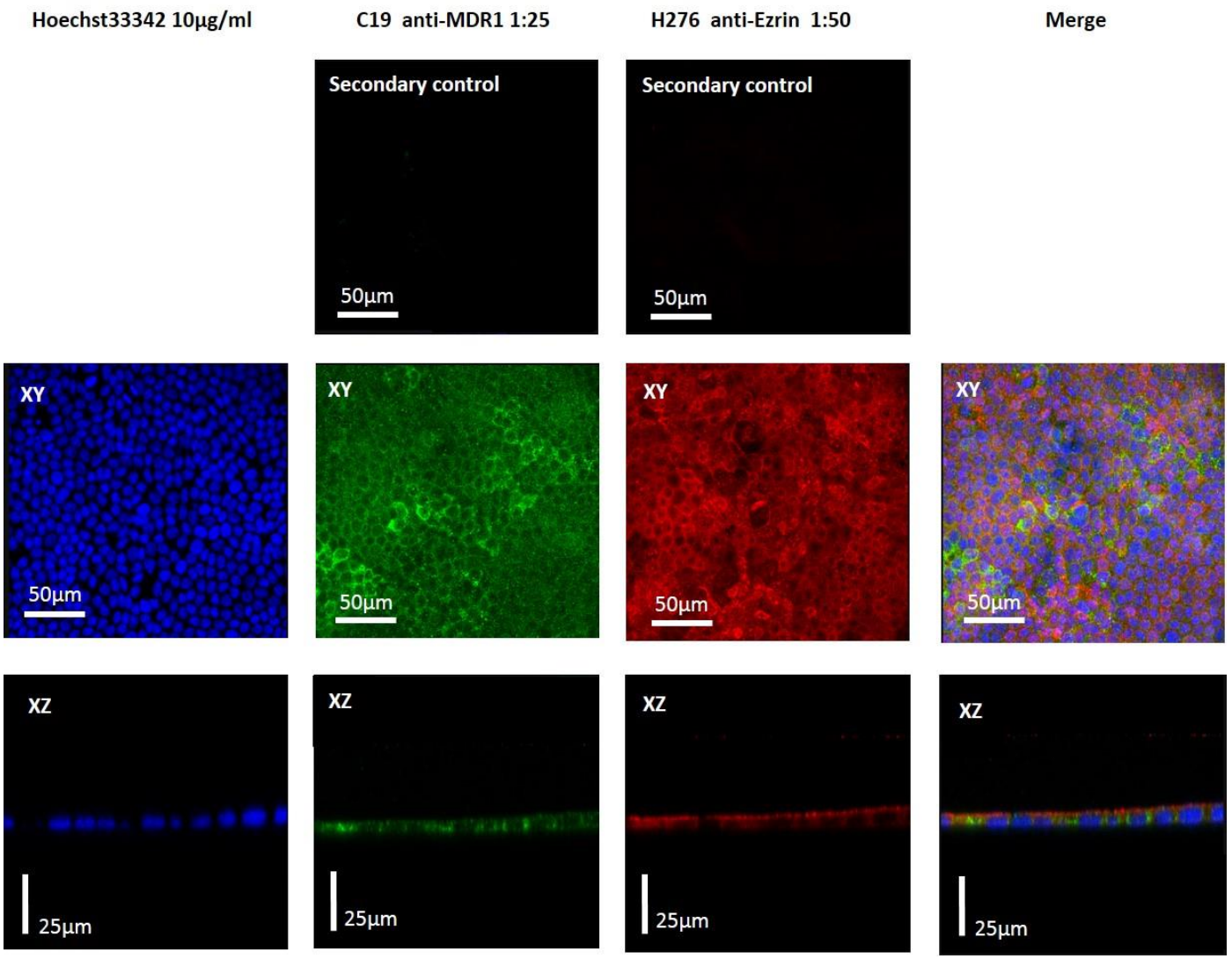
Hoechst33342 10µg/ml
C19 anti-MDR1 1:25
H276 anti-Ezrin 1:50
Merge
Secondary control
Secondary control
50µm
50µm
XY
XY
XY
XY
50µm
50µm
50µm
50µm
XZ
XZ
XZ
XZ
25µm
25µm
25µm
25µm

Figure 5.5 Immunocytochemical detection of MDR1 and Ezrin in native MDCKII cell monolayers using anti-MDR1 antibody C19 and anti-Ezrin H276

Native MDCKII cells were cultured on transwell filters for a period of seven days. Filters were co-stained for MDR1 (C19 goat polyclonal primary antibody, 1:25), and Ezrin (H-276 rabbit polyclonal primary antibody, 1:50). Secondary antibodies directed against C19 and H-276 were donkey anti-goat 488nm (AbCam, UK) and donkey anti-rabbit 566nm (SantaCruz, UK) respectively. Control images show fluorescence in absence of primary antibody. Gain settings were set against secondary only controls, allowing comparison between native MDCKII and MDCKII-MDR1 cells. Cell nuclei were counterstained using Hoechst33342 (10µg/ml). Merged images show Hoechst33342 nuclear stain, MDR1 and Ezrin expression. Images were taken using a Leica CS SP2 UV confocal laser scanning microscopy with a x63 oil immersion objective, sections were approximately 1µm thick. XY images show a stack of images taken throughout the cell monolayer and XZ images confirm apical localisation of Ezrin.

Figure 5.6:

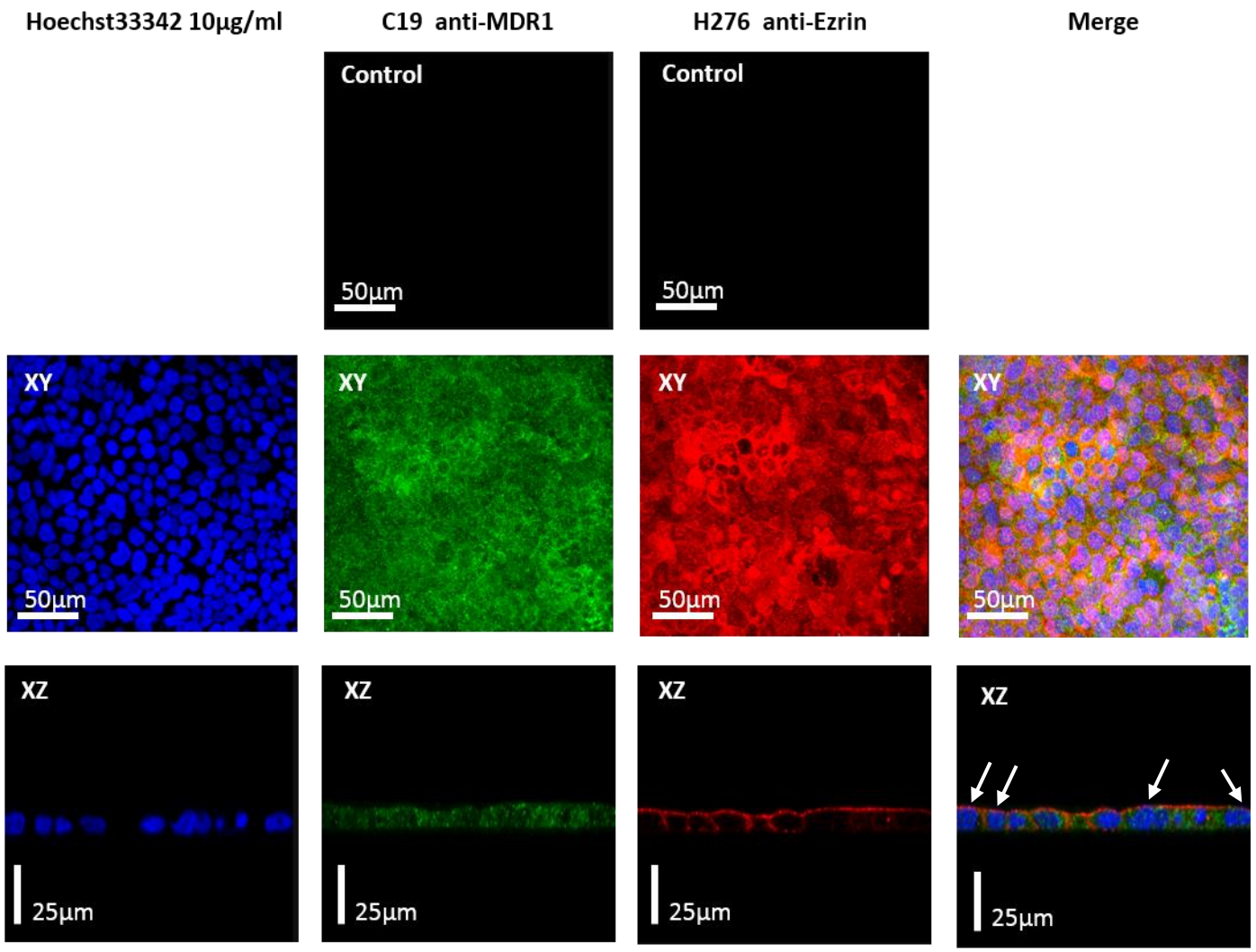
Hoechst33342 10µg/ml
C19 anti-MDR1
H276 anti-Ezrin
Merge
Control
Control
50µm
50µm
XY
XY
XY
XY
50µm
50µm
50µm
50µm
XZ
XZ
XZ
XZ
25µm
25µm
25µm
25µm

Figure 5.6 Immunocytochemical detection of MDR1 and Ezrin in MDCKII-MDR1 cell monolayers using anti-MDR1 antibody C19 and anti-Ezrin H276

MDCKII-MDR1 cells were cultured on transwell filters for a period of seven days. Filters were co-stained for MDR1 (C19 goat polyclonal primary antibody, 1:25), and Ezrin (H-276 rabbit polyclonal primary antibody, 1:50). Secondary antibodies directed against C19 and H-276 were donkey anti-goat (AbCam, UK) 488nm and donkey anti-rabbit 566nm (SantaCruz, UK) respectively. Control images show fluorescence in the absence of primary antibody. Gain settings were set against secondary only controls, allowing comparison between native MDCKII and MDCKII-MDR1. Cell nuclei were counterstained using Hoechst33342 (10µg/ml). Merged images show Hoechst33342 nuclear stain, MDR1 and Ezrin expression. Images were taken using a Leica CS SP2 UV confocal laser scanning microscopy with a x63 oil immersion objective, sections were approximately 1µm thick. XY images show stack of images taken throughout the cell monolayer and indicate co-localisation of Mdr1 and Ezrin however XZ images suggest only sporadic co-localisation of MDR1 and Ezrin at the apical cell membrane (white arrows).

Figure 5.7:

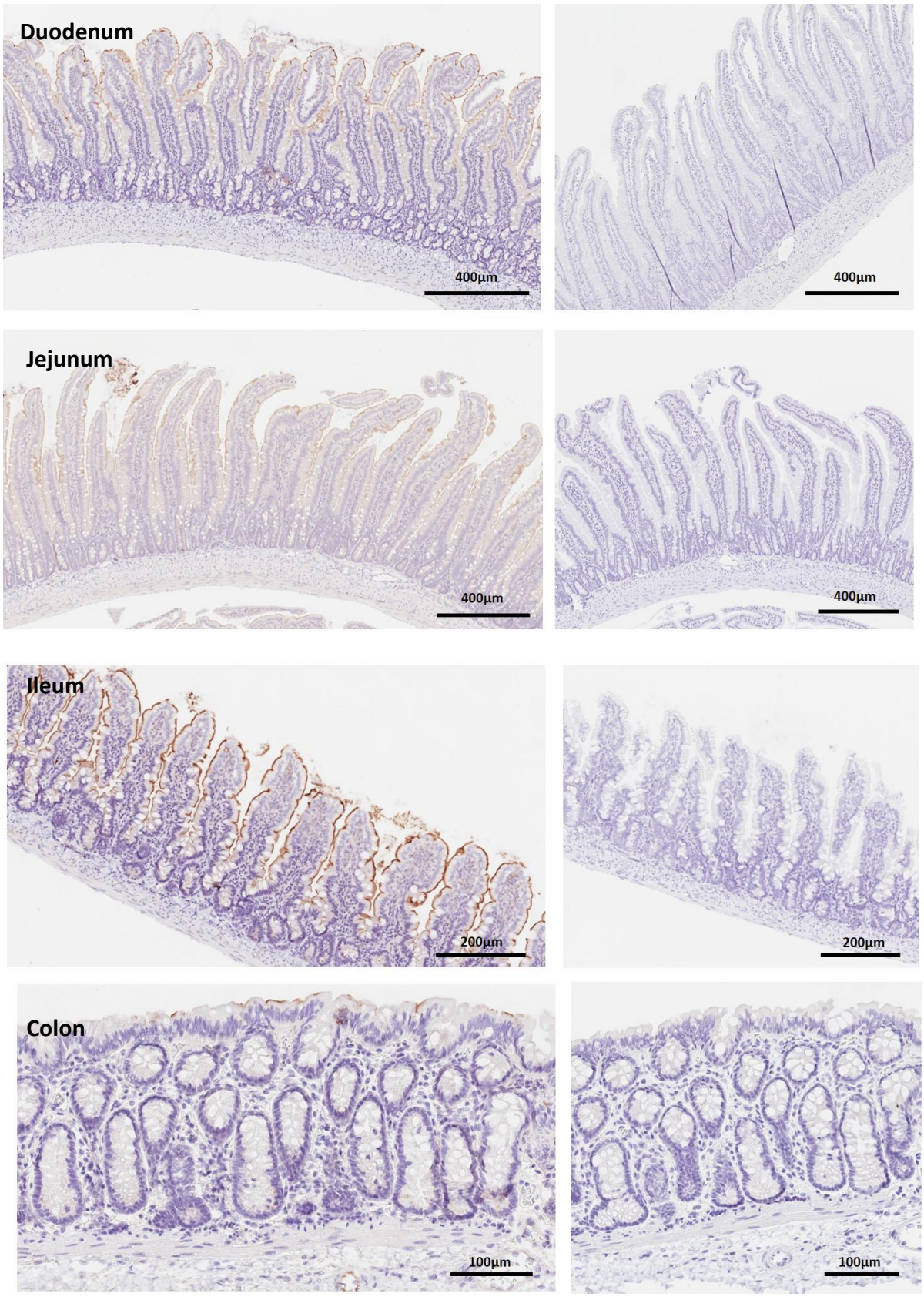
Duodenum
400µm
400µm
Jejunum
400µm
400µm
Ileum
200µm
200µm
Colon
100µm
100µm

Figure 5.7 Immunohistochemical localisation of Mdr1 in formalin fixed, paraffin embedded male rat intestine using the C19 primary antibody.

Immunohistochemical localisation of Mdr1 in the duodenum, jejunum, ileum and colon of rat intestine using primary goat polyclonal C19 antibody, 1:25 dilution, (left) and primary antibody omitted controls (right). Staining is visible at the apical brush-border villus membrane in all intestinal segments. Formalin fixed, paraffin embedded intestinal sections (4µm thickness) were stained using an automated Ventana benchmark XT staining platform with citric acid and protease based antigen retrieval, DAB antigen stain with haematoxylin counter stain, all regional sections were stained simultaneously. Sections were rehydrated and cover slips mounted. Slides were scanned electronically using Aperio ScanScope.

Figure 5.8:

A

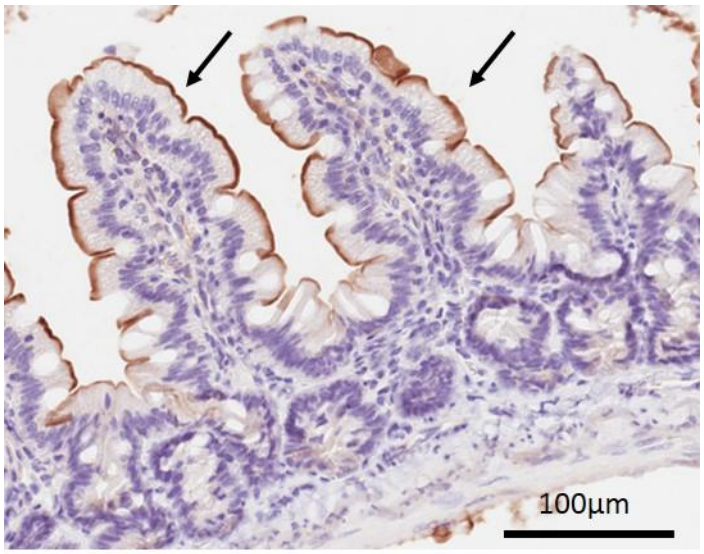

B

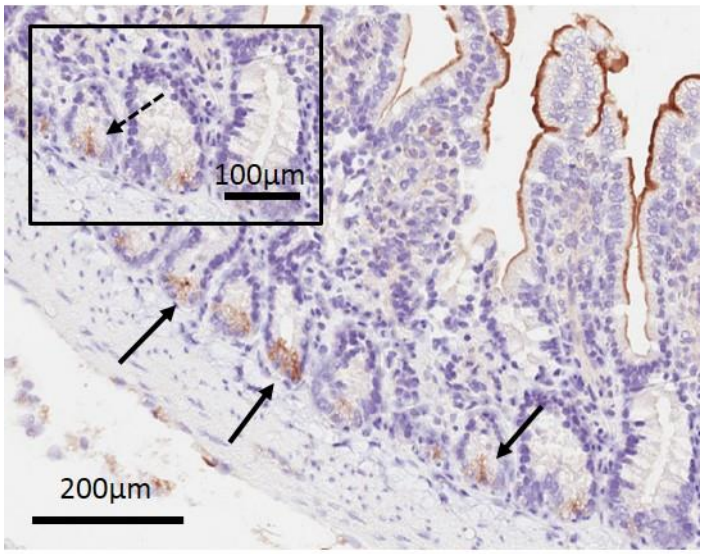

C

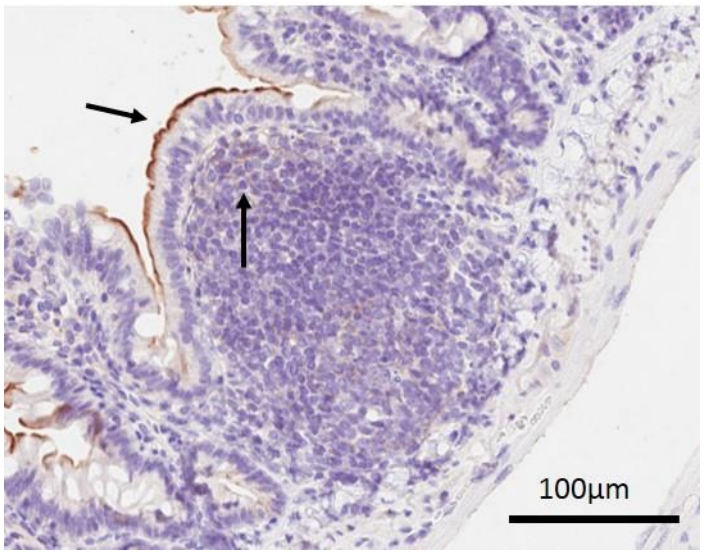

Figure 5.8 Immunohistochemical localisation of Mdr1 to brush-border villus membrane, crypt region and follicular associated epithelium in rat intestine.

Images show Mdr1 localisation using primary goat polyclonal antibody C19, 1:25 dilution, in formalin fixed, paraffin embedded ileal male rat intestinal sections (4µm thickness). **(A)** Intense staining is apparent at the apical brush-border villus membrane, with decreasing intensity down the villus toward the crypt-villus junction **(B)** sporadic staining is shown toward the base of the crypt unit, inset shows immunoreactivity to be localised to cells with a minimal cytoplasmic volume and triangular nuclei (dashed arrow)**. (C)** Mdr1 is interspersed within and localised to the apical membrane of follicular associated epithelium**.** Sections were stained using an automated Ventana benchmark XT staining platform with citric acid and protease based antigen retrieval, DAB antigen stain with haematoxylin counter stain. Regional sections were stained simultaneously. Sections were rehydrated and cover slips mounted. Slides were then scanned electronically using Aperio ScanScope.

Figure 5.9:

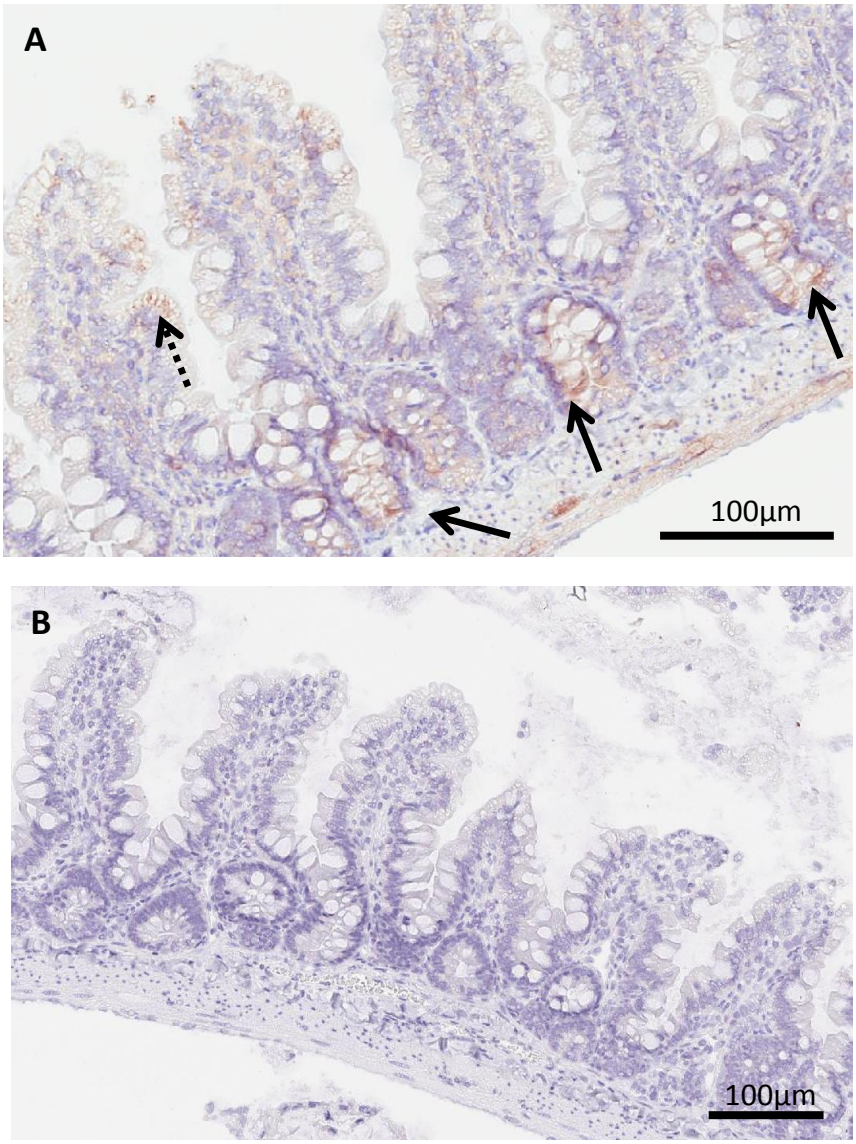

Figure 5.9 Immunohistochemical detection of Lgr5 in rat ileum sections using the anti-GPR49 antibody.

Images show formalin fixed, paraffin embedded rat ileum sections at a thickness of 4µm. **(A)** Immunohistochemical detection of Lgr5 using the anti-GPR49 antibody diluted 1:50 **(B)** primary antibody omitted control image. Image **(A)** shows increased immunoreactivity of GPR49 in cells located to the bottom of the crypt with distinct staining shown sporadically in villus epithelial cells, indicated by the black solid and dashed arrows respectively. Primary antibody omitted control shows no immunoreactivity. Sections were stained using an automated Ventana benchmark XT staining platform with Tris based antigen retrieval, DAB antigen stain with haematoxylin counter stain, sections were stained simultaneously. Sections were rehydrated and cover slips mounted. Slides were then scanned electronically using Aperio ScanScope.

5.3.2 Immunohistochemical detection of Mrp2/MRP2 in rat and human intestine using the primary antibody, M2-III-6

Despite high mRNA expression levels in all small intestine sections only very low Mrp2 protein expression was observed in the rat ileum at the apical membrane of villus epithelium, using the mouse monoclonal M2-III-6 antibody (figure 5.10). Protein expression detected is however questionable and may result from experimental variations in counterstaining procedures. We failed to detect Mrp2 protein expression in any other region of the small intestine. In agreement with NanoString RNA data a lack of Mrp2 expression was also apparent in the colon.

M2-III-6 is raised against a carboxy-terminal immunogen of the human MRP2 protein and is recommended for the detection of MRP2 of human and rat origin (table 5.1). We examined M2-III-6 reactivity in rat liver tissue as a control for Mrp2 expression. Despite questionable M2-III-6 immunoreactivity above the level of mouse IgG_{2a} negative controls in rat ileum sections, positive Mrp2 detection is shown in the liver using the same experimental conditions except for a reduced antibody concentration (figure 5.11). As reported previously (Maher et al., 2005, Mayer et al., 1995), intense Mrp2 staining at the lateral and bile canalicular membranes was observed (figure 5.11). Hepatic Mrp2 staining was observed at dilutions as low as 1:400.

To confirm M2-III-6 reactivity with MRP2/Mrp2 protein Western blot experiments using MDCKII-MRP2 cells and rat ileum and liver protein samples were conducted. Samples were prepared as described in materials and methods section 2.2.7. In support of M2-III-6 antibody specificity Western blot analysis revealed intense protein bands at approximately 170KDa, the molecular weight of MRP2/Mrp2, in MDCKII-MRP2 cells and rat liver. No protein band was detected using M2-III-6 in rat mucosal ileum samples, despite loading of high protein concentrations. Note 50µg of rat ileum and rat liver proteins were loaded compared with only 10µg of MDCKII-MRP2 protein (figure 5.12). Whilst detection of actin as a loading control was not performed, the lack of Mrp2 protein expression in rat ileum samples is supported by immunohistochemical results shown in figure 5.10, and is therefore not surprising. Western blot experiments strongly support reactivity of M2-III-6 with MRP2/Mrp2 of both human and rat origin and show only minimal levels of nonspecific binding in rat samples at a low molecular weight of approximately 26KD, well below the known molecular weight of the MRP2/Mrp2 protein.

The suitability of the M2-III-6 antibody for immunohistochemical staining was shown using indirect immunocytochemistry in the MRP2 transfected MDCKII cell line, with native MDCKII cells utilised as a negative control (figure 5.14 and 5.13). Cell lines were cultured and fixed (4%

PFA) as described in materials and methods section 2.2.8. Cell monolayers were counterstained for both MRP2 and the apical marker Ezrin. Ezrin is shown to be abundantly expressed at the apical cell membrane, as represented by the intense green fluorescence following detection with anti-mouse 488nm secondary antibody in both native and transfected cell lines (figure 5.13 and 5.14). Primary omitted controls are shown for Ezrin in native MDCKII cells (figure 5.13).

Native MDCKII 566nm fluorescence was set arbitrarily to zero (figure 5.13) such that any observed increase results directly from the detection of MRP2 following its stable transfection in the cell line. An intense increase in fluorescence above control level was apparent at the apical cell membrane following incubation of MDCKII-MRP2 cells with M2-III-6 (figure 5.14). Imaging of native MDCKII cells using the same settings failed to detect MRP2 protein (figure 5.13). The intense staining observed in MRP2 transfected cells confirms binding of M2-III-6 to the MRP2 antigen of human origin when the protein is expressed in its tertiary form. Co-localisation with Ezrin is shown in the merged XY panel, represented as mauve fluorescence (figure 5.14).

Immunocytochemical data combined with the appearance of 170KDa bands in Western blot experiments in MDCKII-MRP2 and rat liver protein samples, where MRP2 expression levels are high, in addition to literature supported localisation of Mrp2 to the rat bile canalicular membrane, indicate specific immunoreactivity of M2-III-6 with MRP2/Mrp2 and support the use of this antibody for immunohistochemical detection of the protein. Furthermore, the M2-III-6 antibody is well validated amongst peer reviewed literature with regards to successful detection of MRP2/Mrp2 protein using various techniques.

Confirmation of M2-III-6 Mrp2 specificity indicates a lack of Mrp2 protein expression in the rat small intestine and colon. To determine if this lack of expression observed in rat is attributable to species differences MRP2 protein expression in human jejunum and colon tissue samples was investigated (figure 5.15). Primary incubated sections are shown to the right hand side whilst primary omitted controls are visible to the left. As with rat intestine sections primary antibody dilution was 1:25 and antigen retrieval methods were identical to those used in rat liver and intestinal sections.

A visual increase in immunoreactivity is observed in human jejunum sections incubated with M2-III-6 compared with the lack of staining evident in rat intestine and with primary omitted negative controls. Diffuse staining is shown throughout the absorptive enterocytes (figure 5.15), with a stronger immunoreactivity evident at the apical brush border membrane in agreement with current literature (Fromm et al., 2000, Sandusky et al., 2002). No specific

protein localisation is observed in the cryptal region of human jejunum indicating a lack of MRP2 expression. Primary antibody omitted controls show no staining. Similar staining patterns are observed in human colon sections with a faint immunoreactivity at the epithelial brush border membrane and a lack of cryptal expression (figure 5.16).

Whilst immunohistochemical data indicate a slightly higher MRP2 expression in the human intestine compared with rat, differences may be attributable to experimental variation and/or differential affinity of the M2-III-6 antibody for human and rat MRP2/Mrp2. The apparent lack of intestinal Mrp2/MRP2 expression poses the question as to the involvement of this ABC transporter in intestinal drug disposition, especially in the rat, and suggests a lack of correlation between mRNA (chapter 4) and protein expression.

Figure 5.10:

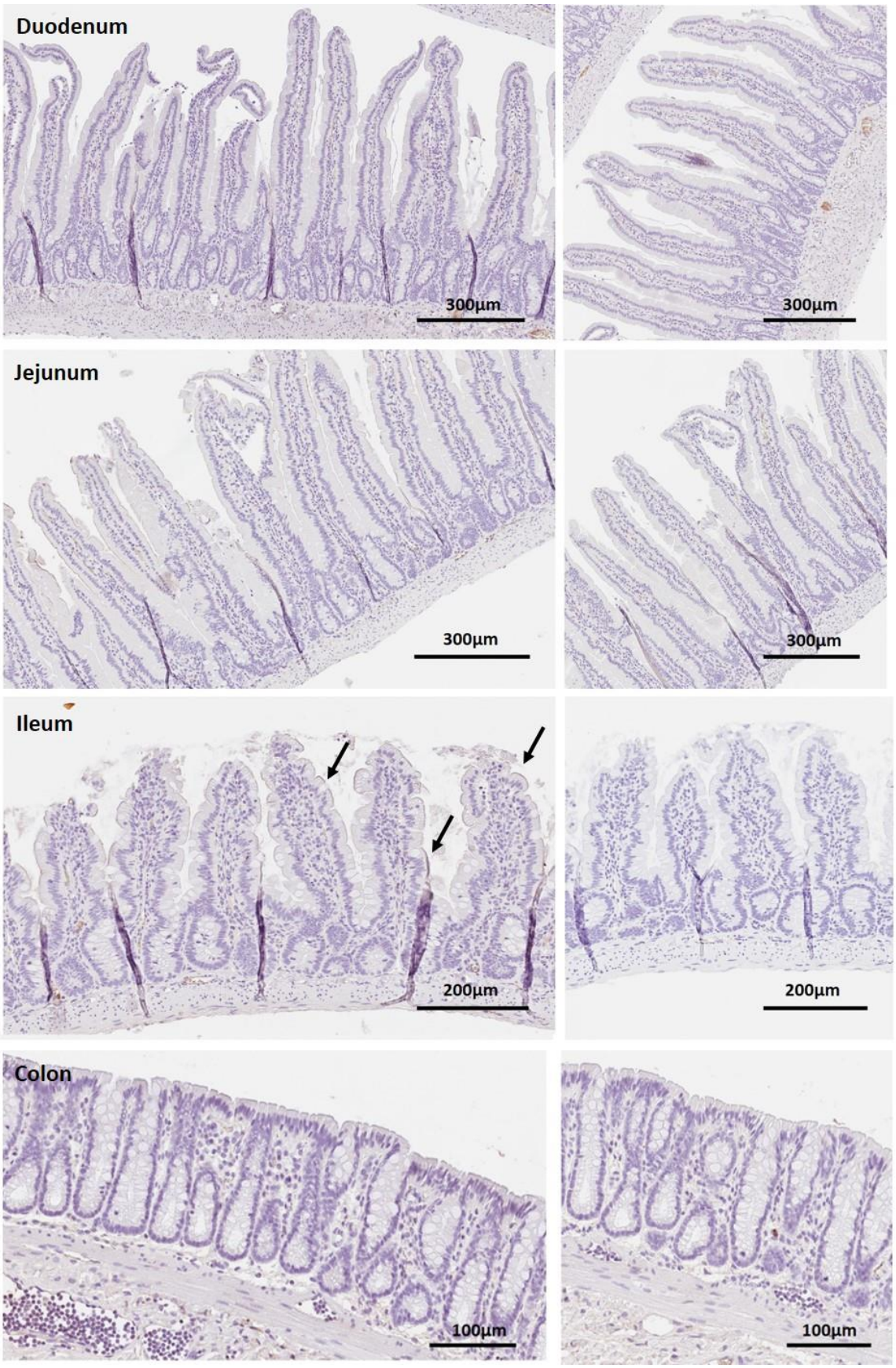
Duodenum
300µm
300µm
Jejunum
300µm
300µm
Ileum
200µm
200µm
Colon
100µm
100µm

Figure 5.10 Immunohistochemical localisation of Mrp2 in formalin fixed, paraffin embedded male rat intestine.

Immunohistochemical localisation of Mrp2 in the duodenum, jejunum, ileum and colon of rat intestine using primary mouse monoclonal antibody M2-III-6, 1:25 dilution, (left) and IgG_{2a} negative controls (right). Very faint staining is visible on the apical brush border membrane in ileum sections (black arrows) compared with negative controls. Duodenal, jejunal and colonic staining looks visually indifferent between M2-III-6 positive sections and negative controls. Intestinal sections (4µm thickness) were stained using an automated Ventana benchmark XT staining platform with citric acid based antigen retrieval, DAB antigen stain and haematoxylin counter stain, sections shown were all stained simultaneously. Sections were rehydrated and cover slips mounted. Slides were then scanned electronically using Aperio ScanScope.

Figure 5.11:

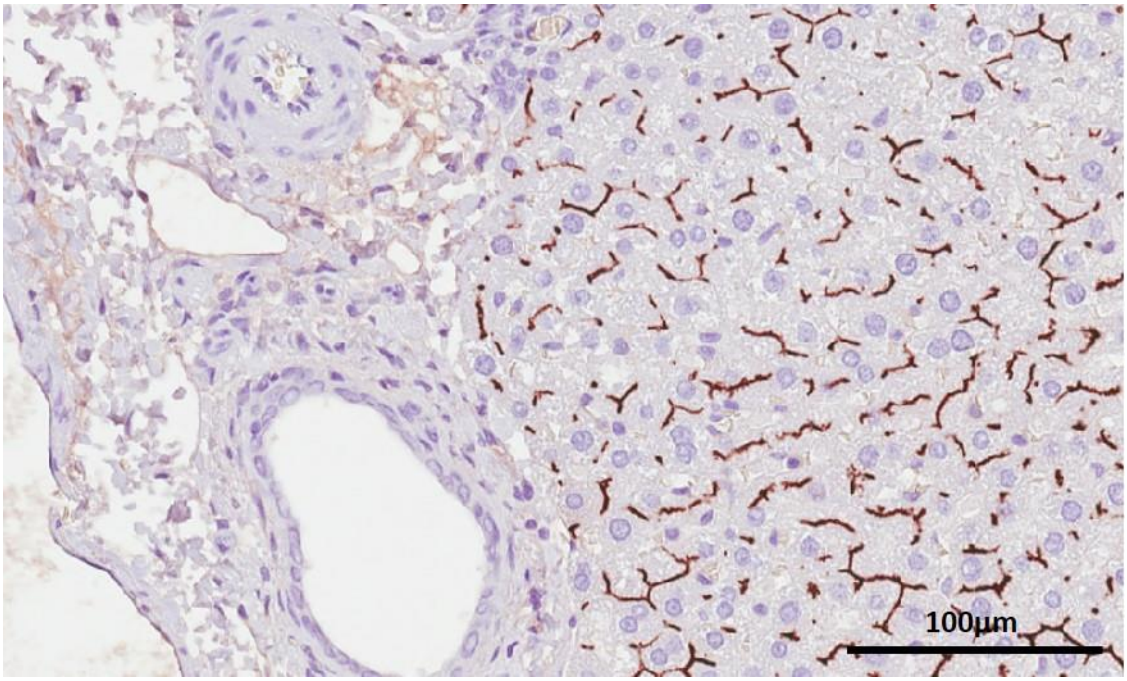

Figure 5.11 Immunohistochemical localisation of Mrp2 in formalin fixed, paraffin embedded rat liver using mouse monoclonal M2-III-6 antibody.

Image shows extensive staining of MRP2 at the canaliculi in rat liver using primary mouse monoclonal Mrp2 antibody M2-III-6, diluted 1:100. Liver section (4µm thickness) was stained using an automated Ventana benchmark XT staining platform with citric acid based antigen retrieval, DAB antigen stain and haematoxylin counter stain. Sections were rehydrated and cover slips mounted. Slides were then scanned electronically using Aperio ScanScope.

Figure 5.12:

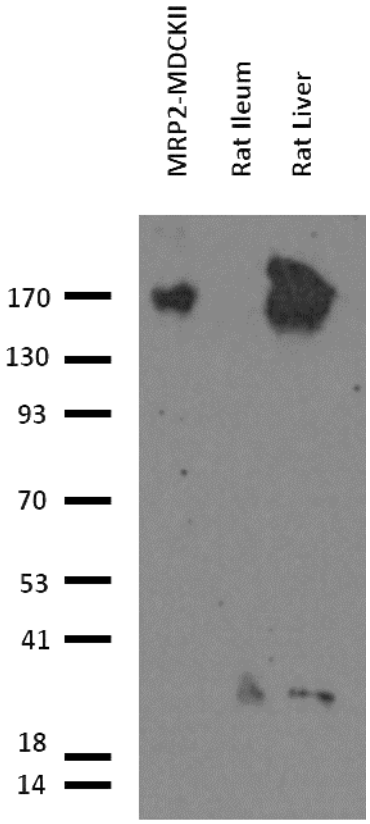

Figure 5.12 Western blot analysis of MRP2 expression in the MDCKII-MRP2 cell line and rat ileum and rat liver homogenate.

Image shows 10µg loaded MDCKII-MRP2 protein and 50µg of loaded rat ileum and rat liver protein. Following transfer, the nitrocellulose membrane was probed with mouse monoclonal M2-III-6 primary antibody, diluted 1:50 overnight at 4˚C with secondary detection using anti-mouse HRP conjugated antibody. M2-III-6 yielded bands at 170KDa in both MDCKII-MRP2 cell lysate and rat liver, however no band was apparent in the lane containing rat ileum protein. Image shown represents one gel.

Figure 5.13:

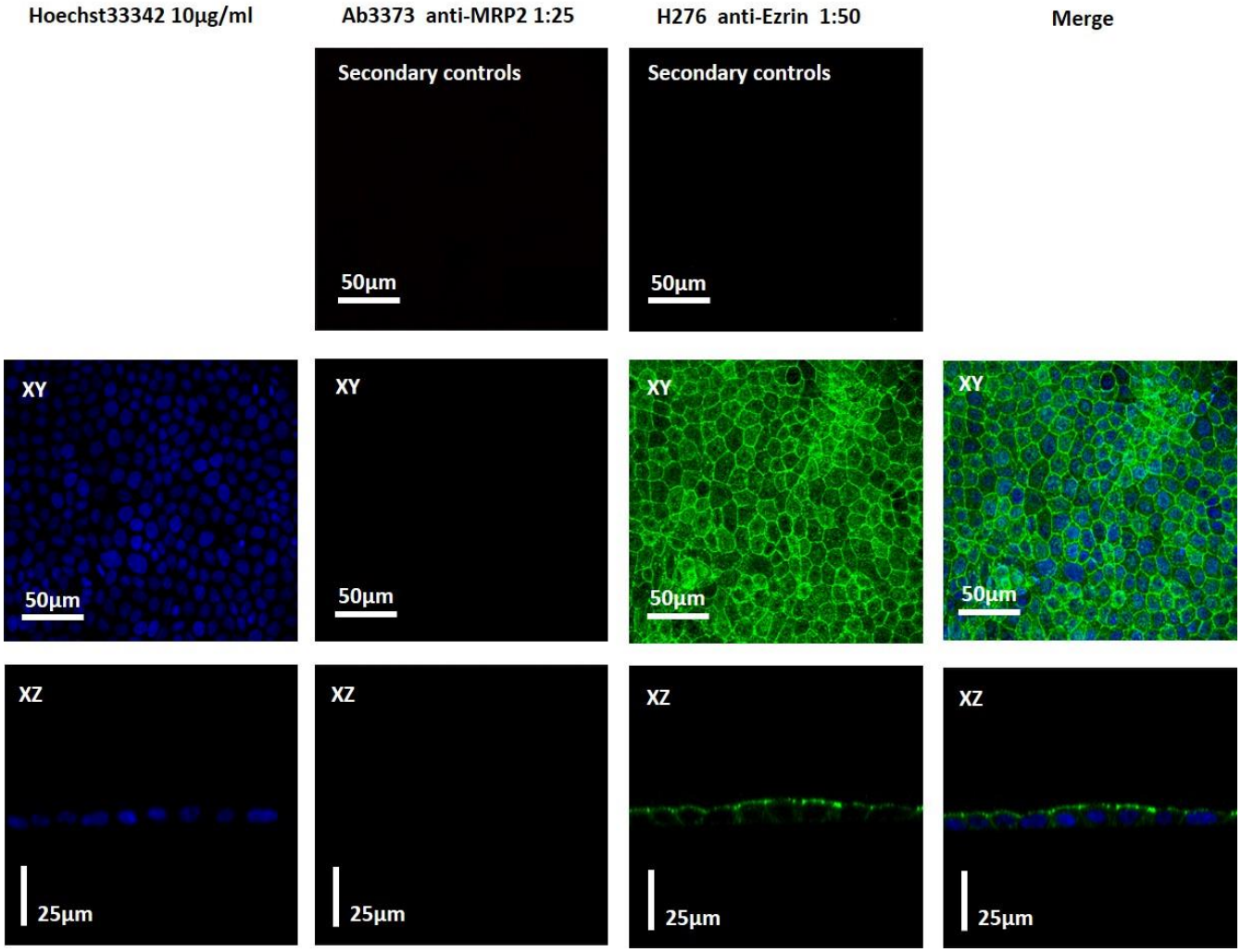
Hoechst33342 10µg/ml
Ab3373 anti-MRP2 1:25
H276 anti-Ezrin 1:50
Merge
Secondary controls
Secondary controls
50µm
50µm
XY
XY
XY
XY
50µm
50µm
50µm
50µm
XZ
XZ
XZ
XZ
25µm
25µm
25µm
25µm

Figure 5.13 Detection of MRP2 (M2-III-6) and Ezrin (H-276) in native MDCKII cell monolayers using indirect immunofluorescence.

Native MDCKII cells were cultured on transwell filters for a period of seven days. Filters were co-stained for MRP2, (M2-III-6 mouse monoclonal primary antibody, 1:25), and Ezrin (H-276 rabbit polyclonal primary antibody, 1:50). Secondary antibodies directed against M2-III-6 and H-276 were donkey anti-mouse 566nm (AbCam, UK) and donkey anti-rabbit 488nm (AbCam, UK) respectively. Cell nuclei were counterstained using Hoechst33342 (10µg/ml). Merged image showing Hoechst33342 nuclear stain, MRP2 and Ezrin expression. Gain settings were adjusted accordingly to within the limits of secondary only controls such that native 566nm fluorescence was arbitrarily set to zero, allowing direct comparison between native MDCKII and MDCKII-MDR1. Images were taken using Leica CS SP2 UV confocal laser scanning microscopy with a x63 oil immersion objective, sections were approximately 1µm thick. XY images show a stack of images taken throughout the depth of the cell monolayer and XZ images confirm apical localisation of Ezrin.

Figure 5.14:

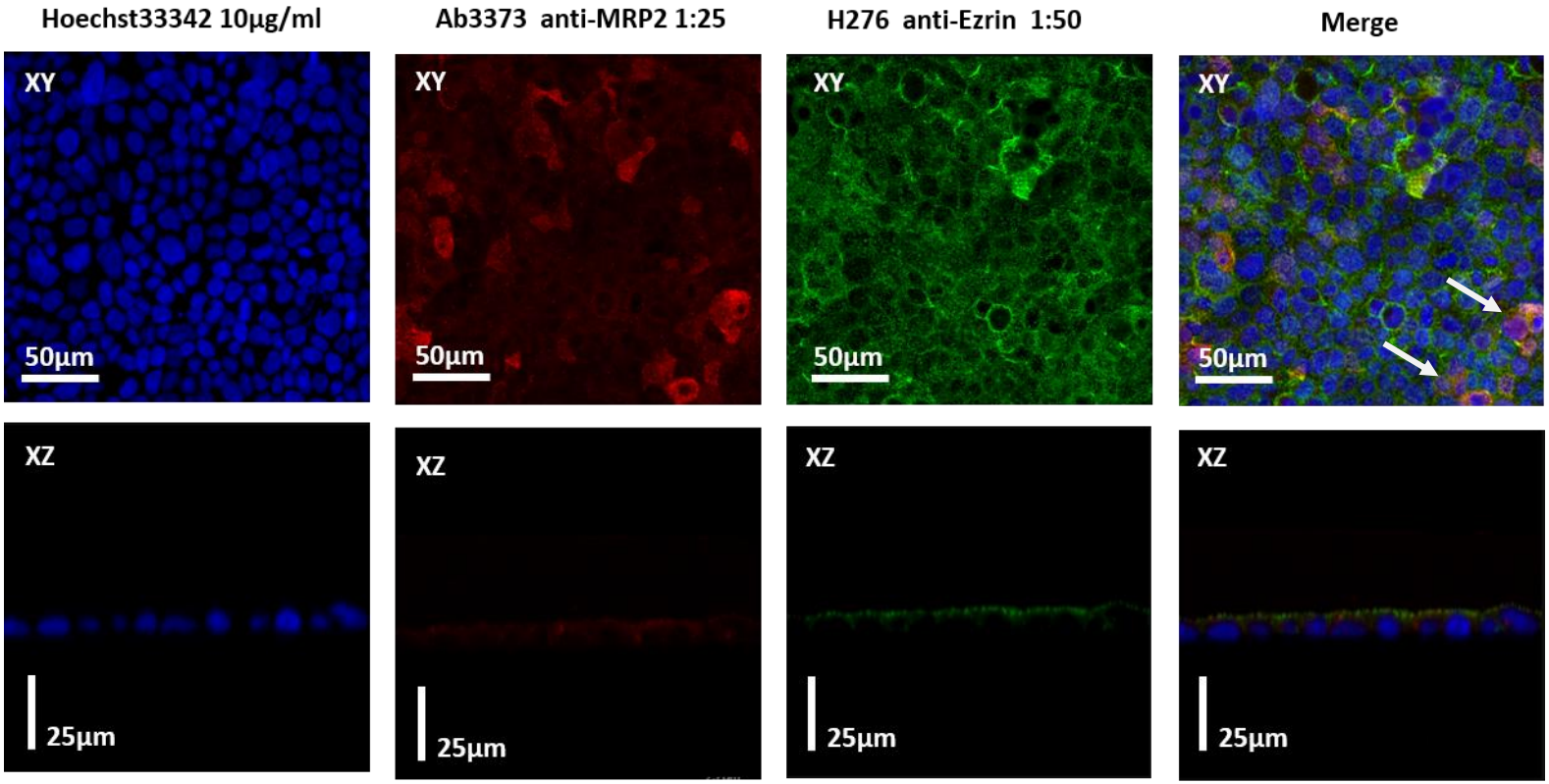
Hoechst33342 10µg/ml
Ab3373 anti-MRP2 1:25
H276 anti-Ezrin 1:50
Merge
XY
XZ
50µm
25µm

Figure 5.14 Detection of MRP2 (M2-III-6) and Ezrin (H-276) in MDCKII-MRP2 cell monolayers using indirect immunofluorescence.

MDCKII-MRP2 cells were cultured on transwell filters for a period of seven days. Filters were co-stained for MRP2, (M2-III-6 mouse monoclonal primary antibody, 1:25), and Ezrin (H-276 rabbit polyclonal primary antibody, 1:50). Secondary antibodies directed against M2-III-6 and H-276 were donkey anti-mouse 546nm (AbCam, UK) and donkey anti-rabbit 488nm (AbCam, UK) respectively. Cell nuclei were counterstained using Hoechst33342 (10µg/ml). Merged image showing Hoechst33342 nuclear stain, MRP2 and Ezrin expression. Gain settings were set at the same levels as native controls to allow direct comparison between native MDCKII and MDCKII-MRP2 cells. Images were taken using Leica CS SP2 UV confocal laser scanning microscopy with a x63 oil immersion objective, sections were approximately 1µm thick. XY images were taken throughout the depth of the cell monolayer and show co-localisation of Mrp2 and Ezrin (solid white arrows) and XZ images confirm apical localisation of MRP2 and Ezrin.

Figure 5.15:

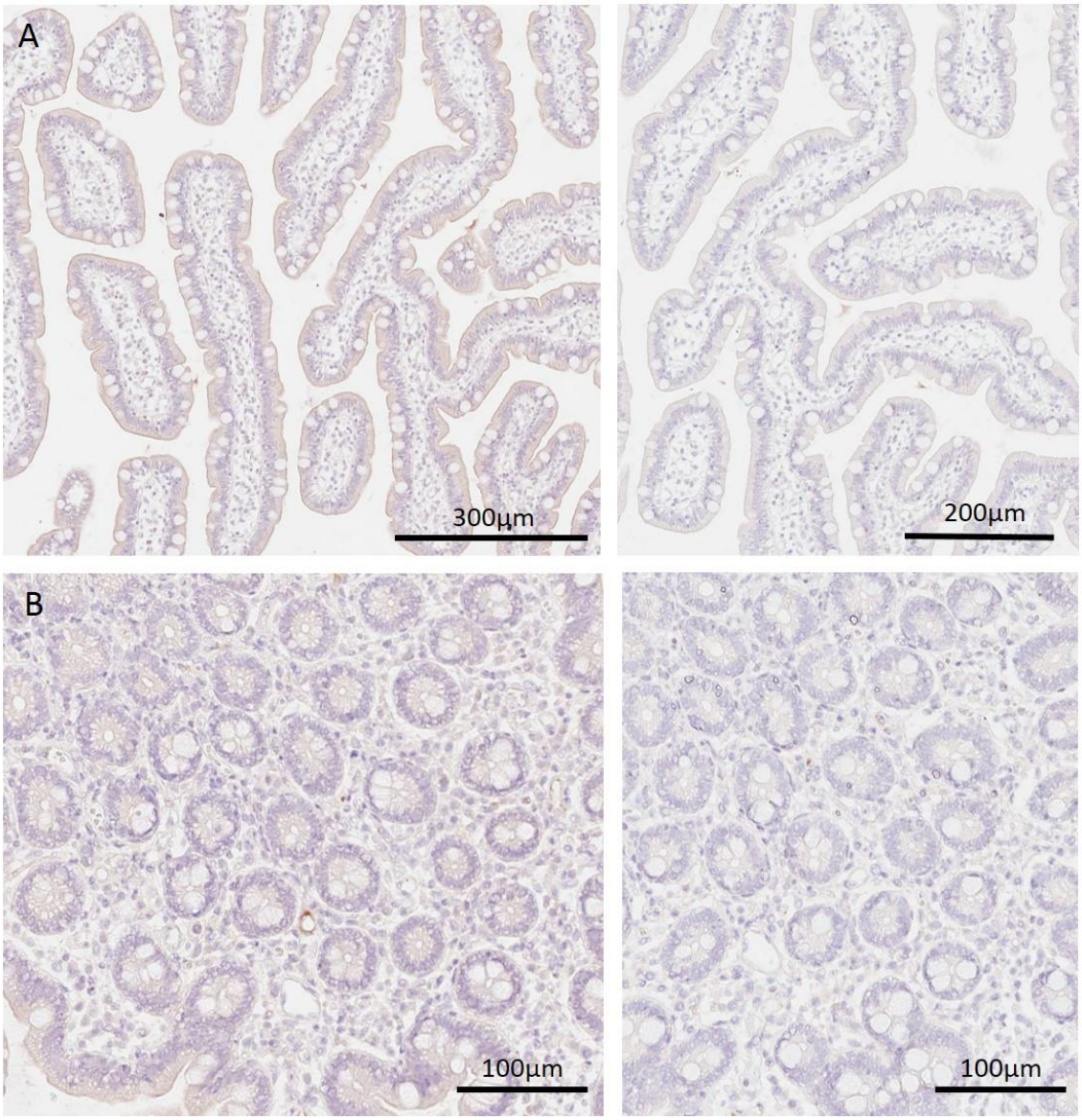

Figure 5.15 Immunohistochemical detection MRP2 protein in human jejunum using the M2-III-6 primary antibody.

Images show detection of MRP2 using primary antibody M2-III-6 diluted 1:25 in formalin fixed paraffin embedded human jejunum. Primary omitted controls (right) are negative and show no staining. **(A)** Diffuse MRP2 staining is observed throughout the epithelial cells of the villus with increased staining intensity visible at the apical membrane. **(B)** No specific immunoreactivity of M2-III-6 is shown in the crypt of human jejunum. Jejunum tissue was stained using an automated Ventana benchmark XT staining platform with citric acid based antigen retrieval, DAB antigen stain and haematoxylin counter stain, sections shown were all stained simultaneously. Sections were rehydrated and cover slips mounted. Slides were then scanned electronically using Aperio ScanScope.

Figure 5.16:

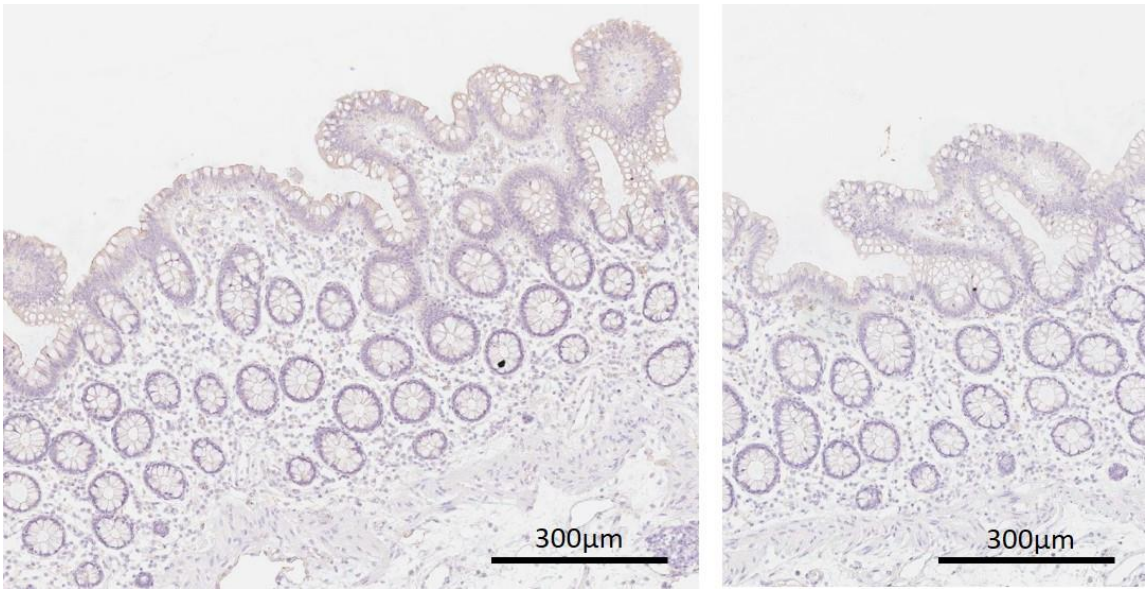

Figure 5.16 Immunohistochemical detection MRP2 protein in human colon using the M2-III-6 primary antibody.

Images show detection of MRP2 using primary antibody M2-III-6 diluted 1:25 in formalin fixed paraffin embedded human colon. Primary omitted controls (right) are negative and show no staining. **(A)** Diffuse MRP2 staining is observed throughout the epithelial cells lining the intestinal lumen with increased staining intensity visible at the apical membrane. **(B)** No specific immunoreactivity of M2-III-6 is shown in the colonic crypt region. Colon tissue was stained using an automated Ventana benchmark XT staining platform with citric acid based antigen retrieval, DAB antigen stain and haematoxylin counter stain, sections shown were all stained simultaneously. Sections were rehydrated and cover slips mounted. Slides were then scanned electronically using Aperio ScanScope.

5.3.3 Immunohistochemical detection of Bcrp in rat and human intestine using M70 and BXP21 antibodies respectively

M70 is a rabbit polyclonal serum purified IgG antibody raised against amino acids 301-370 of the mouse Bcrp protein (table 5.1) and is indicated for the detection of Bcrp of mouse and rat origin. Mouse and rat Bcrp protein sequences are 92% identical, with the rat Bcrp protein sequence differing from the M70 immunogen by only ten amino acids (figure 5.17).

Figure 5.18 shows staining of 4µm thick sections taken from the rat duodenum, jejunum, ileum and colon with the M70 antibody, diluted 1:25 (left), compared with pre-immunised rabbit IgG purified serum negative controls (right). Intense staining is localised to lateral cell membranes of cryptal epithelial cells, with a complete lack of villus M70 immunoreactivity (figure 5.18). Staining appears to visually increase in intensity in the crypt regions from the jejunum to the duodenum and ileum, with only very low expression apparent at the base of crypt units in the colon, although it should be noted that no quantification of staining was performed. No staining is observed in any section of the corresponding rabbit IgG purified serum controls (figure 5.18), similarly no staining was visible in primary omitted controls (results not shown). Higher magnification images in figure 5.19 show lateral Bcrp staining is of highest intensity at the crypt base with decreasing immunoreactivity toward the crypt-villus junction. M70 immunoreactivity ceases at the crypt-villus junction with no villus expression. Colonic immunoreactivity is very low with only sparse staining of epithelial cells located in the lower region of some crypt units. Low level immunoreactivity is observed to the lateral cell membranes of these cells (figure 5.19).

Immunohistochemical localisation of Bcrp in rat intestine was attempted using several alternative Bcrp antibodies including, B25, D20 and 10180-1-AP (table 5.1), all of which were indicated to react with the rat Bcrp protein, however no specific staining was detected. Mouse monoclonal anti-Bcrp antibody clone5d3 (table 5.1) yielded immunoreactivity in the extra-nuclear cytoplasmic region of epithelial cells up the villus and within the crypt unit (figure 5.20). Clone5d3 staining was however not reproducible using immunocytochemistry in human BCRP transfected MDCKII cells in which BXP-21 showed positive localisation to the apical cell membrane (results not shown), additionally no specific signal was generated by clone5d3 in Western blot experiments with MDCKII-hBCRP cell protein (results not shown). Given that the clone5d3 antibody is a mouse IgG_{2b} monoclonal antibody it was not possible to used MDCKII-mBcrp transfected cells as a positive control in either Western blot or immunocytochemistry. Furthermore the clone5d3 epitope is unknown, with the antibody being raised against whole 3T3 cells known to express human ABCG2, thereby drawing the specificity of this antibody into

question. For these reasons ability of clone5d3 to selectively bind Bcrp is doubted and as such clone5d3 immunohistochemical data were disregarded.

Following localisation of Bcrp to lateral cell membranes of crypt epithelia antibody validity was investigated to ensure M70 antibody specificity. M70 reactivity was therefore assessed using native and mBcrp transfected MDCKII cell lines with Western blot and immunocytochemical techniques. Native MDCKII cells were used as a negative control throughout Western blot and immunocytochemistry experiments, due to the absence of endogenous Bcrp protein expression as shown by our laboratory (Wright, 2011). Proteins were extracted from native and MDCKII-mBcrp cells (as described previously, section 2.2.7) and were incubated with M70, at a dilution of 1:100. Western blot resulted in a diffuse band at approximately 84KDa, a molecular weight slightly larger than that of the predicted 72KDa core BCRP protein (figure 5.21). The band was however in accordance with the size indicted on the antibody data sheet (82KDa). It should be noted that mature BCRP/Bcrp is glycosylated (see below). No band was present in native MDCKII cells, despite a higher protein loading concentration (15µg vs. 10µg MDCKII-mBcrp) (figure 5.21).

Following detection of Bcrp using the M70 antibody the nitrocellulose membrane was stripped and probed using an alternative rat monoclonal Bcrp antibody, BXP9 (see table 5.1). Raised against a fragment of mouse Bcrp within amino acid region 221-394, BXP9 is indicated for the detection of Bcrp of mouse origin. Immunoblot analysis revealed a band of similar molecular weight following incubation of MDCKII-mBcrp with BXP9 as was observed with M70 at 84KDa. Since film exposure time was reduced following BXP9 incubation, increased signal density likely reflects an increased antibody affinity of BXP9 for mBcrp. A second band of higher molecular weight ~140KDa was also detected using BXP9. Bcrp is a half transporter which requires dimerisation for functional activity (Kage et al., 2002), it is therefore proposed that the band of molecular weight 140KDa corresponds to the Bcrp homodimer protein. The presence of this band further reinforces an increased antibody affinity of BXP9 for Bcrp, since the M70 antibody failed to detect this dimer protein. Actin loading controls confirm protein presence and separation by gel electrophoresis. Failure to detect a signal in native (control) MDCKII cells and the detection of an 84KDa protein, following stable transfection of mBcrp, by both M70 and BXP9 strongly indicates that these antibodies specifically bind mBcrp protein. Detection of the same protein band with two different Bcrp antibodies strongly supports the use of M70 as a Bcrp specific antibody. Given that BXP9 is a rat IgG_1 monoclonal antibody it was not possible to perform immunohistochemistry experiments using BXP9 on rat intestinal sections. Similarly, a band of molecular weight 84KDa was detected by M70 in rat ileum mucosal samples, with an increased intensity observed at higher loading concentrations (figure

5.22). The distinct identification of an 84KDa band in rat ileal samples supports specific binding of M70 to rat Bcrp.

BCRP is a glycoprotein and is therefore subject to post translational modifications in the endoplasmic reticulum, particularly N-glycosylation (Diop and Hrycyna, 2005). Indeed, both human and rat BCRP/Bcrp proteins have previously been shown to be N-glycosylated with PNGase F treatment reducing the apparent molecular weight of both BCRP and Bcrp as determined by Western blot (Diop and Hrycyna, 2005, Hori et al., 2004). N-linked glycosylation is the addition of sugar molecules to asparagine amino acids (N amino acids), and has previously been shown to alter protein characteristics including stability and protein targeting (Mohrmann et al., 2005). Analysis of the human, mouse and rat BCRP protein sequence revealed four potential sites for N-linked glycosylation, predicted by the recognition of the consensus amino acid sequence asparagine (Asn)-X-threonine/serine, where X can be substituted with any amino acid except proline (figure 5.17)(human sequence not shown) (Diop and Hrycyna, 2005, Hori et al., 2004, Mohrmann et al., 2005). To allow glycosylation these sites must be exposed to the lumen of the endoplasmic reticulum (Diop and Hrycyna, 2005). Of the four predicted glycosylation sites, Asn596 and Asn600 are predicted to be exposed to the endoplasmic reticulum and hence show potential for N-glycosylation of these residues. It is predicted that potential glycosylation sites Asn316 and Asn338 are located extracellularly following insertion of the BCRP/Bcrp protein into the plasma membrane are not exposed to the endoplasmic reticulum and as such show no potential for N-linked glycosylation (Diop and Hrycyna, 2005, Hori et al., 2004). Species conservation of Asn596 indicates a physiological role for this amino acid, with Diop & Hrycyna (2005) and Morhmann et al., (2005) showing site directed mutagenesis of this Asn residue to reduce the detected protein molecular weight. Mutation of Asn596 to glutamine reduced the molecular weight of human BCRP to approximately 60KDa, presented as a single distinct band under Western blot analysis (Diop and Hrycyna, 2005). The mutation of Asn prevented protein N-linked glycosylation as represented by the reduced molecular weight of human BCRP. Similarly treatment of rat Bcrp with PNGase F, which cleaves asparagine residues of carbohydrate molecules, reduced the apparent molecular weight from 85KDa to approximately 62KDa (Mohrmann et al., 2005).

We therefore treated mBcrp protein with the amidase enzyme PNGase F to remove any protein associated N-linked glycosylation (figure 5.23). PNGase F treatment resulted in the separation of large diffuse band ranging from 70 to 90KDa to give two distinct bands with molecular weights 85 and 70KDa. A third band of lower molecular weight, 65KDa, was also evident in both the mBcrp deglycosylated and non-deglycosylated 5µg samples (figure 5.23).

Despite loading of equal protein amounts of deglycosylated and wild type mBcrp protein samples (5µg), protein migration of deglycosylated samples appeared to be compromised, with protein aggregation visible at the top of the blot and a lower actin expression being apparent for the deglycosylated sample (figure 5.23). M70 band intensities were therefore quantified densitometrically and expressed in relation to lane sample actin expression (data not shown). The ratio of M70 band intensity relative to actin intensity shows a relative 2 fold increase between the 140KDa band (2.47 arbitrary units) and the diffuse band of range 70 – 90KDa (4.96 arbitrary units) in the 10µg mBcrp sample, with higher expression of the lower molecular weight protein. Relative to actin, a two-fold increase in expression of the 65KDa protein expression was observed in the deglycosylated sample (1.11 arbitrary units) compared with PNGase F untreated mBcrp protein (0.58 arbitrary units). The apparent inability of PNGase F to deglycosylate all mBcrp protein present within the sample likely results from complex glycosylation of the mBcrp protein and insufficient capacity of the PNGase F to deglycosylate extracted protein.

Both the M70 and BXP9 antibodies showed apical expression of mBcrp in MDCKII-mBcrp cell lines cultured on permeable supports which was absent from native MDCKII cells using indirect immunocytochemistry (figures 5.24 and 5.25). Cells were visualised using confocal laser scanning microscopy. Native MDCKII cells were used as negative controls and confocal gain adjustments made such that fluorescence was arbitrarily set to zero in this cell line. M70 primary antibody was detected using an anti-rabbit 488nm fluorescent secondary antibody and cell nuclei were counterstained with Hoechst33342. Figure 5.24 shows intense fluorescence above the level of native MDCKII fluorescence at wavelength 488nm. Images taken in the XZ plane show detection of mBcrp at the apical cell surface. Staining of adjacent filter quarters using BXP9 and the secondary goat anti-rat 488nm antibody showed a highly similar staining pattern, with distinct apical transporter localisation being apparent following transfection of mBcrp protein (figure 5.25). Although co-staining with Ezrin was not possible due to host species primary antibody overlap, figure 5.26 shows staining of adjacent filter quarters to those used for mBcrp expression, following culture of native and MDCKII-mBcrp on permeable supports and incubation with anti-Ezrin antibody H276 primary antibody with secondary detection using an anti-rabbit 566nm fluorescent antibody. Ezrin expression is, as shown previously, localised to the apical cell membrane of both native and MDCKII-mBcrp cells (figure 5.26). It is expected that co-staining of mBcrp and Ezrin would show significant overlap in protein expression.

The high fluorescence intensity apparent following stable transfection of mBcrp compared with native MDCKII controls strongly supports the binding of both M70 and BXP9 antibodies to

the mBcrp protein immunogen. Replication of immunoblot and immunocytochemical data obtained with M70 by BXP9 in model systems confirms M70 antibody specificity. Immunolocalisation of Bcrp to lateral cell membranes of crypt epithelia using the M70 antibody is therefore concluded to accurately reflect rat intestinal Bcrp protein expression.

Apical expression of Bcrp protein in MDCKII-mBcrp cells contrasts markedly with that found in the rat intestine. As an additional control to show expected Bcrp expression patterns using the M70 antibody, M70 immunostaining was determined in paraffin embedded rat liver sections. M70 showed low level immunoreactivity at the lateral membrane of endothelial cells lining hepatic blood vessels and also within hepatic sinusoids, in agreement with past studies (figure 5.27).

BCRP localisation in human jejunum and colon sections using the human specific BXP21 antibody was also determined (figure 5.28 and 5.29). BXP21 is a mouse monoclonal antibody raised against amino acids 271-396 (table 5.1). BXP21 is well validated in peer reviewed literature and has been used extensively for the detection of human BCRP. A strong immunoreactivity of BXP21 is shown at the apical membrane of villus enterocytes of the jejunum (figure 5.28), with a definite absence of the BCRP protein in mucus secreting goblet cells. Primary omitted controls were negative (figure 5.28B). High magnification images of the human jejunum show very strong staining at the apical membrane with staining also being apparent on lateral cell membranes of these absorptive enterocytes. With regards to cryptal BCRP expression a similar pattern is observed with both apical membrane staining and lateral immunoreactivity (figure 5.28D).

High levels of BXP21 immunoreactivity are shown in the human colon (figure 5.29). Very intense staining is observed at the apical membrane of luminal and cryptal epithelial cells. Decreased staining is also shown in those cells of the crypts which are more deeply invaginated. Lateral membrane staining is observed on all BXP21 positive cells (figure 5.29). This data indicates that there is a marked species difference in the expression of BCRP/Bcrp in the intestines of human versus rat.

Figure 5.17:

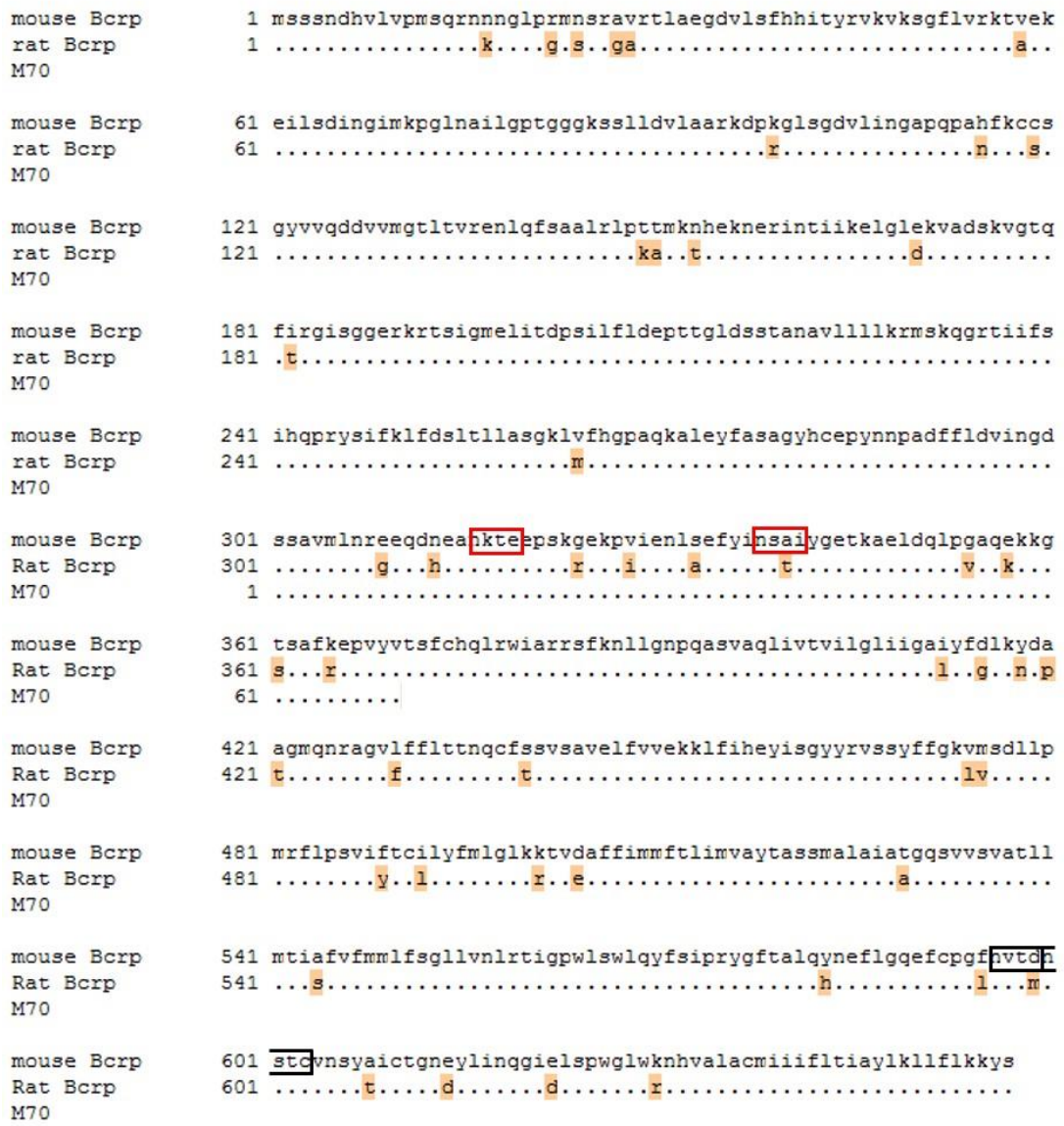

Figure 5.17 shows sequence alignment of mouse and rat Bcrp protein sequences with the M70 antibody epitope.

Protein sequences were obtained from NCBI and alignment performed using Clone Manager software. Non-identical bases which differ between the rat and the mouse protein sequence and M70 epitope are highlighted in orange. There are a total of ten non-identical amino acids within the 69 amino acid length of the M70 antigen. Potential N-linked glycosylation sites are shown, extracellularly located Asn316 and Asn338 (red boxes) and intracellularly located Asn596 and Asn600 (black boxes).

Figure 5.18:

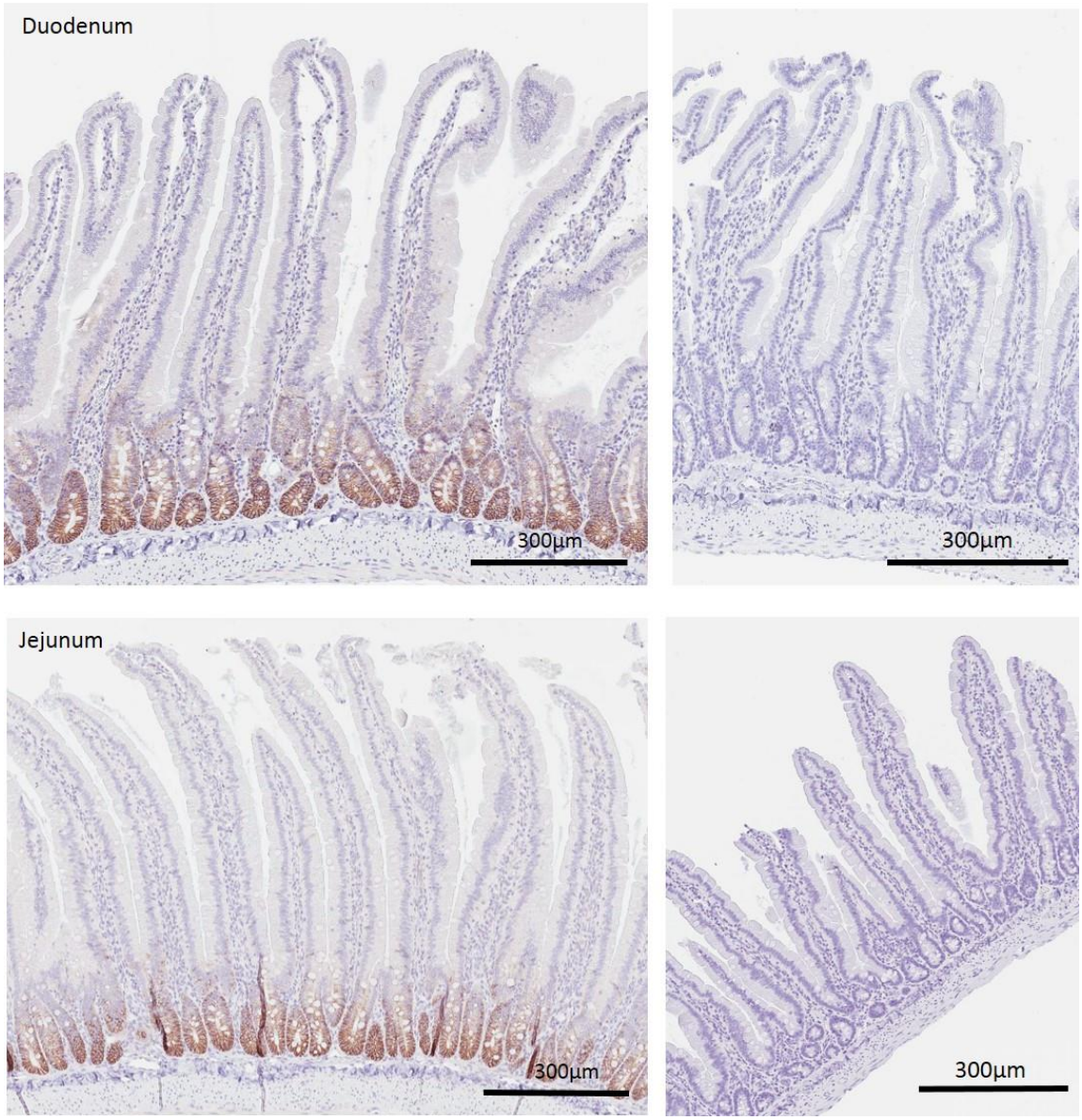

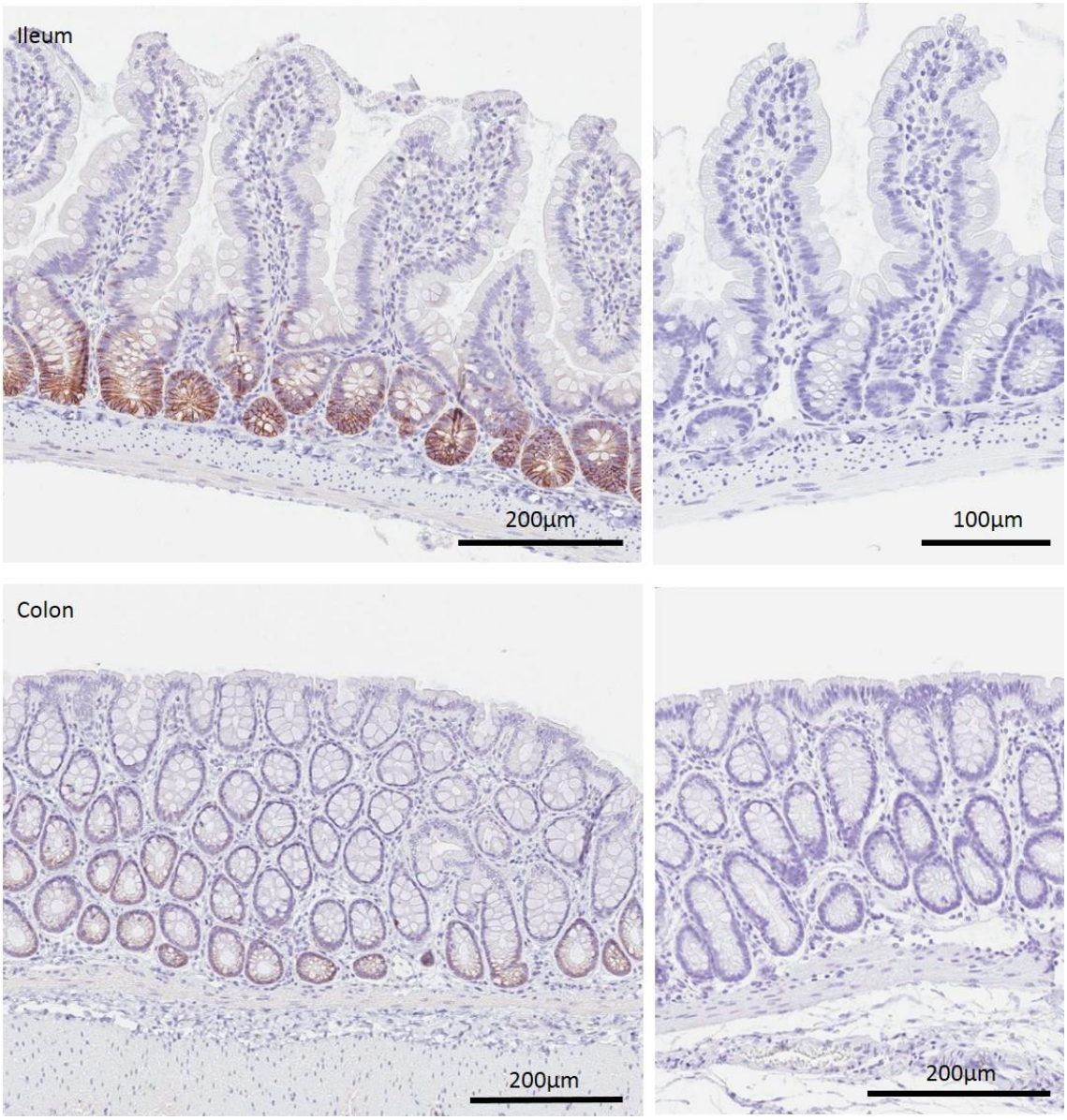

Figure 5.18 Immunohistochemical localisation of Bcrp in rat intestine using the M70 primary antibody.

Immunohistochemical detection of Bcrp in the duodenum, jejunum, ileum and colon of rat intestine using primary rabbit polyclonal antibody M70, 1:25 dilution, (left) and IgG negative controls (right). Staining is visible on lateral cell membranes within crypt units in all intestinal regions. Intestinal sections (4µm thickness) were stained using an automated Ventana benchmark XT staining platform with citric acid based antigen retrieval, DAB antigen stain and haematoxylin counter stain, sections shown were all stained simultaneously. Sections were rehydrated and cover slips mounted. Slides were scanned electronically using Aperio ScanScope.

Figure 5.19:

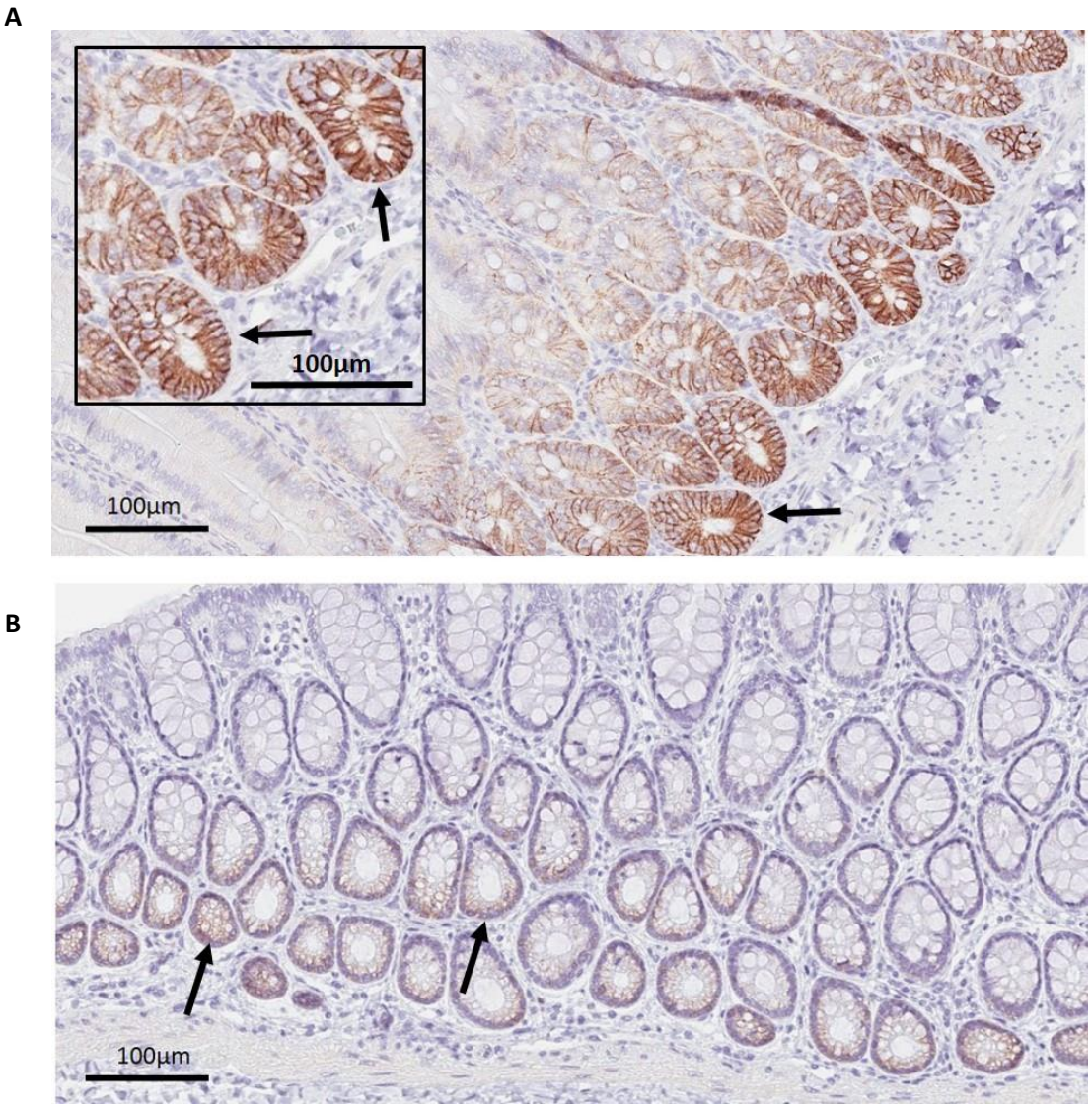

Figure 5.19 Immunohistochemical localisation of Bcrp to lateral cell membranes in rat ileum and colon sections.

Images show Bcrp localisation using primary rabbit polyclonal antibody M70, 1:25 dilution, in formalin fixed, paraffin embedded ileal male rat intestinal sections (4µm thickness). Intense staining is apparent to lateral cell membranes in the ileum **(A)** with minimal staining to the base of colonic crypts **(B)** (black arrows). Sections were stained using an automated Ventana benchmark XT staining platform with citric acid based antigen retrieval, DAB antigen stain and haematoxylin counter stain, sections were stained simultaneously. Sections were rehydrated and cover slips mounted. Slides were then scanned electronically using Aperio ScanScope.

Figure 5.20:

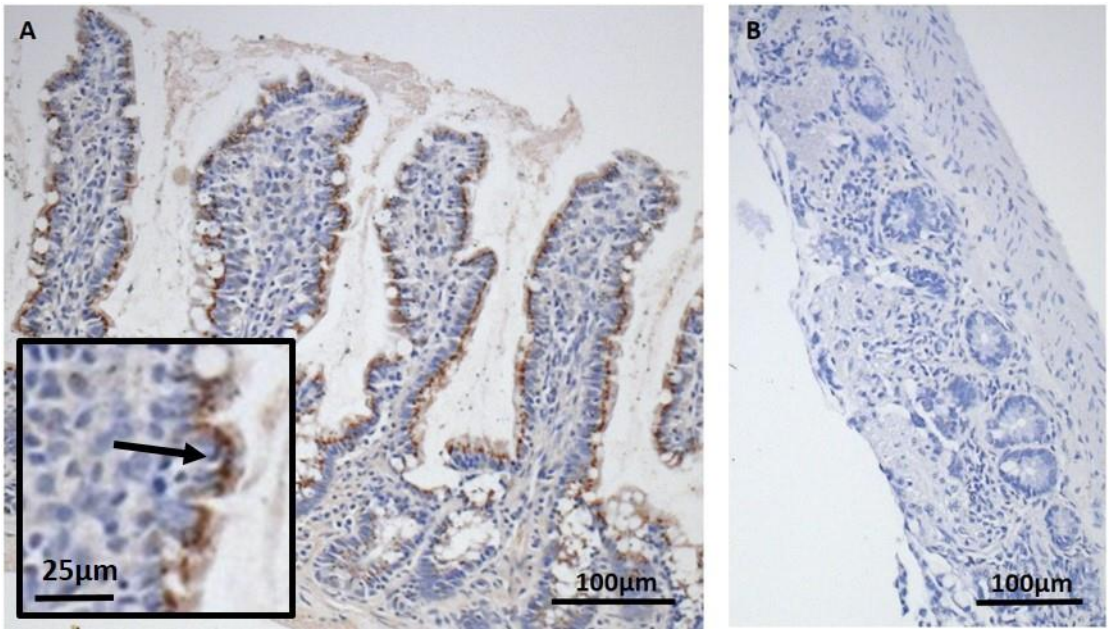

Figure 5.20 shows immunohistochemical detection using the anti-Bcrp monoclonal mouse clone5d3 antibody in rat ileum sections with accompanying primary omitted negative control.

Images show Bcrp localisation using primary mouse monoclonal clone5d3 antibody at a 1 in 50 dilution, in formalin fixed, paraffin embedded ileal male rat intestinal sections (4µm thickness). **(A)** Immunoreactivity is observed in the extra nuclear cytoplasmic (inset, black arrow) region of villus epithelial cells with high magnification images showing a lack of brush border expression. **(B)** Primary omitted controls are negative. Images were stained using a Benchmark staining platform and counterstained using Ventana blueing agent and haematoxylin. Sections were dehydrated using increasing alcohol concentrations and cover slips mounted. Sections were imaged using a Zeiss Axioimager with a x20 lens objective.

Figure 5.21:

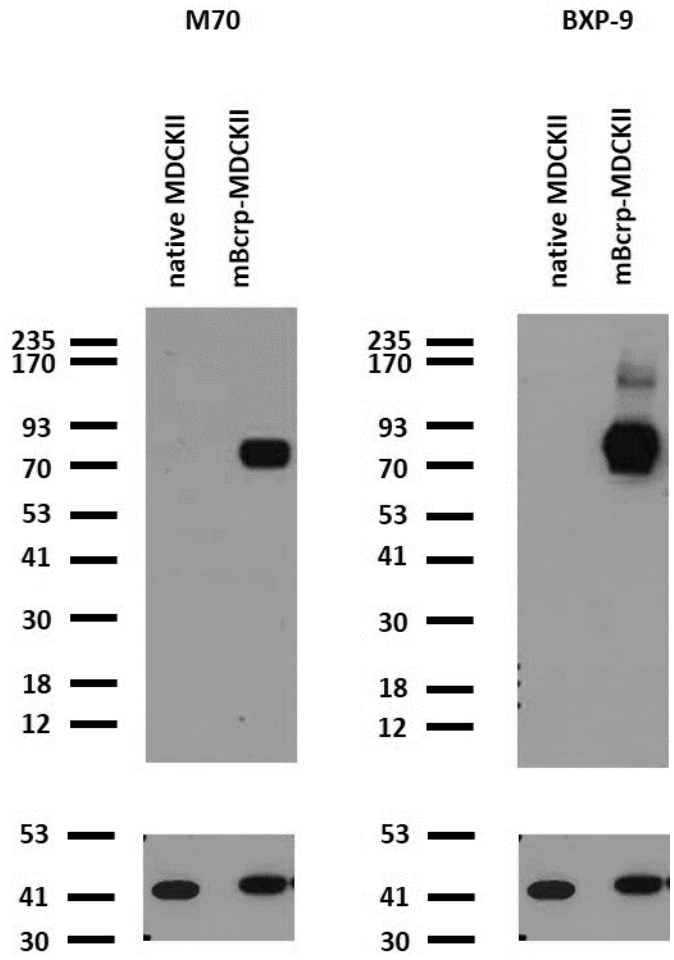

Figure 5.21 Western blot analysis of Bcrp expression in native MDCKII and MDCKII-mBcrp cell lines.

Image shows 15µg loaded native MDCKII protein and 10µg loaded MDCKII-mBcrp protein. Following transfer, nitrocellulose membranes were probed with rabbit polyclonal M70 primary antibody, diluted 1:100 (left) overnight at 4˚C. Nitrocellulose membrane was then stripped and re-probed with rat monoclonal BXP9 primary antibody (1:100) overnight at 4˚C. Both anti-Bcrp antibodies yielded diffuse bands at approximately 84KDa. Primary M70 and BXP9 antibodies were detected using anti-rabbit and anti-rat HRP conjugated secondary. Membranes were stripped and re-probed using a cross species anti-actin I-19 antibody as a loading control, 43KDa. Western blot image shown is one gel showing the same samples which were probed with two different anti-Bcrp antibodies.

Figure 5.22:

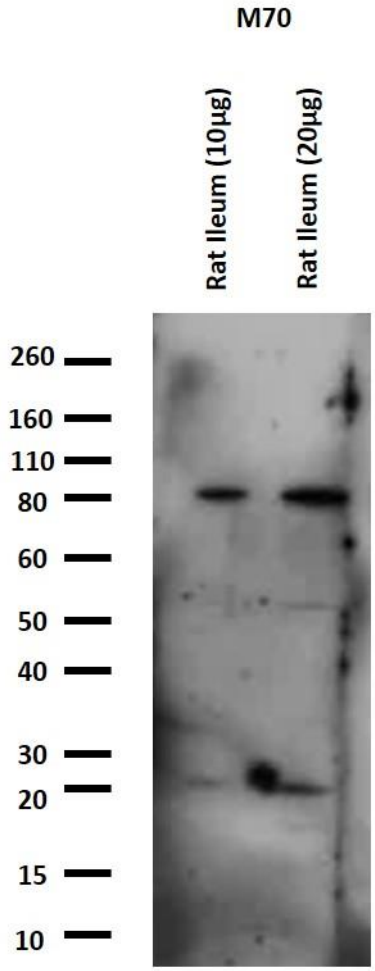

Figure 5.22 Western blot analysis of Bcrp expression in rat ileum mucosa

Image shows 10µg and 20µg of loaded protein extracted from male rat ileum mucosal scrapes. Following transfer, the PVDF membrane was probed with rabbit polyclonal M70 primary antibody (1:200) overnight at 4˚C to yield bands of molecular weight approximately 85KDa. Primary antibody was detected using anti-rabbit HRP conjugated secondary.

Figure 5.23:

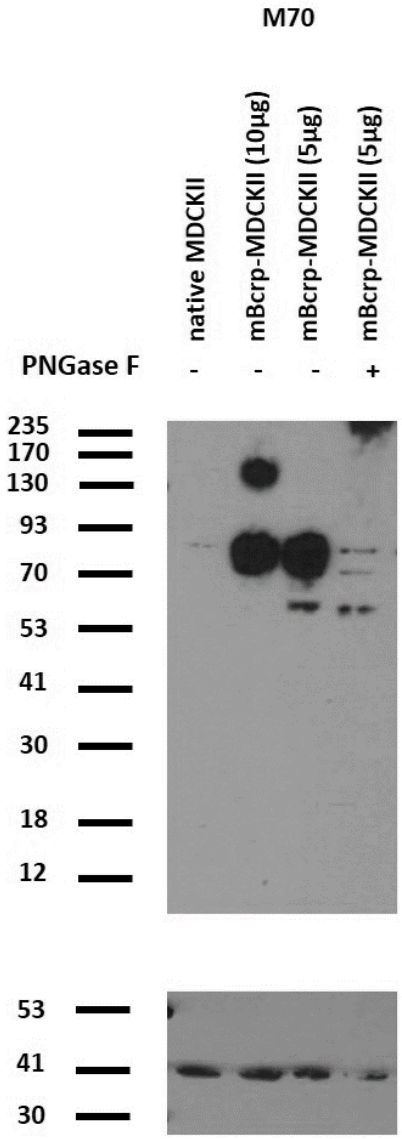

Figure 5.23 Western blot analysis of Bcrp expression in native MDCKII and MDCKII-mBcrp cell lines following mBcrp deglycosylation using PNGase F.

Image shows 10µg loaded native MDCKII protein, 10µg and 5µg loaded MDCKII-mBcrp protein and 5µg loaded PNGase F deglycosylated MDCKII-mBcrp protein. Following transfer, the nitrocellulose membrane was probed with rabbit polyclonal M70 primary antibody, diluted 1:100 overnight at 4˚C. Bands of 140KDa, a diffuse band ranging 70-90KDa and a distinct band at approximately 65KDa were yielded in the MDCKII-mBcrp 10µg and 5µg protein lanes combined. Bands of alternative size, 85, 70 and 65KDa were yielded in the deglycosylated MDCKII-mBcrp protein lane. Nitrocellulose membrane was stripped and re-probed using a cross species anti-actin I-19 antibody as a loading control, 43KDa. Western blot image shown is one gel.

Figure 5.24:

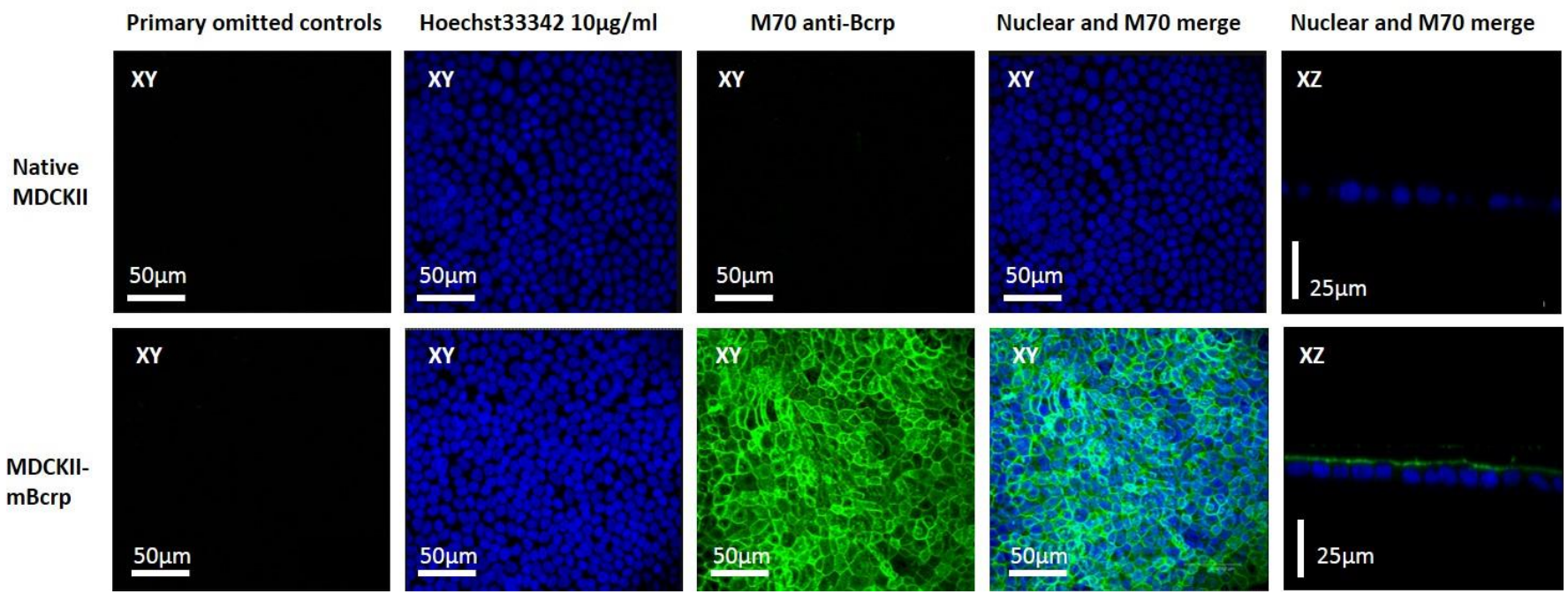
Primary omitted controls
Hoechst33342 10µg/ml
M70 anti-Bcrp
Nuclear and M70 merge
Nuclear and M70 merge
Native MDCKII
MDCKII-mBcrp
XY
XZ
50µm
25µm

Figure 5.24 M70 anti-Bcrp staining in native MDCKII and MDCKII-mBcrp cell monolayers confirms apical localisation of Bcrp in MDCKII-mBcrp cells using indirect immunofluorescence.

Native MDCKII and MDCKII-mBcrp cells were cultured on transwell filters for a period of seven days. Filters were stained for Bcrp using rabbit polyclonal M70 primary antibody, diluted 1:25. Secondary antibody directed against M70 was donkey anti-rabbit 488nm (AbCam, UK). Cell nuclei were counterstained using Hoechst33342 (10µg/ml). Merged image shows Hoechst33342 nuclear stain and M70 Bcrp expression. Gain settings were adjusted accordingly, within the limits of secondary only controls, such that fluorescence measured at 488nm in native MDCKII cells was arbitrarily set to zero, allowing direct comparison between native MDCKII and MDCKII-mBcrp. Images were taken using Leica CS SP2 UV confocal laser scanning microscopy with a x63 oil immersion objective, sections were approximately 1µm thick. XY images show stack of images taken throughout the depth of the cell monolayer and XZ images confirm apical localisation of mBcrp.

Figure 5.25:

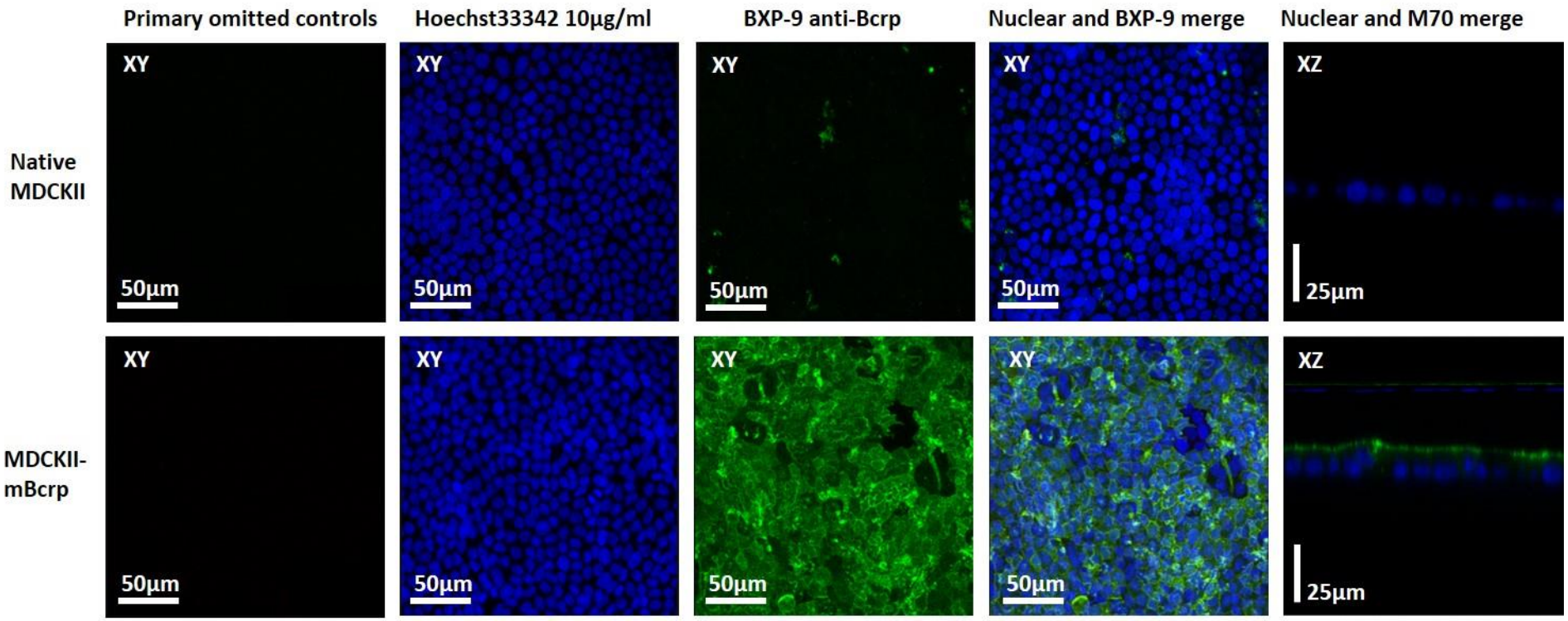
Primary omitted controls
Hoechst33342 10µg/ml
BXP-9 anti-Bcrp
Nuclear and BXP-9 merge
Nuclear and M70 merge
Native MDCKII
MDCKII-mBcrp
XY
XZ
50µm
25µm

Figure 5.25 BXP9 anti-Bcrp staining in native MDCKII and MDCKII-mBcrp cell monolayers confirms apical localisation of Bcrp in MDCKII-mBcrp cells using indirect immunofluorescence.

Native MDCKII and MDCKII-mBcrp cells were cultured on transwell filters, for a period of seven days. Filters were stained for Bcrp using rat polyclonal BXP9 primary antibody, diluted 1:25. Secondary antibody directed against BXP9 was goat anti-rat 488nm (SantaCruz, UK). Cell nuclei were counterstained using Hoechst33342 (10µg/ml). Merged image shows Hoechst33342 nuclear stain and BXP9 dependent fluorescence. Gain settings were adjusted accordingly, within the limits of secondary only controls, such that fluorescence measured at 488nm in native MDCKII cells was arbitrarily set to zero, allowing direct comparison between native MDCKII and MDCKII-mBcrp. Images were taken using Leica CS SP2 UV confocal laser scanning microscopy with a x63 oil immersion objective, sections were approximately 1µm thick. XY images show a stack of images taken throughout the depth of the cell monolayer and XZ images confirm apical localisation of mBcrp.

Figure 5.26:

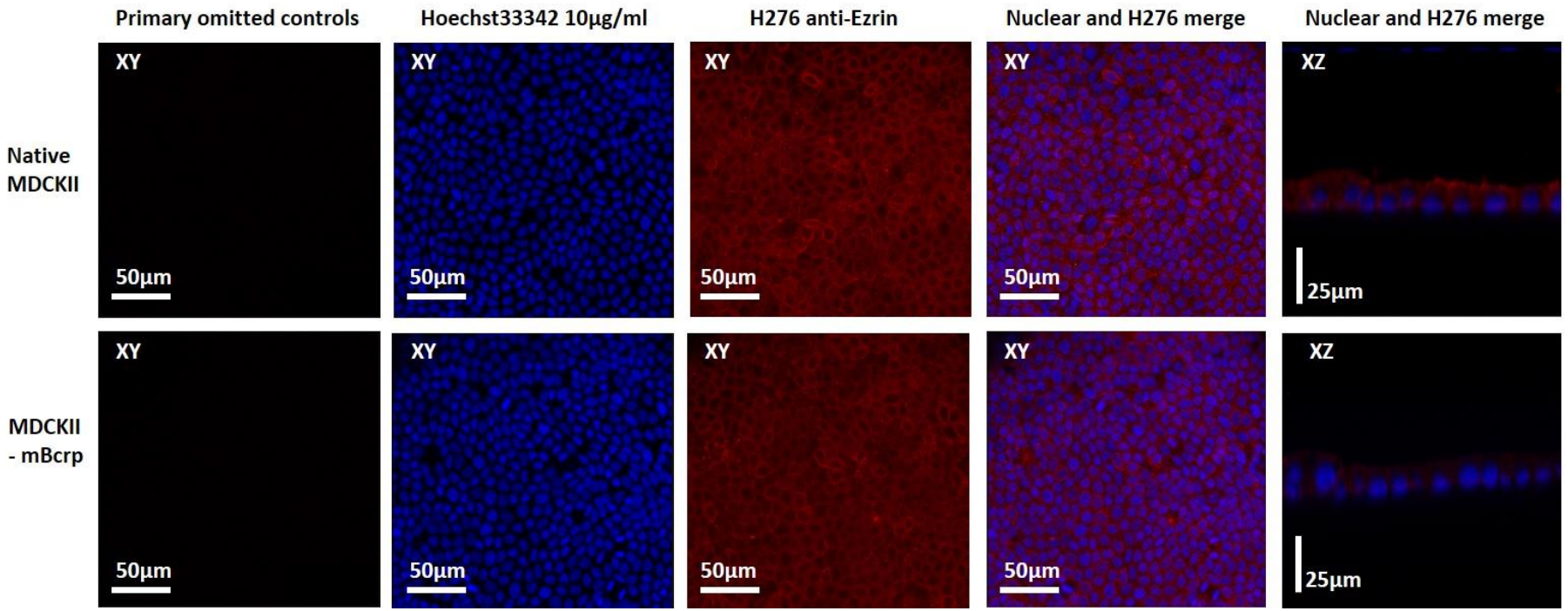
Primary omitted controls
Hoechst33342 10µg/ml
H276 anti-Ezrin
Nuclear and H276 merge
Nuclear and H276 merge
Native MDCKII
MDCKII - mBcrp
XY
XZ
50µm
25µm

Figure 5.26 Ezrin (H-276) staining in native MDCKII and MDCKII-mBcrp cell monolayers confirms apical localisation of Ezrin in these cell lines using indirect immunofluorescence.

Native MDCKII and MDCKII-mBcrp cells were cultured on transwell filters for a period of seven days. Filters were stained for Ezrin using rabbit polyclonal H-276 primary antibody, diluted 1:50. Secondary antibody directed against H-276 was donkey anti-rabbit 566nm (SantaCruz, UK). Cell nuclei were counterstained using Hoechst33342 (10µg/ml). Merged image showing Hoechst33342 nuclear stain and H-276 Ezrin expression. Gain settings were adjusted to secondary only controls. Images were taken using Leica CS SP2 UV confocal laser scanning microscopy with a x63 oil immersion objective, sections were approximately 1µm thick. XY images show a stack of images taken throughout the depth of the cell monolayer and XZ images confirm apical localisation Ezrin.

Figure 5.27:

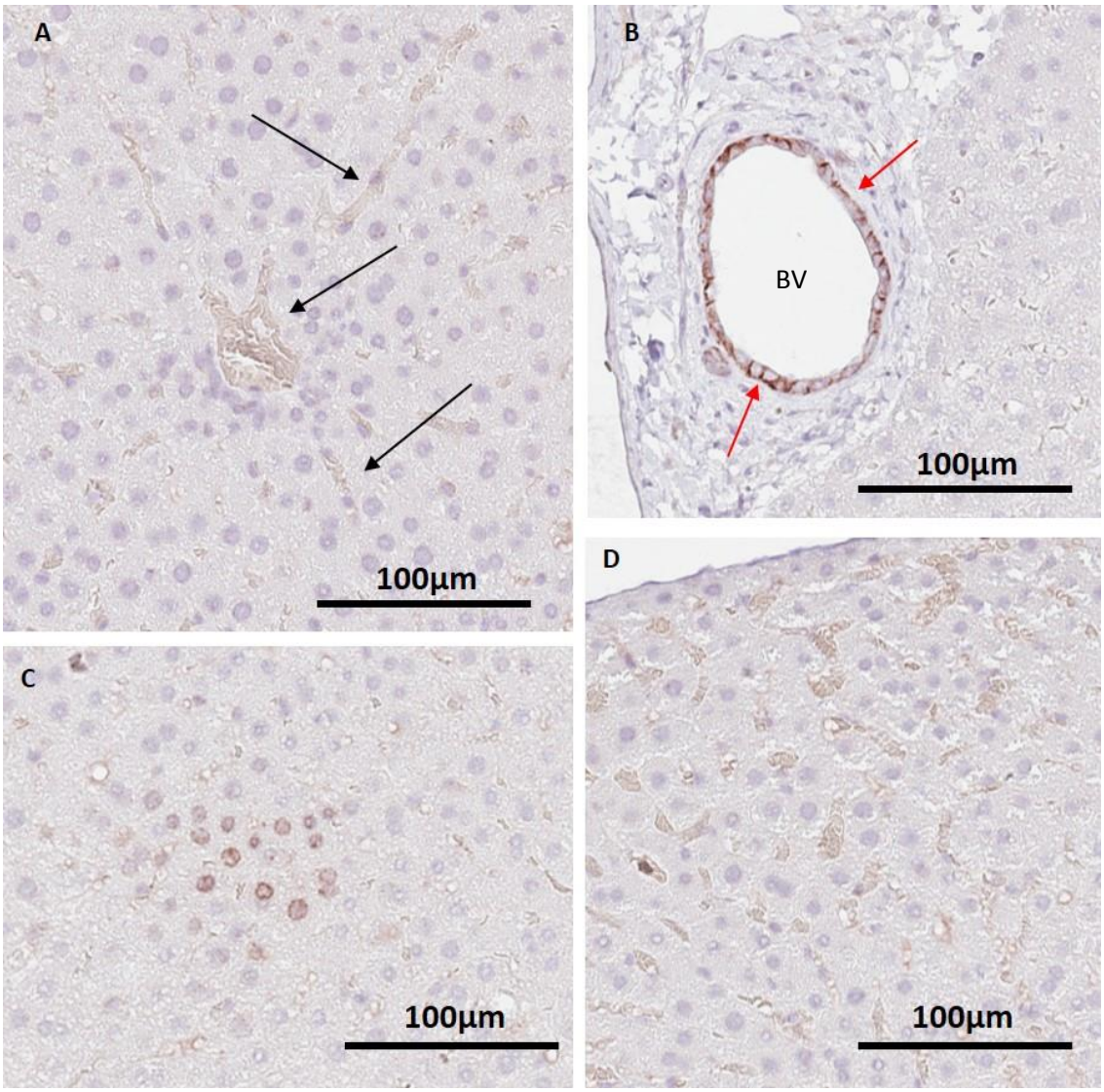

Figure 5.27 Immunohistochemical localisation of Bcrp to hepatic sinusoids, vacuolated hepatocytes and endothelial cells in rat liver sections.

Images show Bcrp localisation using primary rabbit polyclonal antibody M70, 1:25 dilution, in formalin fixed, paraffin embedded rat liver sections (4µm thickness). Staining is apparent within hepatic sinusoids **(A & D)**, vacuolated hepatocytes **(C & D)** and on the lateral membrane on endothelial cells lining hepatic blood vessel (BV) **(B)**. All images are taken from one section stained using an automated Ventana benchmark XT staining platform with citric acid based antigen retrieval, DAB antigen stain and haematoxylin counter stain. Sections were rehydrated and cover slips mounted. Slides were then scanned electronically using Aperio ScanScope.

Figure 5.28:

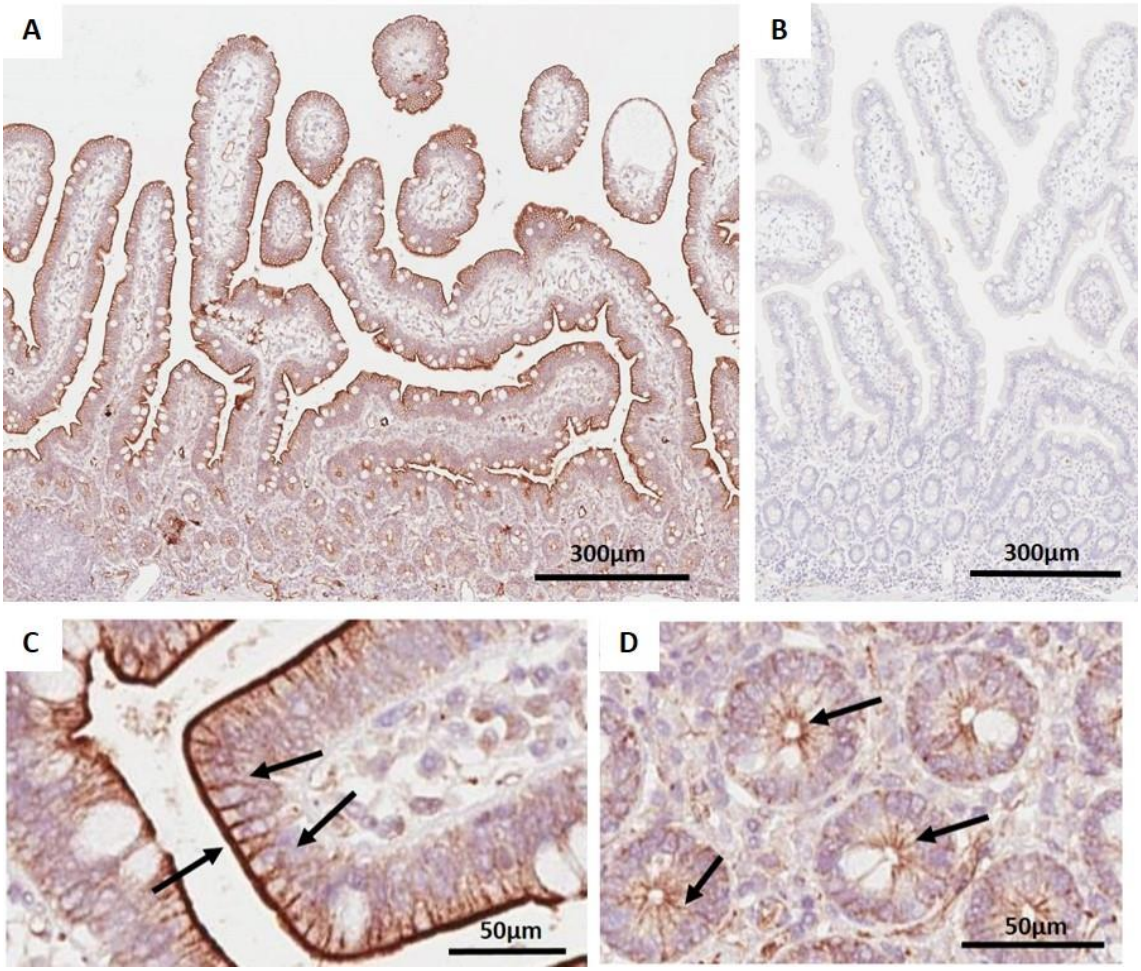

Figure 5.28 Immunohistochemical detection of BCRP protein in human jejunum using the mouse monoclonal BXP21 antibody.

Images show detection of BCRP using primary antibody BXP21 diluted 1:100 in formalin fixed paraffin embedded human jejunum tissue. Primary omitted controls **(B)** were negative and show no staining. **(A)** Strong immunoreactivity is observed at the apical epithelial cell membrane of the jejunal villus with detection of BCRP to the apical membrane of crypt cells. Higher magnification image highlights immunoreactivity of BXP21 at lateral cell membranes in both villus **(C)** and crypt epithelia **(D)**. Jejunal tissue was stained using an automated Ventana benchmark XT staining platform with citric acid based antigen retrieval, DAB antigen stain and haematoxylin counter stain, sections shown were all stained simultaneously. Sections were rehydrated and cover slips mounted. Slides were then scanned electronically using Aperio ScanScope.

Figure 5.29:

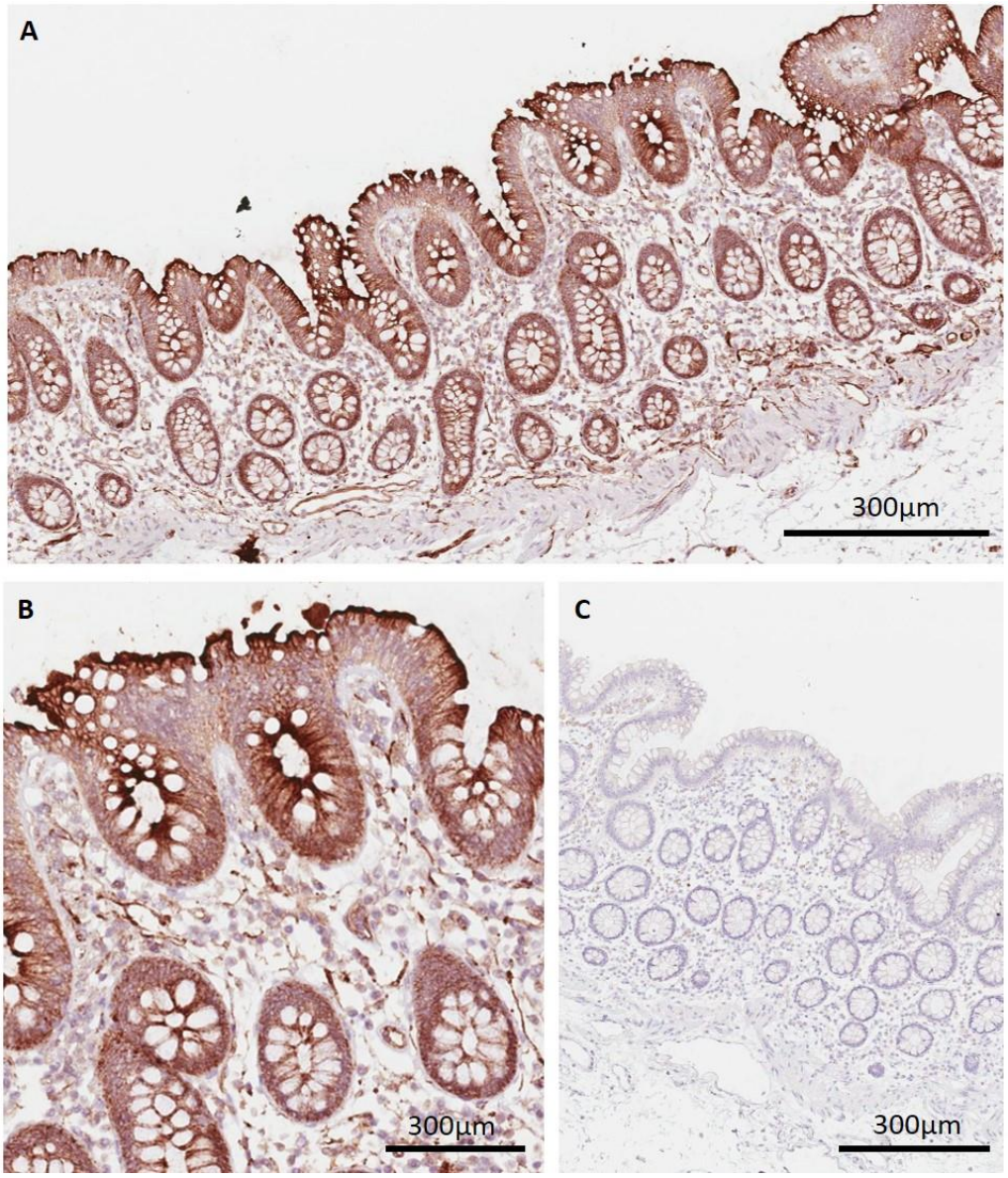

Figure 5.29 shows immunohistochemical detection BCRP protein in human colon using the mouse monoclonal BXP21 antibody.

Images show detection of BCRP using primary antibody BXP21 diluted 1:100 in formalin fixed paraffin embedded human colon tissue. Primary omitted controls **(C)** are negative and show no staining. Strong immunoreactivity is observed at the cell membrane of epithelial cells lining the intestinal lumen and at the apical membrane of cryptal epithelial cells **(A)**. Higher magnification image highlights immunoreactivity of BXP21 at lateral cell membranes in both epithelial cells lining the lumen and crypt epithelia **(B)**. Colonic tissue was stained using an automated Ventana benchmark XT staining platform with citric acid based antigen retrieval, DAB antigen stain and haematoxylin counter stain, sections shown were all stained simultaneously. Sections were rehydrated and cover slips mounted. Slides were then scanned electronically using Aperio ScanScope.

5.4 Discussion

Following the determination of mRNA expression levels of drug transporters and Cyp450 enzymes in the rat intestine (chapter 4) it was decided that protein localisation studies should be performed for three ABC transporters proposed to play a key role in intestinal drug resistance (Chan et al., 2004, Szakacs et al., 2008). Immunohistochemistry was therefore utilised to determine how mRNA data correlates with protein expression, and to confirm or add to current literature regarding intestinal membrane localisation of these proteins. Commercially available peptide antibodies were therefore employed to detect Mdr1, Mrp2 and Bcrp in rat intestine and MRP2 and BCRP in human jejunum and colon sections. Given that key protein motifs, for example the nucleotide binding domains, are conserved across ABC transporter family members it proves difficult to ensure antibody specificity. Further complications arise when the immunogen is raised against peptide sequences of other mammals, for example, C19 is raised against human MDR1 but is recommended for the detection of Mdr1 in rats, mice and dogs amongst other species (table 5.1). Antibody specificity must therefore be tested rigorously. Ideally the immunogen should be wholly specific for the protein of interest, should allow Western blotting to assess likelihood of identifying the protein, singularly and at an appropriate molecular size, and finally be suitable for protein localisation in tissue sections by immunohistochemistry and/or immunocytochemistry.

Details of all antibodies used in the present study are shown in table 5.1. Western blot and immunocytochemical techniques were employed as controls of antibody specificity. All antibodies (except BXP21) raised against ABC transporters were shown to identify proteins of correct predicted molecular weights by Western blot, in both stably transfected cell lines and rat mucosa (with the exception of BXP9). Furthermore, ability of all antibodies to bind MDR1, MRP2 and mBcrp was shown using transfected MDCKII cells.

In the present chapter the use of MDCKII epithelial cells stably transfected with MDR1, MRP2 and mBcrp, allows the parent dog cell-line (MDCKII) to act as a control for transfection in Western blotting. Importantly the use of immunofluorescent staining also allows the localisation of the protein to be assessed within confluent epithelial monolayers of MDCKII cells. Extensive testing of the antibodies used in the present study therefore supports intestinal protein localisation. As an additional experimental control, all intestine sections were stained simultaneously with each individual antibody using a Ventana staining platform to remove inter-experiment variation in staining intensities and sample handling.

The role of Mdr1 in conferring drug resistance is well established following extensive characterisation of the transporter since its discovery in 1976 (Juliano and Ling, 1976, Zhou, 2008). In agreement with increased Mdr1a mRNA expression at the villus tip (3.8 ± 0.9 fold difference, villus tip vs. crypt mRNA expression) reported in chapter 4, decreased immunoreactivity of the anti-Mdr1 C19 antibody is observed from the villus tip to the villus base, with minimal crypt staining. Good correlation between mRNA and protein expression of Mdr1 across the rat crypt villus axis is therefore evident and is in agreement with increased expression resulting from epithelial cell differentiation (Barker et al., 2008). Apical expression of Mdr1 is consistent with the role of this transporter in efflux of substrates into the intestinal lumen and supports the polarised expression of MDR1 reported previously (Blokzijl et al., 2007, Glaeser et al., 2007).

Although little is known with regards to intestinal protein expression of Mdr1, Chianale et al., (2007) showed a 5- to 6- fold increase in protein expression between the duodenum and ileum. Similarly, Mouly and Paine, (2003) report increased protein expression from the proximal to distal intestine. Whilst mRNA concentrations of Mdr1a were shown to increase from the duodenum to ileum (chapter 4) immunohistochemical staining presented here suggests Mdr1 protein expression to be greatest in the ileum, with an expression profile of ileum > duodenum > jejunum > colon, although quantification of immunoreactivity has not been performed. Conflicting data with regards to intestinal protein expression of Mdr1 may result from inter-individual/inter-animal variation or inter-species differences and may potentially arise from experimental variation.

In addition to Mdr1 apical protein expression, cytoplasmic immunoreactivity of the validated anti-Mdr1 antibody C19 in a distinct subset of cryptal cells is shown. Protein expression within this region is supported by detection of Mdr1a mRNA within isolated crypt samples (chapter 4). Each epithelial crypt contains a population of approximately 4-6 stem cells which have been shown to produce all four cell lineages present within the entire enterocyte barrier (Barker et al., 2008, Pinto and Clevers, 2005). Recent identification of Lgr5 (GPR49) as an intestinal stem cell marker has allowed localisation of cryptal stem cells to the crypt base region (Barker et al., 2007). Found interspersed between differentiated Paneth cells, Lgr5 positive stem cells have a distinctive flat, triangular nucleus and a scant cell cytoplasmic volume (Barker et al., 2007). The present study shows a darkened immunoreactivity of selected cells within the crypt following staining with an anti-Lgr5 antibody, although complete antibody specificity remains to be validated. These cells appear to be located to the bottom of the crypt and to be separated by Paneth cells, proposed to have migrated down to the crypt base from a Mix cell population present within the crypt (Barker et al., 2008, Pinto and Clevers, 2005). Indeed Lgr5 staining

observed here is reflective of that reported by Barker et al., (2007). Lgr5 staining is localised to the cytoplasmic cell compartment which appears to have a reduced volume compared with neighbouring cells.

Expression of Mdr1 in a subset of cells located to the base of the crypt suggests potential for Mdr1 expression within intestinal stem cells. Due to poor section morphology it is not possible to conclude co-localisation of Mdr1 and Lgr5 staining. Further studies must be performed to determine if Mdr1 is indeed expressed in intestinal stem cells, however Mdr1 positive cells do share morphological similarities to those reported for the intestinal stem cell (Barker et al., 2007). The cells appear to be interspersed between what are most likely Paneth cells and show distinctive triangular nuclei and minimal cytoplasmic volumes. Expression of Mdr1 in intestinal stem cells suggests potential of this transporter to play a role in protection of this long lived proliferative cell niche. Although studies have focused on the ability of BCRP to generate the side-population phenotype associated with stem cells, Hoechst33342 is also a MDR1 substrate (as shown in chapter 3) and as such MDR1 may contribute somewhat to the SP profile.

Scharenberg et al., (2002) showed a decreased Hoechst33342 efflux in cells displaying an SP phenotype in the presence of 2.5µg/ml verapamil, a concentration sufficient to inhibit MDR1 only (Scharenberg et al., 2002). The decreased efflux of Hoechst33342 in the presence of verapamil indicates MDR1 to contribute to the SP phenotype. Furthermore, whilst BCRP mRNA expression levels in A549 cells, which present an SP like phenotype, were found to be significantly higher than MDR1, MDR1 mRNA was detected (Scharenberg et al., 2002). Although knockout mouse models have demonstrated MDR1 is not required for the SP phenotype (Zhou et al., 2001) this does not conclude a lack of MDR1 contribution.

Although localised within the cell cytoplasm of cryptal epithelia, re-localisation of cellular Mdr1 protein to the cell membrane, as a result of stress responses and/or exposure to toxic/foreign xenobiotics, may serve to protect this crucial cell niche against cell damage from toxic and foreign compounds. Expression of the Mdr1 efflux transporter at the cell membrane could potentially reduce intracellular accumulation of toxic compounds thereby preventing cell damage/cytotoxicity of the stem cell niche. Loss of a single cryptal stem cell has been shown to reduce cell production by up to 64 cells (based on six rounds of cell division) (Marshman et al., 2002), further highlighting physiological requirement for stem cell protection. Studies to determine co-localisation of Mdr1 and Lgr5, and identify cryptal Paneth cells may provide further insight into the potential role of Mdr1 in the crypt region.

MRP2 was discovered following identification of a hepatocyte canalicular membrane transporter responsible for the efflux of conjugated organic anions, including bilirubin, from

hepatocytes into bile (Borst et al., 2000, Mayer et al., 1995). This transporter was found to be expressed at high levels on the bile canalicular and lateral membrane of hepatocytes in both humans and normal rats (Mayer et al., 1995, Nies and Keppler, 2007). Since cloning of the transporter in 1996 (Buchler et al., 1996), MRP2 has been shown to transport various drug compounds including anthracyclines and vinka alkaloids in addition to its role in the physiological transport of glutathione and glucoronide conjugated anions (Jedlitschky et al., 2006, Nies and Keppler, 2007). The ability of this transporter to confer drug resistance and reported intestinal expression (Fromm et al., 2000, Mottino et al., 2000, Sandusky et al., 2002) indicate a role for this protein in intestinal drug disposition.

In agreement with current literature, prominent localisation of Mrp2 to the bile canalicular and lateral membranes of rat hepatocytes using the M2-III-6 primary antibody is shown, however, immunohistochemistry using the M2-III-6 antibody failed to detect substantial Mrp2 protein expression along the length of the rat intestine using the same methodology, except for minimal immunoreactivity in the ileum, indicating absence of Mrp2 protein in rat intestine. Low level immunoreactivity was observed in human jejunal and colonic sections. We have shown an ability of M2-III-6 to detect both rat and human Mrp2/MRP2 denatured protein using Western blot analysis. Furthermore suitability of this antibody in detection of human MRP2 at the apical membrane of MDCKII-MRP2 cells was confirmed.

Past studies have reported expression of Mrp2/MRP2 at the apical membrane of villi cells of rat (Mottino et al., 2000) and human intestine (Fromm et al., 2000, Sandusky et al., 2002) however results are somewhat dubious with low level immunoreactivity, high levels of background staining and absence of immunohistochemical images adding doubt to such findings. Given the accepted role of MRP2 in intestinal drug handling it is somewhat surprising that protein expression in both rat and human intestine was low however antibody validation experiments and immunohistochemistry performed in rat liver prove ability of M2-III-6 to bind MRP2/Mrp2 protein.

We have shown measurement of high Mrp2 mRNA expression levels both along the length of the rat small intestine and across the crypt villus axis, however protein expression is negligible, indicating Mrp2 mRNA and protein expression do not correlate. An apparent lack of correlation between mRNA and protein expression of MRP2 was also reported by Berggren et al., (2007) who failed to detect correlation when individual intestinal sections were studied in isolation, reporting relatively high mRNA expression levels compared with minimal protein along the length of the human intestine. We therefore suggest, as observed by Fromm et al., (2000), that Mrp2 protein expression may be induced in response to exposure of intestinal epithelial cells to xenobiotics. Fromm et al., (2000) show similar low levels of immunoreactivity

when using the M2-III-6 antibody in normal human duodenum sections, although a significant increase in both mRNA and protein expression was observed following oral exposure to the drug compound rifampin (600mg). An increased expression of Mrp2/MRP2 protein, particularly on the villus enterocyte membrane, would ultimately allow efflux of drug compounds from absorptive epithelial cells out into the intestine, thereby increasing intestinal excretion and lowering systemic absorption. As suggested by Benet, (2009) for MDR1, Mrp2 may also serve to cause enterocytic recirculation of drug compounds and potentiate interaction with enteric CYP450 enzymes.

Post-transcriptional regulation, a key aspect of gene regulation in eukaryotes, may also play an important role in accounting for the observed differences between mRNA and protein expression levels of Mrp2, with recent studies reporting the importance of micro RNAs (miRNAs) in regulating the expression of key drug transporters and CYP450 enzymes and as such their ability to influence drug disposition (Koturbash et al., 2012, Valencia-Sanchez et al., 2006). It is predicted that miRNA molecules may regulate the expression of up to 60% of human genes (Koturbash et al., 2012). miRNAs are short nucleotide sequences which are derived from longer primary transcripts via formation of hairpin loops and subsequent cleavage by an RNase III enzyme, Drosha, prior to export from cell the nucleus into the cell cytoplasm (Koturbash et al., 2012). Once within the cytoplasm an RNase III enzyme processes these pre-miRNAs to form miRNA-miRNA hybrids, later unwinding of these hybrids produces a mature miRNA molecule, 22 nucleotides in length (Ambros, 2004, Koturbash et al., 2012).

Following transcription and modification of pre-miRNAs the resultant mature miRNA is processed into a RNA-induced silencing complex (RISC) where is interacts directly with an Argonaute protein which facilitates binding to target mRNA sequences and post-transcriptional modification (Bartel, 2004, Benet, 2009). miRNA incorporated into the RISC binds directly to miRNA binding sites located within the 3'UTR of the target mRNA sequence and directs translational repression, and hence a decrease in the transcribed protein, and/or mRNA destabilisation via cleavage of the target mRNA sequence or acceleration of mRNA capping (Bartel, 2004, Valencia-Sanchez et al., 2006). The mechanism by which miRNA molecules exert their effects is believed to result from the specificity of miRNA-mRNA binding (Benet, 2009). It is believed that miRNAs which shown only partial complementary base pairing cause translational repression whilst miRNA molecules which show a higher degree of complementarity to the target mRNA sequence binding site mediate degradation of target mRNA (Benet, 2009, Valencia-Sanchez et al., 2006).

Given that miRNAs are expressed in a tissue and time dependent manner it is possible that intestinally expressed miRNAs bind to 3' UTR binding sites within the MRP2/Mrp2 mRNA

sequences and prevent mRNA transcription and protein expression. Indeed, past studies have shown that the miRNA molecule, miR-379, binds to and negatively regulates human MRP2 protein expression in the HEPG2 (human hepatoblastoma cells) cell line (Haenisch et al., 2011). Haenisch et al., (2011) showed a minimal decrease of ABCC2 mRNA to 72% of control expression following transfection of 50nM pre-miR-379 into HEPG2 cells. The minimal decrease in RNA expression was not reflected at protein level, with a 46.2 ± 12.1% decrease in protein expression following transfection of 50nM pre-miR-379, as determined using Western blot analysis. The lack of correlation evident between the observed decrease in mRNA and protein levels indicates miR-379 to act via repression of MRP2 mRNA translation, as evident by the exaggerated decrease in MRP2 protein levels (Haenisch et al., 2011). It is therefore possible that a similar miRNA mediated post-transcriptional regulation may account for the apparent lack of correlation between intestinal mRNA and protein expression of Mrp2 in the rat.

Despite the recognised role of BCRP in conferring drug resistance, both in the intestine and other tissues (Hegedus et al., 2009, Robey et al., 2009), little work has been performed to establish the protein expression and membrane localisation profile of this transporter. To our knowledge only two studies have investigated BCRP localisation in human intestine, one of which localised BCRP to the apical membrane of villus epithelial cells (Maliepaard et al., 2001), whilst the second showed cytoplasmic staining in both the small intestine and colon (Fetsch et al., 2006). However no study, to our knowledge, has focused on the expression of rat Bcrp protein despite the common use of rats in the study of *in vivo* drug pharmacokinetics.

This study therefore aimed to determine Bcrp protein expression along the length of the rat intestine and subsequent comparison of protein localisation in human intestine samples. Furthermore, the role of BCRP in the generation of the SP phenotype of stem cells (Scharenberg et al., 2002) and the apparent need for protection of the highly regulated proliferative capacity of the crypt led to the hypothesis of a physiological role of BCRP in crypt protection. High mRNA expression levels determined by us using NanoString analysis within the crypt samples (chapter 4) provide additional support for this theory.

Strongly contradicting with the current consensus we show localisation of Bcrp protein to the lateral cell membranes of cryptal epithelia only, with no villus M70 immunoreactivity. The rabbit polyclonal anti-Bcrp primary antibody M70, showed high level immunoreactivity at the lateral cell membranes of cryptal epithelia along the length of the small intestine with a lack of Bcrp expression above the level of the crypt-villus junction. Antibody validation experiments using mouse Bcrp transfected MDCKII cells show ability of this antibody to detect Bcrp protein both in its denatured and tertiary forms using Western blot and indirect

immunocytochemistry. Furthermore, antibody validation experiments were replicated using the alternative Bcrp antibody, BXP9. Rat intestinal sections incubated with rabbit purified IgG serum only showed no immunoreactivity, therefore confirming observed staining to be attributable to M70 epitope-antigen binding. Colonic Bcrp expression was low, with minimal levels of immunoreactivity observed at lateral cell membranes in several crypt units only.

A recent study highlighted species differences with regards to BCRP protein localisation in human and rat liver tissues (Vander Borght et al., 2006). It is known that, like MRP2, BCRP is expressed in bile canaliculi of the human liver (Diestra et al., 2002) however whilst detection of Bcrp in rat liver showed staining of interlobular bile ducts and the endothelial layer of small veins, arterioles and capillaries, a consistently negative staining of rat hepatocytes at the canalicular membrane using the M70 anti-Bcrp antibody was reported (Vander Borght et al., 2006). Again, as shown here, M70 antibody specificity was validated using Western blot (Vander Borght et al., 2006). Replication of findings by Vander-Borght et al., (2006) is reported here with M70 immunoreactivity localised to endothelial cells lining hepatic blood vessels with an apparent staining of hepatic sinusoids. It is therefore unlikely that results observed here do not result from antigen retrieval methods used in the current study since no antigen retrieval was performed by Vander-Borght et al., (2006). The consistent lack of Bcrp staining at bile canalicular membrane of rat hepatocytes shows differences in BCRP/Bcrp protein expression between human and rat liver. Given the reported differences in hepatic BCRP/Bcrp expression it is not unreasonable to suggest altered Bcrp expression profile to be evident in rat intestine. Species differences with regards to BCRP/Bcrp expression question the reliability of the rat model in prediction of human drug pharmacokinetic profiles, particularly given the extensive role of this transporter in drug efflux.

We therefore evaluated human BCRP expression in jejunum and colon samples. Like that shown by Maliepaard et al., (2001), strong BXP21 immunoreactivity was apparent at the apical membrane of villus and crypt epithelial cells. The strong level of apical BCRP expression on villus enterocytes supports current consensus with regards to the role of this transporter in intestinal drug disposition and drug resistance (Robey et al., 2009, Szakacs et al., 2008). In additional to villus expression it is shown here that BCRP is expressed at the apical membrane of crypt epithelia in the jejunum and colon of adult human intestine. Similarly, Englund et al., (2006) showed localisation of BCRP to the apical membrane of crypt epithelial in non-inflamed colonic human sections of ulcerative colitis patients. Expression of this transporter at the apical membrane of human crypt cells strongly supports a role for it in the protection of the crypt niche, since efflux of xenobiotics into the crypt lumen ultimately lowers cellular accumulation and potential for toxic insult. Furthermore, cryptal BCRP expression may contribute toward

reduced intestinal absorption and enteric metabolism of orally administered drugs through enterocytic recycling (Benet, 2009).

In addition to apical localisation of BCRP in human samples, BXP-21 staining is shown at lateral cell membranes of both villus and crypt epithelia. Interestingly, BXP-21 mediated detection of BCRP in human gall bladder was also found to show staining of lateral cell membranes, with a prominent associated apical expression (Aust et al., 2004), showing lateral BCRP expression is not confined to the intestine.

The observed difference in apical BCRP/Bcrp expression between human and rat samples may result from increased exposure of the human intestine to environmental modulators such as dietary components, drug compounds and ingested foreign and toxic xenobiotics (compared with the sterile housing and the regulated diet of laboratory animals), to allow adequate protection against environmental toxins. Given detection of high mRNA expression levels within isolated villus tip fractions and the contrasting lack of protein expression (chapter 4) it is proposed that, like Mrp2, Bcrp may be subject to post-transcriptional modification and/or protein expression may be upregulated or subject to alterations in protein trafficking should the intestine be exposed to xenobiotic compounds to allow proposed efflux of substrates into the intestinal lumen.

As described earlier, miRNA molecules are becoming increasingly recognised as key players in determination of expression levels of drug transporters and CYP450 enzymes (Koturbash et al., 2012), it is therefore not surprisingly that miRNA molecules which interact with the 3'UTR of BCRP mRNA have been identified. Interacting miRNAs include miR-328 and miR-519c (Pan et al., 2009, To et al., 2008). Pan et al., (2009) analysed the 3' UTR sequence of BCRP mRNA to determine potential for interaction with miRNA molecules and determined miR-328 to be the top candidate for miRNA-mRNA binding. Investigation as to the expression levels of BCRP mRNA and miR-328 in the parental MCF-7 and the mitoxantrone resistant MCF-7/MX100 cell line showed a -30 fold higher mRNA expression in the MCF-7/MX100 line in comparison to drug sensitive MCF-7 cells. Moreover, miR-328 expression was shown to be inversely related to mRNA expression, with MCF-7/MX100 cells expression only 1% of the total miR-328 present in MCF-7 cells (Pan et al., 2009). Transfection of MCF7-MX100 cells with miR-328 was found to down regulate BCRP protein in a dose dependent manner, with an associated decrease in mRNA expression. The correlation between decreased mRNA and protein expression levels following transfection of miR-328 suggest miRNA mediated mRNA degradation to account for the associated loss of BCRP protein (Pan et al., 2009). Contrastingly, To et al., (2008) showed ability of a transfected miR-519c inhibitor to cause a two and six-fold increase in BCRP mRNA and protein expression respectively suggesting miR-519c to exert its activities via both

degradation of BCRP mRNA and inhibition of translation and protein production. The ability of miRNA molecules to interact with human BCRP may also be reflected in the rat, with miRNA-Bcrp mRNA interactions potentially being responsible for the lack of villus tip Bcrp protein expression, due either to, mRNA degradation, and hence decreased mRNA stability and/or inhibition of translation of mRNA to expressed protein.

With regards to lateral BCRP/Bcrp localisation three potential hypothesise are proposed; 1. Cell specific BCRP trafficking mechanisms may cause altered protein distribution patterns; 2. Heterodimerisation of the BCRP monomer may ultimately alter cell surface expression of the protein; 3. Lateral membrane expression may serve to increase flux of drug compounds from within the crypt region into the portal vein and thereby promote hepatic metabolism and drug clearance.

Despite acceptance of strict apical BCRP localisation, only one study has localised BCRP to the apical enterocyte membrane (Maliepaard et al., 2001). Although overlooked, a study by Fetsch et al., (2006) reported cytoplasmic staining using two different anti-BCRP antibodies in paraffin embedded sections. Cytoplasmic BCRP expression was shown in placenta, bladder, prostrate, small and large intestinal epithelium, renal cortical tubules and hepatocytes amongst other human tissue types (Fetsch et al., 2006). Cytoplasmic BCRP expression may support the theory presented here of increased BCRP insertion into the cell membrane in response to epithelial stress/exposure to xenobiotics. As such cytoplasmic BCRP, may potentially serve as a cellular BCRP protein reservoir which undergoes protein translocation in response to environmental variations. Alternatively, intracellular cytoplasmic staining of BCRP may indicate a potentially unrecognised role of the transporter in the intracellular compartment (Fetsch et al., 2006).

Interestingly, Kobuchi et al., (2012) have recently shown localisation of BCRP to the inner mitochondrial membrane using confocal microscopy and Western blot analysis following subcellular fragmentation. Confocal microscopy studies in A549 cells showed high levels of BCRP expression within the perinuclear region, with substantial expression overlap between BCRP and mitochondria. Furthermore, protein bands of intense density were recognised using Western blot analysis of mitochondrial subcellular fractions (Kobuchi et al., 2012). Current literature therefore indicates a highly complex pattern/regulation of BCRP protein expression with potential for expression differences between *in vitro* and *in vivo* cells and across tissue types and species.

As discussed earlier (section 3.1) Caco2 cells are often used in the assessment of BCRP functional activity and as such serve as a model cell line. Our laboratory has previously shown apical BCRP expression in low passage Caco2 cells using immunocytochemistry (Wright, 2011).

Interestingly, whilst apical BCRP protein expression in Caco2 cells appears unchanged from day 5 to 19 in culture, cytoplasmic and lateral BCRP staining is apparent 2 days post seeding (Xia et al., 2005). Immunofluorescence and confocal microscopy showed expression of BCRP at the apical and lateral cell membranes prior to establishment of cell confluency. Basolateral and cytoplasmic expression in Caco2 cells prior to reaching confluence suggests potential for transporter redistribution in model systems to occur over extended growth periods. Indeed cell culture techniques have previously been shown to alter drug transporter expression levels (Xia et al., 2005). Similarly, it is not unreasonable to suggest alterations in transporter expression *in vivo* compared with model cell lines, nor is it hard to imagine differences in expression to result in response to differing cell selection pressures.

BCRP may also undergo posttranslational modification resulting in an altered protein expression pattern however a study performed by Mohrmann et al., (2005) showed mutation of the single putative BCRP N-glycosylation site, Asn596, did not alter cellular trafficking in CHO9 cells. However, N-linked glycosylation has been shown to be cell dependent and may therefore alter protein trafficking in alternative cell lines and/or *in vivo* (Mohrmann et al., 2005). As discussed previously BCRP undergoes cell/tissue specific N-linked glycosylation, as demonstrated by a reduced molecular weight following cleavage of mature mannose structures by PNGase F (Diop and Hrycyna, 2005, Hori et al., 2004, Mohrmann et al., 2005). Alternatively other post translational modifications may influence BCRP protein trafficking.

To allow epithelial cells to perform their physiological functions, including absorption, secretion and vectoral transport they undergo polarisation, such that separate apical and basolateral cell membrane domains are defined by their separation with tight junctions (Deborde et al., 2008). Furthermore definition of membrane localised protein expression ultimately determines cell function and fate (Mellman and Nelson, 2008). Protein localisation is determined by sorting signals associated with individual plasma membrane proteins (Deora et al., 2005, Mellman and Nelson, 2008). Glycophosphatidylinositol anchors, O-glycans and N-glycans are all examples of apical protein sorting signals and have been localised to within the transmembrane or cytoplasmic domains of the protein structure (Deora et al., 2005).

Basolateral trafficking results from cytoplasmic expression of consensus signalling sequences which are also required for cellular recycling of plasma membrane proteins (Mellman and Nelson, 2008). With regard to proteins which express both an apical and basolateral trafficking sequence, the basolateral sequence dominates and as such translocation to the basolateral membrane will pursue (Mellman and Nelson, 2008). Vesicular deactivation of the basolateral consensus signalling sequence can however occur and allow subsequent transcytosis of the protein to the apical cell membrane (Mellman and Nelson, 2008). Such transcytosis permits

alterations in membrane polarisation of one protein between membranes within one cell type, and across different cell types (Mellman and Nelson, 2008). A loss of cell polarity is observed when cells switch to a disease state, for example in cancer where the role of BCRP is well established (Mellman and Nelson, 2008). The loss of epithelial cell polarity disrupts normal cell protein trafficking and as such redistribution of membrane transporters may be observed. In agreement with this, Zhou et al., 2013 report loss of membrane BCRP expression observed in normal breast tissue compared with increased expression levels showing a highly cytoplasmic BCRP profile in tumours.

With regards to altered polarisation of plasma membrane proteins, several proteins including normally basolaterally expressed monocaboxylate transporter (MCT1) and the transmembrane glycoprotein CD147 (cluster of differentiation 147 protein) are transcytosed to the apical cell membrane in retinal pigment epithelium (RPE) (Deora et al., 2005). Interestingly a recent study has shown association of the chaperone protein CD147, proposed to be involved in breast cancer drug resistance, with BCRP, both *in vitro* and *in vivo* (Zhou et al., 2013). The reported co-localisation of the two membrane proteins, and proven ability of CD147 to regulate MDR1 activity (Zhou et al., 2013) suggests a potential role for this glycoprotein in BCRP function.

Zhou et al., (2013) observed a significant increase in BCRP expression, as determined using Western blot, following co-transfection of BCRP and CD147 into MCF7 cells, although only changes in protein expression levels were detected with no accompanying rise in mRNA. Furthermore, increased BCRP apical expression was observed using immunofluorescent staining, and a strong co-localisation evident between BCRP and CD147. Western blot analysis showed a substantial increase in the presence of a protein with approximate molecular weight 140KDa, proposed to be a BCRP homodimer. However, co-immunoprecipitation experiments confirm existence of a BCRP/CD147 complex in transfected MCF7 cells (Zhou et al., 2013). Since CD147 is reported to show extensive variation in protein size due to heterogeneous N-glycosylation (31-65KDa) (Tang et al., 2004), it is suggested that the increased molecular weight observed following co-transfection of BCRP and CD147 may result from heterodimerisation of the two proteins, and thus subsequent alterations in protein expression as have been reported for MCT1 and CD147 (Deora et al., 2005).

CD147 possesses a sorting signal present within the cytoplasmic domain of the protein which contains a leucine residue at position 252 and as such is targeted to the basolateral membrane in MDCKII cells (Deora et al., 2005). Past studies have suggested an obligate relationship between CD147, MCT1 and plasma membrane localisation (Deora et al., 2005). Co-transfection of WT MCT1 and CD147 into MDCK cells results in a strong basolateral (90%) expression of the MCT1/CD147 complex, however mutation of the Leu-252 residue of CD147 to alanine (L252A)

redistributes protein expression, such that approximately 86% of MCT1 is expressed apically (Deora et al., 2005). Transcytosis observed following mutation of the consensus sorting sequence of CD147 confirms CD147 to be the dominant MCT1/CD147 complex partner with regards to determination of polarised localisation (Zhou et al., 2013). Dominant signalling capabilities of CD147 may therefore alter normal BCRP protein expression *in vivo* should CD147 complex with BCRP, via mediation of lateral BCRP membrane insertion (Deora et al., 2005, Zhou et al., 2013).

Lateral BCRP/Bcrp expression may result from altered cellular protein trafficking, compared with the literature proposed apical localisation, due to protein heterodimerisation. BCRP is a member of the ABCG subfamily of ABC transporters. The human ABCG family comprises five members, ABCG1, ABCG2, ABCG4, ABCG5 and ABCG8 (Cserepes et al., 2004). Phylogenetic analysis of the human ABCG family revealed all members to be equally divergent with the exception of ABCG1 and ABCG4, which show closer relation to each other (Cserepes et al., 2004). Like BCRP, other subfamily members are half transporters and, like their drosophila counterparts, have been shown to form heterodimers (Cserepes et al., 2004, Graf et al., 2003). ABCG5 and ABCG8 are involved in the regulation of intestinal sterol absorption and biliary sterol excretion and as such have been localised to apical membrane of epithelial cells lining both the intestine and gall bladder (Graf et al., 2003). Studies have shown obligate ABCG5 and ABCG8 protein dimerisation is required to facilitate transporter trafficking from the endoplasmic reticulum to the Golgi body and subsequent insertion into the apical membrane (Graf et al., 2003). Expression of ABCG5 or ABCG8 alone, in both transfected cell lines and ABCG5/ABCG8 knockout mice models lead to a failure to detect apical membrane insertion of either protein, with protein retention confirmed at the endoplasmic reticulum. Contrastingly, co-transfection of ABCG5 and ABCG8 in both model systems promoted protein heterodimerisation and translocation through the Golgi network with later membrane insertion (Graf et al., 2003).

Furthermore, it has been speculated that ABCG1 and ABCG4 may also form heterodimers (Cserepes et al., 2004). Colorimetric measurement of inorganic phosphate liberation due to ATPase mediated ATP hydrolysis was measured for ABCG1 transfected in the Sf9 insect cell expression system. Rhodamine123 was shown to stimulate ATPase activity above the levels of background controls when ABCG1 was expressed alone, indicating homodimerisation of the ABCG1 protein (Cserepes et al., 2004). However, over-expression of the catalytic $ABCG4_{K108M}$ functionally inactive mutant in combination with WT ABCG1 reduced ATPase activity to the level of constitutive Sf9 background activity (Cserepes et al., 2004). Since it has previously been shown that inactivation of one ATPase catalytic unit in the protein dimer structure is able to

account for a complete loss of function, ABCG1/ABCG4$_{K108M}$ heterodimerisation was assumed (Cserepes et al., 2004). It is likely that ABCG1/ABCG4 $_{K108M}$ heterodimerisation occurs and as such the catalytic ABCG4 mutant exerts a dominant negative effect on ABCG1. It is therefore postulated that ABCG1 and ABCG4 are able to form functional homodimers or heterodimers *in vitro* (Cserepes et al., 2004). Similarly, heterodimerisation of the drosophila ABCG1 and ABCG4 homologs has also been reported (Ewart et al., 1994).

Whilst many have speculated BCRP may form a heterodimer to allow functional protein activity, little investigation has been undertaken in this area. The reported ability of ABCG1/ABCG4 (Cserepes et al., 2004) and requirement of ABCG5/ABCG8 (Graf et al., 2003) protein heterodimerisation and the known ability of the Abcg drosophila family homologs to heterodimerise (Ewart et al., 1994) strongly suggests that, like other ABCG subfamily members, BCRP may heterodimerise. Therefore, it may be that heterodimerisation of the BCRP/Bcrp protein monomer with a currently unknown heterodimer partner may alter protein trafficking and cause expression of the resultant BCRP/Bcrp-heterodimer complex at the lateral cell membranes of crypt epithelia.

Finally, expression of BCRP/Bcrp at the lateral cell membrane of cryptal epithelial may serve to protect this vital region against toxic insult. Whilst vectoral transport of apically expressed BCRP/Bcrp substrates promotes intestinal elimination (Robey et al., 2009, Szakacs et al., 2008), lateral BCRP/Bcrp expression may simply serve to ensure efflux of substrates from the cell cytoplasm. The exclusive localisation of BCRP to the cryptal region of all sections, small intestine and colon, of the rat intestine rather than the apical brush-border membrane of villus enterocytes suggests that the direction of xenobiotic or drug transfer is not back to the lumen of the intestine, but rather is directed to the portal circulation for presentation to the liver and its large metabolic capacity (Suzuki and Sugiyama, 2004). Since the crypts lie deep within the normal intestinal structure diffusion of substrates to the crypts will only occur at high luminal concentrations or when the villi are lost through pathophysiological insult thereby neccessating the requirement for efflux of potentially toxic substances.

Previously in the laboratory a functional role for BCRP was sought using ciprofloxacin secretion as a probe BCRP substrate (Haslam et al., 2011). In the rat, Bcrp mRNA was detected in all intestinal segments by qPCR with the greatest concentration (relative to GAPDH) being present in the ileum. Although ciprofloxacin secretion by ileum was greatest of the rat segments tested, it was notably insensitive to the BCRP-inhibitor, K0143. Indeed the Ki was estimated at approximately 5µM with 1µM being only partially effective. This contrasts to a Ki of 0.1µM in MDCKII-mBcrp. Given the high K0143 concentration required to reduce transepithelial secretion of ciprofloxacin it is unlikely that Bcrp contributes to apical efflux. Rather the

insensitivity of this system to K0143 indicates that ciprofloxacin is not entirely dependent on Bcrp mediated transport and that alternative, unknown, secretory mechanisms may also regulate movement of ciprofloxacin.

6. Response of drug transporter and P450 enzymes to oral imatinib

6.1 Introduction

The apparent lack of correlation between mRNA and protein expression of Mrp2 and Bcrp in the rat intestine indicates potential for post transcriptional regulation of protein expression, especially on exposure to xenobiotics. mRNA transcripts for Mrp2 were previously detected in all regions of the rat small intestine (chapter 4) however immunohistochemistry using the well validated M2-III-6 antibody failed to detect expression of Mrp2 protein in the duodenum and jejunum with only very low immunoreactivity in the ileum (chapter 5). With regards to Bcrp, mRNA concentrations detected using quantitative NanoString analysis were highest of all ABC transporters investigated in all regions of the small intestine, and were found to be significantly higher within villus tip than crypt samples (chapter 4). According to current literature, BCRP plays a vital role in determination of intestinal drug handling due to expression of the transporter at the apical cell membrane of absorptive enterocytes and subsequent efflux of drug compounds/substrates into the lumen of the intestine (Maliepaard et al., 2001, Robey et al., 2009). Movement of substrates against their concentration out into the intestine ultimately increases intestinal elimination and reduces systemic drug concentrations (Szakacs et al., 2008). Despite the presence of mRNA expression in villus tip samples, an absence of Bcrp protein was observed in villus epithelial cells of the rat intestine using immunohistochemistry (chapter 5). In contrast apical expression of BCRP was evident in villus enterocytes of the human jejunum (chapter 5). The transcription of cellular mRNA and apparent lack of translation to expressed protein may reflect cellular energy conservation in that mRNA translation and protein expression occur only in response to intestinal exposure of xenobiotics and/or cellular stress, supported by the apparent differences in apical BCRP/Bcrp expression between humans and rat. Whilst human samples will have been exposed to environmental modulators such as oral drug compounds and dietary constituent's laboratory rats have been housed under sterile conditions and have consumed a controlled diet.

As described in chapter 1, drug molecules have the ability to induce mRNA and protein expression of key proteins (ABC transporters and CYP450 enzymes) involved in drug disposition following oral exposure via alterations in nuclear transcription and translation (Tirona and Kim, 2005). Therefore, following on from determination of mRNA and protein expression in untreated rat intestine, the response of transporters and CYP450 enzymes in rat intestine to oral exposure of imatinib mesylate (imatinib) was investigated. Comparison between mRNA expression levels, intestinal protein expression and localisation and alterations

in the pharmacokinetic profile of imatinib in vehicle treated and imatinib treated animals were addressed.

Imatinib mesylate (Gleevec, STI571), an orally administered drug, is used as standard in the treatment of chronic myeloid leukaemia (CML) and metastatic gastrointestinal stromal tumours (GIST) (Eechoute et al., 2010, Leveque and Maloisel, 2005). Patients are often treated with imatinib for extended periods of time, with drug withdrawal only following development of unacceptable levels of toxicity or decreased imatinib efficacy (Leveque and Maloisel, 2005, Scholler and Levěque, 2011). Designed by Novartis, Imatinib was the first rationally designed specific tyrosine kinase (TK) inhibitor (Eechoute et al., 2010). Normally administered as a 400mg dose, with progression up to 800mg in adult non-responders, imatinib is formulated as a salt, imatinib mesylate, and is administered in tablet form once daily (Leveque and Maloisel, 2005, Manley et al., 2002).

Tyrosine kinases (TKs) prove an attractive target for therapeutic intervention since dysregulation of these enzymes accounts for derivation of approximately one third of oncogenes involved in human malignancies (Özvegy-Laczka et al., 2005). Although design of a drug compound which inhibits TK activity is not difficult, the apparent high levels of protein conservation between up to 800 serine/threonine and tyrosine kinases encoded by the human genome makes development of a drug which specifically targets a single TK extremely difficult (Manley et al., 2002). Imatinib inhibits the activity of the constitutively active BCR-ABL (Breakpoint cluster- Abelson tyrosine kinase gene) hybrid-gene product, via binding and inhibition of ABL (Abelson murine leukaemia viral oncogene homolog) at the ATP binding domain, and also shows inhibitory actions at the c-Kit and PDGFR (platelet derived growth factor receptor) TK receptors (Manley et al., 2002). Given the difficulty in production of a highly specific TK inhibitor, the inhibition profile of imatinib is considered to be good due to low level non-specific reactivity (Manley et al., 2002).

The TK family is subdivided into receptor TKs and intracellular or non-receptor TKs. BCR-ABL is a non-receptor TK protein which was derived following fusion of the c-ABL TK and breakpoint cluster region (BCR) genes as a result of chromosome 9 and 22 translocation in hematopoietic stem cells (HSCs), and is expressed in up to 95% of CML patients (Manley et al., 2002, White et al., 2007, Özvegy-Laczka et al., 2005). Whilst non-receptor TKs are activated independently of extracellular signals and instead are regulated by intracellular and cell adhesion signals under normal physiological conditions, the BCR-ABL fusion protein is constitutively active (Özvegy-Laczka et al., 2005). Dysregulation of the BCR-ABL protein activates intracellular TK signalling pathways which lead to uncontrolled cell growth, inhibition of apoptosis and reduced ability of HSCs to adhere to bone marrow stroma (Manley et al., 2002, Özvegy-Laczka et al., 2005).

Susceptibility to infection is also observed due to a lack of mature lymphocytes in circulation resulting from lowered granulocyte development. Imatinib induces apoptosis of BCR-ABL transformed leukemic cells by binding to the ATP binding domain of ABL kinase and preventing ATP hydrolysis. Inability of BCR-ABL to hydrolyse ATP prevents TK mediated autophosphorylation of intracellular tyrosine residues (Manley et al., 2002, Özvegy-Laczka et al., 2005). Prevention of ATP hydrolysis, and subsequent transfer of γ-phosphate to a tyrosine residue, by imatinib, stops docking of signal transducer proteins to the TK protein and inhibits downstream activation of signalling cascades which induce cellular differentiation, proliferation and survival (Manley et al., 2002, Özvegy-Laczka et al., 2005). BCR-ABL regulates downstream signalling of Ship (SH2-containing inositol 5'-Phosphatase), PI3K (Phosphatidylinositol-4,5-bisphosphate 3-kinase), Stat5 *(*Signal Transducer and Activator of Transcription 5) and Crkl (Crk-like protein) signalling pathways and also influences cytoskeleton proteins (Manley et al., 2002).

In addition to its action on the non-receptor BCR-ABL TK, imatinib also prevents autophosphorylation of the stem cell factor receptor, c-KIT TK, a member of the PDGFR family (Özvegy-Laczka et al., 2005). Mutations within the c-Kit receptor lead to constitutive activation of this TK causing development of GIST, via a similar mechanism to that described for BCR-ABL. As such imatinib is now considered the drug of choice in long term treatment of both CML and GIST despite development of more potent inhibitors due to its exceptional efficacy, high specificity and high levels of tolerability (Manley et al., 2002).

Determination of absolute oral bioavailability of imatinib by comparison with plasma concentrations following continuous infusion showed very high levels of absorption, with a calculated oral bioavailability of 99.3% (Leveque and Maloisel, 2005). Similarly other studies have shown oral bioavailability to be > 98% (Kralj et al., 2014). Following oral administration imatinib must be absorbed across the enterocyte barrier to allow absorption into the systemic circulation and delivery of the drug compound to target organs. As described previously the enterocyte barrier is known to express a variety of transporters and CYP450 enzymes which may influence the bioavailability of a drug compound, either through facilitated absorption, intestinal efflux and elimination or through biotransformation by cytochrome P50 enzymes. The high bioavailability of imatinib however suggests little impact of the enterocyte barrier in contribution to first pass effects of imatinib (Eechoute et al., 2010).

Although the majority of patients initially respond well to imatinib, some show disease progression and decreased imatinib efficacy over longer periods of treatment. The loss of effectiveness observed is attributed to development of imatinib resistance which may result from a variety of different physiological changes such as over expression of TK enzymes to

which imatinib binds or TK mutations (Eechoute et al., 2010). Altered expression of drug transporters and CYP450 enzymes is also proposed as a mechanism responsible for the development of imatinib resistance following long term imatinib treatment, due to involvement of these proteins in determination of imatinib pharmacokinetics (Eechoute et al., 2010). Studies have shown reduced uptake of imatinib in experiments performed at 4°C due to temperature mediated inhibition of active transport processes (Kralj et al., 2014, Thomas et al., 2004). Furthermore, in support of transporter mediated intestinal absorption of imatinib, Kralj et al., (2014) showed increased absorption of imatinib from the duodenum to ileum using excised rat segments. If intestinal absorption of imatinib relied solely on passive diffusion it is expected that absorption levels would remain relatively constant along the length of the intestine therefore the increased absorption levels reported in the ileum compared with the duodenum implicate transporters in the uptake of imatinib from the intestinal lumen into the sinusoidal blood. In support of this, past studies have shown imatinib interacts with several transporter proteins and is metabolised extensively by CYP450 enzymes despite high levels of oral bioavailability (Eechoute et al., 2010, Scholler and Levěque, 2011).

OCT1, a member of the SLC transporter family, is proposed to contribute to uptake of imatinib across the basolateral membrane. This organic cation transporter utilises the cell's electrochemical gradient to influx cationic substrates across the basolateral membrane into the cell cytoplasm however as the cytoplasmic substrate concentration is increased the electrochemical gradient is altered and the direction of vectoral transport reversed to allow efflux of substrates from within the cell across the basolateral membrane (Eechoute et al., 2010). Past studies have shown interaction of imatinib with Oct1. Thomas et al., (2004) showed incubation of a CEM cell line, derived from an acute lymphoblastic leukaemia patient, with the OCT1 and MDR1 inhibitor verapamil caused a decrease in uptake of radiolabelled ^{14}C-imatinib. Since inhibition of MDR1 by verapamil would increase intracellular accumulation of radiolabelled imatinib, the reduced cellular accumulation likely results from inhibition of an uptake pathway present within this CEM cell line (Thomas et al., 2004). Further work showed additional inhibitors of OCT1 function (amantadine, procainamide, prazosin) caused reduced intracellular uptake of ^{14}C-imatinib, whilst specific inhibitors of OCT2 and OCT3, (N-methylnicotinamide and corticosterone), had no effect on cellular imatinib concentration (Thomas et al., 2004). It was therefore concluded that OCT1 directly influences cellular uptake of imatinib at least within the CEM cell line studied. Similar work by Kralj et al., (2014) showed inhibition of Oct1 activity using prazosin and procainamide in rat ileum tissue, as demonstrated by a reduced efflux ratio for imatinib compared with that generated both under control conditions and in the presence of Oct2 inhibitor corticosterone. These works indicate

that the uptake of imatinib across the plasma membrane (apical in the CEM cell line and basolateral in excised rat intestinal tissue) is mediated by the OCT1/Oct1 transporter. In a study by White et al., (2006) it was shown that the IC_{50} of imatinib, as measured by the imatinib concentration required to reduce BCR-ABL mediated phosphorylation of the adaptor protein Crkl by 50%, varied within a small patient cohort. Analysis of OCT1 expression levels showed a correlation between mRNA expression, intracellular uptake and retention of imatinib and imatinib IC_{50} concentration. Inhibition of OCT1 by prazosin and procainamide reduced observed variations in intracellular imatinib accumulation such that levels were similar between patients with a high and low imatinib IC_{50}. Cellular accumulation of imatinib following inhibition of OCT1 likely results from passive diffusion since accumulation is fairly stable between individuals (White et al., 2006). In addition to its role in the intestine, OCT1 is also localised to the basolateral membrane of hepatocytes, where is it believed to facilitate accumulation of imatinib in hepatocytes and therefore promote metabolism hence lowering systemic availability of the parent drug molecule (Hu et al., 2008).

However, the involvement of OCT1 in imatinib transport was questioned by Hu et al., (2008) who showed only 14.5% and 20% higher uptake of radiolabelled imatinib in OCT1 cRNA (complementary RNA) injected Xenopus laevis oocytes and in OCT1 over-expressing HEK293 cells respectively compared with controls. Further, no alteration in the pharmacokinetic profile of imatinib was observed in patients expressing reduced function OCT1 genetic variants, compared with those patients expressing the reference genotype, suggesting only partial involvement of OCT in the uptake of imatinib at target tissue sites (Hu et al., 2008).

Given that imatinib undergoes pH dependent protonation and exists as a cation (~80%) at pH 5 to 6 (Szakács et al., 2005), the pH of duodenal luminal content, it is proposed that the organic cation transporter OCTN2 and may also contribute to the uptake of imatinib from the intestinal lumen across the apical cell membrane (Eechoute et al., 2010). Genetic polymorphisms have previously been shown to alter OCTN2 substrate transport *in vitro*, as such differences in OCTN2 mediated imatinib transport may contribute to the observed inter-individual differences in treatment response (Yamakawa et al., 2011). Hu et al., (2008) showed a significant increase in the uptake of imatinib following injection of OCTN2 cRNA into Xenopus laevis oocytes compared with water injected controls. In addition, studies have shown imatinib uptake, as measured using HPLC to be reduced in OATP1A2 transfected HEK cells, Caco2 cells, and in the BCR-ABL expressing K562 cell line in the presence of OATP1A2 inhibitor naringin (Yamakawa et al., 2011). In addition to expression within the enterocyte barrier, both OCTN2 and OATP1A2 are expressed in the liver and in the kidney, key sites known to influence drug pharmacokinetics and could therefore play an important role in imatinib absorption and

disposition (Eechoute et al., 2010, Yamakawa et al., 2011). Potential roles for the ABC transporters MRP1, MRP4 and MRP7 in imatinib drug disposition have also been suggested, although information regarding interaction of imatinib with these transporters is lacking (Eechoute et al., 2010).

Several studies, discussed below, have shown the ability of imatinib to interact with the ABC efflux transporters MDR1 and BCRP, with potential for an imatinib induced increase in expression. This could contribute to reduced intestinal absorption and decreased systemic drug concentrations. Following initial reports of development of imatinib resistance by over-expression of MDR1 in BCR-ABL expressing cells, more recent studies have confirmed imatinib to be an MDR1 substrate. Hamada et al., (2003) showed decreased accumulation of imatinib in cells known to over-express MDR1, with restoration of intracellular imatinib levels in the presence of 1μM CsA, additionally MDR1 mediated Rhodamine123 efflux was shown to be reduced in the presence of imatinib. Similar work showed Hoechst33342 export to be abolished in the presence of imatinib in murine HSCs known to express both Mdr1 and Bcrp (Dohse et al., 2010). Furthermore, expression of MDR1 or BCRP in BCR-ABL K562 expressing cells was shown to increase BCR-ABL mediated phosphorylation of Crkl compared with the K562 parental cell line. Increased BCR-ABL mediated phosphorylation results from decreased intracellular imatinib concentrations, and subsequent reduction of BCR-ABL inhibition, due to MDR1 and BCRP mediated efflux of imatinib from the cell (Dohse et al., 2010). Thomas et al., (2004) showed a net secretion of radiolabelled imatinib by MDCKII-MDR1 cells which was substantially increased compared with the native MDCKII cell line, thus indicating radiolabeled imatinib to be effluxed from the cell by MDR1. Similarly, Kralj et al., (2014) showed reduced flux of imatinib from the serosal to mucosal chambers (and reversal of transport asymmetry), across rat intestine segments, in the presence of specific MDR1 and BCRP inhibitors PSC-833 and K0143. These studies suggest imatinib to be a substrate for both MDR1 and BCRP.

Conflicting reports are however presented as to whether imatinib is a BCRP substrate or a non-competitive inhibitor. In agreement with others, Burger et al., (2004) showed expression of BCRP in the MCF7 cell line reduced intracellular accumulation of radiolabelled imatinib, with restoration of intracellular imatinib concentrations following incubation of cells with K0143. Decreased accumulation of imatinib in cells over-expressing BCRP indicates BCRP mediated efflux of imatinib and as such shows imatinib to be a substrate. In sharp contrast Houghton et al., (2004) showed the inability of BCRP transfection to lead to imatinib resistance in Saos2 cells, with IC_{50} values for cells transfected with functional or non-functional variants of BCRP of 9.6μM and 9.5μM respectively. Resistance of cells to the BCRP substrate topetecan however was sensitised in the presence of low imatinib concentrations. The concentration of topetecan

required to inhibit cell growth by 50% was decreased from 250nM to 10nM with increasing concentration of imatinib suggesting imatinib mediated inhibition of BCRP activity and topetecan efflux. Furthermore, imatinib accumulation in cells expressing either functional or mutated, non-functional, BCRP was similar following a five minute incubation period indicating a lack of BCRP mediated imatinib efflux (Houghton et al., 2004). Incubation of Saos2 cells with sodium azide to deplete cellular ATP did not cause an increased intracellular accumulation of imatinib, as would be expected if BCRP functional activity was inhibited, but instead was found to reduce cellular imatinib accumulation, consistent with an active uptake mechanism responsible for the absorption of the imatinib drug compound (Houghton et al., 2004).

Like all TK inhibitors imatinib is metabolised by the cytochrome P450 family of enzymes with the majority of metabolism catalysed by CYP3A4, which contributes toward metabolism of up to 70% of therapeutic drugs (Paine et al., 2006, Scholler and Levěque, 2011). The major metabolite of imatinib, the N-desymethyl imatinib derivative, is produced by CYP3A4/3A5 with a lesser contribution from CYP1A1 and CYP2D6 mediated imatinib biotransformation (Scholler and Levěque, 2011). N-desymethyl exhibits comparable levels of activity at TK enzymes to the imatinib parent drug compound (Leveque and Maloisel, 2005). Metabolism by CYP3A4 and CYP1A1 is however suggested to generate other imatinib metabolites which show a decreased affinity compared with the parent compound (Rochat et al., 2008). *In vitro* studies have shown imatinib to also be metabolised by CYP2C8 (Scholler and Levěque, 2011).

Despite high levels of oral bioavailability the potential for *in vivo* interaction between imatinib and members of the ABC, SLC and CYP450 families makes it essential to understand the effects of oral imatinib exposure on gene expression levels, both in tissues involved in drug disposition and also in target tissues. The ability of imatinib to induce transporter expression in the enterocyte barrier may alter the bioavailability of imatinib and as such lower systemic concentrations of active drug compound. This study therefore aimed to determine effects of oral imatinib administration on mRNA expression levels of drug transporters and cytochrome P450 enzymes in rat intestine using NanoString technology. Specific focus is placed on changes in expression of the efflux transporters Mdr1 and Bcrp, for which imatinib is proposed to be a substrate, as such changes in protein expression and localisation of Mdr1 and Bcrp following imatinib treatment were determined using immunohistochemistry. To assess whether short term exposure to imatinib alters the pharmacokinetic profile of the drug, plasma drug concentration profiles were measured on days one and four of treatment, with the hypothesis that induced functional activity of ABC transporter proteins would alter absorption and elimination of imatinib.

6.2 Methods

6.2.1 Details of animals used in study

All work performed in this *in vivo* study was granted ethical approval under an in-house licence at AstraZeneca, Alderley Edge UK and works planned and recorded under study number NOMNO KKR. Details of animals used in the current in vivo study can be found in methods section 2.2.2 and were the same as those used in chapter 4. Animal weights and general health were monitored throughout the entirety of the study. PBS control treated animals were of weights within the range 317g to 363g three days prior to study initiation and 351g – 387g on the day of sacrifice, with a weight gain range of 16g – 32g. Imatinib dosed animals were of weights within the range 298g to 330g three days prior to study initiation and 320g – 359g on the day of sacrifice, giving a weight gain of range 17g – 32g. Animals within each treatment group therefore showed similar weight gain over the period of study.

6.2.2 Imatinib dose justification and delivery

In this study a total of eight animals were dosed with 150mg/kg of oral imatinib dissolved in PBS daily over a period of 5 days by oral gavage. The dose of imatinib administered was determined using clinically relevant human doses ranging 400-800mg/day and literature reported studies showing effects of imatinib, with compensation allowed for ABC transporter mediated efflux of imatinib in the intestine and to optimise the probability of observing gene induction.

Past studies have shown administration of imatinib at a dose of 150mg/kg to cause measureable effects. Nurmio et al., (2007) showed delayed formation of germ-line stem cell pool, reduced proliferation of type A spermatogonia and induced germ cell apoptosis in immature rats following administration of 150mg/kg imatinib. Furthermore 150mg/kg imatinib was shown to reduce destruction in ankle and subtalar joints of collagen induced arthritic rats (Ando et al., 2006). Effects of imatinib described above were observed following only short term administration, a requirement of this study given the high rate of epithelial cell turnover in the intestine. From initial cell proliferation of intestinal stem cells to apoptosis of epithelia at the villus tip the crypt to villus migration process takes approximately five days, therefore any effect of imatinib on transporter expression must be observed within this short time frame. As such, it is likely that, should imatinib cause alterations in expression levels of intestinal genes such changes will be detected using a high imatinib concentration of 150mg/kg.

According to the imatinib mesylate safety data sheet 450mg/kg imatinib is the lowest dose reported to have toxic effects in rats following a three day treatment window. The use of 150mg/kg therefore complies with past toxicity studies and is unlikely to cause adverse effects.

No animal used in this study showed substantial weight loss or displayed any signs of degeneration, with no change in animal health observed.

In the present study imatinib was dissolved in PBS to allow administration by oral gavage. PBS has previously been used as a vehicle for imatinib administration (Ando et al., 2006). Furthermore, imatinib solubility was high, with no requirement for extensive mixing or sonification. Imatinib remained in solution with PBS over extended time periods, with no observation of precipitation.

6.2.3 RNA extraction and determination of mRNA expression levels

RNA was extracted and mRNA concentrations determined using NanoString technology, as described in materials and methods section 2.2.6. Details of the NanoString codeset used are shown in table 2.1. RIN values for in vivo samples were varied (range 1 – 6.7) however Nanodrop 260/280 ratios were all > 1.96 and as such samples were deemed to be of good enough quality for RNA analysis. Low RIN values likely reflect prolonged time taken to acquire tissue samples following excision of the rat intestines.

6.2.4 Intestinal protein localisation

Sections of rat duodenum, jejunum, ileum and colon were prepared as described in materials and methods section 2.2.9. Sections were stained using a Ventana staining platform, details of antibodies and detection systems used are shown in tables 2.4 and 5.1

6.2.5 Determination of plasma imatinib concentrations and generation of pharmacokinetic profiles

Plasma samples were taken over a twenty-four hour period following imatinib dosing on day one and day four of treatment and imatinib concentrations determined using HPLC. Full details of methods used and analysis of samples are detailed in materials and methods section 2.2.11.

6.3 Results

6.3.1 Evidence for interaction of imatinib with MDR1 and mBcrp

In order to confirm a potential interaction between imatinib and MDR1/mBcrp the Hoechst33342 dye efflux assay was used. As already shown in chapter 3 stable transfection and over-expression of MDR1 and mBcrp at the apical cell membrane of MDCKII cells reduces intracellular accumulation of Hoechst33342 represented by a decreased absolute cellular fluorescence between native and MDCKII-MDR1 or MDCKII-mBcrp cells under control conditions. Measured fluorescence decreased from 437.1 ± 32.0 arbitrary units (mean n=18 wells ± SEM) in native MDCKII cells to 73.4 ± 5.75 arbitrary units in mBcrp transfected MDCKII cells (mean n=18 wells ± SEM) (figure 6.1). No significant (not shown) decrease in Hoechst33342 retention was observed between native and MDR1 transfected cells in the absence of imatinib, this likely reflects an anomaly within the data since earlier works (section 3.3.3) showed a marked decrease in fluorescence in MDR1 transfected cells. The specificity of MDR1 or mBcrp transfection was also established previously using specific MDR1 and mBcrp inhibitors CsA and K0143, which were shown to increase Hoechst33342 cellular fluorescence (section 3.3.3).

Despite high levels of measured fluorescence under control conditions imatinib was shown to increase intracellular Hoechst33342 retention in the MDCKII-MDR1 cell line, with a highly significant rise observed at concentrations greater than 30μM (*** $p < 0.001$) (figure 6.1). Similarly, a significant increase in cellular fluorescence was observed in the MDCKII-mBcrp cell line following incubation with imatinib at concentrations greater than 30μM (*** $p > 0.001$) (figure 6.1). Incubation with imatinib did not increase fluorescence in the native cell line (figure 6.1). The observed increase in intracellular retention is therefore attributed to reduced ability of MDR1 and mBcrp to efflux Hoechst33342 from the cell in the presence of imatinib. This inhibition could arise due to the competitive inhibition, via transport of imatinib, of either MDR1 or mBcrp by imatinib, or due to the pharmacological action of imatinib, as such conclusions regarding the interaction between MDR1 and mBcrp and imatinib cannot be drawn from this experiment other than to say imatinib alters the transporter activity of both proteins.

Figure 6.1:

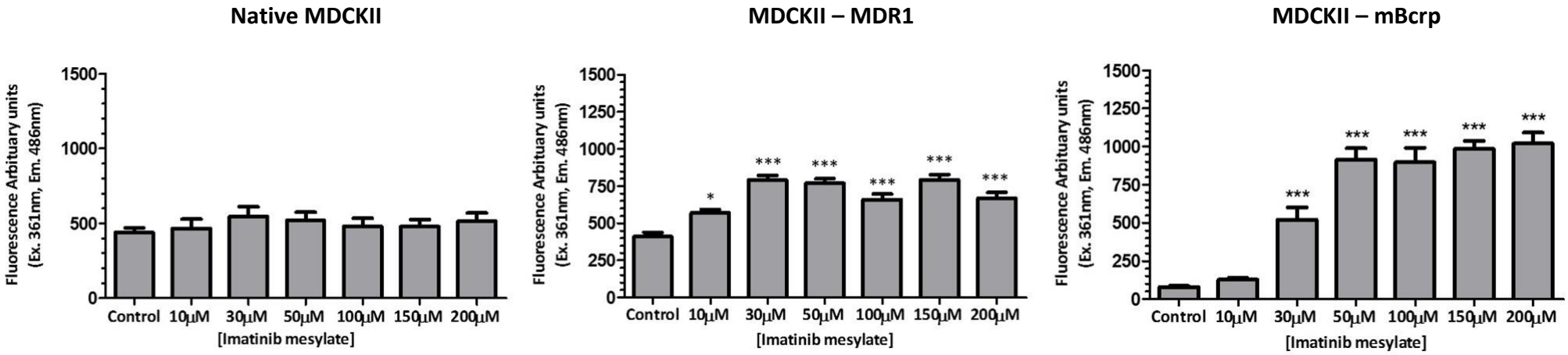

Figure 6.1 Concentration dependent effect of imatinib mesylate on intracellular Hoechst33342 dye retention in native MDCKII, MDCKII-MDR1 and MDCKII-mBcrp cells.

Hoechst33342 retention was measured in a fluorescence-dependent manner in native MDCKII, MDCKII-MDR1 and MDCKII-mBcrp cells following incubation with imatinib at increasing concentrations. Cells were incubated with Hoechst33342 at a concentration of 3μM. Cells were excited at 361nm and emitted fluorescence at 486nm measured. Cells were grown on 96 well plates for 5-7 days, data shown represent n=18 (native MDCKII and MDCKII-mBcrp) and n=12 (MDCKII-MDR1) wells from three independent experiments ± SEM and have been normalised against control fluorescence. * $p < 0.05$ and *** $p < 0.001$ One way ANOVA with Tukey post-test analyses vs. control. Imatinib was dissolved in DMSO.

In support of the Hoechst33342 data transepithelial flux measurements (figure 6.2) were conducted. In these experiments the transepithelial secretion of the MDR1 and mBcrp substrates, ^{3}H-digoxin and ^{14}C-ciprofloxacin, were measured in MDCKII-MDR1 and MDCKII-mBcrp cells respectively. Our laboratory has previously shown digoxin and ciprofloxacin to be substrates for MDR1 and mBcrp, with net flux of radiolabelled digoxin and ciprofloxacin being significantly reduced following specific inhibition of MDR1 and mBcrp by verapamil and K0143 (Haslam, 2007, Wright, 2011). Given the apical expression of MDR1 and mBcrp, as shown using indirect immunocytochemistry (chapter 5, sections 5.3.1 and 5.3.3), it was expected that functional activity of MDR1 and mBcrp would result in a net secretory transport of ^{3}H-digoxin and ^{14}C-ciprofloxacin respectively (figure 6.2). The flux of radiolabelled substrates was substantially lower in the absorptive direction ($J_{(a-b)}$) than in the secretory direction ($J_{(b-a)}$) indicating active efflux of ^{3}H-digoxin and ^{14}C-ciprofloxacin across the apical cell membrane. In agreement, calculated net flux values ($J_{(net)} = J_{(b-a)} – J_{(a-b)}$) are positive, indicative of secretory movement (figure 6.2, control conditions).

As shown in figure 6.2, net secretion of ^{3}H-digoxin and ^{14}C-ciprofloxacin decreases as cells are exposed to increasing concentrations of imatinib. The decreased net secretion reflects both the increased movement of radiolabelled substrates from the apical donor chamber, through the cell monolayer, into the basolateral receiver compartment and the reduced flux of ^{3}H-digoxin and ^{14}C-ciprofloxacin across the apical membrane. It is suggested that incubation with imatinib reduces functional activity of both MDR1 and mBcrp due to the specificity of substrates used and inability of imatinib to increase cellular Hoechst33342, a dual MDR1 and mBcrp substrate, accumulation within the native cell line (figure 6.1). Inhibition of ABC transporter function, either by direct inhibition or competitive substrate inhibition, results in the observed profile of increased absorptive flux and decreased secretory flux suggesting an increased cellular accumulation of ^{3}H-digoxin and ^{14}C-ciprofloxacin within MDCKII epithelial cells.

Figure 6.2:

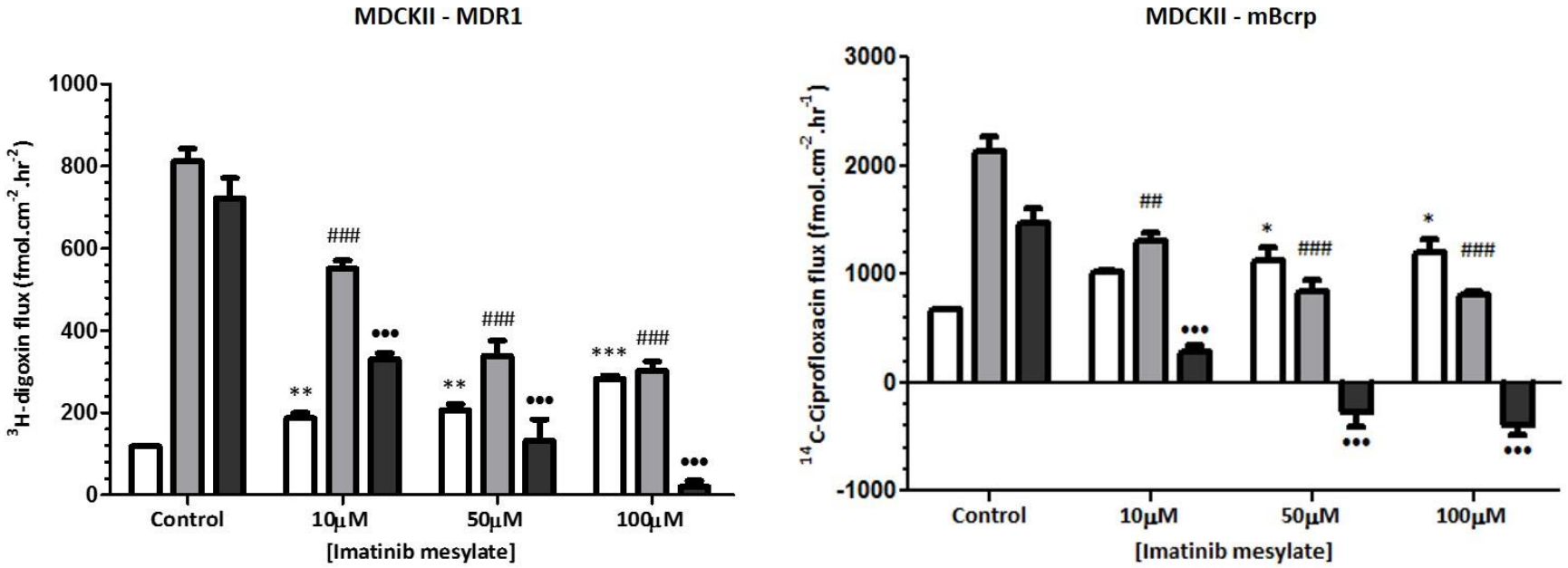

Figure 6.2 Transepithelial flux of ^{3}H-digoxin and ^{14}C-ciprofloxacin across MDCKII-MDR1 and MDCKII-mBcrp cell monolayers respectively in the absence and presence of imatinib mesylate.

Transepithelial flux of ^{3}H-digoxin and ^{14}C-ciprofloxacin across confluent monolayers of MDCKII-MDR1 and MDCKII-mBcrp cells respectively in the absence or presence of imatinib. Donor ^{3}H-digoxin and ^{14}C-ciprofloxacin concentrations were 10nM and 1µM respectively. Imatinib concentrations are shown on x-axis. Fluxes were determined in the apical-basal direction ($J_{(a-b)}$) (clear bars), basal to apical ($J_{(b-a)}$) (grey bars) and net flux calculated ($J_{(net)} = J_{(b-a)} - J_{(a-b)}$) (black bars). Data shown represents n=3 wells taken from a single experiment ± SEM. One-way ANOVA analysis with Tukey post-test * $p < 0.05$, ** $p < 0.01$, *** $p < 0.001$ versus $J_{(a-b)}$ in absence of imatinib, $^{\#\#}$ $p < 0.01$, $^{\#\#\#}$ $p < 0.001$ verses $J_{(b-a)}$ in absence of imatinib and ••• $p < 0.001$ versus $J_{(net)}$ in absence of imatinib. Imatinib was dissolved in DMSO.

6.3.2 Effects of oral imatinib on mRNA and protein expression of selected ABC, SLC and CYP family members and on the pharmacokinetic profile of imatinib

In chapters 4 and 5 a lack of correlation between mRNA and protein expression for Bcrp and Mrp2 was observed in the rat intestine. Past studies have shown increased expression of MDR transporters following oral exposure to drug compounds, with the majority of drug-drug interactions resulting from alterations in expression and function of transporters and CYP450 enzymes leading to changes in drug disposition. The ability of drug compounds to induce expression of transporters and enzymes involved in drug disposition may lead to drug-drug interactions when patients undergo polypharmacy. Imatinib is currently the standard treatment for CML and GIST patients and is administered orally over prolonged periods of time, furthermore imatinib has been shown to interact with several drug transporters and CYP450 enzymes (Eechoute et al., 2010). This study therefore aimed to determine how oral exposure to imatinib alters expression of selected membrane transporters and CypP450 enzymes in the intestinal mucosa at both an mRNA and protein level. It was also determined if oral administration of imatinib alters the pharmacokinetic (PK) profile of imatinib between days 1 and 4 of treatment. Whilst four day treatment is minimal, with clinical treatment with imatinib spanning years (Manley et al., 2002), the intestinal enterocyte barrier, is subject to fast turnover such that epithelial cells are shed into the intestinal lumen only five days following initial differentiation of the crypt stem cells (Barker et al., 2008, Pinto and Clevers, 2005). Therefore any ability of imatinib to induce transporter expression/function in intestinal enterocytes should be evident over this short time period.

mRNA expression levels were determined in the duodenum, jejunum, ileum and colon of both vehicle and imatinib treated animals using NanoString technology and the CodeSet of target genes detailed in table 2.1. Log_2 fold change values were calculated to allow easy identification of fold changes irrelevant of the ability of imatinib to increase or decrease mRNA expression levels of each gene investigated. Log2 fold change values of 1 and -1 represent a two fold increase and decrease in mRNA expression respectively. As with untreated animals (chapter 4) mRNA transcript levels of genes encoding Mdr1b, Mrp4, Oat3, Oatp3, Cyp2c6v11, Cyp2c11, Cyp2d3 and Cyp3a1/3a23 were detected at only very low levels, with similar expression profiles to negative controls, suggesting mRNA expression levels were not upregulated following oral exposure to imatinib, as such these genes were excluded from analysis and will not be discussed further. Housekeeping gene expression levels of all sample groups detailed were not significantly different from the average of all samples studied (n=48 samples) (section 2.6), including samples taken from normal rats (chapter 4) and samples taken from animals treated with either PBS or 150mg/kg imatinib. A lack of significant difference of HSKP gene

expression levels following treatment with 150mg/kg imatinib suggests stability of Hprt1, Hmbs and Gapdh expression levels, independent of experimental treatments.

Average mRNA concentrations of ABC transporters are shown in table 6.1 alongside calculated log_2 fold change values for vehicle versus imatinib treated animals. It is clear that imatinib treatment is not associated with large induction of those ABC genes tested with significant changes measured only for Mdr1a in the jejunum and ileum and for Mrp3, Mrp7 and Bcrp in the ileum.

Mdr1a mRNA expression was found to increase in the jejunum (* $p < 0.05$) with a calculated log_2 fold change of 1.47 ± 0.31 between vehicle and imatinib treated animals (table 6.1). Surprisingly, an approximate 2-fold reduction in average Mdr1a expression from 8.76 ± 0.75 fmol/sample in vehicle treated animals to 4.63 ± 1.13 fmol/sample in imatinib treated animals was detected in the ileum (*$p < 0.05$) (mean mRNA expression of n=3 animals per group ± SEM). Similarly, Mrp7, a basolaterally expressed transporter suggested to transport imatinib (Eechoute et al., 2010) and Bcrp mRNA expression levels were also decreased in the ileum of imatinib treated animals. Mrp7 mRNA concentrations decreased from 2.86 ± 0.12 fmol/sample to 1.37 ± 0.14 fmol/sample (**$p < 0.05$) (mean mRNA expression of n=3 animals per group ± SEM) whilst a greater than 2-fold decrease in ileal Bcrp mRNA expression was apparent following treatment with oral imatinib (log_2 fold change -1.14 ± 0.44) (*$p < 0.05$). mRNA expression levels for Bcrp were decreased from 27.58 ± 3.19 fmol/sample in vehicle treated animals to 12.76 ± 2.45 fmol/sample in imatinib treated animals (mean mRNA expression of n=3 animals per group ± SEM). Although studies to date have not shown an involvement of Mrp3 in the transport of imatinib, it should be noted that Mrp3 expression levels were significantly decreased from 6.65 ± 1.20 fmol/sample in vehicle treated animals to 2.96 ± 0.41 fmol/sample in the ileum of imatinib treated animals (* $p < 0.05$) (mean mRNA expression of n=3 animals per group ± SEM). Despite the potential involvement of Mrp1 in imatinib transport (Eechoute et al., 2010), no significant change in mRNA expression levels was observed following imatinib treatment (table 6.1).

It was of interest to determine how changes in mRNA expression levels of Mdr1a, Mrp2 and Bcrp translated with regards to intestinal protein expression. Protein localisation was therefore determined in paraffin embedded rat intestinal sections of the duodenum, jejunum, ileum and colon taken from both vehicle and imatinib treated animals using the anti-Mdr1, anti-Mrp2 and anti-Bcrp antibodies C19, M2-III-6 and M70 respectively (table 5.1). All antibodies were previously validated using Western blot and indirect immunocytochemistry (chapter 5). Vehicle and imatinib treated intestinal sections were stained simultaneously using each

antibody to remove inter-experimental variation. Whilst attempts were made to quantify staining intensities they proved unsuccessful.

As observed in untreated animals (chapter 5), Mrp2 protein expression was not detected in any section of the rat intestine from either vehicle or imatinib treated animals and results are therefore not shown. As such it is concluded that Mrp2 mRNA expression evident along the length of the intestine under normal physiological conditions is not translated to protein following oral exposure to high concentrations of imatinib administered over a 5 day period.

Mdr1 (C19) immunolocalisation appears largely unchanged along the length of the small intestine between vehicle and imatinib treated animals (figure 6.3). Staining is visible to the apical membrane of villus epithelia and in a specific subset of cells within the crypt. Given that imatinib has a high oral bioavailability (~98%), with low levels of faecal elimination, (Leveque and Maloisel, 2005) it was somewhat surprising to observe expression of Mdr1 at the apical membrane of superficially located colonic crypt units following imatinib treatment (figure 6.3). Expression of Mdr1 protein at the apical membrane of crypt epithelia indicates a role for this transporter in the efflux of substrates into the crypt lumen to aid in protection of the stem cell niche. Vehicle only controls show a complete absence of staining in all colonic crypts (figure 6.3), as was observed in untreated animals (chapter 5). Despite apparently higher Mdr1 protein expression (note, protein quantification was not performed) within colonic crypts of imatinib treated animals no significant change in Mdr1a mRNA expression levels was apparent in the colon following exposure to oral imatinib (table 6.1). The standard error of Mdr1a mRNA expression in colon mucosa of imatinib treated animals is approximately 55% of the total mRNA expression, suggesting considerable inter-animal variation as reflected by the calculated $\log_2$ fold change value of 0.35 ± 0.90 (table 6.1). It should also be recognised that only minimal, non-consistent C19 immunoreactivity was visualised at the apical membrane of colonic crypts in sections taken from a second animal treated with imatinib, suggestion the inter-animal variation observed at mRNA level to be reflected in translated protein expression.

Despite expression of Bcrp mRNA within the villus tip region, no change in Bcrp protein localisation was observed following treatment with imatinib (figure 6.4). As observed in chapter 5, M70 immunoreactivity was localised only to lateral cell membranes of crypt epithelia. Although no measurements of Paneth cell size were made, Paneth cells do appear to be visually enlarged within the crypts of imatinib treated animals in all regions of the small intestine (figure 6.4, magnified insets). Paneth cells are the fourth lineage of cells generated by the intestinal stem cells, but unlike absorptive enterocytes and secretory cells they migrate down to the base of the small intestinal crypt (Porter et al., 2002). Paneth cells have long been known to secrete apically generated vesicular contents into the crypt lumen, with potential for

interaction between vesicular content and villus epithelial (Ouellette, 1997). The mechanism responsible for the possible increase in Paneth cell volume following imatinib treatment is unknown although amongst other secretagogues, the Paneth cells are known to synthesise and secrete α-defensins, cytokines and inflammatory mediators including TNFα (tumour necrosis factor – α) and CD1, suggesting a possible inflammatory associated response following oral administration of imatinib (Ouellette, 1997). Probable intestinal stem cells are shown interspersed between the Paneth cells, with morphological characteristics reflecting those described previously (chapter 5)(Barker et al., 2008). M70 immunoreactivity is clearly shown to be localised to the cell membrane of this specific cell niche (figure 6.4).

Several members of the SLC family have been implicated in the absorption of imatinib. OCT1, OCTN2 and OATP1A2 have all been shown to transport imatinib across the cell membrane (Hu et al., 2008). Although Oatp1a2 was not included as a target gene in the design of the codeset used presently, changes in mRNA expression levels of Oct1 and Octn2 are shown in table 6.2. No significant change in Oct1 mRNA expression levels was observed following treatment with oral imatinib although a decrease in expression levels is suggested in both the duodenum and ileum (table 6.2). High levels of variation observed between animals are reflective of clinical findings which have shown variation in human OCT1 expression levels in both CML cell lines and primary tissues (White et al., 2007). Similarly, down-regulation of Octn2 mRNA expression is suggested (non-significant) in both the duodenum and ileum, although only the ileum shows a non-significant > 2-fold difference in expression with no indication of change in either the jejunum or colon.

mRNA expression levels of other SLC transporters investigated are shown in table 6.2. A significant decrease in the mRNA expression of Octn1 was measured in the ileum, with a decreased mRNA concentration from 6.01 ± 0.91 fmol/sample in vehicle treated animals to 2.19 ± 0.59 in imatinib treated rats (table 6.2). Although no significant change in expression was measured in the duodenum or colon, approximate two and three- fold decreases in mRNA expression of Octn1 were shown in each region respectively (table 6.2). Despite a lack of change in Cnt2 expression in the jejunum, ileum and colon following imatinib treatment a significant decrease in mRNA concentrations from 81.11 ± 6.45 fmol/sample to 49.07 ± 5.43 fmol/sample was measured in the duodenum (table 6.2). Due to time constraints investigation of protein expression was not performed for any SLC transporters, although given the potentially important roles of Oct1 and Octn2 in the intestinal absorption of imatinib (Hu et al., 2008, Kralj et al., 2014, White et al., 2006, Yamakawa et al., 2011) future work should focus on determination of how observed changes in mRNA expression are reflected at a protein level.

CYP3A4 is responsible for the majority of imatinib metabolism in humans with contributory effects of CYP3A5, CYP2D6, CYP1A1 AND CYP2C8 (Rochat et al., 2008, Scholler and Levěque, 2011). mRNA expression levels of the rat homologs to CYP3A4 and CYP2D6, Cyp3a9 and Cyp2d1/2d9 respectively, are shown in table 6.3. Cyp3a9 mRNA expression remains unchanged following treatment with oral imatinib with no significant difference observed between the two animal groups in any region of the intestine. Any differences observed between Cyp3a9 mRNA expressions in vehicle or imatinib treatment animals is negated by large inter-animal variation in expression. Cyp2d1/2d9 mRNA levels are suggested to be reduced in the duodenum, ileum and colon following imatinib treatment however none of these changes achieved statistical significance. As with Cyp3a9, large variation in the mRNA expression of Cyp2d1/2d9 was observed in all regions of the intestine as reflected by the log2 fold change values shown in table 6.3.

Attention is brought to the significant induction of Cyp1a1/1a2 mRNA following treatment with imatinib. As mentioned previously Cyp1a2 is predominantly expressed in hepatocytes with an absence of, or only weak expression, in extrahepatic tissues (Martignoni et al., 2006), it is therefore likely that the observed increase in Cyp1a1/1a2 target expression is attributable to Cyp1a1 induction. The Cyp1a1/1a2 NanoString target will therefore be referred to as Cyp1a1 from this point forward. Average jejunal mRNA expression was shown to increase from 1.24 ± 0.57 fmol/sample to 119.29 ± 30.75 fmol/sample (* $p < 0.05$), with a maximal fold change of 283 in an individual animal. Average $\log_2$ fold change in the jejunum was 6.97 ± 0.85 (fold change 169.5) much higher than that observed for any other target gene. Average ileal Cyp1a1 mRNA expression increased to 78.50 ± 9.37 fmol/sample from 1.52 ± 0.66 fmol/sample ($\log_2$ fold change 6.28 ± 0.94) (** $p < 0.01$) following treatment with oral imatinib (table 6.3). Duodenal Cyp1a1 mRNA levels showed a non-significant change from 3.16 ± 2.55 in vehicle treated animals to 75.64 ± 41.93 in imatinib treated rats, with an associated $\log_2$ fold change of 5.98 ± 1.57 (table 6.3), it is likely that the substantial variation in expression levels observed for Cyp1a1 accounts for the lack of significance reported. Changes in colonic mRNA expression levels were far less pronounced than those observed in the small intestine with a $\log_2$ fold change of 1.70 ± 0.82. mRNA expression levels of other Cyp450 enzymes Cyp2b1/2b2, Cyp2d1/2d9, Cyp2j4 and Cyp3a62 also remained relatively unchanged following oral treatment of imatinib with only Cyp2d4/2d6, Cyp2s1 and Cyp3a18 showing a significant change in only one intestinal region (table 6.3). Given the lack of major changes in other CYP mRNA expression levels, the induction of Cyp1a1 mRNA by imatinib appears to be a major adaptation to imatinib oral dosing in the rat.

In order to determine how observed increases in mRNA expression levels for Cyp1a1 were represented with regards to translated protein, immunohistochemistry was performed using the Ab111868 primary anti-Cyp1a1/1a2 antibody (table 5.1). Attempts were made to confirm antibody specificity by Western blot, but were unsuccessful. It should also be noted that no studies using the Ab111868 antibody have been published to date, as such it is emphasised that determination of changes in Cyp1a1/1a2 protein expression is preliminary work only and future studies should look to confirm antibody specificity or employ alternative antibodies to confirm changes in protein expression observed here. The Ab111868 primary antibody visually appears to show increased immunoreactivity in intestine sections of imatinib treated animals compared with vehicle only treated animals, although no quantification of staining intensity has been performed to confirm such observations (figure 6.5). Ab111868 immunoreactivity observed in both vehicle and imatinib treated animals in the all regions of the intestine (top) was above that seen in the respective primary antibody omitted controls (bottom), confirming immunoreactivity to be attributable to the primary antibody. Background staining is detected in some primary omitted controls and should be considered if quantitative analysis of the images is performed.

In addition to Cyp1a1 a significant increase in mRNA expression of Cyp2s1 is observed in the rat jejunum following treatment with oral imatinib (table 6.3), however no significant change was detected in any other region. Log2 fold change differences of 1.01 ± 0.71, 1.38 ± 0.17 and 1.45 ± 0.68 were calculated for the duodenum, jejunum and ileum respectively (vehicle treated animals versus imatinib treated animals).

In addition to determination of mRNA expression levels of drug transporters and cytochrome P450 enzymes in the intestine, miscellaneous gene targets (previously used to validate NanoString technology and regional separation of samples in chapter 4) were also included in the CodeSet. Of note is the altered expression of villin (figure 6.6) which shows replication of trends observed for ABC transporters, with an increased jejunal expression (* $p < 0.05$) and a decreased ileal expression (* $p < 0.05$). Villin mRNA concentrations in the ileum were shown to decrease from 207.90 ± 8.93 fmol/sample to 113.7 ± 19.51 fmol/sample (average n=3 animals per group ± SEM). Jejunal mRNA levels increased from 89.65 ± 17.73 fmol/sample to 147.28 ± 9.64 fmol/sample (average n=3 animals per group ± SEM).

It is suggested that long term treatment with imatinib may contribute toward to development of imatinib resistance observed in some patients. Of several potential reasons for development of such resistance changes in transporter expression and or metabolism both in the intestine and target tissues is proposed. Particularly, alterations in expression and function of MDR1 and BCRP may cause reduced uptake of imatinib from the intestine and/or increase efflux in target

tissues thereby altering the pharmacokinetic (PK) profile. To determine if any changes detected by us, either using NanoString technology and immunohistochemistry, or otherwise, resulted in altered pharmacokinetics of orally administered imatinib the PK profile of imatinib was determined over a twenty-four hour period both on day 1 and day 4 of treatment in rats (figure 6.7 and table 6.4). Figure 6.7 shows three representative PK profiles on day 1 and day 4 of treatment in individual animals, with the average PK profile of all eight animals treated with imatinib, shown in figure 6.7D.

Animal A, which is representative of three of eight imatinib treated rats tested, showed a complex PK profile (figure 6.7A.) The PK profile shows an apparent 2-phase increase in plasma concentration and a delay in the time taken to reach maximal plasma concentration to between 6 and 12 hours post oral gavage. The reason for this is unclear but may represent a pH-dependent change in solubility with delay due to gut transit or altered uptake of imatinib by facilitated absorption. Table 6.4 displays the calculated respective area under the curve (AUC) and maximal plasma concentration (Cmax) values for each individual animal as determined using non-compartmental analysis. Average AUC was calculated using mean profile of all animals as opposed to the mean of all individuals AUCs. All animals showed increased plasma concentrations of imatinib with fold increases of day four versus day one ranging from 1.2 to 2.4 (average 1.5), similarly maximal plasma concentration (Cmax) was shown also to increase (table 6.4). The Cmax fold increase ranged from 1.1 to 2.7 with an average of 1.4. Figure 6.7 clearly shows increased plasma concentration of imatinib over a twenty-four hour period on day four of treatment compared with day one (*** $p = 0.0015$) consistent with drug accumulation and does not therefore support a decreased absorption profile due to altered transporter/metabolism functional induction nor an increased clearance from biliary, intestinal or renal action. It should however be noted that the high concentration of imatinib used here may obscure changes in the PK profile following treatment.

Table 6.1:

		Mdr1a		Mrp1		Mrp2		Mrp3		Mrp5		Mrp6		Mrp7		Bcrp	
		Vehicle	Imatinib	Vehicle	Imatinib	Vehicle	Imatinib	Vehicle	Imatinib	Vehicle	Imatinib	Vehicle	Imatinib	Vehicle	Imatinib	Vehicle	Imatinib
Duodenum	AVG mRNA concentration fmol/sample ± SEM	1.26 ± 0.28	2.47 ± 0.49	1.50 ± 0.63	2.07 ± 0.68	7.58 ± 1.57	7.37 ± 1.06	5.44 ± 0.66	5.23 ± 0.77	1.87 ± 0.59	1.03 ± 0.06	13.84 ± 8.22	7.49 ± 2.10	1.84 ± 0.83	1.24 ± 0.32	20.33 ± 6.66	17.76 ± 2.33
	Log2 fold change ± SEM	0.98 ± 0.62		0.55 ± 1.02		0.01 ± 0.30		-0.07 ± 0.38		-0.72 ± 0.5		-0.49 ± 1.05		-0.39 ± 0.82		-0.04 ± 0.7	
	t-test	0.0990		0.5697		0.9177		0.8432		0.2250		0.4957		0.5349		0.7348	
Jejunum	AVG mRNA concentration fmol/sample	1.61 ± 0.36	4.35 ± 0.62	1.62 ± 0.25	2.28 ± 0.55	6.78 ± 2.045	12.70 ± 2.79	3.68 ± 0.39	4.07 ± 0.19	1.19 ± 0.15	1.76 ± 0.56	14.94 ± 4.99	18.01 ± 4.85	1.71 ± 0.29	1.89 ± 0.26	7.52 ± 2.17	11.85 ± 0.75
	Log2 fold change	1.47 ± 0.31		0.42 ± 0.61		0.94 ± 0.36		0.16 ± 0.09		0.42 ± 0.35		0.33 ± 0.13		0.16 ± 0.05		0.82 ± 0.48	
	t-test	0.0193	*	0.3323		0.1624		0.4229		0.3817		0.6818		0.6654		0.1318	
Ileum	AVG mRNA concentration fmol/sample	8.76 ± 0.75	4.63 ± 1.13	2.11 ± 0.11	2.24 ± 0.32	6.70 ± 1.56	9.20 ± 2.38	6.65 ± 1.20	2.96 ± 0.41	1.16 ± 0.04	0.90 ± 0.23	13.45 ± 1.93	12.29 ± 2.46	2.86 ± 0.12	1.37 ± 0.14	27.58 ± 3.19	12.76 ± 2.45
	Log2 fold change ± SEM	-1.00 ± 0.33		0.06 ± 0.29		0.47 ± 0.45		-1.16 ± 0.46		-0.46 ± 0.34		- 0.17 ± 0.10		-1.07 ± 0.20		-1.14 ± 0.44	
	t-test	0.0381	*	0.7030		0.4296		0.0439	*	0.3308		0.7309		0.0013	**	0.0211	*
Colon	AVG mRNA concentration fmol/sample	2.09 ± 0.16	3.59 ± 2.00	3.99 ± 0.81	2.62 ± 0.24	0.35 ± 0.06	0.27 ± 0.11	24.41 ± 2.59	23.95 ± 2.56	4.28 ± 1.60	2.58 ± 0.51	1.31 ± 0.48	0.69 ± 0.20	1.71 ± 0.64	1.03 ± 0.20	8.86 ± 2.00	12.18 ± 3.51
	Log2 fold change ± SEM	0.35 ± 0.90		-0.56 ± 0.16		-0.61 ± 0.79		-0.03 ± 0.30		-0.61 ± 0.35		-0.87 ± 0.41		-0.62 ± 0.34		0.42 ± 0.49	
	t-test	0.4956		0.1802		0.5630		0.9060		0.3672		0.2973		0.3645		0.4575	

Table 6.1 mRNA concentrations of ABC transporters in the duodenum, jejunum, ileum and colon of rat intestine following administration of 150mg/kg/day oral imatinib or PBS vehicle only over a five day period.

mRNA concentration (fmol/sample) of ABC transporters in rat intestine following exposure to oral imatinib. Data show mean mRNA concentration determined using NanoString mRNA analysis from n=3 animals ± SEM in PBS vehicle and 150mg/kg/day imatinib treated animals over a five day period. Accompanying $\log_2$ fold change values are shown (mRNA expression imatinib treated versus vehicle treated animals) ± SEM and two-tailed Student's t-test statistical analyses performed. Welche's correction was applied to Student's statistical test if vehicle and imatinib treated populations showed unequal variance, as determined using Levene's test, Welche's test was therefore applied when Levene's statistic < 0.05. T-test statistical analysis * $p < 0.05$. mRNA expression data are normalised against positive and negative assay controls and against expression of housekeeping genes, Gapdh, Hprt1 and Hmbs.

Figure 6.3:

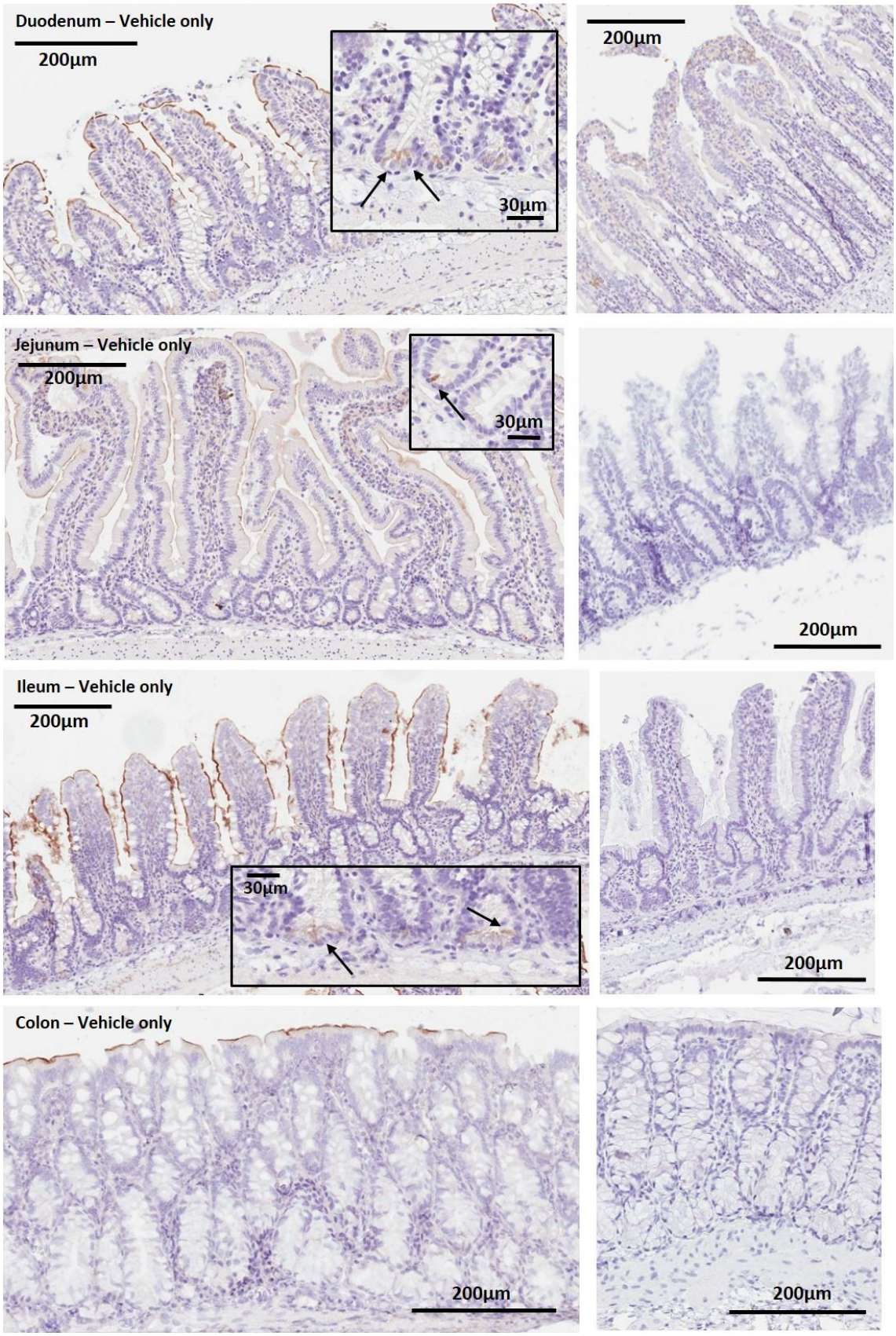
Duodenum – Vehicle only
200µm
30µm
200µm
Jejunum – Vehicle only
200µm
30µm
200µm
Ileum – Vehicle only
200µm
30µm
200µm
Colon – Vehicle only
200µm
200µm

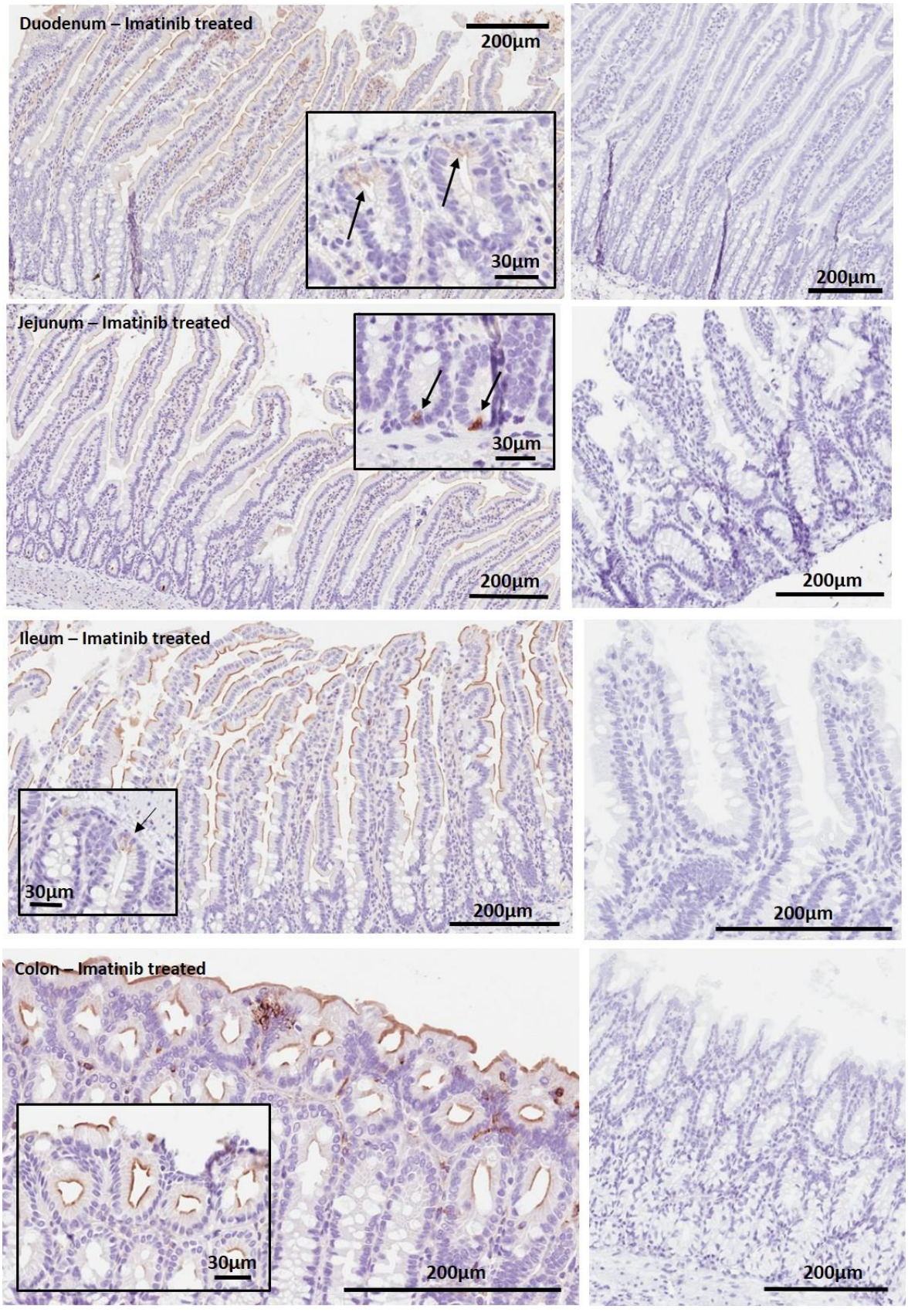
Duodenum – Imatinib treated
200µm
30µm
200µm
Jejunum – Imatinib treated
30µm
200µm
200µm
Ileum – Imatinib treated
30µm
200µm
200µm
Colon – Imatinib treated
30µm
200µm
200µm

Figure 6.3 Immunohistochemical localisation of Mdr1 in formalin fixed, paraffin embedded male rat intestine of PBS vehicle and imatinib treated animals.

Protein expression of Mdr1 in duodenum, jejunum, ileum and colon of rat intestine treated with PBS vehicle only and following oral administration of 150mg/kg/day imatinib over a five day period. Images show Mdr1 localisation using primary goat polyclonal antibody C19 (1:25 dilution) in respective rat intestine section (left) and primary antibody omitted controls (right). Inset shows magnified image of staining in each respective regional intestinal crypt. Intestinal sections (4µm thickness) were stained simultaneously using an automated Ventana benchmark XT staining platform with tris-based antigen retrieval, DAB antigen stain with haematoxylin counter stain. Sections were rehydrated and cover slips mounted. Slides were scanned electronically using Aperio ScanScope.

Figure 6.4:

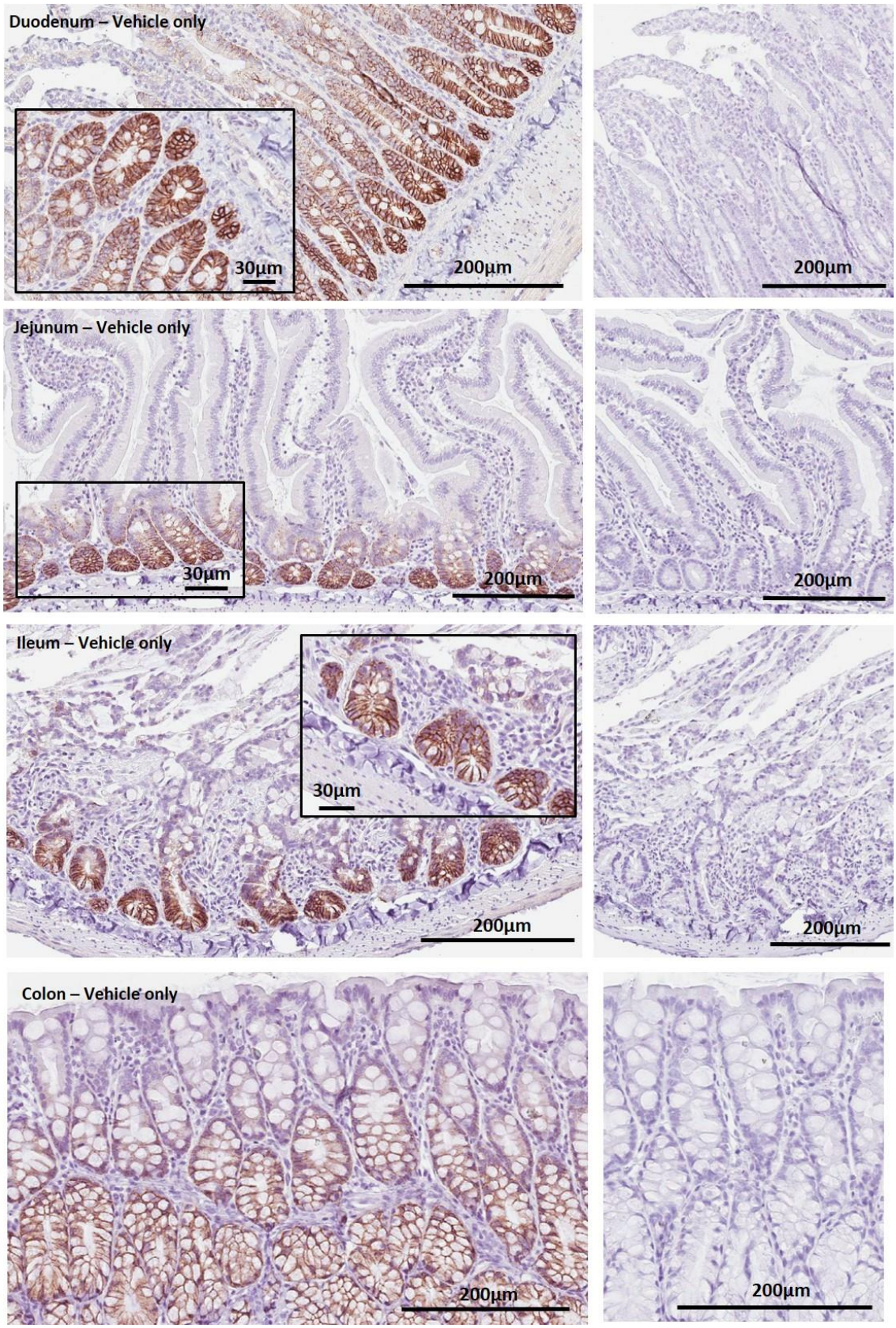
Duodenum – Vehicle only
30µm
200µm
200µm
Jejunum – Vehicle only
30µm
200µm
200µm
Ileum – Vehicle only
30µm
200µm
200µm
Colon – Vehicle only
200µm
200µm

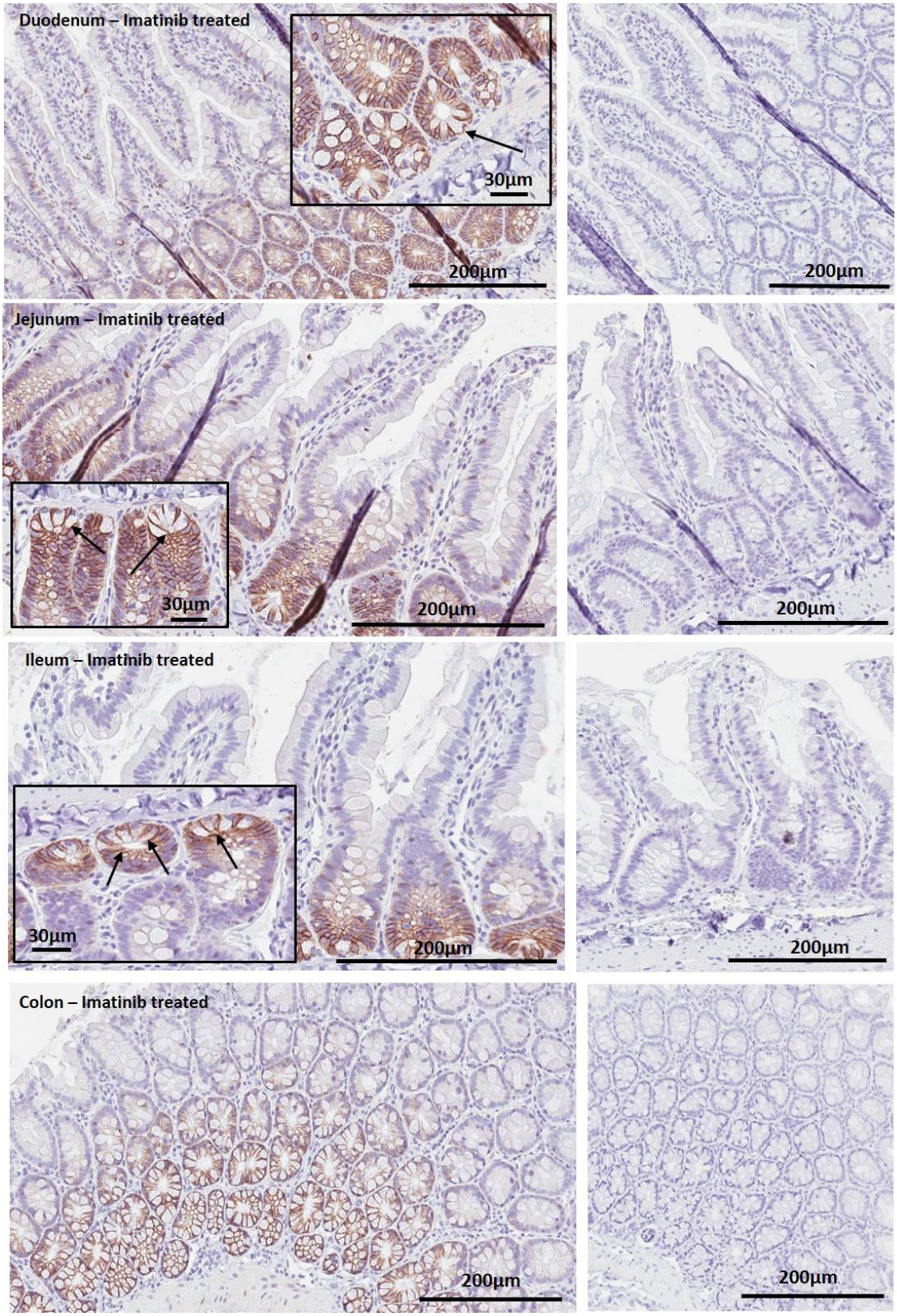
Duodenum – Imatinib treated
30µm
200µm
200µm
Jejunum – Imatinib treated
30µm
200µm
200µm
Ileum – Imatinib treated
30µm
200µm
200µm
Colon – Imatinib treated
200µm
200µm

Figure 6.4 Immunohistochemical localisation of Bcrp in formalin fixed, paraffin embedded male rat intestine of PBS vehicle and imatinib treated animals.

Protein expression of Bcrp in duodenum, jejunum, ileum and colon of rat intestine treated with PBS vehicle only and following oral administration of 150mg/kg/day imatinib over a five day period. Images show Bcrp localisation using primary rabbit polyclonal antibody M70 (1:25 dilution) in each respective rat intestine section (left) and primary antibody omitted controls (right). Inset shows magnified image of staining in respective regional intestinal crypt. Intestinal sections (4µm thickness) were stained simultaneously using an automated Ventana benchmark XT staining platform with citric acid based antigen retrieval, DAB antigen stain with haematoxylin counter stain. Sections were rehydrated and cover slips mounted. Slides were scanned electronically using Aperio ScanScope.

Table 6.2:

		Cnt2		PepT1		Oct1		Octn1		Octn2		Oatpb	
		Vehicle	Imatinib	Vehicle	Imatinib	Vehicle	Imatinib	Vehicle	Imatinib	Vehicle	Imatinib	Vehicle	Imatinib
Duodenum	AVG mRNA concentration fmol/sample	81.11 ± 6.45	49.07 ± 5.43	5.65 ± 1.13	3.06 ± 0.70	11.86 ± 2.43	7.14 ± 1.70	3.05 ± 0.40	1.47 ± 0.18	17.12 ± 1.95	11.21 ± 1.42	1.20 ± 0.52	0.90 ± 0.16
	Log2 fold change	-0.73 ± 0.06		-0.89 ± 0.64		-0.75 ± 0.64		-1.05 ± 0.05		-0.61 ± 0.10		-0.22 ± 0.74	
	t-test	0.0191	*	0.1236		0.1874		0.0234		0.0703		0.6017	
Jejunum	AVG mRNA concentration fmol/sample	46.97 ± 9.15	43.21 ± 10.36	4.47 ± 1.28	5.47 ± 1.86	8.83 ± 2.98	8.69 ± 2.28	1.99 ± 0.38	2.72 ± 0.73	11.72 ± 3.07	10.20 ± 3.47	1.48 ± 0.39	1.90 ± 0.28
	Log2 fold change	-0.14 ± 0.44		0.24 ± 0.91		0.06 ± 0.19		0.41 ± 0.69		-0.22 ± 0.37		0.41 ± 0.31	
	t-test	0.7988		0.6809		0.9719		0.4222		0.7591		0.4251	
Ileum	AVG mRNA concentration fmol/sample	37.41 ± 5.23	23.84 ± 3.53	17.54 ± 2.01	8.30 ± 3.58	7.61 ± 2.15	4.70 ± 1.17	6.01 ± 0.91	2.19 ± 0.59	20.99 ± 3.10	9.48 ± 3.18	3.44 ± 0.75	1.83 ± 0.41
	Log2 fold change	-0.66 ± 0.26		-1.48 ± 0.99		-0.71 ± 0.46		-1.52 ± 0.56		-1.26 ± 0.41		-0.92 ± 0.38	
	t-test	0.0978		0.0873		0.2996		0.0242	*	0.0606		0.1318	
Colon	AVG mRNA concentration fmol/sample	5.76 ± 2.34	3.32 ± 0.79	0.59 ± 0.12	0.29 ± 0.09	2.21 ± 1.00	1.66 ± 0.26	0.21 ± 0.09	0.08 ± 0.05	7.63 ± 1.70	5.92 ± 2.92	1.94 ± 0.47	2.38 ± 0.44
	Log2 fold change	-0.65 ± 0.78		-1.08 ± 0.58		-0.15 ± 0.74		-1.47 ± 1.06		-0.62 ± 0.41		0.32 ± 0.10	
	t-test	0.3796		0.1296		0.6271		0.2697		0.6404		0.5279	

Table 6.2 mRNA concentrations of selected SLC transporters in the duodenum, jejunum, ileum and colon of rat intestine following administration of 150mg/kg/day oral imatinib or PBS vehicle only.

mRNA concentration (fmol/sample) of selected SLC transporters in rat intestine following exposure to oral imatinib. Data show mean mRNA concentration determined using NanoString mRNA analysis from n=3 animals ± SEM in PBS vehicle and 150mg/kg/day imatinib treated animals over a five day period. Accompanying $\log_2$ fold change values (imatinib versus vehicle treated animal mRNA expression) are shown ± SEM and two-tailed Student's t-test statistical analyses performed. Welche's correction was applied to Student's statistical test if vehicle and imatinib treated populations showed unequal variance, as determined using Levene's test, Welche's test was therefore applied when Levene's statistic < 0.05. T-test statistical analysis * $p < 0.05$. mRNA expression data are normalised against positive and negative assay controls and against expression of housekeeping genes, Gapdh, Hprt1 and Hmbs.

Table 6.3:

		Cyp1a1		Cyp2b2		Cyp2d1/2d9		Cyp2d4/2d6		Cyp2j4		Cyp2s1		Cyp3a9		Cyp3a18		Cyp3a62	
		Vehicle	Imatinib	Vehicle	Imatinib	Vehicle	Imatinib	Vehicle	Imatinib	Vehicle	Imatinib	Vehicle	Imatinib	Vehicle	Imatinib	Vehicle	Imatinib	Vehicle	Imatinib
Duodenum	AVG mRNA concentration fmol/sample	3.16 ± 2.55	75.64 ± 41.93	0.83 ± 0.34	1.12 ± 0.10	3.36 ± 0.85	1.48 ± 0.19	7.95 ± 122	4.49 ± 0.49	12.26 ± 2.75	10.46 ± 2.71	10.73 ± 2.62	21.12 ± 4.38	157.61 ± 32.71	95.14 ± 14.15	5.40 ± 1.35	3.02 ± 0.71	16.14 ± 7.18	10.77 ± 1.56
	Log2 fold change	5.98 ± 1.57		0.67 ± 0.76		-1.12 ± 0.37		-0.81 ± 0.23		-0.25 ± 0.54		1.01 ± 0.71		-0.71 ± 0.31		-0.83 ± 0.68		-0.15 ± 1.01	
	t-test	0.1595		0.4605		0.0982		0.0577		0.6652		0.1113		0.1545		0.1941		0.5056	
Jejunum	AVG mRNA concentration fmol/sample	1.24 ± 0.57	118.29 ± 30.75	1.03 ± 0.35	1.85 ± 0.51	1.33 ± 0.40	0.76 ± 0.26	5.62 ± 1.46	6.27 ± 1.46	11.35 ± 4.17	15.82 ± 5.60	6.90 ± 0.89	18.14 ± 3.15	91.01 ± 26.42	136.92 ± 43.67	4.14 ± 1.09	3.86 ± 1.54	5.92 ± 2.06	5.25 ± 0.08
	Log2 fold change	6.97 ± 0.85		0.90 ± 0.97		-0.84 ± 0.85		0.18 ± 0.68		0.5 4± 0.30		1.38 ± 0.17		0.54 ± 1.00		-0.29 ± 0.82		0.05 ± 0.63	
	t-test	0.0190	*	0.2530		0.2960		0.7693		0.5571		0.0265	*	0.4193		0.8879		0.7611	
Ileum	AVG mRNA concentration fmol/sample	1.52 ± 0.66	78.50 ± 9.37	11.06 ± 4.43	3.70 ± 1.54	1.55 ± 0.70	0.60 ± 0.14	11.02 ± 1.04	5.33 ± 1.64	15.54 ± 3.85	13.00 ± 4.71	5.23 ± 3.54	9.57 ± 3.38	110.45 ± 67.98	61.41 ± 7.20	18.02 ± 2.77	7.97 ± 4.84	24.58 ± 10.91	8.42 ± 2.92
	Log2 fold change	6.28 ± 0.94		-1.81 ± 1.45		-1.21 ± 0.98		-1.18 ± 0.56		-0.22 ± 0.49		1.45 ± 0.68		-0.28 ± 0.99		-1.93 ± 1.28		-1.45 ± 0.99	
	t-test	0.0012	**	0.1913		0.2506		0.0429	*	0.8128		0.4257		0.5127		0.1459		0.2257	
Colon	AVG mRNA concentration fmol/sample	0.88 ± 0.61	2.80 ± 1.62	0.36 ± 0.18	0.19 ± 0.02	15.86 ± 4.39	13.86 ± 2.96	2.19 ± 0.35	1.45 ± 0.05	2.20 ± 0.70	1.50 ± 0.57	0.90 ± 0.30	0.94 ± 0.36	50.10 ± 4.97	37.11 ± 8.30	0.77 ± 0.08	0.38 ± 0.11	4.97 ± 0.69	5.82 ± 0.82
	Log2 fold change	1.70 ± 0.82		-0.61 ± 0.51		-0.16 ± 0.57		-0.56 ± 0.25		-0.63 ± 0.16		0.01 ± 0.69		-0.49 ± 0.38		-1.18 ± 0.56		0.23 ± 0.41	
	t-test	0.3309		0.4011		0.7253		0.1060		0.4828		0.9447		0.2503		0.0409	*	0.4714	

Table 6.3 mRNA concentrations of selected Cyp450 enzymes in the duodenum, jejunum, ileum and colon of rat intestine following administration of 150mg/kg/day oral imatinib or PBS vehicle only.

mRNA concentration (fmol/sample) of selected Cyp450 enzymes in rat intestine following exposure to oral imatinib. Data show mean mRNA concentration determined using NanoString mRNA analysis from n=3 animals ± SEM in PBS vehicle and 150mg/kg imatinib treated animals over a five day period. Accompanying log_2 fold change values (imatinib versus vehicle treated animal mRNA expression) are shown ± SEM and two-tailed Student's t-test statistical analyses performed. Welche's correction was applied to Student's statistical test if vehicle and imatinib treated populations showed unequal variance, as determined using Levene's test, Welche's test was therefore applied when Levene's statistic < 0.05. T-test statistical analysis * $p < 0.05$, ** $p < 0.01$. mRNA expression data are normalised against positive and negative assay controls and against expression of housekeeping genes, Gapdh, Hprt1 and Hmbs.

Figure 6.5:

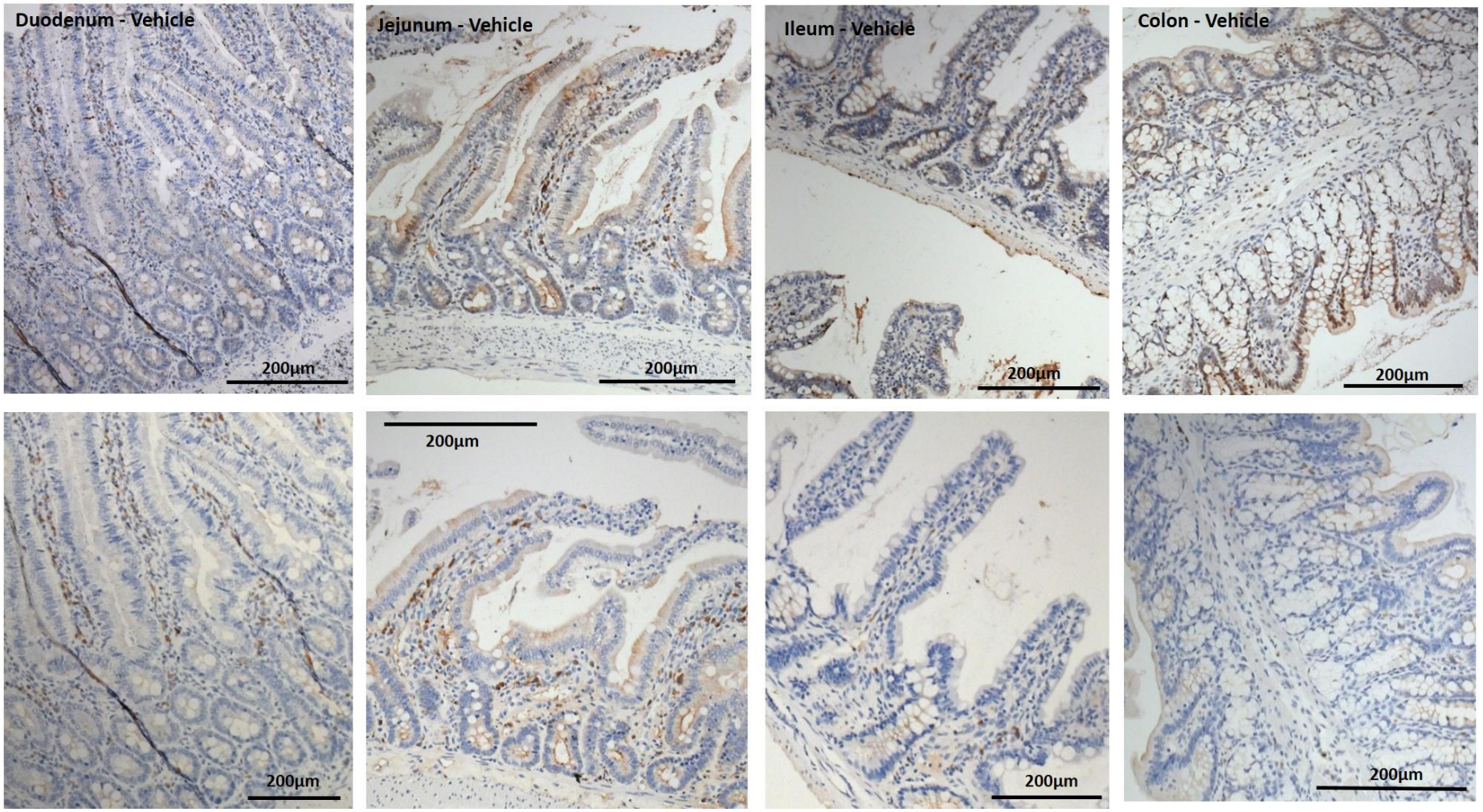
Duodenum - Vehicle
200µm
Jejunum - Vehicle
200µm
Ileum - Vehicle
200µm
Colon - Vehicle
200µm
200µm
200µm
200µm
200µm

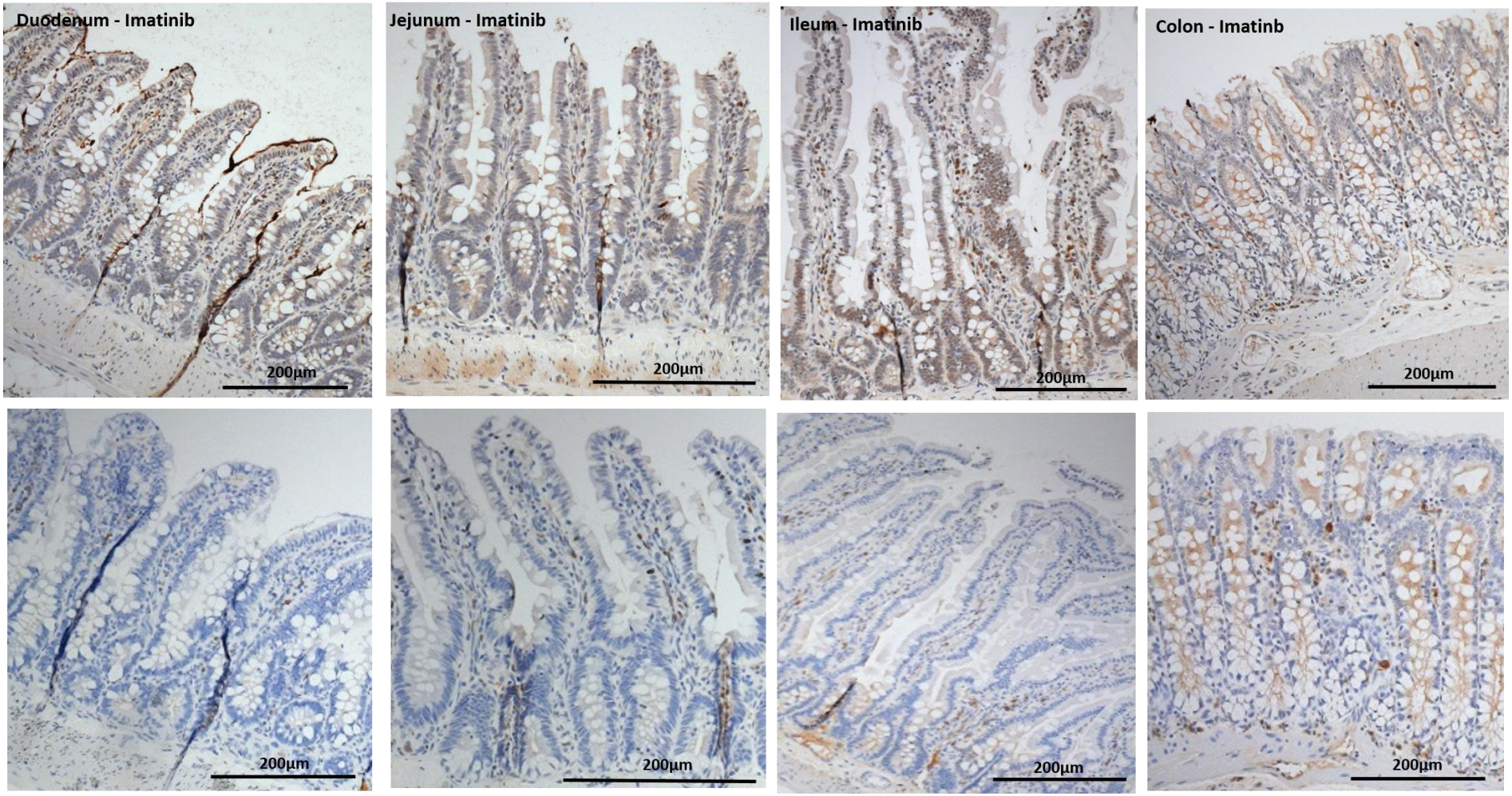
Duodenum - Imatinib
200µm
Jejunum - Imatinib
200µm
Ileum - Imatinib
200µm
Colon - Imatinb
200µm
200µm
200µm
200µm
200µm

Figure 6.5 Immunohistochemical localisation of Cyp1a1 in formalin fixed, paraffin embedded male rat intestine of PBS vehicle only and imatinib treated animals.

Protein expression of Cyp1a1 in duodenum, jejunum, ileum and colon of rat intestine treated with PBS vehicle control only and following oral administration of 150mg/kg/day imatinib. Images show Cyp1a1 localisation using primary mouse monoclonal antibody Ab111868 (1:50 dilution) in each respective rat intestine section (top) and primary antibody omitted controls (bottom). Intestinal sections (4µm thickness) were stained simultaneously using an automated Ventana benchmark staining platform with protease based antigen retrieval and counterstained using Ventana blueing agent and haematoxylin. Sections were rehydrated and cover slips mounted. Slides were viewed and images taken using a Zeiss Axioimager.

Figure 6.6:

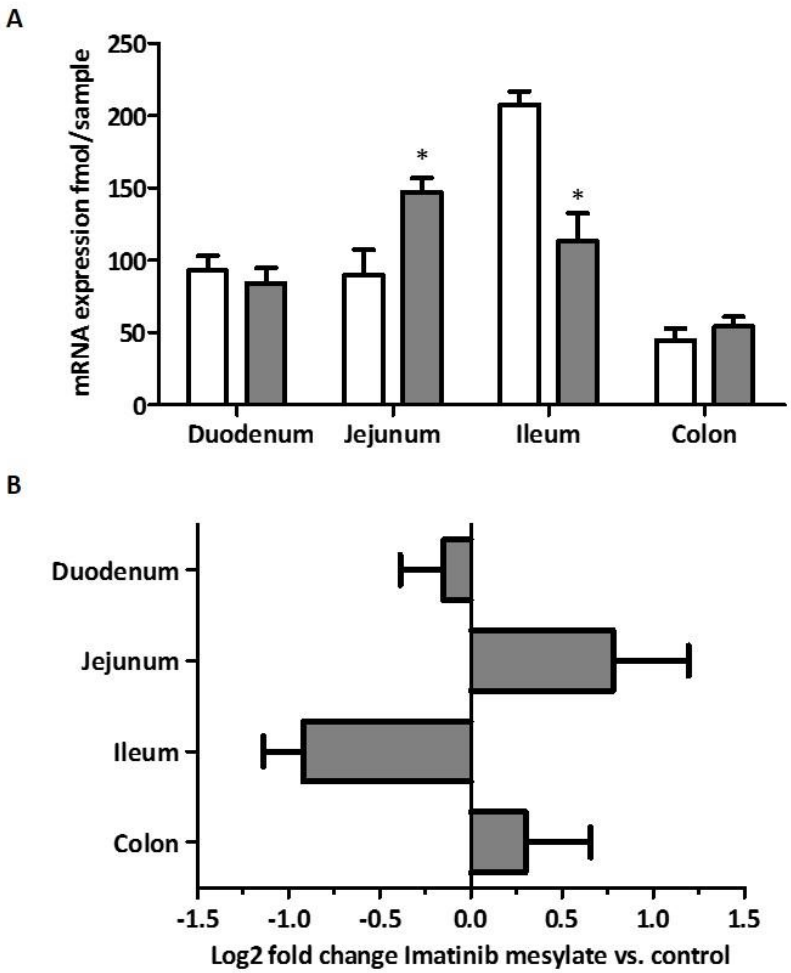

Figure 6.6 Changes in mRNA concentrations of Villin in rat duodenum, jejunum, ileum and colon mucosa following treatment with 150mg/kg/day imatinib or PBS vehicle control only and associated log_2 fold change imatinib vs. vehicle treated animals.

(A) mRNA concentrations (fmol/sample) of Villin in the duodenum, jejunum, ileum and colon in PBS vehicle treated animals (clear bars) and animals treated with 150mg/kg/day imatinib (grey bars) over a five day period by oral gavage. **(B)** Calculated mRNA expression log_2 fold change imatinib treated versus vehicle treated animals. Data show mean mRNA expression, determined using NanoString technology, of n = 3 animals in each treatment group ± SEM. Two tailed t-test statistical analysis * $p < 0.05$ vehicle versus imatinib treatment. mRNA expression data shown has been normalised against positive and negative assay controls and against expression of selected housekeeping genes, Gapdh, Hprt1 and Hmbs.

Figure 6.7:

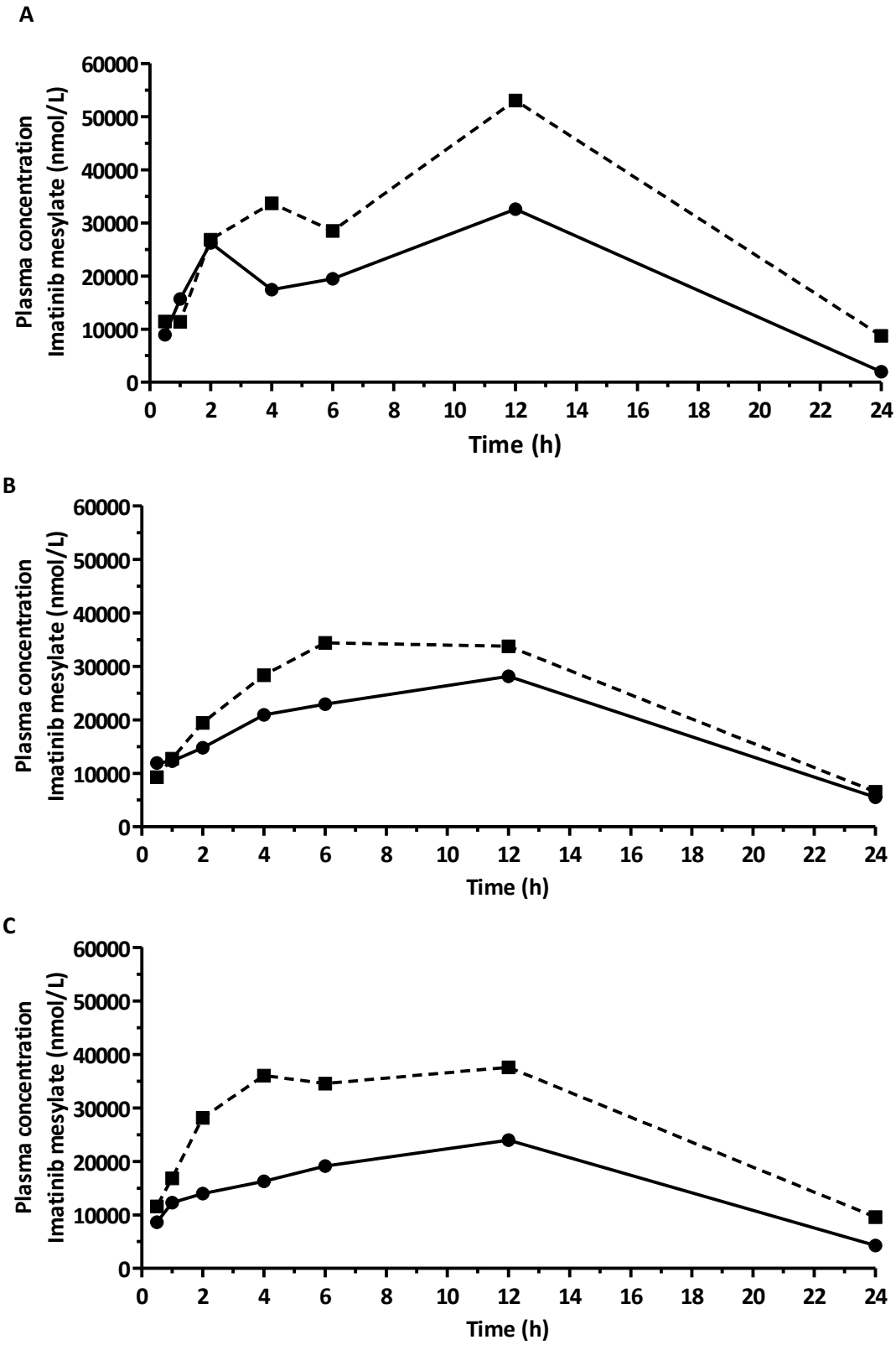
A
Plasma concentration
Imatinib mesylate (nmol/L)
60000
50000
40000
30000
20000
10000
0
0 2 4 6 8 10 12 14 16 18 20 22 24
Time (h)
B
Plasma concentration
Imatinib mesylate (nmol/L)
60000
50000
40000
30000
20000
10000
0
0 2 4 6 8 10 12 14 16 18 20 22 24
Time (h)
C
Plasma concentration
Imatinib mesylate (nmol/L)
60000
50000
40000
30000
20000
10000
0
0 2 4 6 8 10 12 14 16 18 20 22 24
Time (h)

D

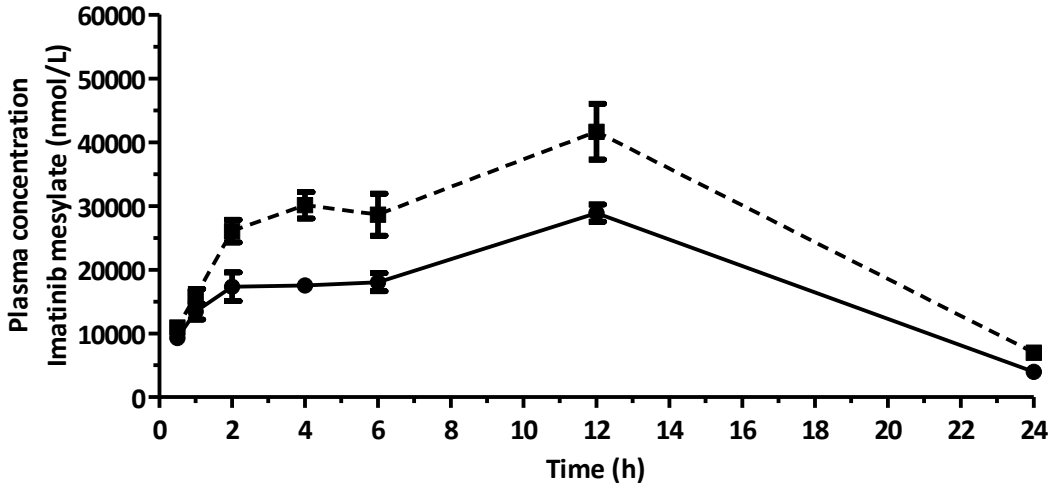

Figure 6.7 Pharmacokinetic profile of imatinib over a 24 hour period following administration of 150mg/kg imatinib for one or four consecutive days.

Imatinib was administered at t=0 at a dose of 150mg/kg to male rats aged approximately eight weeks. Plasma samples were acquired at time points; 0.5, 1, 2, 4, 6, 12 and 24 hours following initial dose administration on day 1 (solid line) and day 4 (dashed line) of treatment and imatinib concentrations determined by HPLC-MS. **(A-C)** Representative PK profiles taken from three individual animals, note drop in plasma drug concentrations observed at 4 and 6 hours following administration in figure A (representative of three of eight imatinib treated animals). **(D)** Average PK profile taken from eight animals, showing plasma imatinib concentrations over a twenty-four hour period ± SEM. Calculated PK parameters for all animals are shown in table 6.4. Average AUC day 1 vs average AUC day 4 *** p = 0.00015, Student's t-test statistical analysis.

Table 6.4:

Animal	AUC (nmol.h/L)		Fold Increase	Cmax (nmol/L)		Fold Increase
	D1	D4	(D4/D1)	D1	D4	(D4/D1)
109	473314	765263	1.6	32576	53030	1.6
110	439886	653479	1.5	30434	49293	1.6
111	332920	808653	2.4	23136	63370	2.7
112	457294	580401	1.3	28117	34388	1.2
113	384851	666636	1.7	23964	37595	1.6
114	526602	624634	1.2	32965	41224	1.3
115	385299	487091	1.3	27709	30180	1.1
116	444850	596316	1.3	32027	37637	1.2
Mean	**431612**	**647809**	**1.5**	**28866**	**41647**	**1.4**

Table 6.4 AUC and Cmax for all individual animals with calculated mean pharmacokinetic parameters and associated fold increase.

AUC (nmol.h/L) and Cmax (nmol/L) for all individual animals on day 1 and day 4 of treatment calculated from plasma imatinib concentrations and resultant pharmacokinetic profile over a twenty-four hour period. AUC (nmol.h/L) and Cmax (nmol/L) determined from mean profile of all animals. Associated fold increase is shown from day 1 to day 4. AUC 0-24h was calculated using non-compartmental analysis, mean AUC was calculated using mean profile of all animals as opposed to mean of all individual AUCs. Student's t-test analysis mean AUC day 1 vs. day 4 *** $p = 0.00015$ and Cmax day 1 vs. day 4 ** $p < 0.01$. All data calculations were performed in WinNonLin Phoenix v 6.3, Pharsight Corp.

6.4 Discussion

Orally administered imatinib is standard treatment for patients with CML or GIST and exerts its therapeutic effect via inhibition of ABL TKs including c-ABL, Tel/ABL, PDGF TK receptors, ARG (ABL related gene kinase) and cKit and macrophage colony stimulating factor (c-fms) and the chimeric BCR-ABL protein expressed in 95% of CML patients (White et al., 2006, Özvegy-Laczka et al., 2005). A lowered affinity at the c-Src TK has also been reported (Seeliger et al., 2007). Although many (70-90%) CML and GIST patients respond well to treatment with imatinib, disease progression and an apparent resistance may develop following long term treatment (Eechoute et al., 2010). One mechanism proposed for onset of imatinib resistance is altered expression of transporter proteins and CYP450 enzymes known to play a role in the disposition of imatinib (Eechoute et al., 2010). Alterations in the expression of such genes, either in the intestine, liver or in target cells may alter the pharmacokinetic profile such that plasma and target tissue concentrations of imatinib do not reach levels of therapeutic effect (Eechoute et al., 2010).

Induction of ABC transporters MDR1, BCRP and CYP450 enzymes within intestinal enterocytes may reduce intestinal absorption of active drug compound thereby leading to the reduced systemic concentrations. A reduced expression of transporters proposed to be involved in the absorption of imatinib (OCT1, OCTN2, OATP1A1, MRP1, MRP4 and MRP7) may reduce intestinal and systemic uptake. This study therefore aimed to determine the effects of orally administered imatinib at a dose of 150mg/kg/day over a five day period on the mRNA expression levels of selected ABC and SLC transporters and CYP450 enzymes in rat intestine. Imatinib induced alterations in protein expression of Mdr1, Mrp2, Bcrp and Cyp1a1/1a2 were also determined.

Initial experiments confirmed ability of imatinib to alter functional activity of both MDR1 and mBcrp using the transfected MDCKII cell line system. Incubation of MDCKII-MDR1 and MDCKII-mBcrp cells with imatinib was shown to increase intracellular accumulation of Hoechst33342 in a concentration dependent manner. Furthermore, imatinib significantly decreased net secretory flux of ^{3}H-digoxin and ^{14}C-ciprofloxacin, known MDR1 and mBcrp substrates (Haslam, 2007, Wright, 2011) in MDCKII-MDR1 and MDCKII-mBcrp cells respectively. If imatinib is indeed a substrate for ABC-transporter mediated efflux the prediction would be that oral absorption should be incomplete due to recycling of drug to the intestinal lumen. In contrast, if imatinib exerted an inhibitory pharmacological action, no effect on absorption would be expected. Both types of experiments performed here (Hoechst33342 dye retention and net transepithelial secretion of digoxin or ciprofloxacin) do not allow conclusion as to whether imatinib is a substrate or inhibitor of MDR1 and mBcrp, and this remains a subject of current

literary debate (Eechoute et al., 2010). Transport experiments using radiolabelled imatinib or mass spectrometry analysis of cold imatinib substrate transport would be required to confirm the type of interaction.

The reported oral bioavailability of imatinib in man is near 100%. As already noted this does not fit the profile of a drug subject to ABC-mediated transport. Temperature sensitive inhibition of active transport processes has previously been shown to reduce cellular uptake of imatinib therefore indicating presence of an active uptake pathway (Kralj et al., 2014, Thomas et al., 2004). Additionally Houghton et al., (2004) reported sodium azide depletion of ATP to reduce intracellular imatinib accumulation. These studies indicate a role for active transport processes in imatinib absorption. However, given that the MDCKII cell line is often used for the study of functional activity of transfected transporter proteins due to low level constitutive transporter expression levels (Giacomini et al., 2010), it is unlikely that transporter mediated uptake of imatinib occurs in MDCKII cells. The concentration dependent reduction in Hoechst33342, ^{3}H-digoxin and ^{14}C-ciprofloxacin transport by imatinib in the MDCKII-MDR1 and MDCKII-mBcrp cell lines shown here therefore indicates ability of imatinib to diffuse passively across the cell membrane.

A comprehensive study of membrane permeable drug compounds lead to identification of four simple rules, which if followed, optimise potential of a drug compound to diffuse passively across the cell membrane (Leeson, 2012). Lipinski's rule of five states that for optimal membrane permeability drug compounds should have a molecular weight (Mr) < 500, a logP (partition coefficient) value < 5, < 5 donor H atoms and < 10 H atoms capable of forming hydrogen bonds (Leeson, 2012). According to DrugBank imatinib has a Mr of 589.7, a logP value between 3.47 and 4.38, 2 donor and 7 acceptor hydrogen atoms, indicating the drug compound should show good levels of membrane permeability (DrugBank, 2014). Although the Mr of imatinib is slightly larger than that suggested to be optimal by Lipinski, Gaussian distribution dictates compounds with Mr values up to 550 to show good levels of membrane permeability (Navia and Chaturvedi, 1996). Furthermore, Lipinski's rule of five is not absolutely definitive as shown by ability of CsA, a compound with a Mr of 1200, to diffuse across the cell membrane (Navia and Chaturvedi, 1996). Whilst the high oral bioavailability of imatinib (98%) indicates no negative involvement of enterocytic proteins in first pass effects of imatinib, high luminal concentrations of imatinib would likely over saturate transporter capabilities. It is therefore likely that high levels of intestinal absorption represents cumulative passive and facilitated diffusion *in vivo*, with passive diffusion supported by compliance of imatinib physiochemical properties with Lipinski's rule of five.

The high levels of imatinib required to alter function of MDR1 and mBcrp compared with clinical concentrations (lowest therapeutic trough levels 1000ng/ml) (Eechoute et al., 2010) may reflect a lack of active uptake in MDCKII cells. Although high extracellular imatinib concentrations were used, correlation between extracellular imatinib and intracellular accumulation is unknown, with Hamada et al., (2003) showing intracellular accumulation to be only ~35% of total dose in the LLC-PK1 cell line. Expression of uptake transporters *in vivo* may therefore allow increased accumulation of imatinib and promote interaction between MDR1 and BCRP at therapeutic concentrations (Hamada et al., 2003).

An approximate 2-fold increase in jejunal mRNA expression levels of Mdr1a, Mrp2, Bcrp, Cyp1a1, Cyp2b2 and Cyp2s1 were observed following treatment with oral imatinib. Induction of Cyp1a1 mRNA levels was greatest with a measured 7-fold increase following imatinib administration. Cyp1a1 mRNA also showed a significant increase in expression in the ileum and a non-significant increase in duodenal samples. The CYP1A family is known to be under the transcriptional control of the aryl-hydrocarbon receptor (AhR) (Deb and Bandiera, 2009). The AhR increases mRNA and protein expression via binding to xenobiotic response elements (XRE) of target sequences (Deb and Bandiera, 2009). Following ligand binding, the cytoplasmic AhR translocates to the nucleus and becomes dissociated from heat shock proteins (HSP90) with which it is associated in the cytoplasm. The AhR then heterodimerises with the AhR nuclear translocator (ARNT) which allows binding to XRE of target genes and induction of mRNA transcription (Deb and Bandiera, 2009, Wang et al., 2011).

Known ligands of the AhR include polycyclic aromatic hydrocarbons (PAHs), TCDD, dietary components (such as flavonoids), and therapeutic agents including omeprazole and thiabendazole (Wang et al., 2011). Since members of the CYP1 family are induced by AhR ligands the observed increase in mRNA transcript expression may result from activation of the AhR by imatinib. Past studies have shown correlation between CYP1A1 tumour expression, genetic CYP1A1 variations and response to treatment of drug compounds (Rochat et al., 2008). Therefore induction of Cyp1a1 expression may alter pharmacokinetics of imatinib *in vivo*. In addition to increased mRNA expression we also show an apparent increase in protein levels, although further work is required to confirm these findings.

Rochat et al., (2008) showed that CYP1A1, amongst other enzymes, metabolises imatinib. Incubation of imatinib with cDNA expressing CYP1A1 microsomes generated three main metabolites (seven structural isomers), produced via CYP1A1 mediated hydroxylation and N-oxidation (Rochat et al., 2008). Since imatinib acts at the ABL kinase (part of the ABL-BCR chimeric protein known to be expressed in CML patients) via docking to the ATP binding site, it was determined how imatinib metabolites of CYP1A1 differ with regards to docking at the ABL

protein, compared with the parent drug molecule (Rochat et al., 2008). Of seven possible metabolite isomers, three showed modified interaction with the ABL binding site compared with the parent drug compound. Of the three metabolites showing altered interaction only one was proposed to show decreased affinity, with others showing potential for increased affinity due to formation of additional hydrogen bonds (Rochat et al., 2008). Therefore if changes in mRNA and protein expression levels correlate with functional activity, Cyp1a1 mediated metabolism may in fact increase the affinity of imatinib for ABL and therefore cause increased inhibition of BCR-ABL, potentiating the therapeutic effects of the imatinib TK inhibitor.

However, in addition to the reported increase in affinity of selective Cyp1a1 metabolites at ABL kinase they may also show increased affinity for transporter mediated efflux (Rochat et al., 2008). If Cyp1a1 metabolites bind MDR1 and BCRP with increased affinity their efflux from intestinal enterocytes may be promoted, therefore lowering oral bioavailability and systemic concentrations of supposedly pharmacologically active drug metabolites. Should Cyp1a1 metabolites show increased affinity for Mdr1 and Bcrp, the effects of Cyp1a1 imatinib metabolism may be amplified by the associated increase in expression levels of the ABC transporter Mdr1a in the jejunum. Quantitative measurement of changes in absolute levels of cellular protein following imatinib treatment by Western blot could potentially provide confirmation with regards to ability of imatinib to alter Mdr1 and Bcrp expression, this was not however possible due to time constraints of the present study.

In addition to their role at the enterocyte barrier, MDR1, MRP2 and BCRP contribute toward efflux of drug compounds at the blood brain barrier (Wang et al., 2011). In support of imatinib as an AhR ligand, recent studies have shown upregulation of Mdr1, Mrp2 and Bcrp protein and functional activity in rat brain capillaries following *in vivo* exposure to the AhR ligand TCDD (Wang et al., 2011). A TCDD concentration dependent increase in transport of fluorescently labelled Mdr1, Mrp2 and Bcrp substrates NSD-CsA, Texas-Red and BODIPY-Prazosin respectively was observed following intraperitoneal injection of TCDD, with increased MDR1 activity been abolished by AhR antagonists resveratrol and α-napthoflavone (Wang et al., 2011). Furthermore, *in vitro* studies have shown upregulation of BCRP by benzopryine, a known AhR ligand, and showed ability of the anti-cancer drug Romidepsin to increase association between the AhR-ARNT dimer at the XRE present within the BCRP gene (To et al., 2011). Whilst only Mdr1a mRNA expression was shown to be significantly increased in the present study indication of Mrp2 and Bcrp mRNA upregulation was observed. Such changes require confirmation and may show significance should the study size be increased to include a larger number of animals within each treatment group.

Finally, in addition to AhR regulation of the CYP1 family, a weaker agonistic effect of AhR ligands is confirmed for the CYP2 family of enzymes (Deb and Bandiera, 2009). In agreement with this we observed an approximate 2.5 fold increase in mRNA expression levels of Cyp2s1 in the duodenum following treatment with imatinib.

Cyp2s1 is a recently identified member of the CYP2 family and has been identified in humans, mice and rats, with high levels of mRNA detected in the human small intestine (Deb and Bandiera, 2009). CYP2S1 protein has been detected in all regions of the intestine (Deb and Bandiera, 2009). Cyp2s1 mRNA expression in mouse Hepa-1 cells was shown to increase following 6 hour incubation with the AhR ligand TCDD. A lack of induction was however observed in Hepa-1 cells deficient for AhR, ARNT or XRE (Deb and Bandiera, 2009).

Given the reported ability of AhR ligands to induce expression of Cyp1a1, Mdr1, Mrp2, Bcrp and Cyp2s1 the upregulation of Cyp1a1, Cyp2s1 and Mdr1a reported here following oral imatinib exposure strongly suggests imatinib to be an AhR ligand. Measured changes in mRNA expression due to AhR mediated induction may contribute to inter-individual variation and response to imatinib treatment in the clinic, should these changes be translated to a functional level. Further importance of imatinib-AhR interaction is apparent due to confirmation of imatinib interaction with these proteins, at least *in vitro* (Eechoute et al., 2010).

In contrast to increased mRNA expression observed in the jejunum the expression of several genes was shown to be decreased in ileum mucosal samples following treatment with imatinib, with Mdr1a, Mrp3, Mrp7, Bcrp, Cyp2b2, Cyp2d1/2d9, Cyp2d4, Cyp3a1, Cyp3a62, PepT1, Octn2, Octn1 and Villin showing a greater than 2-fold reduction in mRNA expression following imatinib treatment (not all genes mentioned showed a significant decrease in expression and rather data is only suggestive of such changes).

Villin is an actin bundling protein found to be highly expressed in differentiated enterocytes with earlier assessment in untreated animals showing an average fold increase of 2.4 ± 0.4 between crypt and villus tip samples (chapter 4). Expressed at the cell surface, and involved in formation of the epithelial brush border membrane villin is known to play a role in cytoskeleton remodelling, apoptosis and cell migration, with phosphorylation of the villin protein required for normal physiological processes (Mathew et al., 2008). Mathew et al., (2008) showed loss of villin phosphorylation, and hence cell surface localisation *in vitro* following transfection of SFY cells with super enhanced yellow fluorescent protein (SEYFP) full length villin in the absence of TK enzymes c-Src, c-Yes and c-Fyn. However, transfection of c-Src in SEYFP-villin cells promoted redistribution of villin protein such that the vast majority of cells

(~85%) showed expression at the cell margin (Mathew et al., 2008), thus indicating a role for c-Src in villin phosphorylation and physiological function.

The c-Src TK is ubiquitously expressed throughout the body and is known to be expressed in the intestinal brush border membrane. Although not a primary target of imatinib, imatinib inhibits the actions of c-Src TK with reduced affinity. An IC_{50} value for imatinib inhibition of c-Src was previously determined to be > 100μM. This is much higher than the IC_{50} values of imatinib for Abl and c-KIT (0.025 – 2μM and 0.4μM respectively) (Mathew et al., 2008) however it may be possible that concentrations of imatinib used in the present study cause partial inhibition of c-Src activity leading to reduced phosphorylation of the villin protein, with an accompanied retraction from the cell surface to give an intracellular, cytoplasmic expression profile. Reduced mRNA transcription may therefore follow due to a lack of requirement for further protein translation.

In addition to the role of c-Src in villin expression and cell migration other members of the Src family have been linked with epithelial cell differentiation, although data is lacking in this area. The activity of Src was shown to be increased in less differentiated cells present within the crypt whilst lower Src activity levels were apparent in intestinal villus tip cells (Basson et al., 1998). Epithelial cells undergo extensive differentiation as they migrate up the crypt-villus axis. In chapter 4 we showed significantly increased mRNA expression levels of many genes involved in drug disposition in villus tip compared with crypt samples, suggesting expression patterns of many genes oppose measured Src TK activity across the crypt-villus axis. Potential for imatinib inhibition of Src kinase activity, and therefore reduced epithelial differentiation compared with vehicle treated animals may account for the observed decrease in expression of target genes in ileum samples.

In support of altered cell signalling being responsible for observed decreases in expression, work by Nakanishi et al., (2006) showed decreased BCRP protein expression in response to imatinib exposure to be mediated by inhibition of PI3K-Akt signalling. Human K562 cells, a CML BCR-ABL expressing cell line, selected for resistance to the BCRP substrate mitoxantrone showed increased resistance to both mitoxantrone and imatinib with an associated increase in cellular BCRP protein, indicative of increased BCRP function and mitoxantrone and imatinib efflux (Nakanishi et al., 2006). No increase in BCR-ABL expression was apparent in the BCRP expressing K562 cell line. Incubation of BCRP expressing K562 cells with 5μM imatinib however showed an approximate 60% reduction in cell surface expression of BCRP measured using flow cytometry, and a decreased total cellular BCRP protein content as measured by Western blot (Nakanishi et al., 2006). In contrast, no decrease in BCRP expression was observed in the BCR-ABL non-expressing MCF7/AdrVp cell line (Nakanishi et al., 2006). Knowing murine Bcrp

protein expression was regulated by PI3K-Akt signalling and that PI3K activation is increased in BCR-ABL expression cells, Nakanishi et al., (2006) treated cells with the PI3K inhibitor LT294002 and showed BCRP expression to decrease to a similar level to that observed following incubation with 5μM imatinib. In agreement with this work data presented here suggests that M70 immunoreactivity is decreased following imatinib treatment. The ability of imatinib to down regulate BCRP protein expression and cause retraction of BCRP from the cell surface via inhibition of BCR-ABL mediated phosphorylation of PI3K-Akt signalling, provides an alternative potential model for the decreased mRNA expression levels observed here; via alterations in cellular signalling pathways. Furthermore, the apparent imatinib induced inhibition of BCRP may actually reflect reduced protein expression and function as opposed to direct interaction of imatinib with the BCRP protein (Nakanishi et al., 2006).

With regards to observed differences in the effect of imatinib on mRNA expression levels in the jejunum and ileum no comprehensive explanation can currently be provided. Potentially, ileal enterocytes may show altered expression of TK enzymes and/or AhRs and so respond differently to imatinib exposure. Alternatively, observed changes in target gene expression may result from altered expression of villin. Given the roles of villin in cell migration, the loss of villin mRNA may decrease motility of enterocytes and as such prevent movement toward the villus tip. During migration from the crypt to villus tip enterocytes undergo extensive differentiation, as reflected in the observed increase in villus tip mRNA expression levels of many genes in chapter 4. Therefore, effects of imatinib on villin may indirectly alter ability of enterocytes to migrate and differentiate, reflected as an increased/decreased mRNA expression compared with vehicle control animals. This theory, however, does not provide explanation as to why some target genes (Cyp1a1 and Cyp2s1) show higher expression levels in the ileum following imatinib treatment whilst villin mRNA expression levels are decreased.

The PK profiles of imatinib following 4 day dosing show an increased Cmax. This does not therefore support a decreased absorption profile or increased first pass metabolism/biliary secretion due to functional transporter/metabolism induction nor an increased clearance from biliary, intestinal or renal action. The reason for such an increase in Cmax is not apparent. With regard to the apparent 2-phase increase in plasma concentrations of imatinib shown in the PK profile of three out of a total eight animals treated with imatinib (represented in figure 6.7A), it is proposed that regional specific intestinal absorption may be responsible for such differences in the absorption profile between animals. The $\log K_1$ value of imatinib protonation is 7.7 ± 0.1 and as such imatinib will exist as a charged molecule in the intestinal lumen (Szakács et al., 2005). As discussed previously past studies have suggested involvement of transporter proteins OCTN2, OATP1A2 and OCT1 in facilitated absorption of orally

administered imatinib (Eechoute et al., 2010). As such the apparent 2-phase increase in plasma concentration may reflect decreased uptake of imatinib in the mid-ileum, due to altered transporter expression, with an associated lag in reduced plasma concentrations due to intestinal drug transit. Indeed lower level expression of Octn2 and Oct1 transporters is observed in the mid-ileum, compared with the jejunum. Absorption may therefore resume with progression toward the more distal regions of the intestine. It should not however be disregarded that these observations come from a very small sample set so any inferences drawn from the data are speculative. For confirmation, further investigations of the absorption profile of imatinib in rat intestine are required.

As demonstrated here mechanisms regulating transcriptional expression of intestinal drug transporter and CYP450 enzymes are extremely complicated, with potential for differences in induction between regions of the intestine and numerous mechanisms capable of altering protein function. As such, it is not surprising that many drug compounds exhibit interaction when co-administered, nor is it surprising that inter-individual variation in response to treatments is apparent. With regards to ability of imatinib administration to alter drug disposition such that intestinal absorption is reduced, further work is required to establish clear interaction of imatinib with potential target genes, and to characterise by what mechanism imatinib exerts its effects on transcriptional regulation. Furthermore, the majority of changes reported here are shown only at an mRNA level and may not correlate with changes in protein functional activity, as suggested by the lack of change observed in the pharmacokinetic profile of imatinib on day one and day four of treatment, indicating a need to understand how such changes may be represented in a clinical setting.

7. Final conclusions and future work

The primary aim of this thesis was to quantitate mRNA expression levels of key transporter and CYP450 genes involved in intestinal drug disposition, both along the length of the rat intestine and along the ileal crypt-villus axis. Additionally, protein expression and localisation of three ABC transporters, Mdr1, Mrp2 and Bcrp, proposed to play important roles in intestinal drug resistance was evaluated using immunohistochemistry (Szakacs et al., 2008). Finally, since drug exposure has previously been reported to induce the expression of both ABC transporters and CYP450 enzymes via activation of nuclear receptor proteins (Nakata et al., 2006, Tirona and Kim, 2005, Urquhart et al., 2007) it was determined how mRNA and protein expression profiles were altered following oral administration of the tyrosine kinase inhibitor imatinib mesylate.

Although primarily involved in the absorption of dietary nutrients by facilitated transport, epithelium lining the intestine also serves to protect against invasion from foreign and toxic compounds, including oral pharmaceuticals (Paine et al., 2006, Snoeck et al., 2005, Szakacs et al., 2008). It is generally accepted that MDR1, MRP2 and BCRP are expressed together on the apical cell of intestinal enterocytes where they form a functional transporter network which acts to prevent cellular absorption of drug compounds via efflux of orally administered substrates out of the cell and into the intestinal lumen (Dietrich et al., 2003, Szakacs et al., 2008). More recently, a significant role for enteric CYP450 enzymes in determination of oral bioavailability has been established and it is now suggested that enteric CYP450 metabolism contributes equally toward the detoxification of drug compounds as does the liver (Paine et al., 2006). A model proposed by Benet, (2009) suggests ABC transporters and CYP450 enzymes may in fact work synergistically such that ABC transporters efflux drug substrates from enterocytes so as not to overload CYP450 enzymes and to allow re-entry of drug compounds into epithelial cells thereby promoting interaction with metabolising enzymes (Benet, 2009). As such it is vital to determine how potential drug compounds interact with ABC transporters and/or CYP450 enzymes and how such interactions alter their pharmacokinetic profiles following oral administration. By gaining a more comprehensive understanding of the relationship between CYP450 and ABC transporter expression along the length of the intestine it may allow for optimisation of bioavailability of drug compounds following oral administration.

Formed by a single layer of epithelial cells the entire enterocyte barrier is populated by intestinal stem cells which reside toward the base of crypt units (Barker et al., 2008). Strict self-regulation of intestinal stem cell number is therefore required, since loss or gain of one single stem cell may cause fluctuation in cell number by up to 64 cells (Marshman et al., 2002).

Given the vital physiological role of the intestinal stem cell niche it was hypothesised that some mechanism exists to minimise toxic insult toward these cells. BCRP has previously been detected in a range of progenitor stem cell populations and is known to cause development of the SP stem cell phenotype (Scharenberg et al., 2002, Zhou et al., 2001). Since it is reported that BCRP plays a functional role in drug efflux at the apical cell membrane of villus enterocytes it was postulated that such a role may also be recognised within the crypt unit. It was therefore of interest to determine mRNA expression profiles of key intestinal drug transporters and CYP450 enzymes in both villus tip and crypt regions and determine how crypt-villus cell migration alters epithelial gene and protein expression.

A modified crypt-villus isolation technique, as reported by McNicholas et al., (1994) was therefore employed to allow distinct separation of villus tip and crypt cell rich populations. Successful isolation of two distinct cell populations was confirmed using phase and TEM microscopy, Alph and Lap enzyme activities were also compared between villus tip and crypt samples. In addition, NanoString technology confirmed samples to be rich in villus and crypt cells with mRNA expression levels of brush borders enzymes Lap, Ca2 and Sglt1 showing a 4.9 ± 1.4, 3.6 ± 0.8 and 2.7 ± 0.8 fold increase in expression in villus tip versus crypt samples, with similar findings being reported previously (Freeman et al., 1993, Himmelhoch, 1969, Lenzen et al., 1996, Mariadason et al., 2005, McNicholas et al., 1994). Conversely, Pcna and Nkcc1 showed increased mRNA expression in cryptal cells in agreement with past literature (Jakab et al., 2010, Mariadason et al., 2005).

For the sake of this discussion emphasis will be placed on main thesis findings and how such results relate to current literature. Given the complexity of intestinal drug disposition and importance of the enterocyte barrier in determination of oral drug bioavailability focus was placed upon evaluation of Mdr1a, Mrp2, Bcrp and Cyp450 expression patterns in the rat intestine.

MDR1 is well characterised and is known to transport a wide variety of pharmacologically and structurally unrelated drug compounds in a wide range of tissues (Szakacs et al., 2008, Zhou, 2008). Expression of MDR1 on the apical cell membrane is known to substantially reduce intestinal absorption of many drug compounds (Szakacs et al., 2008, Zhou, 2008), with data presented here supporting the role of MDR1 in intestinal drug resistance. Immunohistochemical protein detection and NanoString mRNA detection showed consistent results, indicating strong correlation between mRNA and protein expression. Mdr1 protein was localised to the apical membrane of rat villus enterocytes in all regions of the small intestine with a reduced antibody immunoreactivity observed in rat colon sections. For the first time MDR1 immunoreactivity was also detected in the follicle associated epithelium overlying

Peyer's patches, suggesting that these modified enterocytes are also protected in a similar fashion to absorptive enterocytes. Both mRNA and protein data indicates expression to be greatest in rat ileum, although quantification of stain intensities was not performed. Localisation of Mdr1 protein to the apical enterocyte membrane, as reported previously (Blokzijl et al., 2007, Glaeser et al., 2007), supports the proposed role of this transporter in efflux of substrates across the apical enterocyte membrane out into the intestinal lumen, thereby increasing intestinal elimination or potentiating enterocytic drug recirculation and enteric Cyp450 metabolism (discussed in chapter 1) (Benet, 2009). Further work may look to quantitatively determine Mdr1 expression levels along the length of the rat intestine using Western blot analysis. It would be of particular interest to compare absolute Mdr1 protein expression with that of key metabolising enzymes such as Cyp3a9.

The observed increasing gradient of both Mdr1 mRNA and protein from the crypt to villus tip reflects physiological requirements for increased expression on villus cells which project into the intestinal lumen, thereby allowing increased interaction with luminal contents. Apical, villus expression of Mdr1 in rat intestine, with increasing expression from duodenum to ileum samples is in agreement with human expression data (Blokzijl et al., 2007, Englund et al., 2006, Glaeser et al., 2007) and suggests the rat to be a good representation of human physiology with regard to MDR1/Mdr1 mediated drug disposition, although caution should still be applied when extrapolating rodent data to human subjects.

A model proposed by Benet, (2009) suggests enterocytic drug recirculation to serve as a mechanism by which interaction between drug compounds and enteric CYP450 enzymes is potentiated (Benet, 2009). In agreement with the proposed synergistic actions of Cyp450 enzymes and Mdr1, mRNA expression levels of key Cyp450 enzymes involved in rat enteric metabolism, including the human CYP3A4 homolog, Cyp3a9, were detected in all regions of the rat intestine. As observed for Mdr1 a general trend of increased Cyp450 mRNA expression was observed from the duodenum to the jejunum, the ileum expression levels were generally equal to those in the jejunum. Although past studies have shown decreased mRNA, protein and functional activity of CYP450 enzymes, both in rat and human (Martignoni et al., 2006, Matsubara et al., 2004, Mitschke et al., 2008), from the proximal to distal small intestine it should be noted that substantial levels of inter-animal variation in expression were observed here, particularly in ileal mucosa. Furthermore, it has not been determined how mRNA expression correlates with regards to protein levels and further work should look to determine expression profiles of key Cyp3a family members particularly along both the longitudinal and crypt-villus axis to allow further insight into the relationship between Mdr1 and Cyp3a functional activity and allow for optimisation of oral drug delivery.

Interesting findings are reported for both Mrp2 and Bcrp expression in rat intestine. Mrp2 is proposed to play an important role in regulation of drug absorption across intestinal enterocytes, with previous immunohistochemical studies showing localisation of Mrp2 protein to the apical membrane of human intestinal cells (Fromm et al., 2000, Sandusky et al., 2002). Although mRNA expression levels of Mrp2 were found to be higher than those of Mdr1a in the duodenum, jejunum and ileum, immunohistochemistry showed only minimal staining at the apical membrane of ileal villus enterocytes in the ileum, with no visual staining detected in any other area of the intestine. Strong M2-III-6 antibody immunoreactivity was however apparent in rat liver sections with specific localisation to canalicular membranes in agreement with the known function of Mrp2 in biliary excretion (Mayer et al., 1995). Western blot analysis also failed to detect expression of Mrp2 protein in rat ileum samples although dense protein bands were observed for both MRP2 transfected MDCKII cells and rat liver samples. In agreement with earlier studies (Fromm et al., 2000, Sandusky et al., 2002), it was shown that MRP2 is expressed on the apical membrane of human jejunal enterocytes, showing differences in expression of this key drug resistance protein between species. It is possible that mRNA translation and protein expression is induced following intestinal exposure to xenobiotics as reported by Fromm et al., (2000) following oral administration of rifampin in healthy human volunteers. However it was found that oral exposure of rat intestine to high concentrations of imatinib mesylate (150mg/kg) did not induce intestinal MRP2 protein expression nor cause any significant increase in mRNA expression.

Despite only one study showing expression of BCRP at the apical membrane of intestinal enterocytes (Maliepaard et al., 2001) it is widely accepted that BCRP protein co-localises to this region along with Mdr1. Results presented in this thesis strongly contradict such localisation and failed to detect apical expression of Bcrp in any region of the intestine, rather, strong levels of immunoreactivity were detected on lateral cell membranes of crypt epithelia with apparent expression also evident to lateral cell membranes of intestinal stem cells using the anti-Bcrp primary antibody M70.

Whilst it was hypothesised that Bcrp may be expressed within the crypt region it was expected that the protein would localise to the apical membrane and mediate efflux of xenobiotics, including drug compounds, into the crypt lumen, thereby increasing intestinal elimination. Apparent localisation of Bcrp to the lateral cell membranes of crypt cells however suggests active efflux of substrates into the underlying blood supply, with subsequent transport via the hepatic portal vein to the liver. Since the liver possess exceptionally high capacity to detoxify xenobiotics (Suzuki and Sugiyama, 2004), such lateral efflux may serve to decrease xenobiotic

accumulation within the crypt, thereby preventing stem cell damage, and maximise potential for xenobiotic detoxification.

Although lateral membrane staining was observed in human jejunal sections immunoreactivity was stronger at the apical membrane of both villus and crypt epithelia. Therefore, despite validation of M70 antibody specificity using immunocytochemistry in mouse Bcrp transfected MDCKII cell lines and Western blot detection of a protein with apparent molecular weight representative of N-glycosylated Bcrp in both MDCKII-mBcrp cells and rat intestine, further work must be conducted to confirm BCRP/Bcrp protein expression differences between the human and rat intestine. If lateral expression of Bcrp in rat crypt epithelia were to hold against further scrutiny future work should investigate the polarity of Bcrp with regard to membrane targeting and the potential for heterodimerisation of the Bcrp protein to alter membrane localisation of this protein.

The apparent lack of Mrp2 protein expression in rat intestine and the accompanying localisation of Bcrp to lateral crypt membrane only, strongly suggests Mdr1a to be the most important ABC transporter involved in intestinal drug resistance in rat enterocytes. As such data presented here suggest that use of the rat as a preclinical model, particularly for Mrp2 and Bcrp substrates, to be ill-advised and further work should look to confirm relativity of the rat model to human drug pharmacokinetics. It would also be of interest to evaluate expression of key drug disposition proteins in the mouse intestine.

Oral administration of drug compounds has previously been shown to alter expression and function of key ABC transporters and CYP450 enzymes either by induction or repression of gene transcription or by inhibition of protein activity (Fromm et al., 2000, Greiner et al., 1999, Haslam et al., 2008, Tirona and Kim, 2005). Changes in protein function may alter PK profiles of drug compounds such that plasma drug concentrations are reduced or elevated above the levels of the therapeutic window (Tirona and Kim, 2005, Urquhart et al., 2007). Oral administration, and subsequent alterations in protein function alters bioavailability of drug compounds and pharmacokinetic profiles. Given that mRNA expression levels of Mrp2 and Bcrp were detected in all regions of the intestine, with an apparent lack of correlation in protein expression it was of interest to investigate how oral administration of the MDR1/BCRP substrate/inhibitor imatinib mesylate altered intestinal gene expression and function and how such changes influence oral pharmacokinetic profiles of imatinib. Indeed past data regarding ability of imatinib to induce BCRP expression is contradictory (Burger et al., 2005, Nakanishi et al., 2006) highlighting a need to understand how imatinib effects BCRP expression and function in vivo, and if any such differences in expression modify the PK profile.

Oral administration of imatinib mesylate caused a significant increase in jejunal Mdr1a mRNA expression with no significant change in mRNA expression levels of either Mrp2 of Bcrp within this region. Conversely, ileal mRNA expression of both Mdr1a and Bcrp was reduced significantly following intestinal exposure. Colonic Mdr1a mRNA expression increased with associated high levels of inter-animal variation. Additionally, increased Mdr1 protein expression at the apical membrane of epithelial cells lining the intestinal lumen was apparent. Mdr1 protein expression was also detected at the apical membrane of crypt cells consistent with a potential role for this transporter in protection of the crypt unit. In agreement with reduced BCRP expression reported by Nakanishi et al., (2006) following imatinib exposure, an apparent decrease in protein expression of Bcrp is suggested by immunohistochemistry although any such changes require quantitative confirmation (Nakanishi et al., 2006). High luminal concentrations of imatinib mesylate did not alter the expression profile for Bcrp and protein was not detected in villus epithelia. Similarly, no significant change in mRNA expression levels of Mrp2 was evident with protein expression being only minimal compared with IgG negative controls.

Cyp1a1 mRNA expression levels were shown to be markedly increased in both the jejunum and ileum. Induction of Cyp1a1 mRNA expression was much greater than observed for any other target gene. Although immunohistochemistry suggests upregulation of Cyp1a1 protein expression, antibody validation experiments were not performed and future work should look to quantitatively assess protein changes, particularly given the reported ability of Cyp1a1 to metabolise imatinib (Rochat et al., 2008). It is established that Cyp1a1 is under the transcriptional regulation of the AhR (Deb and Bandiera, 2009, Nakata et al., 2006), it is therefore proposed that the observed increase in mRNA expression is attributable to imatinib ligand activation of the AhR with subsequent translocation to the nucleus and binding to xenobiotic response elements of the Cyp1a1 gene. Further work should look to confirm imatinib to be an AhR ligand and determine if AhR activation is responsible for the observed induction of Cyp1a1.

Further work is required to determine if functional activity of ABC transporter proteins and/or Cyp1a1 is altered following oral administration of imatinib. Oral administration of imatinib over a four day period however showed a PK profile consistent with drug accumulation as opposed to increased elimination or metabolism of the parent drug molecule.

This thesis highlights the complexity of the enterocyte barrier in determination of intestinal drug absorption and bioavailability, particularly with regard to correlation between mRNA and protein expression of the three main ABC transporters proposed to confer intestinal drug resistance. Overall this work indicates potential for substantial differences in drug handling

between the well-used rodent model and human intestine and as such indicate a requirement for further work in establishing concordance of rat oral dosing studies in pre-clinical studies to human data. In agreement with current literature it is also emphasised that oral drug exposure shows potential to alter expression levels of key drug disposition proteins and highlights the importance of inter-individual responses to drug treatment.

8. References

AIBA, T., YOSHINAGA, M., ISHIDA, K., TAKEHARA, Y. & HASHIMOTO, Y. 2005. Intestinal expression and metabolic activity of the CYP3A subfamily in female rats. *Biological and Pharmaceutical Bulletin,* 28**,** 311-315.

AL-SHAWI, M. K. & OMOTE, H. 2005. The remarkable transport mechanism of P-glycoprotein: a multidrug transporter. *Journal of bioenergetics and biomembranes,* 37**,** 489-496.

ALLIKMETS, R., SCHRIML, L. M., HUTCHINSON, A., ROMANO-SPICA, V. & DEAN, M. 1998. A human placenta-specific ATP-binding cassette gene (ABCP) on chromosome 4q22 that is involved in multidrug resistance. *Cancer Research,* 58**,** 5337-5339.

AMBROS, V. 2004. The functions of animal microRNAs. *Nature,* 431**,** 350-355.

ANDERLE, P., SENGSTAG, T., MUTCH, D. M., RUMBO, M., PRAZ, V., MANSOURIAN, R., DELORENZI, M., WILLIAMSON, G. & ROBERTS, M.-A. 2005. Changes in the transcriptional profile of transporters in the intestine along the anterior-posterior and crypt-villus axes. *BMC genomics,* 6**,** 69.

ANDO, W., HASHIMOTO, J., NAMPEI, A., TSUBOI, H., TATEISHI, K., ONO, T., NAKAMURA, N., OCHI, T. & YOSHIKAWA, H. 2006. Imatinib mesylate inhibits osteoclastogenesis and joint destruction in rats with collagen-induced arthritis (CIA). *Journal of bone and mineral metabolism,* 24**,** 274-282.

ANZENBACHER, P. & ANZENBACHEROVA, E. 2001. Cytochromes P450 and metabolism of xenobiotics. *Cellular and Molecular Life Sciences CMLS,* 58**,** 737-747.

AUST, S., OBRIST, P., JAEGER, W., KLIMPFINGER, M., TUCEK, G., WRBA, F., PENNER, E. & THALHAMMER, T. 2004. Subcellular localization of the ABCG2 transporter in normal and malignant human gallbladder epithelium. *Laboratory investigation,* 84**,** 1024-1036.

BARKER, G. & SIMMONS, N. L. 1981. Identification of two strains of cultured canine renal epithelial cells (MDCK cells) which display entirely different physiological properties. *Experimental Physiology,* 66**,** 61-72.

BARKER, N., VAN ES, J. H., KUIPERS, J., KUJALA, P., VAN DEN BORN, M., COZIJNSEN, M., HAEGEBARTH, A., KORVING, J., BEGTHEL, H. & PETERS, P. J. 2007. Identification of stem cells in small intestine and colon by marker gene Lgr5. *Nature,* 449**,** 1003-1007.

BARKER, N., VAN DE WETERING, M. & CLEVERS, H. 2008. The intestinal stem cell. *Genes & development,* 22**,** 1856-1864.

BARRETT, K. E., BROOKS, K. L., BOITANO, S. & BARMAN, S. M. 2010. *Review of medical physiology*, 23rd edition: The McGraw-Hill companies, pages 449-451.

BARTEL, D. P. 2004. MicroRNAs: genomic, mechanism and function. *Cell,* 116**,** 281-297.

BASSON, M. D., EMENAKER, N. J. & RASHID, Z. 1998. Effects of modulation of tyrosine phosphorylation on brush border enzyme activity in human Caco-2 intestinal epithelial cells. *Cell and tissue research,* 292**,** 553-562.

BENET, L. Z. 2009. The drug transporter metabolism alliance: uncovering and defining the interplay. *Molecular pharmaceutics,* 6**,** 1631-1643.

BERGGREN, S., GALL, C., WOLLNITZ, N., EKELUND, M., KARLBOM, U., HOOGSTRAATE, J., SCHRENK, D. & LENNERNÄS, H. 2007. Gene and protein expression of P-glycoprotein, MRP1, MRP2, and CYP3A4 in the small and large human intestine. *Molecular pharmaceutics,* 4**,** 252-257.

BERRYMAN, M., FRANCK, Z. & BRETSCHER, A. 1993. Ezrin is concentrated in the apical microvilli of a wide variety of epithelial cells whereas moesin is found primarily in endothelial cells. *Journal of Cell Science,* 105**,** 1025-1043.

BJERKNES, M. & CHENG, H. 1981. Methods for the isolation of intact epithelium from the mouse intestine. *The Anatomical Record,* 199**,** 565-574.

BLOKZIJL, H., VANDER BORGHT, S., BOK, L. I. H., LIBBRECHT, L., GEUKEN, M., VAN DEN HEUVEL, F. A. J., DIJKSTRA, G., ROSKAMS, T. A. D., MOSHAGE, H. & JANSEN, P. L. M. 2007. Decreased P-glycoprotein (P-gp/MDR1) expression in inflamed human intestinal

epithelium is independent of PXR protein levels. *Inflammatory bowel diseases,* 13**,** 710-720.

BOLLER, K., ARPIN, M., PRINGAULT, E., MANGEAT, P. & REGGIO, H. 1988. Differential distribution of villin and villin mRNA in mouse intestinal epithelial cells. *Differentiation,* 39**,** 51-57.

BORON, W. F. & BOULPAEP, E. L. 2009. *Medical Physiology,* 2nd edition: Philadelphia, PA, Saunders, Elsevier, pages 432, 883-884, 908-909, 934-935 and 951.

BORST, P., EVERS, R., KOOL, M. & WIJNHOLDS, J. 2000. A family of drug transporters: the multidrug resistance-associated proteins. *Journal of the National Cancer Institute,* 92**,** 1295-1302.

BORST, P., DE WOLF, C. & VAN DE WETERING, K. 2007. Multidrug resistance-associated proteins 3, 4, and 5. *Pflügers Archiv-European Journal of Physiology,* 453**,** 661-673.

BUCHLER, M., KONIG, J., BROM, M., KARTENBECK, J., SPRING, H., HORIE, T. & KEPPLER, D. 1996. cDNA cloning of the hepatocyte canalicular isoform of the multidrug resistance protein, cMrp, reveals a novel conjugate export pump deficient in hyperbilirubinemic mutant rats. *Journal of Biological Chemistry,* 271**,** 15091-15098.

BURGER, H., VAN TOL, H., BROK, M. L., WIEMER, E. A. C., DE BRUIJN, E. A., GUETENS, G., DE BOECK, G., SPARREBOOM, A., VERWEIJ, J. & NOOTER, K. 2005. Research Paper Chronic Imatinib Mesylate Exposure Leads to Reduced Intracellular Drug Accumulation by Induction of the ABCG2 (BCRP) and ABCB1 (MDR1) Drug Transport Pumps. *Cancer biology & therapy,* 4**,** 747-752.

BURLEY, S. K., DAVID, P. R., TAYLOR, A. & LIPSCOMB, W. N. 1990. Molecular structure of leucine aminopeptidase at 2.7-A resolution. *Proceedings of the National Academy of Sciences,* 87**,** 6878-6882.

CARR, G., WRIGHT, J. A. & SIMMONS, N. L. 2010. Epithelial barrier resistance is increased by the divalent cation zinc in cultured MDCKII epithelial monolayers. *The Journal of membrane biology,* 237**,** 115-123.

CAVET, M. E., WEST, M. & SIMMONS, N. L. 1996. Transport and epithelial secretion of the cardiac glycoside, digoxin, by human intestinal epithelial (Caco2) cells. *British journal of pharmacology,* 118**,** 1389-1396.

CHAN, L., LOWES, S. & HIRST, B. H. 2004. The ABCs of drug transport in intestine and liver: efflux proteins limiting drug absorption and bioavailability. *European journal of pharmaceutical sciences,* 21**,** 25-51.

CHAWLA, G. & BANSAL, A. 2003. A means to address regional variability in intestinal drug absorption. *Pharm tech,* 27**,** 50-68.

CHENG, H. & LEBLOND, C. P. 1974. Origin, differentiation and renewal of the four main epithelial cell types in the mouse small intestine I. Columnar cell. *American Journal of Anatomy,* 141**,** 461-479.

CHIANALE, J., VOLLRATH, V., WIELANDT, A. M., MIRANDA, S., GONZALEZ, R., FRESNO, A. M., QUINTANA, C., GONZALEZ, S., ANDRADE, L. & GUZMAN, S. 1995. Differences between nuclear run-off and mRNA levels for multidrug resistance gene expression in the cephalocaudal axis of the mouse intestine. *Biochimica et Biophysica Acta (BBA)-Gene Structure and Expression,* 1264**,** 369-376.

COLE, S. P. C. & DEELEY, R. G. 1998. Multidrug resistance mediated by the ATP-binding cassette transporter protein MRP. *Bioessays,* 20**,** 931-940.

COLEMAN, J. E. 1992. Structure and mechanism of alkaline phosphatase. *Annual review of biophysics and biomolecular structure,* 21**,** 441-483.

CONYERS, R. A. J., BIRKETT, D. J., NEALE, F. C., POSEN, S. & BRUDENELLWOODS, J. 1967. The action of EDTA on human alkaline phosphatases. *Biochimica et Biophysica Acta (BBA)-Enzymology,* 139**,** 363-371.

CSEREPES, J., SZENTPÉTERY, Z., SERES, L., ÖZVEGY-LACZKA, C., LANGMANN, T., SCHMITZ, G., GLAVINAS, H., KLEIN, I., HOMOLYA, L. & VÁRADI, A. 2004. Functional expression and characterization of the human ABCG1 and ABCG4 proteins: indications for

heterodimerization. *Biochemical and biophysical research communications,* 320**,** 860-867.

DE JONGE, H. J. M., FEHRMANN, R. S. N., DE BONT, E. S. J. M., HOFSTRA, R. M. W., GERBENS, F., KAMPS, W. A., DE VRIES, E. G. E., VAN DER ZEE, A. G. J., TE MEERMAN, G. J. & TER ELST, A. 2007. Evidence Based Selection of Housekeeping Genes. *PLoS ONE,* 2**,** e898.

DEAN, M., HAMON, Y. & CHIMINI, G. 2001. The human ATP-binding cassette (ABC) transporter superfamily. *Journal of lipid research,* 42**,** 1007-1017.

DEB, S. & BANDIERA, S. M. 2009. Characterization and expression of extrahepatic CYP2S1. *Expert opinion on drug metabolism & toxicology,* 5**,** 367-380.

DEBORDE, S., PERRET, E., GRAVOTTA, D., DEORA, A., SALVAREZZA, S., SCHREINER, R. & RODRIGUEZ-BOULAN, E. 2008. Clathrin is a key regulator of basolateral polarity. *Nature,* 452**,** 719-723.

DEELEY, R. G., WESTLAKE, C. & COLE, S. P. C. 2006. Transmembrane transport of endo-and xenobiotics by mammalian ATP-binding cassette multidrug resistance proteins. *Physiological reviews,* 86**,** 849-899.

DEORA, A. A., PHILP, N., HU, J., BOK, D. & RODRIGUEZ-BOULAN, E. 2005. Mechanisms regulating tissue-specific polarity of monocarboxylate transporters and their chaperone CD147 in kidney and retinal epithelia. *Proceedings of the National Academy of Sciences,* 102**,** 16245-16250.

DIESTRA, J. E., SCHEFFER, G. L., CATALA, I., MALIEPAARD, M., SCHELLENS, J. H. M., SCHEPER, R. J., GERMÁ-LLUCH, J. R. & IZQUIERDO, M. A. 2002. Frequent expression of the multidrug-resistance associated protein BCRP/MXR/ABCP/ABCG2 in human tumours detected by the BXP-21 monoclonal antibody in paraffin embedded material. *The Journal of pathology,* 198**,** 213-219.

DIETRICH, C. G., GEIER, A. & ELFERINK, R. P. J. O. 2003. ABC of oral bioavailability: transporters as gatekeepers in the gut. *Gut,* 52**,** 1788-1795.

DIOP, N. K. & HRYCYNA, C. A. 2005. N-Linked glycosylation of the human ABC transporter ABCG2 on asparagine 596 is not essential for expression, transport activity, or trafficking to the plasma membrane. *Biochemistry,* 44**,** 5420-5429.

DOHSE, M., SCHARENBERG, C., SHUKLA, S., ROBEY, R. W., VOLKMANN, T., DEEKEN, J. F., BRENDEL, C., AMBUDKAR, S. V., NEUBAUER, A. & BATES, S. E. 2010. Comparison of ATP-binding cassette transporter interactions with the tyrosine kinase inhibitors imatinib, nilotinib, and dasatinib. *Drug Metabolism and Disposition,* 38**,** 1371-1380.

DOYLE, L. A., YANG, W., ABRUZZO, L. V., KROGMANN, T., GAO, Y., RISHI, A. K. & ROSS, D. D. 1998. A multidrug resistance transporter from human MCF-7 breast cancer cells. *Proceedings of the National Academy of Sciences,* 95**,** 15665-15670.

DRESSER, G. K., SCHWARZ, U. I., WILKINSON, G. R. & KIM, R. B. 2003. Coordinate induction of both cytochrome P4503A and MDRI by St John's wort in healthy subjects. *Clinical Pharmacology And Therapeutics,* 73**,** 41-50.

DRUGBANK. 2014. Available: www.drugbank.ca [Accessed August 2014].

DULUC, I., LORENTZ, O., FRITSCH, C., KEDINGER, M. & FREUND, J.-N. 1997. Changing intestinal connected tissue interactions alters homeobox gene expression in epithelial cells. *J. Cell Science,* 110**,** 1317-1324.

EECHOUTE, K., SPARREBOOM, A., BURGER, H., FRANKE, R. M., SCHIAVON, G., VERWEIJ, J., LOOS, W. J., WIEMER, E. A. C. & MATHIJSSEN, R. H. J. 2010. Drug transporters and imatinib treatment: implications for clinical practice. *Clinical Cancer Research,* 17**,** 406-415.

EJENDAL, K. F. K. & HRYCYNA, C. A. 2005. Differential sensitivities of the human ATP-binding cassette transporters ABCG2 and P-glycoprotein to cyclosporin A. *Molecular pharmacology,* 67**,** 902-911.

ENGLUND, G., RORSMAN, F., RÖNNBLOM, A., KARLBOM, U., LAZOROVA, L., GRASJÖ, J., KINDMARK, A. & ARTURSSON, P. 2006. Regional levels of drug transporters along the

human intestinal tract: co-expression of ABC and SLC transporters and comparison with Caco-2 cells. *European journal of pharmaceutical sciences,* 29**,** 269-277.

ENSINGER, H. A., PAULY, H. E., PFLEIDERER, G. & STIEFEL, T. 1978. The role of Zn (II) in calf intestinal alkaline phosphatase studied by the influence of chelating agents and chemical modification of histidine residues. *Biochimica et Biophysica Acta (BBA)-Enzymology,* 527**,** 432-441.

EWART, G. D., CANNELL, D., COX, G. B. & HOWELLS, A. J. 1994. Mutational analysis of the traffic ATPase (ABC) transporters involved in uptake of eye pigment precursors in Drosophila melanogaster. Implications for structure-function relationships. *Journal of Biological Chemistry,* 269**,** 10370-10377.

FERRUZZA, S., ROSSI, C., SCARINO, M. L. & SAMBUY, Y. 2011. A protocol for in situ enzyme assays to assess the differentiation of human intestinal Caco-2 cells. *Toxicology in Vitro,* 26**,** 1247-1251.

FETSCH, P. A., ABATI, A., LITMAN, T., MORISAKI, K., HONJO, Y., MITTAL, K. & BATES, S. E. 2006. Localization of the ABCG2 mitoxantrone resistance-associated protein in normal tissues. *Cancer letters,* 235**,** 84-92.

FLEMING, R. E., PARKKILA, S., PARKKILA, A.-K., RAJANIEMI, H., WAHEED, A. & SLY, W. S. 1995. Carbonic anhydrase IV expression in rat and human gastrointestinal tract regional, cellular, and subcellular localization. *Journal of Clinical Investigation,* 96**,** 2907.

FLINT, N., COVE, F. L. & EVANS, G. S. 1991. A low-temperature method for the isolation of small-intestinal epithelium along the crypt-villus axis. *Biochem. J,* 280**,** 331-334.

FORD, D., HOWARD, A. & HIRST, B. H. 2003. Expression of the peptide transporter hPepT1 in human colon: a potential route for colonic protein nitrogen and drug absorption. *Histochemistry and cell biology,* 119**,** 37-43.

FREEMAN, T. C., COLLINS, A. J., HEAVENS, R. P. & TIVEY, D. R. 1993. Genetic regulation of enterocyte function: a quantitative in situ hybridisation study of lactase-phlorizin hydrolase and Na^+-glucose cotransporter mRNAs in rabbit small intestine. *Pflügers Archiv,* 422**,** 570-576.

FREEMAN, T. C., BENTSEN, B. S., THWAITES, D. T. & SIMMONS, N. L. 1995. H^+/di-tripeptide transporter (PepT1) expression in the rabbit intestine. *Pflügers Archiv,* 430**,** 394-400.

FREUND, J.-N., BOUKAMEL, R. & BENAZZOUZ, A. 1998a. Gradient expression of Cdx along the rat intestine throughout postnatal development. *FEBS Letters,* 314**,** 163-166.

FREUND, J.-N., DOMON-DELL, C., KEDLINGER, M. & DULUC, I. 1998b. The Cdx-1 and Cdx-2 homeobox genes in the intestine. *Biochem. Cell Biol,* 76**,** 957-969.

FRICKER, G. & MILLER, D. S. 2002. Relevance of multidrug resistance proteins for intestinal drug absorption in vitro and in vivo. *Pharmacology & toxicology,* 90**,** 5-13.

FRIEDERICH, E., PRINGAULT, E., ARPIN, M. & LOUVARD, D. 1990. From the structure to the function of villin, an actin-binding protein of the brush border. *Bioessays,* 12**,** 403-408.

FROMM, M. F., KAUFFMANN, H.-M., FRITZ, P., BURK, O., KROEMER, H. K., WARZOK, R. W., EICHELBAUM, M., SIEGMUND, W. & SCHRENK, D. 2000. The effect of rifampin treatment on intestinal expression of human MRP transporters. *The American journal of pathology,* 157**,** 1575-1580.

FUKUDA, Y. & SCHUETZ, J. D. 2012. ABC transporters and their role in nucleoside and nucleotide drug resistance. *Biochemical pharmacology,* 83**,** 1073-1083.

GEISS, G. K., BUMGARNER, R. E., BIRDITT, B., DAHL, T., DOWIDAR, N., DUNAWAY, D. L., FELL, H. P., FERREE, S., GEORGE, R. D., GROGAN, T., JAMES, J. J., MAYSURIA, M., MITTON, J. D., OLIVERI, P., OSBORN, J. L., PENG, T., RATCLIFFE, A. L., WEBSTER, P. J., DAVIDSON, E. H., HOOD, L. & DIMITROV, K. 2008. Direct multiplexed measurement of gene expression with color-coded probe pairs. *Nat Biotech,* 26**,** 317-325.

GIACOMINI, K. M., HUANG, S.-M., TWEEDIE, D. J., BENET, L. Z., BROUWER, K. L. R., CHU, X., DAHLIN, A., EVERS, R., FISCHER, V. & HILLGREN, K. M. 2010. Membrane transporters in drug development. *Nature reviews Drug discovery,* 9**,** 215-236.

GLAESER, H., BAILEY, D. G., DRESSER, G. K., GREGOR, J. C., SCHWARZ, U. I., MCGRATH, J. S., JOLICOEUR, E., LEE, W., LEAKE, B. F. & TIRONA, R. G. 2007. Intestinal drug transporter expression and the impact of grapefruit juice in humans. *Clinical Pharmacology & Therapeutics,* 81**,** 362-370.

GLAVINAS, H., MÉHN, D., JANI, M. R., OOSTERHUIS, B., HERÉDI-SZABÓ, K. & KRAJCSI, P. 2008. Utilization of membrane vesicle preparations to study drug-ABC transporter interactions. *Expert opinion on drug metabolism & toxicology,* 4**,** 721-732.

GOMEZ-ORELLANA, I. 2005. Strategies to improve oral drug bioavailability. *Expert Opinion on Drug Delivery,* 2**,** 419-433.

GRAF, G. A., YU, L., LI, W.-P., GERARD, R., TUMA, P. L., COHEN, J. C. & HOBBS, H. H. 2003. ABCG5 and ABCG8 are obligate heterodimers for protein trafficking and biliary cholesterol excretion. *Journal of Biological Chemistry,* 278**,** 48275-48282.

GRAY, J. H., OWEN, R. P. & GIACOMINI, K. M. 2004. The concentrative nucleoside transporter family, SLC28. *Pflügers Archiv,* 447**,** 728-734.

GREINER, B., EICHELBAUM, M., FRITZ, P., KREICHGAUER, H.-P., VON RICHTER, O., ZUNDLER, J. & KROEMER, H. K. 1999. The role of intestinal P-glycoprotein in the interaction of digoxin and rifampin. *Journal of Clinical Investigation,* 104**,** 147-153.

GRIFFITHS, N. M., HIRST, B. H. & SIMMONS, N. L. 1993. Active secretion of the fluoroquinolone ciprofloxacin by human intestinal epithelial Caco2 cell layers. *British journal of pharmacology,* 108**,** 575-576.

GU, Y., WU, Z. H., XIE, J. X., JIN, D. Y. & ZHUO, H. C. 2001. Effects of growth hormone (rhGH) and glutamine supplemented parenteral nutrition on intestinal adaptation in short bowel rats. *Clinical Nutrition,* 20**,** 159-166.

GUTMANN, H., HRUZ, P., ZIMMERMANN, C., BEGLINGER, C. & DREWE, J. 2005. Distribution of breast cancer resistance protein (BCRP/ABCG2) mRNA expression along the human GI tract. *Biochemical pharmacology,* 70**,** 695-699.

HAENISCH, S., LAECHELT, S., BRUCKMUELLER, H., WERK, A., NOACK, A., BRUHN, O., REMMIER, C. & CASCORBI, I. 2011. Down-Regulation of ATP-Binding Cassette C2 Protein Expression in HepG2 Cells after Rifampicin Treatment is Mediated by MicroRNA-379. *Molecular Pharmacology,* 80**,** 314-320.

HAMADA, A., MIYANO, H., WATANABE, H. & SAITO, H. 2003. Interaction of imatinib mesilate with human P-glycoprotein. *Journal of Pharmacology and Experimental Therapeutics,* 307**,** 824-828.

HARRISON, D. D. & WEBSTER, H. L. 1969. The preparation of isolated intestinal crypt cells. *Experimental cell research,* 55**,** 257-260.

HASLAM, I. S. 2007. *Regulation of the expression and function of P-glycoprotein by the nuclear xenobiotic receptor PXR.* Doctor of Philosophy, Newcastle University.

HASLAM, I. S., JONES, K., COLEMAN, T. & SIMMONS, N. L. 2008. Rifampin and digoxin induction of MDR1 expression and function in human intestinal (T84) epithelial cells. *British journal of pharmacology,* 154**,** 246-255.

HASLAM, I. S., WRIGHT, J. A., O'REILLY, D. A., SHERLOCK, D. J., COLEMAN, T. & SIMMONS, N. L. 2011. Intestinal ciprofloxacin efflux: the role of breast cancer resistance protein (ABCG2). *Drug Metabolism and Disposition,* 39**,** 2321-2328.

HEDIGER, M. A., ROMERO, M. F., PENG, J.-B., ROLFS, A., TAKANAGA, H. & BRUFORD, E. A. 2004. The ABCs of solute carriers: physiological, pathological and therapeutic implications of human membrane transport proteins. *Pflügers Archiv,* 447**,** 465-468.

HEGEDUS, C., SZAKA¡CS, G., HOMOLYA, L., ORBAN, T., TELBISZ, Ã., JANI, M. & SARKADI, B. 2009. Ins and outs of the ABCG2 multidrug transporter: An update on *in vitro* functional assays. *Advanced drug delivery reviews,* 61**,** 47-56.

HIGGINS, C. F. & LINTON, K. J. 2004. The ATP switch model for ABC transporters. *Nature structural & molecular biology,* 11**,** 918-926.

HILGENDORF, C., AHLIN, G., SEITHEL, A., ARTURSSON, P., UNGELL, A.-L. & KARLSSON, J. 2007. Expression of thirty-six drug transporter genes in human intestine, liver, kidney, and organotypic cell lines. *Drug Metabolism and Disposition,* 35**,** 1333-1340.

HIMMELHOCH, S. R. 1969. Leucine aminopeptidase: a zinc metalloenzyme. *Archives of biochemistry and biophysics,* 134**,** 597-602.

HODGES, L. M., MARKOVA, S. M., CHINN, L. W., GOW, J. M., KROETZ, D. L., KLEIN, T. E. & ALTMAN, R. B. 2011. Very important pharmacogene summary: ABCB1 (MDR1, P-glycoprotein). *Pharmacogenetics and genomics,* 21**,** 152.

HOMOLYA, L., ORBAN, T. I., CSANADY, L. & SARKADI, B. Z. 2011. Mitoxantrone is expelled by the ABCG2 multidrug transporter directly from the plasma membrane. *Biochimica et Biophysica Acta (BBA)-Biomembranes,* 1808**,** 154-163.

HOPPER-BORGE, E., CHEN, Z.-S., SHCHAVELEVA, I., BELINSKY, M. G. & KRUH, G. D. 2004. Analysis of the Drug Resistance Profile of Multidrug Resistance Protein 7 (ABCC10) Resistance to Docetaxel. *Cancer Research,* 64**,** 4927-4930.

HORI, S., OHTSUKI, S., TACHIKAWA, M., KIMURA, N., KONDO, T., WATANABE, M., NAKASHIMA, E. & TERASAKI, T. 2004. Functional expression of rat ABCG2 on the luminal side of brain capillaries and its enhancement by astrocyte-derived soluble factor (s). *Journal of neurochemistry,* 90**,** 526-536.

HOUGHTON, P. J., GERMAIN, G. S., HARWOOD, F. C., SCHUETZ, J. D., STEWART, C. F., BUCHDUNGER, E. & TRAXLER, P. 2004. Imatinib mesylate is a potent inhibitor of the ABCG2 (BCRP) transporter and reverses resistance to topotecan and SN-38 in vitro. *Cancer Research,* 64**,** 2333-2337.

HU, S., FRANKE, R. M., FILIPSKI, K. K., HU, C., ORWICK, S. J., DE BRUIJN, E. A., BURGER, H., BAKER, S. D. & SPARREBOOM, A. 2008. Interaction of imatinib with human organic ion carriers. *Clinical Cancer Research,* 14**,** 3141-3148.

IRVINE, J. D., TAKAHASHI, L., LOCKHART, K., CHEONG, J., TOLAN, J. W., SELICK, H. E. & GROVE, J. R. 1999. MDCK (Madin–Darby canine kidney) cells: A tool for membrane permeability screening. *Journal of Pharmaceutical Sciences,* 88**,** 28-33.

ISENBERG, G. & KLOCKNER, U. 1982. Calcium tolerant ventricular myocytes prepared by preincubation in a KB medium. *Pflügers Archiv,* 395**,** 6-18.

JAKAB, R. L., COLLACO, A. M. & AMEEN, N. A. 2010. Physiological relevance of cell-specific distribution patterns of CFTR, NKCC1, NBCe1, and NHE3 along the crypt-villus axis in the intestine. *American Journal of Physiology-Gastrointestinal and Liver Physiology,* 300**,** G82-G98.

JAMES, R. & KAZENWADEL, J. 1991. Homeobox Gene Expression in the Intestinal Epithelium of Adult Mice. *The journal of Biological Chemsitry,* 266**,** 3246-3251.

JEDLITSCHKY, G., HOFFMANN, U. & KROEMER, H. K. 2006. Structure and function of the MRP2 (ABCC2) protein and its role in drug disposition. *Expert opinion on drug metabolism & toxicology,* 2**,** 351-366.

JULIANO, R. L. & LING, V. 1976. A surface glycoprotein modulating drug permeability in Chinese hamster ovary cell mutants. *Biochimica et Biophysica Acta (BBA)-Biomembranes,* 455**,** 152-162.

KAGE, K., TSUKAHARA, S., SUGIYAMA, T., ASADA, S., ISHIKAWA, E., TSURUO, T. & SUGIMOTO, Y. 2002. Dominant-negative inhibition of breast cancer resistance protein as drug efflux pump through the inhibition of S-S dependent homodimerization. *International journal of cancer,* 97**,** 626-630.

KAMINSKY, L. S. & ZHANG, Q.-Y. 2003. The small intestine as a xenobiotic-metabolizing organ. *Drug Metabolism and Disposition,* 31**,** 1520-1525.

KATO, Y., SUGIURA, M., SUGIURA, T., WAKAYAMA, T., KUBO, Y., KOBAYASHI, D., SAI, Y., TAMAI, I., ISEKI, S. & TSUJI, A. 2006. Organic cation/carnitine transporter OCTN2 (Slc22a5) is responsible for carnitine transport across apical membranes of small intestinal epithelial cells in mouse. *Molecular pharmacology,* 70**,** 829-837.

KERB, R. 2006. Implications of genetic polymorphisms in drug transporters for pharmacotherapy. *Cancer letters,* 234**,** 4-33.

KIM, M., TURNQUIST, H., JACKSON, J., SGAGIAS, M., YAN, Y., GONG, M., DEAN, M., SHARP, J. G. & COWAN, K. 2002. The multidrug resistance transporter ABCG2 (breast cancer resistance protein 1) effluxes Hoechst 33342 and is overexpressed in hematopoietic stem cells. *Clinical Cancer Research,* 8**,** 22-28.

KIS, O., ROBILLARD, K., CHAN, G. N. Y. & BENDAYAN, R. 2009. The complexities of antiretroviral drug-drug interactions: role of ABC and SLC transporters. *Trends in pharmacological sciences,* 31**,** 22-35.

KIVELA, A. J., KIVELA, J., SAARNIO, J. & PARKKILA, S. 2005. Carbonic anhydrases in normal gastrointestinal tract and gastrointestinal tumours. *World J Gastroenterol,* 11**,** 155-163.

KOBAYASHI, D., NOZAWA, T., IMAI, K., NEZU, J.-I., TSUJI, A. & TAMAI, I. 2003. Involvement of human organic anion transporting polypeptide OATP-B (SLC21A9) in pH-dependent transport across intestinal apical membrane. *Journal of Pharmacology and Experimental Therapeutics,* 306**,** 703-708.

KOBUCHI, H., MORIYA, K., OGINO, T., FUJITA, H., INOUE, K., SHUIN, T., YASUDA, T., UTSUMI, K. & UTSUMI, T. 2012. Mitochondrial localization of ABC transporter ABCG2 and its function in 5-aminolevulinic acid-mediated protoporphyrin IX accumulation. *PLOS ONE,* 7**,** e50082.

KOEPSELL, H. & ENDOU, H. 2004. The SLC22 drug transporter family. *Pflügers Archiv,* 447**,** 666-676.

KOTURBASH, I., BELAND, F. A. & POGRIBNY, I. P. 2012. Role of microRNAs in the regulation of drug metabolising and transporting genes and the response to environmental toxicants. *Expert Opinion on Drug Metabolism & Toxicology,* 8**,** 597-606.

KRALJ, E., ZAKELJ, S., TRONTELJ, J., ROŚKAR, R., CERNELC, P. & KRISTL, A. 2014. Absorption and elimination of imatinib through the rat intestine in vitro. *International journal of pharmaceutics,* 460**,** 144-149.

KRALJEVIC, S., STAMBROOK, P. J. & PAVELIC, K. 2004. Accelerating drug discovery. *EMBO reports,* 5**,** 837-842.

KRUH, G. D. & BELINSKY, M. G. 2003. The MRP family of drug efflux pumps. *Oncogene,* 22**,** 7537-7552.

KUTEYKIN-TEPLYAKOV, K., LUNA-TORTOS, C., AMBROZIAK, K. & LOSCHER, W. 2010. Differences in the expression of endogenous efflux transporters in MDR1-transfected versus wildtype cell lines affect P-glycoprotein mediated drug transport. *British journal of pharmacology,* 160**,** 1453-1463.

LAMBERT, M., COLNOT, S., SUH, E. R., L-HORSET, F., BLIN, C., CALLIOT, M., RAYMONJEAN, M., THOMASSET, M., TRABER, P. G. & PERRET, C. 1996. Cis-acting elements and transcription factors involved in the intestinal specific expression of the rat calbindin-D9k gene. Binding of the intestin-specific transcription factor Cdx-2 to the TATA box. *European Journal of Biochemistry,* 236**,** 778-788.

LANGMANN, T., MAUERER, R., ZAHN, A., MOEHLE, C., PROBST, M., STREMMEL, W. & SCHMITZ, G. 2003. Real-time reverse transcription-PCR expression profiling of the complete human ATP-binding cassette transporter superfamily in various tissues. *Clinical chemistry,* 49**,** 230-238.

LEE, E. J. D., LEAN, C. B. & LIMENTA, L. M. G. 2009. Role of membrane transporters in the safety profile of drugs. *Expert opinion on drug metabolism & toxicology,* 5**,** 1369-1383.

LEESON, P. 2012. Drug discovery: Chemical beauty contest. *Nature,* 481**,** 455-456.

LENZEN, S., LORTZ, S. & TIEDGE, M. 1996. Effects of metformin on SGLT1, GLUT2, and GLUT5 hexose transporter gene expression in small intestine from rats. *Biochemical pharmacology,* 51**,** 893-896.

LEVEQUE, D. & MALOISEL, F. D. R. 2005. Clinical pharmacokinetics of imatinib mesylate. *In Vivo-Attiki,* 19**,** 77-84.

LI, Y.-F., POLGAR, O., OKADA, M., ESSER, L., BATES, S. E. & XIA, D. 2007. Towards understanding the mechanism of action of the multidrug resistance-linked half-ABC transporter ABCG2: a molecular modeling study. *Journal of Molecular Graphics and Modelling,* 25**,** 837-851.

LIN, J. H., CHIBA, M. & BAILLIE, T. A. 1999. Is the role of the small intestine in first-pass metabolism overemphasized? *Pharmacological reviews,* 51**,** 135-158.

LINDELL, M., LANG, M. & LENNERNÃS, H. 2003. Expression of genes encoding for drug metabolising cytochrome P450 enzymes and P-glycoprotein in the rat small intestine; comparison to the liver. *European journal of drug metabolism and pharmacokinetics,* 28**,** 41-48.

LITMAN, T., JENSEN, U., HANSEN, A., COVITZ, K.-M., ZHAN, Z., FETSCH, P., ABATI, A., HANSEN, P. R., HORN, T. & SKOVSGAARD, T. 2002. Use of peptide antibodies to probe for the mitoxantrone resistance-associated protein MXR/BCRP/ABCP/ABCG2. *Biochimica et Biophysica Acta (BBA)-Biomembranes,* 1565**,** 6-16.

LU, H., CHEN, C. & KLAASSEN, C. 2004. Tissue distribution of concentrative and equilibrative nucleoside transporters in male and female rats and mice. *Drug Metabolism and Disposition,* 32**,** 1455-1461.

LYNCH, T. & PRICE, A. 2007. The effect of cytochrome P450 metabolism on drug response, interactions, and adverse effects. *Am Fam Physician,* 1**,** 391-396.

MADIN, S. H. & DARBY N, B. J. 1958. Established kidney cell lines of normal adult bovine and ovine origin. *Proc Soc Exp Biol Med,* 98**,** 574-6.

MAHER, J. M., SLITT, A. L., CHERRINGTON, N. J., CHENG, X. & KLAASSEN, C. D. 2005. Tissue distribution and hepatic and renal ontogeny of the multidrug resistance-associated protein (Mrp) family in mice. *Drug Metabolism and Disposition,* 33**,** 947-955.

MAIER, T., GÜELL, M. & SERRANO, L. 2009. Correlation of mRNA and protein in complex biological samples. *FEBS Letters,* 583**,** 3966-3973.

MALIEPAARD, M., SCHEFFER, G. L., FANEYTE, I. F., VAN GASTELEN, M. T. A., PIJNENBORG, A. C. L. M., SCHINKEL, A. H., VAN DE VIJVER, M. J., SCHEPER, R. J. & SCHELLENS, J. H. M. 2001. Subcellular localization and distribution of the breast cancer resistance protein transporter in normal human tissues. *Cancer Research,* 61**,** 3458-3464.

MANLEY, P. W., COWAN-JACOB, S. W., BUCHDUNGER, E., FABBRO, D., FENDRICH, G., FURET, P., MEYER, T. & ZIMMERMANN, J. 2002. Imatinib: a selective tyrosine kinase inhibitor. *European Journal of Cancer,* 38**,** S19-S27.

MARCHETTI, S., MAZZANTI, R., BEIJNEN, J. H. & SCHELLENS, J. H. M. 2007. Concise review: clinical relevance of drug-drug and herb-drug interactions mediated by the ABC transporter ABCB1 (MDR1, P-glycoprotein). *The oncologist,* 12**,** 927-941.

MARIADASON, J. M., NICHOLAS, C., L'TALIEN, K. E., ZHUANG, M., SMARTT, H. J. M., HEERDT, B. G., YANG, W., CORNER, G. A., WILSON, A. J., KLAMPFER, L., ARANGO, D. & AUGENLICHT, L. H. 2005. Gene expression profiling of intestinal epithelial cell maturation along the crypt-villus axis. *Gastroenterology,* 128**,** 1081-1088.

MARSHMAN, E., BOOTH, C. & POTTEN, C. S. 2002. The intestinal epithelial stem cell. *Bioessays,* 24**,** 91-98.

MARTIGNONI, M., GROOTHUIS, G. M. M. & DE KANTER, R. 2006. Species differences between mouse, rat, dog, monkey and human CYP-mediated drug metabolism, inhibition and induction. *Expert opinion on drug metabolism & toxicology,* 2**,** 875-984.

MATHEW, S., GEORGE, S. P., WANG, Y., SIDDIQUI, M. R., SRINIVASAN, K., TAN, L. & KHURANA, S. 2008. Potential molecular mechanism for c-Src kinase-mediated regulation of intestinal cell migration. *Journal of Biological Chemistry,* 283**,** 22709-22722.

MATSSON, P., PEDERSEN, J. M., NORINDER, U., BERGSTRÖM, C. A. S. & ARTURSSON, P. 2009. Identification of novel specific and general inhibitors of the three major human ATP-binding cassette transporters P-gp, BCRP and MRP2 among registered drugs. *Pharmaceutical research,* 26**,** 1816-1831.

MATSUBARA, T., KIM, H. J., MIYATA, M., SHIMADA, M., NAGATA, K. & YAMAZOE, Y. 2004. Isolation and characterization of a new major intestinal CYP3A form, CYP3A62, in the rat. *Journal of Pharmacology and Experimental Therapeutics,* 309**,** 1282-1290.

MAYER, R., KARTENBECK, J., BÜCHLER, M., JEDLITSCHKY, G., LEIER, I. & KEPPLER, D. 1995. Expression of the MRP gene-encoded conjugate export pump in liver and its selective absence from the canalicular membrane in transport-deficient mutant hepatocytes. *The Journal of cell biology,* 131**,** 137-150.

MCNICHOLAS, C. M., BROWN, C. D. & TURNBERG, L. A. 1994. Na-K-Cl cotransport in villus and crypt cells from rat duodenum. *American Journal of Physiology-Gastrointestinal and Liver Physiology,* 30**,** G1004.

MELLMAN, I. & NELSON, W. J. 2008. Coordinated protein sorting, targeting and distribution in polarized cells. *Nature Reviews Molecular Cell Biology,* 9**,** 833-845.

MILLER, C. P., MCGEHEE JR., R. E. & HABENER, J. F. 1994. IDX-1: a new homeodomain transcription factor expression in rat pancreatic islets and duodenum that transactivates the somatostatin gene. *The EMBO journal,* 13**,** 1145-1156.

MIRSKI, S. E. L., GERLACH, J. H. & COLE, S. P. C. 1987. Multidrug resistance in a human small cell lung cancer cell line selected in adriamycin. *Cancer Research,* 47**,** 2594-2598.

MITSCHKE, D., REICHEL, A., FRICKER, G. & MOENNING, U. 2008. Characterization of cytochrome P450 protein expression along the entire length of the intestine of male and female rats. *Drug Metabolism and Disposition,* 36**,** 1039-1045.

MIYAKE, K., MICKLEY, L., LITMAN, T., ZHAN, Z., ROBEY, R., CRISTENSEN, B., BRANGI, M., GREENBERGER, L., DEAN, M. & FOJO, T. 1999. Molecular Cloning of cDNAs Which Are Highly Overexpressed in Mitoxantrone-resistant Cells Demonstration of Homology to ABC Transport Genes. *Cancer Research,* 59**,** 8-13.

MOHRMANN, K., VAN EIJNDHOVEN, M. A. J., SCHINKEL, A. H. & SCHELLENS, J. H. M. 2005. Absence of N-linked glycosylation does not affect plasma membrane localization of breast cancer resistance protein (BCRP/ABCG2). *Cancer chemotherapy and pharmacology,* 56**,** 344-350.

MOLDOVAN, G.-L., PFANDER, B. & JENTSCH, S. 2007. PCNA, the Maestro of the Replication Fork. *Cell,* 129**,** 665-679.

MOOLENBEEK, C. & RUITENBERG, E. J. 1981. The 'Swiss roll': a simple technique for histological studies of the rodent intestine. *Laboratory Animals,* 15**,** 57-59.

MOTTINO, A. D., HOFFMAN, T., JENNES, L. & VORE, M. 2000. Expression and localization of multidrug resistant protein mrp2 in rat small intestine. *Journal of Pharmacology and Experimental Therapeutics,* 293**,** 717-723.

MOULY, S. P. & PAINE, M. F. 2003. P-glycoprotein increases from proximal to distal regions of human small intestine. *Pharmaceutical research,* 20**,** 1595-1599.

MÜLLER, H., KLINKHAMMER, W., GLOBISCH, C., KASSACK, M. U., PAJEVA, I. K. & WIESE, M. 2007. New functional assay of P-glycoprotein activity using Hoechst 33342. *Bioorganic & medicinal chemistry,* 15**,** 7470-7479.

MULLER, J., LIPS, K. S., METZNER, L., NEUBERT, R. H. H., KOEPSELL, H. & BRANDSCH, M. 2005. Drug specificity and intestinal membrane localization of human organic cation transporters (OCT). *Biochemical pharmacology,* 70**,** 1851-1860.

MUTCH, D. M., ANDERLE, P., FIAUX, M., MANSOURIAN, R., VIDAL, K., WAHLI, W., WILLIAMSON, G. & ROBERTS, M.-A. 2004. Regional variations in ABC transporter expression along the mouse intestinal tract. *Physiological reviews,* 17**,** 11-20.

NAKANISHI, T., SHIOZAWA, K., HASSEL, B. A. & ROSS, D. D. 2006. Complex interaction of BCRP/ABCG2 and imatinib in BCR-ABL expressing cells: BCRP-mediated resistance to imatinib is attenuated by imatinib-induced reduction of BCRP expression. *Blood,* 108**,** 678-684.

NAKATA, K., TANAKA, Y., NAKANO, T., ADACHI, T., TANAKA, H., KAMINUMA, T. & ISHIKAWA, T. 2006. Nuclear receptor-mediated transcriptional regulation in Phase I, II, and III

xenobiotic metabolizing systems. *Drug metabolism and pharmacokinetics,* 21**,** 437-457.

NAVIA, M. A. & CHATURVEDI, P. R. 1996. Design principles for orally bioavailable drugs. *Drug discovery today,* 1**,** 179-189.

NEBERT, D. W. & RUSSELL, D. W. 2002. Clinical importance of the cytochromes P450. *The Lancet,* 360**,** 1155-1162.

NIES, A. T. & KEPPLER, D. 2007. The apical conjugate efflux pump ABCC2 (MRP2). *Pflügers Archiv-European Journal of Physiology,* 453**,** 643-659.

OHLAND, C. L. & MACNAUGHTON, W. K. 2010. Probiotic bacteria and intestinal epithelial barrier function. *American Journal of Physiology-Gastrointestinal and Liver Physiology,* 298**,** G807-G819.

OUELLETTE, A. J. 1997. Paneth cells and innate immunity in the crypt microenvironment. *Gastroenterology,* 113**,** 1779-1784.

PAGEOT, L.-P., PERREAULT, N., BASORA, N., FRANCOEUR, C., MAGNY, P. & BEAULIEU, J.-F. 2000. Human cell models to study small intestinal functions: Recapitulation of the crypt-villus axis. *Microscopy Research and Technique,* 49**,** 394-406.

PAINE, M. F., KHALIGHI, M., FISHER, J. M., SHEN, D. D., KUNZE, K. L., MARSH, C. L., PERKINS, J. D. & THUMMEL, K. E. 1997. Characterization of interintestinal and intraintestinal variations in human CYP3A-dependent metabolism. *Journal of Pharmacology and Experimental Therapeutics,* 283**,** 1552-1562.

PAINE, M. F., HART, H. L., LUDINGTON, S. S., HAINING, R. L., RETTIE, A. E. & ZELDIN, D. C. 2006. The human intestinal cytochrome P450 ''pie''. *Drug Metabolism and Disposition,* 34**,** 880-886.

PAN, Y.-Z., MORRIS, M. E. & YU, A.-M. 2009. MicroRNA-328 Negatively Regulations the Expression of Breast Cancer Resistance Protein (BCRP/ABCG2) in Human Cancer Cells. *Molecular pharmacology,* 75**,** 1374-1379.

PERREAULT, N. & BEAULIEU, J.-F. O. 1998. Primary cultures of fully differentiated and pure human intestinal epithelial cells. *Experimental cell research,* 245**,** 34-42.

PINTO, D. & CLEVERS, H. 2005. Wnt control of stem cells and differentiation in the intestinal epithelium. *Experimental cell research,* 306**,** 357-363.

PLOCKE, D. J. & VALLEE, B. L. 1962. Interaction of Alkaline Phosphatase of E. coli with Metal Ions and Chelating Agents. *Biochemistry,* 1**,** 1039-1043.

PORTER, E. M., BEVINS, C. L., GHOSH, D. & GANZ, T. 2002. The multifaceted Paneth cell. *Cellular and Molecular Life Sciences CMLS,* 59**,** 156-170.

POTTEN, C. S. 1977. Extreme sensitivity of some intestinal crypt cells to X and γ irradiation. *Nature,* 269**,** 518-521

PROULX, P. 1991. Structure-function relationships in intestinal brush border membranes. *Biochimica et Biophysica Acta (BBA)-Reviews on Biomembranes,* 1071**,** 255-271.

ROBEY, R. W., TO, K. K. K., POLGAR, O., DOHSE, M., FETSCH, P., DEAN, M. & BATES, S. E. 2009. ABCG2: a perspective. *Advanced drug delivery reviews,* 61**,** 3-13.

ROCHAT, B., ZOETE, V., GROSDIDIER, A., VON GRÜNIGEN, S., MARULL, M. & MICHIELIN, O. 2008. In vitro biotransformation of imatinib by the tumor expressed CYP1A1 and CYP1B1. *Biopharmaceutics & drug disposition,* 29**,** 103-118.

ROSENBERG, M. F., KAMIS, A. B., CALLAGHAN, R., HIGGINS, C. F. & FORD, R. C. 2003. Three-dimensional structures of the mammalian multidrug resistance P-glycoprotein demonstrate major conformational changes in the transmembrane domains upon nucleotide binding. *Journal of Biological Chemistry,* 278**,** 8294-8299.

ROST, D., MAHNER, S., SUGIYAMA, Y. & STREMMEL, W. 2002. Expression and localization of the multidrug resistance-associated protein 3 in rat small and large intestine. *American Journal of Physiology-Gastrointestinal and Liver Physiology,* 282**,** G720-G726.

SAI, Y. & TSUJI, A. 2004. Transporter-mediated drug delivery: recent progress and experimental approaches. *Drug discovery today,* 9**,** 712-720.

SAI, Y. 2005. Biochemical and molecular pharmacological aspects of transporters as determinants of drug disposition. *Drug metabolism and pharmacokinetics,* 20**,** 91-99.

SANDUSKY, G. E., MINTZE, K. S., PRATT, S. E. & DANTZIG, A. H. 2002. Expression of multidrug resistanceâ€associated protein 2 (MRP2) in normal human tissues and carcinomas using tissue microarrays. *Histopathology,* 41**,** 65-74.

SASTRY, S. V., NYSHADHAM, J. R. & FIX, J. A. 2000. Recent technological advances in oral drug delivery - a review. *Pharmaceutical science & technology today,* 3**,** 138-145.

SATO, T., VRIES, R. G., SNIPPERT, H. J., VAN DE WETERING, M., BARKER, N., STANGE, D. E., VAN ES, J. H., ABO, A., KUJALA, P. & PETERS, P. J. 2009. Single Lgr5 stem cells build crypt villus structures in vitro without a mesenchymal niche. *Nature,* 459**,** 262-265.

SCHARENBERG, C. W., HARKEY, M. A. & TOROK-STORB, B. 2002. The ABCG2 transporter is an efficient Hoechst 33342 efflux pump and is preferentially expressed by immature human hematopoietic progenitors. *Blood,* 99**,** 507-512.

SCHEFFER, G. L., KOOL, M., HEIJN, M., DE HAAS, M., PIJNENBORG, A. C. L. M., WIJNHOLDS, J., VAN HELVOORT, A., DE JONG, M. C., HOOIJBERG, J. H. & MOL, C. A. A. M. 2000. Specific detection of multidrug resistance proteins MRP1, MRP2, MRP3, MRP5, and MDR3 P-glycoprotein with a panel of monoclonal antibodies. *Cancer Research,* 60**,** 5269-5277.

SCHOLLER, J. & LEVĚQUE, D. 2011. Molecular pharmacokinetic determinants of anticancer kinase inhibitors in humans. *Oncology Reviews,* 5**,** 77-92.

SEELIGER, M. A., NAGAR, B., FRANK, F., CAO, X., HENDERSON, M. N. & KURIYAN, J. 2007. c-Src binds to the cancer drug imatinib with an inactive Abl/c-Kit conformation and a distributed thermodynamic penalty. *Structure,* 15**,** 299-311.

SHAPIRO, A. B., CORDER, A. B. & LING, V. 1997. P-Glycoprotein Mediated Hoechst 33342 Transport Out of the Lipid Bilayer. *European Journal of Biochemistry,* 250**,** 115-121.

SHEPPARD, D. N. & WELSH, M. J. 1999. Structure and function of the CFTR chloride channel. *Physiological reviews,* 79**,** S23-S45.

SHIGETA, J., KATAYAMA, K., MITSUHASHI, J., NOGUCHI, K. & SUGIMOTO, Y. 2010. BCRP/ABCG2 confers anticancer drug resistance without covalent dimerization. *Cancer science,* 108**,** 1813-1821.

SHIN, H.-C., KIM, H.-R., CHO, H.-J., YI, H., CHO, S.-M., LEE, D.-G., ABD EL-ATY, A. M., KIM, J.-S., SUN, D. & AMIDON, G. L. 2009. Comparative gene expression of intestinal metabolizing enzymes. *Biopharmaceutics & drug disposition,* 30**,** 411-421.

SILBERG, D. G., SWAIN, G. P., SUH, E. R. & TRABER, P. G. 2000. Cdx1 and Cdx2 expression during intestinal development. *Gastroenterology,* 119**,** 961-971.

SIMMONS, N. L. 1981. The action of ouabain upon chloride secretion in cultured MDCK epithelium. *Biochimica et Biophysica Acta (BBA)-Biomembranes,* 646**,** 243-250.

SMIT, J. J. M., SCHINKEL, A. H., ELFERINK, R. P. J., GROEN, A. K., WAGENAAR, E., VAN DEEMTER, L., MOL, C., OTTENHOFF, R., VAN DER LUGT, N. M. T. & VAN ROON, M. A. 1993. Homozygous disruption of the murine MDR2 P-glycoprotein gene leads to a complete absence of phospholipid from bile and to liver disease. *Cell,* 75**,** 451-462.

SMIT, J. J., SCHINKEL, A. H., MOL, C. A., MAJOOR, D., MOOI, W. J., JONGSMA, A. P., LINCKE, C. R. & BORST, P. 1994. Tissue distribution of the human MDR3 P-glycoprotein. *Laboratory investigation; a journal of technical methods and pathology,* 71**,** 638-649.

SMITH, P. C., KARPOWICH, N., MILLEN, L., MOODY, J. E., ROSEN, J., THOMAS, P. J. & HUNT, J. F. 2002. ATP binding to the motor domain from an ABC transporter drives formation of a nucleotide sandwich dimer. *Molecular cell,* 10**,** 139-149.

SNOECK, V., GODDEERIS, B. & COX, E. 2005. The role of enterocytes in the intestinal barrier function and antigen uptake. *Microbes and infection,* 7**,** 997-1004.

STAUD, F. & PAVEK, P. 2005. Breast cancer resistance protein (BCRP/ABCG2). *The international journal of biochemistry & cell biology,* 37**,** 720-725.

STEFFANSEN, B., NIELSEN, C. U., BRODIN, B., ERIKSSON, A. H., ANDERSEN, R. & FROKJAER, S. 2004. Intestinal solute carriers: an overview of trends and strategies for improving oral drug absorption. *European journal of pharmaceutical sciences,* 21**,** 3-16.

SUH, E. R., CHEN, L., TAYLOR, J. & TRABER, P. G. 1994. A homeodomain protein related to caudal regulates intestine-specific gene transcription. *Molecular and cellular biology,* 14**,** 7340-7351.

SUH, E. & TRABER, P. G. 1996. An Intestine-Specific Homeobox Gene Regulates Proliferation and Differentiation. *Molecular And Cellular Biology,* 16**,** 619-625.

SUZUKI, H. & SUGIYAMA, Y. 2004. Hepatic Drug Metabolism. *Molecular Pathogenesis of Cholestasis***,** 135-148.

SZAKACS, G., VARADI, A., ÖZVEGY-LACZKA, C. & SARKADI, B. 2008. The role of ABC transporters in drug absorption, distribution, metabolism, excretion and toxicity (ADME-Tox). *Drug discovery today,* 13**,** 379-393.

SZAKÁCS, Z., BÉNI, S., VARGA, Z., ÖRFI, L., KÉRI, G. & NOSZÁL, B. 2005. Acid-base profiling of imatinib (gleevec) and its fragments. *Journal of medicinal chemistry,* 48**,** 249-255.

TAIPALENSUU, J., TÖRNBLOM, H., LINDBERG, G., EINARSSON, C., SJÖQVIST, F., MELHUS, H. K., GARBERG, P., SJÖSTRÖM, B., LUNDGREN, B. & ARTURSSON, P. 2001. Correlation of gene expression of ten drug efflux proteins of the ATP-binding cassette transporter family in normal human jejunum and in human intestinal epithelial Caco-2 cell monolayers. *Journal of Pharmacology and Experimental Therapeutics,* 299**,** 164-170.

TAKAKURA, Y., HINOI, T., OUE, N., SASADA, T., KAWAGUCHI, Y., OKAJIMA, M., AKYOL, A., FEARON, E. R., YASUIE, W. & OHDAN, H. 2010. CDX2 Regulates Multidrug Resistance 1 Gene Expression in Malignant Intestinal Epithelium. *Molecular and Cellular Pathology,* 70**,** 6767-6778.

TANG, W., CHANG, S. B. & HEMLER, M. E. 2004. Links between CD147 function, glycosylation, and caveolin-1. *Molecular biology of the cell,* 15**,** 4043-4050.

TEETER, L. D., BECKER, F. F., CHISARI, F. V., LI, D. J. & KUO, M. T. 1990. Overexpression of the multidrug resistance gene mdr3 in spontaneous and chemically induced mouse hepatocellular carcinomas. *Molecular and cellular biology,* 10**,** 5728-5735.

TERADA, T. & INUI, K.-I. 2007. Gene expression and regulation of drug transporters in the intestine and kidney. *Biochemical Pharmcology,* 73**,** 440-449.

THOMAS, J., WANG, L., CLARK, R. E. & PIRMOHAMED, M. 2004. Active transport of imatinib into and out of cells: implications for drug resistance. *Blood,* 104**,** 3739-3745.

THWAITES, D. T., CAVET, M., HIRST, B. H. & SIMMONS, N. L. 1995. Angiotensin-converting enzyme (ACE) inhibitor transport in human intestinal epithelial (Caco2) cells. *British journal of pharmacology,* 114**,** 981-986.

TIRONA, R. G. & KIM, R. B. 2005. Nuclear receptors and drug disposition gene regulation. *Journal of Pharmaceutical Sciences,* 94**,** 1169-1186.

TO, K. K. K., ZHAN, Z., LITMAN, T. & BATES, S. 2008. Regulation of ABCG2 Expression at the 3' Untralsation Region of Its mRNA through Modulation of Transcript Stability and Protein Translation by a Putative MicroRNA in the S1 Colon Cancer Cell Line. *Molecular and cellular biology,* 28**,** 5147-5161.

TO, K. K. W., ROBEY, R., ZHAN, Z., BANGIOLO, L. & BATES, S. E. 2011. Upregulation of ABCG2 by romidepsin via the aryl hydrocarbon receptor pathway. *Molecular Cancer Research,* 9**,** 516-527.

TREZISE, A. E., ROMANO, P. R., GILL, D. R., HYDE, S. C., SEPULVEDA, F. V., BUCHWALD, M. & HIGGINS, C. F. 1992. The multidrug resistance and cystic fibrosis genes have complementary patterns of epithelial expression. *The EMBO journal,* 11**,** 4291.

TUCKER, M. J. 1997. *Diseases of the Wistar Rat*, 1st edition: Taylor & Francis, page 4.

UAUY, R., QUAN, R. & GIL, A. 1994. Role of Nucleotides in Intestinal Development and Repair: Implications for Infant Nutrition1. *J Nutr,* 124**,** 1436S-1441S.

URQUHART, B. L., TIRONA, R. G. & KIM, R. B. 2007. Nuclear Receptors and the Regulation of Drug-Metabolizing Enzymes and Drug Transporters: Implications for Interindividual Variability in Response to Drugs. *The Journal of Clinical Pharmacology,* 47**,** 566-578.

VALENCIA-SANCHEZ, M. A., LIU, J., HANNON, G. J. & PARKER, R. 2006. Control of trasnaltion anf mRNA degradation by miRNAs and siRNAs. *Genes & development,* 20**,** 515-524.

VANDER BORGHT, S., LIBBRECHT, L., KATOONIZADEH, A., VAN PELT, J., CASSIMAN, D., NEVENS, F., VAN LOMMEL, A., PETERSEN, B. E., FEVERY, J. & JANSEN, P. L. 2006. Breast cancer resistance protein (BCRP/ABCG2) is expressed by progenitor cells/reactive ductules and hepatocytes and its expression pattern is influenced by disease etiology and species type: possible functional consequences. *Journal of Histochemistry & Cytochemistry,* 54**,** 1051-1059.

VANDESOMPELE, J., DE PAEPE, A. & SPELEMAN, F. 2002a. Elimination of primer-dimer artifacts and genomic coamplification using a two-step SYBR Green I real-time RT-PCR. *Anal Biochem,* 303**,** 95 - 98.

VANDESOMPELE, J., DE PRETER, K., PATTYN, F., POPPE, B., VAN ROY, N., DE PAEPE, A. & SPELEMAN, F. 2002b. Accurate normalization of real-time quantitative RT-PCR data by geometric averaging of multiple internal control genes. *Genome Biology,* 3**,** research0034.1 - research0034.11.

VASILIOU, V., VASILIOU, K. & NEBERT, D. W. 2009. Human ATP-binding cassette (ABC) transporter family. *Human genomics,* 3**,** 281.

VOLPE, D. A. 2008. Variability in Caco2 and MDCK Cell-Based Intestinal Permeability Assays. *Journal of Pharmaceutical Sciences,* 97**,** 712-725.

WALKER, J. M. 2009. The bicinchoninic acid (BCA) assay for protein quantitation. *The Protein Protocols Handbook.* Springer.

WALTER, E. & KISSEL, T. 1995. Heterogeneity in the human intestinal cell line Caco-2 leads to differences in transepithelial transport. *European journal of pharmaceutical sciences,* 3**,** 215-230.

WALTERS, J. R. F., HOWARD, A., RUMBLE, H. E. E., PRATHALINGAM, R. S., SHAW-SMITH, C. J. & LEGON, S. 1997. Differences in expression of Homeobox Transcription Factors in Proximal and Distal Human Small Intestine. *Gastroenterology,* 113**,** 472-477.

WANG, F., WANG, J., LIU, D. & SU, Y. 2010. Normalizing genes for real-time polymerase chain reaction in epithelial and nonepithelial cells of mouse small intestine. *Analytical Biochemistry,* 399**,** 211-217.

WANG, X., HAWKINS, B. T. & MILLER, D. S. 2011. Aryl hydrocarbon receptor-mediated up-regulation of ATP-driven xenobiotic efflux transporters at the blood-brain barrier. *The FASEB Journal,* 25**,** 644-652.

WEBSTER, M. J. 2011. *MDR1 and BCRP mediated transport; identification and regulation of MDR1 and BCRP in renal and intestinal cell lines.* Master of Research, Newcastle Univeristy.

WEISER, M. M. 1973. Intestinal epithelial cell surface membrane glycoprotein synthesis I. An indicator of cellular differentiation. *Journal of Biological Chemistry,* 248**,** 2536-2541.

WHITE, D. L., SAUNDERS, V. A., DANG, P., ENGLER, J., ZANNETTINO, A. C. W., CAMBARERI, A. C., QUINN, S. R., MANLEY, P. W. & HUGHES, T. P. 2006. OCT-1 mediated influx is a key determinant of the intracellular uptake of imatinib but not nilotinib (AMN107): reduced OCT-1 activity is the cause of low in vitro sensitivity to imatinib. *Blood,* 108**,** 697-704.

WHITE, D. L., SAUNDERS, V. A., DANG, P., ENGLER, J., VENABLES, A., ZRIM, S., ZANNETTINO, A., LYNCH, K., MANLEY, P. W. & HUGHES, T. 2007. Most CML patients who have a suboptimal response to imatinib have low OCT-1 activity: higher doses of imatinib may overcome the negative impact of low OCT-1 activity. *Blood,* 110**,** 4064-4072.

WILKINSON, G. R. 2005. Drug metabolism and variability among patients in drug response. *New England Journal of Medicine,* 352**,** 2211-2221.

WRIGHT, J. A., HASLAM, I. S., COLEMAN, T. & SIMMONS, N. L. 2010. Breast cancer resistance protein BCRP (ABCG2)-mediated transepithelial nitrofurantoin secretion and its regulation in human intestinal epithelial (Caco-2) layers. *European journal of pharmacology,* 672**,** 70-76.

WRIGHT, J. A. 2011. *BCRP (ABCG2) expression, function and regulation in model and intestinal epithelial cells.* Doctor of Philosophy, Newcastle University.

XIA, C. Q., LIU, N., YANG, D., MIWA, G. & GAN, L.-S. 2005. Expression, localization, and functional characteristics of breast cancer resistance protein in caco-2 cells. *Drug Metabolism and Disposition,* 33**,** 637-643.

XIA, C. Q., LIU, N., MIWA, G. T. & GAN, L.-S. 2007. Interactions of cyclosporin a with breast cancer resistance protein. *Drug Metabolism and Disposition,* 35**,** 576-582.

XU, J., LIU, Y., YANG, Y., BATES, S. & ZHANG, J.-T. 2004. Characterization of oligomeric human half-ABC transporter ATP-binding cassette G2. *Journal of Biological Chemistry,* 279**,** 19781-19789.

XU, J., PENG, H., CHEN, Q., LIU, Y., DONG, Z. & ZHANG, J.-T. 2007. Oligomerization Domain of the Multidrug Resistance Associated Transporter ABCG2 and Its Dominant Inhibitory Activity. *Cancer Research,* 67**,** 4373-4381.

YAMAKAWA, Y., HAMADA, A., SHUTO, T., YUKI, M., UCHIDA, T., KAI, H., KAWAGUCHI, T. & SAITO, H. 2011. Pharmacokinetic impact of SLCO1A2 polymorphisms on imatinib disposition in patients with chronic myeloid leukemia. *Clinical Pharmacology & Therapeutics,* 90**,** 157-163.

YAN, L.-H., WEI, W.-Y., CAO, W.-L., ZHANG, X.-S., XIE, Y.-B. & XIAO, Q. 2015. Overexpression of CDX2 in gastric cancer cells promotes the development of multidrug resistance. *Am J Cancer Res,* 5**,** 321-332.

YOSHIKAWA, T., INOUE, R., MATSUMOTO, M., YAJIMA, T., USHIDA, K. & IWANAGA, T. 2011. Comparative expression of hexose transporters (SGLT1, GLUT1, GLUT2 and GLUT5) throughout the mouse gastrointestinal tract. *Histochemistry and cell biology,* 135**,** 183-194.

YUMOTO, R., MURAKAMI, T., NAKAMOTO, Y., HASEGAWA, R., NAGAI, J. & TAKANO, M. 1999. Transport of rhodamine 123, a P-glycoprotein substrate, across rat intestine and Caco-2 cell monolayers in the presence of cytochrome P-450 3A-related compounds. *Journal of Pharmacology and Experimental Therapeutics,* 289**,** 149-155.

ZHANG, L., BUCHET, R. & AZZAR, G. R. 2004. Phosphate binding in the active site of alkaline phosphatase and the interactions of 2-nitrosoacetophenone with alkaline phosphatase-induced small structural changes. *Biophysical journal,* 86**,** 3873-3881.

ZHANG, Q.-Y., DING, X. & KAMINSKY, L. S. 1997. cDNA cloning, heterologous expression, and characterization of rat intestinal CYP2J4. *Archives of biochemistry and biophysics,* 340**,** 270-278.

ZHANG, Q.-Y., RANER, G., DING, X., DUNBAR, D., COON, M. J. & KAMINSKY, L. S. 1998. Characterization of the cytochrome P450 CYP2J4: expression in rat small intestine and role in retinoic acid biotransformation from retinal. *Archives of biochemistry and biophysics,* 353**,** 257-264.

ZHOU, S., SCHUETZ, J. D., BUNTING, K. D., COLAPIETRO, A.-M., SAMPATH, J., MORRIS, J. J., LAGUTINA, I., GROSVELD, G. C., OSAWA, M. & NAKAUCHI, H. 2001. The ABC transporter Bcrp1/ABCG2 is expressed in a wide variety of stem cells and is a molecular determinant of the side-population phenotype. *Nature medicine,* 7**,** 1028-1034.

ZHOU, S., LIAO, L., CHEN, C., ZENG, W., LIU, S., SU, J., ZHAO, S., CHEN, M., KUANG, Y. & CHEN, X. 2013. CD147 mediates chemoresistance in breast cancer via ABCG2 by affecting its cellular localization and dimerization. *Cancer letters,* 337**,** 285-292.

ZHOU, S. F. 2008. Structure, function and regulation of P-glycoprotein and its clinical relevance in drug disposition. *Xenobiotica,* 38**,** 802-832.

ZIMMERMANN, C., GUTMANN, H., HRUZ, P., GUTZWILLER, J.-P., BEGLINGER, C. & DREWE, J. 2005. Mapping of multidrug resistance gene 1 and multidrug resistance-associated protein isoform 1 to 5 mRNA expression along the human intestinal tract. *Drug Metabolism and Disposition,* 33**,** 219-224.

ÖZVEGY-LACZKA, C., CSEREPES, J., ELKIND, N. B. & SARKADI, B. 2005. Tyrosine kinase inhibitor resistance in cancer: role of ABC multidrug transporters. *Drug resistance updates,* 8**,** 15-26.

9. Appendices

Appendix 9.1:

1. *** Start Time Steps ***
2. *** Select EZ Prep ***
3. Warmup slide to 75 Deg C and incubation for 8 minutes
4. Apply EZPrep volume adjust (DXT)
5. Apply depar volume adjust (DXT)
6. Apply coverslip (DXT)
7. Incubate for 8 minutes
8. Rinse slide
9. Apply depar volume adjust (DXT)
10. Apply coverslip (DXT)
11. Warmup slide to 37 Deg C and incubation for 4 minutes
12. *** Select SSC wash ***
13. *** Select EZ prep ***
14. *** Select EZ prep ***
15. Rinse slide
16. Jet drain (DXT)
17. Apply long cell conditioner #1 (DXT)
18. Apply CC coverslip (DXT)
19. Apply long cell conditioner #1 (DXT)
20. Apply CC coverslip (DXT)
21. Warmup slide to 95 Deg C and incubate for 8 minutes
22. Apply coverslip (DXT)
23. Apply medium cell conditioner #1 (DXT)
24. Warmup slide to 100 Deg C and incubate for 4 minutes
25. Apply coverslip (DXT)
26. Apply cell conditioner #1 (DXT)
27. Incubate for 4 minutes
28. Apply coverslip (DXT)
29. Apply cell conditioner #1 (DXT)
30. Incubate for 4 minutes
31. Apply coverslip (DXT)
32. Apply medium cell conditioner #1 (DXT)
33. Incubate for 4 minutes
34. Apply coverslip (DXT)
35. Apply medium cell conditioner #1 (DXT)
36. Incubate for 4 minutes
37. Apply coverslip (DXT)
38. Apply cell conditioner #1 (DXT)
39. Incubate for 4 minutes
40. Apply coverslip (DXT)
41. Apply cell conditioner #1 (DXT)
42. Incubate for 4 minutes
43. Apply coverslip (DXT)

44. Disable slide heater
45. Incubate for 8 minutes
46. Rinse slide with reaction buffer
47. Adjust slide volume with reaction buffer
48. Apply coverslip (DXT)
49. *** Select EZ prep ***
50. *** Select SSC wash ***
51. Warmup slide to 36 Deg C and incubate for 4 minutes
52. Rinse slide with reaction buffer
53. Adjust slide volume with reaction buffer
54. Apply coverslip (DXT)
55. Apply one drop on Inhibitor CM and incubate for 4 minutes
56. Rinse slide with reaction buffer
57. Adjust slide volume with reaction buffer
58. Apply coverslip (DXT)
59. *** Mixers off ***
60. *** Wait for button (Hold Step) ***
61. *** Mixers on ***
62. Rinse slide with reaction buffer
63. Adjust slide volume with reaction buffer
64. Apply coverslip (DXT)
65. *** Mixers off ***
66. *** Hand Apply primary antibody (titration) ***
67. *** Mixers on ***
68. Incubate for [32 minutes] (Primary antibody incubation)
69. Rinse slide with reaction buffer
70. Adjust slide volume with reaction buffer
71. Apply coverslip (DXT)
72. Rinse slide with reaction buffer
73. Adjust slide volume with reaction buffer
74. Apply coverslip (DXT)
75. Rinse slide with reaction buffer
76. Adjust slide volume with reaction buffer
77. Apply one drop of [OMap anti-Ms HRP] (Multimer HRP), apply coverslip and incubate for [20 minutes]
78. Rinse slide with reaction buffer
79. Adjust slide volume with reaction buffer
80. Apply coverslip (DXT)
81. Rinse slide with reaction buffer
82. Adjust slide volume with reaction buffer
83. Apply coverslip (DXT)
84. Rinse slide with reaction buffer
85. Adjust slide volume with reaction buffer
86. Apply coverslip (DXT)
87. Rinse slide with reaction buffer
88. Adjust slide volume with reaction buffer

89. Apply one drop of DAB CM and one drop of H2O2, apply coverslip and incubate for 8 minutes
90. Rinse slide with reaction buffer
91. Adjust slide volume with reaction buffer
92. Apply one drop of copper CM, apply coverslip and incubate for 4 minutes
93. Rinse slide with reaction buffer
94. Adjust slide volume with reaction buffer
95. Apply coverslip (DXT)
96. *** Select EZ prep ***
97. Rinse slide with reaction buffer
98. Adjust slide volume with reaction buffer
99. Apply coverslip (DXT)
100. Disable slide heater
101. *** Mixers off ***
102. *** Wait for button (Hold counterstain/cleaning) ***
103. *** Mixers on ***
104. *** Select EZ prep ***

Appendix 9.1 Example ventana staining protocol showing methodology for Mouse_sCC1 treatment for sections with the Omni-UltraMap HRP antibody detection system.

Appendix 9.2:

	Duodenum					Jejunum				Ileum			Colon	
	AVG mRNA expression (fmol/sample)	SEM	Duo vs. Jej	Duo vs. Ileum	Duo vs. Colon	AVG mRNA expression (fmol/sample)	SEM	Jej vs. Ileum	Jej vs. Colon	AVG mRNA expression (fmol/sample)	SEM	Ileum vs. Colon	AVG mRNA expression (fmol/sample)	SEM
Alph	0.1	0.0				0.1	0.0			0.1	0.1		0.0	0.0
Sglt1	326.4	40.5	*		##	583.6	69.7		##	517.3	133.1	##	29.4	5.1
Cftr	13.7	0.8	**		###	20.6	1.5		###	20.0	2.8	#	6.2	0.9
Villin	183.5	18.0	**	•••	#	301.2	14.5		###	334.8	12.5	###	96.2	20.3
Ca2	92.3	24.7		•		55.0	15.4		#	23.9	4.7	##	186.8	41.7
Lap3	177.2	14.9	***	••	##	402.6	13.6		###	529.4	63.4	##	43.7	1.8
Pcna	29.8	0.9			##	27.2	3.2		#	27.7	3.8	#	14.0	3.3
Nkcc1	13.7	2.5				9.8	2.4			18.8	6.6		38.0	10.0
Mdr1a	2.4	0.4	*	•		4.5	0.6	•		10.2	2.2		4.6	1.6
Mdr1b	0.3	0.1				0.2	0.0			0.2	0.1		0.1	0.1
Mrp1	2.6	0.7			#	2.0	0.2		###	2.5	0.3	###	5.6	0.4
Mrp2	8.8	2.0			#	14.8	2.9		#	14.5	5.5		0.5	0.2
Mrp3	8.0	0.7			##	7.3	0.3		##	9.3	2.5	##	41.8	7.6
Mrp4	0.3	0.1				0.1	0.1		#	0.3	0.1		0.4	0.1
Mrp5	2.9	0.9				2.2	0.4		#	1.5	0.2	##	4.0	0.5
Mrp6	12.6	2.8			#	13.0	2.9		##	11.6	2.3	##	0.8	0.2
Mrp7	2.7	0.6				2.9	0.4		#	3.4	0.2	##	1.7	0.2
Bcrp	24.2	2.9		•		30.6	2.4		#	46.4	8.4	#	19.1	3.5
Cnt2	115.5	11.2	**		###	192.6	12.2		###	129.1	36.5	##	12.4	3.6
PepT1	12.0	0.9	*	•	###	22.9	3.7		##	33.1	6.6	###	2.5	0.9
Oct1	11.1	1.5			###	9.5	1.9		##	7.6	0.9	##	1.8	0.5
Octn1	3.7	0.6	*	••	##	6.5	0.6		###	7.4	0.6	###	0.4	0.1
Octn2	18.7	1.3		•		25.3	3.5		#	25.5	2.0	##	11.6	2.8
Oat3	0.1	0.1	*	••		0.3	0.0		###	0.3	0.1	###	0.0	0.0
Oatp-3	0.0	0.0		•		0.0	0.0			0.1	0.0	##	0.0	0.0
Oatp-b	2.0	0.3				1.9	0.3			3.3	0.9		2.5	0.4

-

Cont.

	Duodenum					Jejunum				Ileum			Colon	
	AVG mRNA expression (fmol/sample)	SEM	Duo vs. Jej	Duo vs. Ileum	Duo vs. Colon	AVG mRNA expression (fmol/sample)	SEM	Jej vs. Ileum	Jej vs. Colon	AVG mRNA expression (fmol/sample)	SEM	Ileum vs. Colon	AVG mRNA expression (fmol/sample)	SEM
Cyp1a1	9.0	5.2				15.1	3.2		##	12.2	3.9	#	0.7	0.2
Cyp2b2	2.4	1.0				7.8	2.6		#	16.8	6.3	#	1.1	0.3
Cyp2c11	0.1	0.0			#	0.1	0.0		#	0.1	0.0		0.0	0.0
Cyp2c6v1	0.1	0.0				0.1	0.0		##	0.2	0.1	#	0.0	0.0
Cyp2d1/2d9	5.0	0.5			##	6.5	0.9		##	3.9	0.7	##	31.2	5.3
Cyp2d3	0.1	0.0				0.2	0.0			0.2	0.1		0.6	0.3
Cyp2d4/2d6	11.2	1.0	**	•	##	18.3	1.1		###	18.8	2.2	###	4.4	0.8
Cyp2j4	22.2	4.5			#	25.8	3.8		##	25.1	5.6	#	3.5	0.7
Cyp2s1	21.9	2.3	*		###	37.1	3.7		###	21.9	7.0	#	1.9	0.6
Cyp3a1/3a23	0.1	0.0	*			0.2	0.0		###	0.1	0.0	#	0.0	0.0
Cyp3a18	10.0	2.6		•		19.6	4.4		#	29.8	6.5	##	2.0	0.2
Cyp3a62	20.3	4.9				38.9	6.2		##	44.1	10.2	#	12.2	2.1
Cyp3a9	183.7	22.7	***			389.7	17.0		###	300.5	99.7		121.0	23.6

Appendix 9.2 Expression of NanoString codeset genes in the duodenum, jejunum, ileum and colon of male rat intestine with accompanying statistical comparison between intestinal sections.

mRNA concentrations (fmol/sample) for each gene within specificed regions were calculated from an average n = 4 male rats and are shown ± SEM. Data shown has been normalised against assay controls and expression of HSKP genes, Gapdh, Hmbs and Hprt1. Student's t-test analyses were performed with tests in which Welche's correction was applied shaded light grey. Welche's correction was applied to remove assumption of equal population variance of any two regions being compared following sample variance assessment between two populations using Levene's test. Where Levene's test showed probability < 0.05 (results not shown) population variances were concluded to be different and Welche's correction applied to prevent occurance of false statistical significance. Resultant p-values with p-summaries are shown. * $p < 0.05$, ** $p < 0.01$ and *** $p < 0.001$ vs. jejunum. • $p < 0.05$, •• $p < 0.01$, and •••$p < 0.001$ vs. ileum. # $p < 0.05$, ## $p < 0.01$ and ### $p < 0.001$.

Appendix 9.3:

	mRNA concentration fmol/sample										Average fold change	SEM	Average Log2 fold change	SEM	P summary
	Villus tip				Average	Crypt				Average					
Alph	0.2	0.2	0.1	0.0	0.1 ± 0.0	0.0	0.0	0.0	0.0	0.0 ± 0.0					
Lap3	1252.0	1512.5	1587.1	827.2	1294.7 ± 171.6	175.9	220.3	380.2	614.1	347.6 ± 99.1	4.9	1.4	2.0	0.6	**
Ca2	39.4	48.9	59.8	38.7	46.7 ± 5.0	8.2	10.4	16.2	32.4	16.8 ± 5.5	3.6	0.8	1.7	0.5	**
Sglt1	1476.9	1935.4	434.7	734.5	1145.4 ± 342.5	463.4	392.4	357.2	459.7	418.2 ± 26.1	2.7	0.8	1.2	0.5	
Villin	639.8	762.4	553.4	541.6	624.3 ± 51.0	219.3	236.1	300.9	398.9	288.8 ± 40.7	2.3	0.4	1.1	0.3	**
PCNA	10.6	8.0	14.3	11.3	11.0 ± 1.3	27.7	28.8	31.1	21.4	27.2 ± 2.1	0.4	0.1	-1.3	0.2	***
Nkcc1	5.0	4.7	10.4	6.0	6.5 ± 1.3	45.3	43.6	32.1	18.2	34.8 ± 6.3	0.2	0.1	-2.4	0.5	**
Cftr	37.5	28.6	32.7	18.2	29.2 ± 4.1	17.5	15.2	11.1	11.4	13.8 ± 1.5	2.1	0.3	1.1	0.2	*
Mdr1a	58.8	85.0	37.4	24.9	51.5 ± 13.2	12.1	15.3	12.0	16.1	13.9 ± 1.1	3.8	0.9	1.8	0.4	
Mdr1b	0.3	0.5	0.3	0.1	0.3 ± 0.1	0.1	0.1	0.1	0.0	0.1 ± 0.0					
Mrp1	2.5	3.7	4.2	3.2	3.4 ± 0.4	1.9	2.4	1.7	2.3	2.1 ± 0.2	1.7	0.3	0.7	0.2	*
Mrp2	64.6	77.3	22.9	18.6	45.9 ± 14.8	10.9	10.8	7.9	10.5	10.0 ± 0.7	4.4	1.3	1.9	0.5	
Mrp3	15.8	18.3	20.7	17.6	18.1 ± 1.0	7.0	10.0	9.1	12.3	9.6 ± 1.1	2.0	0.2	0.9	0.2	**
Mrp4	0.1	0.4	0.3	0.3	0.3 ± 0.1	0.3	0.4	0.4	0.3	0.3 ± 0.0					
Mrp5	6.0	5.6	8.9	4.6	6.3 ± 0.9	1.2	0.9	1.0	2.1	1.3 ± 0.3	5.5	1.3	2.3	0.4	**
Mrp6	42.8	51.7	29.8	20.6	36.3 ± 6.9	9.8	11.4	7.7	7.4	9.1 ± 1.0	3.9	0.4	1.9	0.2	*
Mrp7	5.6	7.4	9.5	5.7	7.0 ± 0.9	1.6	1.8	1.6	2.3	1.8 ± 0.2	4.0	0.7	1.9	0.3	**
Bcrp	126.5	186.1	154.5	111.7	144.7 ± 16.4	35.3	38.9	53.2	84.3	52.9 ± 11.2	3.2	0.7	1.5	0.4	**
Cnt2	312.2	156.3	360.8	110.1	234.9 ± 60.3	37.3	52.7	46.4	67.0	50.9 ± 6.2	5.2	1.7	2.1	0.6	
PepT1	141.0	199.4	110.3	122.1	143.2 ± 19.8	27.8	34.5	34.7	74.9	43.0 ± 9.1	3.9	0.9	1.8	0.4	**
Oct1	8.5	10.6	13.9	9.2	10.5 ± 1.2	5.1	6.7	5.2	6.6	5.9 ± .1	1.8	0.3	0.8	0.2	*
Octn1	16.6	28.0	18.9	11.3	18.7 ± 3.5	6.2	6.5	7.5	6.5	6.7 ± .1	2.8	0.5	1.4	0.3	*
Octn2	99.9	111.6	89.0	39.2	84.9 ± 15.9	13.7	14.0	16.3	21.4	16.3 ± 1.2	5.6	1.4	2.3	0.5	**
Oatp-b	2.2	2.5	2.3	4.2	2.8 ± 0.5	5.2	6.2	4.4	4.2	5.0 ± 0.5	0.6	0.1	-0.9	0.3	*
Oat3	0.9	1.0	1.0	0.5	0.9 ± 0.1	0.1	0.2	0.3	0.4	0.2 ± 0.3					
Oatp-3	0.3	0.3	0.4	0.2	0.3 ± 0.0	0.0	0.0	0.0	0.1	0.0 ± 3.3					

Cont.

	mRNA concentration fmol/sample										Average fold change	SEM	Average Log2 fold change	SEM	
	Villus tip				Average	Crypt				Average					P summary
Cyp1a1	20.3	26.4	30.3	17.1	23.5 ± 3.0	3.0	3.8	4.3	9.4	5.1 ± 1.4	5.6	1.3	2.3	0.5	**
Cyp2b2	60.5	54.8	114.5	49.3	69.8 ± 15.1	7.3	9.5	8.8	37.1	15.7 ± 7.2	7.1	2.5	2.4	0.7	*
Cyp2c11	0.0	0.0	0.0	0.0	0.0 ± 0.0	0.0	0.0	0.0	0.0	0.0 ± 0.0					
Cyp2c6v1	1.8	1.6	1.5	0.7	1.4 ± 0.2	0.1	0.2	0.2	0.4	0.2 ± 0.0					
Cyp2d1/2d9	6.8	12.7	7.6	5.3	8.1 ± 1.6	1.1	1.4	1.0	2.9	1.6 ± 0.4	6.2	1.6	2.4	0.5	**
Cyp2d3	0.6	0.7	0.3	0.2	0.5 ± 0.1	0.1	0.1	0.0	0.1	0.1 ± 0.0					
Cyp2d4/2d6	47.8	72.4	57.9	44.1	55.5 ± 6.3	8.7	10.8	8.9	18.3	11.7 ± 2.3	5.3	1.0	2.3	0.3	***
Cyp2j4	44.2	59.2	59.2	32.8	48.9 ± 6.4	6.8	7.6	16.3	14.6	11.3 ± 2.4	5.0	1.3	2.2	0.4	**
Cyp2s1	89.1	31.3	38.4	13.4	43.1 ± 16.2	13.1	5.4	6.3	8.2	8.3 ± 1.7	5.1	1.2	2.2	0.5	
Cyp3a1/3a23	0.4	0.6	0.4	0.2	0.4 ± 0.1	0.1	0.1	0.1	0.3	0.1 ± 0.0					
Cyp3a18	72.9	113.9	101.4	67.8	89.0 ± 11.1	18.4	20.1	17.7	47.3	25.9 ± 7.1	4.2	1.0	1.9	0.5	**
Cyp3a62	212.2	255.7	200.0	49.4	179.3 ± 44.9	30.7	36.7	38.2	43.6	37.3 ± 2.6	5.1	1.4	2.0	0.6	*
Cyp3a9	532.6	466.3	634.8	151.2	446.2 ± 104.3	52.0	43.8	39.0	108.6	60.8 ± 16.1	9.6	3.1	2.8	0.8	*

Appendix 9.3 mRNA concentrations (fmol/sample) of genes included in the NanoString codeset in villus tip and crypt samples from ileal samples of male rats, including fold change, log_2 fold change and statistical analysis.

Replicate mRNA concentrations (fmol/sample) from n=4 animals are shown, with average mRNA concentrations ± SEM. Average fold change villus tip versus crypt is shown alongside relative log_2 fold change. Data shown has been normalised against assay controls and expression of HSKP genes, Gapdh, Hmbs and Hprt1. Student's t-test analyses were performed with tests in which Welche's correction was applied are shaded grey. Welche's correction was applied to remove assumption of equal population variance of any two regions being compared following sample variance assessment between two populations using Levene's test. Where Levene's test showed probability < 0.05 (results not shown) population variances were concluded to be different and Welche's correction applied to prevent occurance of false statistical significance. Resultant p-values with p-summaries are shown, * $p < 0.05$, ** $p < 0.01$ and *** $p < 0.001$. Average fold change values were calculated using pairwise comparisons of animal replicate mRNA concentrations as opposed to fold change of average mRNA concentration in villus tip and crypt samples.